energies

Special Issue Reprint

Advanced Energy Systems in Energy Resilient, Zero/ Positive Energy Buildings, Communities and Districts

Edited by
Ala Hasan and Hassam Ur Rehman

mdpi.com/journal/energies

MDPI

Advanced Energy Systems in Energy Resilient, Zero/Positive Energy Buildings, Communities and Districts

Advanced Energy Systems in Energy Resilient, Zero/Positive Energy Buildings, Communities and Districts

Guest Editors

Ala Hasan
Hassam Ur Rehman

MDPI

Basel • Beijing • Wuhan • Barcelona • Belgrade • Novi Sad • Cluj • Manchester

Guest Editors

Ala Hasan
Independent Researcher
Baghdad
Iraq

Hassam Ur Rehman
VTT Technical Research
Centre of Finland
Espoo
Finland

Editorial Office
MDPI AG
Grosspeteranlage 5
4052 Basel, Switzerland

This is a reprint of the Special Issue, published open access by the journal *Energies* (ISSN 1996-1073), freely accessible at: https://www.mdpi.com/journal/energies/special_issues/2YA064JBV2.

For citation purposes, cite each article independently as indicated on the article page online and as indicated below:

Lastname, A.A.; Lastname, B.B. Article Title. *Journal Name* **Year**, *Volume Number*, Page Range.

ISBN 978-3-7258-4187-5 (Hbk)
ISBN 978-3-7258-4188-2 (PDF)
https://doi.org/10.3390/books978-3-7258-4188-2

© 2025 by the authors. Articles in this book are Open Access and distributed under the Creative Commons Attribution (CC BY) license. The book as a whole is distributed by MDPI under the terms and conditions of the Creative Commons Attribution-NonCommercial-NoDerivs (CC BY-NC-ND) license (https://creativecommons.org/licenses/by-nc-nd/4.0/).

Contents

About the Editors . . . . . **vii**

Preface . . . . . **ix**

Hassam ur Rehman and Ala Hasan
Advanced Energy Systems in Energy-Resilient and Zero/Positive Energy Buildings, Communities, and Districts
Reprinted from: *Energies* **2025**, *18*, 1218, https://doi.org/10.3390/en18051218 . . . . . **1**

Ieva Pakere, Kirils Goncarovs, Armands Grāvelsiņš and Marita Agate Zirne
Dynamic Modelling of Data Center Waste Heat Potential Integration in District Heating in Latvia
Reprinted from: *Energies* **2024**, *17*, 445, https://doi.org/10.3390/en17020445 . . . . . **4**

Wassila Tercha, Sid Ahmed Tadjer, Fathia Chekired and Laurent Canale
Machine Learning-Based Forecasting of Temperature and Solar Irradiance for Photovoltaic Systems
Reprinted from: *Energies* **2024**, *17*, 1124, https://doi.org/10.3390/en17051124 . . . . . **16**

Paraskevas Koukaras, Akeem Mustapha, Aristeidis Mystakidis and Christos Tjortjis
Optimizing Building Short-Term Load Forecasting: A Comparative Analysis of Machine Learning Models
Reprinted from: *Energies* **2024**, *17*, 1450, https://doi.org/10.3390/en17061450 . . . . . **36**

Eugenia Rossi di Schio, Vincenzo Ballerini, Jan Kašpar, Manuela Neri, Mariagrazia Pilotelli, Edoardo Alessio Piana and Paolo Valdiserri
Applicability of Face Masks as Recyclable Raw Materials for Self-Made Insulation Panels
Reprinted from: *Energies* **2024**, *17*, 1648, https://doi.org/10.3390/en17071648 . . . . . **62**

Jaume Fitó and Julien Ramousse
Multi-Stakeholder Decision Support Based on Multicriteria Assessment: Application to Industrial Waste Heat Recovery for a District Heating Network in Grenoble, France
Reprinted from: *Energies* **2024**, *17*, 2009, https://doi.org/10.3390/en17092009 . . . . . **77**

Henriqueta Teixeira, A. Moret Rodrigues, Daniel Aelenei and M. Glória Gomes
Simulation-Based Evaluation of the Impact of an Electrochromic Glazing on the Energy Use and Indoor Comfort of an Office Room
Reprinted from: *Energies* **2024**, *17*, 2110, https://doi.org/10.3390/en17092110 . . . . . **102**

Irene Bertolami, Adriano Bisello, Marco Volpatti and Marta Carla Bottero
Exploring Multiple Benefits of Urban and Energy Regeneration Projects: A Stakeholder-Centred Methodological Approach
Reprinted from: *Energies* **2024**, *17*, 2862, https://doi.org/10.3390/en17122862 . . . . . **131**

Qin Xiaoxiang, Yin Junjia, Nuzul Azam Haron, Aidi Hizami Alias, Teik Hua Law and Nabilah Abu Bakar
Status, Challenges and Future Directions in the Evaluation of Net-Zero Energy Building Retrofits: A Bibliometrics-Based Systematic Review
Reprinted from: *Energies* **2024**, *17*, 3826, https://doi.org/10.3390/en17153826 . . . . . **153**

Alexios Papaioannou, Asimina Dimara, Christoforos Papaioannou, Ioannis Papaioannou, Stelios Krinidis, Christos-Nikolaos Anagnostopoulos, et al.
Simulation of Malfunctions in Home Appliances' Power Consumption
Reprinted from: *Energies* **2024**, *17*, 4529, https://doi.org/10.3390/en17174529 . . . . . **176**

Georgios Martinopoulos, Alexandros Tsimpoukis, Vasileios Sougkakis, Petros Dallas, Komninos Angelakoglou, Paraskevi Giourka and Nikolaos Nikolopoulos
A Comprehensive Approach to Nearly Zero Energy Buildings and Districts: Analysis of a Region Undergoing Energy Transition
Reprinted from: *Energies* **2024**, *17*, 5581, https://doi.org/10.3390/en17225581 . . . . . **207**

Ran Wang, Zijian He, Xue Zhai and Shilei Lu
Application and Performance Evaluation of Key Technologies in Green Buildings
Reprinted from: *Energies* **2024**, *17*, 6418, https://doi.org/10.3390/en17246418 . . . . . **225**

Pengqiang Nie, Song Xu, Zhenlin Wang, Seiji Hashimoto, Linfeng Sun and Takahiro Kawaguchi
Design and Implementation of a Wireless Power Transfer System Using LCL Coupling Network with Inherent Constant-Current and Constant-Voltage Output for Battery Charging
Reprinted from: *Energies* **2025**, *18*, 341, https://doi.org/10.3390/en18020341 . . . . . **248**

Maurizio Cellura, Alberto Fichera, Francesco Guarino and Rosaria Volpe
Leveraging Positive Energy Districts Surplus for the Achievement of the Sustainable Development Goals
Reprinted from: *Energies* **2025**, *18*, 506, https://doi.org/10.3390/en18030506 . . . . . **265**

Helmut Bruckner, Svitlana Alyokhina, Simon Schneider, Manuela Binder, Zain Ul Abdin, Rudi Santbergen, et al.
Lessons Learned from Four Real-Life Case Studies: Energy Balance Calculations for Implementing Positive Energy Districts
Reprinted from: *Energies* **2025**, *18*, 560, https://doi.org/10.3390/en18030560 . . . . . **285**

Kangji Li, Shiyi Zhou, Mengtao Zhao and Borui Wei
Short-Term Building Electrical Load Prediction by Peak Data Clustering and Transfer Learning Strategy
Reprinted from: *Energies* **2025**, *18*, 686, https://doi.org/10.3390/en18030686 . . . . . **301**

Muhyiddine Jradi
A Decision-Making Tool for Sustainable Energy Planning and Retrofitting in Danish Communities and Districts
Reprinted from: *Energies* **2025**, *18*, 692, https://doi.org/10.3390/en18030692 . . . . . **323**

About the Editors

Ala Hasan

Dr. Ala Hasan was a Principal Scientist in the Smart Energy and Built Environment Research Area at VTT, the Technical Research Centre of Finland. He had worked in the field of energy in buildings since 1982. He joined VTT in 2013. Prior to that, he worked at the Helsinki University of Technology and Aalto University since 1998. He held the position of Research Fellow of the Academy of Finland and was PI of several Academy of Finland research projects. He was evaluated as a University Full Professor in 2015. Dr. Hasan has an excellent portfolio in research, scientific publications, earning research funding, as well as offering services to the international scientific community. He has more than 120 publications in international scientific journals, conferences, book chapters, and reports. He was listed within the top 2% most cited scientists in the world in his field as published by Elsevier BV and Stanford University in years 2020 and 2021. He is a member of the Editorial Board of the Buildings journal MDPI Switzerland and is a member of the Editorial Board of the International Journal of Low Carbon Technologies–Oxford Journals UK. He acted as advisor and examiner of several PhD and Licentiate degree students in Finland, Sweden, and Denmark. He was elected in 2021 as a Fellow of IBPSA (The International Building Performance Simulation Association). He initiated IBPSA-Nordic and was its first president. He was a member of the IBPSA-World Board of Directors for several years. He was a member of the Executive Committee of the International Energy Agency (IEA), Energy in Buildings and Communities (EBC).

Hassam Ur Rehman

Dr. Hassam Ur Rehman (D.Sc.) has completed a Ph.D. in the field of Energy Engineering from Aalto University, Finland. Presently, he has been working as a senior scientist at VTT Technical Research Centre of Finland. He is also a Postdoctoral researcher fellow at the Research Council of Finland (Suomen Akatemia) and a PI. He is supporting the research work with his experience in building energy simulation, energy system design for buildings, community-sized energy systems, energy storage, electric vehicles, and multi-objective optimization in order to plan a stable and carbon-neutral society. Currently, he is involved in developing positive energy building concepts and energy resilience at the national and European level along with technical, social, and business-related studies. He is representing Finland in the International Energy Agency (IEA), Energy in Buildings and Communities (EBC) as Executive Committee and leading the IEA EBC Annex 93 on Energy resilience (operating agent) and coordinating IEA EBC Annex83.

Preface

Climate action efforts to reduce greenhouse gas emissions in the building sector are important for cities around the world. In general, this sector is responsible for approximately 40% of the EU's energy consumption and 36% of its emissions. Therefore, energy in buildings, communities, and districts is at the forefront of mitigating emissions and ensuring a sustainable, self-sufficient, and safe future. These goals can be achieved by enhancing energy efficiency and using advanced onsite renewable energy generation, conversion, and storage technologies in buildings, communities, and districts, which can offset the energy imported from grids. Various concepts for net-zero/positive energy buildings and districts (NZPEBDs) have emerged in recent years to shape cities into carbon-neutral communities in the near future. In addition to this, climate change and energy crises (disruptive events) can reduce a building's energy performance and impact occupants' well-being and habitability conditions, especially during a power outage. These buildings and districts can also help reach self-sufficiency, engage users, and provide energy resiliency during outages.

This Special Issue presents innovative research in the domain of buildings, districts and built environment while providing pathways to the new, challenging research avenues for further research. We found that large amount of research topics that were covered showing the diversity and evolving field. We hope that the research results presented will contribute to the future development and research in the field of build environment.

As the Guest Editor of this Special Issue, we would like to say thanks and appreciate to the authors and coauthors who published their articles. We are also grateful to the wonderful reviewers whose valuable time, comments and suggestions helped in improving the quality of the articles and also the MDPI editorial staff who helped us during the entire process of producing the Special Issue.

Ala Hasan and Hassam Ur Rehman
Guest Editors

energies

MDPI

Editorial

Advanced Energy Systems in Energy-Resilient and Zero/Positive Energy Buildings, Communities, and Districts

Hassam ur Rehman [1,*] and Ala Hasan [2]

[1] VTT Technical Research Centre of Finland Ltd., P.O. Box 1000, FI-02044 Espoo, Finland
[2] Independent Researcher, Hai Al-Mustansiriya, Baghdad 02044, Iraq
* Correspondence: hassam.rehman@vtt.fi; Tel.: +358-40-621-5917

The pursuit of sustainable energy solutions has become a critical focus in addressing the challenges of climate change and urbanization. This Special Issue provides a comprehensive overview of recent research in the field of energy and sustainability, encompassing diverse topics such as urban energy planning, short-term electrical load forecasting, energy resilience, energy flexibility, energy efficiency, nearly zero-energy buildings and districts, and the development of Positive Energy Districts (PEDs). The studies included in this Special Issue demonstrate the importance of combining innovative technologies, community engagement, and policy support to achieve energy efficiency and sustainability goals. By exploring the practical applications and impacts of these advancements, this Special Issue fosters a holistic understanding of the current state of energy research and its potential to drive positive change in urban environments. This Special Issue includes a total of 16 papers covering different aspects of building and district planning, technologies and their economics, building design and retrofitting, citizen engagement and the collection of energy data, energy resilience, and energy flexibility.

Multiple studies discuss the development and benefits of Positive Energy Districts (PEDs), which aim to achieve net-zero energy imports and CO_2 emissions while producing surplus renewable energy [1]. PEDs, defined as urban areas that produce more renewable energy than they consume, are explored through various case studies [2]. This Special Issue highlights the importance of building renovations, renewable energy integration, and community engagement in achieving sustainable urban development. PEDs have the potential to support energy accessibility, alleviate energy poverty, and contribute to carbon reduction [3]. Key sustainable development goals can be achieved through PEDs, such as energy accessibility, sustainable cities, and climate action [4]. Different methodologies to evaluate the multiple benefits of PEDs are developed with the use of stakeholder engagement to align project strategies with broader perspectives [5]. The advancements in energy and sustainability research presented in this Special Issue underscore the critical role of innovative technologies, predictive modeling, and community engagement in achieving sustainable urban development. The integration of automated data collection, energy demand prediction, and renewable energy sources into urban energy planning and retrofitting frameworks has demonstrated significant potential in reducing energy consumption and emissions and enhancing efficiency. Positive Energy Districts (PEDs) have emerged as a promising solution to urban sustainability challenges, offering benefits such as energy self-sufficiency, energy resilience, energy flexibility, reduced carbon emissions, and improved social equity and energy resilience [6]. Therefore, future cities and districts require planning that can accommodate such innovative districts and buildings based on local conditions in order to provide carbon-neutral, sustainable, and resilient districts that are socially acceptable and economically feasible.

Evaluations of green building technologies and post-evaluation studies underscore the need for continuous improvement in energy efficiency and occupant satisfaction [7]. While green buildings generally meet energy performance standards, the effectiveness of certain technologies, particularly energy-saving ones, can be improved. Research on novel technologies such as wireless power transfer for battery-charging smart controls, glazing, and the reuse of advanced building materials demonstrates their potential to contribute to sustainability. In addition, producing energy through waste (using heat recovery) is another method that can support sustainability goals [8]. Hence, further research is needed to introduce these innovative solutions to society in a way that is economical, scalable, and can be replicated.

The benefits of district-level energy strategies over individual building retrofits are highlighted in this Special Issue, including significant reductions in CO_2 emissions and energy use. Effective stakeholder engagement can lead to new, more effective solutions; however, new methods are needed to achieve this [9] in order to provide feasible solutions. Advances in machine learning and data analysis are highlighted for improving the accuracy of energy demand predictions [10]. Various machine learning models for short-term load forecasting in buildings are discussed, with the most accurate methods identified based on different data resolutions and time steps. The Special Issue highlights the importance of data preparation in model accuracy, error calculations, forecasting, and performance analysis [10].

This Special Issue highlights the importance of energy-efficient technologies, renewable integration, the circular economy, and advanced data-driven prediction models in creating sustainable and resilient urban environments. From Positive Energy Districts (PEDs) to waste heat recovery and building retrofitting, these approaches are paving the way for the achievement of net-zero and positive energy goals. Technologies such as machine learning and energy simulation tools can enhance the accuracy of energy predictions and the optimization of resources.

We would like to thank the authors of the papers for their valuable contributions to this Special Issue. We also wish to express our gratitude to the reviewers of the papers for their time and effort.

Funding: This Special Issue was supported and funded by the Research Council of Finland, "Energy Resilience in Buildings in Extreme Cold Weather Conditions in Finland 2022–2025 (FinERB), grant number 348060" and "Integration of Building Flexibility into Future Energy Systems 2020–2024 (FlexiB), grant number 333364" and by the European Union's Horizon 2020 research and innovation program [H2020-LC-EEB-03-2019] and the Euratom research and training program 2014–2018 under the project 'EXCESS (FleXible user-CEntric Energy poSitive houseS)' grant agreement No [870157].

Acknowledgments: IEA EBC Annex 93 Energy Resilience of the Buildings in Remote Cold Regions and IEA EBC Annex 83 Positive Energy Districts.

Conflicts of Interest: Author Hassam ur Rehman is employed by the VTT Technical Research Centre of Finland Ltd. The remaining authors declare that the research was conducted in the absence of any commercial or financial relationships that could be construed as a potential conflict of interest. All authors declare no conflicts of interest. The funders had no role in the design of the study; in the collection, analyses, or interpretation of data; in the writing of the manuscript; or in the decision to publish the results.

References

1. Gondeck, M.; Triebel, M.A.; Steingrube, A.; Albert-Seifried, V.; Stryi-Hipp, G. Recommendations for a Positive Energy District Framework—Application and Evaluation of Different Energetic Assessment Methodologies. *Smart Energy* **2024**, *15*, 100147. [CrossRef]
2. Healey Trulsrud, T.; van der Leer, J. Towards a Positive Energy Balance: A Comparative Analysis of the Planning and Design of Four Positive Energy Districts and Neighbourhoods in Norway and Sweden. *Energy Build.* **2024**, *318*, 114429. [CrossRef]
3. Bruckner, H.; Alyokhina, S.; Schneider, S.; Binder, M.; Abdin, Z.U.; Santbergen, R.; Verkou, M.; Zeman, M.; Isabella, O.; Pagliarini, M.; et al. Lessons Learned from Four Real-Life Case Studies: Energy Balance Calculations for Implementing Positive Energy Districts. *Energies* **2025**, *18*, 560. [CrossRef]
4. Schreiber, F. The Long Road from Urban Experimentation to the Transformation of Urban Planning Practice: The Case of Tactical Urbanism in the City of Barcelona. *J. Urban Mobil.* **2025**, *7*, 100100. [CrossRef]
5. Mueller, L.; Marcroft, T.P.; von Beck, C.; Zeiss, J.P.; Schwanitz, V.J.; Wierling, A.; Holstenkamp, L. "First Come, First Served" or "the More, the Merrier"? Organizational Dynamics of Citizen-Led Solar Initiatives and the Presence of Photovoltaic Installations in Germany. *J. Clean. Prod.* **2024**, *449*, 141861. [CrossRef]
6. Ur Rehman, H.; Nik, V.M.; Ramesh, R.; Ala-Juusela, M. Quantifying and Rating the Energy Resilience Performance of Buildings Integrated with Renewables in the Nordics under Typical and Extreme Climatic Conditions. *Buildings* **2024**, *14*, 2821. [CrossRef]
7. Yue, N.; Li, L.; Caini, M.; Xie, X. Occupant Information Computer Vision Sensing-Based Displacement Ventilation in Large Space Building for Improving Indoor Environment and Energy Efficiency. *Build. Environ.* **2025**, *269*, 112364. [CrossRef]
8. Miškić, J.; Dorotić, H.; Pukšec, T.; Schneider, D.R.; Duić, N. Holistic Method for Determining the Techno-Economic Feasibility of Waste Heat for the Planning of the Low-Temperature District Heating Systems. *Energy* **2024**, *313*, 133968. [CrossRef]
9. Bertolami, I.; Bisello, A.; Volpatti, M.; Bottero, M.C. Exploring Multiple Benefits of Urban and Energy Regeneration Projects: A Stakeholder-Centred Methodological Approach. *Energies* **2024**, *17*, 2862. [CrossRef]
10. Purna Prakash, K.; Pavan Kumar, Y.V.; Reddy, C.P.; Pradeep, D.J.; Flah, A.; Alzaed, A.N.; Al Ahamdi, A.A.; Ghoneim, S.S.M. A Comprehensive Analytical Exploration and Customer Behaviour Analysis of Smart Home Energy Consumption Data with a Practical Case Study. *Energy Rep.* **2022**, *8*, 9081–9093. [CrossRef]

Disclaimer/Publisher's Note: The statements, opinions and data contained in all publications are solely those of the individual author(s) and contributor(s) and not of MDPI and/or the editor(s). MDPI and/or the editor(s) disclaim responsibility for any injury to people or property resulting from any ideas, methods, instructions or products referred to in the content.

energies

MDPI

Article

Dynamic Modelling of Data Center Waste Heat Potential Integration in District Heating in Latvia

Ieva Pakere *, Kirils Goncarovs, Armands Grāvelsiņš and Marita Agate Zirne

Institute of Energy Systems and Environment, Faculty of Natural Sciences and Technology, Riga Technical University, Azenes Street 12/1, LV-1048 Riga, Latvia; kirils.goncarovs@edu.rtu.lv (K.G.); armands.gravelsins@rtu.lv (A.G.); marita-agate.zirne@edu.rtu.lv (M.A.Z.)

* Correspondence: ieva.pakere@rtu.lv

Abstract: As demand for data centers (DC) has increased rapidly, so has their electricity consumption. Cooling DCs is essential to maintain optimal temperatures for the operation of servers and equipment. The consequence of the cooling process is that most of the electricity consumed in DCs, including cooling, is eventually dissipated as heat that is released into the atmosphere without any useful application. Recovering and reusing waste heat offers a sustainable solution to reduce primary energy consumption and minimize the environmental impact. Using waste heat from DCs to heat buildings can significantly improve the energy efficiency and environmental sustainability of DCs. Therefore, this research analyzes the existing potential of waste heat recovery from data centers in Latvia and proposes a system dynamic modelling approach for evaluation of the future impact of waste heat on the national heat supply. The overall waste heat generated by DCs in 2022 was 51.37 GWh at a temperature of 65 °C. By 2050, the total heat energy production potential from DCs will increase to 257 GWh, with 201 GWh being utilized.

Keywords: data center; waste heat; district heating; renewable energy; heat pumps; system dynamic modelling; stella modelling

1. Introduction

Sustainable digital infrastructure is a critical policy area in the European Union (EU). As stated in the decision to establish the Digital Decade Policy Program 2030, digital transformation is key for reaching the European Green Deal objectives and such technologies must maximize the impact of policies dealing with climate change and environmental protection [1]. The overall industrialization strategy is directed towards simultaneous environmental improvement and digital transition development [2]. Data centers (DCs) are a crucial digital infrastructure that processes and stores data using electricity [3].

The energy efficiency of DCs is an emerging concern, as more and more data are saved, processed, and transferred to offer a multitude of digital services. It has been suggested that centralized DCs are more energy efficient than individual and distributed information technology. Moreover, to direct electricity consumed by the information and communication technology hardware and basic infrastructure, DCs require vast amounts of cooling energy, traditionally produced with air conditioning units, however, the electricity consumed in a DC almost completely converts to heat. The heat from data centers is mostly not utilized, even though various solutions already exist. As the capacity and size of data centers increase, their energy consumption and associated CO_2 emissions increase [4]. Recovering and reusing waste heat offers a sustainable solution to reduce energy waste and minimize the environmental impact. Using waste heat from DCs to heat buildings can significantly improve the energy efficiency and environmental sustainability of DCs, as buildings are responsible for around 40% of the total energy consumption and 36% of GHG emissions worldwide. In the EU, more than 75% of the energy used to heat a building

comes from fossil fuels, so district heating (DH) operators have focused on recovering and using this waste heat in DH, limiting energy consumption, and reducing CO_2 emissions [5].

Globally, DCs consume 3% of the energy available, creating 4% of greenhouse gas emissions [6]. During use of the equipment in the DC, waste heat is created. The impact of waste heat on technical equipment is alleviated using cooling technological solutions, which increases energy use by 40% [7]. Waste heat recovery and reuse within DCs provides a possibility to both reduce the electricity consumption of DCs and increase the use of renewable energy in heating. The reuse of waste heat within DCs was identified as one of the cheapest heat energy production solutions compared to the use of natural gas and other electricity solutions [8].

The use of waste heat as an energy source in Latvia has been studied in several areas. One study investigated the total national waste heat potential of industrial plants and the distribution of its sources. The total waste heat potential was 272 GWh per year and 14% of the total supply was in rural areas [9]. In another study, a total of the industrial waste heat potential was evaluated for a part of the capital city of Riga [10]. However, the use of low-temperature waste heat from other sources, including DCs, is understudied in Latvia.

2. Literature Review

2.1. Data Centers as Heat Energy Producers

The use of DC's waste heat for district heating (DH) has been evaluated in different global regions and climates. A heat pump is the main technology to increase the outlet temperature to be aligned with the heating network temperature. In the following section, the results of several case studies [11–16] will be described to evaluate the potential results of waste heat recovery system design in DCs.

Jang et al. have evaluated the performance characteristics of a water-source heat pump system to use as a heat energy producer in the residential area of Incheon City in South Korea. The proposed system decreased the overall energy use in the DC by 12.3% and 21.2% in residential housing. The most significant use of the recovered waste heat was observed in January with 65% of the energy from the DC used in residential housing [11].

Güğül et al. assessed the feasibility of the creation of a zero-energy consumption DC with a waste heat recovering system in Kocaeli, Turkey. As a result, the proposed system design decreased electricity consumption by 40% and saved 30,793 m^3 of natural gas with a payback time of six years in combination with a photovoltaic panel instalment [16].

He et al. proposed a DH system design for DC waste heat recovery in Hohhot, China. With a supply heating water temperature of 54 °C, the heat pump produced 73.92 MW of heat load, which alleviated the use of coal by 18 thousand tons per year and decreased the power usage effectiveness (PUE) by 0.13 to 1.17 [12].

Oró et al. evaluated the use of waste heat recovery systems from air-cooled DCs focusing on a DC with 1 MW power in Barcelona, Spain. The overall heat reuse reached 55%, but economically the solution was unfeasible for most of the cases due to the low demand for heat energy in the region [14].

The case studies show significant potential for using the waste heat from DCs as an energy source in domestic heating. Especially, use in colder climates has a high potential to increase the energy efficiency of DCs as well as supply energy to close-by communities.

2.2. Evaluation of Heat Production

Several methods are used for the evaluation of waste heat potential in DCs as energy sources. Primarily, the use of an empirical model or TRNSYS are two main techniques for evaluation [11,14,17–19].

The waste heat potential in TRNSYS is evaluated by recreating a possible system design for a case study [11,14,17]. To perform the evaluation, information on the building, the temperature variations, heat demand, and technical information on each of the elements is required to assess the waste heat potential. The empirical models require fewer data

points to evaluate the waste heat potential compared with TRNSYS models [18,19]. This enables evaluation of the potential on a national level with multiple DCs involved.

In addition, empirical models could be used to create SD models for evaluation of the waste heat over time. Pakere et al. evaluated the national potential of industrial waste heat use and proposed further development scenarios based on the possible policy scenarios created [9]. The same framework has been used in the evaluation of waste heat potential on the district level in Riga, Latvia [10].

2.3. Aim and Scope of the Article

Previous studies on waste heat potential from DCs have mainly assessed the overall potential for utilization locally or in district heating systems. However, the technical feasibility and economic benefits of waste heat integration are dynamic depending on several aspects of the overall energy system, e.g., availability of RES electricity for heat pumps, and the development of investments. Therefore, this article proposes a novel methodology by using an SD approach for the in-depth forecasting of waste heat potential from DCs. This paper aims to evaluate the waste heat potential from DCs and the possible development scenarios for waste heat implementation as an energy source on the national level.

3. Methodology

The methodological framework (Figure 1) in the study is divided into three main sections. The first section includes a waste heat potential assessment through a stakeholder survey to identify the waste heat sources and energy consumption, an empirical waste heat assessment, and the mapping of the quantitative results to evaluate the technical potential and conduct spatial analyses. In the second section, an SDs submodel is developed to evaluate possible adoption scenarios of the technological solutions. In the third step, the developed submodel is integrated within the national energy sector model to evaluate the future role of low-temperature waste heat sources in DH systems.

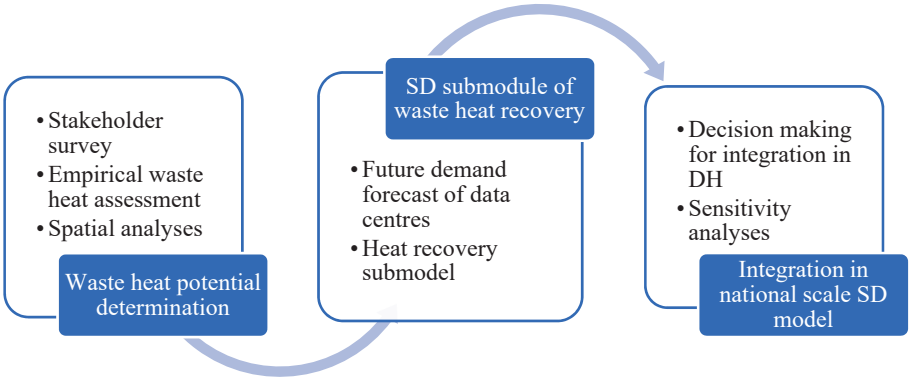


Figure 1. Methodology framework of the current research.

3.1. Waste Heat Potential Determination

The power of information technology (IT) equipment is required to evaluate the waste heat potential of a DC. Several methods for the evaluation of IT equipment power exist. The methodological framework, which uses the nominal power and number of different pieces of equipment, has been developed by Cheung et al. [19].

To reduce the number of data points required, an alternative framework is proposed with the use of the power usage effectiveness (PUE) coefficient used by Oró et al. [14]. The PUE coefficient describes the proportion of the total energy consumed with the energy consumption of IT equipment [20]. Alternatively, if no information on the DC's PUE coefficient was available, the estimation from Cho et al. of a typical DC's energy consumption with a PUE coefficient of 2.27 was used. To evaluate the waste heat potential of a DC, the assumption from Cho et al. that 80% of the electricity power used by the IT equipment

creates waste heat as a side product to perform computational operations was used [21]. The information was gathered via a stakeholder survey with three data submission options: the first option contained only the information on annual electricity consumption, the second option contained both electricity consumption and the DC's PUE coefficient and the third option contained the nominal power and a number of different technical components of the DCs to perform the calculation by the methodology developed by Cheun et al. [18]. As the survey was distributed among the operators of data centers containing technical parameters available for the target audience, the reliability of data is considered high by the authors of the publication. A total of 40 possible DCs were identified, which were operated by 29 different organizations. The survey was disseminated to the operators of the data centers from October 2022 to January 2023.

For the evaluation of the coefficient of performance (COP) for heat pumps, assumptions on the heat source and heat sink temperatures are used. The outlet temperature from the DC is assumed to be around 18.7 °C, but the necessary inlet temperature for the DH is 65 °C [22]. The calculation was performed based on the Lorenz efficiency method [23]. The COP was used to determine the total heat energy produced by the heat pump and electricity consumption. Heat energy production was evaluated annually without the differentiation of the seasons.

To evaluate the technical feasibility of heat pump use in DCs, an energy reuse factor (ERF) was calculated for every DC based on the relation of the waste heat recovered compared to the total electricity consumption [14]. Additionally, the distances between the DC and the domestic heating network were evaluated by the proximity analysis via the ArcGIS Online software. The payback time (PBP) and the levelized cost of energy (LCOE) were calculated for the economic feasibility evaluation. The payback time was used as a metric based on Jovet et al. assessment of the decision-making in industrial waste heat recovery long-term project planning and the same calculation method was used in this study [24]. The calculation of LCOE was based on the method described in Lotfi et al. on the evaluation of LCOE for microgrids [25].

After the evaluation was completed for every DC, the waste heat potential on the national level was summarized, and the average values of the ERF, PBP, and LCOE were calculated to evaluate the effectiveness of the intervention. The calculated values were used as a base scenario for the SD model.

3.2. SD Submodule of Waste Heat Recovery and Integration in the National Scale SD Model

The SD model evaluates the DC's potential waste heat production with heat pumps on the national level. The comparison of the energy solutions is based on the average heat production cost of different solutions. The heat energy costs for waste heat from DCs are evaluated based on the investment cost for heat pumps, connection costs for DCs to DH networks based on the results of the proximity analysis, electricity prices, and heat supply shortages. The overall system model loop diagram is summarized in Figure 2. Three basic loops are observed: a balancing loop between potential and utilized energy, a balancing loop in the form of investment decisions, and a reinforcing loop in the form of a lack of thermal energy.

The balancing loop between potential and used energy describes a diffusion system with a process of decision-making. The potential of energy generated from waste heat passes to the energy used and returns to the thermal energy potential at the end of the technical life of heat pumps. The second balancing loop describes the creation of investment decisions. Capital investment is one of the main aspects of the investment decision, which is calculated using (1) [26].

$$KI = \frac{II * (1 - AESF) * CS}{\left(1 - \frac{1}{(1+AESF)^{TDC}}\right) * OHDC} \quad (1)$$

where:

KI—capital investment in data centers, EUR/MWh,
II—data center investments, EUR/MW,
AESF—a fraction of available EU funding,
CS—price change fraction,
TDC—technical life cycle of heat pumps, years,
OHDC—DC heat pump working hours, hours/year.

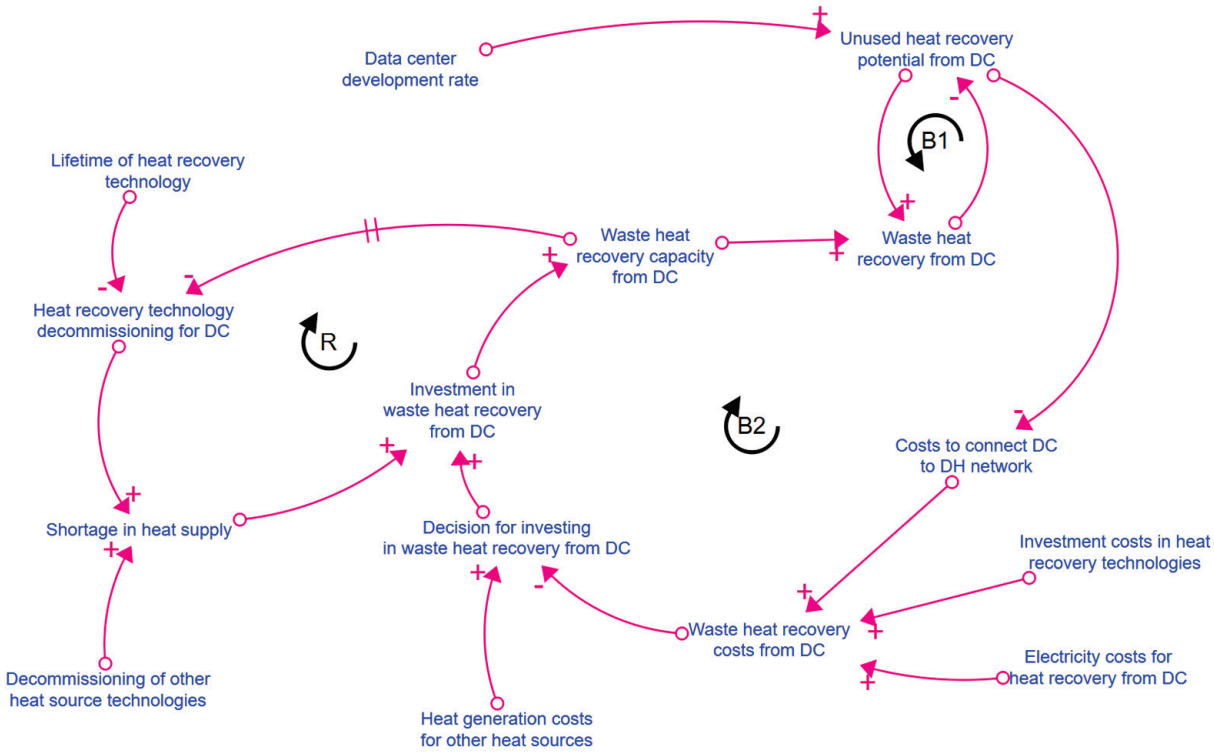


Figure 2. System model loop diagram for waste heat integration.

Reduction in the heat energy tariff is also facilitated by a decrease in the total investment and electricity costs. As the tariff for the generated heat decreases or other energy sources of heat generation increase, the investment decision is reinforced using (2) [26]. After increasing the total investment, the installation capacity of waste heat recovery systems and the amount of energy generated from waste heat used in the future also increases.

$$ILDC = IF * \frac{(KII + ST)}{\frac{PL}{OHDC}} * 1000 \quad (2)$$

where:

ILDC—investment decision for the installation of a data center waste heat recovery system, MW/year,
IF—investment fraction for data center waste heat recovery systems,
KII—total annual investment, GWh/year,
ST—lack of heat energy, GWh/year,
PL—order time, years.

The initial waste heat recovery system potential was estimated from the results of the static evaluation described in Section 2.1. Furthermore, the increase of the waste heat potential in DCs is impacted by the macroeconomic performance prediction for the IT industry. The assumption of Liao et al. on the role of the investment-GDP ratio was used

to evaluate the increase in energy consumption overall [27]. Based on historical data, a fraction of the IT industry's turnover from the total national turnover was used to determine the fraction of energy consumption increase within the IT industry [28]. The GDP and investment ratio was calculated dynamically based on the average rates of change in the 2012–2021 period [29,30]. Based on it, the total electricity consumption was calculated.

The difference between the values in the previous and current year are used to calculate the available power capacity for building DCs. In it, the power is distributed from larger to smaller DCs. The available capacity is divided among a priority order from largest to smallest DC, which uses average electricity capacity for three categories: with electricity capacity above 0.9 MW, from 0.4 to 0.9 MW, and below 0.4 MW. The electricity capacity of the planned newly built data centers is subtracted from the total available capacity, reducing the value of the stock.

The heat energy production potential created by existing and new DCs is dispersed to the waste heat utilization after the implementation of the solution. Based on the 25-year technical life cycle of the heat pumps, the waste heat utilization decreases over time [23]. The decision for the DC's waste heat utilization is based on the energy tariff of the solution compared to other heat energy production technologies. For the evaluation of the energy tariff, four criteria are used: investment cost for the heat pump, new pipeline building cost, operation and maintenance costs for the heat pumps, and electricity price [9,23,31].

The overall tariff evaluation framework is summarized in Figure 3. After evaluation of the cost of heat energy produced with heat pumps, it is compared with other heat energy sources' costs and possible production rates to evaluate the most cost-effective method to meet the heat energy demand. The heat energy demand is estimated on an annual basis without seasonal variation.

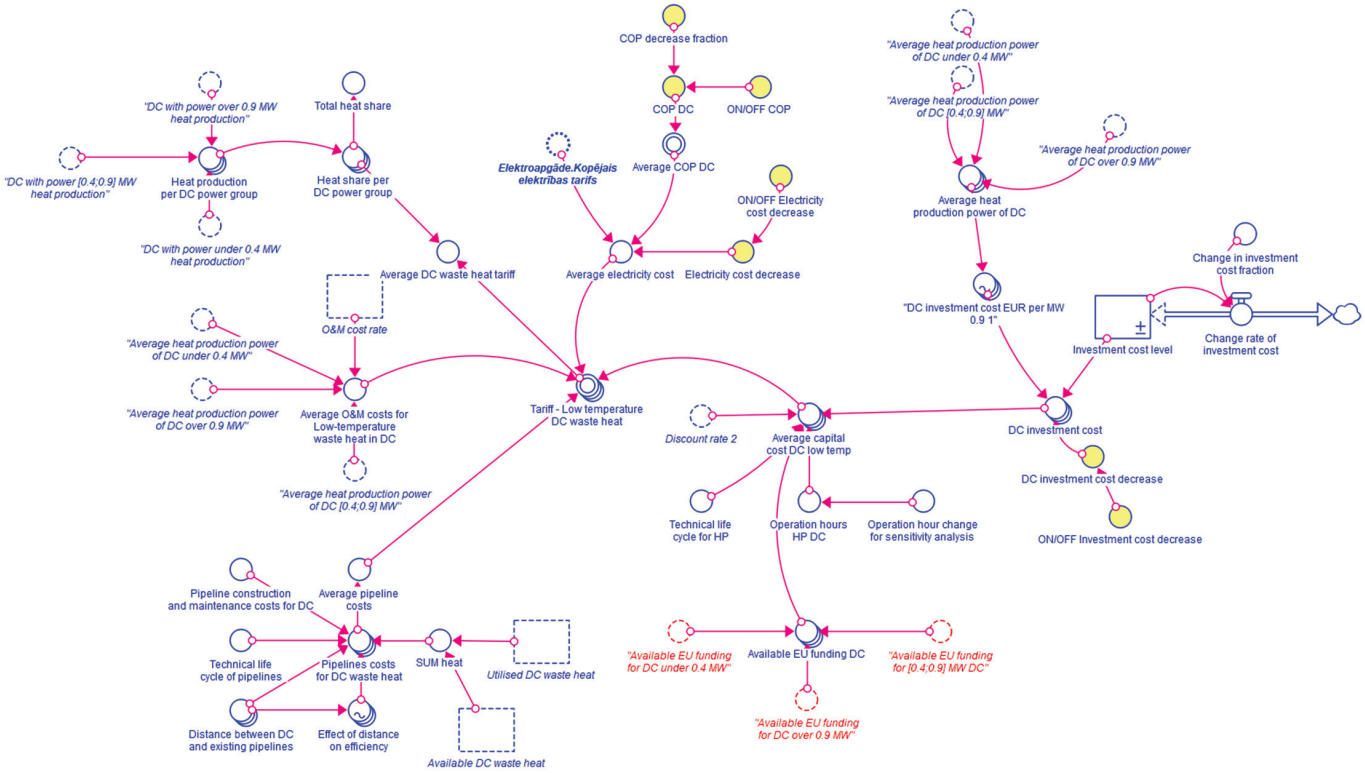


Figure 3. Heat energy tariff evaluation.

The developed waste recovery submodel is integrated within the national SD model developed and described by Pakere et al. [9]. The national scale SD model developed in previous studies encompasses both energy production and consumption, resulting in a more precise description of the entire energy supply system [26]. The optimal resource for

heat or power production is selected based on a comprehensive cost analysis that compares different technologies. The model also includes power generation by using both fossil and renewable energy sources and sectoral linkage of the heating and power sector through cogeneration plants and heat pumps.

4. Results

40 possible DCs were identified from the initially created dataset. 26 out of 40 were confirmed DCs, whereas the operators denied the remaining 14 possible DC locations or did not have additional public information. Based on the results of the survey, a map of DCs was created, see Figure 4. Of 26 DCs, 11 submitted information on energy consumption and the data for the remaining 15 was filled out using the publicly available data. Most of the DCs (24) were in Riga and one was in the city of Ogre and Valmiera. The distribution of DCs is shown in Figure 4.



(**a**) (**b**)

Figure 4. Distribution of DCs (marked with orange dots) in (**a**) Latvia, (**b**) Riga based on survey results.

The electricity consumption of identified DCs and server rooms ranges from 0.02 to 20.15 GWh/year, with an average value of 3.83 GWh/year. The PUE coefficient value ranges from 1.24 to 2.27 with an average of 1.9. The national waste heat potential of DCs is 51.37 GWh/year, which can be utilized to create 63.12 GWh of heat energy with air-to-water heat pumps with COP 4.37. The values of the ERF coefficient are between 0.40 and 0.69 with the highest ERF value being in the DC with the lowest PUE coefficient. The distances between the DCs and DH networks are in the range of 3 to 2265 m, with an average of 371.7 m. The summary of distances between DCs and DH networks is shown in Figure 5. The payback time for the introduction of heat pumps in DCs is from 6.44 years for the biggest DC to 14.98 years for the smallest.

The results of the static assessment of waste heat utilization in DCs were used in the SD model to evaluate the further development of the industry. The energy tariff was evaluated for the three different sizes of DC identified and is summarized in Figure 6. The national value for the heat energy tariff is higher by 59.08 EUR/MWh compared with the average of the three DC types. Furthermore, the use of waste heat in small DCs is economically feasible only up to the year 2034, by which the modelled national heat energy tariff becomes lower. The energy tariff evaluation shows the economic feasibility of heat pump use for waste heat utilization in DCs over 0.4 MW.

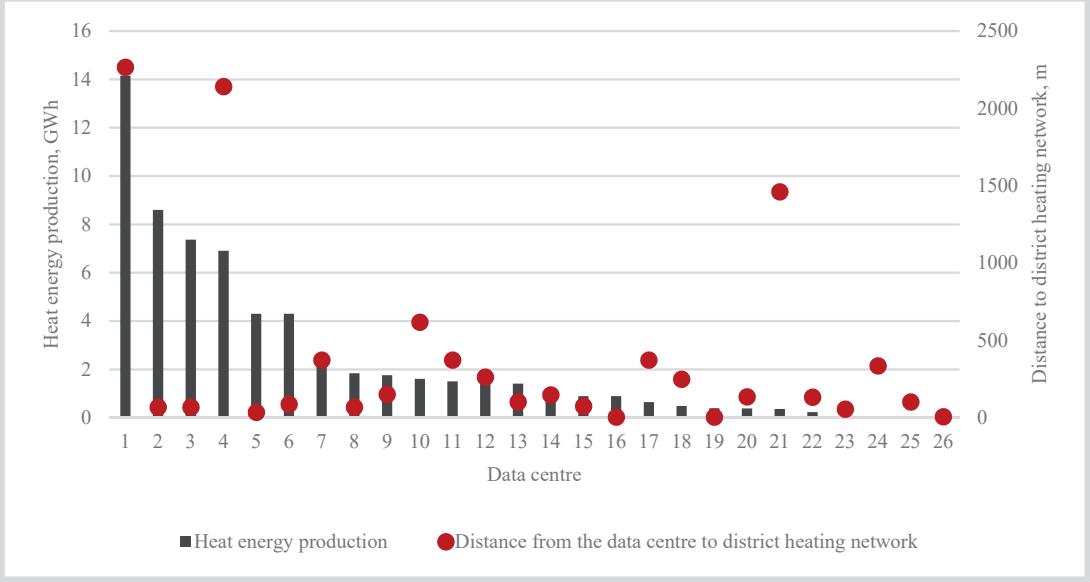


Figure 5. Waste heat production of DCs compared to the distance to the DH network based on survey results.

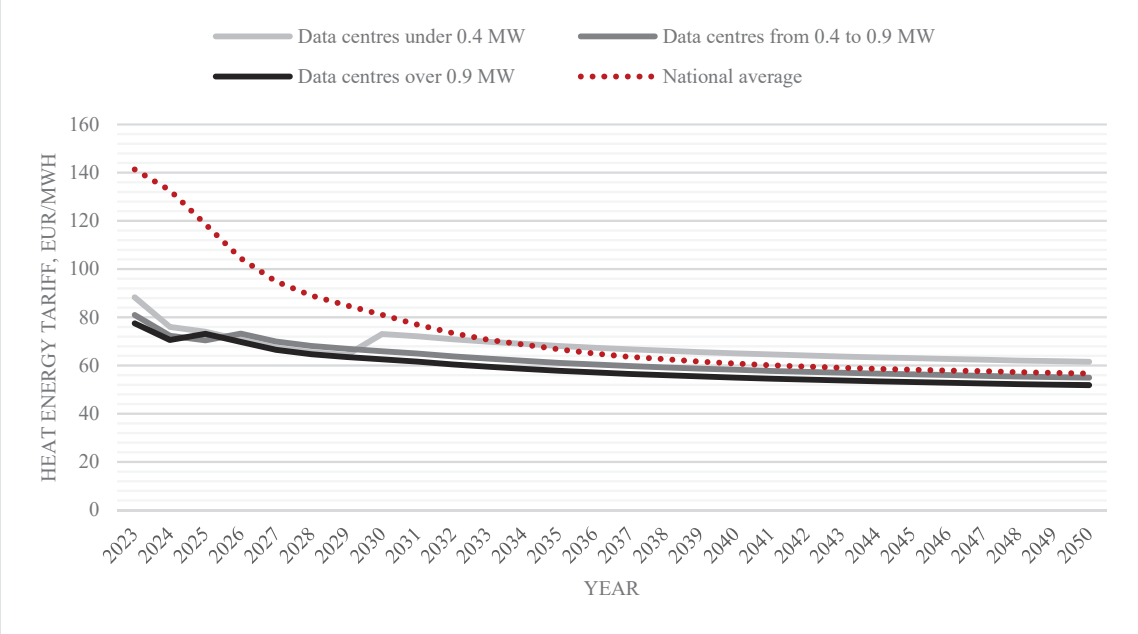


Figure 6. System dynamics results on heat energy tariff calculation for the different sizes of DC.

The overall trend shows the lower application of heat pump technologies in small DCs due to the lack of economic feasibility. After the year 2035, all the DCs with power over 0.9 MW should utilize the waste heat due to the lower price of heat energy which is estimated within the larger SD model, which takes into account the overall development trends in the energy sector and has shown high accuracy in predicting the energy prices.

The overall trend of waste heat utilization on the national level can be seen in Figure 7. With the increase in the number of DCs due to macroeconomic indicators, the overall heat energy generation potential from DCs increases. The lower economic cost of heat energy produced by DCs compared to other heat energy production technologies increases the overall utilization value. By the year 2050, out of 256.69 GWh of total waste heat, 200.62 GWh will be utilized.

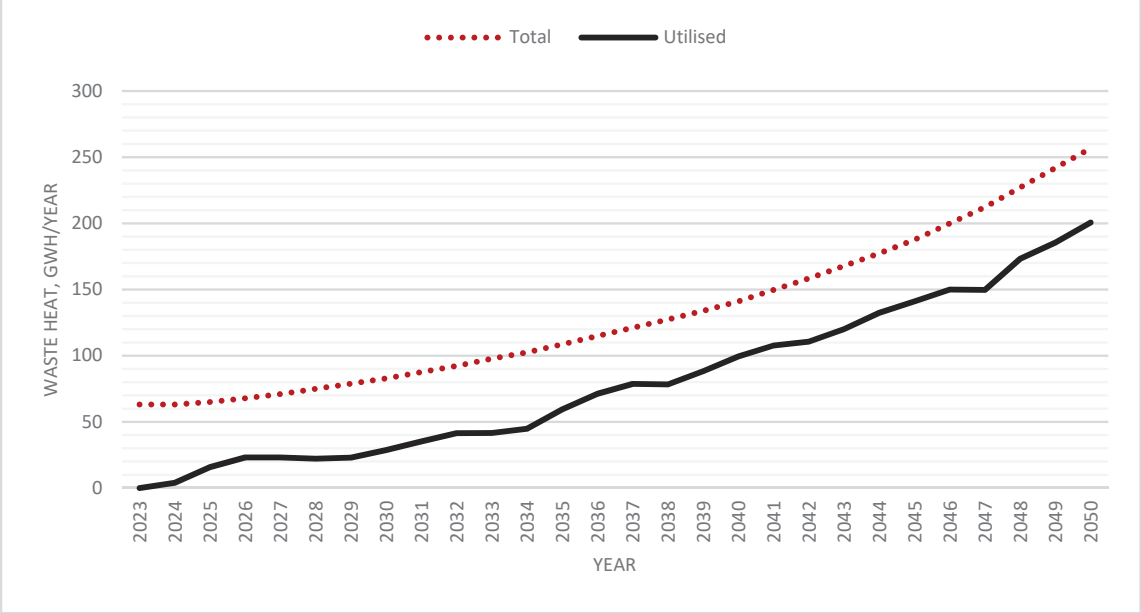


Figure 7. DC waste heat utilization rate on the national level based on system dynamics results.

The modelled national energy portfolio for DH is summarized in Figure 8. A total of 2.6% of the national heat supply is DC's waste heat regeneration systems in 2050. An overall relative increase in the national energy portfolio is observed between 2023 and 2050, which is created by the utilization rate described in Figure 7.

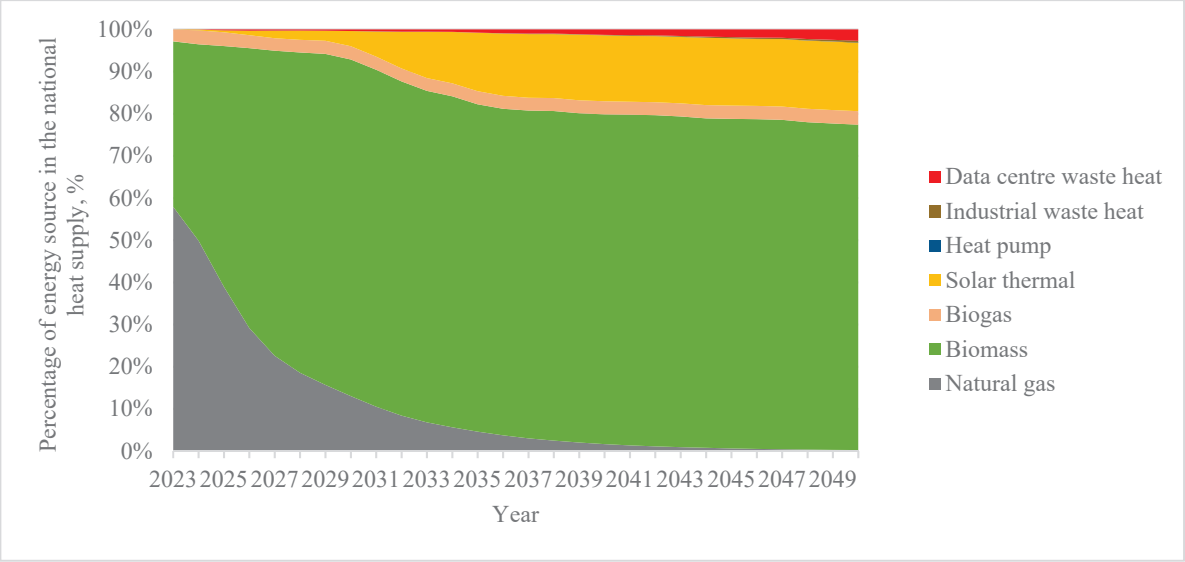


Figure 8. National relative energy portfolio for Latvia in the 2023–2050 period based on system dynamics results.

Furthermore, a sensitivity analysis of the model on the price of electricity and operational hours was performed. The results of the sensitivity analysis are summarized in Figure 9. The model showed high sensitivity to electricity prices over 260 EUR/MWh with a decrease in the total amount of utilized heat. The model showed high sensitivity to the operational time of heat pumps below 6570 h/year and a COP coefficient below 4.75.

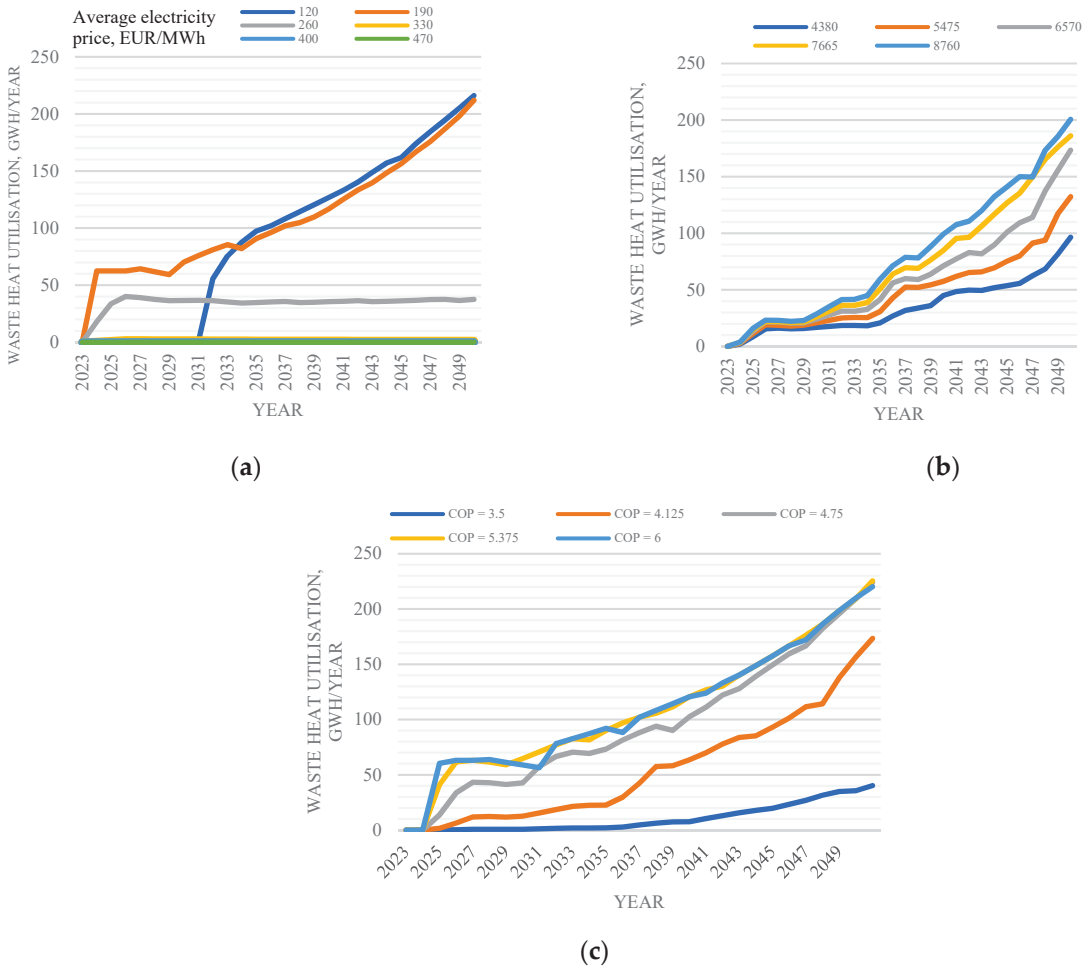


Figure 9. The sensitivity analysis (**a**) on the average prices of electricity, (**b**) operational hours of heat pumps, and (**c**) COP coefficient of heat pumps.

5. Discussion and Conclusions

This paper evaluated the use of waste heat generated by DCs as a heat energy resource in Latvia. A methodological framework consisting of empirical calculation of the existing waste heat and SD model was proposed. The results described both the static and dynamic evaluations of waste heat potential and its implementation in Latvia. The results reveal the pathways to facilitate technology adoption on a national level.

The evaluation of the preliminary assessment of DCs revealed the heterogenic distribution pattern concentrated in the capital city of Latvia, which limits the use of DC's waste heat as an energy source on the national level. The development of a decentralized network of DCs regionally is required for more equal use of its waste heat, which would increase the use of renewable energy in the DH networks as the current distribution of data centers is concentrated in the capital city. On the one hand, the distributional pattern allows for the centralization of the production of renewable heat energy due to the geographical proximity, but at the same time, it significantly increases the peak demand for electricity, especially during the winter months. In this regard, decentralization of the DC network would increase the use of waste heat in DH, evenly distributing the increases in peak electricity demand.

The overall waste heat generated by DCs is 51.37 GWh, which could be used to create 63.12 GWh of heat energy at the temperature of 65 °C. The assessment of individual DCs revealed the correlation between the payback time and waste heat production: the DCs with a higher waste heat potential have a shorter payback period for the heat pumps. The implications of that require an additional incentive for smaller DCs to participate in the

waste heat regeneration system installation. This notion furthermore is confirmed by the evaluation of the heat energy tariffs between different DCs and utilization rates within different DC types in the modelled scenario.

The SD model evaluated the changes in waste heat utilization potential. By 2050, the total heat energy production potential increased to 257 GWh, with 201 GWh being utilized. The overall waste heat utilization rate is highly sensitive to electricity prices and the COP coefficient, which posits a higher feasibility with the decrease of national electricity prices and temperatures of DH as the overall performance of heat pumps and operational costs generating heat energy would improve. This furthermore amplifies the notion of greening the electricity grid to support the transition to renewable heat energy generation.

The findings revealed the necessity for stakeholder engagement to support the use of heat energy created by DC's waste heat. This is particularly important for the DCs with the highest energy consumption and waste heat production due to the decreased payback time and lower price for the implementation of such solutions. Furthermore, the biggest DC analyzed is operated by the same market operators. The overall incentive framework and cooperation between DC operators and DH companies are necessary for the utilization of waste heat.

Author Contributions: Methodology, I.P. and K.G.; Software, K.G. and A.G.; Validation, K.G. and A.G.; Formal analysis, I.P. and K.G.; Investigation, K.G.; Data curation, K.G. and M.A.Z.; Writing—original draft, K.G.; Writing—review & editing, M.A.Z.; Visualization, K.G.; Project administration, I.P.; Funding acquisition, I.P. All authors have read and agreed to the published version of the manuscript.

Funding: The results presented in the paper were made possible thanks to funding from Nordic Energy Research in the frame of the joint Baltic–Nordic Energy Research Program project no.: 117686 «Waste heat in smart energy systems».

Data Availability Statement: The used data is not publicly available.

Conflicts of Interest: The authors declare no conflicts of interest.

References

1. European Parliament and the Council of the European Union. Decision (EU) 2022/2481 of the European Parliament and of the Council of 14 December 2022 Establishing the Digital Decade Policy Programme 2030. 2022. Available online: https://eur-lex.europa.eu/eli/dec/2022/2481/oj (accessed on 14 December 2023).
2. European Commission. Communication from the Commission to the European Parliament, the Council, the European Economic and Social Committee and the Committee of the Regions Updating the 2020 New Industrial Strategy: Building a Stronger Single Market for Europe's Recovery. Available online: https://eur-lex.europa.eu/legal-content/EN/TXT/?uri=CELEX:52021SC0352 (accessed on 14 December 2023).
3. Geng, H. Data Centers-Strategic Planning, Design, Construction, and Operations. In *Data Center Handbook*; Wiley: Hoboken, NJ, USA, 2014. [CrossRef]
4. Wahlroos, M.; Pärssinen, M.; Rinne, S.; Syri, S.; Manner, J. Future views on waste heat utilization—Case of data centers in Northern Europe. *Renew. Sustain. Energy Rev.* **2018**, *82*, 1749–1764. [CrossRef]
5. Lu, T.; Lü, X.; Välisuo, P.; Zhang, Q.; Clements-Croome, D. Innovative approaches for deep decarbonization of data centers and building space heating networks: Modeling and comparison of novel waste heat recovery systems for liquid cooling systems. *Appl. Energy* **2024**, *357*, 122473. [CrossRef]
6. Luo, Y.; Andresen, J.; Clarke, H.; Rajendra, M.; Maroto-Valer, M. A decision support system for waste heat recovery and energy efficiency improvement in data centres. *Appl. Energy* **2019**, *250*, 1217–1224. [CrossRef]
7. Energy Efficiency in Industry—Markus Blesl, Alois Kessler—Google Grāmatas. Available online: https://books.google.com.hk/books/about/Energy_Efficiency_in_Industry.html?id=1aSDzgEACAAJ&redir_esc=y (accessed on 19 December 2023).
8. Li, J.; Yang, Z.; Li, H.; Hu, S.; Duan, Y.; Yan, J. Optimal schemes and benefits of recovering waste heat from data center for district heating by CO2 transcritical heat pumps. *Energy Convers. Manag.* **2021**, *245*, 114591. [CrossRef]
9. Pakere, I.; Gravelsins, A.; Lauka, D.; Blumberga, D. Will there be the waste heat and boiler house competition in Latvia? Assessment of industrial waste heat. *Smart Energy* **2021**, *3*, 100023. [CrossRef]
10. Ziemele, J.; Dace, E. An analytical framework for assessing the integration of the waste heat into a district heating system: Case of the city of Riga. *Energy* **2022**, *254*, 124285. [CrossRef]
11. Jang, Y.; Lee, D.; Kim, J.; Ham, S.H.; Kim, Y. Performance characteristics of a waste-heat recovery water-source heat pump system designed for data centers and residential area in the heating dominated region. *J. Build. Eng.* **2022**, *62*, 105416. [CrossRef]

12. He, Z.; Ding, T.; Liu, Y.; Li, Z. Analysis of a district heating system using waste heat in a distributed cooling data center. *Appl. Therm. Eng.* **2018**, *141*, 1131–1140. [CrossRef]
13. Keskin, I.; Soykan, G. Optimal cost management of the CCHP based data center with district heating and district cooling integration in the presence of different energy tariffs. *Energy Convers. Manag.* **2022**, *254*, 115211. [CrossRef]
14. Oró, E.; Taddeo, P.; Salom, J. Waste heat recovery from urban air cooled data centres to increase energy efficiency of district heating networks. *Sustain. Cities Soc.* **2019**, *45*, 522–542. [CrossRef]
15. Huang, P.; Copertaro, B.; Zhang, X.; Shen, J.; Löfgren, I.; Rönnelid, M.; Fahlen, J.; Andersson, D.; Svanfeldt, M. A review of data centers as prosumers in district energy systems: Renewable energy integration and waste heat reuse for district heating. *Appl. Energy* **2020**, *258*, 114109. [CrossRef]
16. Güğül, G.N.; Gökçül, F.; Eicker, U. Sustainability analysis of zero energy consumption data centers with free cooling, waste heat reuse and renewable energy systems: A feasibility study. *Energy* **2023**, *262*, 125495. [CrossRef]
17. Oró, E.; Allepuz, R.; Martorell, I.; Salom, J. Design and economic analysis of liquid cooled data centres for waste heat recovery: A case study for an indoor swimming pool. *Sustain. Cities Soc.* **2018**, *36*, 185–203. [CrossRef]
18. Pan, Q.; Peng, J.; Wang, R. Application analysis of adsorption refrigeration system for solar and data center waste heat utilization. *Energy Convers. Manag.* **2021**, *228*, 113564. [CrossRef]
19. Cheung, H.; Wang, S.; Zhuang, C.; Gu, J. A simplified power consumption model of information technology (IT) equipment in data centers for energy system real-time dynamic simulation. *Appl. Energy* **2018**, *222*, 329–342. [CrossRef]
20. Deymi-Dashtebayaz, M.; Valipour-Namanlo, S. Thermoeconomic and environmental feasibility of waste heat recovery of a data center using air source heat pump. *J. Clean. Prod.* **2019**, *219*, 117–126. [CrossRef]
21. Cho, J.; Yang, J.; Lee, C.; Lee, J. Development of an energy evaluation and design tool for dedicated cooling systems of data centers: Sensing data center cooling energy efficiency. *Energy Build.* **2015**, *96*, 357–372. [CrossRef]
22. Zajacs, A.; Bogdanovičs, R.; Zeiza-Seleznova, A.; Valančius, R.; Zemītis, J. Integration of decentralized solar collectors into a district heating system. *Sustain. Cities Soc.* **2022**, *83*, 103920. [CrossRef]
23. Technology Data-Energy Plants for Electricity and District Heating Generation. Available online: http://www.ens.dk/teknologikatalog (accessed on 19 December 2023).
24. Jovet, Y.; Lefèvre, F.; Laurent, A.; Clausse, M. Combined energetic, economic and climate change assessment of heat pumps for industrial waste heat recovery. *Appl. Energy* **2022**, *313*, 118854. [CrossRef]
25. Lotfi, H.; Khodaei, A. Levelized cost of energy calculations for microgrids. In Proceedings of the IEEE Power and Energy Society General Meeting, Boston, MA, USA, 17–21 July 2016. [CrossRef]
26. Pakere, I.; Gravelsins, A.; Lauka, D.; Bazbauers, G.; Blumberga, D. Linking energy efficiency policies toward 4th generation district heating system. *Energy* **2021**, *234*, 121245. [CrossRef]
27. Liao, H.; Peng, Y.; Wang, F.Z.; Zhang, T. Understanding energy use growth: The role of investment-GDP ratio. *Struct. Chang. Econ. Dyn.* **2022**, *63*, 15–24. [CrossRef]
28. Komersantu Peļņa vai Zaudējumi pēc Nodokļiem un Neto Apgrozījums pa Darbības Veidiem (NACE 2. Red.), (milj. eiro)—Laika Periods. PxWeb. Available online: https://data.stat.gov.lv/pxweb/lv/OSP_PUB/START__ENT__UA__UFF/UFF030/table/tableViewLayout1/ (accessed on 14 December 2023).
29. Bruto Kapitālieguldījumi pa Darbības Veidiem (Faktiskajās Cenās, Tūkst. Eiro) | Oficiālās Statistikas Portāls. Available online: https://stat.gov.lv/lv/statistikas-temas/uznemejdarbiba/finanses/tabulas/ufi010c-bruto-kapitalieguldijumi-pa-darbibas (accessed on 14 December 2023).
30. Iekšzemes Kopprodukts Pavisam, uz Vienu Iedzīvotāju un uz Vienu Nodarbināto 1995–2022. PxWeb. Available online: https://data.stat.gov.lv/pxweb/lv/OSP_PUB/START__VEK__IK__IKP/IKP010 (accessed on 14 December 2023).
31. Volkova, A.; Koduvere, H.; Pieper, H. Large-scale heat pumps for district heating systems in the Baltics: Potential and impact. *Renew. Sustain. Energy Rev.* **2022**, *167*, 112749. [CrossRef]

Disclaimer/Publisher's Note: The statements, opinions and data contained in all publications are solely those of the individual author(s) and contributor(s) and not of MDPI and/or the editor(s). MDPI and/or the editor(s) disclaim responsibility for any injury to people or property resulting from any ideas, methods, instructions or products referred to in the content.

energies

MDPI

Article

Machine Learning-Based Forecasting of Temperature and Solar Irradiance for Photovoltaic Systems

Wassila Tercha [1], Sid Ahmed Tadjer [1], Fathia Chekired [2] and Laurent Canale [3,*]

[1] Electrification of Industrial Enterprises Laboratory, University of Boumerdes, Boumerdes 35000, Algeria; wassilatercha@gmail.com (W.T.); s.tadjer@univ-boumerdes.dz (S.A.T.)
[2] Unité de Développement des Équipements Solaires, UDES, Centre de Développement des Energies Renouvelables, CDER, Tipaza 42004, Algeria; f.chekired@udes.dz
[3] CNRS, LAPLACE Laboratory, UMR 5213, 31062 Toulouse, France
* Correspondence: laurent.canale@laplace.univ-tlse.fr

Abstract: The integration of photovoltaic (PV) systems into the global energy landscape has been boosted in recent years, driven by environmental concerns and research into renewable energy sources. The accurate prediction of temperature and solar irradiance is essential for optimizing the performance and grid integration of PV systems. Machine learning (ML) has become an effective tool for improving the accuracy of these predictions. This comprehensive review explores the pioneer techniques and methodologies employed in the field of ML-based forecasting of temperature and solar irradiance for PV systems. This article presents a comparative study between various algorithms and techniques commonly used for temperature and solar radiation forecasting. These include regression models such as decision trees, random forest, XGBoost, and support vector machines (SVM). The beginning of this article highlights the importance of accurate weather forecasts for the operation of PV systems and the challenges associated with traditional meteorological models. Next, fundamental concepts of machine learning are explored, highlighting the benefits of improved accuracy in estimating the PV power generation for grid integration.

Keywords: forecasting; machine learning; photovoltaic; solar irradiance; temperature; regression models

1. Introduction

The proliferation of photovoltaic (PV) has brought about significant changes in the global energy landscape. With the sun as an abundant and renewable energy resource, PV installations have become a vital component of efforts to reduce greenhouse gas emissions and transition towards a greener future. However, the proficiency and functioning of PV systems are inherently linked to the availability of sunlight, which is subject to dynamic fluctuations driven by meteorological factors such as temperature and solar irradiance. Solar energy is produced using PV cells, which transform sunlight to produce electricity. The efficacy and staging of solar power systems are strongly influenced by solar irradiance, which is the amount of sunlight received on a specified surface during a specific period. Due to the growing use of electricity from solar energy on the one hand and the growth of this energy integration into the electricity grid on the other hand [1,2], it is becoming increasingly important to predict the amount of this renewable energy source. This prediction must imperatively involve the forecasting of meteorological data such as irradiation and temperature. In this context, as mentioned by Yagli et al. [3], an improvement in the accuracy of photovoltaic energy production forecasting by 25% could reduce 1.56% (USD 46.5 million) in net production costs. Consequently, weather and photovoltaic power forecasting is essential to assess solar potential.

Numerous photovoltaic power-forecasting approaches have been studied. According to Mellit et al. [4] and taking into account the horizon [5], these approaches can be classified into four categories: (1) very short-term forecasting (VSTF), (2) short-term forecasting

(STF), (3) medium-term (MTF), and (4) long-term forecasting (LTM). According to the same authors [4], each category has its precise application; for example, very short-term forecasting is used in the management of microgrids. Accurate prediction of temperature and solar irradiance is essential for the optimization of a grid-connected PV system operation. Numerous works have been done to recommend an accurate solar energy prediction. The authors in [6,7] discussed two main approaches: traditional (conventional) approaches and AI (artificial intelligence) approaches. Traditional approaches contain physical methods, statistical methods, and regression methods used for energy prediction [8]. These methods served as a cornerstone for weather forecasting. They can deliver good accuracy, but they mostly depend on the stability of weather conditions. However, the implementation of conventional models is comparatively difficult and requires different parameters and expensive equipment.

On the other hand, over the past decades, AI methods have become very popular in different engineering fields [6]. Among AI algorithms, machine learning (ML) has become a powerful tool, offering the potential to advance the accuracy and reliability of forecasts. The forecasting horizon, spatial resolution, and the accessibility of historical data are just some of the variables that affect the accuracy of temperature and solar irradiance forecasts [4]. Smaller spatial areas and shorter forecast lead times often result in more accurate forecasts. When you have a wealth of reliable historical data, forecasts are also more accurate. The principle of ML relies on models learned from large data sets and uses these models to forecast unknown data by learning from mistakes and comparing errors [9]. Machine learning frequently deals with classification and regression problems using different algorithms and techniques such as random forest, XGBoost, support vector machine, and the decision tree.

This article presents an in-depth analysis of existing machine-learning models used in temperature and solar irradiance prediction. The present work shows how ML models can be trained on historical data to learn the relationships between temperature, irradiance, and other relevant factors, such as month, season, and weather conditions. Once trained, these models can be used to predict future temperature and irradiance values accurately. This study evaluates the effectiveness and accuracy of presented ML models for weather forecasting. Moreover, given the self-adaptive nature of ML models, this study and the application of these models to weather forecasts for PV systems remain sustainable since they are based on models that are capable of evolution [10].

The rest of this paper is organized as follows: Section 2 presents the motivation of the present study; related works are presented in Section 3; Section 4 brings together the ML algorithms employed to predict solar irradiance and temperature proposed and studied in this work. In Section 5, the results found are discussed. Section 6 presents some conclusions.

2. Motivation of This Study

Electricity production and consumption must always be precisely balanced by an electric operator. The ability of the electricity system to absorb anticipated and unanticipated changes and interruptions (in production and consumption) while maintaining quality and consistency of service to customers is then what determines the reliability of the electricity system. The energy supplier will then be responsible for monitoring the system during different periods. The intermittent nature of sustainable energy sources makes it more difficult to manage the network and maintain the production/consumption balance when added to a network [11], which can cause certain problems regarding the security of the network [12]. In addition to voltage fluctuations, poor local power quality, and stability issues, solar power generation is sporadic and unpredictable, leading to several other problems. For example, maintenance operations are necessary on the network because various power plants should be frequently stopped or restarted to ensure the balance between energy production and energy consumption [13]. As a result, the failure rate will increase,

and maintenance will require more components [14]. All of these problems increase the cost of photovoltaic energy [15] and greenhouse gas emissions [16].

For this reason, it is essential to develop accurate electricity production projections to strengthen the stability of the integration of a solar PV system's production into the grid and help producers successfully implement their operational strategies [17]. It is also necessary for reserve estimation, electricity system planning, congestion control, optimal storage management with stochastic production, the exchange of produced energy on the electricity market, and, in the long term, minimizing the cost of electricity production. Several works have been carried out to achieve all these goals, focusing on the accuracy of solar irradiance prediction, which has recently been improved through the use of deep learning and machine learning approaches [18,19].

The choice of decision trees, support vector machines (SVMs), random forest, and XGBoost is based on some good reasons. Decision trees help us understand the decision-making process, making it easier to interpret solar and temperature predictions. These models are great at handling complex, non-linear relationships in weather patterns. SVMs work well with lots of variables, like in meteorological data, ensuring accurate forecasting. They are also robust, meaning they avoid making predictions that are too specific, making them more reliable. Random forest combines multiple decision trees, giving us better predictions and telling us which weather factors matter most. XGBoost improves itself over time, learning from mistakes to refine forecasts. Plus, it handles missing data, which is important in real-world situations where we might not have all the meteorological information. In simple terms, these models are ideal for obtaining accurate temperature and solar energy forecasts for PV systems.

3. Related Work

In the context of photovoltaic systems, there is a renewed interest and creativity in research on temperature and solar irradiation prediction based on machine learning.

Table 1 illustrates some research works related to the present study, and Table 2 highlights the advantages/disadvantages of the ML methods used.

Table 1. Bibliographic summary of the main methods and applications.

Ref.	Description	Forecasting Target	Year
[17]	Utilization of a" Partial Functional Linear Regression Model" (PFLRM) for forecasting the daily power generation in photovoltaic (PV) systems in order to capitalize on the substantial trajectory data inherent in daily power output.	PV power	2022
[18]	A comprehensive examination of various resources and techniques employed in predicting solar irradiance across different timeframes.	Solar irradiance	2020
[20]	Determination of a range for ambient temperature and the sun radiant, utilizing MAE as a metric for irradiance, the proportion of variation in these factors.	Temperature and solar	2021
[21]	Various forecasting challenges, comprising eight papers that delve into methods for maximizing the output power of PV systems, the sun radiant, and power generation forecasting.	Solar irradiance, temp., thermal energy production	2022
[22]	Overview of recent studies emphasizing solar irradiance forecasting using ensemble methods categorized into two main forecasting ensembles: competitive and cooperative.	PV power	2023
[23]	A critical and systematic review of current machine learning forecasters for wind and solar power, specifically focusing on (ANNs), (RNNs), (SVMs), and (ELMs).	PV power	2021
[24]	Emerging utilization of alternative methods, including regression trees, random forests, gradient boosting, and various others, in the context of solar irradiation prediction.	Solar irradiance	2017

Table 1. *Cont.*

Ref.	Description	Forecasting Target	Year
[25]	Ability to pinpoint seven crucial perspectives and trends for prospective investigations in solar forecasting. These findings are designed to help readers better utilize these approaches for more profound future research.	Solar irradiance, PV power	2023
[26]	Examining the current state of the art and assessing different methodologies, not solely based on their performance and generalization of this. Evaluation of these approaches to perform not only on the designated dataset but also on alternative datasets or varied case studies.	PV power	2018

Table 2. Disadvantages and advantages of ML methods.

Ref.	Machine Learning Method	Advantages	Disadvantages
[17]	Partial functional linear regression model (PFLRM)	Introduces the PFLRM as a generalization of traditional multiple linear regression, allowing the modeling of non-linearity structures in the data.	Acknowledges the need for further investigation and considering additional time-varying meteorological variables as functional predictors.
[18]	RNN, LSTM, GRU, TCN	Leverages deep learning and machine learning techniques for very short-term solar forecasting, demonstrating irradiance and practical application of advanced technologies in renewable energy optimization.	The study's findings are tailored to the local city of Karachi, potentially limiting the generalizability of the results to other regions with different climatic conditions.
[20]	Machine learning, linear statistical models, numerical weather prediction (NWP)	Guide future research by highlighting the most suitable forecasting methods and confirm the importance of forecasting terms, revealing up to 95% power output variation between short and long-term predictions.	Limitations related to the availability of historical information for site-specific applications potentially impact the model's accuracy and generalizability.
[21]	Numerical weather prediction models (NWP), physical techniques, machine learning techniques, linear statistical models	Demonstrating a practical strategy for overcoming challenges in inaccurately predicting power generation.	Lack of universally applicable models and the need for customization based on regional characteristics.
[22]	Competitive ensemble (bagging, boosting, ensemble Kalman filter), cooperative ensemble (ARMA-ANN, ARIMA-SVM. . .)	Demonstrated that ensemble models perform better than standalone ones. The artificial neural network (ANN) and space vector machine (SVM) are widely used with ensemble models (WD-ANN, EMD BPNN, and W-SVM) due to their ability to solve complex.	It did not present the various intelligent techniques and machine learning algorithms used in the field of forecasting, showing the advantages and disadvantages.
[23]	ANN, RNN, SVM, ELM	Compares machine learning methods, metaheuristics, and hybrid approaches, aiding scientists and engineers in choosing suitable prediction methods for diverse circumstances.	Extreme learning machines (ELMs) might be suitable only for simple models and could struggle to capture enough features and learn adequately, requiring careful optimization or extension to become deep networks.
[24]	Regression tree, random forest, gradient boosting	Recognizes the potential of hybrid models and ensemble forecast approaches to enhance prediction performance, addressing the challenges posed by the diversity of solar radiation data.	Due to the variety in data conditions and parameters, determining the superior method becomes challenging, leading to comparable prediction errors among different approaches.

Table 2. *Cont.*

Ref.	Machine Learning Method	Advantages	Disadvantages
[25]	128 forecasting methods of solar irradiance and power	Reviews five classifications and seven pre-processing methods for solar forecasting data, enhancing forecasting accuracy and providing a solid foundation for further research.	Despite the comprehensive comparisons, the diversity of forecasting methods and associated characteristics makes it challenging to draw definitive conclusions, highlighting the complexity of solar forecasting evaluation.
[26]	Probabilistic forecasting of solar power (PSPF) and load forecasting (PLF)	Recognizes the need to combine PSPF and PLF in the review, emphasizing the growing interest in net demand forecasting and exploring common ground between these areas.	Research gaps such as the impact of net demand forecasting on probabilistic performance metrics and the importance of benchmark datasets.

When comparing forecasting models based on criteria such as efficiency, complexity, response time, data size, scalability, evaluation methods, difficulty of implementation, and the overall cost of implementation, various considerations come into play (Table 3). Statistical methods, known for their simplicity, demonstrate their efficiency in terms of computational resources and response time, making them suitable for smaller datasets. However, they may have difficulty dealing with complex patterns. Machine learning methods, while potentially offering high accuracy, often require significant computing resources and have slower response times. Physical methods, incorporating fundamental principles, offer moderate efficiency and scalability but may encounter challenges in diverse datasets. Numerical weather prediction (NWP) models, designed for atmospheric forecasting, demonstrate high accuracy but come with high implementation costs and computational requirements. Hybrid models aim to strike a balance between accuracy and efficiency by combining machine learning and physical components. Ensemble methods, focusing on diversity for accuracy, have moderate scalability but may require additional computational resources. Implementation costs vary, with statistical models being cost-effective, machine learning and physical models having moderate to high costs, and hybrid and ensemble models providing a balance between accuracy and implementation expense. The choice of model depends on the specific task requirements, available resources, and acceptable tradeoffs between accuracy, efficiency, and cost.

New irradiation and temperature prediction methods quantify the impact of proposed improvements on the overall efficiency, sustainability, and profitability of photovoltaic systems using more complex models and more precise data. They integrate climate variability, site-specific characteristics, and solar panel performance to provide more reliable forecasts. Compared to traditional forecasting methods, which often rely on simplified models and historical data, new methods provide a better understanding of future weather conditions, enabling more accurate planning and optimized use of photovoltaic systems.

Table 3. Comparison between ML methods and different "traditional" forecasting methods.

Methods	Accuracy	Complexity Level	Response	Data Size	Scalability	Evaluation	Difficulty of Implementation	Cost
Machine Learning Methods [23,24]	High	high	Slow	Large	Scalable	Statistical metrics (MAE, MSE) and specialized metrics (accuracy, F1-score)	May range from easy to hard	May vary from moderate to high
Statistical Methods [17,19,20]	Good	Simple	Fast	Small	Generally scalable	Statistical metrics (MAE, MSE, RMSE)	Generally easy	Generally low
Physical Methods [9,11]	Good	Varied	Varied	Varied	Moderate	Utilizing physical principles	Can be challenging	Can vary from moderate to high

Table 3. *Cont.*

Methods	Accuracy	Complexity Level	Response	Data Size	Scalability	Evaluation	Difficulty of Implementation	Cost
Numerical Weather Prediction (NWP) Models [12,13]	Good	Varied	slow	Large	Typically scalable	Brier score, continuous ranked probability score	Can be challenging	Generally high
Hybrid Models [25,27]	High	high	Varied	Varied	Moderate	Combine metrics from both statistical and machine learning evaluation	May range from easy to hard	Can vary from moderate to high
Ensemble Forecasting [22]	High	Moderate to high	Varied	Varied	Scalable	Combine metrics from both statistical and machine learning evaluation	May range from easy to hard	Can vary from moderate to high

4. Methods

The subfield of machine learning in computer science is classified as an artificial intelligence technique. It has the advantage of allowing models to solve problems that explicit methods cannot, and it can be used in a variety of domains [24]. Analyzing data using machine learning (ML) allows computer systems to gain insights from data over time. Unlike statistical models, ML approaches can generally capture non-linearity and adapt data instability, producing more accurate predictors. As a result, ML algorithms have been used in recent years to forecast a variety of problems, including forecasting renewable energy sources [23].

4.1. Decision Tree

A decision tree (DT) functions as a classification model, illustrating a recursive division of instance space. The structure comprises nodes, forming a rooted tree where the "root" node lacks outgoing edges, and subsequent nodes possess exactly one incoming edge. Internal or test nodes, with exterior edges, partition the instance space based on discrete functions of input attribute values. Each internal node creates two or more subspaces, where, in the simplest scenario, each test assesses a single attribute, dividing the instance space based on attribute values. Numeric attributes are split based on range conditions.

It is common practice to assign a class corresponding to the ideal target value to each leaf. Alternatively, a leaf may store a probability vector indicating the likelihood of the target characteristic having a specific value. Instances are categorized by traversing the tree from the root to a leaf based on test results. The representation employs circles for internal nodes and triangles for leaves [28].

Figure 1 illustrates a straightforward decision tree model with two variables, k1 and k2 (ranging from 0 to 1) and a binary objective variable, Y (0 or 1). A decision tree model has key components, including nodes, branches, and essential modeling operations such as stopping, splitting, and pruning.

- Nodes: Three node types exist. (a) A root node, or decision node, divides records into mutually exclusive sets. (b) Inner nodes, or chance nodes, elucidate options at a particular position in the tree structure, connecting to parent nodes above and child or leaf nodes below. (c) Leaf nodes, or final nodes, signify the result of a sequence of choices or events.
- Branches: Replacing random events from internal and root nodes, branches form a hierarchy, defining decision paths. Each route (from the root node through inner nodes to a leaf node) depicts a rule of classification decision, expressible as 'if-then' rules. For instance, "If condition 1 and condition 2 and... condition i occur, then outcome j occurs".

- Splitting: Parent nodes are divided into purer child nodes related to the target variable, using input variables associated with the target. Continuous and discrete input variables, categorized into two or more bins, are employed. Criteria like entropy, Gini index, classification error, information gain, gain ratio, and towing criteria determine the most crucial input variables, ensuring the purity of resulting child nodes (i.e., the proportion with the target condition) [29].

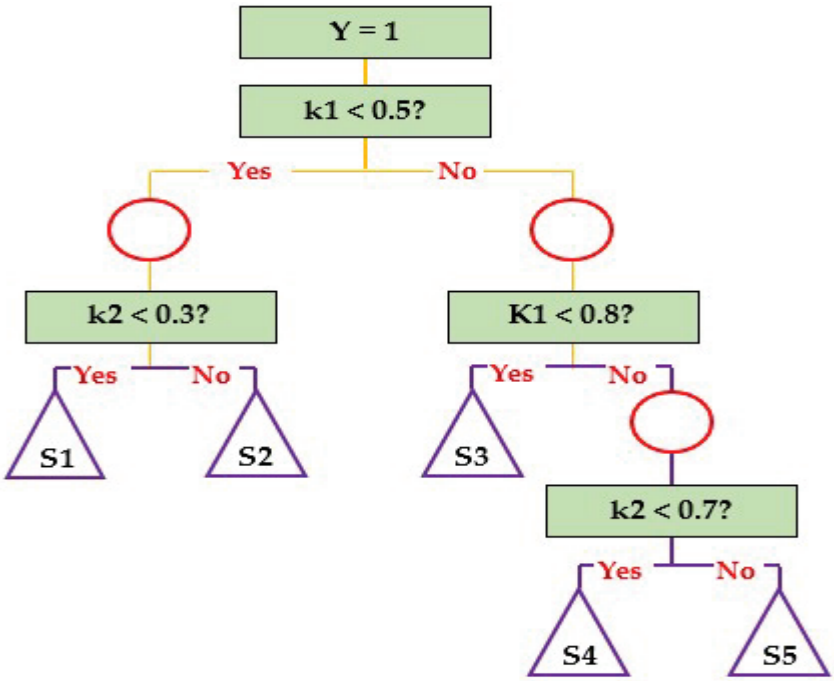


Figure 1. An example of the decision tree model's algorithm.

4.2. Random Forest

In the realm of machine learning, the random forest (RF) stands out as a widely embraced ensemble learning technique, frequently employed for tasks related to classification and regression (Figure 2). The essence of ensemble learning lies in combining predictions from multiple machine learning models to enhance forecast accuracy and reliability.

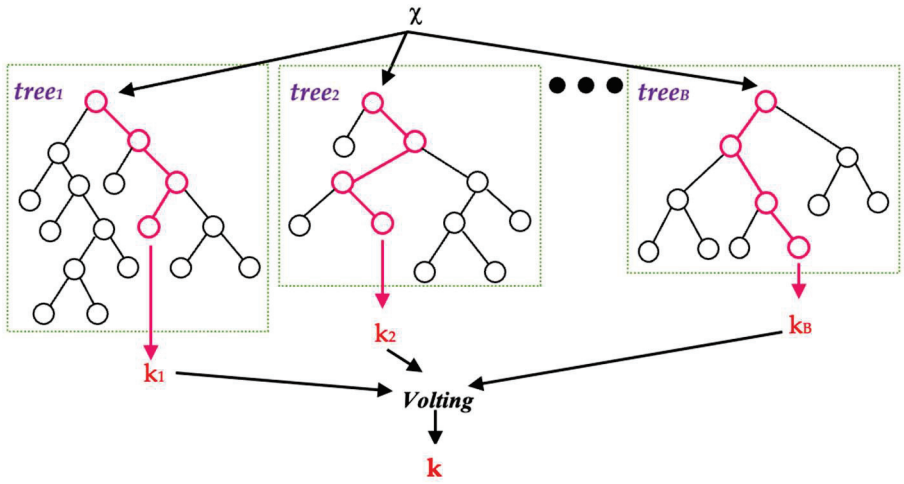


Figure 2. An example of the random forest model's algorithm.

Contrary to linear regression, which assumes data linearity, random decision trees within the RF framework demonstrate superior predictive capabilities by swiftly adapting to non-linearities inherent in the data. While the simplicity of linear regression aids in

model comprehension, it often falls short in predictive performance due to its reliance on the linearity assumption. Random forests exhibit enhanced prediction accuracy, particularly on medium to large datasets, as they effectively navigate and capture non-linear patterns.

In situations where the number of independent variables surpasses the number of observations, logistic regression and linear regression algorithms encounter limitations since there are more parameters to estimate than available data points. The random forest circumvents this constraint by selectively utilizing predictor variables, ensuring effective model performance [30].

The predictive process of the random forest model involves computing a forecast through the averaging of projections derived from individual decision trees. This aggregation mitigates model variance and contributes to an overall improvement in predictive accuracy [31].

Here is a detailed description of how a random forest model works:

1. Divide the training data into different groups. The process used for this is called bagging.
2. Use each subset of training data to train a decision tree. Only a random subset of features is considered at each split in the decision tree.
3. Repeat steps 1 and 2 to create a forest of the decision tree.
4. To predict something, take the average of all the projections from all the individual decision trees.

4.3. Support Vector Machine (SVM)

Another kernel-based machine learning approach employed for classification tasks and regression challenges is the support vector machine (SVM), pioneered by Vapnik in 1986 (Figure 3). This method is particularly utilized in support vector regression (SVR) to address regression problems. Successful applications of support vector machines in time series forecasting have been documented [24].

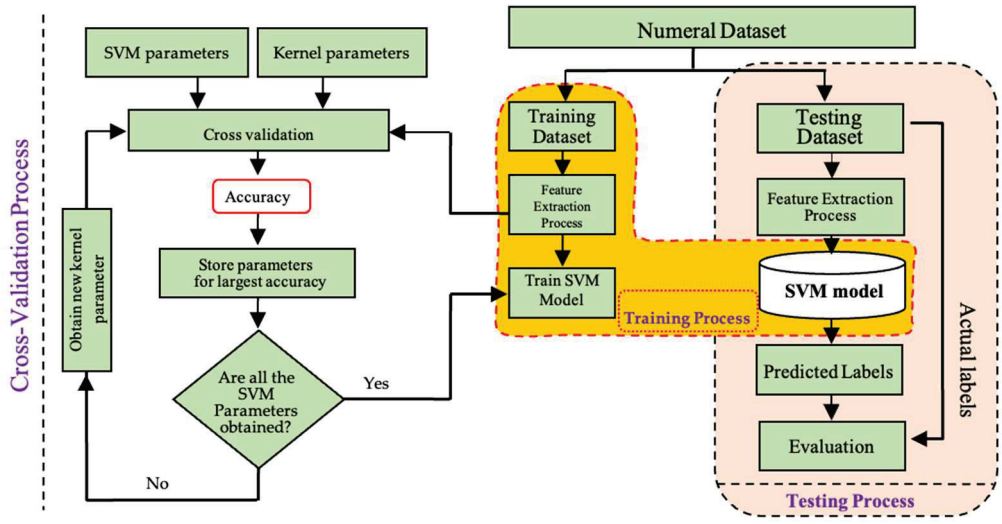


Figure 3. Schematic description of the SVM model algorithm.

The SVM technique partitions data points into two classes with the widest margin by identifying a hyperplane within the input space. The margin represents the separation between the nearest data points for each class and the hyperplane. The hyperplane is determined through the resolution of a quadratic programming problem. A set of support vector data points closest to the hyperplane provides the solution to this problem. Once the support vectors are identified, new data points can be classified using SVM by projecting them onto the hyperplane. If data points lie on one side of the hyperplane, they are classified into a specific class; otherwise, they are grouped into the opposing class. SVMs are a potent machine learning technique applicable to regression and classification tasks, particularly effective with high-dimensional data and data exhibiting non-linear relationships [32,33].

The primary objective of model classification is to construct a model that performs optimally based on the training dataset. Conventional training methods often result in models that accurately memorize each input-output combination, leading to a decreased ability to generalize if the model is overly tailored to the training data. Conversely, SVM aims to categorize classes within the training set into as many distinct groups as possible using a surface that maximizes the separation between them. In essence, SVM facilitates the maximization of a model's generalization potential [34].

4.4. XGBoost (XGB)

XGBoost (XGB) is a collection of decision trees based on gradient boosting, known for its high scalability (Figure 4). It achieves incremental expansion of the objective function by minimizing a loss attributed to gradient ascent. XGBoost utilizes a distinct loss function designed specifically for decision trees, the sole base classifiers employed in XGBoost. To expedite the training of decision trees without compromising ensemble accuracy, XGBoost implements various techniques. XGBoost addresses the computational complexity of decision tree construction, particularly the time-consuming step of determining optimal distribution. It targets this by optimizing the split search process. While conventional split search algorithms explore all potential candidate splits and choose the one with the highest gain, XGBoost streamlines this process by pre-sorting and storing data in a compressed column format. This reduces the need for repeated sorting at each node, ensuring each feature is sorted only once. Moreover, XGBoost incorporates randomization strategies to improve training efficiency and prevent overfitting. Random subsamples are employed during the training of individual trees, and column subsampling is applied at both the tree and tree node levels as part of XGBoost's randomization approaches [35].

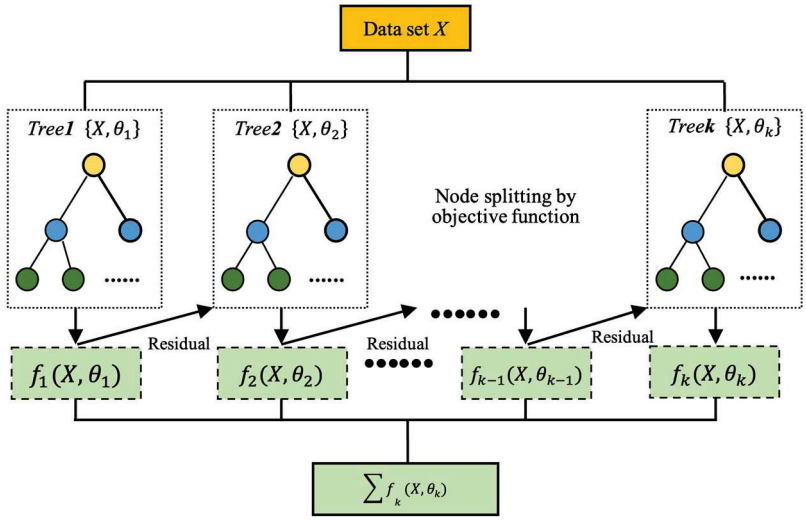


Figure 4. Example of XGBoost model's algorithm.

Each decision tree has learned to predict the residual error of the previous tree. The disparity between the actual target value and the predicted value of the previous tree is called residual error. The XGBoost algorithm uses a method known as gradient boosting to train decision trees. One additional decision tree is added to the set at a time using the iterative gradient boosting approach. Each new decision tree undergoes training to reduce the residual error of the previous trees. Other methods, such as regularization and early stopping, are also used by the XGBoost algorithm to improve model performance [36–38].

4.4.1. Case Study

In this case study, a dataset containing historical information on the energy production of a solar farm located in Hassi R'mel, Laghouat, is used, Algeria (Latitude: 33°7′29.728″ N; Longitude: 3°21′22.484″ E). Figure 5 shows a satellite image of the Hassi R'Mel power plant.



Figure 5. Satellite image of the Hassi R'Mel power plant.

The Hassi R'Mel power installation, boasting a capacity of 150 MW, stands as a pioneering facility in the realm of thermo-solar and combined cycle hybrid electricity generation. Positioned within the largest natural gas field in Algeria, Hassi R'Mel, the installation incorporates two (02) gas turbines (40 MW), two 75 MW combustion systems, a steam turbine with a capacity of 80 MW, and two (02) parabolic solar fields contributing 25 MW to the production capacity. The solar fields encompass 224 parabolic collectors organized into 56 loops across an expansive area of 180,000 m^2. Figure 6 provides a visual representation, showcasing the power plant adorned with its distinctive parabolic-shaped collectors.



Figure 6. Parabolic Collector of the Power Plant.

Historical data for temperatures and solar irradiance were collected daily from solar stations [39], covering a 7-month period from January to July (comprising 212 entries indexed from 0 to 211, each containing five columns: year, month, day, temperature, and irradiance).

The dataset is pre-processed by handling missing values and extracting relevant temporal features. The data used in this study are available at (Figure 7):

- NASA/POWER CERES/MERRA2 Native Resolution Daily Data
- Dates (month/day/year): 1 January 2023 through 31 April 2023
- Location: Longitude 3.356; Latitude 33.125;

```
Range Index: 212 entries, 0 to 211
Data columns (total 5 columns):
#   Column  Non-Null Count  Dtype
---  ------  --------------  -----
0   YEAR    212 non-null    int64
1   MONTH   212 non-null    int64
2   DAY     212 non-null    int64
3   TEMP    212 non-null    float64
4   IRR     203 non-null    float64
    dtypes: float64(2), int64(3)
```

Figure 7. Description of data shown using Python.

Data may disappear due to file loss, equipment malfunction, or other reasons. This can reduce the statistical power of the analysis, making it less likely that true effects or relationships will be detected because missing data may be systematically related to the variables of interest. As shown in the table above, which was extracted from the program via Python, no value is lost as a result of processing the data used in this study (non-null).

In this study, the four models are employed for temperature and solar irradiance forecasting, with "YEAR", "MONTH", and "DAY" serving as design variables across all models. The decision tree model dynamically adapts its structure during training, utilizing a decision tree regressor with default parameters. The random forest model, employing the random forest regressor, determines its structure based on the number of trees and their configurations. The support vector machine (SVM) with a linear kernel characterizes its structure with the optimal hyperplane during training. In contrast, the XGBoost model utilizes the XGBoost Regressor with specific hyperparameters, including n_estimators = 100, learning_rate = 0.1, and max_depth = 3. All models share temporal features as input measures, offering predictions for temperature and solar irradiance.

Figure 8 illustrates the variations in temperature and solar irradiance throughout the month of January. The daily values represent the averages recorded per day, explaining the temperature drop of up to 2 °C during the first months, as observed in Figure 8.

4.4.2. Model Evaluation

The performance evaluation of each model involved the use of key metrics, including mean absolute error (MAE), mean squared error (MSE), and root mean square error (RMSE). The definitions of these metrics are provided using Equations (1)–(3), respectively, as outlined in the pertinent literature [26,27,39].

$$MAE = \frac{1}{N}\sum_{i=1}^{N}|\hat{x}_i - x_i| \quad (1)$$

$$MSE = \frac{1}{N}\sum_{i=1}^{N}(\hat{x}_i - x_i)^2 \quad (2)$$

$$RMSE = \sqrt{\frac{1}{N}\sum_{i=1}^{N}(\hat{x}_i - x_i)^2} \quad (3)$$

Here, "N" represents the length of the time series, "$\hat{x}_i$" denotes the forecasted value, and "x_i" represents the measured value.

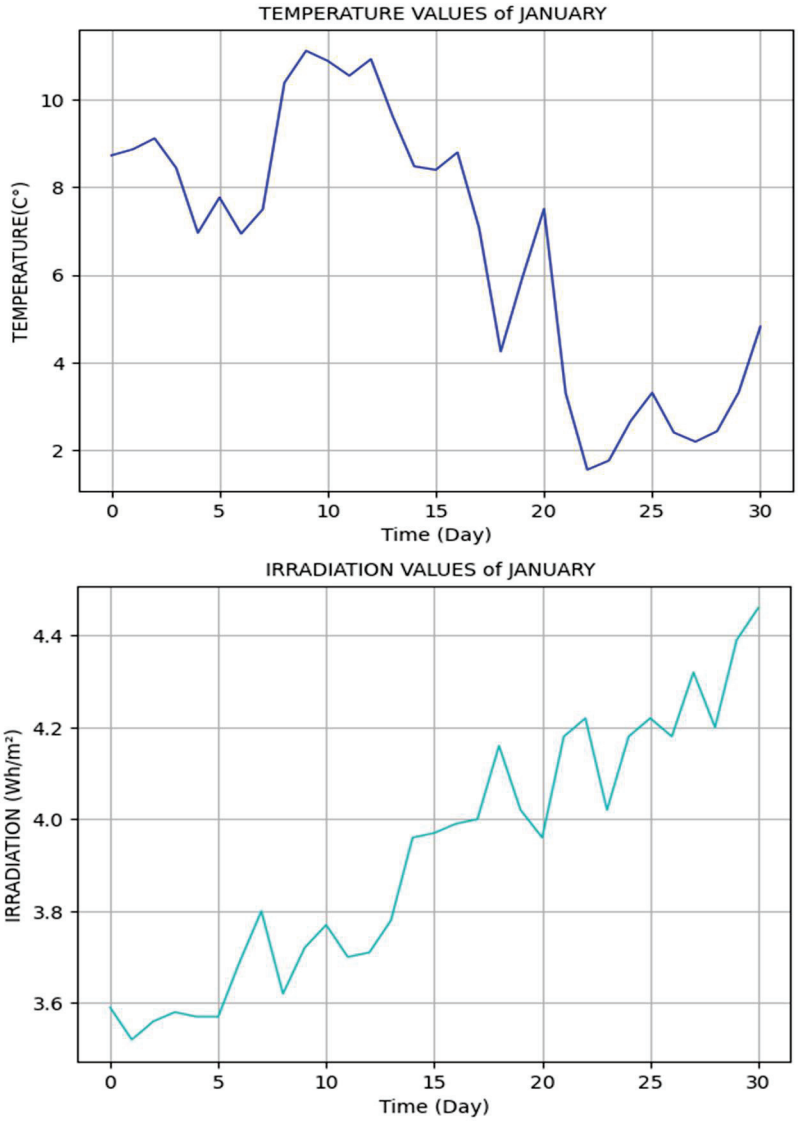


Figure 8. The dataset from the month of January in Hassi R'Mel used in this study is presented as follows: (**Top**) the daily average temperature recorded per day, (**Bottom**) the daily solar irradiance data for the month of January.

5. Discussion of Results

The initial section of the verification results focuses on visual comparison to evaluate the concordance between actual and predicted values within the test data for irradiance and temperature predictions. Moreover, quantitative evaluation employs metrics such as mean absolute error (MAE), mean squared error (MSE), and root mean square error (RMSE). Moving to the next section, the comparison of models expands to encompass various criteria, including complexity level, stability, response time, and implementation complexity. This multifaceted evaluation aims to offer a comprehensive understanding of the models' performance beyond numerical metrics alone.

5.1. Temperature Prediction

The accuracy of temperature forecasts is contingent upon several factors, including the chosen forecast method, the quality of input data, and the complexity of prevailing weather conditions. Machine learning algorithms prove effective by being trained on extensive datasets comprising historical temperature data, which may encompass information from extreme weather events. This training enables algorithms to discern patterns and relationships associated with diverse climatic scenarios. Once trained, these algorithms exhibit

the capability to provide more precise predictions about future temperatures, even when faced with conditions beyond the range of historical data. In the specific case outlined, the program leverages data spanning several months to enhance its training, capturing the nuances of climate changes throughout different seasons. Figure 9 visually represents the variation in temperature within the study area over a duration of seven months.

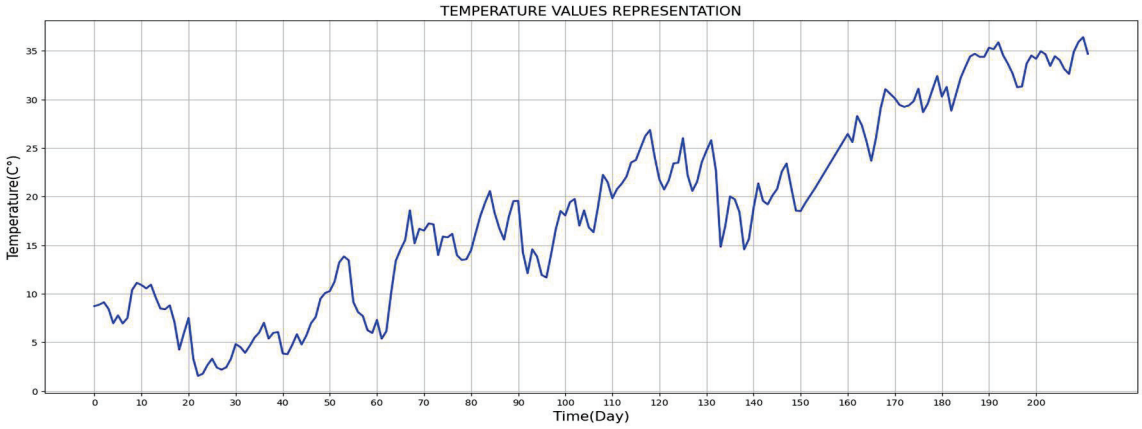


Figure 9. Representation of the temperature data.

Note

In this process, the decision tree model registers a value of 0 in the metrics, signifying that the studied model perfectly fits the training data. This exceptional case implies that the model attains flawless accuracy in predicting the values of the target variable for all training data points. Such a scenario is uncommon and is more likely to occur with smaller training datasets. In this instance, 80% of the data is allocated for the model training, corresponding to 167 days. Figure 10 provides a visual comparison of the predicted temperature values among the four models, highlighting the distinctive characteristics and performance of each. For each studied model, the values of the MAE, MSE, and RMSE for temperature forecasting are shown in Table 4.

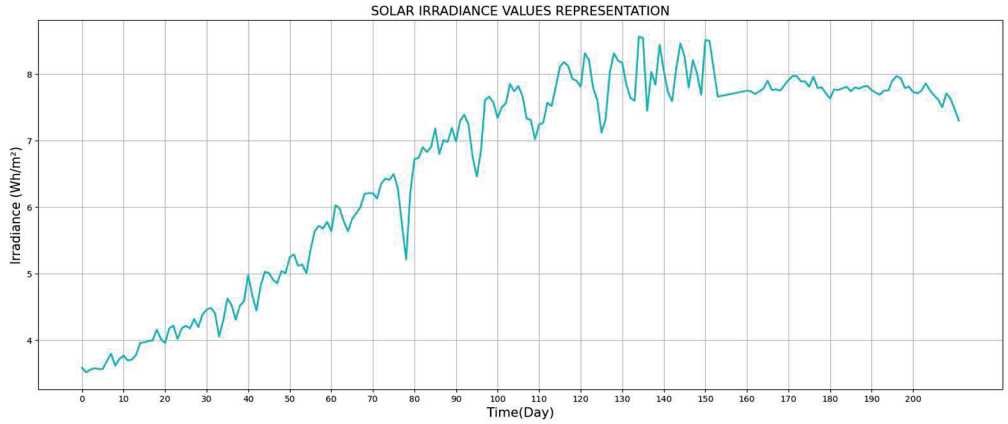


Figure 10. Representation of the solar irradiance data.

Table 4. The values of metrics for temperature forecasting.

Model	MAE	MSE	RMSE
DT	0.00000 *	0.00000 *	0.00000 *
RF	0.32031	0.15355	25.15817
SVM	1.18382	2.25412	24.38985
XGBoost	0.59879	0.58510	0.76492

* Raw result obtained from data treatment.

5.2. Solar Irradiance Prediction

Solar irradiation forecasting involves the complex process of predicting how much sunlight will reach a specific location at a given time in the future. However, this process has become more complex due to ongoing climate change. As the planet warms, we observe an increase in extreme weather events, such as thick clouds and dust storms, which are becoming more frequent. These extreme weather conditions can significantly reduce the amount of sunlight reaching the Earth's surface, making it extremely difficult to predict solar irradiation levels accurately.

This increased complexity explains the relatively low solar irradiation scores recorded during the first months of the study. Figure 11, shown above, provides a visual overview of the collected solar irradiation data, highlighting the challenges of forecasting this vital resource. Figure 12 illustrates a comparison between the different models for predicted irradiance values. Values of MAE, MSE, and RMSE for solar irradiance forecasting are presented in Table 5.

Table 5. The values of metrics for solar irradiance forecasting.

Model	MAE	MSE	RMSE
DT	0.00000 *	0.00000 *	0.00000 *
RF	0.02702	0.027029	0.03940
SVM	0.75297	0.75297	0.84729
XGBoost	0.06601	0.06601	0.08301

* Data raw result obtained from data treatment, a decision tree works by recursively splitting the data based on the features, creating decision nodes to differentiate between different classes (in this case, we are concerned with regression, not classification, as such we are not going to work with classes). Thus, achieving 0 error in a DT model is theoretically possible, especially if you have a small and well-structured dataset.

5.2.1. Interpretation

In this study, the models underwent training with the exclusion of the last 40 days that were selected for the test set. Upon evaluation of its accuracy, the SVM model emerged with the highest mean absolute error (MAE) value, indicating its relatively weaker performance compared to the other models. The XGBoost model secured the second position, followed by the RF model, with the simple DT model ranking last. Graphical analysis unveiled that the representation of temperature values generated by the decision tree model closely resembled the original representation. This observation implies that the decision tree model retained the fundamental characteristics of the original data, offering valuable insights into temperature patterns within the study.

5.2.2. Measuring Forecast Speed

The forecasting speed of a model varies depending on the model architecture, the size of the dataset, and the hardware the model is running on. However, measuring forecast speed can be useful for comparing different models or for optimizing a model's performance. As we can see in Table 6, both DT and XGB achieve a low prediction speed (unit is second). Table 7 presents a comparison between different models according to their complexity of implementation, their speed, and their efficiency.

Table 6. The values of forecasting speed (s).

Model	DT	RF	SVM	XGB
Temperature	0.00588	0.01296	0.01292	0.00199
Irradiance	0.00399	0.02592	0.00793	0.00426

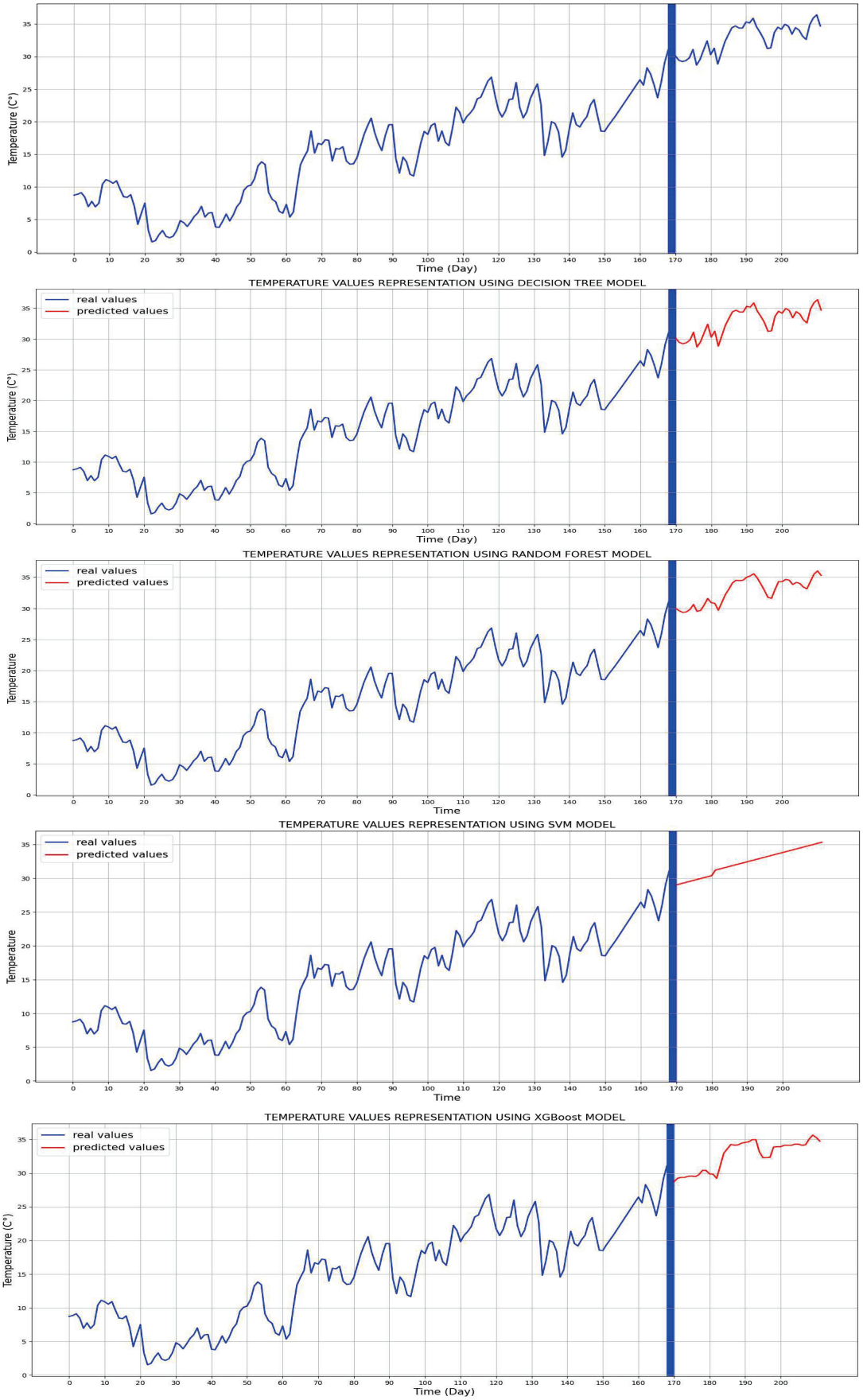


Figure 11. Comparison between different models for predicted temperature values.

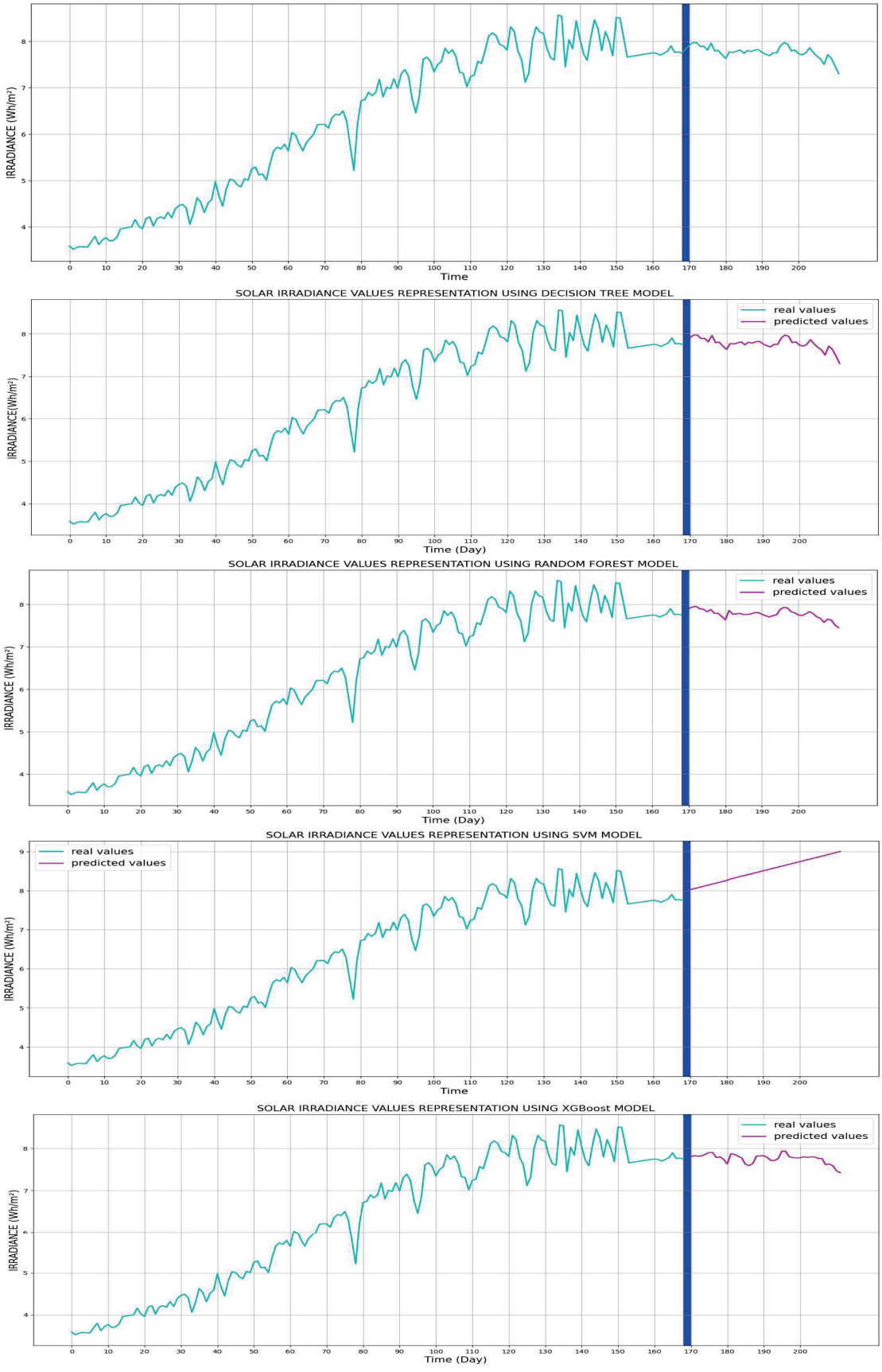


Figure 12. Comparison between the different models for predicted irradiance values.

Table 7. Comparison of the different models using other factors.

Model	Complexity	Speed	Efficiency
DT	Simple	Very fast	More efficient
RF	Simple	Fairly fast	Efficient
SVM	Simple	Fairly fast	Not enough
XGB	Medium	Very fast	Efficient

The evaluation results indicate that the decision tree stands out as an accurate and robust forecasting tool for both temperature and solar irradiance. The model demonstrates the capability to achieve low mean absolute error (MAE), mean squared error (MSE), and root mean square error (RMSE) values, along with optimal forecasting speed. However, the selection of the most suitable forecasting model is contingent on the specific requirements of the application. In the current study, where forecasting accuracy and speed are paramount, the decision tree model excels on both fronts. Decision trees exhibit high accuracy by adeptly learning intricate relationships between features and the target variable. Through recursive data division based on feature values, decision trees discern complex patterns, contributing to their accurate predictions.

Decision trees are notably fast due to their avoidance of complex calculations. The algorithm's efficiency lies in comparing the feature values of a data point with those of the training data and, upon finding a match, assigning a label to the data point. Moreover, decision trees showcase versatility by accommodating both continuous and categorical features, rendering them a versatile and adaptable machine-learning algorithm for various applications.

Differential privacy techniques provide a robust framework for injecting controlled noise into the training process, thereby protecting individual data points such as federated learning and homomorphic encryption. By integrating these advanced privacy-preserving techniques, our future research aims to strike a delicate balance between accuracy, model complexity, and computational efficiency, thereby contributing to the development of secure and privacy-friendly ML models for predicting energy production photovoltaic. By exchanging model parameters rather than private data, the intended FedDRL (federated deep reinforcement learning) can produce an accurate prediction model in a decentralized manner, thus avoiding sensitive privacy issues [40]. Moreover, homomorphic encryption (HE), with its security guarantees and computability on encrypted data, has become one of the most promising techniques to protect data privacy [41]. This proactive approach aligns with the evolving data protection landscape and highlights our commitment to ensuring responsible and ethical use of energy-related data in the context of renewable energy forecasting.

6. Conclusions

In this paper, four ML algorithms were designed to predict future temperature and irradiance values with high accuracy: decision tree, support vector machine, random forest, and XGBoost.

The effectiveness of these methods was evaluated based on different simulation studies. A comparative study between these algorithms is presented according to three parameters: the mean absolute error, the absolute error, and the mean square error.

Based on the results, the present study highlights the importance of accurate temperature and solar irradiation estimates to optimize photovoltaic systems. The simple decision tree algorithm allows the model to make predictions very quickly. However, it is important to note that the accuracy of a decision tree model depends on the quality of the training data and the choice of features. We also propose using ensemble methods like gradient boosting to improve accuracy in photovoltaic energy production forecasting. These methods combine multiple models for higher accuracy while remaining computationally efficient. They also recommend streamlining model complexity by focusing on relevant features, using techniques like recursive feature elimination (RFE) or feature importance analysis.

Additionally, fine-tuning model hyperparameters is crucial for finding the right balance between accuracy and efficiency. On another note, researchers emphasize advanced feature engineering to capture nuanced relationships in meteorological data for better accuracy, particularly in the context of climate change-induced variability. Integrating climate models into forecasting processes helps understand long-term climate trends, and real-time data assimilation techniques enhance accuracy amidst climate variability by continuously incorporating the latest observational data. These strategies effectively manage tradeoffs in forecasting accuracy, model complexity, and computational efficiency in photovoltaic energy production.

By providing the tools needed for efficient and sustainable solar energy production, machine learning models, particularly decision trees, have the potential to transform the energy sector. Furthermore, given the self-adaptive nature of ML models, this article can be used as a reference because the results mentioned can be considered sustainable.

Concerning our future research on forecasting photovoltaic energy production, this study will be developed subsequently via other machine learning models and, in particular, on the improvement of model architectures, the search for new approaches, and the integration of technology techniques to improve forecast accuracy. The results of this study pave the way for better consumption of renewable energies in areas rich in solar resources.

The results obtained in this article make a notable contribution to the field of photovoltaic energy production forecasting by shedding light on the choice of predictive models used in the development of solar energy infrastructures in order to obtain forecasts. They are more accurate and reliable for efficient energy management and predicting energy and financial gains.

Author Contributions: Conceptualization, W.T. and S.A.T.; methodology, W.T., S.A.T. and F.C.; software, W.T. and S.A.T.; validation, W.T., S.A.T. and F.C.; formal analysis, W.T., S.A.T. and F.C.; investigation, W.T., S.A.T. and F.C.; resources, W.T., S.A.T. and F.C.; data curation, W.T., S.A.T., F.C. and L.C.; writing—original draft preparation, W.T., S.A.T., F.C. and L.C.; writing—review and editing, S.A.T., F.C. and L.C.; visualization, W.T., S.A.T., F.C. and L.C.; supervision, S.A.T., F.C. and L.C.; project administration, S.A.T. and F.C.; funding acquisition, S.A.T., F.C. and L.C. All authors have read and agreed to the published version of the manuscript.

Funding: This research work is supported by the "Directorate General for Scientific Research and technological Development DGRSDT"—"Ministry of Higher Education and Scientific Research", Algeria, as well as the fruit of the collaboration established via the "PHC Maghreb international research program": PHC *MELINA* "Mastering Efficient Lighting In North Africa", Grant number 43981ZG, led by Dr L. Canale.

Data Availability Statement: Data are contained within the article.

Conflicts of Interest: The authors of this article declare that they have no conflicts of interest to report regarding the present work.

References

1. Mierzwiak, M.; Kroszczyński, K. Impact of Domain Nesting on High-Resolution Forecasts of Solar Conditions in Central and Eastern Europe. *Energies* **2023**, *16*, 4969. [CrossRef]
2. Wolniak, R.; Skotnicka-Zasadzień, B. Development of Photovoltaic Energy in EU Countries as an Alternative to Fossil Fuels. *Energies* **2022**, *15*, 662. [CrossRef]
3. Yagli, G.M.; Yang, D.; Srinivasan, D. Reconciling solar forecasts: Sequential reconciliation. *Sol. Energy* **2019**, *179*, 391–397. [CrossRef]
4. Mellit, A.; Massi Pavan, A.; Ogliari, E.; Leva, S.; Lughi, V. Advanced Methods for Photovoltaic Output Power Forecasting: A Review. *Appl. Sci.* **2020**, *10*, 487. [CrossRef]
5. Wan, C.; Zhao, J.; Song, Y.; Xu, Z.; Lin, J.; Hu, Z. Photovoltaic and solar power forecasting for smart grid energy management. *IEEE CSEE J. Power Energy Syst.* **2015**, *1*, 38–46. [CrossRef]
6. Lima, M.A.F.B.; Carvalho, P.C.M.; Fernandez-Ramírez, L.M.; Braga, A.P.S. Improving solar forecasting using deep learning and portfolio theory integration. *Energy* **2020**, *195*, 117016. [CrossRef]
7. Tian, J.; Ooka, R.; Lee, D. Multi-scale solar radiation and photovoltaic power forecasting with machine learning algorithms in urban environment: A state-of-the-art review. *J. Clean. Prod.* **2023**, *426*, 139040. [CrossRef]

8. Sharma, A.; Kakkar, A. Forecasting daily global solar irradiance generation using machine learning. *Renew. Sustain. Energy Rev.* **2018**, *82*, 2254–2269. [CrossRef]
9. Zhou, Y. Advances of Machine Learning in Multi-Energy District Communities—Mechanisms, Applications and Perspectives. *Energy AI* **2022**, *10*, 100187. [CrossRef]
10. Gheibi, O.; Weyns, D.; Quin, F. Applying machine learning in self-adaptive systems: A systematic literature review. *ACM Trans. Auton. Adapt. Syst.* **2021**, *15*, 1–37. [CrossRef]
11. Denholm, P.; Margolis, R.M. Evaluating the limits of solar photovoltaics (PV) in traditional electric power systems. *Energy Policy* **2007**, *35*, 2852–2861. [CrossRef]
12. Adewuyi, O.B.; Lotfy, M.E.; Olabisi Akinloye, B.; Howlader Hor, R.; Senjyu, T.; Narayanan, K. Security-constrained optimal utility-scale solar PV investment planning for weak grids: Short reviews and techno-economic analysis. *Appl. Energy* **2019**, *245*, 16–30. [CrossRef]
13. Pérez-Arriaga, I.J.; Batlle, C. Impacts of Intermittent Renewables on Electricity Generation System Operation. *Econ. Energy Environ. Policy* **2012**, *1*, 3–18. [CrossRef]
14. Batlle, C.; Rodilla, P. *Generation Technology Mix, Supply Costs, and Prices in Electricity Markets with Strong Presence of Renewable Intermittent Generation 2011*; IIT Working Paper IIT-11-020A; Institute for International Trade: Adelaide, Australia, 2011.
15. Rehman, S.; Bader, M.A.; Al-Moallem, S.A. Cost of solar energy generated using PV panels. *Renew. Sustain. Energy Rev.* **2007**, *11*, 1843–1857. [CrossRef]
16. Majdi, A.; Alqahtani, M.D.; Almakytah, A.; Saleem, M. Fundamental Study Related to The Development of Modular Solar Panel for Improved Durability and Repairability. *IET Renew. Power Generation. (RPG)* **2021**, *15*, 1382–1396. [CrossRef]
17. Wang, G.; Su, Y.; Shu, L. One-day-ahead daily power forecasting of photovoltaic systems based on partial functional linear regression models. *Renew Energy* **2016**, *96*, 469–478. [CrossRef]
18. Khan, H.A.; Alam, M.; Rizvi, H.A.; Munir, A. Solar Irradiance Forecasting Using Deep Learning Techniques. *Eng. Proc.* **2023**, *46*, 15. [CrossRef]
19. Kumar, D.S.; Yagli, G.M.; Kashyap, M.; Srinivasan, D. Solar irradiance resource and forecasting: A comprehensive review. *IET* **2020**, *14*, 1641–1656. [CrossRef]
20. Ramirez-Vergara, J.; Bosman, L.B.; Leon-Salas, W.D.; Wollega, E. Ambient temperature and solar irradiance forecasting prediction horizon sensitivity analysis. *Mach. Learn. Appl.* **2021**, *6*, 100128. [CrossRef]
21. Cotfas, D.T.; Marzband, M.; Cotfas, P.A.; Siroux, M.; Sera, D. Editorial: Forecasting solar radiation, photovoltaic power and thermal energy production applications. *Front. Energy Res.* **2022**, *10*, 1115096. [CrossRef]
22. Rahimi, N.; Park, S.; Choi, W.; Oh, B.; Kim, S.; Cho, Y.H.; Ahn, S.; Chong, C.; Kim, D.; Jin, C.; et al. A Comprehensive Review on Ensemble Solar Power Forecasting Algorithms. *J. Electr. Eng. Technol.* **2023**, *18*, 719–733. [CrossRef]
23. Alkabbani, H.; Ahmadian, A.; Zhu, Q.; Elkamel, A. Machine Learning and Metaheuristic Methods for Renewable Power Forecasting: A Recent Review. *Front. Chem. Eng.* **2021**, *3*, 665415. [CrossRef]
24. Voyant, C.; Notton, G.; Kalogirou, S.; Nivet, M.L.; Paoli, C.; Motte, F.; Fouilloy, A. Machine learning methods for solar radiation forecasting: A review. *Renew. Energy* **2017**, *105*, 569–582. [CrossRef]
25. Yang, B.; Zhu, T.; Cao, P.; Guo, Z.; Zeng, C.; Li, D.; Chen, Y.; Ye, H.; Shao, R.; Shu, H.; et al. Classification and Summarization of Solar Irradiance and Power Forecasting Methods: A Thorough Review. *CSEE J. Power Energy Syst.* **2023**, *9*, 978–995. [CrossRef]
26. Van Der Meer, D.W.; Widén, J.; Munkhammar, J. Review on probabilistic forecasting of photovoltaic power production and electricity consumption. *Renew. Sustain. Energy Rev.* **2018**, *81*, 1484–1512. [CrossRef]
27. Okumus, I.; Dinler, A. Current status of wind energy forecasting and a hybrid method for hourly predictions. *Energy Convers. Manag.* **2016**, *123*, 362–371. [CrossRef]
28. Rokach, L.; Maimon, O. Decision Trees. In *Data Mining and Knowledge Discovery Handbook*; Springer: Berlin/Heidelberg, Germany, 2006; pp. 165–192.
29. Song, Y.Y.; Lu, Y. Decision tree methods: Applications for classification and prediction. *Shanghai Arch Psychiatry* **2015**, *27*, 130–135. [CrossRef] [PubMed]
30. Schonlau, M.; Zou, R.Y. The random forest algorithm for statistical learning. *Stata J.* **2020**, *20*, 3–29. [CrossRef]
31. Breiman, L. Random Forests. *Mach. Learn.* **2001**, *45*, 5–32. [CrossRef]
32. Pisner, D.A.; Schnyer, D.M. Support vector machine. In *Machine Learning: Methods and Applications to Brain Disorders*; Elsevier: Amsterdam, The Netherlands, 2019; pp. 101–121.
33. Jun, Z. The Development and Application of Support Vector Machine. *Stata J. Promot. Commun. Stat. Stata* **2020**, *20*, 3–29. [CrossRef]
34. Cervantes, J.; Garcia-Lamont, F.; Rodríguez-Mazahua, L.; Lopez, A. A comprehensive survey on support vector machine classification: Applications, challenges and trends. *Neurocomputing* **2020**, *408*, 189–215. [CrossRef]
35. Bentéjac, C.; Csörgő, A.; Martínez-Muñoz, G. A comparative analysis of XGBoost. *Artif. Intell. Rev.* **2021**, *54*, 1937–1967. [CrossRef]
36. Chen, T.; Guestrin, C. XGBoost: A scalable tree boosting system. In Proceedings of the ACM SIGKDD International Conference on Knowledge Discovery and Data Mining, San Francisco, CA, USA, 13–17 August 2016; Association for Computing Machinery: New York, NY, USA, 2016; pp. 785–794.
37. Sabri, M.; Hassouni, M. El: Photovoltaic Power Forecasting with a Long Short-Term Memory Autoencoder Networks. *Soft Comput.* **2022**, *27*, 10533–10553. [CrossRef]

38. NASA. Prediction of Worldwide Energy Resources.: Power Data Access Viewer. 2023. Available online: https://power.larc.nasa.gov/data-access-viewer/ (accessed on 1 February 2024).
39. Hu, T.; Song, T. Research on XGBoost academic forecasting and analysis modelling. *J. Phys. Conf. Ser.* **2019**, *1324*, 012091. [CrossRef]
40. Li, Y.; Wang, R.; Li, Y.; Zhang, M.; Long, C. Wind power forecasting considering data privacy protection: A federated deep reinforcement learning approach. *Appl. Energy* **2023**, *329*, 120291. [CrossRef]
41. Xu, W.; Sun, J.; Cardell-Oliver, R.; Mian, A.; Hong, J.B. A Privacy-Preserving Framework Using Homomorphic Encryption for Smart Metering Systems. *Sensors* **2023**, *23*, 4746. [CrossRef] [PubMed]

Disclaimer/Publisher's Note: The statements, opinions and data contained in all publications are solely those of the individual author(s) and contributor(s) and not of MDPI and/or the editor(s). MDPI and/or the editor(s) disclaim responsibility for any injury to people or property resulting from any ideas, methods, instructions or products referred to in the content.

energies

MDPI

Article

Optimizing Building Short-Term Load Forecasting: A Comparative Analysis of Machine Learning Models

Paraskevas Koukaras, Akeem Mustapha, Aristeidis Mystakidis and Christos Tjortjis *

School of Science and Technology, International Hellenic University, 57001 Thessaloniki, Greece; p.koukaras@ihu.edu.gr (P.K.); amustapha@ihu.edu.gr (A.M.); a.mystakidis@ihu.edu.gr (A.M.)
* Correspondence: c.tjortjis@ihu.edu.gr

Abstract: The building sector, known for its high energy consumption, needs to reduce its energy use due to rising greenhouse gas emissions. To attain this goal, a projection for domestic energy usage is needed. This work optimizes short-term load forecasting (STLF) in the building sector while considering several variables (energy consumption/generation, weather information, etc.) that impact energy use. It performs a comparative analysis of various machine learning (ML) models based on different data resolutions and time steps ahead (15 min, 30 min, and 1 h with 4-step-, 2-step-, and 1-step-ahead, respectively) to identify the most accurate prediction method. Performance assessment showed that models like histogram gradient-boosting regression (HGBR), light gradient-boosting machine regression (LGBMR), extra trees regression (ETR), ridge regression (RR), Bayesian ridge regression (BRR), and categorical boosting regression (CBR) outperformed others, each for a specific resolution. Model performance was reported using R^2, root mean square error (RMSE), coefficient of variation of RMSE (CVRMSE), normalized RMSE (NRMSE), mean absolute error (MAE), and execution time. The best overall model performance indicated that the resampled 1 h 1-step-ahead prediction was more accurate than the 15 min 4-step-ahead and the 30 min 2-step-ahead predictions. Findings reveal that data preparation is vital for the accuracy of prediction models and should be model-adjusted.

Keywords: time series forecasting; energy load forecasting; machine learning; prediction model; smart building

1. Introduction

Energy use and surrounding issues are critically important today as these challenges directly impact society's wellbeing and security [1]. Among the three main economic sectors described as having very high energy consumption, buildings have been identified to contribute a large share of this consumption [2]. According to the International Energy Agency (IEA) report 2021, energy use in buildings has significantly increased from 115 EJ in 2010 to 135 EJ in 2021. The latter represents 30% of global final energy consumption, with electricity accounting for 35% of building energy use and a significant amount catering to space cooling needs [3]. Because people spend most of their time in buildings, homes, and offices, they rely heavily on heating and cooling systems. Electricity and heat generated for use in buildings account for substantial carbon emissions in the energy industry. In residential houses, electricity use is growing faster than any other energy source and is projected to increase through 2050, regardless of the efficiency gains.

A power grid that relies heavily on renewable energy is one of the most essential steps toward carbon neutrality [4]. According to estimates, 60% of the world's power will be generated from renewable energy by 2035 [5]. This growth in renewable energy generations and their sporadic nature has made it necessary to have smart grids and microgrids to ensure power system stability, operability, and reliability [6,7]. The developed variability in the energy demanded and power generated, introduced by several power sources,

particularly solar and wind, is causing an impending transition in the power systems and infrastructure. Several strategies have been conceived and implemented to lessen the adverse ramping effects, such as demand response (DR), resource allocation, total energy forecasting, peer-to-peer energy transfer, microgrids, and bigger storage capabilities.

Accurate energy forecasting makes managing imbalances between energy production and consumption easier and supports smart grid architecture procedures like demand response management (DRM) [8]. DR allows households to actively participate in efforts to improve power system reliability and emissions reduction [9]. Proper implementation of DR programs requires forecasting households' energy requirements. To assess the impact of both current and prospective energy plans, stakeholders in the energy sectors, such as the distribution system operators (DSOs) and aggregators, rely on prediction algorithms to anticipate demand and supply. The power sectors use long-term load requirement forecasts to guide current investments and planning while using short-term energy forecasts to ensure supply and dependability [10].

The development of powerful prediction tools for building energy consumption has been facilitated by the rapid growth of the Internet of Things (IoT) and artificial intelligence (AI) technologies exploiting data contained in complex information networks [11]. Energy recommendation systems continue to be deployed and implemented to foster energy-saving behavior and reduce carbon emissions [12]. These systems can propose models for short-term load forecasting (STLF) for various buildings, considering their physical and operational characteristics and time series data on energy consumption.

Load forecasting has transitioned over the years and has become a pillar for energy planning and operation. However, load forecasting for buildings does not receive the necessary attention from the power engineering community. The growing impacts of smart meters have driven the attention of building engineers, researchers, and practitioners to building load forecasting primarily to pursue operational excellence. This study aims to use different machine learning (ML) algorithms for very-short-term load forecasting (VSTLF) of energy requirements in a household and evaluate the performance of algorithms on different time resolutions (15 min, 30 min, and 1 h) to observe the errors in the predictions.

VSTLF has found high relevance in energy load forecasting (ELF). Hence, this paper elaborates on short-term ELF, comparing the performance of different traditional models on the same data with different features like data time resolution and forecasting time steps [13]. The study explores the effect of different time steps on the prediction models' performance by resampling the data into 30 min and 1 h time steps. While analyzing the resampled datasets, the models were compared to their 1 h ahead predictions using 1, 2, and 4 steps for each resolution. The results showed that the most accurate prediction was achieved with the resampled 1 h 1-step-ahead prediction, outperforming the 15 min 4-step-ahead and the 30 min 2-step-ahead predictions.

The study reveals the relevance of energy forecasting in transitioning from conventional to sustainable, smart buildings with greater control over their energy resources by spelling out the importance of high-performing ML prediction models.

2. Background

The design and operation of power systems rely on ELF. To monitor and balance future energy generation with consumption, DSOs use forecasting as a tool. It lets utility providers predict electricity usage and plan for future power loads. Given the rapidly changing infrastructure for energy distribution and its growing capabilities, the need for precise predictions for quicker response times and resource allocation is very apparent. It can be generalized that ELF is essential for the proper and continuous operation of power systems. Compared to other types of loads, the accuracy of residential ELF has proven challenging due to many uncertainties.

In the past, it was a usual practice to forecast residential energy usage by estimating the hourly average electricity usage of many households [14]. This gives the ability to predict peak electricity demand times and allows power system operators to switch on

additional power plants to avoid severe electrical shortages. Recently, buildings have incorporated solar panels, wind turbines, and battery storage, which require accurate ELF for proper implementation [15]. The nature of renewable energy sources necessitates accurate forecasting of residential electricity consumption at disaggregated levels.

Energy consumption forecasting would be straightforward if the process depended only on the energy data. In reality, this is not the case. Energy use also relies heavily on several other factors, including the environment and the weather. Household energy consumption patterns vary according to temperature, humidity, time of day, occupancy level, and socioeconomic characteristics. Researchers have reported several factors significantly affecting the energy consumption in residential buildings. In [16], the number of bedrooms accounts for almost 35% of the difference in the electricity consumption of houses in Leicester and Sheffield, United Kingdom.

Similarly, another study revealed that the number of rooms per house is the most significant factor influencing energy consumption [17]. While this is obvious, at the city and national levels, population density is directly linked to aggregated energy consumption [18]. These variables are very related. The higher the number of rooms in a house, the higher the number of occupants in the building, hence the higher the use of electrical appliances. These factors can be directly linked to household spaces, which is also a significant factor. A large space area will require a large amount of heat or cooling. In the case of electric heating systems, the impact of the space area per square meter on electricity consumption was investigated [19]. Another factor that has been attributed to influence energy consumption is household income. A high-income household may imply a larger, warmer house with more appliances.

2.1. Factors Affecting Energy Use in Building

The energy behavior of a building is impacted by such factors as the weather conditions, the thermal characteristics of construction materials, the level of occupancy, occupants' behavior and performance, and schedules of components—lighting and heating, ventilating, and air-conditioning (HVAC) systems [20].

2.1.1. Weather

The weather plays a significant role in determining how much energy buildings use. Parameters such as temperature, relative humidity, and wind speed, which define the weather conditions, vary with time. Commercial building heating and cooling loads using the external dry-bulb temperature as a weather factor were estimated [21]. To forecast monthly building energy usage, authors in [22] used the typical monthly temperatures. Their prediction is more accurate than conventional methods, which often use heating and cooling degree days. The annual heating and cooling load of nonresidential buildings was predicted based on a few weather variables, such as the monthly average of maximum and lowest temperatures, relative humidity, air pressure, and cloud cover [23]. Comparing their findings to energy simulation tools, predictions for low-mass envelope buildings were more accurate.

Time series prediction models estimate future demand using historical energy and climate data. As a result, once the weather pattern changes, the prediction error will significantly increase. The lower performance of time series predictions with changing weather conditions is considered a challenge.

2.1.2. Building Characteristics

A building's characteristics are another critical aspect of its energy performance. These entail the physical design of the building, the shape, window-to-wall ratio, type of facade, orientation, roof and wall insulation, the number of floors, the type of window, and glazing. It is a significant but complicated factor in determining energy performance is the building. A simple method of predicting energy consumption in a residential building with a renewable energy system was conceived [19]. Appliances, hot water, and space

heating were included in the definition of the total energy use of the building. A particular modeling technique was used for each component, using statistical data on average end-use consumption.

Just a few studies considered building characteristics as a predictor in the forecast models according to their reviews [24]. Using statistical ML algorithms, the effect of eight building characteristics on the cooling and heating of a building was also investigated [25]. The authors further compared the strength of each factor on the performance of a linear and nonlinear regression model to ascertain the potential of using an ML model to predict building energy load.

2.1.3. Type of Appliance Used

The number, type, and occupants' appliance use pattern explain the household's electricity consumption. These appliances account for up to 30% of energy use in the residential sector [26]. Appliance energy consumption can be divided into components, including HVAC equipment like air conditioners. Another study analyzed household electrical appliances, including dish and clothes washers, to determine their energy use pattern. It was demonstrated that the use of these appliances depends highly on the user and varies with time from house to house [27]. The use of these appliances also affects indoor conditions such as temperature, humidity, light, and noise.

The influence of appliances on thermal gains is very significant and relevant for highly insulated buildings in terms of a building's energy performance [27]. The problem of predicting appliance aggregated energy use was addressed by applying four regression models: support vector regression (SVR), gradient-boosting regression (GBR), random forest (RF), and multiple linear regression (MLR) models with several combinations of features [28].

2.2. Time Series Energy Forecasting

Energy forecasting has made it possible to solve real-world issues by developing a system of predicting energy demand and production. These systems are developed by creating models that learn about past events from historical data represented by many observations, each corresponding to a specific moment in time. These sequential observations indexed by time are called time series data and are expressed as a vector of n variables. The primary goal of analyzing these time series data is to create a mathematical model to learn from available data to predict future observations. This has made time series forecasting an extensive research field in science and engineering [29].

Time series modeling and prediction are approached with linear or nonlinear forecasting models. Autoregressive (AR), moving average (MA), and autoregressive moving average (ARMA) are the three most common linear models for time series forecasting [30]. These models do not perform well for nonlinear time series. They rarely produce accurate predictions because they exhibit linear dependencies over time and assume that the time series is constant. However, there have been numerous studies on the application of AI to solve forecasting problems using nonlinear time series [31–33].

Four statistical models were developed to forecast aggregated appliance energy consumption for a passive house in Belgium [28]. These models were MLP, SVM with radial kernel, RF, and GBMs using R programming language. The extensive data analysis approach to the model development indicated that the best model performance was achieved with GBMs. The evaluation considered the metric values of root mean square error (RMSE), mean absolute percentage error (MAPE), and mean absolute error (MAE) and was compared with the three other employed models. In [34], authors adopted a homogeneous and heterogeneous transfer learning approach using boosting to learn a set of multiple kernel regressors. The results of this experiment on the residential dataset showed that knowledge gained from other households could significantly reduce forecasting errors.

2.3. Energy Load Forecasting

ELF can be divided into the following categories, each with a distinct goal and time frame. According to [35], short-, medium-, and long-term are the three main types of ELF in energy operations planning and control. VSTLF is the term used to describe forecasts for extremely small time frames. Using past energy loads observed on the same day to train the prediction model, they vary from one minute to one or several hours in the future (often in five-minute steps) [36]. In addition to being used in transmission lines load management, VSTLF assists in intraday power trading and handling ancillary tasks that ensure the electricity system's stability [10].

STLF is intended to estimate electrical demand for 30 min up to two weeks [37] and is applied to the day-ahead load, energy network planning, and maintenance. STLF can improve operational safety and reduce power system costs [8].

Medium-term load forecasting (MTLF) covers one week to a couple of months up to one year in advance [10]. It allows running the power networks' energy switching, maintenance, and outage planning [38]. Retailers and large customers need accurate long-term probabilistic energy forecasting to optimize their energy scheduling and operation and adjust in the short-term market and profitable sign agreements [10].

The time ranges covered by long-term load forecasting (LTLF) may range from one to ten years or even longer [39]. Energy management and system capacity planning heavily rely on long-term energy forecasts. The long-term annual energy demand forecast is crucial because it plays a part in developing and planning the nation's energy mix and power system infrastructure investment.

Compared to the middle and long-term, short-term forecasts provide more accurate and precise predictions. Though studies on short-term energy have been conducted, the accuracy of forecasting performance differs due to the lack of real-time data [40–42]. Recently, day-ahead forecasting of residential customers' electricity consumption has also undergone extensive analysis. Other researchers claimed that their 1-step-ahead method for STLF can be used consistently for any energy load prediction problem irrespective of the type of load forecasting. The study further suggests that forecasts depend on the context and the input data for the hypothetical energy demand [8].

2.4. Related Work

Recently, much research has been conducted on how electrical energy is used in buildings. The effect of meteorological factors on the monthly power demand in buildings has been the subject of many studies. Variables such as the daytime, weekend, month, outdoor temperature, holiday, previous day consumption, rainfall index, global solar radiation, wind speed, and occupancy have been incorporated in models for predicting electricity demand in buildings [43,44].

The electricity data of 1628 households were studied, containing information on the weather, building envelope characteristics, number of appliances, occupancy level, location, age of the building, floor area, ownership, energy-efficient light gadgets, and income level of occupants. The researcher concluded that the weather, location, floor area, number of refrigerators, and entertainment appliances were the most crucial factors affecting minimum daily consumption [45]. It was demonstrated that weather variables can be used to forecast how much electricity is used in buildings. In another study, the same author correlated the energy use efficiency in the building with the time of occupancy and attributed the low efficiency of appliance energy use with a high level of occupancy [46]. Also, data-driven prediction models were used to establish the relationship between appliance energy consumption and the predicting variables for a house in Stambruges [28]. The statistical analysis of the data collected and prediction models showed the prevalence of weather data and time information as better predictors among the variables used.

Several deep learning techniques were used to forecast the energy consumption of a building, and the long short-term memory network/gated recurrent unit (LSTM/GRU)

model performed the best [47]. A strategy for predicting energy usage in residential buildings using a deep extreme ML approach was proposed by [48].

A comparative analysis of different ML models on household energy data was performed in South Korea to determine the behavioral pattern of the occupants and develop an optimal energy use plan for each house [49]. The authors applied linear regression (LR), SVR, and k-nearest neighbor (KNN) regression on the dataset using WEKA (Waikato Environment for Knowledge Analysis—a data mining tool) before using times series models, ARIMA, and vector autoregression (VAR) to forecast energy consumption. They found that ARIMA and VAR did not perform well on the test data, but better performance was recorded for SVM regression.

Examining the energy use in all German industries, including residential structures, it was reported that multiple regression was the best forecasting method [50]. Likewise, an analysis of different factors that affected home energy usage in France concluded that MLR is the best method to identify the critical factors [51]. For buildings in London, the influence of economic, sociodemographic, and building characteristics on energy consumption and using LR models was also investigated [52].

To optimize HVAC systems, a data-driven predictive control approach that combines reinforcement learning (RL) and time-series forecasting to analyze different sensor metadata was proposed [53]. This entails creating and validating sixteen architectures based on long short-term memory (LSTM) with attention, convolution, and bidirectional processing processes. The findings demonstrated that recursive prediction significantly lowers model accuracy. This effect was more noticeable in the model that predicts temperature and humidity.

The extreme weather identification and STLF model based on the bagging-extreme gradient-boosting (XGBoost) algorithm may provide an early warning on the time period and detailed value of peak demand [54]. First, the concept of bagging was presented to lower the output variance and improve the algorithm's capacity for generalization based on the XGBoost algorithm. Next, to increase the model's ability to follow changes in the weather, the mutual information (MI) between weather-affecting factors and load was evaluated. The extreme weather detection model was then constructed to ascertain the occurrence range of peak load, taking into account the load, weather, and timing aspects.

Furthermore, to estimate building loads, a novel hybrid technique that incorporates convolutional neural networks (CNNs), grey wolf optimization (GWO), and bidirectional long short-term memory (BiLSTM) was introduced [55]. The CNN and BiLSTM algorithms' ideal set of parameters was obtained using the GWO. To extract the time series data feature efficiently, one-dimensional CNN was used. Four buildings with unique characteristics acted as case studies to examine the performance of the suggested technique utilizing hourly resolution data. The outcomes validated that the same method may be successfully employed on other architectures.

Home energy consumption was predicted in the United States using an MLR method [56]. Multiple regression was employed to predict building gas and electricity consumption using the average number of rooms, heating degree days, and median household income as the model inputs [57]. Finally, the number of occupants and rooms in a building were utilized as input to model an algorithm for predicting electricity consumption [58].

2.5. Challenges in Household Energy Forecasting

Anticipating energy consumption in a building is difficult due to the intricate nature of energy systems. The primary energy sources discussed in the literature are heating/cooling load, hot water, and electricity [23,43,59]. Individuals' decision-making processes influence their electricity consumption, which is unpredictable. Each occupant's behavior is rendered insignificant when forecasting energy consumption at an aggregated level. However, it becomes more important when forecasting is carried out at disaggregated levels. That way, noticeable variations can be observed in individual consumption, consequently introducing errors in the prediction model.

Data gathering and access are the main challenges in building ELF. Much research on individual electricity consumption forecasting uses consumer survey data or sub-metered appliances. However, this is not practically feasible on a large scale, partly due to privacy concerns. Therefore, it is crucial to conduct research in this field using data from fiscal smart meters that include integrated local weather data. A combination of several ML techniques to manage data inconsistencies from the fiscal smart meter modeling user behavior and forecast individual users' residential electricity consumption was conceived [14]. Such studies focus on forecasting the next day's hourly energy consumption of residential households [60].

Despite the success achieved with data-driven forecasting models, there are certain drawbacks in capturing residential consumers' irregular but highly periodic energy habits. Generalizing occupant behavioral patterns is one of the main flaws in the current models. When only electricity consumption, calendar information, and external weather data are accessible, they reflect user behavior, climate, and seasonal variations. However, it is difficult to infer the user behavior as it is independent of these seasonal dependencies. Another study emphasized the high correlation between the occupancy profile and energy consumption relative to people's activity. This occupancy profile predicted the electricity demand for heating and cooling appliances [61].

After exploring the main challenges in household ELF, this study addresses the urgent need to lower energy usage by presenting a novel method for optimizing short-term load forecasting (STLF). The research performs a comparative examination of multiple ML models, investigating varying data resolutions and time steps ahead, and demonstrates the specificity of each model's performance for various resolutions. Although the study provides insightful information about the relative advantages of different models, it also emphasizes the importance of improving data preparation procedures to increase forecasting accuracy, underscoring the necessity of ongoing adaptation to attain the best outcomes.

3. Methodology

Comparative analysis of the performance of conventional ML models for predicting the energy consumption of the building under study is carried out using its historical energy consumption and weather data. The effect of engineered features and hyperparameter tuning on the model's performance is also analyzed. The study explored the model's performance based on different time steps, i.e., 15 min, 30 min, and 1 h. The computation stage is divided into the training stage and the test stage. The evaluation of the models is based on the estimation error and the computational time to train the model.

Having all the 1-step-ahead predictions for all three resolutions, a 1-step-ahead vs. direct multistep-ahead (i.e., 4-step and 2-step) comparison was performed to identify the best method for 1 h ahead prediction. The goal was to test the original 15 min resolution on a 4-step-ahead prediction against a 2-step-ahead resampled 30 min resolution and 1-step-ahead resampled 1 h resolution.

3.1. Dataset Description

Data from the ITI/CERTH Smart House [62], the first smart net-zero building in Thessaloniki, Greece, were explored for the experimental test. The energy data include energy consumption, photovoltaic (PV) energy generation, battery storage, and electricity price. These energy data were logged at 15 min intervals over two years between October 2018 and September 2020 by IoT devices, smart meters, and sensors. The weather data include temperature, relative humidity, wind speed, and cloud cover, which were interpolated at 15 min intervals from a local weather station. All in all, the data comprised 63,612 observations with 15 min time intervals.

3.2. Data Preprocessing

Data preprocessing is a crucial step in time series forecasting model development. This critical process determines model success. To gain insights and make predictions using ML algorithms, smart meter data need to be analyzed using robust techniques due to missing data and outliers. Data preprocessing quality directly affects forecasting model performance.

3.2.1. Handling Missing Data

Missing observations or null values pose a big problem to the learning algorithms. Making the algorithm work and connecting all the signals in the features is impossible if some values are missing. Initially, the weather data had some missing values, whichwere filled by using linear interpolation. This approach is commonly employed in time series data to fill the missing values with the preceding or succeeding ones.

3.2.2. Outliers Removal

Communication errors in data collection and storage may result in inaccurate data that exceed the normal measurable limits. Outliers, also known as anomalies, are typically data points that deviate significantly from the expected values, being either very low or very high. Outliers pose a significant risk to ML algorithms as they can potentially disrupt the patterns and rules that the algorithm has learned. To address this issue, a statistical analysis was conducted to assess the deviation of median values from the mean, as well as the difference between the 25th and 75th percentiles.

Energy Consumption: Sorting the frequency of unique values in ascending and descending order detects the outliers in the energy consumption data. These outliers were replaced by the 99.8th percentile of the energy consumption data. The frequency of the data represented by the histogram in Figure 1 shows the occurrences of different energy consumptions that range from 0–2.4 kiloWatt hour (kWh) after removing outliers. Figure 2 shows the hourly energy consumption profile. The low values in this profile represent a period of low energy consumption, reflecting the diminishing occupant's energy use.

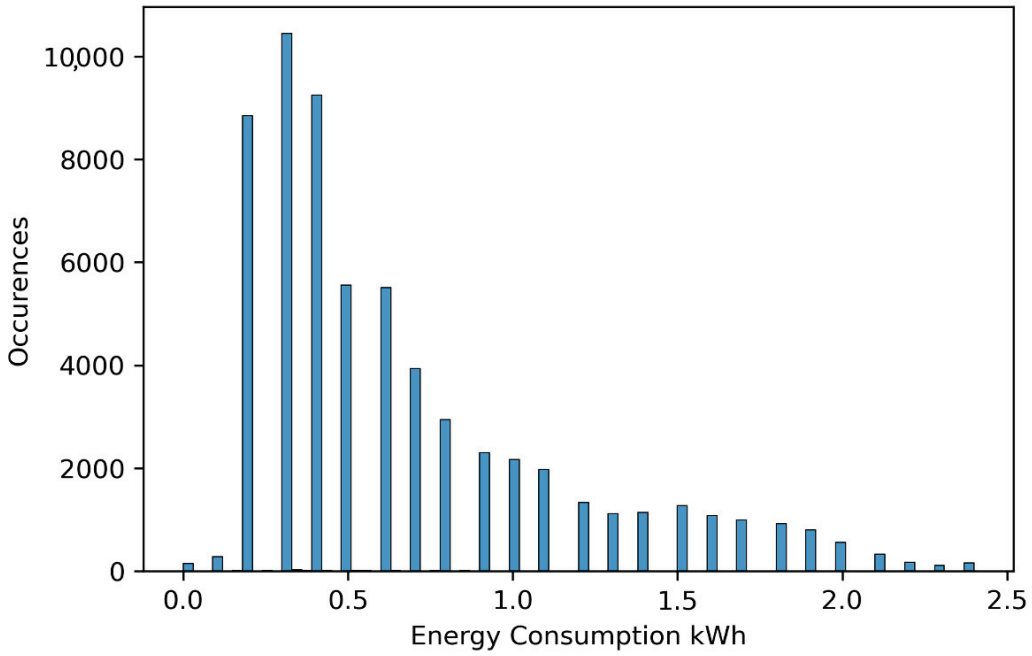


Figure 1. Histogram of the energy consumption data.

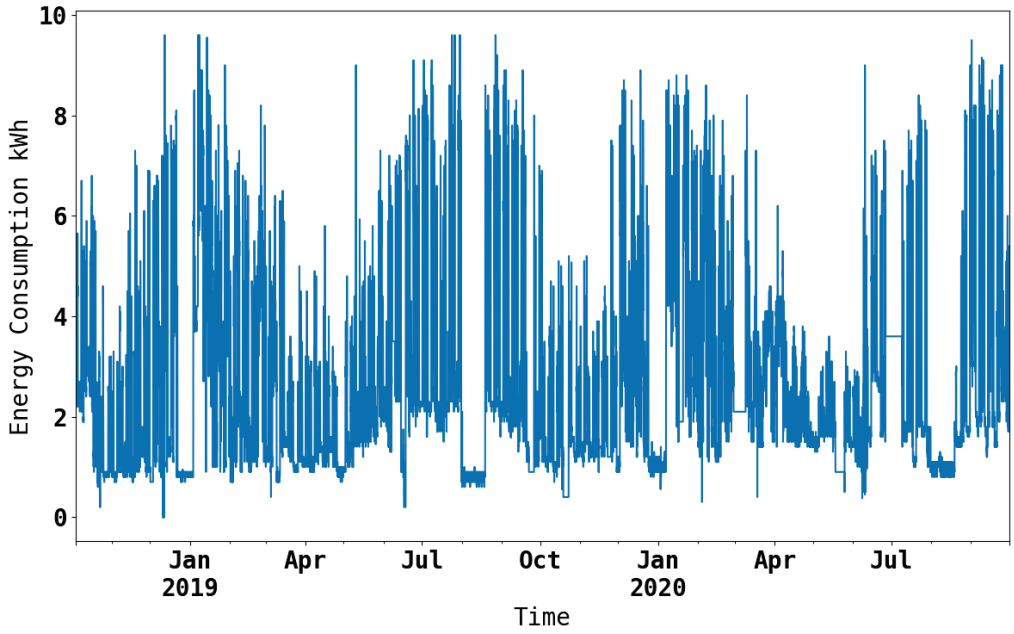


Figure 2. Energy consumption profile aggregated per hour.

Weather data: These data feature temperature, relative humidity, wind speed, and cloud cover data. The outliers in temperature were removed by replacing the outrageous values with the 99th percentile of the data values, found to be approximately 41 °C. This is important because the temperature is fundamentally related to the energy consumption of any building.

Energy generation: The PV energy generation data contain no missing and extreme values. The 0th and 100th percentile of PV energy generation lie between 0 and 3.6 kWh. Outliers were eliminated by replacing data values exceeding the 99th percentile with the 99th percentile value of the data. The hourly energy generation profile is shown in Figure 3.

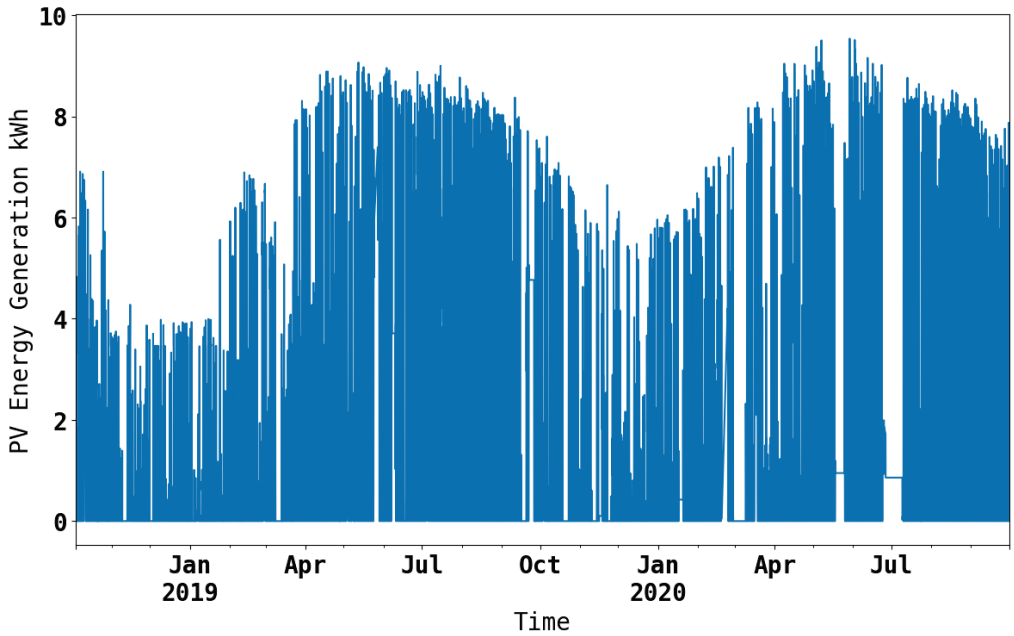


Figure 3. PV energy generation profile aggregated per hour.

3.2.3. Data Rescaling

The performance of ML models is often affected by the scale of numeric values. Therefore, rescaling the distribution is necessary for the approach to converge more quickly and provide a more accurate result. Rescaling changes the feature values' range, and it may also impact variance [63]. In this study, the scikit-learn "StandardScaler" was employed [64]. This preprocessing method uses min–max transformation to rescale the data from 0 to 1 by subtracting the minimum values from the current value and dividing by the range. This method was preferred because the data observations have a very small deviation from the mean values.

3.2.4. Feature Extraction and Engineering

Feature extraction highlights parts of the time series and reduces dimensionality. In this step, the time series is modified to produce a few distinctive features that will be passed as input variables for the prediction model. In addition to the energy consumption, generation, and weather data, time-related features extracted from the time series form the bulk of data for analysis. Research demonstrated that integrating time-related data improves the performance of electricity forecasting algorithms [65].

Dummy variables were created from the time-related features extracted using one hot encoding. The intention behind feature generation was to create a more complex feature matrix that could help the model achieve better results rather than building complex models.

3.3. Exploratory Data Analysis

As originally used in his book Exploratory Data Analysis (EDA), the American statistician John Tukey discussed the need for greater integration between graphical analysis and descriptive measure [66]. Visualizing observable trends in 1 h resolution can enhance comprehension of the data. Figure 2 shows that the 1 h energy consumption profile has higher energy consumption during the winter and the summer months due to high cooling and heating demands. The lower energy consumption in August and December implies periods of inactivity in the building. The PV energy generation data show a gradual increase in energy generation from January through April, as shown in Figure 3. The peak of energy generation spans from June to October due to the intense and prolonged sunlight, followed by a gradual decline until December.

3.3.1. Energy Consumption—Weather Data Relationship

Scatter plots visualize the relationship between energy consumption and weather variables. As shown in Figure 4, temperature reveals a clear pattern with energy consumption. When the ambient temperature is high or low, there is a corresponding proportion of energy consumption. Figure 5 shows the hourly mean aggregation of the energy consumption and the temperature in the dataset. This illustrates high energy consumption when the temperature is high. Daytime temperatures coincide with increased electrical energy consumption, particularly for cooling purposes. Utilizing a sliding window (SW) for the model training, as described in Section 3.4.3, necessitates a large number of parameters, rendering it impractical to showcase feature importance for numerous variables. Thus, Figure 6 shows a feature matrix that filters out and displays the most significant correlations defining the variables with the greatest impact to be used for the model training.

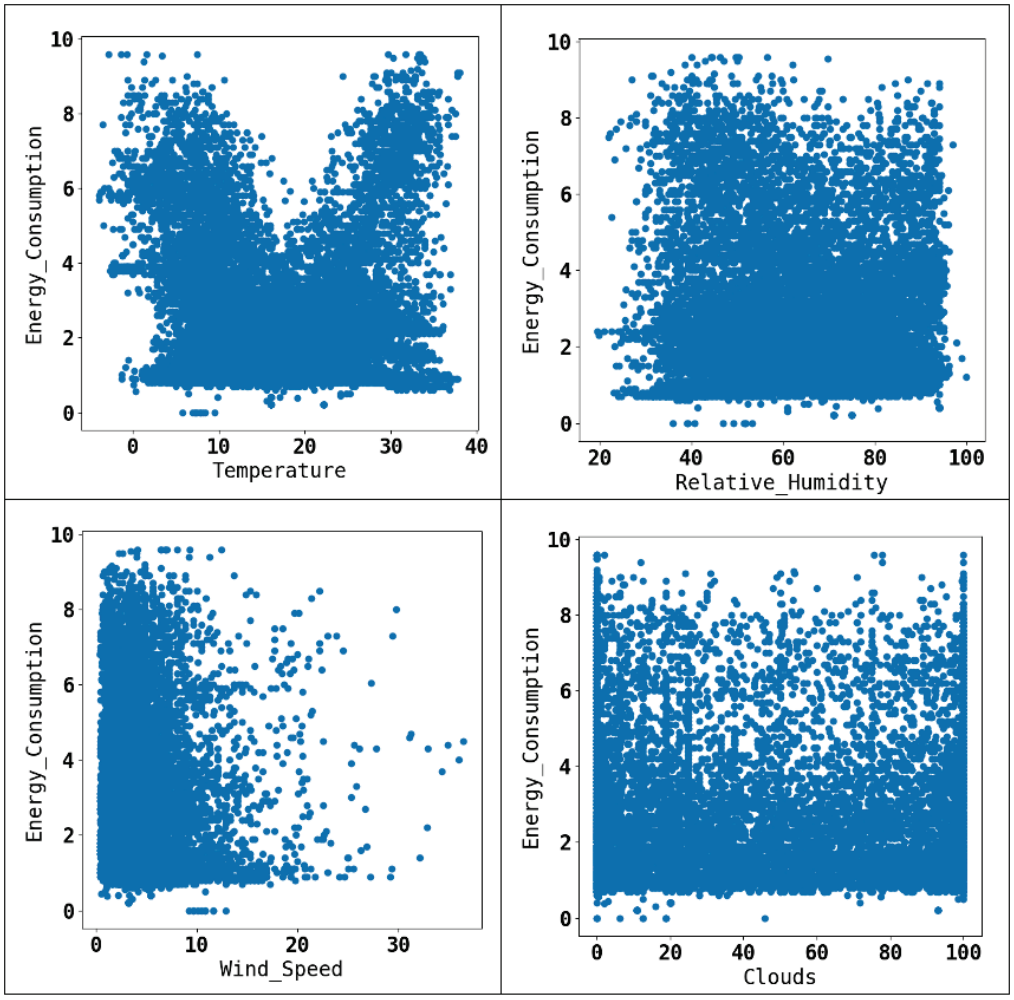


Figure 4. Scatter plot of the weather variables.

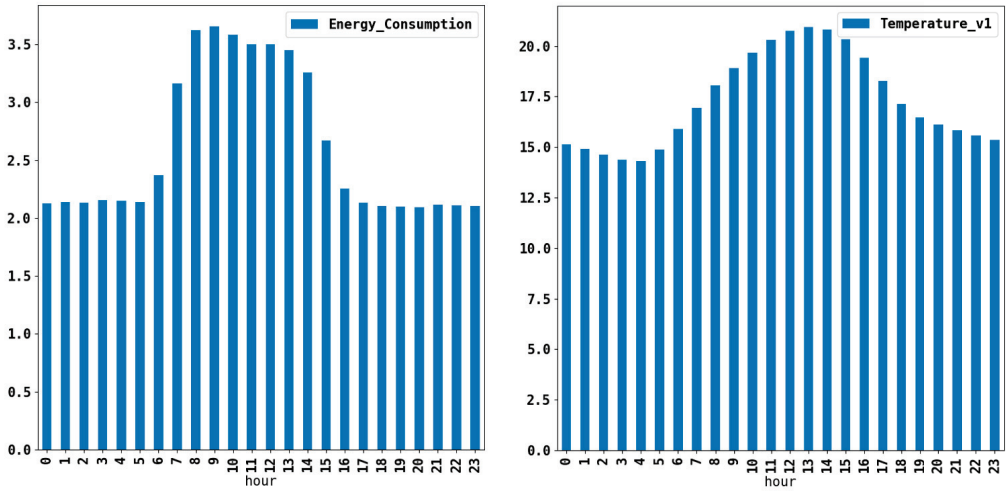


Figure 5. Hourly aggregation of energy consumption and temperature data.

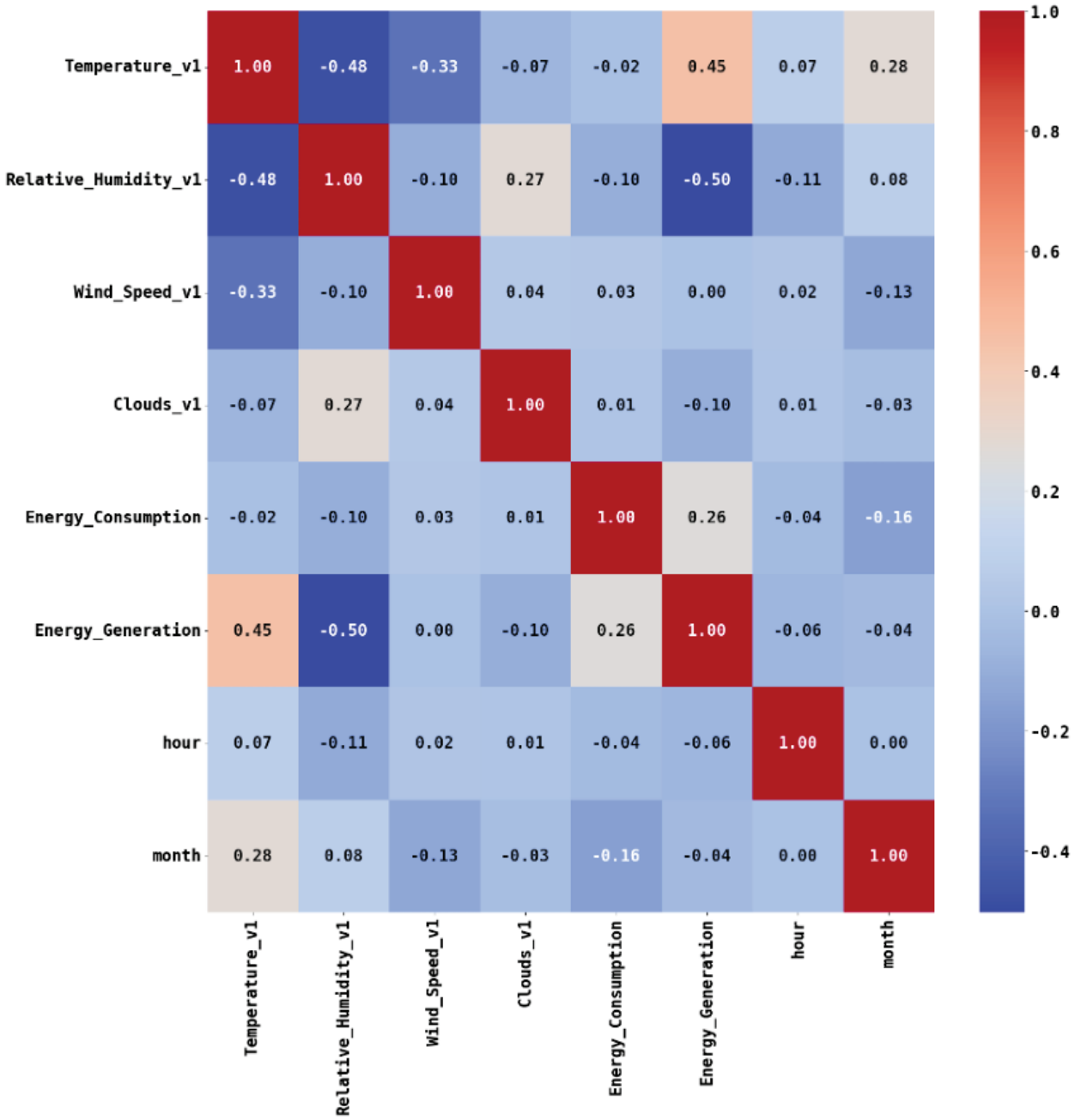


Figure 6. Feature correlation matrix.

3.3.2. Autocorrelation Analysis

Time series data result from collecting the same repetitive observation over a period. Considering the correlation between the observations specified by the lag is essential to understanding the persistent relation in the time series data. This also helps to determine the stationarity of the dataset, as it is commonly assumed in time series problems that the data is stationary. The properties defining stationarity are the unaltered pattern in the mean, fluctuation, and autocorrelation over time. Figure 7 shows the autocorrelation plot of the hourly energy consumption in the dataset, which indicates a strong correlation between hourly energy consumption throughout the dataset. Moreover, the blue area represents a 95% confidence interval and serves as a signal of the significance threshold. Inside this area, values are statistically insignificant, while beyond this area, values are statistically significant. To establish the model's order, we must consider all spikes that fall beyond the significance threshold (blue region).

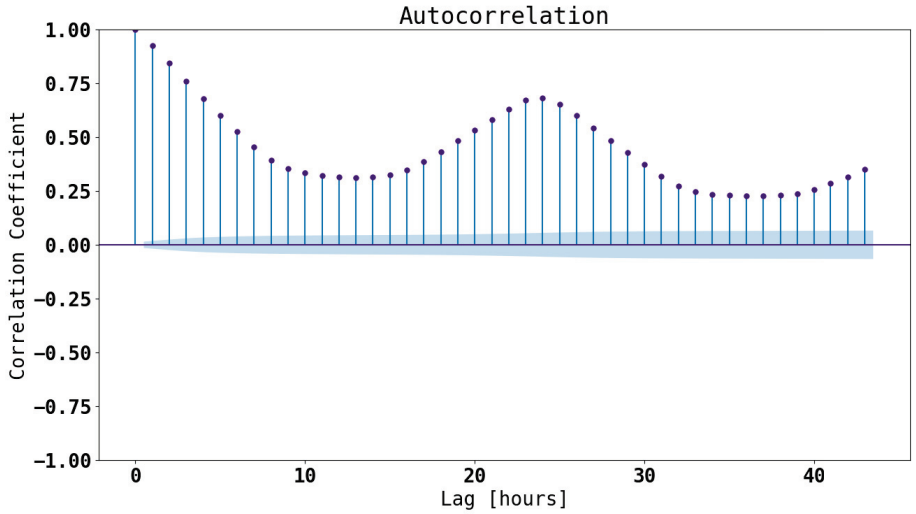


Figure 7. Autocorrelation plot of the hourly energy consumption.

3.4. Algorithmic Modeling

Over the years, several techniques have been developed to predict building energy consumption accurately. The widely used methods include engineering, statistics, and AI.

3.4.1. Linear Models

The most fundamental regression algorithm is LR. Simple LR is used when there is only a single input variable, while MLR is applied when there are several variables, usually referred to as a matrix of features. A linear model predicts by adding the bias term (also known as the intercept term) to the weighted sum of the input features. More complexity is not required if a linear model sufficiently captures the facts. A cost function is often used to validate the performance of LR. The goal is to reduce this distance between the predictions of the linear model and the training samples.

Ridge regression (RR) is a regularized version of LR. Regularization of the linear model is an effective way to reduce the problem of overfitting. This is achieved by constraining the model and reducing the number of polynomial degrees to reduce its degree freedom and make it hard to overfit. Another regularized form of LR is the least absolute shrinkage and selection operator regression, lasso. Like RR, it adds a regularization element to the cost function [67].

Support vector regression (SVR) is based on high-dimensional feature space created by modifying the original variables and penalizing the resulting complexity with a term added to the error function. The model generated by SVR only depends on a subset of the training data because the cost function for building the model ignores any training data relatively close to the model prediction [68].

One of the main drawbacks of LR models is that they should not be used when a nonlinear relationship exists between the independent and dependent variables.

3.4.2. Tree-Based and Boosting Models

Tree-based models are a family of ML models that perform regression or classification tasks by building decision trees to classify the target variable or determine its values. Because of their capacity to handle outliers, tree models provide a major advantage over linear models. Regression trees are likely to perform better than linear models when no attributes have been found to have a linear relationship with the target variable [69]. They are robust algorithms that can successfully fit complex datasets.

RF is an ensemble of decision trees trained on several random subsets of the training via the bagging method. This method combines classification and regression by growing many decision trees in parallel [70]. Due to its simplicity, ease of usage, and straightforward interpretation, RF is one of the most popular and efficient ML algorithms currently accessible [63]. It proves very useful for data with very high dimensionality.

The extremely randomized trees ensemble, shortened as extra-trees, is a forest of extremely random trees. When growing a tree in an RF, only a random subset of the features is considered for splitting at each node. Instead of looking for the best possible thresholds like conventional decision trees, random entries can be used for each feature to make trees even more random. This method sacrifices a higher bias for a reduced variance. As a result, extra-trees are considerably faster to train than conventional RFs. This is due to the short time it takes to figure out the optimal threshold for each feature at each node of the trees.

Boosting models are ensemble methods that combine and turn several weak learners into strong learners [63]. The main concept behind most boosting techniques is to train predictors in succession, each attempting to correct the one before it. GBR operates by adding predictors to an ensemble one at a time, with each one correcting the one before it. It achieves this by fitting the new predictor to the residual errors made by the previous predictor rather than adjusting the instance weights at each iteration [63]. The prediction of building energy consumption has been made using GB in such research as simulating the energy usage of commercial buildings [71]. In forecasting commercial building energy usage [72], GB outperformed MLR and RF models implemented in comparison to it.

Extreme gradient-boosting regression (XGBR) is an optimized implementation of GB, usually used with decision trees [14,69]. This efficient, fast, and scalable machine learning method is frequently used along with neural networks. The model is enhanced so that each decision tree incorporates lessons from the one before it and influences the one after it [73]. GB models surpass other ML algorithms (such as KNN and SVMs) in accuracy and robustness [74]. A method for predicting energy usage in a large-scale scenario using GB is presented [75].

The light gradient-boosting machine regressor (LGBMR) uses one-side sampling to determine the ideal split for input data. But, unlike other boosting algorithms, the LGBMR expands on a leaf basis for developing a decision tree. The LGBMR is considered lightweight and resource-efficient compared to other gradient-boosting techniques, allowing quicker training times and lower computational demands while producing excellent accuracy [76].

3.4.3. Model Selection and Training

Model selections for prediction depend on the data available [77]. The models selected for this study consist of linear and nonlinear ML models informed by past works in ELF. The linear regression (LR), elastic net regression (ENR) [78], lasso least-angle regression (LLR) [79], RR [67], and SVR [68] were selected because of the interesting facts about them. LLR can zero out the coefficient of the parameters that are unimportant in the model by automatically selecting the best features on its own; RR regression can deal with multicollinearity in a dataset with many predictors; and SVR is effective for multifeature modeling.

The gradient models—GBR [73], XGBR [77], LGBMR [80], and categorical boosting regressor (CBR) [81]—were included as they rely on the ensembling of weaker models to obtain better performance. The tree algorithms, random forest regressor (RFR) [82], and extra trees regressor (ETR) [83] have been reported as suitable when dealing with models whose features have almost zero linear correlation with the target vector [69]. Other models utilized were histogram-based gradient-boosting regressor (HGBR) [73], bagging regressor (BR) [84], and Bayesian ridge regression (BRR) [85].

The dataset was divided horizontally into training and testing sets in proportions of 80% and 20%, respectively. This is equivalent to using approximately the first 18 months of

the data to train the models and the last six months to test the models. The train–test split is in this order to avoid randomization, which results in poor performance of the model.

Since the correlation between the target variable (energy consumption) and weather features is very little, the approach adopted is to check, by trial and error method, the impact of each feature group on the model's performance to identify the right combination of features that gives optimal performance. Having features that do not correlate with the target variable in the feature matrix impacts the model's performance and takes a long time for the computation.

The data comprised 63,612 observations with 15 min time intervals. Resampling the data into 30 min and 1 h time steps reduces the size of the training and test sets for the experiments. Thus, the time resolution and size of the dataset affect the model's performance and establish the best time frame for short-time load forecasting.

The selected algorithms were first trained with the default parameters, and the performance obtained formed the preliminary results. Hyperparameter optimization was employed to improve the models' performance. The process involves tweaking the parameters. Primarily, hyperparameters are defined as ones that must be provided to the models before training because they cannot learn. Numerous methods for hyperparameter optimization have been proposed. For this study, grid search with cross-validation from the scikit-learn library [64] was employed. Furthermore, the SW technique [86] was utilized for all three resolutions, including previous observations up to one day before. This means that a 96-step SW was utilized for the 15 min resolution, a 48-step SW for the 30 min resolution, and a 24-step SW for the 1 h resolution. Figure 8 shows the chart of the experimental framework.

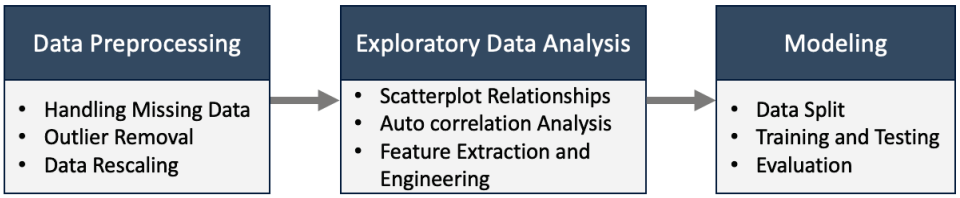


Figure 8. Overview of the experimental process.

3.5. Performance Measures

The performance of prediction models is evaluated using statistical metrics, which represent the key performance indicators of the models. The common metrics used for time series models are RMSE, MAE, R^2, CVRMSE, and NRMSE. They all quantify the variability of observations around the mean, but they are not the same, and their values are different. These metrics were rationally selected based on a combination of absolute (MAE, RMSE, time) and relative (CVRMSE, NRMSE, R^2) measures to comprehensively assess the models' performance in terms of accuracy, error, computational time, and resources.

3.5.1. Root Mean Square Error (RMSE)

RMSE is a general-purpose error metric for prediction. The standard deviation of the prediction errors gives the difference between the regression line and the data points [87]. It is defined as the square root of the average squared difference of the actual and prediction values. RMSE is widely used as it is measured in the same units as the variable in question. According to its mathematical definition (Equation (1)), RMSE applies more weight to larger errors, given that the impact of a single error on the total is proportional to its square and not its magnitude [88].

$$RMSE = \sqrt{\frac{1}{N}\sum_{i=1}^{N}(y_i - f_i)^2} \quad (1)$$

where y_i is the actual and f_i is the forecasted value, and N is the number of values.

3.5.2. Mean Absolute Error (MAE)

Calculating MAE involves summing the absolute error values (i.e., the difference between the actual and the predicted value) and then dividing the total error by the number of observations (Equation (2)). Unlike other statistical methods, MAE considers the same weight for all errors.

$$MAE = \frac{1}{N}\sum_{i=1}^{N}|y_i - f_i| \tag{2}$$

where y_i is the actual and f_i is the forecasted value, and N is the number of values.

3.5.3. Coefficient of Determination (R^2)

The coefficient of determination (R^2) constitutes the comparison of the variance of the errors to the variance of the data that are to be modeled. It describes the proportion of variance "explained" by the forecasting model (Equation (3)). Unlike other error-based metrics, the higher its value, the better the fit.

$$R^2 = 1 - \frac{SS_{res}}{SS_{tot}} = 1 - \frac{\sum(y_i - f_i)^2}{\sum(y_i - \overline{y})^2} \tag{3}$$

where SS_{res} is the sum of squares of residuals (errors) and SS_{tot} is the total sum of squares (proportional to the variance of the data), y_i is the actual energy load value, $\overline{y}$ is the mean of the actual values, and f_i is the forecasted value.

3.5.4. Coefficient of Variation of Root Mean Square Error (CVRMSE)

The CVRMSE is often used to measure relative error. It is calculated as the ratio of the RMSE to the mean of the observed values. The formula for CVRMSE is given by Equation (4):

$$\text{CVRMSE} = \frac{\text{RMSE}}{\bar{Y}} \times 100\% \tag{4}$$

where

$\bar{Y}$: Mean of the observed values.

3.5.5. Normalized Root Mean Square Error (NRMSE)

The NRMSE is a common metric for assessing the accuracy of a model's predictions. It is calculated as the ratio of the RMSE to the range of the observed values. The formula for NRMSE is provided in Equation (5):

$$\text{NRMSE} = \frac{\text{RMSE}}{\text{Range}(\bar{Y})} \times 100\% \tag{5}$$

where

$\bar{Y}$: Mean of the observed values

Range($\bar{Y}$): Range of the observed values (max–min).

4. Results

This section presents and discusses the experimental procedure results and the models' performance evaluation based on the evaluation metrics. The experimentation is broken down into different parts. The first part evaluates the models using a 15 min resolution (Section 4.1). The second part evaluates the models based on a 30 min resolution (Section 4.2), with the third part extending the second part with a 1 h resolution (Section 4.3). Finally, a one- vs. multistep comparison is conducted to identify the best method for 1 h ahead forecasting in Section 4.4.

Forecasting using different time series resolutions is crucial for gaining a thorough insight into trends, patterns, and anomalies across various temporal scales. This approach enhances prediction accuracy and facilitates the comparison of results for optimal outcomes [89,90].

4.1. Dataset with 15 min Resolution

The first set of experiments was carried out with processed data in the default 15 min resolution and 1-step-ahead prediction. The 10 best-performing models are illustrated in Table 1.

Table 1. Model performance metrics for 1-step-ahead and 15 min resolution.

Model	R^2	RMSE	MAE	CVRMSE	NRMSE	Time (s)
HGBR	0.939	0.115	0.070	0.186	0.048	30.12
ETR	0.939	0.115	0.073	0.186	0.048	1759.75
LGBMR	0.938	0.116	0.071	0.188	0.048	11.20
CBR	0.929	0.124	0.079	0.201	0.052	17.51
LLR	0.929	0.124	0.079	0.201	0.052	14.81
ENR	0.929	0.124	0.079	0.201	0.052	19.48
GBR	0.928	0.125	0.077	0.202	0.052	333.32
BR	0.928	0.125	0.081	0.203	0.052	8.63
RR	0.928	0.125	0.082	0.203	0.052	11.92
LR	0.927	0.126	0.082	0.204	0.052	4.92

In addition to the training time, the table also presents the performance metrics for various regression models. HGBR and extra tree regression (ETR) stand out with high R^2 values of 0.939, indicating strong predictive performance. However, ETR has a notably longer computational time of 1759.75 s. LGBMR also performs with an R^2 of 0.938 and a relatively low computational time of 11.20 s. Regarding MAE, HGBR and LGBMR show lower errors, followed by ETR, while from an RMSE (as well as CVRMSE and NRMSE) perspective, HGBR and ETR have lower values, followed by LGBMR. After these three top-performing models, all the others provide lower but similar performance metrics in terms of R^2, RMSE, MAE, CVRMSE, and NRMSE.

Table 2 provides results for 15 min resolution for 4-step-ahead. HGBR and LGBMR lead with an R^2 of 0.884, demonstrating robust predictive capabilities, followed by ETR and GBR. However, ETR, despite achieving a high R^2, exhibits a significantly longer computational time of 1731.49 s, the second after RFR, which has the highest computational time of 1944.22 s. In terms of error, again, HGBR and LGBMR show lower scores, followed either by GBR (in the case of MAE) or ETR (in the case of RMSE, CVRMSE, and NRMSE).

Table 2. Model performance metrics for 4-step-ahead and 15 min resolution.

Model	R^2	RMSE	MAE	CVRMSE	NRMSE	Time (s)
HGBR	0.884	0.158	0.092	0.257	0.066	29.06
LGBMR	0.884	0.159	0.092	0.257	0.066	7.86
ETR	0.879	0.162	0.099	0.263	0.068	1731.49
GBR	0.878	0.163	0.095	0.264	0.068	335.05
RFR	0.868	0.169	0.109	0.274	0.071	1944.22
CBR	0.855	0.177	0.106	0.287	0.074	31.86
ENR	0.855	0.177	0.106	0.287	0.074	25.02
LLR	0.855	0.177	0.106	0.287	0.074	14.35
BR	0.855	0.177	0.108	0.287	0.074	8.55
RR	0.855	0.177	0.109	0.288	0.074	8.83

4.2. Dataset with 30 min Resolution

With a 30 min 1-step-ahead time step, the total number of observations was reduced to half compared to the 15 min resolution. Therefore, fewer data remained for the training and test sets. Initially, models were trained and tested for 1-step-ahead (30 min ahead) forecasting, followed by a 2-step-ahead (1 h ahead) implementation.

Regarding the performance metrics with a 1-step-ahead 30 min resolution, Table 3 illustrates that GBR and HGBR stand out with high R^2 values of 0.957 and 0.956, indicating strong predictive capabilities. LGBMR also performs well, with an R^2 of 0.954. These models exhibit low RMSE, CVRMSE, NRMSE and MAE, suggesting accurate predictions. However, the computation time varies significantly, with GBR being the most time-consuming, taking 116.15 s. In general, all 10 illustrated models show good performance, indicating a strong fit to the dataset.

Table 3. Model performance metrics for a 1-step-ahead and 30 min resolution.

Model	R^2	RMSE	MAE	CVRMSE	NRMSE	Time (s)
GBR	0.957	0.229	0.129	0.157	0.048	116.15
HGBR	0.956	0.231	0.131	0.158	0.048	8.67
LGBMR	0.954	0.237	0.143	0.163	0.049	4.31
CBR	0.953	0.240	0.131	0.165	0.050	12.63
LLR	0.953	0.240	0.131	0.165	0.050	6.17
ENR	0.953	0.240	0.132	0.165	0.050	6.16
RR	0.953	0.241	0.137	0.165	0.050	3.76
BR	0.953	0.241	0.137	0.165	0.050	2.44
XGBR	0.953	0.241	0.137	0.165	0.050	1.45
LR	0.952	0.241	0.138	0.166	0.050	1.84

Furthermore, a 2-step-ahead implementation was conducted, targeted for 1 h ahead forecasting. Table 4 showcases the performance metrics for the 10 best-performing regression models.

Table 4. Model performance metrics for 2-step-ahead and 30 min resolution.

Model	R^2	RMSE	MAE	CVRMSE	NRMSE	Time (s)
RR	0.920	0.314	0.182	0.215	0.065	3.51
BRR	0.919	0.314	0.182	0.215	0.065	2.73
CBR	0.919	0.314	0.183	0.215	0.065	30.25
LR	0.919	0.314	0.183	0.216	0.065	2.62
ENR	0.919	0.315	0.176	0.216	0.066	6.69
LLR	0.919	0.315	0.176	0.216	0.066	6.42
GBR	0.917	0.318	0.181	0.218	0.066	117.95
HGBR	0.908	0.335	0.193	0.230	0.070	13.26
ETR	0.908	0.335	0.197	0.230	0.070	373.49
LGBMR	0.906	0.339	0.204	0.233	0.071	3.16

RR and BRR lead with high R^2 values of 0.920 and 0.919, indicating strong predictive performance. These models, along with CBR, LR, and ENR, demonstrate low RMSE and MAE, suggesting accurate predictions. GBR and ETR, although slightly less accurate, stand out negatively for their relatively high computational times of 117.95 and 373.49 s, respectively. From RR to HGBR and LGBMR, all the models in the table show generally good performance, indicating a strong fit to the dataset.

4.3. Dataset with 1 h Resolution

Resampling the dataset into 1 h resolution resulted in 17,702 observations, i.e., two times less than the 30 min dataset and four times less than the 15 min dataset. Initially, it was expected that the performance might deteriorate due to the smaller number of observations. However, the model performed better for the 1 h ahead (Table 5) compared to the first two cases (4-step-ahead for 15 min and 2-step-ahead prediction for 30 min resolutions) described in Sections 4.1 and 4.2, respectively. This outcome can be attributed to the fact that the data were smoothened by resampling to remove some extremities, such as long periods of no energy production or low energy consumption. The resampled data take the hourly sum of energy consumption to compute the hourly resolution and the mean of the weather variables.

More detailed results are presented in Table 5, providing details regarding the 10 best-performing models. The top three of them are LGBMR, HGBR, and ETR. LGBMR is

computationally efficient, taking only 1.08 s, obtaining a high R^2 score of 0.927, indicating a significant correlation between predicted and real values. Furthermore, low RMSE (0.486) (as well as CVRMSE, NRMSE) and MAE (0.252) show reliable predictions with minimal mistakes.

Table 5. Model performance metrics for 1-step-ahead and 1 h resolution.

Model	R^2	RMSE	MAE	CVRMSE	NRMSE	Time (s)
LGBMR	0.927	0.486	0.252	0.191	0.053	1.078
HGBR	0.926	0.489	0.252	0.192	0.054	5.517
ETR	0.925	0.493	0.260	0.194	0.054	79.933
GBR	0.922	0.502	0.265	0.197	0.055	35.093
RFR	0.911	0.535	0.294	0.211	0.059	139.682
RR	0.906	0.550	0.303	0.216	0.060	0.547
BR	0.906	0.551	0.302	0.217	0.060	0.533
LR	0.906	0.552	0.305	0.217	0.060	0.422
ENR	0.904	0.556	0.293	0.219	0.061	1.625
LLR	0.904	0.556	0.293	0.219	0.061	1.578

Similar to LGBMR, with an R^2 of 0.926, HGBR performs quite closely to the former, with RMSE (0.489), CVRMSE (0.192), and NRMSE (054) being marginally higher than those of LGBMR, with MAE (0.252) being equal. Overall, HGBR is still a robust performer, taking 5.52 s to train.

Regarding ETR, while having a high R^2 of 0.925 (very close to LGBMR and HGBR), it exhibits a slightly higher RMSE (0.493) and MAE (0.260) compared to the previous models. The computational cost is higher, taking approximately 79.93 s.

Overall, all 10 illustrated models perform well, indicating a strong fit to the 1 h resolution dataset.

4.4. Final Models' Comparison for 1 h Ahead Forecasting

A thorough comparison of the performance metrics for the three best distinct ML models that were applied to forecasting tasks at different resolutions (15 min, 30 min, and 1 h) is shown in Table 6, as provided in Sections 4.1–4.3. Every row corresponds to a distinct set of resolutions, steps ahead, and regression models. Also, it is important to highlight that since the energy load target parameter was measured in kWh, downgrading the resolutions provides higher MAE and RMSE metrics for 30 min and 1 h datasets.

Table 6. Model performance metrics comparison for 1 h ahead forecasting.

Resolution	Steps	Model	R^2	RMSE	MAE	CVRMSE	NRMSE	Time (s)
15 min	4	HGBR	0.884	0.158	0.092	0.257	0.066	29.06
15 min	4	LGBMR	0.884	0.159	0.092	0.257	0.066	7.86
15 min	4	ETR	0.879	0.162	0.099	0.263	0.068	173.49
30 min	2	RR	0.920	0.314	0.182	0.215	0.065	3.51
30 min	2	BRR	0.919	0.314	0.182	0.215	0.065	2.73
30 min	2	CB	0.919	0.314	0.183	0.215	0.065	1.25
1 h	1	LGBMR	0.927	0.486	0.252	0.191	0.053	1.078
1 h	1	HGBR	0.926	0.489	0.252	0.192	0.054	5.517
1 h	1	ETR	0.925	0.493	0.260	0.194	0.054	79.933

For the 4-step-ahead and 15 min resolution implementation, models HGBR, LGBMR, and ETR performed best, with shorter intervals and with a finer temporal granularity. These models have strong predictive performance, as seen by their high R^2 values. Particularly, HGBR and LGBMR have similar performance but different computation times.

For the 2-step-ahead and 30 min resolution, models RR, BRR, and CB are the best performing, with the 2-step-ahead at a slightly coarser 30 min resolution. Each of these models has a strong R^2 and comparable performance metrics. This stands in terms of R^2, where RR performs slightly better than the others with a 2-step-ahead 30 min resolution, providing better results compared to the 4-step-ahead 15 min resolution.

For the 1-step-ahead and 1 h resolution, the models LGBMR, HGBR, and ETR are the best performing. Each of these models at the 1-step-ahead and 1 h resolution has a higher R^2 and lower CVRMSE and NRMSE compared to the two previous resolutions.

Overall, although the dataset size was resampled to 1 h resolution, results indicate higher R^2 and lower CVRMSE and NRMSE compared to the 2-step-ahead and 15 min resolution or the 2-step-ahead and 30 min resolution.

4.5. Discussion

It was observed that the models performed differently for different time resolutions on the same data. The difference in the number of observations from the original data is by half (for 30 min resolution) and a quarter (for 1 h resolution). This shows that models reported to have good prediction performance may perform poorly on different datasets, provided the preprocessing stage is performed adequately.

For time series data, our analysis shows the dependency and important predicting power of time- and calendar-related predictors in the model's performance. In this study, several parameters were included, like the day of the week, the hour of the day, the week of the year, and the month of the year. Based on the data, the temperature is the only weather feature with the highest correlation with the target variable, and is ranked as the most important feature for all the algorithms used. This suggests that temperature is an adequate weather predictor for household energy consumption when weather data cannot be easily obtained.

Implications

Developing energy prediction models is essential to managing and improving building energy efficiency and reducing carbon emissions. In developed and developing countries, with growing populations, rising economies, and a desire for a better quality of life, energy consumption prediction in buildings is required to support national and municipal energy strategies.

Energy forecasting is capable of tracking changes in building energy usage towards the directive of the European Parliament on the energy performance of buildings, which supports nearly-zero-energy buildings. Energy consumption forecast in the buildings sector at the sub-national level, such as regions, local governments, and cities, can be used to identify areas that will be the focus of future investments, thereby enhancing the success of energy-saving measures in buildings there [77].

Forecasting energy requirements in residential buildings is part of the effort to achieve a community of high-energy-efficient buildings. It forms the core of building energy management systems, building design optimization, and retrofit evaluation. The benefits of accurate energy forecasting cut across energy consumers, generating companies and stakeholders in the distribution line, DSOs, and aggregators. Knowing the consumption and potential future consumption empowers households to manage energy use operations efficiently.

It also allows them to participate effectively in DR programs, providing recommendations for optimal energy usage and playing their end roles in energy management. If occupants or house owners know their likely consumption at a particular time, they are better informed to take precautions to curtail it to meet the DR deal. By doing so, households can contribute to the stability of the power system and the reduction of emissions.

It is advisable to utilize forecasting recommendation systems to develop building energy management systems that optimize real-time building operations management, minimize expenses, and facilitate informed decision making. Such tools serve as valuable resources for selecting forecasting models to predict building energy consumption.

This study identified the most effective models for STLF, yet such a finding is specific to the building being examined. Based on the outcome of the performance evaluation, the most effective models can be incorporated into developing a scalable model-based recommendation system. Such a system could identify the appropriate models for energy

prediction in a specific building by utilizing its historical energy data during the training process. For example, a building energy model recommendation system with a meta-learning approach to automatically identify the most effective models for various building types was introduced in [91]. This methodology minimized redundant computations and promised precise modeling outcomes.

5. Conclusions

This study focused on optimizing building STLF by performing a comparative analysis of various ML models. State-of-the-art preprocessing techniques were employed for detailed data analysis, emphasizing the crucial role of data preprocessing in the accuracy of ML models. Time-related and dummy features were engineered, transforming the dataset into a supervised learning problem. Various linear, tree-based, and gradient-boosting models were utilized for energy consumption prediction in the ITI/CERTH Smart House at different resolutions (15 min, 30 min, and 1 h).

The accuracy of selected forecasting models was evaluated based on key performance metrics and training time. Notably, the best-boosting models (HGBR, LGBMR) outperformed tree-based models (ETR) for 15 min and 1 h resolutions, while both were surpassed by RR in the 30 min resolution. The overall best performance for 1-step-ahead forecasting was observed for the resampled 30 min resolution.

Additionally, a one- vs. multistep comparison identified the most effective method for 1 h ahead forecasting. Findings showed that the 1-step-ahead resampled 1 h resolution outperformed other methods, followed by the 2-step-ahead resampled 30 min resolution. Despite the reduced dataset sizes for these resampled resolutions, they exhibited a stronger fit compared to the original 4-step-ahead forecasting target with a 15 min resolution.

In the future, testing with more diverse and vast datasets can assist in ensuring our approach's resilience and generalizability. In a more technical context, potential areas for further research are the following:

- Improve ELF data preprocessing by tailoring it to different models and investigating model-specific challenges, such as addressing multicollinearity in linear models and handling missing data for nonlinear models.
- Explore model variability by investigating alternatives to neural network approaches while considering computational costs and dataset sizes. Also, examine the potential of stacking tree-based models, especially in scenarios with limited historical data.
- Improve the model evaluation by incorporating additional regression problem evaluation metrics, such as SMAPE and MAPE, with the aim of providing an even more comprehensive analysis.
- Include building attributes that expand beyond weather-related data for a more holistic understanding of the building's energy consumption. Consider the type of home and its physical characteristics, the number, type, and efficiency of energy-consuming devices, and the number of occupants and their energy consumption behavior.

Author Contributions: Conceptualization, P.K., A.M. (Aristeidis Mystakidis) and A.M. (Akeem Mustapha); methodology, A.M. (Akeem Mustapha), P.K. and A.M. (Aristeidis Mystakidis); validation, P.K., A.M. (Aristeidis Mystakidis) and C.T.; formal analysis, P.K. and A.M. (Aristeidis Mystakidis); investigation, A.M. (Akeem Mustapha), P.K. and C.T.; resources, P.K.; data curation, A.M. (Aristeidis Mystakidis) and A.M. (Akeem Mustapha); writing—original draft preparation, P.K. and A.M. (Akeem Mustapha); writing—review and editing, A.M. (Aristeidis Mystakidis) and P.K.; visualization, A.M. (Akeem Mustapha); supervision, P.K.; project administration, P.K. and C.T.; funding acquisition, C.T. All authors have read and agreed to the published version of the manuscript.

Funding: This research received no external funding.

Data Availability Statement: The data presented in this study are available upon request from the authors. The data are not publicly available due to working on more research analyses.

Conflicts of Interest: Researchers in School of Science and Technology, International Hellenic University.

Abbreviations

The following abbreviations are used in this manuscript:

AI	Artificial intelligence
AR	Autoregressive
ARMA	Autoregressive moving average
BiLSTM	Bidirectional long short-term memory
CNN	Convolutional neural network
CVRMSE	Coefficient of the variation of the root mean square error
DR	Demand response
DRM	Demand response management
DSO	Distribution system operator
EDA	Explorative data analysis
EJ	Exajoule
ELF	Energy load forecasting
ETR	Extra tree regression
GBR	Gradient-boosting regression
GBM	Gradient-boosting machine
GWO	Grey wolf optimization
HGBR	Histogram gradient-boosting regression
HVAC	Heating, ventilating, and air-conditioning
IEA	International Energy Agency
IoT	Internet of Things
ITI/CERTH	Information Technologies Institute/Centre for Research and Technology
KNN	k-nearest neighbor
kWh	kiloWatt hour
LGBMR	Light gradient-boosting machine regressor
LR	Linear regression
LSTM	Long short-term memory network
LSTM/GRU	Long short-term memory network/gated recurrent unit
LTLF	Long-term load forecasting
MA	Moving average
MAE	Mean absolute error
MAPE	Mean absolute percentage error
MI	Mutual information
ML	Machine learning
MLP	Multilayer perceptron
MLR	Multiple linear regression
MTLF	Medium-term load forecasting
NRMSE	Normalized root mean square error
nZEB	Net-zero building
PV	Photovoltaic
RF	Random forest
RL	Reinforcement learning
RMSE	Root mean square error
R^2	Coefficient of determination
SMAPE	Symmetric mean absolute percentage error
STLF	Short-term load forecasting
SVM	Support vector machine
SVR	Support vector regression
SW	Sliding window
VAR	Vector autoregression
VSTLF	Very-short-term load forecasting
WEKA	Waikato Environment for Knowledge Analysis
XGBoost	Extreme gradient boosting
XGBR	Extreme gradient-boosting regressor

References

1. Shahriar, M.S.; Rahman, M.S. Urban sensing and smart home energy optimisations: A machine learning approach. In Proceedings of the IoT-App 2015—2015 International Workshop On Internet of Things Towards Applications, Co-Located with SenSys 2015, Seoul, Republic of Korea, 1 November 2015; pp. 19–22. [CrossRef]
2. Himeur, Y.; Alsalemi, A.; Bensaali, F.; Amira, A. Building power consumption datasets: Survey, taxonomy and future directions. *Energy Build.* **2020**, *227*, 110404. [CrossRef]
3. International Energy Agency (IEA). World Energy Outlook 2022. p. 524. Available online: https://www.iea.org/reports/world-energy-outlook-2022 (accessed on 21 January 2024).
4. Cai, Q.; Xu, Q.; Qing, J.; Shi, G.; Liang, Q.M. Promoting wind and photovoltaics renewable energy integration through demand response: Dynamic pricing mechanism design and economic analysis for smart residential communities. *Energy* **2022**, *261*, 125293. [CrossRef]
5. McKinsey Company. Global Energy Perspective 2022—Executive Summary. 2022. Available online: https://www.mckinsey.com/~/media/McKinsey/Industries/OilandGas/OurInsights/GlobalEnergyPerspective2022/Global-Energy-Perspective-2022-Executive-Summary.pdf (accessed on 8 February 2024).
6. Hong, T.; Fan, S. Probabilistic electric load forecasting: A tutorial review. *Int. J. Forecast.* **2016**, *32*, 914–938. [CrossRef]
7. Koukaras, P.; Tjortjis, C.; Gkaidatzis, P.; Bezas, N.; Ioannidis, D.; Tzovaras, D. An interdisciplinary approach on efficient virtual microgrid to virtual microgrid energy balancing incorporating data preprocessing techniques. *Computing* **2021**, *104*, 209–250. [CrossRef]
8. Koukaras, P.; Bezas, N.; Gkaidatzis, P.; Ioannidis, D.; Tzovaras, D.; Tjortjis, C. Introducing a novel approach in one-step ahead energy load forecasting. *Sustain. Comput. Inform. Syst.* **2021**, *32*, 100616. [CrossRef]
9. Shakeri, M.; Shayestegan, M.; Abunima, H.; Reza, S.M.; Akhtaruzzaman, M.; Alamoud, A.R.; Sopian, K.; Amin, N. An intelligent system architecture in home energy management systems (HEMS) for efficient demand response in smart grid. *Energy Build.* **2017**, *138*, 154–164. [CrossRef]
10. Ahmad, T.; Zhang, H.; Yan, B. A review on renewable energy and electricity requirement forecasting models for smart grid and buildings. *Sustain. Cities Soc.* **2020**, *55*, 102052. [CrossRef]
11. Koukaras, P.; Berberidis, C.; Tjortjis, C. A Semi-supervised Learning Approach for Complex Information Networks. In *Intelligent Data Communication Technologies and Internet of Things*; Hemanth, J., Bestak, R., Chen, J.I.Z., Eds.; Springer: Singapore, 2021; pp. 1–13. [CrossRef]
12. Himeur, Y.; Alsalemi, A.; Al-Kababji, A.; Bensaali, F.; Amira, A.; Sardianos, C.; Dimitrakopoulos, G.; Varlamis, I. A survey of recommender systems for energy efficiency in buildings: Principles, challenges and prospects. *Inf. Fusion* **2021**, *72*, 1–21. [CrossRef]
13. Mystakidis, A.; Ntozi, E.; Afentoulis, K.; Koukaras, P.; Giannopoulos, G.; Bezas, N.; Gkaidatzis, P.A.; Ioannidis, D.; Tjortjis, C.; Tzovaras, D. One Step Ahead Energy Load Forecasting: A Multi-Model Approach Utilizing Machine and Deep Learning. In Proceedings of the 2022 57th International Universities Power Engineering Conference (UPEC), Istanbul, Turkey, 30 August–2 September 2022; pp. 1–6. [CrossRef]
14. Lazzari, F.; Mor, G.; Cipriano, J.; Gabaldon, E.; Grillone, B.; Chemisana, D.; Solsona, F. User behaviour models to forecast electricity consumption of residential customers based on smart metering data. *Energy Rep.* **2022**, *8*, 3680–3691. [CrossRef]
15. Langevin, A.; Cheriet, M.; Gagnon, G. Efficient deep generative model for short-term household load forecasting using non-intrusive load monitoring. *Sustain. Energy Grids Netw.* **2023**, *34*, 101006. [CrossRef]
16. Baker, K.J.; Rylatt, R.M. Improving the prediction of UK domestic energy-demand using annual consumption-data. *Appl. Energy* **2008**, *85*, 475–482. [CrossRef]
17. Brounen, D.; Kok, N.; Quigley, J.M. Residential energy use and conservation: Economics and demographics. *Eur. Econ. Rev.* **2012**, *56*, 931–945. [CrossRef]
18. Urquizo, J.; Calderón, C.; James, P. Metrics of urban morphology and their impact on energy consumption: A case study in the United Kingdom. *Energy Res. Soc. Sci.* **2017**, *32*, 193–206. [CrossRef]
19. Jones, R.V.; Lomas, K.J. Determinants of high electrical energy demand in UK homes: Socio-economic and dwelling characteristics. *Energy Build.* **2015**, *101*, 24–34. [CrossRef]
20. Zhao, H.X.; Magoulès, F. A review on the prediction of building energy consumption. *Renew. Sustain. Energy Rev.* **2012**, *16*, 3586–3592. [CrossRef]
21. Dhar, A.; Reddy, T.A.; Clarid, D.E. A Fourier series model to predict hourly heating and cooling energy use in commercial buildings with outdoor temperature as the only weather variable. *J. Sol. Energy Eng.* **1999**, *121*, 47–53. [CrossRef]
22. White, J.; Reichmuth, R. Simplified method for predicting building energy consumption using average monthly temperatures. In Proceedings of the IECEC 96, 31st Intersociety Energy Conversion Engineering Conference, Washington, DC, USA, 11–16 August 1996; Volume 3, pp. 1834–1839. [CrossRef]
23. Westphal, F.S.; Lamberts, R. The use of simplified weather data to estimate thermal loads of non-residential buildings. *Energy Build.* **2004**, *36*, 847–854. [CrossRef]
24. Al-Shargabi, A.A.; Almhafdy, A.; Ibrahim, D.M.; Alghieth, M.; Chiclana, F. Buildings' energy consumption prediction models based on buildings' characteristics: Research trends, taxonomy, and performance measures. *J. Build. Eng.* **2022**, *54*, 104577. [CrossRef]

25. Tsanas, A.; Xifara, A. Accurate quantitative estimation of energy performance of residential buildings using statistical machine learning tools. *Energy Build.* **2012**, *49*, 560–567. [CrossRef]
26. Cetin, K.S.; Tabares-Velasco, P.C.; Novoselac, A. Appliance daily energy use in new residential buildings: Use profiles and variation in time-of-use. *Energy Build.* **2014**, *84*, 716–726. [CrossRef]
27. Ruellan, M.; Park, H.; Bennacer, R. Residential building energy demand and thermal comfort: Thermal dynamics of electrical appliances and their impact. *Energy Build.* **2016**, *130*, 46–54. [CrossRef]
28. Candanedo, L.M.; Feldheim, V.; Deramaix, D. Data driven prediction models of energy use of appliances in a low-energy house. *Energy Build.* **2017**, *140*, 81–97. [CrossRef]
29. Bezzar, N.E.H.; Laimeche, L.; Meraoumia, A.; Houam, L. Data analysis-based time series forecast for managing household electricity consumption. *Demonstr. Math.* **2022**, *55*, 900–921. [CrossRef]
30. Hong, T.; Pinson, P.; Wang, Y.; Weron, R.; Yang, D.; Zareipour, H. Energy Forecasting: A Review and Outlook. *IEEE Open Access J. Power Energy* **2020**, *7*, 376–388. [CrossRef]
31. Zhao, H. Artificial Intelligence Models for Large Scale Buildings Energy Consumption Analysis. Ph.D. Thesis, Ecole Centrale, Paris, France, 2011.
32. Elbeltagi, E.; Wefki, H. Predicting energy consumption for residential buildings using ANN through parametric modeling. *Energy Rep.* **2021**, *7*, 2534–2545. [CrossRef]
33. Liu, T.; Tan, Z.; Xu, C.; Chen, H.; Li, Z. Study on deep reinforcement learning techniques for building energy consumption forecasting. *Energy Build.* **2020**, *208*, 109675. [CrossRef]
34. Wu, D.; Wang, B.; Precup, D.; Boulet, B. Multiple Kernel Learning-Based Transfer Regression for Electric Load Forecasting. *IEEE Trans. Smart Grid* **2020**, *11*, 1183–1192. [CrossRef]
35. Arora, S.; Taylor, J.W. Rule-based autoregressive moving average models for forecasting load on special days: A case study for France. *Eur. J. Oper. Res.* **2018**, *266*, 259–268. [CrossRef]
36. Guan, C.; Luh, P.B.; Michel, L.D.; Wang, Y.; Friedland, P.B. Very short-term load forecasting: Wavelet neural networks with data pre-filtering. *IEEE Trans. Power Syst.* **2013**, *28*, 30–41. [CrossRef]
37. Jacob, M.; Neves, C.; Greetham, D.V. *Forecasting and Assessing Risk of Individual Electricity Peaks*; Springer Nature: Berlin/Heidelberg, Germany, 2020; Volume 1, pp. 1–161. [CrossRef]
38. Abu-Shikhah, N.; Elkarmi, F. Medium-term electric load forecasting using singular value decomposition. *Energy* **2011**, *36*, 4259–4271. [CrossRef]
39. Daneshi, H.; Shahidehpour, M.; Choobbari, A.L. Long-term load forecasting in electricity market. In Proceedings of the 2008 IEEE International Conference on Electro/Information Technology, IEEE EIT 2008 Conference, Rochester, MI, USA, 3–5 May 2008; pp. 395–400. [CrossRef]
40. Ruiz-Abellón, M.C.; Fernández-Jiménez, L.A.; Guillamón, A.; Falces, A.; García-Garre, A.; Gabaldón, A. Integration of demand response and short-term forecasting for the management of prosumers' demand and generation. *Energies* **2019**, *13*, 11. [CrossRef]
41. Zheng, Z.; Chen, H.; Luo, X. A Kalman filter-based bottom-up approach for household short-term load forecast. *Appl. Energy* **2019**, *250*, 882–894. [CrossRef]
42. Shaikh, A.K.; Nazir, A.; Khan, I.; Shah, A.S. Short term energy consumption forecasting using neural basis expansion analysis for interpretable time series. *Sci. Rep.* **2022**, *12*, 22562. [CrossRef] [PubMed]
43. Bacher, P.; Madsen, H.; Nielsen, H.A. Online short-term heat load forecasting for single family houses. In Proceedings of the IECON Proceedings (Industrial Electronics Conference), Brussels, Belgium, 17–20 October 2013; pp. 5741–5746. [CrossRef]
44. Sandels, C.; Widén, J.; Nordström, L.; Andersson, E. Day-ahead predictions of electricity consumption in a Swedish office building from weather, occupancy, and temporal data. *Energy Build.* **2015**, *108*, 279–290. [CrossRef]
45. Kavousian, A.; Rajagopal, R.; Fischer, M. Determinants of residential electricity consumption: Using smart meter data to examine the effect of climate, building characteristics, appliance stock, and occupants' behavior. *Energy* **2013**, *55*, 184–194. [CrossRef]
46. Kavousian, A.; Rajagopal, R.; Fischer, M. Ranking appliance energy efficiency in households: Utilizing smart meter data and energy efficiency frontiers to estimate and identify the determinants of appliance energy efficiency in residential buildings. *Energy Build.* **2015**, *99*, 220–230. [CrossRef]
47. Lee, Y.J.; Choi, H.J. Forecasting building electricity power consumption using deep learning approach. In Proceedings of the 2020 IEEE International Conference on Big Data and Smart Computing, BigComp, Busan, Republic of Korea, 19–22 February 2020; pp. 542–544. [CrossRef]
48. Fayaz, M.; Kim, D. A prediction methodology of energy consumption based on deep extreme learning machine and comparative analysis in residential buildings. *Electronics* **2018**, *7*, 222. [CrossRef]
49. Bilal, M.; Kim, H.; Fayaz, M.; Pawar, P. Comparative Analysis of Time Series Forecasting Approaches for Household Electricity Consumption Prediction. *arXiv* **2022**, arXiv:2207.01019. Available online: http://arxiv.org/abs/2207.01019 (accessed on 15 January 2024).
50. Tabasi, S.; Aslani, A.; Forotan, H. Prediction of Energy Consumption by Using Regression Model. *Comput. Res. Prog. Appl. Sci. Eng.* **2016**, *2*, 110–115. Available online: https://www.crpase.com/archive/CRPASE-2016-VOL%2002-ISSUE%2003-04.pdf (accessed on 8 February 2024).
51. Belaïd, F. Understanding the spectrum of domestic energy consumption: Empirical evidence from France. *Energy Policy* **2016**, *92*, 220–233. [CrossRef]

52. Huebner, G.; Shipworth, D.; Hamilton, I.; Chalabi, Z.; Oreszczyn, T. Understanding electricity consumption: A comparative contribution of building factors, socio-demographics, appliances, behaviours and attitudes. *Appl. Energy* **2016**, *177*, 692–702. [CrossRef]
53. Zhuang, D.; Gan, V.J.; Tekler, Z.D.; Chong, A.; Tian, S.; Shi, X. Data-driven predictive control for smart HVAC system in IoT-integrated buildings with time-series forecasting and reinforcement learning. *Appl. Energy* **2023**, *338*, 120936.
54. Deng, X.; Ye, A.; Zhong, J.; Xu, D.; Yang, W.; Song, Z.; Zhang, Z.; Guo, J.; Wang, T.; Tian, Y.; et al. Bagging–XGBoost algorithm based extreme weather identification and short-term load forecasting model. *Energy Rep.* **2022**, *8*, 8661–8674. [CrossRef]
55. Sekhar, C.; Dahiya, R. Robust framework based on hybrid deep learning approach for short term load forecasting of building electricity demand. *Energy* **2023**, *268*, 126660.
56. Fumo, N.; Biswas, M.A.R. Regression analysis for prediction of residential energy consumption. *Renew. Sustain. Energy Rev.* **2015**, *47*, 332–343. [CrossRef]
57. Morris, J.; Allinson, D.; Harrison, J.; Lomas, K.J. Benchmarking and tracking domestic gas and electricity consumption at the local authority level. *Energy Effic.* **2016**, *9*, 723–743. [CrossRef]
58. Lorimer, S. A housing stock model of non-heating end-use energy in England verified by aggregate energy use data. *Energy Policy* **2012**, *50*, 419–427. [CrossRef]
59. Maltais, L.G.; Gosselin, L. Forecasting of short-term lighting and plug load electricity consumption in single residential units: Development and assessment of data-driven models for different horizons. *Appl. Energy* **2022**, *307*, 118229. [CrossRef]
60. Koukaras, P.; Gkaidatzis, P.; Bezas, N.; Bragatto, T.; Carere, F.; Santori, F.; Antal, M.; Ioannidis, D.; Tjortjis, C.; Tzovaras, D. A Tri-Layer Optimization Framework for Day-Ahead Energy Scheduling Based on Cost and Discomfort Minimization. *Energies* **2021**, *14*, 3599. [CrossRef]
61. Palacios-García, E.J.; Moreno-Munoz, A.; Santiago, I.; Flores-Arias, J.M.; Bellido-Outeiriño, F.J.; Moreno-Garcia, I.M. Modeling human activity in Spain for different economic sectors: The potential link between occupancy and energy usage. *J. Clean. Prod.* **2018**, *183*, 1093–1109. [CrossRef]
62. ITI-CERTH. ITI Smart Home, a Digital Innovation Hub powered by ITI/CERTH. Available online: Https://smarthome.iti.gr (accessed on 5 October 2023).
63. Géron, A. *Hands-on Machine Learning with Scikit-Learn, Keras, and TensorFlow (2019, O'reilly)*; O'Reilly Media: Sebastopol, MA, USA, 2019; p. 510.
64. Pedregosa, F.; Varoquaux, G.; Gramfort, A.; Michel, V.; Thirion, B.; Grisel, O.; Blondel, M.; Prettenhofer, P.; Weiss, R.; Dubourg, V.; et al. Scikit-learn: Machine Learning in Python. *J. Mach. Learn. Res.* **2011**, *12*, 2825–2830. [CrossRef]
65. Ramos, D.; Teixeira, B.; Faria, P.; Gomes, L.; Abrishambaf, O.; Vale, Z. Using diverse sensors in load forecasting in an office building to support energy management. *Energy Rep.* **2020**, *6*, 182–187. [CrossRef]
66. John, P.M.; Massaron, L. *Machine Learning for Dummies*, 2nd ed.; John Wiley & Sons, Inc.: Hoboken, NJ, USA, 2021; pp. 1–467.
67. Hoerl, A.E.; Kennard, R.W. Ridge regression: Biased estimation for nonorthogonal problems. *Technometrics* **1970**, *12*, 55–67. [CrossRef]
68. Asadi, M.; TaghaviGhalesari, A.; Kumar, S. Machine learning techniques for estimation of Los Angeles abrasion value of rock aggregates. *Eur. J. Environ. Civ. Eng.* **2022**, *26*, 964–977. [CrossRef]
69. Rambabu, M.; Ramakrishna, N.; Polamarasetty, P.K. Prediction and Analysis of Household Energy Consumption by Machine Learning Algorithms in Energy Management. *E3S Web Conf.* **2022**, *350*, 02002. [CrossRef]
70. Gassar, A.A.A.; Yun, G.Y.; Kim, S. Data-driven approach to prediction of residential energy consumption at urban scales in London. *Energy* **2019**, *187*, 115973. [CrossRef]
71. Touzani, S.; Granderson, J.; Fernandes, S. Gradient boosting machine for modeling the energy consumption of commercial buildings. *Energy Build.* **2018**, *158*, 1533–1543. [CrossRef]
72. Robinson, C.; Dilkina, B.; Hubbs, J.; Zhang, W.; Guhathakurta, S.; Brown, M.A.; Pendyala, R.M. Machine learning approaches for estimating commercial building energy consumption. *Appl. Energy* **2017**, *208*, 889–904. [CrossRef]
73. Friedman, J.H. Greedy Function Approximation: A Gradient Boosting Machine. *Ann. Stat.* **2001**, *29*, 1189–1232. [CrossRef]
74. Yu, H.F.; Lo, H.Y.; Hsieh, H.P.; Lou, J.K.; McKenzie, T.G.; Chou, J.W.; Chung, P.H.; Ho, C.H.; Chang, C.F.; Wei, Y.H.; et al. Feature engineering and classifier ensemble for KDD cup 2010. In Proceedings of the JMLR: Workshop and Conference Proceedings, Sardinia, Italy, 13–15 May 2010; pp. 1–12. Available online: https://pslcdatashop.web.cmu.edu/KDDCup/workshop/papers/kdd2010ntu.pdf. (accessed on 8 February 2024).
75. Sepulveda, L.F.; Diniz, P.S.; Diniz, J.O.; Netto, S.M.; Cipriano, C.L.; Araújo, A.C.; Lemos, V.H.; Pessoa, A.C.; Quintanilha, D.B.; Almeida, J.D.; et al. Forecasting of individual electricity consumption using Optimized Gradient Boosting Regression with Modified Particle Swarm Optimization. *Eng. Appl. Artif. Intell.* **2021**, *105*, 104440. [CrossRef]
76. Sun, Y.; Haghighat, F.; Fung, B.C. A review of the-state-of-the-art in data-driven approaches for building energy prediction. *Energy Build.* **2020**, *221*, 110022. [CrossRef]
77. Chen, T.; Guestrin, C. XGBoost: A scalable tree boosting system. In Proceedings of the ACM SIGKDD International Conference on Knowledge Discovery and Data Mining, San Francisco, CA, USA, 13–17 August 2016; pp. 785–794. [CrossRef]
78. Zou, H.; Hastie, T. Regularization and variable selection via the elastic net. *J. R. Stat. Soc. Ser. B (Stat. Methodol.)* **2005**, *67*, 301–320. [CrossRef]
79. Efron, B.; Hastie, T.; Johnstone, I.; Tibshirani, R. Least angle regression. *Ann. Stat.* **2004**, *32*, 407–499. [CrossRef]

80. Ke, G.; Meng, Q.; Finley, T.; Wang, T.; Chen, W.; Ma, W.; Ye, Q.; Liu, T.Y. LightGBM: A Highly Efficient Gradient Boosting Decision Tree. In Proceedings of the Advances in Neural Information Processing Systems, Long Beach, CA, USA, 4–9 December 2017; Guyon, I., Luxburg, U.V., Bengio, S., Wallach, H., Fergus, R., Vishwanathan, S., Garnett, R., Eds.; Curran Associates, Inc.: Red Hook, NY, USA, 2017; Volume 30. Available online: https://api.semanticscholar.org/CorpusID:3815895 (accessed on 8 February 2024).
81. Prokhorenkova, L.; Gusev, G.; Vorobev, A.; Dorogush, A.V.; Gulin, A. CatBoost: Unbiased boosting with categorical features. *Adv. Neural Inf. Process. Syst.* **2018**, *31*. [CrossRef]
82. Breiman, L. Random Forests. *Mach. Learn.* **2001**, *45*, 5–32. [CrossRef]
83. Geurts, P.; Ernst, D.; Wehenkel, L. Extremely randomized trees. *Mach. Learn.* **2006**, *63*, 3–42. [CrossRef]
84. Breiman, L. Bagging predictors. *Mach. Learn.* **1996**, *24*, 123–140. [CrossRef]
85. MacKay, D.J.C. Bayesian interpolation. *Neural Comput.* **1992**, *4*, 415–447. [CrossRef]
86. Mystakidis, A.; Stasinos, N.; Kousis, A.; Sarlis, V.; Koukaras, P.; Rousidis, D.; Kotsiopoulos, I.; Tjortjis, C. Predicting COVID-19 ICU needs using deep learning, XGBoost and random forest regression with the sliding window technique. IEEE Smart Cities 2021. Available online: https://smartcities.ieee.org/newsletter/july-2021/predicting-covid-19-icu-needs-using-deep-learning-xgboost-and-random-forest-regression-with-the-sliding-window-technique (accessed on 20 January 2024).
87. Reyes, C.; Hilaire, T.; Paul, S.; Mecklenbräuker, C.F. Evaluation of the root mean square error performance of the PAST-consensus algorithm. In Proceedings of the 2010 International ITG Workshop on Smart Antennas, WSA, Bremen, Germany, 23–24 February 2010; pp. 156–160. [CrossRef]
88. Mystakidis, A.; Ntozi, E.; Afentoulis, K.; Koukaras, P.; Gkaidatzis, P.; Ioannidis, D.; Tjortjis, C.; Tzovaras, D. Energy generation forecasting: Elevating performance with machine and deep learning. *Computing* **2023**, *105*, 1623–1645. [CrossRef]
89. Reikard, G. Predicting solar radiation at high resolutions: A comparison of time series forecasts. *Sol. Energy* **2009**, *83*, 342–349. [CrossRef]
90. Wu, X.; Shi, B.; Dong, Y.; Huang, C.; Faust, L.; Chawla, N.V. RESTFul: Resolution-Aware Forecasting of Behavioral Time Series Data. In Proceedings of the 27th ACM International Conference on Information and Knowledge Management, CIKM '18, Torino, Italy, 22–26 October 2018; pp. 1073–1082. [CrossRef]
91. Cui, C.; Wu, T.; Hu, M.; Weir, J.D.; Li, X. Short-term building energy model recommendation system: A meta-learning approach. *Appl. Energy* **2016**, *172*, 251–263. [CrossRef]

Disclaimer/Publisher's Note: The statements, opinions and data contained in all publications are solely those of the individual author(s) and contributor(s) and not of MDPI and/or the editor(s). MDPI and/or the editor(s) disclaim responsibility for any injury to people or property resulting from any ideas, methods, instructions or products referred to in the content.

energies

MDPI

Article

Applicability of Face Masks as Recyclable Raw Materials for Self-Made Insulation Panels

Eugenia Rossi di Schio [1], Vincenzo Ballerini [1], Jan Kašpar [2], Manuela Neri [3], Mariagrazia Pilotelli [3], Edoardo Alessio Piana [3] and Paolo Valdiserri [1,*]

[1] Department of Industrial Engineering, Alma Mater Studiorum—University of Bologna, Viale Risorgimento 2, 40136 Bologna, Italy; eugenia.rossidischio@unibo.it (E.R.d.S.); vincenzo.ballerini2@unibo.it (V.B.)
[2] Department of Chemical and Pharmaceutical Sciences, University of Trieste, Via L. Giorgieri 1, 34127 Trieste, Italy; kaspar@units.it
[3] Department of Mechanical and Industrial Engineering, University of Brescia, Via Branze 38, 25123 Brescia, Italy; manuela.neri@unibs.it (M.N.); mariagrazia.pilotelli@unibs.it (M.P.); edoardo.piana@unibs.it (E.A.P.)
* Correspondence: paolo.valdiserri@unibo.it

Abstract: The circular economy model is based on the 4R framework—reduce, reuse, recycle, and recover. While recycling was the primary focus in the past, the shortage of raw materials and the desire to reduce carbon footprints have led to a change in focus: end-of-life materials are now considered resources rather than waste. When discharged, end-of-life materials still possess properties that can be exploited. For this reason, a comprehensive characterization of reusable materials is mandatory to reduce waste and increase material availability. The reuse of waste materials, such as surgical masks, is of particular interest in giving people in disadvantaged contexts the opportunity to self-produce and self-install panels within their homes, with the dual result of improving indoor comfort and increasing human capital. This paper focuses on the identification of a possible second application for surgical face masks through experimental characterization. Panels made of masks were tested for water vapor permeability, thermal conductivity, and fire resistance and their use as insulating material in the building sector was discussed. Based on the results, surgical face masks are suitable as thermal insulating materials, do not pose safety concerns, and can reduce energy consumption and improve thermal comfort when installed indoors.

Keywords: surgical face masks; circular economy; sustainable materials; energy efficiency

1. Introduction

The United Nations calls for strategies aimed at environmental quality, economic prosperity, social equity, decent standards of living, and future generations [1]. As a reaction to the increasing energy costs, and pushed by the need to reduce carbon dioxide emissions, sustainability and the circular economy are now becoming integral parts of the building sector. In 2021, the operation of buildings accounted for 30% of global final energy consumption [2]. Despite several regulations and the availability of efficient and renewable energy sources, the decarbonization of the construction sector requires investments that not all realities can afford. The circular economy is based on business models able to replace the 'end-of-life' concept with the 4R framework—reduce, reuse, recycle, and recover [3]. Reusing aims at extending product life and reducing waste [4]. In contexts where material procurement is not feasible due to limited economic resources, reuse is a viable solution but, so far, it has been analyzed only partially. On the other hand, thermal insulating materials obtained by recycling waste are now very common, and they include materials derived from textiles [5,6], rubber [7], agriculture [7–9], cigarettes [10], and construction elements [11]. There has been an increase in the analysis of end-of-life materials (EoLHMs), such as plastic bottles [12], sponges [13], egg cartons [14], and clothes [15] as, when disposed

of, they still retain properties that can be exploited in other activities. Through local labor, EoLHMs could be converted into building elements for social inclusion.

One aspect that cannot be neglected is the possibility to support sustainable development, promoted by the United Nations through 1 of its 17 goals [1]. As part of this call, steps will be taken to reduce inequalities, improve health and education, and protect the environment. Moreover, Europe is facing the challenge of energy poverty in many contexts. As a result of their inability to pay the bills, people living in energy poverty are suffering from a lack of sufficient heating, cooling, and lighting. Symptoms of this situation include disease, death, and social isolation. Multidisciplinary approaches are necessary to eradicate this problem, considering technical, social, and policy factors. However, such interventions often require an initial budget that is only available to a limited number of people. The study presented in this paper seeks to shorten this gap by offering cost-effective solutions; to do this, building elements that can be obtained by residents of the dwellings to be improved were considered. Through the implementation of these solutions, residents can achieve decent living conditions.

An environmental threat was represented by the significant number of face masks used to face the COVID-19 pandemic. The use of masks is affected by demographic factors such as age, gender, urbanicity, and education levels, with more intensive use for older people, females, and those with higher education levels [16]. Due to the difficulty of separating face masks' basic materials and their contained size, in most municipal systems, face masks are not recyclable [17]: surgical masks along with plastic gloves in coastal regions are emerging sources of microplastic particles and secondary microfibers in marine environments [18] and urban rivers [19].

The littering of masks has presented a big problem, with consequent plastic debris ending up in urban rivers [19] and, consequently, in oceans, where the biodegradation process can take hundreds of years, resulting in pollution by micro- and nano-plastic particles [20]. Several other solutions have been proposed, including biodegradable, disposable masks; mask-only trash cans; guidelines; and strict waste management. From the perspective of reuse, a possible disinfection method was investigated in [21]. This method was based on a sustainable and fast vacuum ultraviolet (VUV) treatment for the disinfection of N95 masks that had no structural damage and functional decline and were up to the reuse standard. Reusing masks outside surgical settings offers notable benefits in waste management while maintaining the safety of the individuals who use them, whether in the general population, industries, or hospitals [22]. Moreover, Alcaraz et al. [22] examined the feasibility of cleaning medical masks to ensure their safety and functionality for reuse, exploring the environmental advantages associated with managing medical disposable waste, despite the current designation of masks as single-use by regulatory frameworks. Indeed, IIR, namely, medical face masks classified as Type II according to bacterial filtration efficiency and splash resistance, are polypropylene medical masks that can be washed up to 10 times, washed 5 times and autoclaved 5 times, or washed and then sterilized with radiation or ethylene oxide, without any degradation of their filtration or breathability properties, although there is loss of the anti-projection properties. In detail, the breathability and filtration efficiency of face masks after washing and decontamination processes were investigated in [23]. Other studies focused on reusing bulk residuals from the face mask production process to realize panels with thermal and acoustic properties [24] and for cement production [25–27]. In [25], shredded and cut single-use face masks were added as fiber in a mortar that enhanced flexural strength and mitigated shrinkage, carbonation degree, and water absorption. Both scenarios withstand crack propagation and offer gradual failure.

In [26], Kilmartin-Lynch et al. proposed the reuse of face masks to improve the quality of concrete. The authors cut up single-use masks by first removing the ear loops and inner nose wire to size and spread them throughout five different mix designs to explore possible benefits and uses within concrete in percentages of 0.10%, 0.15%, 0.20%, and 0.25% by concentrating on compressive strength, indirect tensile strength, modulus of elasticity, and ultrasonic pulse velocity to test the overall quality of the concrete. The inclusion of

single-use face masks resulted in an increase in the strength properties of the concrete samples, as well as an increase in the overall quality of the concrete. However, beyond 0.20%, the trend of increasing strength decreased.

The analysis presented by Koniorczyk et al. [27] instead focused on processed face masks that were converted into fiber to be added to mortar. The results obtained indicated that the addition of processed masks slightly increased the compressive strength (by about 5%) and decreased the tensile strength (by about 3%). It was also reported that the addition of the masks did not affect material properties related to concrete durability such as frost resistance, water permeability, and fire performance. Experiments were performed on bound composite materials using the discarded face masks and wood adhesive as a binder. Initially, the discarded face masks underwent a heating process lasting one and a half hours at 120 °C to eliminate any potential contaminants, be they biological or otherwise. Subsequently, five different composites were created: the first incorporated the complete face masks, the second used face masks with iron nose clips only, the third used face masks lacking both ear loops and iron nose clips, the fourth contained the elastic ear loops exclusively, and the fifth had face masks with only elastic ear loops [28]. The polymerized binder percentage significantly affected the thermal conductivity coefficient.

In the present study, surgical face masks (hereafter referred to as SFMs) were analyzed experimentally to propose self-realizable panels to be installed indoors to reduce the energy demand in the heating season and improve thermal comfort in disadvantaged contexts (such as social housing). SFMs' structure, water vapor permeability, thermal conductivity, and fire resistance were investigated experimentally and the effect of their arrangement, dimension, and density was analyzed along with the effect of sanitation and fire retardant treatments. As far as the authors are concerned, this experimental characterization has never been performed in the literature. Water vapor permeability and thermal conductivity measurement tests were performed at the Laboratory of Thermal Engineering and Industrial Energy Systems at the University of Bologna and the Ecam Ricert in Vicenza (Italy). Tests to assess fire resistance were performed at the Department of Chemical and Pharmaceutical Sciences at the University of Trieste (Italy).

2. Materials and Methods

Experimental and numerical analyses were performed to assess the suitability of SFMs for applications in the construction sector and building energy refurbishment. The SFMs analyzed (Figure 1) were made of 67% non-woven fabric and 33% melt-blown fabric for a total of three layers: the outmost layer was made of polypropylene spun-bonded non-woven fabric and had waterproof and bacteriostatic properties, the filtrating intermediate layer was made of PP melt-blown superfine fiber, and the innermost layer was made of non-woven fabric with water-absorbing and skin-friendly properties [29]. A metal insert in the top part (white strip in Figure 1) facilitated positioning on the nose.

Both untreated and treated SFMs were considered. The first treatment considered was sanitization. A subset of the sanitized masks also received an additional fire retardant treatment. The sanitization process consisted of a 60 °C dishwasher cycle for a duration of 60 min followed by a one-week drying process in ambient air. This was consistent with the observation that a significant degree of inactivation of pathogenic species occurs at 60 °C, and several virus types, e.g., COVID-19, are among those highly sensitive to thermal degradation [30,31]. The wet impregnation of the fire retardant was performed using a commercial flame retardant (FEUERFEST®Fire protection impregnation for textiles, DIN 4102). SMFs were soaked for 5 min in the fire retardant liquid, then drained and dried for 3 days. SFM loading of 8 wt% was attained.

2.1. Experimental Activities

The analyzed SFM properties were morphology, water vapor resistance, fire resistance, and thermal conductivity.

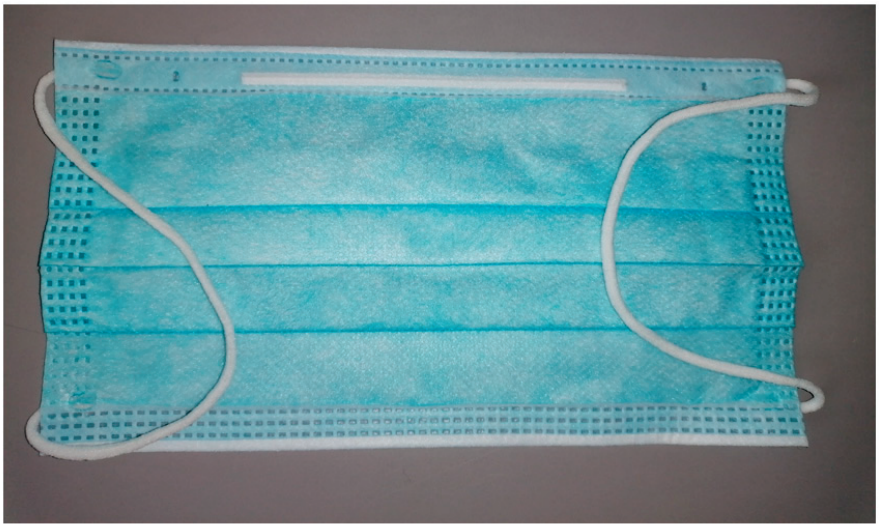


Figure 1. Surgical face masks analyzed in this study.

2.1.1. Sample Morphology Detected by Optical Microscopy

SFM samples were analyzed using an optical microscope equipped with a Dino-lite AM4023 digital eyepiece camera with a 1.3 Megapixel resolution. The morphology of the face masks was compared to that of two widely employed insulating materials, i.e., polystyrene and rock wool. The images are shown in Figure 2. The observed patterns appeared well in line with the origin of the materials: polystyrene showed typical features of an irregular foam-type surface with diffuse porosity (pore diameter $\leq$ 85 μm) (Figure 2C), whereas both rock wool and SFM featured typical aspects of a fibrous type of insulation material, with a ratio length/diameter well over 10. The diameter of the fibers in the rock wool appeared slightly thinner compared to the SFM layer of PP melt-blown superfine fibers and, more importantly, the web of the rock wool fibers featured a higher density of fibers compared to SFM. A perusal of the SFM micrograph revealed that there was a soft compact layer under the fibrous level consistent with the multilayer structure of the SFM.

2.1.2. Fire Resistance Analysis

The fire resistance of the SFMs, both untreated and fire retardant-treated, was tested using the Temperature Programmed Oxidation technique [32]. This technique, which consisted of heating a sample of the SFM in a flow reactor using a constant heating rate of 10 °C/min from room temperature up to 500 °C with a flow of air (200 mL/min), allowed us to directly detect the auto-ignition temperature of the material, i.e., the temperature at which the material spontaneously combusted. In a typical experiment, a rectangular piece (ca. 10–15 × 2–3 mm, 7–15 mg) was cut out from the central part of the SFM, loaded into a U-shaped flow microreactor (Figure 3), and then subjected to the above quoted thermal treatment. The reactor out-flow was continuously analyzed using a Multigas 2030 FTIR analyzer made by MKS instrument Inc., Andover (MA), USA.

An inspection of Figure 4 reveals similar features for both untreated and fire retardant-treated samples; both samples ignited at about 200 °C, although there was some change in the combustion pattern, as denoted by CO_2 evolution: the broad peak with a maximum at about 400 °C in the untreated sample was split into two overlapping peaks at 295 °C and 415 °C. The molar compositions of the emitted gases were not significantly affected, 65% vs. 65 % for CO_2, 20% vs. 24% for CO, 3% vs. 3% for CH_4 12% and 12% vs. 13% for acetaldehyde, respectively, in the untreated and retardant-treated SFMs. Conversely, the total amount of evolved gases in the retardant-treated SFM decreased by 20% mol with respect to the untreated one. Consistently, some solid uncharacterized deposit was found in a cold zone at the outlet of the TPO reactor.

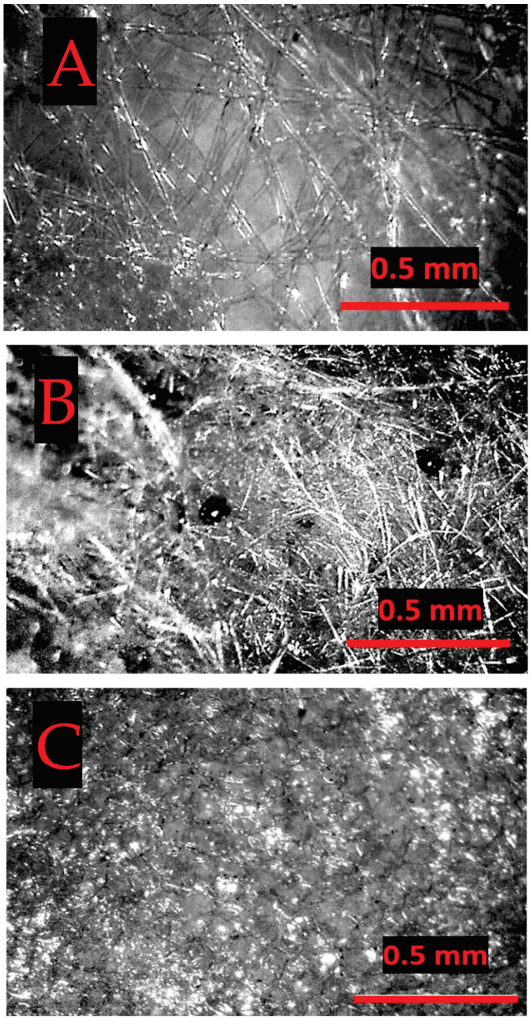


Figure 2. Micrographs of surgical face mask (**A**), rock wool (**B**), and polystyrene (**C**).

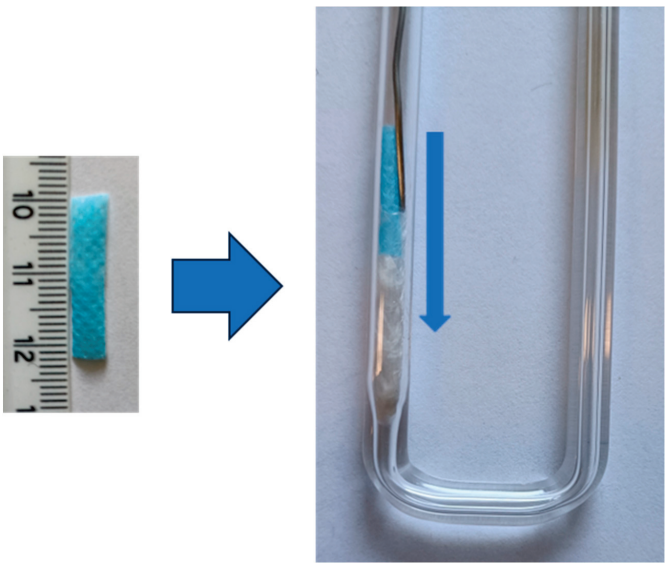


Figure 3. Test specimen made for the fire resistance analysis (SFM sample) and the flow microreactor loaded with the SFM (right arrow): The vertical arrow indicates the direction of the airflow. A K-thermocouple was vertically inserted into the SFM layer to continuously monitor the temperature. The SFM was held in place using glass wool.

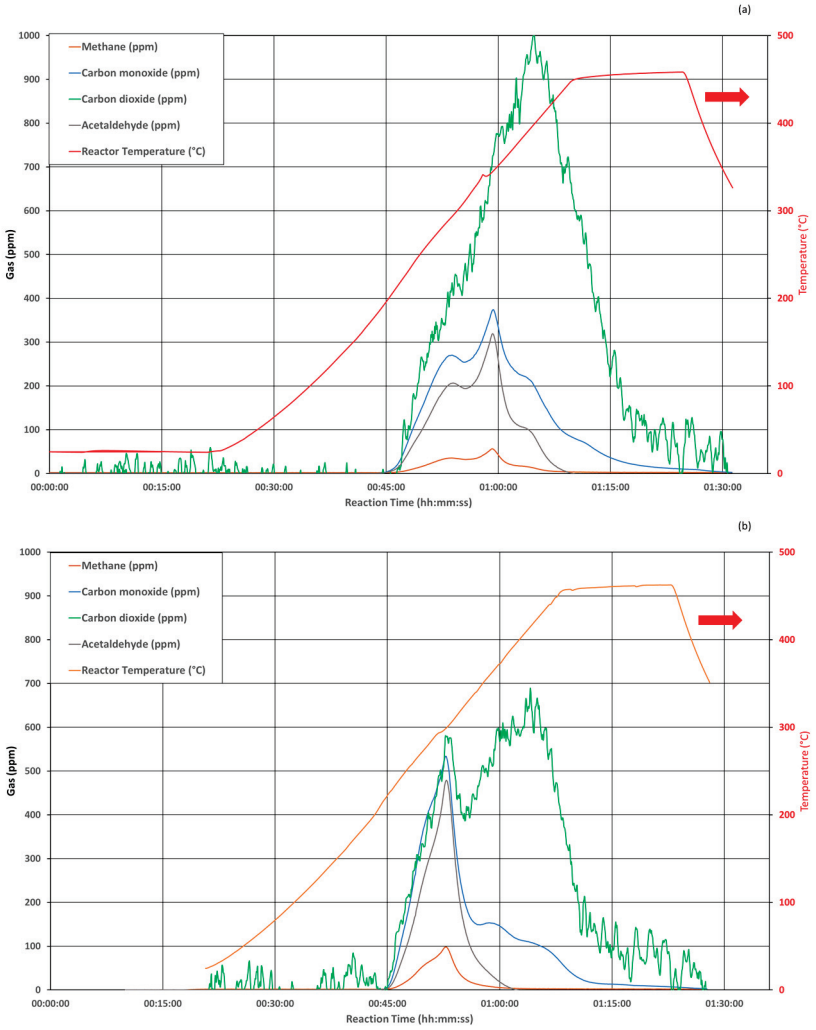


Figure 4. Examples of Temperature Programmed Oxidation profiles obtained on (**a**) untreated and (**b**) fire retardant-treated SFMs. Gas concentration (ppm) and temperature profile (°C) are reported as a function of time (hh:mm:ss).

2.1.3. Water Permeability

The water vapor transmission rate of a sample made by stacking 20 SFMs for a total of 6.3 cm in thickness was evaluated through a water vapor permeability test carried out in accordance with the EN 12086 [33] standard. As shown in Figure 5, the sample was placed at the top of a holder element while, at the bottom, there was a desiccant-saturated solution of water and potassium nitrate KNO_3.

The sample was placed in a chamber with controlled humidity and temperature. At regular time intervals, the sample was weighed using a precision weighing scale to determine the total mass of the vapor passed through the mask layer (Figure 6). The test was performed in a condition defined as 'A', which required a pressure difference of 1400 Pa for the determination of the water vapor permeability. The resulting water vapor permeability δ was about 176×10^{-12} kg/(m s Pa).

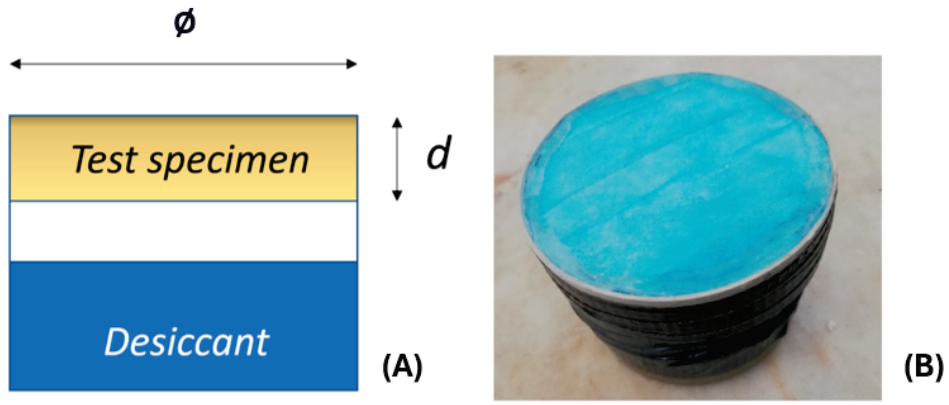


Figure 5. Section of the test specimen made for the water vapor (**A**) test and picture of the sample (**B**). The sample diameter (Ø) was 9 cm, while the sample thickness *d* was 6.3 cm. A total of 20 face masks were used.

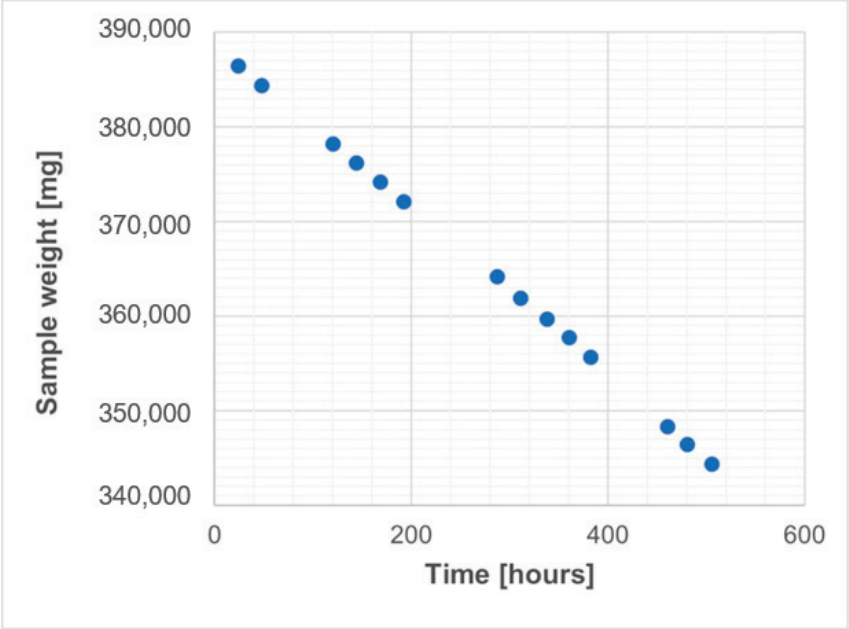


Figure 6. Sample weight along the water vapor permeability test.

2.1.4. Thermal Conductivity

The analyzed sample, shown in Figure 7, was made of a cardboard frame measuring 0.5 m × 0.5 m × 0.08 m in which SFMs were placed in different manners. The masks were weighed, folded (if necessary), and stacked in the frame to achieve the desired density. Finally, the SFMs were compacted by closing the shell.

Thermal conductivity tests were conducted at the University of Bologna (Italy) and the Ecam Ricert Institute of Monte di Malo—Vicenza (Italy). The first case involved a heat flow meter designed to analyze material with a thermal conductivity of less than 5 W/(m K), following the ISO 8301 [34] standard. The test apparatus used in the second laboratory was a commercial guarded hot plate (model Lambda Meter EP500) manufactured by Lambda Messtechnik GmbH Dresden (Dresden, Germany), in accordance with the EN 1946-2 [35] standard. In the test, the sample was placed between a hot and a cold plate kept at constant temperatures by two thermostatic baths, and an insulating layer reduced lateral heat losses. Data were acquired by means of a multimeter, a switch control unit, and an ice point reference.

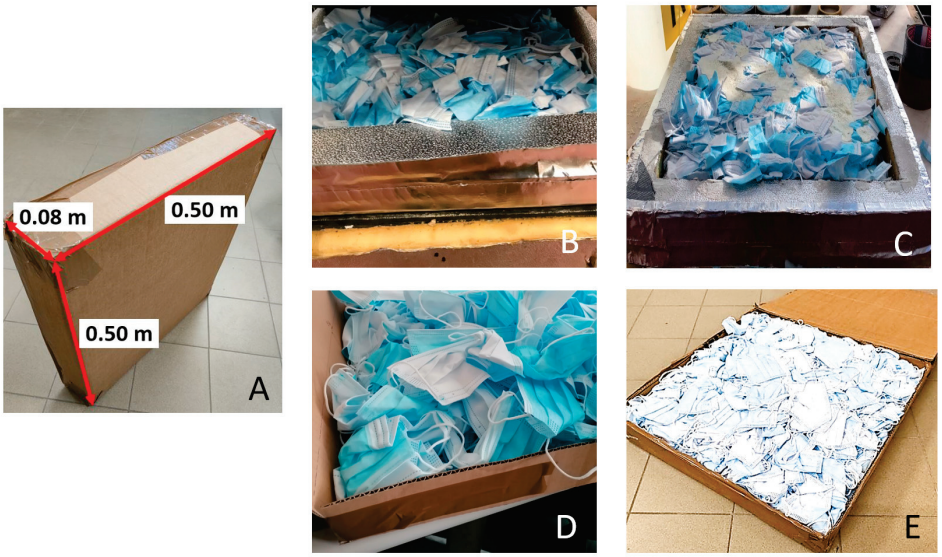


Figure 7. Test specimens made for the thermal conductivity tests: dimensions of the specimens (**A**), shredded masks (**B**), shredded masks with polyurethane foam (**C**), and two phases of the panel realization with crumpled masks (**D**,**E**).

Several aspects were analyzed, such as panel density, operator manual skills, the presence of metallic elements and foams, and the effect of some treatments. Panel density ranged between 30 and 90 kg/m^3 (corresponding to a number of masks in the panel of about 200 and 600, respectively, considering the unit weight of a mask to be 0.003 kg), which are typical values for commercial insulating materials. In view of panel self-realization, SFMs were crumpled and/or shredded to assess the influence on operator manual skills. The effect of polyurethane foam and metal elements in the panel was also analyzed.

Tests performed on untreated SFMs—non-sanitized and without fire retardants—are summarized in Table 1. SFM arrangement and density are identified by an acronym: the letters refer to the masks' arrangement—ordered (O), casual arrangement (D), crumpled (C), and shredded (S)—while the number refers to the panel density (in kg/m^3). For the ordered, disordered, and crumpled arrangements, the masks were left intact, while, for the shredded arrangement, they were cut to facilitate their packing. To assess how the thermal conductivity was affected by the assembling phase, for the samples filled with crumpled masks, two repetitions were performed for some tests (denoted with the number 2) in which the masks were casually rearranged. Tests where the metallic nose clip was removed are identified with the letter W. Finally, two tests (S_54_W and S_63_W) were performed by adding a polyurethane foam both superficially and laterally through a nozzle. The results are reported in Table 1 and displayed in Figure 8.

Since end-of-life SFMs cannot be used directly after being used by people and need to undergo a fire retardant process, the effect of two treatments was analyzed. The sanitization was carried out through a washing machine process, while the fire retardant process consisted of the application of a flame retardant designed for textiles. Table 2 summarizes the tests performed, while the results are displayed in Figure 9, where they are compared to the reference case T1 performed on untreated SFMs.

Table 1. Tests performed on non-sanitized masks to determine the panels' thermal conductivity.

Test Name	Sample Characteristics	ρ (kg/m^3)	λ_{eq} (W/mK)
O_60	Masks in an ordered arrangement	60	0.046
O_90	Masks in an ordered arrangement	90	0.039
D_90	Masks in a disordered arrangement	90	0.042
C_30_1	Crumpled masks	30	0.072
C_30_2	Crumpled masks—repetition	30	0.064
C_40_1	Crumpled masks	40	0.055
C_40_2	Crumpled masks—repetition	40	0.047
C_50_1	Crumpled masks	50	0.051
C_50_2	Crumpled masks—repetition	50	0.059
C_60_1	Crumpled masks	60	0.047
C_60_2	Crumpled masks—repetition	60	0.052
C_70_1_W	Crumpled masks without clip-on	70	0.045
C_70_2_W	Crumpled masks without clip-on	70	0.047
C_76_1	Crumpled masks	76	0.052
C_76_2	Crumpled masks—repetition	76	0.052
S_30	Shredded masks without clip-on	30	0.052
S_50	Shredded masks without clip-on	50	0.043
S_54_W	0.355 kg of shredded masks in polyurethane foam (44%) without clip-on	54	0.048
S_63_W	0.59 kg of shredded masks in polyurethane foam (21%) without clip-on	63	0.041

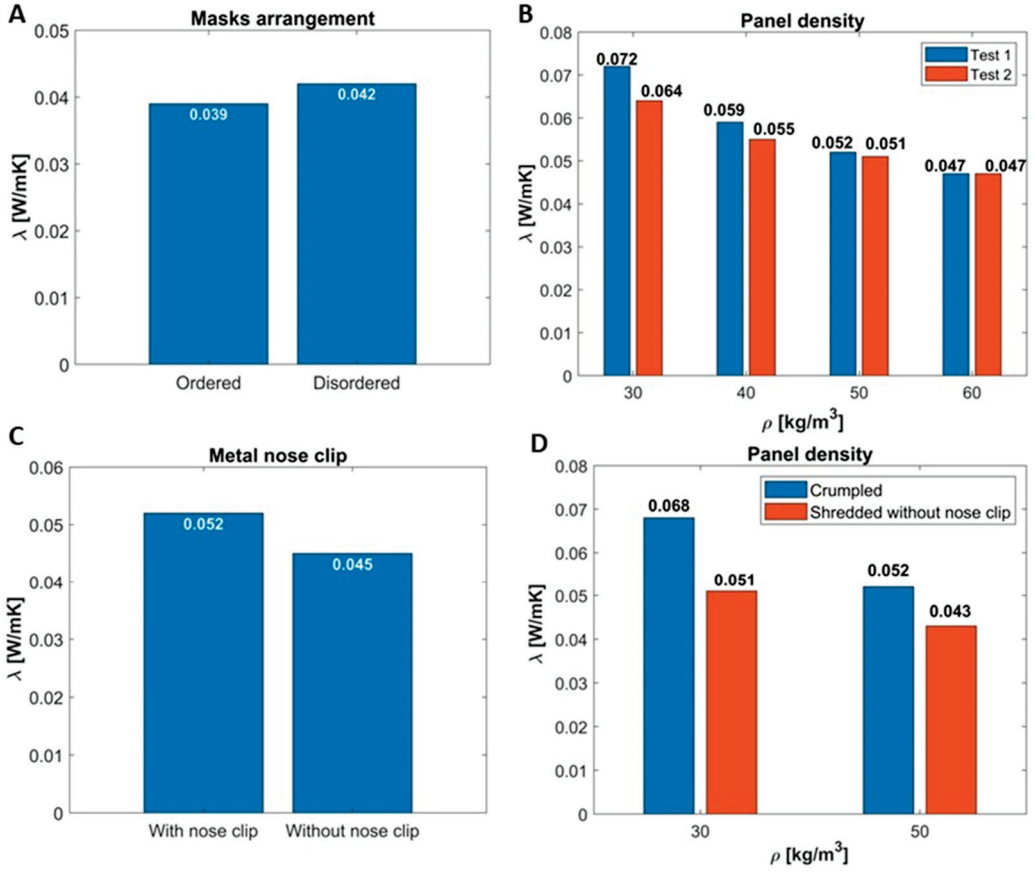
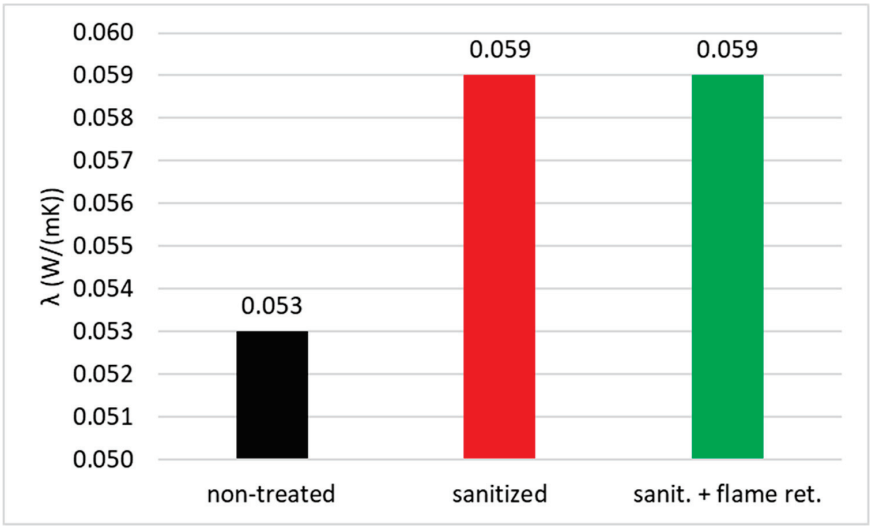


Figure 8. Thermal conductivity as a function of the mask arrangement (ϱ = 90 kg/m^3) (**A**), density and arrangement (the second test was performed by casually reshuffling the masks) (**B**), presence of the nose clip-on (**C**), SFM dimensions (**D**).

Table 2. Tests performed on SFMs sanitized and treated with flame retardant. Crumpled masks were used to realize the panel. Each test is identified by an acronym: "Sa" indicates sanitized; "SFR" sanitized and fire retardant treatment. The final number is the panel density. The uncertainty of the measurement is ±0.001.

Test Name	Sanitized	Flame Retardant	ρ (kg/m^3)	λ_{eq} (W/(mK))
T1			75	0.053
Sa_60	✔		60	0.066
Sa_70	✔		70	0.060
Sa_75	✔		75	0.059
Sa_80	✔		80	0.054
Sa_90	✔		90	0.050
SFR_60	✔	✔	60	0.053
SFR_64	✔	✔	64	0.052
SFR_70	✔	✔	70	0.050
SFR_75	✔	✔	75	0.059
SFR_80	✔	✔	80	0.044
SFR_83	✔	✔	83	0.043
SFR_90	✔	✔	90	0.052

(**A**)



(**B**)

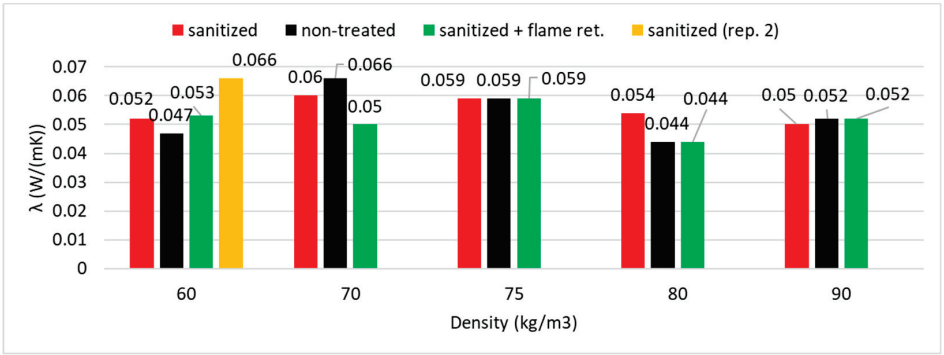


Figure 9. Thermal conductivity as a function of the treatment (density 75 kg/m^3 made with crumpled masks) (**A**) and the density (**B**). Values were measured for panels made with non-treated, sanitized (where "sanitized (rep. 2)" is the second test repetition conducted at the same density), and impregnated with flame retardant (sanit. + flame ret.) masks.

3. Discussion

The experimental and numerical results are here discussed to determine whether SFMs are suitable for the realization of panels to be installed indoors to improve comfort and reduce energy demands during the heating season.

3.1. SFM Characterization and Fire-Resistance of SFMs

The microscope analysis (Figure 2) clearly revealed that the morphology of the SFMs represented similar features to fibrous types of insulating materials such as rock wool, with comparable thickness and length of the fibers; yet, the density of the fibrous web appeared less dense than that of the rock wool. Consequently, thermal conductivity comparable to that of fibrous materials was expected. Moreover, compaction or any treatment affecting the space distribution of the web of fibrous elements could in principle affect thermal behavior.

As far as the fire resistance of SFMs is concerned, it must be recalled that PP ignition temperature is reported in the literature to be 570 °C [36]; yet, this value is related to massive, extruded PP. Our results appear to be very consistent with those reported in [37], where it was observed that the combustion of SFMs started at about 200 °C in thermogravimetric measurements carried out in air. Large PP particles showed lower reactivity compared to fine ones, indicating that the larger the exposed surface, the higher the reactivity [38]. Figure 2 shows a fibrous structure of a PP layer with a typical fiber diameter of 3.2×10^{-4} cm. Assuming an average length of the fibers of 1 cm, a surface area of 1.39×10^{4} cm^2/g was calculated for the fiber, which would drop to 6.67 cm^2/g for a single cubic piece. Such an order of magnitude variation of the surface area is clearly expected to change the reactivity of the material.

The observation that the starting temperature of the combustion was slightly affected by the fire retardant can be attributed to the mechanism of the fire retardancy effect [36], which, in our case, was related to an endothermic effect, as checked by separate experiments (data not reported). These experiments were carried out using glass wool impregnated with a pure fire retardant, which showed a neat endothermic phenomenon that started at around 200 °C, i.e., the temperature at which the samples ignited. Consistently, we found some increase in CO production in the treated sample, indicating a slightly higher extension of the partial combustion and fewer gases evolving compared to the untreated sample. With both ignition and endothermic phenomena occurring at the same temperature, significant fire retardancy was not expected. There are several studies reporting the effects of fire retardants on the combustion behavior of PP, all indicating that, due to the high flammability of PP, the use of a combination of fire retardants is necessary to achieve significant protection (see, for example, [39]); moreover, endothermal effect-based fire retardants generally require the use of high loading, which was not applicable in our case. Other results clearly explain our observations; although, we must keep in mind that for the targets of this research, only simple, cheap, and easy-to-apply solutions must be employed for panel production.

3.2. Vapor Permeability and Thermal Conductivity

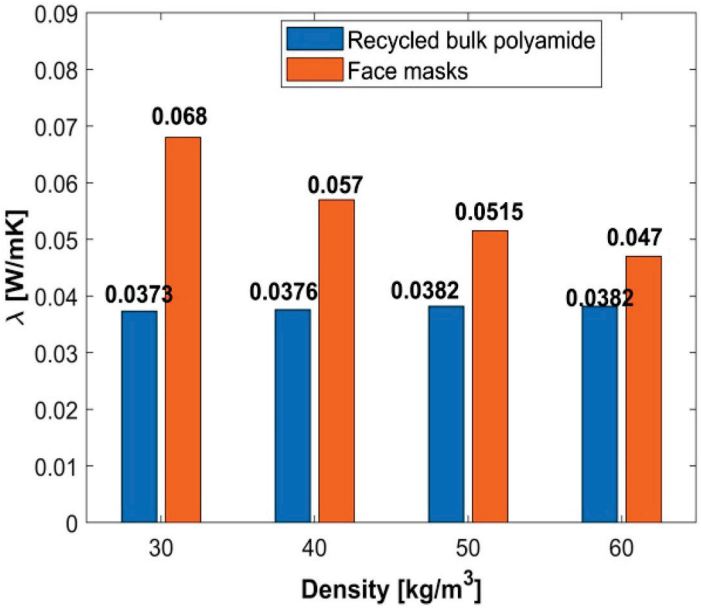
The measured water vapor permeability, equal to 1.76×10^{-10} kg/(m s Pa), was comparable to that of other fibrous insulating materials, such as mineral wools and glass wool (that are in the order of 1.50×10^{-10} kg/(m s Pa).

With regard to thermal conductivity, several aspects were analyzed. As a general comment, the thermal conductivity values here reported for the panels were in the typical range of items made with fibrous materials, consistent with the SFM microstructure depicted in the micrographs (Figure 2): 0.044 and 0.037 W/m K thermal conductivity was reported respectively for rock wool and polystyrene [39]. Data in Figure 8A obtained on non-sanitized masks show that the masks' arrangement in the panel affected the thermal conductivity, which ranged between 0.039 W/mK for ordered masks and 0.042 W/mK for disordered masks. The random shuffling of masks meant that the panel was not uniformly filled, allowing air to circulate and increasing the heat transfer; this aspect was also con-

firmed by the results in Figure 8B, determined by repeating the tests for the same panel density but shuffling the masks: two different thermal conductivity values were obtained for the same panel density. Thermal conductivity was a decreasing function of density, but the masks' positioning was less important for higher density values. This was due to the minor quantity of voids left when masks were tidily stacked. The metallic nose clip affected thermal performance (Figure 8C): when the metal element was removed, the thermal conductivity was reduced from 0.052 to 0.045 W/mK. Cutting the masks resulted in an improvement in thermal performance, as can be seen in Figure 8D, where, in this case, it was also a decreasing function of density. Ideally, the metal element should be removed and the masks should be cut into smaller pieces, but, since both operations are time-consuming, a cost/benefit assessment would be necessary, especially if implemented on a medium/large scale. According to Figure 9, SFM treatment determined an increase in thermal conductivity. However, a clear pattern between sanitized and flame retardant treatment was not evident (Figure 9A), even if it seemed that lower values were detected with higher density. For sanitized masks, the thermal conductivity decreased with density (as seen for the untreated templates), but, for the flame retardant-treated masks, there was no discernible trend since the highest conductivity value was found for the panel with a density of 75 kg/m^3. This may have been due to uneven product application.

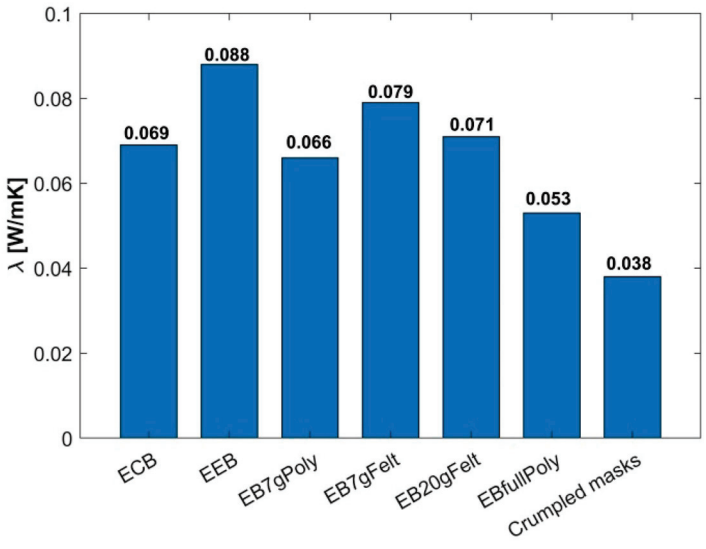
3.3. Comparison with Properties of Materials in the Literature

The thermal conductivity measured for the panels made with SFMs was compared with that given for other EoLHMs reported in the literature. Figure 10 compares the thermal performance of SFMs with those of bulk polyamide, a waste material from the production of non-surgical face masks. The bulk material showed lower thermal conductivity, and this was due to the structure of SFMs, which did not allow for voids to be completely filled in the panel, and the presence of the metal nose clip. On the other hand, the thermal conductivity of panels made with SFMs was lower than that of panels made using EoLHMs such as egg boxes, polyester, and felt.



A

Figure 10. *Cont.*



B

Figure 10. Comparison of the thermal conductivity measured for panels made with recycled polyamide-66 [40] and crumpled face masks (**A**). In (**B**), the comparison of the thermal conductivity measured for panels made with a cardboard box filled with crumpled masks (Crumpled masks) is reported with that measured for panels made of cardboard boxes filled with different materials and presented in [15]. In this latter case, ECB refers to an empty cardboard box 7 cm thick (with air in the box); in EEB, the cardboard box contained egg boxes, and each egg box was filled with 7 g of polyester in EB7gPoly, 7 g felt in EB7gFelt, and 20 g felt in EB20gFelt. The cardboard box was filled with polyester in EBfullyPoly (but no egg boxes).

4. Conclusions

This study explored new ways to foster the circular economy model and encourage the reuse of EoLHMs for applications in the building sector. The focus was on the properties of surgical face masks, and attention was paid to complete face masks, face masks with only iron nose clips, face masks (no loops and iron nose clips), face masks with elastic loops only and a high binder ratio (no iron nose clip), and face masks with elastic loops only but a low binder ratio.

The experimental results show that SFMs' water vapor permeability is comparable to that of other porous materials such as mineral and glass wool. The measured thermal conductivity ranged from 0.039 to 0.072 W/(m K), which is typical of items made with fibrous materials.

However, the thermal conductivity depends on the masks' arrangement, dimensions, and density. Thermal conductivity was affected by sanitization and flame retardant treatment, with higher values for treated masks, but no recognizable pattern was observed. As density increased, thermal conductivity decreased. There was an important influence from the nose clip-on since, when it was removed, the thermal conductivity was reduced. Placing masks neatly and removing the metal element was the best method for making panels, but this method would generate board construction difficulties in large-scale production. The addition of polyurethane foam seems not to be beneficial. The observed ignition temperature and the minimal effect of the flame retardant suggest that the use of an insulating panel with a gypsum board embedded for fire protection is required.

In this paper, the authors reported results that may lead to new ways to use EoLHMs. Attention was paid to surgical face masks, and future analyses will consider other possible materials.

Author Contributions: Conceptualization, E.R.d.S., V.B., J.K., M.N., M.P., E.A.P. and P.V.; methodology, E.R.d.S., V.B., J.K., M.N., M.P., E.A.P. and P.V.; investigation, E.R.d.S., V.B., J.K., M.N., M.P., E.A.P. and P.V.; writing—original draft preparation, E.R.d.S., V.B., J.K., M.N., M.P., E.A.P. and P.V.;

writing—review and editing, E.R.d.S., V.B., J.K., M.N., M.P., E.A.P. and P.V.; visualization, E.R.d.S., V.B., J.K., M.N., M.P., E.A.P. and P.V.; funding acquisition, E.R.d.S., V.B., J.K., M.N., M.P., E.A.P. and P.V. All authors have read and agreed to the published version of the manuscript.

Funding: This research was funded by the Italian Ministry of University and Research (MUR) within the framework of the PRIN2022 project "Sustainable Thermal and Acoustic self-made solutions for buildings refurbishment in disadvantaged social contexts by Reusing poor materials (STAR)" grant 2022MW3CSK; and by the Department of Mechanical and Industrial Engineering of the University of Brescia through the MetATer PRD project.

Data Availability Statement: The data presented in this study are available on request from the corresponding author.

Conflicts of Interest: The authors declare no conflicts of interest.

References

1. United Nations, Department of Economic and Social Affairs, Sustainable Development. The 17 Goals. Available online: https://sdgs.un.org/goals (accessed on 6 November 2023).
2. IEA. *Buildings*; IEA: Paris, France, 2022; Available online: https://www.iea.org/reports/buildings (accessed on 6 November 2023).
3. Kirchherr, J.; Reike, D.; Hekkert, M. Conceptualizing the circular economy: An analysis of 114 definitions. *Resour. Conserv. Recycl.* **2017**, *127*, 221–232. [CrossRef]
4. Neri, M.; Pilotelli, M.; Traversi, M.; Levi, E.; Piana, E.A.; Bannó, M.; Cuerva, E.; Pujadas, P.; Guardo, A. Conversion of end-of-life household materials into building insulating low-cost solutions for the development of vulnerable contexts: Review and outlook towards a circular and sustainable economy. *Sustainability* **2021**, *13*, 4397. [CrossRef]
5. Dissanayake, D.G.K.; Weerasinghe, D.U.; Thebuwanage, L.M.; Bandara, U.A.A.N. An environmentally friendly sound insulation material from post-industrial textile waste and natural rubber. *J. Build. Eng.* **2021**, *33*, 101606. [CrossRef]
6. Hadded, A.; Benltoufa, S.; Fayala, F.; Jemni, A. Thermo physical characterisation of recycled textile materials used for building insulating. *J. Build. Eng.* **2016**, *5*, 34–40. [CrossRef]
7. Wang, J.; Du, B. Experimental studies of thermal and acoustic properties of recycled aggregate crumb rubber concrete. *J. Build. Eng.* **2020**, *32*, 101836. [CrossRef]
8. Limami, H.; Manssouri, I.; Cherkaoui, K.; Khaldoun, A. Physicochemical, mechanical and thermal performance of lightweight bricks with recycled date pits waste additives. *J. Build. Eng.* **2021**, *34*, 101867. [CrossRef]
9. Othmani, C.; Taktak, M.; Zein, A.; Hentati, T.; Elnady, T.; Fakhfakh, T.; Haddar, M. Experimental and theoretical investigation of the acoustic performance of sugarcane wastes based material. *Appl. Acoust.* **2016**, *109*, 90–96. [CrossRef]
10. Gómez Escobar, V.; Maderuelo-Sanz, R. Acoustical performance of samples prepared with cigarette butts. *Appl. Acoust.* **2017**, *125*, 166–172. [CrossRef]
11. Gruhler, K.; Schiller, G. Grey energy impact of building material recycling—A new assessment method based on process chains. *RCR Adv.* **2023**, *18*, 200139. [CrossRef]
12. Taaffe, J.; O'Sullivan, S.; Rahman, M.E.; Pakrashi, V. Experimental characterisation of Polyethylene Terephthalate (PET) bottle Eco-bricks. *Mater. Des.* **2014**, *60*, 50–56. [CrossRef]
13. Kang, C.W.; Kim, M.; Jang, E.S.; Lee, Y.H.; Jang, S.S. Sound absorption coefficient and sound transmission loss of porous sponge attached corrugated cardboard of noise insulation cover. *Palpu Chongi Gisul/J. Korea Tech. Assoc. Pulp Pap. Ind.* **2020**, *52*, 38–44. [CrossRef]
14. Algaily, B.; Puttajukr, S.; Navarat, T. Acoustic absorption, rheological and mechanical characteristics of waste egg boxes fibers filled SBR. *J. Teknol.* **2015**, *77*, 45–52. [CrossRef]
15. Neri, M. Thermal and Acoustic Characterization of Innovative and Unconventional Panels Made of Reused Materials. *Atmosphere* **2022**, *13*, 1825. [CrossRef]
16. Badillo-Goicoechea, E.; Chang, T.H.; Kim, E.; LaRocca, S.; Morris, K.; Deng, X.; Chiu, S.; Bradford, A.; Garcia, A.; Kern, C.; et al. Global trends and predictors of face mask usage during the COVID-19 pandemic. *BMC Public Health* **2021**, *21*, 2099. [CrossRef] [PubMed]
17. Ibn-Mohammed, T.; Mustapha, K.B.; Godsell, J.; Adamu, Z.; Babatunde, K.A.; Akintade, D.D.; Acquaye, A.; Fujii, H.; Ndiaye, M.M.; Yamoah, F.A.; et al. A critical analysis of the impacts of COVID-19 on the global economy and ecosystems and opportunities for circular economy strategies. *Resour. Conserv. Recycl.* **2021**, *164*, 105169. [CrossRef] [PubMed]
18. Akhbarizadeh, R.; Dobaradaran, S.; Nabipour, I.; Tangestani, M.; Abedi, D.; Javanfekr, F.; Jeddi, F.; Zendehboodi, A. Abandoned COVID-19 personal protective equipment along the Bushehr shores, the Persian Gulf: An emerging source of secondary microplastics in coastlines. *Mar. Pollut. Bull.* **2021**, *168*, 112386. [CrossRef]
19. Wang, F.; Wu, H.; Li, J.; Liu, J.; Xu, Q.; An, L. Microfiber released into urban rivers from face masks during COVID-19. *J. Environ. Manag.* **2022**, *319*, 115741. [CrossRef]

20. Tabatabaei, M.; Hosseinzadeh-Bandbafha, H.; Yang, Y.; Aghbashlo, M.; Lam, S.S.; Montgomery, H.; Peng, W. Exergy intensity and environmental consequences of the medical face masks curtailing the COVID-19 pandemic: Malign bodyguard? *J. Clean. Prod.* **2021**, *313*, 127880. [CrossRef] [PubMed]
21. Ye, S.; Li, Y.; Huang, H.; Xu, Y.; Du, S.; Wan, F.; Xie, R.; Huang, P.; Liu, B.; Dong, T.; et al. Fast and deep disinfection for face masks recycle using vacuum ultraviolet irradiation. *J. Clean. Prod.* **2022**, *368*, 133221. [CrossRef]
22. Alcaraz, J.-P.; Le Coq, L.; Pourchez, J.; Thomas, D.; Chazelet, S.; Boudry, I.; Barbado, M.; Silvent, S.; Dessale, C.; Antoine, F.; et al. Reuse of medical face masks in domestic and community settings without sacrificing safety: Ecological and economical lessons from the COVID-19 pandemic. *Chemosphere* **2022**, *288*, 132364. [CrossRef]
23. Whyte, H.E.; Joubert, A.; Leclerc, L.; Sarry, G.; Verhoeven, P.; Le Coq, L.; Pourchez, J. Reusability of face masks: Influence of washing and comparison of performance between medical face masks and community face masks. *Environ. Technol. Innov.* **2022**, *28*, 102710. [CrossRef]
24. Neri, M.; Cuerva, E.; Levi, E.; Pujadas, P.; Müller, E.; Guardo, A. Thermal, acoustic, and fire performance characterization of textile face mask waste for use as low-cost building insulation material. *Dev. Built Environ.* **2023**, *14*, 100164. [CrossRef]
25. Miah, M.J.; Pei, J.; Kim, H.; Sharma, R.; Jang, J.G.; Ahn, J. Property assessment of an eco-friendly mortar reinforced with recycled mask fiber derived from COVID-19 single-use face masks. *J. Build. Eng.* **2023**, *66*, 105885. [CrossRef]
26. Kilmartin-Lynch, S.; Saberian, M.; Li, J.; Roychand, R.; Zhang, G. Preliminary evaluation of the feasibility of using polypropylene fibers from COVID-19 single-use face masks to improve the mechanical properties of concrete. *J. Clean. Prod.* **2021**, *296*, 126460. [CrossRef] [PubMed]
27. Koniorczyk, M.; Bednarska, D.; Masek, A.; Cichosz, S. Performance of concrete containing recycled masks used for personal protection during coronavirus pandemic. *Constr. Build. Mater.* **2022**, *324*, 126712. [CrossRef] [PubMed]
28. Al-Salem, K.; Ali, M.; Almuzaiqer, R.; Al-Suhaibani, Z.; Nuhait, A. Recycling Discarded Facemasks of COVID-19 Pandemic to New Novel Composite Thermal Insulation and Sound-Absorbing Materials. *Sustainability* **2023**, *15*, 1475. [CrossRef]
29. Neubauer, K. The Determination of Metals in Disposable, Non-Medical Face Masks by ICP-OES. *ICP-OES ICP-MS Tech. Today's Spectrosc.* **2021**, *36*, 16–23.
30. Mocé-Llivina, L.; Muniesa, M.; Pimenta-Vale, H.; Lucena, F.; Jofre, J. Survival of bacterial indicator species and bacteriophages after thermal treatment of sludge and sewage. *Appl. Environ. Microbiol.* **2003**, *69*, 1452–1456. [CrossRef] [PubMed]
31. Riddell, S.; Goldie, S.; Hill, A.; Eagles, D.; Drew, T.W. The effect of temperature on persistence of SARS-CoV-2 on common surfaces. *Virol. J.* **2020**, *17*, 145. [CrossRef]
32. Bhatia, S.; Beltramini, J.; Do, D.D. Temperature programmed analysis and its applications in catalytic systems. *Catal. Today* **1990**, *7*, 309–438. [CrossRef]
33. *UNI EN 12086:2013*; Thermal Insulating Products for Building Applications—Determination of Water Vapor Transmission Properties. UNI: Milano, Italy, 2013.
34. *UNI ISO 8301:1991*; Thermal Insulation—Determination of Steady-State Thermal Resistance and Related Properties—Heat Flow Meter Apparatus. ISO: Geneva, Switzerland, 1991.
35. *EN 1946-2:1999*; Thermal Performance of Building Products and Components—Specific Criteria for the Assessment of Laboratories Measuring Heat Transfer Properties—Part 2: Measurements by Guarded Hot Plate Method. UNI: Milano, Italy, 1999.
36. Zhang, S.; Horrocks, A.R. A review of flame retardant polypropylene fibres. *Prog. Polym. Sci.* **2003**, *28*, 1517–1538. [CrossRef]
37. Manić, N.; Janković, B.; Stojiljković, D.; Angelopoulos, P.; Radojević, M. Thermal characteristics and combustion reactivity of coronavirus face masks using TG-DTG-MS analysis. *J. Therm. Anal.* **2022**, *147*, 10131–10143. [CrossRef] [PubMed]
38. Majewsky, M.; Bitter, H.; Eiche, E.; Horn, H. Determination of microplastic polyethylene (PE) and polypropylene (PP) in environmental samples using thermal analysis (TGA-DSC). *Sci. Total Environ.* **2016**, *568*, 507–511. [CrossRef] [PubMed]
39. Seidi, F.; Movahedifar, E.; Naderi, G.; Akbari, V.; Ducos, F.; Shamsi, R.; Vahabi, H.; Saeb, M.R. Flame retardant polypropylenes: A review. *Polymers* **2020**, *12*, 1701. [CrossRef]
40. Dong, Y.; Kong, J.; Mousavi, S.; Rismanchi, B.; Yap, P.S. Wall Insulation Materials in Different Climate Zones: A Review on Challenges and Opportunities of Available Alternatives. *Thermo* **2023**, *3*, 38–65. [CrossRef]

Disclaimer/Publisher's Note: The statements, opinions and data contained in all publications are solely those of the individual author(s) and contributor(s) and not of MDPI and/or the editor(s). MDPI and/or the editor(s) disclaim responsibility for any injury to people or property resulting from any ideas, methods, instructions or products referred to in the content.

energies

MDPI

Article

Multi-Stakeholder Decision Support Based on Multicriteria Assessment: Application to Industrial Waste Heat Recovery for a District Heating Network in Grenoble, France

Jaume Fitó and Julien Ramousse *

Laboratoire Procédés Energie Bâtiment (LOCIE), CNRS UMR 5271—Université Savoie Mont Blanc, Polytech Annecy-Chambéry, Campus Scientifique, Savoie Technolac, 73376 Le Bourget-Du-Lac CEDEX, France; jaume.fito-de-la-cruz@univ-smb.fr

* Correspondence: julien.ramousse@univ-smb.fr

Abstract: The decarbonization and decentralization of district heating networks lead to the shared use of on-site resources by multiple stakeholders. The optimal design of prospective equipment in such contexts should take into account the preferences and objectives of each stakeholder. This article focuses on the adaptation of a 4E multicriteria model (the criteria being energy, exergy, economic, and exergoeconomic) to include and compare the stakeholders' performance criteria around the technical design. In addition, two graphical supports are proposed that represent and cross-analyze the different stakeholders' preferred optima. A preliminary implementation of the methodology is illustrated through a study case in France, which features waste heat recovery for district heating utilization. After presenting the results, a discussion is offered on how to complete the methodology with an iterative negotiation procedure to determine the most suitable design. It was concluded, among other considerations, that the relaxation of the stakeholders' optimality requirements can greatly enable the project's feasibility. Such a relaxation could be implemented in the form of a joint consortium. In addition, the results showed that stakeholder relaxations of requirements can lead to new solutions that may outperform the best solutions pre-relaxation. Lastly, perspectives are suggested toward verifying whether relaxed requirements from upstream stakeholders might be more impactful than those of downstream stakeholders.

Keywords: district heating; waste heat recovery system; multi-stakeholder; techno-economic assessment; thermodynamic assessment; exergoeconomic

1. Introduction

District heating networks are evolving toward renewable energies, low temperatures, decentralized production [1], and on-site exploitation of energy sources [2]. The potential of recovering industrial excess heat is large, as identified in the studied Swedish case, for example [3]. In the past, renewable energy-driven projects have been extensively studied through separate multi-objective [4], multi-agent [5], and multi-stakeholder [6] approaches.

The multi-objective approach has assisted in different parts of the energy chain, for example, with the optimal integration of solar resources on the production side [7], or for energy efficiency renovation measures on the demand side [8]. A classic example of multiple conflicting objectives is that of the economic and the environmental criteria as one seeks the best configuration that minimizes pollutant emissions while remaining cost-effective [9]. For district energy networks, such problems are usually approached through mixed-integer linear programming (MILP) [10], sometimes with a rolling horizon [9]. Multi-objective optimization is often used during the development of decision-making frameworks, as demonstrated by numerous case studies internationally, for example, in China [11] or Germany [12], just to name a few.

Most of the time, the diversity of energy sources and demands implies a variety of stakeholders and decision criteria. The natural consequence of that variety is the arrival of new types of decentralized agents and/or markets [13] and of prosumers, with a notable impact on the structure of energy systems and the modeling approaches [14]. One stakeholder's choices have consequences, sometimes unintended, for other stakeholders [15]. For instance, industrial actors tend to be reluctant to share data about their waste streams [16]. This is understandable, for the sake of public image, and defendable by confidentiality laws. And yet, keeping those data a secret makes it difficult to model new recovery processes accurately. In other instances, new environmentally friendly systems may be socially rejected [17].

An active search for engagement by the stakeholders is identified as a key point for policy changes in order to accelerate the approval of renewable energy projects [18]. Traditionally, studies on the development of energy communities have focused on citizens as the main stakeholders, but some studies have analyzed the motivations of other stakeholders in joining an energy community [19]. In addition, past studies have found that institutional cooperation at different levels has different effects on the efficiency of multi-stakeholder partnerships for the deployment of renewable energies [20].

Socio-technical considerations are more and more frequently included in energy projects from the initial design stage, such as social or urban factors [21,22]. Some approaches, such as the assembly theory [23], model the consequences of one stakeholder's choices on the other stakeholders. In the particular case of industrial heat recovery, this (and the concept of synergies) has also been illustrated [24]. Elsewhere, the concept of a socio-technical optimality gap has been suggested [15], which quantifies the distance between a calculated optimum and the actually desired socio-technical optimal solution.

Decentralized renewable energy projects need to involve the different stakeholders in the planning [25], implementation, and management stages, in order to avoid critical issues in governance [26]. A multi-stakeholder approach can also solve socio-technical barriers in the reconfiguration of district heating towards low-carbon configurations, and the perception that the different stakeholders have on those barriers [27]. Besides, technical models adapted to multi-stakeholder problematics can assist in encouraging investment in more environmentally friendly technologies. For example, the evolutionary multi-objective optimization algorithm proposed by Simeoni et al. [28] considered multiple types of stakeholders (investors, consumers, citizenship, etc.) and indicators (energy, economic, and environmental) to identify Pareto-optimal configurations for an industrial waste heat-driven smart energy system in Italy. Multi-stakeholder approaches could unlock the potential of large-scale heat pumps for district heating in some countries (e.g., Denmark, with an estimated potential of 100 M EUR/y within 2025 [29]).

Several models have been proposed that take into account the variety of criteria, decision-makers, and disciplines. For example, Taylor et al. [30] proposed an interdisciplinary methodology for the planning and operation of future multi-vector energy networks, taking many aspects into account: new technologies, innovative business models, policy and societal changes, and cyber security. Höfer and Madlener [31] proposed a multi-criteria group decision model combining value-focused thinking with multi-attribute utility theory, which evaluates different energy transition scenarios through holistic approaches and involves stakeholders at every step of the decision-making process. Turcksin et al. [32] built a multi-actor multi-criteria (MAMCA) framework to support the implementation of biofuels in Belgium, taking into account all stakeholders of the biofuel supply chain. Hettinga et al. [33] proposed a multi-stakeholder decision support system for energy planning at the local level, identifying boundary conditions that could have been missed at wider scales.

As demonstrated by the above studies, the current state of the art proposes several tools for multi-stakeholder analysis of energy projects. Some of those tools can consider multiple scenarios with varying interactions between stakeholders: ownership over shared equipment, selling/buying prices of boundary resources, etc. Oftentimes, different optimal

solutions will be identified depending on the scenario, the stakeholder, and the performance indicators. In such cases, the discussion is up to the stakeholders. However, such a discussion can be very difficult, especially for real energy projects where multiple criteria are involved. Decision support tools are, thus, needed to evaluate the distances between the different optimal solutions and the possibilities for an agreement. Those tools should also support the negotiation process by providing updated results while taking into account the stakeholders' choices.

With the abovementioned research gap in mind, the authors of this article propose a set of decision support tools to facilitate the technical design of on-site energy projects involving multiple stakeholders, through iterative negotiations over quantified solutions [34]. The methodology applies the notion of a "socio-energetic node" proposed by Tabourdeau and Debizet [35]. Socio-energetic nodes represent parts of a complex energy system, defined as "a set of elements that harvest, convert, or distribute energy and are managed by a decision-maker interacting with other agents" [35].

The methodology relies on the evaluation of multiple quantitative decision criteria for the considered scenarios that are related to the stakeholders' share of the equipment. Then, the stakeholders are asked to convey the weight (or importance) that they give to every decision criterion. In the end, two visual tools cross-evaluate the optimal solution preferred by each stakeholder with the decision criteria of the other stakeholders. The possibility that stakeholders might relax their objectives and be more tolerant of suboptimal solutions is also considered. For each decision by a stakeholder, the visual tools are updated.

Therefore, the methodology is sensitive, responsive, and adaptive to the stakeholders' decisions. It can guide them through iterative negotiations by contrasting the different socio-energetic nodes, and answering questions like: Which design is the most promising among the feasible ones? Which scenario is the most favorable one for all stakeholders? Which are the most constraining and the most conciliating criteria? Can relaxation of the stakeholders' constraints yield solutions that are more promising? Thus, negotiations are guided toward an agreement when possible.

The first part of the methodology is demonstrated in this article through a case study on a district heating system driven by industrial waste heat. The case study involves a multicriteria 4E model (energy, exergy, economic, and exergoeconomic), four possible stakeholders, and the relative scenarios based on the possible ownership of the prospective equipment by stakeholders. An added value of this case study is the exergy criterion and its exergo-economic variant. Despite not yet being included in decision support tools, exergy is slowly but surely gaining its place in energy decision-making and in the planning of low-temperature urban heat networks [34].

Section 2 of this manuscript presents the case study, the prospective energy system, the negotiation support algorithm, the simulation and optimization tools, and the criteria considered (energy, exergy, economic, exergoeconomic, and multi-stakeholder). Section 3 presents and analyzes the main results. Section 4 presents the specific conclusions of this case study, along with more general conclusions concerning multi-stakeholder technical projects.

2. Materials and Method

The case study focuses on the on-site valorization of waste heat from a French laboratory of high-intensity magnetic fields (LNCMI), working in order to cover the heating demand of the Presqu'Île district in Grenoble [36].

2.1. System Description and Ownership Scenarios

Figure 1 presents the case study and the socio-energetic nodes considered for modeling. The LNCMI's electro-intensive processes reject considerable amounts of waste heat that is currently dissipated within the Isère River. Thus, the LNCMI's socio-energetic node is made up of their laboratory experiences (noted as "EXP" in the diagram) and heat dissipation (noted as "DISS"). A nearby district heating network ("DHN") has thermal needs of the

same order of magnitude. That network and its substations ("NS") are managed by the CCIAG, an aggregator that also manages a heat supply plant ("HS"). The LNCMI wants to valorize its waste heat, and the CCIAG wants a higher share of renewables in its energy mix. Both decision-makers are interested in a project that connects their needs.

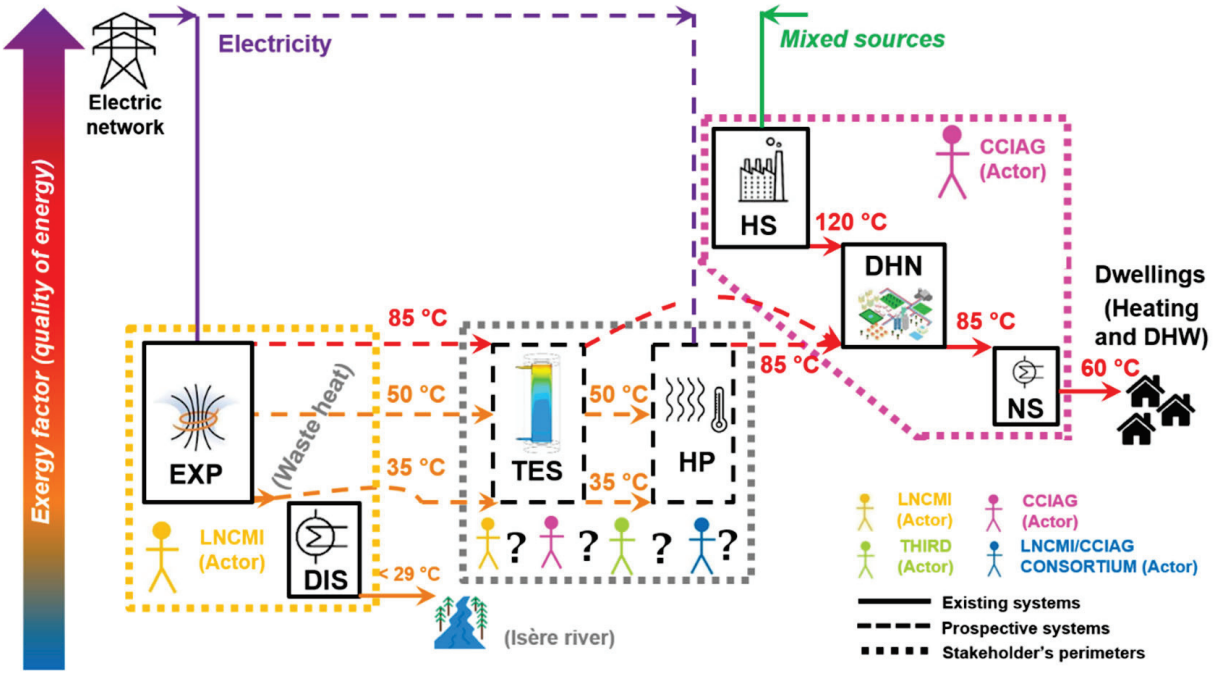


Figure 1. Diagram of the case study, showing the stakeholder's perimeters.

The project consists of implementing a waste heat recovery system capable of upgrading the LNCMI's waste heat, i.e., increasing its temperature and injecting it into the CCIAG's network. The recovery system is made up of a thermal energy storage unit ("TES") to compensate for temporal mismatch and a heat pumping unit ("HP") to increase the waste heat's temperature. The technical pre-design of this system requires the user to determine the optimal waste heat temperature and storage capacity of the system. The potential owners of the prospective system are [37]: (1) the LNCMI; (2) the CCIAG; (3) an unidentified third party (named THIRD); (4) an LNCMI/CCIAG joint consortium.

Three choices exist for the input temperature, namely: 35 °C, which is the current rejection temperature by the LNCMI's electro-magnetic processes; 50 °C, which is theoretically possible with the current cooling loop of the LNCMI's magnets; and 85 °C, granted by a prospective technology for cooling the magnets (nucleate boiling [38]). In terms of storage capacity, five choices are investigated, namely, from 0 MWh (i.e., no storage) to 40 MWh in increments of 10 MWh. This leads to a total of 15 possible pre-designs for this system. The reference case involves heat rejection at 35 °C and complete dissipation to the Isère River.

In addition to the technical layer, this project also has a multi-stakeholder layer, through the notion of the "socio-energetic node" proposed by [35]. The perimeter of a socio-energetic node is defined by material and energy flows, as well as the socio-juridical governance models attached to them. The perimeter and borders of each socio-energetic node depend on the investments made by that stakeholder. The assembly of all socio-energetic nodes forms the overall system. Identifying socio-energetic nodes allows us to understand better the decision-making capacity of each stakeholder. Table 1 presents the socio-energetic nodes of this study for the four ownership scenarios considered. In this study, most of the stakeholders have an existing socio-energetic node that could be enlarged by acquiring a heat recovery system.

Table 1. Configuration of the socio-energetic nodes as a function of the scenario.

Scenario	Stakeholder	Socio-Energetic Node
1	**LNCMI** (Owner)	EXP + DISS + TES + HP
	CCIAG (Not owner)	CDCH + RES + SST
2	**CCIAG** (Owner)	HS + NTW + SST + TES + HP
	LNCMI (Not owner)	EXP + DISS
3	**THIRD** (Owner)	TES + HP
	LNCMI (Not owner)	EXP + DISS
	CCIAG (Not owner)	HS + NTW + SST
4	**CONSORTIUM** (Owner)	EXP + DISS + TES + HP + HS + NTW + SST

Thus, the heat recovery system (TES + HP) may become the property of the LNCMI (already the owner of EXP + DISS)—Scenario 1, or the property of the CCIAG (already owner/manager of HS + NTW + SST)—Scenario 2. It may also belong to an unidentified stakeholder (THIRD) that does not own any unit as yet—Scenario 3, or to an LNCMI/CCIAG alliance (CONSORTIUM) that would join their respective units into one unique node—Scenario 4. It was assumed that THIRD and CONSORTIUM may only be modeled as owners because acquiring the prospective equipment is the only reason for these actors to exist in this study.

Each stakeholder has their own optimization criteria, which suggest the design that would be most interesting for their socio-energetic node (i.e., their perimeter of responsibility [35,39]). Those designs will be interpreted as the stakeholder's preferences in the negotiations. When confronted with other stakeholders' preferences, each stakeholder can accept a degree of tolerance, which is understood as a maximal deviation from the optimal solution that they would prefer. Should tolerance not suffice to find a satisfying solution, a stakeholder can relax their constraints. These aspects of the study are further detailed in Section 2.3.2 (multi-stakeholder model).

2.2. Calculation Procedure and Simulation/Optimization Tools

The study presented in this article implements a portion of a larger method envisaged by the authors (Figure 2). The method consists of an algorithmic procedure for facilitating the technical design of a prospective energy unit that is of common interest to two or more stakeholders [40]. This subsection presents the specific work conducted in this article, which corresponds to Steps 1 and 2 and, partially, to Steps 0 and 4 (with a few assumptions) of the algorithm in Figure 2. Refer to Section 3.4 for a complete and generalized description of the whole algorithm.

The work in this article was conducted to:

1. **Optimize the technical system's yearly management.** This was performed with an open-source tool called OMEGAlpes (v.0.4.0), which stands for "Optimization Model Generation as Linear Programming for Energy Systems" ([41,42]). This tool applies mixed-integer linear programming (MILP) to find the optimal management of energy flows in a study case. This optimization was applied to the 15 possible designs of the waste heat recovery system.
2. **Apply multi-stakeholder and multi-criteria analysis.** This was performed with the multi-stakeholder energy, exergy, economic, and exergoeconomic models presented in the next subsections. These models were applied to the results yielded by OMEGAlpes in the previous step. The analysis gives the system's performance in terms of 4 indicators for each stakeholder, for each possible design.
3. **Relax stakeholders' constraints and repeat step 2.** Some of the stakeholders may relax some of their constraints in order to facilitate the project's feasibility. Those relaxations are detailed in Section 2.3.2. Only decisional or economic relaxations were considered. Thus, it was not necessary to repeat step 1, since OMEGAlpes accounts for technical or operational constraints that were not modified.

4. **Generate the matrices and the radar chart.** This was performed to identify the feasible designs without relaxations, along with the most promising designs after the relaxations were applied. The results presented in this article were selected for the sake of illustrating the method.
5. **Analyze the negotiation possibilities.** Reflections based on the matrices and radar chart inspired an iterative procedure for the conception of these kinds of projects, through cooperation between the stakeholders. That procedure is presented in Section 3.4.

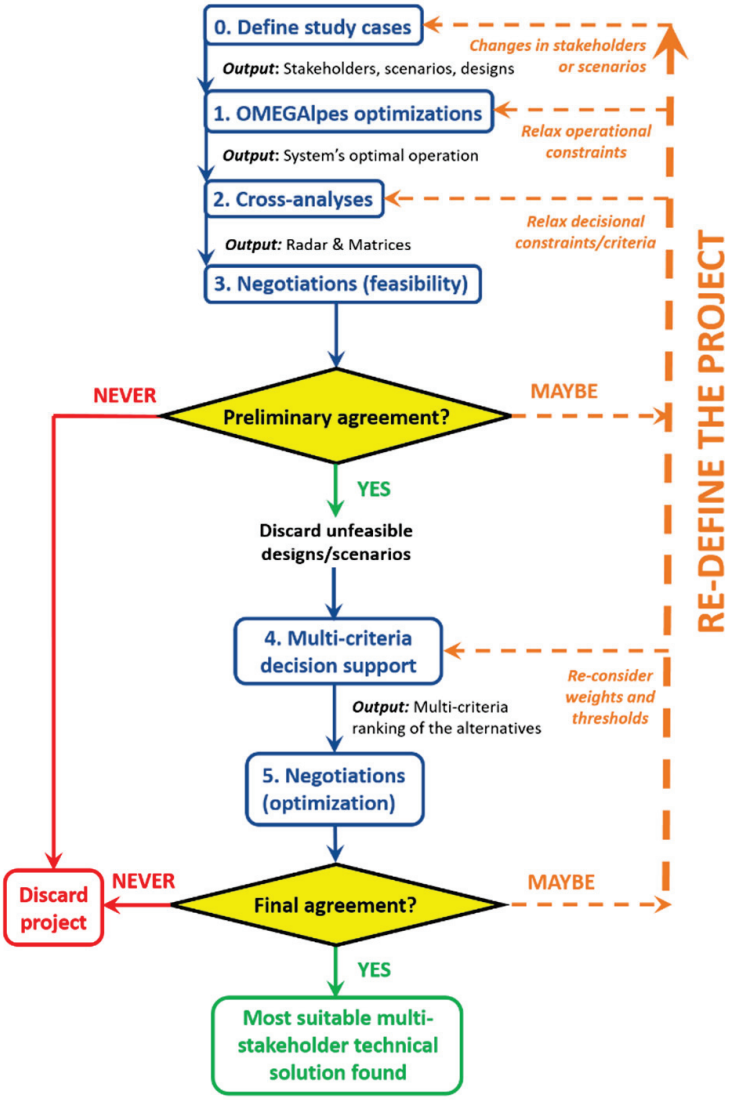


Figure 2. Decision support algorithm with the tools used in this study, plus any prospective ones.

2.3. Models

2.3.1. Energy, Exergy, Economic, and Exergoeconomic Models

A novel multi-stakeholder formulation model was applied to the energy, exergy, economic, and exergoeconomic (4E) sub-models used in previous articles for this case study. The 4E sub-models are only presented succinctly in this sub-section, for the sake of brevity. A slightly more developed description is available in the Supplementary Materials, and a detailed description is available in previous articles by the authors on this case study [36,43].

The energy model is the fundamental one, as the rest of the models were built on it. The general energy balance (Equation (1)) at a certain time step (Δt) was applied unit by unit, considering all heat inlets ($\dot{Q}^{in}$), heat outlets ($\dot{Q}^{out}$), power inlets ($\dot{W}^{in}$), power outlets

($\dot{W}^{out}$), and energy accumulations (ΔU). The term of accumulation was relevant for the thermal storage unit only.

$$\Delta t \cdot \sum \left(\dot{Q}^{in} + \dot{W}^{in} \right) = \Delta t \cdot \sum \left(\dot{Q}^{out} + \dot{W}^{out} \right) + \Delta U \quad (1)$$

The input energy data and the concretized formulation of the energy balances for each unit are presented, respectively, in Tables S1 and S2 (Supplementary Materials).

This energy model was built on the following hypotheses:

- Potential and kinetic energy are neglected.
- Temperature levels of the units remain constant throughout the year.
- Pressure, temperature, and heat losses across the pipelines are neglected.
- Perfect stratification is assumed in the thermal storage unit.
- The initial and final states of charge of the thermal energy storage are the same.
- Heat losses across the different components of the heat pump are neglected.
- The heat production process by the heat supplier has a constant exergy efficiency.

The exergy model was built on the energy model. Thus, it encompasses all the equations, hypotheses, and input parameters mentioned previously and adds additional ones. Its most fundamental equation is for exergy balance (Equation (2)). It allows us to evaluate exergy destruction within a unit by knowing its inputs/outputs of exergy, as well as exergy accumulations within the unit (the latter was only relevant for storage units). It was assumed that all streams exchanging heat remain at a constant temperature. This allowed us to use Equation (2a) in order to evaluate the exergy associated with the heat stream. In order to keep thermodynamic consistency in the study, the dead-state temperature (T_0) was kept at a constant value [44]. The exergy associated with work equals work, as its exergy factor is 1 (2b).

$$\Delta t \cdot \sum \left(\dot{E}^{in} \right) = \Delta t \cdot \left[\sum \left(\dot{E}^{out} \right) + \dot{E}^{D} \right] + \Delta E^{u} \quad (2)$$

$$\text{With } \dot{E}^{q} = \dot{Q} \cdot \left(1 - \frac{T_0}{T_q} \right) \quad (2a)$$

$$\dot{E}^{W} = \dot{W} \quad (2b)$$

The input parameters and unit-by-unit exergy balances are summarized in Tables S3 and S4 (Supplementary Materials), respectively. The exergy model was built on the following hypotheses:

- Potential and kinetic exergy are neglected.
- The heat production process by the heat supplier has a constant exergetic efficiency.

The economic and exergoeconomic models were built on cost flow balances (Equation (3)). These balances establish that the revenue from selling a unit's product ($\dot{C}^{P}$) must cover the unit's fuel costs ($\dot{C}^{F}$), investment amortization ($\dot{Z}^{CI}$), and operation and maintenance costs ($\dot{Z}^{OM}$). The costs of investment amortization were annualized by means of the capital recovery factor, or *CRF* (Equation (3a)). Operation and maintenance costs are typically assumed as a fraction of the investment amortization costs (Equation (3b)). The *CRF* (Equation (3c)) allows us to determine the equivalent yearly cash flows that a project should generate in order to compensate for present investments at a certain return rate (i) and throughout the project's economic life (n).

$$\dot{C}^{F} + \dot{Z}^{CI} + \dot{Z}^{OM} = \dot{C}^{P} \quad (3)$$

$$\dot{Z}^{CI} = Z^{CI} \cdot CRF \tag{3a}$$

$$\dot{Z}^{OM} = \dot{Z}^{CI} \cdot c_k^{OM} \tag{3b}$$

$$CRF = \frac{i \cdot (1+i)^n}{(1+i)^n - 1} \tag{3c}$$

The input data for the economic and exergoeconomic models, along with unit-by-unit cost flow balances, are provided in Tables S5 and S6 (Supplementary Materials), respectively.

2.3.2. Multi-Stakeholder Model

The multi-stakeholder model accomplishes two main functions. The first is defining the performance indicators for each of the actors, as a function of their perimeter of responsibility (considering possible ownership of the new equipment). These perimeter-dependent definitions concern the criteria presented above, i.e., energy, exergy, economic, and exergoeconomic. The second function of this model is to establish the stakeholders' tolerance to sub-optimal solutions (for them) in order to facilitate the feasibility of the overall project. This tolerance was defined as a percentage deviation from each mono-criterion and mono-stakeholder optimal solution. In addition, NO-GO thresholds were considered for some criteria of some stakeholders, including relaxation possibilities on those thresholds for the sake of the project's feasibility.

Perimeter-Dependent Performance Indicators

The preceding sub-section introduces a series of unit-by-unit balances that stay the same in each assessment. However, the decisional indicators change depending on who is the owner of the heat recovery system.

The energy criterion was assessed in all instances as a heat coverage rate but used a different reference point for each stakeholder. The exergy indicator refers to the overall exergy destruction, but its contributions depend on the frontiers of the socio-energetic node under study and, thus, on the units within it (see Table 1). The same consideration is applicable to the exergoeconomic indicator based on overall exergy destruction costs. The economic assessment used the net present value (NPV) as an indicator, but the investments and the economic frontiers differ for each stakeholder as a function of the scenario considered.

Table 2 shows how each indicator is defined for each stakeholder and if it is the owner of the WHRS or not. By definition, the stakeholders named THIRD and CONSORTIUM may only exist as owners of the equipment. The energy indicator for both the LNCMI and the CCIAG is the same, independent of whether they are owners or not. Further details on the chosen indicators are given in the following paragraphs.

For the LNCMI, recovering as much waste heat as possible is a priority energy-wise. The indicator named Recovery Factor *(RF)* quantifies that objective. Exergy-wise, their objective is to minimize overall exergy destruction within their perimeter of responsibility. That perimeter comprises their laboratory and the waste heat dissipation, plus the WHRS if they are the owner of it. The same applies exergoeconomic-wise but involves the costs of exergy destruction instead. Economy-wise, the non-owner LNCMI would sell waste heat to the WHRS's owner, thus aiming at making some profit ($C_{WHRS}^{Q,in}$). If the LNCMI is the owner, they would sell upgraded heat to the CCIAG. Revenues should compensate for the investment, operation and maintenance, and electricity consumption, plus the price that the LNCMI estimates for their waste heat.

The CCIAG's objectives are similar to those of the LNCMI, but their socio-energetic node is different. The Coverage Factor *(CF)* assesses the WHRS's coverage of the network's heat needs. Exergy destruction and exergy destruction costs are assessed on the heat

production plant, the network, and its substations, plus the WHRS if it is the CCIAG's property. Economy-wise, the CCIAG's profits from this project come from fuel savings with respect to the reference scenario. From these profits, they must subtract the cost of acquiring upgraded heat at 85 °C. If they are not the owner, these costs are simply the purchase price fixed by the owner. If they are the owner, the costs include investment, operation, maintenance, electricity to run the WHRS, and the purchase price of LNCMI's waste heat.

Table 2. Definition of the optimization criteria as a function of the system's ownership.

Stakeholder	Criterion	Indicator (Owner)	Indicator (Not Owner)
LNCMI	ENER	$RF = \frac{Q_{WHRS}^{in}}{Q_{WH}}$	
	EXER	$Ex_{LNCMI}^{D,\,TOT} = Ex_{LAB}^{D} + Ex_{TES}^{D} + Ex_{HP}^{D} + Ex_{DISS}^{D}$	$Ex_{LNCMI}^{D,\,TOT} = Ex_{LAB}^{D} + Ex_{DISS}^{D}$
	EXEC	$C_{LNCMI}^{D,\,TOT} = C_{EXP}^{D} + C_{TES}^{D} + C_{HP}^{D} + C_{DISS}^{D}$	$C_{LNCMI}^{D,\,TOT} = C_{LAB}^{D} + C_{DISS}^{D}$
	ECON	$NPV_{LNCMI} = \frac{C_{WHRS}^{Q,out} - C_{WHRS}^{elec,in} - C_{WHRS}^{Q,in} - \dot{Z}^{OM} - \dot{Z}^{CI}}{CRF}$	$NPV_{LNCMI} = \frac{C_{WHRS}^{Q,in}}{CRF}$
CCIAG	ENER	$TDC = \frac{Q_{WHRS}^{out}}{Q_{DHN}^{in,\,tot}}$	
	EXER	$Ex_{CCIAG}^{D,\,TOT} = Ex_{TES}^{D} + Ex_{HP}^{D} + Ex_{HS}^{D} + Ex_{DHN}^{D} + Ex_{SST}^{D}$	$Ex_{CCIAG}^{D,\,TOT} = Ex_{HS}^{D} + Ex_{DHN}^{D} + Ex_{SST}^{D}$
	EXEC	$C_{CCIAG}^{D,\,TOT} = C_{TES}^{D} + C_{HP}^{D} + C_{HS}^{D} + C_{DHN}^{D} + C_{SST}^{D}$	$C_{CCIAG}^{D,\,TOT} = C_{HS}^{D} + C_{DHN}^{D} + C_{SST}^{D}$
	ECON	$NPV_{CCIAG} = \frac{\left(C_{HS,REF}^{En,in} - C_{HS}^{En,in} - C_{WHRS}^{elec,in} - C_{WHRS}^{Q,in} - \dot{Z}^{OM} - \dot{Z}^{CI}\right)}{CRF}$	$NPV_{CCIAG} = \frac{\left(C_{HS,REF}^{En,in} - C_{HS}^{En,in} - C_{WHRS}^{Q,out}\right)}{CRF}$
THIRD	ENER	$VF = \frac{Q_{WHRS}^{out}}{Q_{WHRS}^{in}}$	N/A
	EXER	$Ex_{THIRD}^{D,\,TOT} = Ex_{TES}^{D} + Ex_{HP}^{D}$	N/A
	EXEC	$C_{THIRD}^{D,\,TOT} = C_{TES}^{D} + C_{HP}^{D}$	N/A
	ECON	$NPV_{THIRD} = \frac{\left(C_{WHRS}^{Q,out} - C_{WHRS}^{Q,in} - C_{WHRS}^{elec,in} - \dot{Z}^{OM} - \dot{Z}^{CI}\right)}{CRF}$	N/A
CONSORTIUM	ENER	$RACF = RF \cdot CF$	N/A
	EXER	$Ex_{CSRT}^{D,\,TOT} = Ex_{LNCMI}^{D,\,TOT} + Ex_{CCIAG}^{D,\,TOT} + Ex_{TES}^{D} + Ex_{HP}^{D}$	N/A
	EXEC	$C_{CSRT}^{D,\,TOT} = C_{LNCMI}^{D,\,TOT} + C_{CCIAG}^{D,\,TOT} + C_{TES}^{D} + C_{HP}^{D}$	N/A
	ECON	$NPV_{CSRT} = \frac{\left(C_{HS,REF}^{En,in} - C_{HS}^{En,in}\right) - C_{WHRS}^{elec,in} - \dot{Z}^{OM} - \dot{Z}^{CI}}{CRF}$	N/A

The stakeholder named THIRD represents an external party that is interested in owning the WHRS. Accordingly, this stakeholder was only modeled as an owner, since otherwise they would not be involved in the project. Energy-wise, an important thought for the THIRD stakeholder is that electricity is always available, while waste heat is intermittent. Accordingly, the Valorization Factor *(VF)* quantifies the ratio of output heat to input heat, and it should be maximized. Exergy-wise and exergoeconomic-wise, their objectives are the same as those of other stakeholders, but the perimeter reduces to just the WHRS. Economy-wise, this stakeholder buys waste heat from the LNCMI and sells upgraded heat to the CCIAG in order to recover the investment in the WHRS. This imposes a double constraint on this stakeholder, who must negotiate the costs of both input and output heat.

The CONSORTIUM represents an agreement between the LNCMI and the CCIAG. Accordingly, its indicators account for the objectives and perimeters of both stakeholders. Energy-wise, the Recovery and Coverage Factor *(RACF)* is the product of the *RF* and *CF* presented in the previous paragraphs. The objectives of minimizing exergy destruction and exergy destruction costs comprise all the LNCMI's and CCIAG's units, plus the WHRS. Economy-wise, the project's benefits correspond to the CCIAG's savings on primary fuel. The CCIAG shares those benefits with the consortium. Additionally, the LNCMI does not claim a cost for their waste heat since they are part of the consortium. By definition, this consortium may only exist as an owner, since the sole purpose to form it would be to acquire the new equipment as shared value.

The results for all criteria in each scenario are shown in Table A1 (in Appendix A).

Stakeholder's Tolerance and Relaxation Possibilities

The performance indicators described in the previous subsection will most likely suggest divergent optimal designs. During negotiations, it is improbable that any stakeholder will manage to convince the others in favor of their own optimal design. A compromise will be necessary. This subsection introduces parameters for assisting negotiations. The purpose is not to delve into multi-stakeholder dynamics, which would require expertise in the social sciences. Rather, the objective is to render the mathematical model sensitive to such dynamics. The stakeholders' capacity to search for a compromise was modeled here by means of two concepts:

- Tolerance, understood as a stakeholder's capacity to accept a design that is inferior to the optimal design that they would prefer, from the standpoint of a specific criterion.
- Relaxation, understood as a stakeholder's capacity to decrease or eventually drop a constraint of theirs, potentially increasing the project's feasibility for themselves and for other stakeholders.

It was assumed that a stakeholder's tolerance and relaxation capacity are independent of who is the owner of the prospective system. It was also assumed that the stakeholders' decisions would be based on the rational, quantifiable indicators presented in the previous subsection. Table 3 shows the tolerance limits, NO-GO criteria, and relaxation possibilities per stakeholder and optimization criterion. A NO-GO is a threshold that, if violated, forces a solution to be discarded. Detailed explanations follow in the next paragraphs.

Table 3. Stakeholders' tolerance and relaxation possibilities, shown criterion per criterion.

Stakeholder	Criterion	Tolerance			NO-GO	Relaxation
		Light	Moderate	Heavy		
LNCMI	ENER	<5%	<10%	>10%	N/A	N/A
	EXER	<10%	<25%	>25%	if $\Delta(Ex^D) > 0$	Disregard NO-GO
	ECON	<25%	<50%	>50%	if NPV < 0	Cut C_WH by 50%
	EXEC	<10%	<25%	>25%	if $\Delta(C^D) > 0$	Disregard NO-GO
CCIAG	ENER	<10%	<25%	>25%	N/A	N/A
	EXER	<10%	<25%	>25%	if $\Delta(Ex^D) > 0$	Disregard NO-GO
	ECON	<5%	<10%	>10%	if NPV < 0	Disregard Z_NETW by 50%
	EXEC	<10%	<25%	>25%	if $\Delta(C^D) > 0$	Disregard NO-GO
THIRD	ENER	<25%	<50%	>50%	N/A	N/A
	EXER	<25%	<50%	>50%	N/A	N/A
	ECON	<5%	<10%	>10%	if NPV < 0	N/A
	EXEC	<25%	<50%	>50%	N/A	N/A
CONSORTIUM	ENER	<5%	<10%	>10%	N/A	N/A
	EXER	<10%	<25%	>25%	if $\Delta(Ex^D) > 0$	Disregard NO-GO
	ECON	<5%	<10%	>10%	if NPV < 0	N/A
	EXEC	<10%	<25%	>25%	if $\Delta(C^D) > 0$	Disregard NO-GO

The LNCMI engages in this project to reduce their waste heat emissions. This can be understood as an energy-focused motivation, with underlying ecological notions. Accordingly, the tightest tolerance of this stakeholder was supposed to be on the energy indicator (ENER). More than 10% of underperformance with respect to their energy-optimal design was understood as heavy tolerance. The exergy (EXER) and exergoeconomic (EXEC) criteria are less widely known by industrial partners, but in waste heat recovery, they can be correlated to ecological advantage. Therefore, the heavy tolerance threshold was assumed as 25%. The economic criterion (ECON) was assumed as the least important for this stakeholder since: (1) the LNCMI is a scientific organization, and its waste heat is a by-product; (2) they currently dissipate that waste heat at zero profit. Thus, the heavy tolerance threshold was set at 50%.

Since the CCIAG is a commercial organization, its economic criterion was given the tightest tolerance (a heavy threshold of 10%). The other criteria were assumed to be less important. Still, an operator of a district energy network is sensitive to energy efficiency, renewable sources, and, in the case of district heating, the quality (temperature) of heat and, thus, its exergy. Therefore, the ENER, EXER, and EXEC criteria were given a heavy tolerance threshold of 25%.

The THIRD was modeled as an external party that seeks profit, with an accordingly tight tolerance on the economic criterion (a heavy threshold of 10%). The rest of the criteria were given a large tolerance (a heavy threshold of 50%).

The CONSORTIUM combines the priorities of both the LNCMI and the CCIAG. Accordingly, for each criterion, the most constraining tolerance was selected among both actors. The result is tight tolerance (heavy threshold of 10%) for the energy and economic criteria, and medium tolerance (heavy threshold of 25%) for the exergy and exergoeconomic criteria.

Some NO-GO thresholds were also considered. Economy-wise, for all stakeholders, if the NPV is negative, then the project is a NO-GO. Exergy-wise, if the new system causes an increase in total exergy destruction within a stakeholder's perimeter with respect to the reference scenario, then that design is a NO-GO. The same consideration was applied in the exergoeconomic criterion, although for exergy destruction costs. These considerations were not applied to the THIRD, as it has no exergy destruction in the reference scenario.

It was assumed that the LNCMI would accept relaxing (dropping) the price of their waste heat by 50%. Since the LNCMI's waste heat is currently dissipated, with zero revenue, it should not be an issue for them to be flexible on its price, as long as they make some profit from it.

It was assumed that the CCIAG would accept relaxing (disregarding) the amortization requirements on their existing facilities by 50%. In the current, real negotiations for this project, the CCIAG marked a maximum buying price for the valorized heat. That maximum corresponds to the price of the heat produced by their own production plants and is, of course, lower than the selling price to end-users. This means that the CCIAG demands that the project respect its current amortizations on the district network. Should that constraint be relaxed, the CCIAG would be able to buy the heat at a higher price, thus facilitating the project's feasibility for the system's owner (be it another stakeholder or themselves).

One general relaxation was assumed for all stakeholders: that exergy- and exergoeconomic-related NO-GOs may be disregarded. In the current world situation, exergy analysis is a useful tool for comparing the thermodynamic performance of different systems. This allows us to select the most promising ones on a relative basis. However, defining $\Delta Ex^D \leq 0$ or $\Delta C^{ExD} \leq 0$ as feasibility requirements for a project is a strong condition, like the $NPV \geq 0$ requirement. This application of exergy would be somewhat of an innovation, and it stems from a research question: How might exergy re-shape energy projects if it was just as precisely defined as economy? The above are not only reasons for modeling such NO-GOs but also for countering them with relaxation possibilities.

3. Results and Discussion

3.1. Stakeholder–Stakeholder Interactions (Cross-Analysis Matrix)

This subsection aims to identify the NO-GO thresholds infringed by otherwise optimal designs in order to facilitate agreements and relaxations. To that end, a cross-analysis matrix is proposed for clear visualization of the information.

Figure 3 presents the "cross-analysis matrix" for Scenario 1. It shows each optimal mono-criterion solution in a scenario and evaluates them from the viewpoint of other stakeholders and their decision criteria. The main purpose of this matrix is to spot which criteria render a mono-criterion optimum non-feasible. Its secondary purpose is to display the level of agreement between stakeholders.

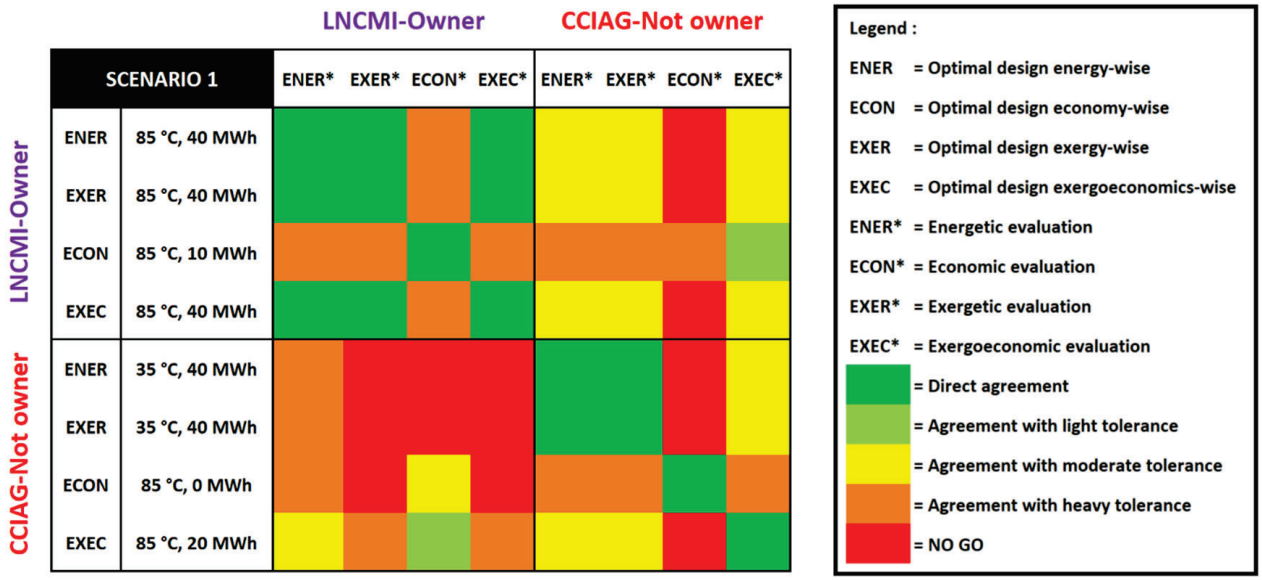


Figure 3. Cross-analysis matrix for Scenario 1 (where LNCMI is the owner of the waste heat recovery system).

Each row represents an optimal design that is preferred by a stakeholder according to a certain criterion. Each column displays the evaluation of the mono-criterion and stakeholder-optimal designs, from the viewpoint of each stakeholder, shown criterion by criterion. In each intersection between a row and a column, a colored cell indicates the possibilities for agreement (refer to the legend), according to the rules presented in Table 3. If a design does not encounter any red cells, that design is feasible. Note that with this layout, the matrix's downward diagonal is always green, but the matrix's content is not symmetrical with respect to that diagonal. Each colored cell has its own unique meaning.

Intersections between stakeholders define the quadrants within the matrix. The sizes of those quadrants are proportional to the number of criteria per stakeholder. Quadrants that confront two different stakeholders may be seen as "negotiation quadrants". Those are the most important quadrants in the matrix since they will support negotiations. Quadrants that confront a stakeholder with I, i.e., quadrants on the downward diagonal, are rather informative. They give an idea of how complex it may be for stakeholders to decide on a multicriteria optimum for themselves. In general, the greener the matrix, the more favorable the scenario.

The matrix for Scenario 1 (Figure 3) indicates that the optimal designs preferred by the CCIAG encounter very difficult negotiations (see the lower-left quadrant). Most of the designs infringe NO-Gos or require heavy tolerance from the LNCMI. The {85 °C, 20 MWh} design is feasible, but it represents an economic NO-GO for the CCIAG itself. A specific conclusion would be that the CCIAG's aspirations are difficult to meet in this scenario.

Conversely, the optimal designs preferred by the LNCMI require slightly easier negotiations (upper-right quadrant). They require a generally lesser tolerance from the CCIAG, although most encounter an economic NO-GO. In addition, in this scenario, the LNCMI is meant to be the system's owner; therefore, their preferences should be prioritized. Without relaxations by the stakeholders, the {85 °C, 10 MWh} design is the only feasible solution.

The conclusions for Scenario 1 (without relaxations) would be as follows. First, only the {85 °C, 10 MWh} design is feasible. Second, the LNCMI's preferences have better chances of prevailing after negotiations. Third, the biggest limitations are exergy- and exergoeconomic-related for the LNCMI and are economy-related for the CCIAG. Relaxations are needed to facilitate a technical compromise. Fourth, the LNCMI prefers designs at 85 °C if they are the owner of the WHRS.

Figure 4 presents the cross-analysis matrices for the other scenarios. The most evident conclusion is that Scenario 4 (i.e., a consortium) is the most feasible scenario. It does not encounter any NO-GO. Another conclusion is that in Scenarios 2 and 3, none of the mono-criterion preferences are feasible. The {85 °C, 10 MWh} solution is feasible, but it is not mono-criterion optimal and, thus, is not displayed in the matrix. It can also be observed that none of the solutions at 50 °C are represented in either of the matrices, which means that they are not very promising.

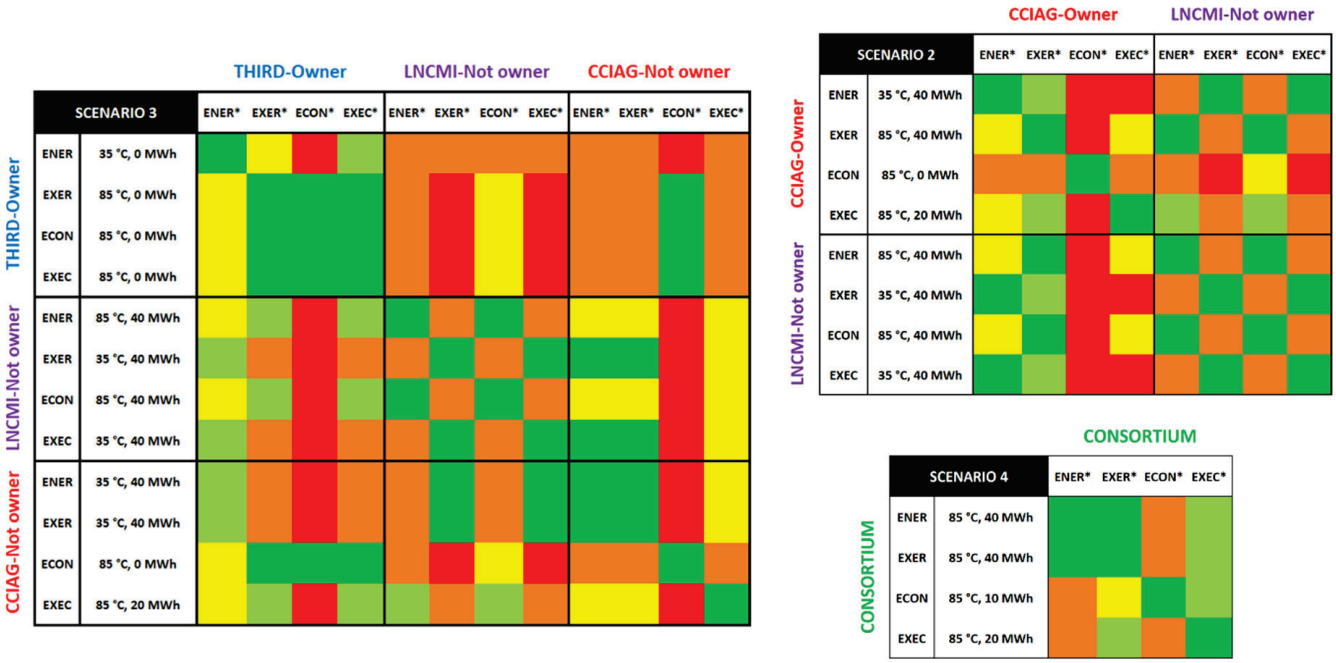


Figure 4. Cross-analysis matrix for Scenarios 2, 3, and 4. The legend is the same as that for Figure 3.

The following subsection displays the matrices after relaxations and analyzes the influence of each type of relaxation.

3.2. Relative Optimality (Multicriteria Radar)

Figure 5 presents the multicriteria evaluation (energy, exergy, economy, and exergoeconomics) of the different technical designs in each ownership scenario. The data are represented in the form of a radar chart.

Each angular position within the chart represents one performance criterion for one stakeholder in one scenario. In each scenario, the owner of the technical system is highlighted with a yellow star. The radial axis represents relative optimality, wherein the values of 1 and 0 correspond to the most and least efficient designs, respectively. Relative optimality is assessed for each criterion and amongst all available designs, before and after relaxations. Only feasible designs are represented, i.e., those that do not violate any NO-GO

from the stakeholders. Designs represented with continuous lines are optimal for at least one criterion. Those represented with dotted lines are not; therefore, they are dominated by other designs. For every criterion, there exists at least one optimal design (value = 1). Mono-criterion optimums not displayed in Figure 5 are unfeasible, due to NO-GO violation on another criterion (see Table A1 in Appendix A). Some of those unfeasible optimums are accessible through relaxations, as Section 3.3 will later prove.

Out of 15 designs analyzed, just 8 are feasible. Of those 8 designs, 7 are feasible if, and only if, a multi-stakeholder consortium is built (the "CSRT" scenario). This approach enables more designs because it enlarges the socio-energetic node. For example, a design may be locally non-feasible for the LNCMI or the CCIAG but may be feasible for the consortium as a whole. It is concluded that a joint consortium is the approach that most contributes to the project's feasibility prior to relaxations. It should be noted, however, that agreeing to form a consortium is, in itself, a sort of relaxation.

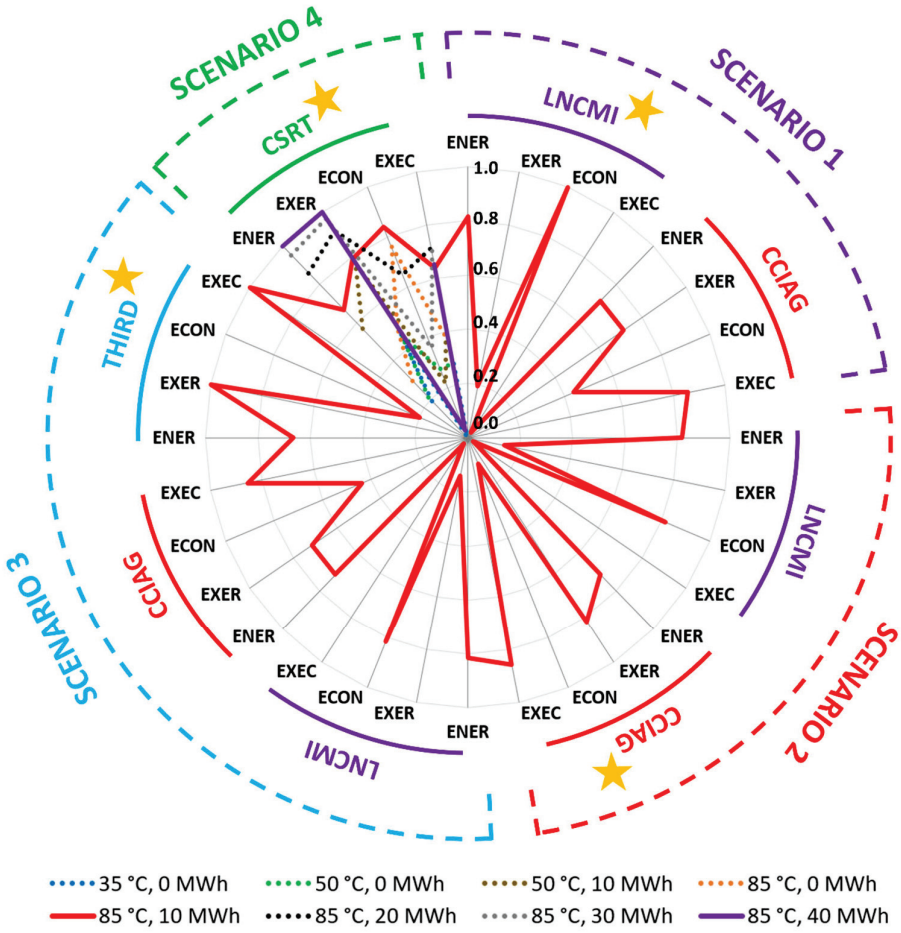


Figure 5. Multi-scenario, multi-stakeholder, and multi-criteria radar chart displaying the relative optimality of different designs. Only feasible designs are displayed. Optimal mono-criterion designs are plotted with continuous lines, the rest are shown with dotted lines. The yellow star indicates the owner of the equipment in each scenario.

Only the {85 °C, 10 MWh} design is feasible without a consortium. In fact, this design is feasible in any scenario. It may be concluded that it is the most versatile design. Nevertheless, its overall performance may be insufficient for agreement. In all scenarios other than "CSRT", this design has serious shortcomings. Those are exergy-related for the LNCMI and are economy-related for the other stakeholders. The feasibility of the project will depend on the weight (importance) that each stakeholder gives to each criterion.

All designs that involve a waste heat temperature of 85 °C are feasible in at least one scenario. Furthermore, all mono-criterion optimums that are feasible are granted by a design at 85 °C. It is, thus, concluded that 85 °C is the most promising design temperature prior to relaxations. In addition, the radar chart allows us to check the influence of storage capacity at 85 °C in Scenario 4, since all designs are feasible in this scenario at this temperature. Increasing storage capacity from 0 MWh to 10 MWh improves performance in all criteria. After that, the energy and exergy indicators improve consistently with storage capacity, while the economic indicator drops consistently. The exergoeconomic indicator reaches its optimum at 20 MWh and decreases past that point.

As expected, no design meets all mono-criterion optimums. This is due to the large variety of scenarios involved, which justifies the need for this type of diagram. The definitive solution would depend on the weight attributed to each criterion. The search for a definitive solution is not covered in this article, but Section 3.4 discusses it theoretically. Assuming the same weight for all criteria, the radar chart suggests {85 °C, 10 MWh} and {85 °C, 20 MWh} as the most balanced designs.

The paragraphs above have illustrated how to build, read, and interpret the radar charts. The authors think that this tool may help project leaders and policymakers in deciding on technical designs when non-technical specialists are involved.

3.3. Effects of Stakeholders' Flexibility

Figure 6 presents the matrices for Scenarios 1, 2, and 3 after applying the relaxations described in Table 3. In each matrix, the new mono-criteria optimums are highlighted in ochre. Scenario 4 is not displayed because its matrix stayed the same as in Figure 4.

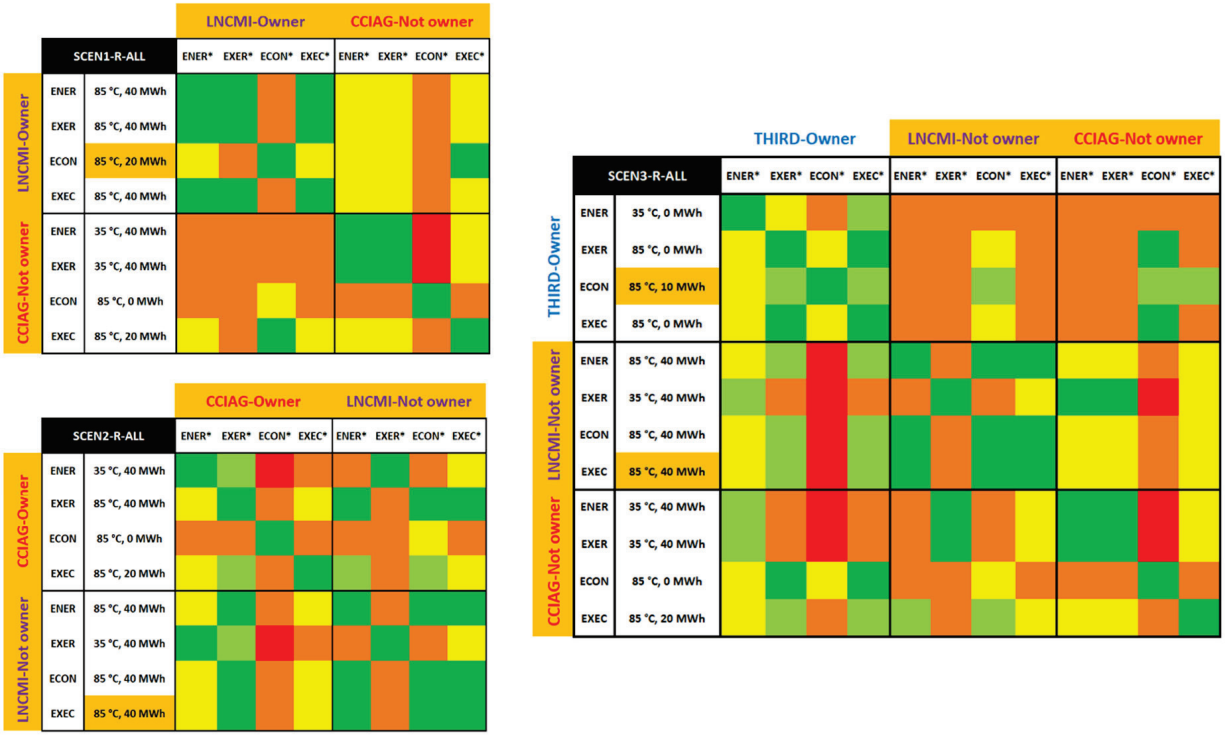


Figure 6. Cross-analysis matrices for Scenarios 1 to 3, after relaxations by the stakeholders. The legend is the same as that in Figure 3. Scenario 4 is not displayed because its matrix remains the same as it was before the relaxations (see Figure 4).

After the relaxations, many more solutions become feasible. The exergy-related NO-GOs have disappeared. The economy-related NO-GOs persist, but their effects have been mitigated. In fact, all designs that infringe the economic NO-GO imply maximal storage

capacity (40 MWh). It is also noticeable that solutions at 50 °C are still not promising regarding mono-criteria, even after the relaxations.

For a more detailed analysis, Figure 7 presents the separate effects of the LNCMI's and CCIAG's relaxations on Scenario 1. As a reminder, the relaxations include: dropping the price of LNCMI's waste heat by 50%; ignoring CCIAG's amortization needs on the existing network by 50%; and disregarding the exergy- and exergoeconomic-related NO-GO thresholds for both stakeholders.

The LNCMI's relaxations seem more impactful. They unlock all exergy-related NO-GOs and one economic NO-GO. Moreover, they mitigate some economy-related tolerance requirements for both them and the CCIAG. Meanwhile, the CCIAG's relaxations do not seem very impactful. They only unlock a NO-GO with the {85 °C, 20 MWh} solution, which is also unlocked by relaxation by the LNCMI. That seems to suggest that relaxations from upstream stakeholders might have a greater impact than those of downstream stakeholders. However, there are insufficient results to assert, let alone generalize such a claim. Since further investigation is needed, the authors are planning on prospective works on the upstream/downstream effects of actors and their choices. Still, some economic NO-GOs can only be unlocked through both relaxations. That suggests that the feasibility of multi-stakeholder projects should be a collective effort. Synergies between stakeholders and their decisions should be maximized. In general, the stakeholders' tolerance can unlock more and better solutions.

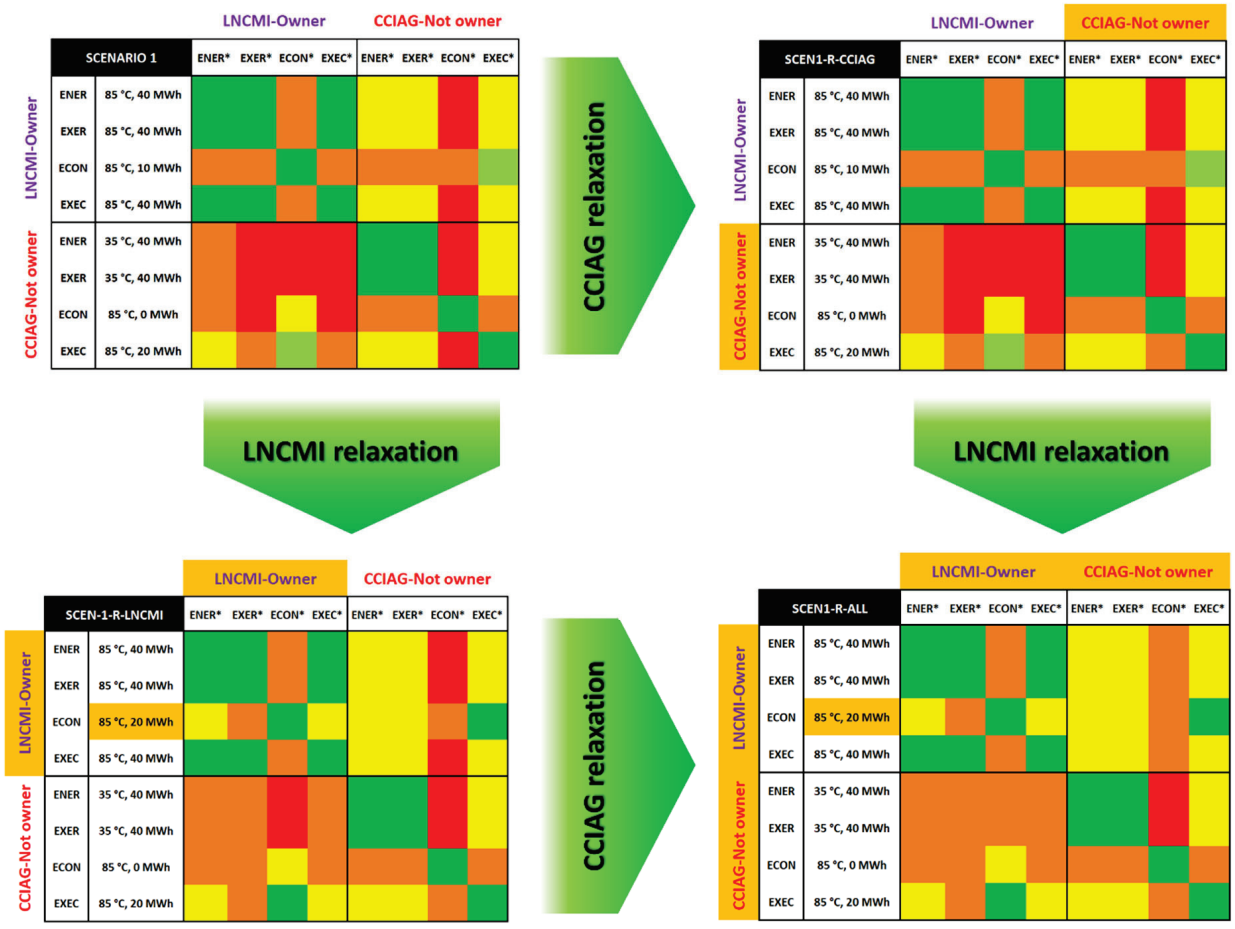


Figure 7. Detailed effects of stakeholders' relaxations on Scenario 1. The legend is the same as that in Figure 3.

This study considered stakeholders' flexibility in terms of relaxation on criteria and certain prices. However, other types of flexibility can be investigated. For instance, the LNCMI has a flexible energy profile, i.e., they can adapt their yearly schedule of experi-

ments [45,46]. This way, they can match their heat rejection more closely with the district's heat needs [37]. The LNCMI's energy flexibility is currently a subject under investigation by the authors, along with some of their peers.

Figure 8 presents the radar chart after relaxations by the stakeholders. The scenarios, stakeholders, criteria, and axes are the same as those in Figure 5, but the relaxations described in Table 3 have also been applied. This discussion focuses on the effects of relaxations.

Overall, relaxations increased the number of promising designs and the possibilities for agreement compared to the base case (Figure 5). The most remarkable example is the {85 °C, 20 MWh} design. It went from the suboptimal and only feasible choice in Scenario 4 (Figure 5) to pluri-criterion optimal and feasible in any scenario (Figure 8). Moreover, if the whole radar chart is scouted, this design is now the most efficient one in 17 out of 32 instances, 6 of which are mono-criterion optimums. Thanks to relaxations, this design has now become the most promising choice.

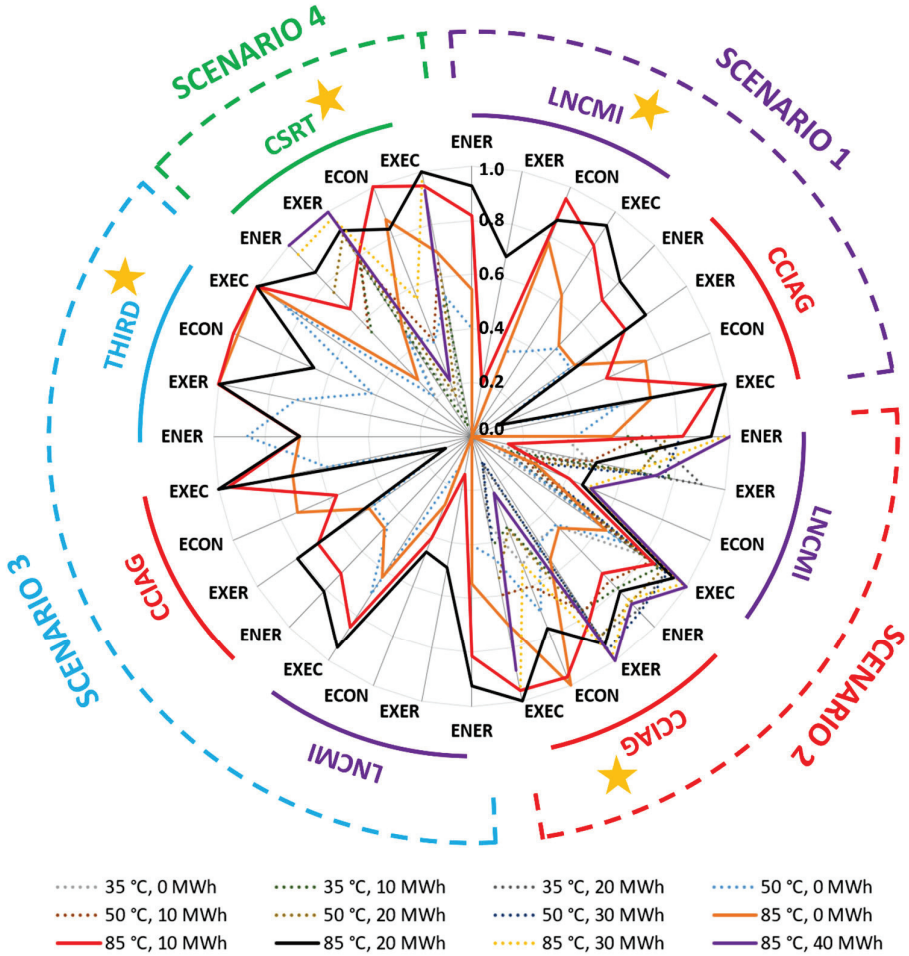


Figure 8. Multi-scenario, multi-stakeholder, and multi-criteria radar chart after relaxations by the stakeholders. Only feasible designs are displayed. Designs plotted with continuous lines are mono-criterion-optimal (value = 1) in at least one instance. Designs plotted with dotted lines are never mono-criterion-optimal, and are, therefore, dominated by other solutions. The yellow star indicates the owner of the equipment in each scenario.

Meanwhile, the {85 °C, 10 MWh} design was relegated to the second-most promising choice. It went from being the most efficient and, often, the only feasible design (Figure 5) to only standing out in 4 out of 32 instances. It showed mixed effects from relaxations: although most of its performances rose, it was outperformed by newly feasible designs. Its economic indicators dropped for the LNCMI due to waste heat price reduction but rose for

the rest of the actors, thanks to this relaxation. This design can still outperform the {85 °C, 20 MWh} design if economic criteria are given more weight than other criteria.

Relaxations unlocked feasibility for four more designs: {35 °C, 10 MWh}, {35 °C, 20 MWh}, {50 °C, 20 MWh}, and {50 °C, 30 MWh}. They also extended the feasibility of the already identified designs to new scenarios. However, most of the newly feasible solutions were dominated by the two favorites: ({85 °C, 10 MWh} and {85 °C, 20 MWh}).

In light of the discussion above, the following ranking of solutions is proposed. Assuming equal weights for all criteria, the most promising approach is Scenario 4 with the {85 °C, 20 MWh} design. Besides this, the {85 °C, 20 MWh} design is the most promising multicriteria candidate in all scenarios. The {85 °C, 10 MWh} design is a promising alternative, especially if the economic criterion is given more weight than the others. These two designs give a decent range of options for agreement between stakeholders, and the feasibility of the project is more likely to be secured than before relaxations were made. In Scenario 4, the {85 °C, 40 MWh} design might be the favorite if the energy and exergy indicators are given more weight than the others.

Besides the absolute and relative performances, the radar chart yields three important pieces of information. First, the density of the solutions points out the most favorable scenarios for reaching an agreement. In this case, these are Scenarios 2 and 4, as they admit 12 and 9 solutions, respectively, out of 15 possible solutions. Second, the flexibility of the different solutions can also be assessed. In this case, the {85 °C, 0 MWh}, {85 °C, 10 MWh}, {85 °C, 20 MWh}, and {50 °C, 0 MWh} solutions are the most flexible, as they are feasible in any scenario. Third, the distances from the outermost radius tell us that there is room available for further improvement. In this case, 14 monocriterion optimums have been unlocked out of 32 possible optimums.

3.4. Toward an Iterative Decision Procedure

The tools and methods presented in this article belong with the negotiation support algorithm presented in Figure 2. The algorithm starts by identifying the stakeholders involved in the project, the possible designs for the energy system, and the possible scenarios of ownership (Step 0). Then, the system's operating performance is optimized for each design (Step 1). In this study, this step was performed by means of OMEGAlpes, an open-source MILP tool (mixed-integer linear programming).

The choice of an energy dispatch optimizer for Step 1 is open. While OMEGAlpes was used here, any other dispatch optimizer could have been used: non-linear (NLP, MINLP), energy management systems (EMS), etc. The only conditions are: (1) that it be state of the art and verified (through peer review); (2) that it considers all the optimization variables, objective functions, and performance indicators necessary to make decisions. Moreover, the robustness of this multi-stakeholder methodology depends on the underlying hypotheses and limitations of the energy dispatch optimizer. For that reason, prospective studies are planned by the authors to analyze the sensitivity of this multi-stakeholder method to other dispatch optimizers.

With the results given by OMEGAlpes, the analysis presented in this article is applied (Step 2). With the radar chart and the matrices, the project enters preliminary negotiations (Step 3) to verify whether at least one scenario and design respects all of the NO-GO criteria. The radar chart indicates whether more interesting solutions can be unlocked through relaxations, and the matrices point out the kinds of relaxations that would be necessary.

The assumption of stakeholders' tolerance and relaxation capacities is a simplification with respect to real-world negotiation complexities. A stakeholder's capacity to accommodate sub-optimal solutions (in terms of their interests) can be a very dynamic and volatile variable. It will depend on quantitative and qualitative factors, as well as on interactions with other stakeholders. The method described in this article is just a preliminary effort to bridge the gap between technical modeling and human decision-making. The goal, rather than governing negotiations through technical modeling, is to make technical models sensitive, adaptive, and responsive to human decisions. The authors' perspectives include

field validation of the methodology. This field validation will rely on interviews for an accurate representation of every stakeholder's criteria, objectives, and tolerance.

Past Step 3, if more than one feasible design/scenario does exist, the decision support stage begins (Step 4). At this point, stakeholders must decide on the weight and tolerance thresholds that they will allocate to each criterion. A multicriteria decision analysis (MCDA) is then possible with any state-of-the-art method (for instance, ELECTRE [47]). These methods may be computationally costly if many alternatives are available, hence the importance of discarding non-feasible designs upon preliminary negotiations (at the end of Step 2). The results from the MCDA support the final negotiation stage (Step 5). At this point, stakeholders must select one design that suits their aspirations, oftentimes through a compromise.

Both preliminary and final negotiations are opportunities for redefining the project, if necessary. This auxiliary procedure may include changes in the ownership scenarios (Step 0), the relaxation of operational constraints (Step 1), the relaxation of NO-GO criteria (Step 2), or changes in criteria weights and thresholds (Step 4). If, despite all redefinitions, relaxations, and negotiations, the stakeholders do not agree on the project's feasibility (Step 3) or optimality (Step 5), then the project will eventually be discarded.

This decision algorithm has two main innovations: (1) it accounts for the system's operating life already in the design phase; (2) it is sensitive and adaptive to the stakeholders' decisions.

4. Conclusions

This article investigated the preliminary implementation of a methodology to support the multicriteria technical conception of an energy project in a multi-stakeholder context. The methodology can consider various decision criteria with different weights, depending on the stakeholder. Then, the project's operation is simulated over a set time period and a multicriteria and multi-scenario analysis is performed. The main innovations are: the multi-stakeholder definition of performance indicators, including the possible relaxations and tolerances; a multi-scenario analysis depending on equipment ownership; and the disposition of visual tools to facilitate negotiations between decision-makers. Thus, the methodology is sensitive, adaptive, and responsive to stakeholders' choices.

This article illustrates the application of this methodology to a real case study, with a special focus on how relaxations of stakeholders' preferences can facilitate the success of a project. The study relied on the use of a MILP optimization tool called OMEGAlpes to optimize yearly management of the energy flows, but any other optimizer could have been used as long as it is verified and state of the art. On top of the optimizer's results, this methodology applies two visual tools to assist negotiations between stakeholders. The first one is a multi-criteria, multi-stakeholder, and multi-scenario radar chart that points out the most promising solutions, the non-acceptable ones, and the most flexible scenarios. The second tool is a multi-criteria and multi-stakeholder matrix that cross-analyzes the optimal technical solutions preferred by the different stakeholders and points out the most impactful relaxations.

For the study case presented in this article, it was found that relaxations by the stakeholders are highly recommendable and almost necessary. Before relaxations, in most of the scenarios, just 1 out of 15 technical designs was feasible. After relaxations, at least three designs were feasible in every scenario, including one that challenged the most suitable design pre-relaxations. It was found that relaxations on economy- and exergy-related indicators were the most impactful. The results of this article showed that the variety of stakeholders can shift the project toward different designs that, even if not ideal for some stakeholders, may be more beneficial in the bigger picture. Such designs may never be identified if some of the stakeholders or some of the criteria were excluded from the analysis.

This methodology can be extended to many types of stakeholders, as long as their involvement has consequences for the technical conception of the project. It can also be

enriched with additional criteria, as long as they can be quantified in some way. The work planned by the authors after this article is to adapt existing multi-criteria decision analysis (MDCA) procedures in order to apply them to multiple-stakeholder scenarios. After that work is conducted, all tools will be ready for the iterative algorithm described in the last subsection of this article.

The decision support tools proposed (a multi-criteria radar chart and cross-analysis matrices) provide visual negotiation aids, but their effectiveness in real-world decision-making processes needs to be empirically tested. Furthermore, the conditions and extent of relaxations by the stakeholders need careful consideration, as they significantly changed project feasibility and design preferences in this case study. They could also affect project sustainability and stakeholder buy-in. For these reasons, a prospective study is envisaged where the criteria, weights, tolerances, and relaxation capacities will be determined through direct interviews with the stakeholders. Then, the matrices and radar charts will be presented to the stakeholders for their feedback.

Supplementary Materials: The following supporting information can be downloaded at: https://www.mdpi.com/article/10.3390/en17092009/s1, Table S1: Input data for the energy model; Table S2: Formulation of the energy balance for every unit in the study case; Table S3: Input data for the exergy model (to be aggregated to that in the energy model); Table S4: Formulation of the exergy balance for every unit in the study case; Table S5: Input data for the economic and exergoeconomic models (to be aggregated to the energy and exergy models); Table S6: Formulation of the cost flow balance for every unit in the study case. Figure S1. Depiction of the socio-energetic nodes in Scenario 1, where LNCMI is the owner of the prospective energy system. Figure S2. Depiction of the socio-energetic nodes in Scenario 2, where CCIAG is the owner of the prospective energy system. Figure S3. Depiction of the socio-energetic nodes in Scenario 3, where THIRD is the owner of the prospective energy system. Figure S4. Depiction of the socio-energetic nodes in Scenario 4, where a LNCMI/CCIAG consortium is the owner of the prospective energy system.

Author Contributions: Conceptualization, J.F. and J.R.; methodology, J.F. and J.R.; software, J.F.; validation, J.R.; formal analysis, J.F. and J.R.; investigation, J.F. and J.R.; resources, J.R.; data curation, J.F.; writing—original draft preparation, J.F. and J.R.; writing—review and editing, J.F. and J.R.; visualization, J.F. and J.R.; supervision, J.R.; project administration, J.R.; funding acquisition, J.R. All authors have read and agreed to the published version of the manuscript.

Funding: The authors are grateful to the ADEME (i.e., the French Agency for Ecological Transition) for their financial support through the RETHINE project (Réseaux Electriques et Thermiques Interconnectés, grant number 1805C0001).

Data Availability Statement: Data are contained within the article (and Supplementary Materials).

Acknowledgments: The authors thank the team involved in the implementation of the optimization tool used in this study, i.e., OMEGAlpes. The authors thank the corresponding representatives and decision-makers from the CCIAG for sharing real operational data from their facilities. The authors thank the corresponding representatives and decision-makers from the French National Laboratory of High Magnetic Fields (LNCMI) for facilitating real operational data to construct the model hourly energy profile of electricity consumption used in this study; allowing us to display that hourly profile in the several published works that this case study has yielded; and for allowing us to make the data available in the OMEGAlpes documentation [34] for public use under license (ODC-By v1.0).

Conflicts of Interest: The authors declare no conflicts of interest.

Abbreviations

The following abbreviations are used in this manuscript:

ch	Chemical	in	Inlet
chrg	Heat charge of the thermal storage unit	ini	Initial
CI	Capital investment	L	Losses
cooling	Magnet's cooling process	magnets	LNCMI's high-intensity magnets
CF	Coverage factor	max	Maximal
COM	Costs of operation and maintenance	min	Minimal
COP	Coefficient of performance	mono	Mono-criterion
D	Destruction	multi	Multi-criterion
dchg	Heat discharge of the thermal storage unit	*NPV*	Net present value
DHN	District heating network	OM	Operation and maintenance
DISS	Dissipation	out	Outlet
ECON	Economic criterion	P	Product
ENER	Energetic criterion	*PEC*	Purchased equipment cost
EXER	Exergetic criterion	piping	Overall pipeline layout
EXEC	Exergo-economic criterion	*RACF*	Recovery and coverage factor
elec	Electrical	REF	Reference scenario
ex	Exergetic	*RF*	Recovery factor
exo	Exogenous	SST	Network sub-stations
F	Fuel	TES	Thermal energy storage
f	Final	*TCI*	Total capital investment
GLOB	Global	use	Useful exergy destruction
HP	Heat pump	wh	Waste heat
HS	Heat supplier	WHRS	Waste heat recovery system

Appendix A. Detailed Results for Each Technical Solution per Criteria and Scenario

Table A1 presents the results before relaxations.

Table A1. Results before relaxations, shown by scenario, stakeholder, and criterion for every possible system design.

Scenario	Stakeholder	Criterion	35 °C—Reference	35 °C—0 MWh	35 °C—10 MWh	35 °C—20 MWh	35 °C—30 MWh	35 °C—40 MWh	50 °C—0 MWh	50 °C—10 MWh	50 °C—20 MWh	50 °C—30 MWh	50 °C—40 MWh	85 °C—0 MWh	85 °C—10 MWh	85 °C—20 MWh	85 °C—30 MWh	85 °C—40 MWh
SCENARIO 1	LNCMI [OWNER]	**ENER**	0.00	0.20	0.33	0.38	0.41	0.42	0.22	0.36	0.42	0.45	0.46	0.30	0.45	0.51	0.54	0.55
		EXER	7.59	8.23	8.68	8.84	8.92	8.96	8.24	8.30	8.32	8.34	8.34	8.09	7.50	7.26	7.15	7.10
		ECON	0.00	0.02	−0.61	−1.91	−3.40	−4.98	1.12	0.99	−0.14	−1.56	−3.10	2.81	3.53	2.95	1.63	0.13
		EXEC	0.99	1.05	1.17	1.25	1.33	1.40	1.08	1.13	1.18	1.23	1.28	1.08	0.98	0.95	0.93	0.92
	CCIAG [NOT OWNER]	**ENER**	0.00	0.23	0.39	0.45	0.48	0.49	0.23	0.37	0.43	0.45	0.47	0.23	0.35	0.40	0.42	0.43
		EXER	29.8	23.2	18.7	17.1	16.2	15.8	23.4	19.2	17.7	16.9	16.5	23.1	19.8	18.5	17.9	17.6
		ECON	0.00	0.00	0.00	0.00	0.00	0.00	0.13	0.00	0.00	0.00	0.00	0.65	0.29	0.00	0.00	0.00
		EXEC	1.86	1.57	1.38	1.35	1.37	1.40	1.54	1.37	1.34	1.36	1.40	1.48	1.35	1.33	1.36	1.41
SCENARIO 2	LNCMI [NOT OWNER]	**ENER**	0.00	0.20	0.33	0.38	0.41	0.42	0.22	0.36	0.42	0.45	0.46	0.30	0.45	0.51	0.54	0.55
		EXER	7.59	7.28	7.06	6.98	6.94	6.91	7.61	7.27	7.14	7.08	7.04	8.09	7.50	7.26	7.15	7.10
		ECON	0.00	0.60	1.02	1.17	1.25	1.29	0.99	1.63	1.88	2.00	2.07	2.16	3.24	3.68	3.87	3.97
		EXEC	0.99	0.93	0.90	0.88	0.88	0.87	0.99	0.94	0.92	0.91	0.90	1.08	0.98	0.95	0.93	0.92
	CCIAG [OWNER]	**ENER**	0.00	0.23	0.39	0.45	0.48	0.49	0.23	0.37	0.43	0.45	0.47	0.23	0.35	0.40	0.42	0.43
		EXER	29.8	24.2	20.3	18.9	18.2	17.9	24.0	20.3	18.8	18.2	17.8	23.1	19.8	18.5	17.9	17.6
		ECON	0.00	−0.58	−1.63	−3.08	−4.65	−6.28	0.26	−0.63	−2.01	−3.56	−5.16	1.30	0.57	−0.73	−2.24	−3.84
		EXEC	1.86	1.69	1.65	1.72	1.82	1.93	1.62	1.56	1.60	1.69	1.78	1.48	1.35	1.34	1.36	1.41

Table A1. *Cont.*

Scenario	Stakeholder	Criterion	35 °C—Reference	35 °C—0 MWh	35 °C—10 MWh	35 °C—20 MWh	35 °C—30 MWh	35 °C—40 MWh	50 °C—0 MWh	50 °C—10 MWh	50 °C—20 MWh	50 °C—30 MWh	50 °C—40 MWh	85 °C—0 MWh	85 °C—10 MWh	85 °C—20 MWh	85 °C—30 MWh	85 °C—40 MWh
SCENARIO 3	LNCMI [NOT OWNER]	ENER	0.00	0.20	0.33	0.38	0.41	0.42	0.22	0.36	0.42	0.45	0.46	0.30	0.45	0.51	0.54	0.55
		EXER	7.59	7.28	7.06	6.98	6.94	6.91	7.61	7.27	7.14	7.08	7.04	8.09	7.50	7.26	7.15	7.10
		ECON	0.00	0.60	1.02	1.17	1.25	1.29	0.99	1.63	1.88	2.00	2.07	2.16	3.24	3.68	3.87	3.97
		EXEC	0.99	0.93	0.90	0.88	0.88	0.87	0.99	0.94	0.92	0.91	0.90	1.08	0.98	0.95	0.93	0.92
	CCIAG [NOT OWNER]	ENER	0.00	0.23	0.39	0.45	0.48	0.49	0.23	0.37	0.43	0.45	0.47	0.23	0.35	0.40	0.42	0.43
		EXER	29.8	23.2	18.7	17.1	16.2	15.8	23.4	19.2	17.7	16.9	16.5	23.1	19.8	18.5	17.9	17.6
		ECON	0.00	0.00	0.00	0.00	0.00	0.00	0.13	0.00	0.00	0.00	0.00	0.65	0.29	0.00	0.00	0.00
		EXEC	1.86	1.57	1.38	1.35	1.37	1.40	1.54	1.37	1.34	1.36	1.40	1.48	1.35	1.33	1.36	1.41
	THIRD [OWNER]	ENER	0.00	1.50	1.50	1.49	1.49	1.49	1.30	1.30	1.30	1.30	1.30	1.00	1.00	1.00	1.00	1.00
		EXER	2.05	0.96	1.62	1.86	1.98	2.05	0.62	1.03	1.18	1.26	1.30	0.00	0.00	0.00	0.00	0.01
		ECON	0.00	−0.58	−1.63	−3.08	−4.65	−6.28	0.13	−0.63	−2.01	−3.56	−5.16	0.65	0.29	−0.73	−2.24	−3.84
		EXEC	525	122	272	369	450	525	83.1	189	261	324	381	0.00	0.20	0.44	0.71	0.98
SCENARIO 4	CONSORTIUM [OWNER]	ENER	0.00	0.05	0.13	0.17	0.19	0.21	0.05	0.13	0.18	0.20	0.22	0.07	0.16	0.20	0.23	0.24
		EXER	37.4	31.5	27.4	25.9	25.2	24.8	31.6	27.6	26.0	25.2	24.8	31.2	27.3	25.7	25.0	24.7
		ECON	0.00	0.02	−0.61	−1.91	−3.40	−4.98	1.25	0.99	−0.14	−1.56	−3.10	3.47	3.82	2.95	1.63	0.13
		EXEC	2.84	2.62	2.55	2.60	2.69	2.80	2.62	2.50	2.52	2.59	2.68	2.56	2.34	2.28	2.29	2.33

Table A2 presents the results after relaxations.

Table A2. Results after relaxations, by scenario, stakeholder, and criterion for every possible system design.

Scenario	Stakeholder	Criterion	35 °C—Reference	35 °C—0 MWh	35 °C—10 MWh	35 °C—20 MWh	35 °C—30 MWh	35 °C—40 MWh	50 °C—0 MWh	50 °C—10 MWh	50 °C—20 MWh	50 °C—30 MWh	50 °C—40 MWh	85 °C—0 MWh	85 °C—10 MWh	85 °C—20 MWh	85 °C—30 MWh	85 °C—40 MWh
SCENARIO 1	LNCMI [OWNER]	ENER	0.00	0.20	0.33	0.38	0.41	0.42	0.22	0.36	0.42	0.45	0.46	0.30	0.45	0.51	0.54	0.55
		EXER	7.59	8.23	8.68	8.84	8.92	8.96	8.24	8.30	8.32	8.34	8.34	8.09	7.50	7.26	7.15	7.10
		ECON	0.00	0.40	0.20	−0.98	−2.42	−3.97	1.11	1.29	0.74	−0.62	−2.13	2.52	3.08	2.81	2.22	1.02
		EXEC	0.85	0.93	1.06	1.15	1.22	1.29	0.91	0.98	1.04	1.09	1.14	0.86	0.81	0.79	0.78	0.78
	CCIAG [NOT OWNER]	ENER	0.00	0.23	0.39	0.45	0.48	0.49	0.23	0.37	0.43	0.45	0.47	0.23	0.35	0.40	0.42	0.43
		EXER	29.8	23.2	18.7	17.1	16.2	15.8	23.4	19.2	17.7	16.9	16.5	23.1	19.8	18.5	17.9	17.6
		ECON	0.00	−0.38	−0.81	−0.92	−0.98	−1.02	0.14	−0.29	−0.88	−0.94	−0.97	0.95	0.73	0.14	−0.59	−0.89
		EXEC	1.86	1.55	1.36	1.33	1.34	1.38	1.52	1.34	1.31	1.32	1.36	1.44	1.29	1.26	1.29	1.33

Table A2. *Cont.*

Scenario	Stakeholder	Criterion	35 °C—Reference	35 °C—0 MWh	35 °C—10 MWh	35 °C—20 MWh	35 °C—30 MWh	35 °C—40 MWh	50 °C—0 MWh	50 °C—10 MWh	50 °C—20 MWh	50 °C—30 MWh	50 °C—40 MWh	85 °C—0 MWh	85 °C—10 MWh	85 °C—20 MWh	85 °C—30 MWh	85 °C—40 MWh
SCENARIO 2	LNCMI [NOT OWNER]	**ENER**	0.00	0.20	0.33	0.38	0.41	0.42	0.22	0.36	0.42	0.45	0.46	0.30	0.45	0.51	0.54	0.55
		EXER	7.59	7.28	7.06	6.98	6.94	6.91	7.61	7.27	7.14	7.08	7.04	8.09	7.50	7.26	7.15	7.10
		ECON	0.00	0.30	0.51	0.59	0.63	0.65	0.50	0.81	0.94	1.00	1.03	1.08	1.62	1.84	1.94	1.99
		EXEC	0.85	0.83	0.81	0.80	0.80	0.79	0.84	0.81	0.80	0.80	0.80	0.86	0.81	0.79	0.78	0.78
	CCIAG [OWNER]	**ENER**	0.00	0.23	0.39	0.45	0.48	0.49	0.23	0.37	0.43	0.45	0.47	0.23	0.35	0.40	0.42	0.43
		EXER	29.8	24.2	20.3	18.9	18.2	17.9	24.0	20.3	18.8	18.2	17.8	23.1	19.8	18.5	17.9	17.6
		ECON	0.00	2.82	1.98	0.60	−0.93	−2.53	3.85	3.28	2.02	0.54	−1.03	5.48	5.30	4.21	2.80	1.24
		EXEC	1.86	1.66	1.61	1.68	1.77	1.88	1.59	1.50	1.54	1.62	1.71	1.44	1.29	1.26	1.29	1.33
SCENARIO 3	LNCMI [NOT OWNER]	**ENER**	0.00	0.20	0.33	0.38	0.41	0.42	0.22	0.36	0.42	0.45	0.46	0.30	0.45	0.51	0.54	0.55
		EXER	7.59	7.28	7.06	6.98	6.94	6.91	7.61	7.27	7.14	7.08	7.04	8.09	7.50	7.26	7.15	7.10
		ECON	0.00	0.30	0.51	0.59	0.63	0.65	0.50	0.81	0.94	1.00	1.03	1.08	1.62	1.84	1.94	1.99
		EXEC	0.85	0.83	0.81	0.80	0.80	0.79	0.84	0.81	0.80	0.80	0.80	0.86	0.81	0.79	0.78	0.78
	CCIAG [NOT OWNER]	**ENER**	0.00	0.23	0.39	0.45	0.48	0.49	0.23	0.37	0.43	0.45	0.47	0.23	0.35	0.40	0.42	0.43
		EXER	29.8	23.2	18.7	17.1	16.2	15.8	23.4	19.2	17.7	16.9	16.5	23.1	19.8	18.5	17.9	17.6
		ECON	0.00	−0.38	−0.81	−0.92	−0.98	−1.02	0.14	−0.29	−0.88	−0.94	−0.97	0.95	0.73	0.14	−0.59	−0.89
		EXEC	1.86	1.55	1.36	1.33	1.34	1.38	1.52	1.34	1.31	1.32	1.36	1.44	1.29	1.26	1.29	1.33
	THIRD [OWNER]	**ENER**	0.00	1.50	1.50	1.49	1.49	1.49	1.30	1.30	1.30	1.30	1.30	1.00	1.00	1.00	1.00	1.00
		EXER	2.05	0.96	1.62	1.86	1.98	2.05	0.62	1.03	1.18	1.26	1.30	0.00	0.00	0.00	0.00	0.01
		ECON	0.00	0.10	−0.31	−1.57	−3.04	−4.61	0.61	0.47	−0.19	−1.62	−3.16	1.43	1.46	0.97	0.28	−0.97
		EXEC	499	110	251	345	425	499	67.8	163	232	292	349	0.00	0.10	0.22	0.35	0.49
SCENARIO 4	CONSORTIUM [OWNER]	**ENER**	0.00	0.05	0.13	0.17	0.19	0.21	0.05	0.13	0.18	0.20	0.22	0.07	0.16	0.20	0.23	0.24
		EXER	37.4	31.5	27.4	25.9	25.2	24.8	31.6	27.6	26.0	25.2	24.8	31.2	27.3	25.7	25.0	24.7
		ECON	0.00	0.50	0.20	−0.98	−2.42	−3.97	1.72	1.76	0.74	−0.62	−2.13	3.95	4.54	3.78	2.50	1.02
		EXEC	2.71	2.49	2.42	2.48	2.57	2.67	2.43	2.32	2.34	2.42	2.51	2.30	2.10	2.06	2.07	2.11

References

1. Lichtenegger, K.; Leitner, A.; Märzinger, T.; Mair, C.; Moser, A.; Wöss, D.; Schmidl, C.; Pröll, T. Decentralized heating grid operation: A comparison of centralized and agent-based optimization. *Sustain. Energy Grids Netw.* **2020**, *21*, 100300. [CrossRef]
2. Lund, H.; Werner, S.; Wiltshire, R.; Svendsen, S.; Thorsen, J.E.; Hvelplund, F.; Vad Mathiesen, B.; Mathiesen, B.V. 4th Generation District Heating (4GDH). *Energy* **2014**, *68*, 1–11. [CrossRef]
3. Broberg, S.; Backlund, S.; Karlsson, M.; Thollander, P. Industrial excess heat deliveries to Swedish district heating networks: Drop it like it's hot. *Energy Policy* **2012**, *51*, 332–339. [CrossRef]
4. Haas, J.; Nowak, W.; Palma-Behnke, R. Multi-objective planning of energy storage technologies for a fully renewable system: Implications for the main stakeholders in Chile. *Energy Policy* **2018**, *126*, 494–506. [CrossRef]
5. Yao, R.; Hu, Y.; Varga, L. Applications of Agent-Based Methods in Multi-Energy Systems—A Systematic Literature Review. *Energies* **2023**, *16*, 2456. [CrossRef]
6. Gährs, S.; Knoefel, J. Stakeholder demands and regulatory framework for community energy storage with a focus on Germany. *Energy Policy* **2020**, *144*, 111678. [CrossRef]
7. Wang, G.; Blondeau, J. Multi-Objective Optimal Integration of Solar Heating and Heat Storage into Existing Fossil Fuel-Based Heat and Power Production Systems. *Energies* **2022**, *15*, 1942. [CrossRef]
8. Battini, F.; Pernigotto, G.; Morandi, F.; Gasparella, A.; Kämpf, J.H. Assessment of Subsidization Strategies for Multi-Objective Optimization of Energy Efficiency Measures for Building Renovation at District Scale. *Energies* **2023**, *16*, 5780. [CrossRef]

9. Alavijeh, N.M.; Steen, D.; Norwood, Z.; Tuan, L.A.; Agathokleous, C. Cost-Effectiveness of Carbon Emission Abatement Strategies for a Local Multi-Energy System—A Case Study of Chalmers University of Technology Campus. *Energies* **2020**, *13*, 1626. [CrossRef]
10. Li, M.; Feng, Y.; Zhou, M.; Mu, H.; Li, L.; Wang, Y. Economic and Environmental Optimization for Distributed Energy System Integrated with District Energy Network. *Energies* **2019**, *12*, 1844. [CrossRef]
11. Ye, B.; Zhou, M.; Yan, D.; Li, Y. Multi-Objective Decision-Making for Hybrid Renewable Energy Systems for Cities: A Case Study of Xiongan New District in China. *Energies* **2020**, *13*, 6223. [CrossRef]
12. Schmeling, L.; Schönfeldt, P.; Klement, P.; Wehkamp, S.; Hanke, B.; Agert, C. Development of a Decision-Making Framework for Distributed Energy Systems in a German District. *Energies* **2020**, *13*, 552. [CrossRef]
13. Thomsen, J.; Saad Hussein, N.; Senkpiel, C.; Hartmann, N.; Schlegl, T. An optimized energy system planning and operation on distribution grid level—The Decentralized Market Agent as a novel approach. *Sustain. Energy Grids Netw.* **2017**, *12*, 40–56. [CrossRef]
14. Lichtenegger, K.; Wöss, D.; Halmdienst, C.; Höftberger, E.; Schmidl, C.; Pröll, T. Intelligent heat networks: First results of an energy-information-cost-model. *Sustain. Energy Grids Netw.* **2017**, *11*, 1–12. [CrossRef]
15. Hinker, J.; Hemkendreis, C.; Drewing, E.; März, S.; Hidalgo Rodríguez, D.I.; Myrzik, J.M.A. A novel conceptual model facilitating the derivation of agent-based models for analyzing socio-technical optimality gaps in the energy domain. *Energy* **2017**, *137*, 1219–1230. [CrossRef]
16. Miró, L.; Brueckner, S.; McKenna, R.; Cabeza, L.F. Methodologies to estimate industrial waste heat potential by transferring key figures: A case study for Spain. *Appl. Energy* **2016**, *169*, 866–873. [CrossRef]
17. Bolwig, S.; Bolkesjø, T.F.; Klitkou, A.; Lund, P.D.; Bergaentzlé, C.; Borch, K.; Olsen, O.J.; Kirkerud, J.G.; Chen, Y.K.; Gunkel, P.A.; et al. Climate-friendly but socially rejected energy-transition pathways: The integration of techno-economic and socio-technical approaches in the Nordic-Baltic region. *Energy Res. Soc. Sci.* **2020**, *67*, 101559. [CrossRef]
18. Martin, N.; Rice, J. Improving Australia's renewable energy project policy and planning: A multiple stakeholder analysis. *Energy Policy* **2015**, *84*, 128–141. [CrossRef]
19. Heuninckx, S.; Boveldt, G.T.; Macharis, C.; Coosemans, T. Stakeholder objectives for joining an energy community: Flemish case studies. *Energy Policy* **2022**, *162*, 112808. [CrossRef]
20. Sanderink, L.; Nasiritousi, N. How institutional interactions can strengthen effectiveness: The case of multi-stakeholder partnerships for renewable energy. *Energy Policy* **2020**, *141*, 111447. [CrossRef]
21. Dashti, R.; Yousefi, S.; Parsa Moghaddam, M. Comprehensive efficiency evaluation model for electrical distribution system considering social and urban factors. *Energy* **2013**, *60*, 53–61. [CrossRef]
22. Jano-Ito, M.A.; Crawford-Brown, D. Investment decisions considering economic, environmental and social factors: An actors' perspective for the electricity sector of Mexico. *Energy* **2017**, *121*, 92–106. [CrossRef]
23. Farías, I.; Bender, T. *Urban Assemblages: How Actor-Network Theory Changes Urban Studies*; Routledge: London, UK; New York, NY, USA, 2010; ISBN 978-0-415-48662-0. [CrossRef]
24. Hampikian, Z. *De la Distribution Aux Synergies? Circulations Locales d'énergie et Transformations des Processus de Mise en Réseau de la Ville*; Université Paris-Est: Créteil, France, 2017.
25. Wehkamp, S.; Schmeling, L.; Vorspel, L.; Roelcke, F.; Windmeier, K.-L. District Energy Systems: Challenges and New Tools for Planning and Evaluation. *Energies* **2020**, *13*, 2967. [CrossRef]
26. Ha, Y.H.; Kumar, S.S. Investigating decentralized renewable energy systems under different governance approaches in Nepal and Indonesia: How does governance fail? *Energy Res. Soc. Sci.* **2021**, *80*, 102214. [CrossRef]
27. Reda, F.; Ruggiero, S.; Auvinen, K.; Temmes, A. Towards low-carbon district heating: Investigating the socio-technical challenges of the urban energy transition. *Smart Energy* **2021**, *4*, 100054. [CrossRef]
28. Simeoni, P.; Ciotti, G.; Cottes, M.; Meneghetti, A. Integrating industrial waste heat recovery into sustainable smart energy systems. *Energy* **2019**, *175*, 941–951. [CrossRef]
29. Lund, R.; Ilic, D.D.; Trygg, L. Socioeconomic potential for introducing large-scale heat pumps in district heating in Denmark. *J. Clean. Prod.* **2016**, *139*, 219–229. [CrossRef]
30. Taylor, P.C.; Abeysekera, M.; Bian, Y.; Ćetenović, D.; Deakin, M.; Ehsan, A.; Levi, V.; Li, F.; Oduro, R.; Preece, R.; et al. An interdisciplinary research perspective on the future of multi-vector energy networks. *Int. J. Electr. Power Energy Syst.* **2021**, *135*, 107492. [CrossRef]
31. Höfer, T.; Madlener, R. A participatory stakeholder process for evaluating sustainable energy transition scenarios. *Energy Policy* **2020**, *139*, 111277. [CrossRef]
32. Turcksin, L.; Macharis, C.; Lebeau, K.; Boureima, F.; Van Mierlo, J.; Bram, S.; De Ruyck, J.; Mertens, L.; Jossart, J.M.; Gorissen, L.; et al. A multi-actor multi-criteria framework to assess the stakeholder support for different biofuel options: The case of Belgium. *Energy Policy* **2011**, *39*, 200–214. [CrossRef]
33. Hettinga, S.; Nijkamp, P.; Scholten, H. A multi-stakeholder decision support system for local neighbourhood energy planning. *Energy Policy* **2018**, *116*, 277–288. [CrossRef]
34. Fitó, J.; Ramousse, J.; Hodencq, S.; Morriet, L.; Wurtz, F.; Debizet, G. Analyse technico-économique multi-acteurs de la conception d'un système de valorisation de chaleur fatale sur réseau de chaleur. In Proceedings of the Communautés Énergétiques, Autoproduction, Autoconsommation: Cadrages, Pratiques et Outils, Paris, France, 15–16 June 2020.

35. Tabourdeau, A.; Debizet, G. Concilier ressources in situ et grands réseaux: Une lecture des proximités par la notion de nœud socio-énergétique. *Flux* **2017**, *109–110*, 87–101. [CrossRef]
36. Fitó, J.; Hodencq, S.; Ramousse, J.; Wurtz, F.; Stutz, B.; Debray, F.; Vincent, B. Energy- and exergy-based optimal designs of a low-temperature industrial waste heat recovery system in district heating. *Energy Convers. Manag.* **2020**, *211*, 112753. [CrossRef]
37. Morriet, L.; Pajot, C.; Delinchant, B.; Marechal, Y.; Wurtz, F.; Debray, F.; Vincent, B. Optimisation multi-acteurs appliquée à la valorisation de chaleur fatale d'un acteur industriel flexible. In Proceedings of the Conférence Francophone de l'International Building Performance Simulation Association (IBPSA), Bordeaux, France, 15–16 May 2018.
38. Hodencq, S.; Debray, F.; Trophime, C.; Vincent, B.; Stutz, B.; Delinchant, B.; Wurtz, F.; Pajot, C.; Morriet, L.; Bentivoglio, F.; et al. Thermohydraulics of High Field Magnets: From microns to urban community scale. In Proceedings of the 24ème Congrès Français de Mécanique, Brest, France, 26–30 August 2019.
39. Morriet, L.; Debizet, G.; Wurtz, F. Multi-actor modelling for MILP energy systems optimisation: Application to collective self-consumption. In *Building Simulation*; 2015; Available online: https://hal.science/hal-02285965/ (accessed on 11 February 2022).
40. Debizet, G.; Pappalardo, M.; Wurtz, F. *Local Energy Communities: Emergence, Places, Organizations, Decision Tools*, 1st ed.; Routledge: London, UK, 2022; ISBN 9781003257547. [CrossRef]
41. Pajot, C.; Morriet, L.; Hodencq, S.; Delinchant, B.; Maréchal, Y.; Wurtz, F.; Reinbold, V. An Optimization Modeler as an Efficient Tool for Design and Operation for City Energy Stakeholders and Decision Makers. (HAL Id: Hal-02285954). In Proceedings of the 16th IBPSA International Conference, Rome, Italy, 2–4 September 2019.
42. Pajot, C. OMEGAlpes: Outil D'aide à la Décision Pour Une Planification Energétique Multi-Fluides Optimale à L'échelle Des Quartiers. Doctoral Thesis, Université de Grenoble, Saint-Martin-d'Hères, France, 2019.
43. Fitó, J.; Ramousse, J.; Hodencq, S.; Wurtz, F. Energy, exergy, economic and exergoeconomic (4E) multicriteria analysis of an industrial waste heat valorization system through district heating. *Sustain. Energy Technol. Assess.* **2020**, *42*, 100894. [CrossRef]
44. Pons, M. On the reference state for exergy when ambient temperature fluctuates. *Int. J. Thermodyn.* **2009**, *12*, 113–121.
45. Pajot, C.; Delinchant, B.; Marechal, Y.; Wurtz, F.; Debray, F.; Vincent, B. Valorisation optimale de chaleur fatale d'un site à forte consommation électrique. In Proceedings of the Conférence des Jeunes Chercheurs en Génie Electrique (JCGE), Oléron, France, 30 May–1 June 2017.
46. Pajot, C.; Delinchant, B.; Maréchal, Y.; Wurtz, F.; Robin, S.; Vincent, B.; Debray, F.; Nguyen, Q. Data-Driven Modeling of Building Consumption Profile for Optimal Flexibility: Application to Energy Intensive Industry. In Proceedings of the Building Simulation Conference, Rome, Italy, 2–4 September 2019; Available online: https://hal.science/hal-02364669/ (accessed on 14 April 2022).
47. Greco, S.; Ehrgott, M.; Figueira, J. *Multiple Criteria Decision Analysis*; Springer: Catania, Italy, 2016.

Disclaimer/Publisher's Note: The statements, opinions and data contained in all publications are solely those of the individual author(s) and contributor(s) and not of MDPI and/or the editor(s). MDPI and/or the editor(s) disclaim responsibility for any injury to people or property resulting from any ideas, methods, instructions or products referred to in the content.

energies

MDPI

Article

Simulation-Based Evaluation of the Impact of an Electrochromic Glazing on the Energy Use and Indoor Comfort of an Office Room

Henriqueta Teixeira [1], A. Moret Rodrigues [1], Daniel Aelenei [2,3] and M. Glória Gomes [1,*]

[1] CERIS, Department of Civil Engineering, Architecture and Environment (DECivil), Instituto Superior Técnico, Universidade de Lisboa, Av. Rovisco Pais, 1049-001 Lisbon, Portugal; henriqueta.teixeira@tecnico.ulisboa.pt (H.T.); moret.rodrigues@tecnico.ulisboa.pt (A.M.R.)
[2] Centre of Technology and Systems/UNINOVA, Department of Civil Engineering, Faculty of Science and Technology, Universidade Nova de Lisboa, 2829-516 Caparica, Portugal; aelenei@fct.unl.pt
[3] Laboratório Associado de Sistemas Inteligentes, LASI, 4800-058 Guimarães, Portugal
* Correspondence: maria.gloria.gomes@tecnico.ulisboa.pt

Abstract: Electrochromic glazing alters its optical properties in the absence/presence of an electrical charge, varying from clear to dark to control daylighting and solar heat gains. This study aims to evaluate the impact of an electrochromic glazing, with indoor glare or temperature control, on the energy performance and thermal and visual comfort of an office room under three European climates, using a calibrated simulation model. The novelty of the paper lies in its combined performance assessment, using different standards and metrics. The results showed reduced climatization energy requirements with temperature control, but significantly increased artificial lighting energy use. Glare control achieved useful illuminance levels during 74–80% of working hours. Concerning temperature control, working hours within thermal comfort increased (21–43%) under a free-float regime. Moreover, the performance of this glazing was compared to that of a clear glazing with/without a reflective film and a thermochromic glazing for different solar orientations. The electrochromic glazing with glare control showed the highest energy savings (14–36%) for a western orientation, and the lowest negative impact on daylighting for a northern orientation. The best glare reduction was achieved with the reflective film. Considering the free-float regime, the electrochromic glazing, with temperature control, showed the highest increase in working hours within thermal comfort (6–9%) for a western orientation.

Keywords: electrochromic glazing; dynamic simulation; thermal performance; visual performance; energy performance; indoor comfort

1. Introduction

Buildings account for a high energy consumption, and consequently, high CO_2 emission levels [1]. A significant amount of the consumed energy [2] is used to provide heating and cooling, along with artificial lighting, to indoor spaces. These two energy end uses are strongly influenced by the building facade [3,4], since it acts as an interface between the outdoor and indoor environments responsible for energy and mass flows.

Glazing systems allow natural light to flow towards the indoors, having a positive impact on visual comfort and artificial lighting needs [5]. However, these elements, particularly conventional clear glazing, tend to have high solar and visible transmittance values that can result in high solar heat gains and potential glare problems [6]. While the inclusion of solar control systems [7–10], such as overhangs, balconies, louvres, and shutters, into the building facade can help improve its performance by providing shade to the glazing elements and reducing excessive solar radiation levels, these solar control systems can have a negative visual impact by partial or totally blocking the outside view. It is also possible

to incorporate solar control directly into the glazing systems through coatings, such as low-emissivity and reflective coatings, and/or films, such as solar control films. Coated or filmed glazing yields a better performance than conventional glazing, since it aims at decreasing climatization energy needs and potential glare [11–14]. Even though these are affordable solutions, largely available on the market, the static behavior of these coated and filmed glazing systems can limit their efficiency, particularly in hot climates with high solar radiation levels. With the ambition of achieving net-zero energy buildings [15,16] and the fact that largely glazed buildings are the tendency of modern architecture, the investment in the improvement and innovation of glazing solutions that surpass conventional glazing performance has become essential.

Smart glazing technologies [17–21], which have been increasing in recent years, can dynamically control the entrance of heat and light through the glazing by adapting to specific stimuli, aiming at improving the global performance of the building. The installation of smart glazing systems can promote the reduction of the energy needs of the building, while providing indoor comfort conditions [20]. Some smart glazing technologies present a passive reaction control, meaning that they independently react to environmental stimuli, as in the case of thermochromic (TC) glazing that autonomously and reversibly alters its optical properties due to temperature variation in the thermochromic material (with the most successfully applied being vanadium dioxide, hydrogels, ionic liquids, or perovskites [22,23]) incorporated in a thin coating in the glazing. When it reaches temperature levels higher that a specific value (transition temperature), the TC material darkens, reducing solar gains through the glazing [24,25]. If temperature levels are lower than the transition temperatures, the clear state is restored. When assessing the energy performance of TC glazing in an office environment, research studies obtained energy savings of up to 17–23% for large-area windows under temperate climates, when compared to the results for static glazing [26,27]. Under arid and continental climates, cooling energy savings were also reduced with TC glazing [28,29]. When investigating the impact of TC glazing on the visual comfort of office rooms, it was found that daylight exploitation increased by 5–20% and glare reduced by 10–50%, for higher and lower latitude locations, respectively [30,31]. Regarding thermal comfort, TC glazing can reduce the occurrence of uncomfortable conditions during summer by 36% [32]. However, the lack of control of the chromatic change by the users inherent in passive technologies acts as a disadvantage. Active smart glazing technologies [33], such as liquid crystals, suspended particles, and electrochromic (EC) glazing, can be directly controlled by users or through a computerized building management system, offering a more flexible dynamic behavior. Both liquid crystals [34,35] and suspended particle [36] glazing technologies make it possible to achieve energy savings when compared with static windows; nevertheless, their performance is usually surpassed by that of EC glazing [37], which is a more established and deeply investigated smart glazing.

EC glazing, a property-changing smart glazing technology, can reversibly alter its optical properties (transmittance and absorptance) in response to an electrical stimulus [18–20,38]. This dynamic behavior is possible due to the presence of an EC coating comprising five layers: an electron accumulation layer, an ion conductor layer, an electrode layer, and two transparent conductive oxide outer layers. When voltage is applied to the EC coating of the glazing, the transfer of ions from the electron accumulation layer to the electrode layer causes a chromatic change from a clear to a tinted state, with the possibility of achieving intermediate tinted states. The change between tinted states usually requires low energy use, with even lower energy consumption required to maintain a specific tinted state. In the absence of the electrical stimulus, the chromatic change is reversed, and the glazing returns to its clear state.

EC glazing can be manually controlled by the occupant or automatically controlled (based on control parameters, such as solar radiation, glare levels, indoor temperature, and outdoor temperature) when connecting the glazing to a terminal box, a sensor, and a control panel that can be programmed to manage tinting, based on different inputs. The type of control of an EC glazing has a strong impact on its performance [38]. Considering

EC glazing systems controlled by solar radiation and/or illuminance levels, energy saving potentials were obtained in previous studies [39–41], particularly cooling energy savings. When trying to combine indoor comfort with energy performance objectives in the EC glazing control [42–45], comfort conditions are improved, but energy requirements increase.

Existing research studies that explore the performance of smart EC glazing systems, either through a numerical simulation, experimental testing, or in combination, conclude that this innovative glazing technology contributes to the reduction of the cooling energy needs and indoor glare levels, being more suitable for hot climates. A brief description and the main findings of these studies is presented in Table 1.

Existing studies tend to focus on the energy performance of EC, evaluating energy savings and the reduction of peak energy demand. These studies concluded that EC glazing makes it possible to reduce cooling energy needs, when compared to the results for clear and low-emissivity glazing systems, particularly during summer in hot climates. However, an increase in the artificial lighting energy consumption was generally observed in those cases. Also, existing studies do not consider the energy consumption of the control of the dynamic glazing. Even though this energy end use can be low for small glazing areas, it should be considered in the energy performance analysis of this type of glazing.

Regarding the impact on the conditions of the indoor environment, some studies assess the thermal and/or visual comfort of occupants in spaces with EC glazing installed. The thermal comfort of EC glazing is poorly explored by existing studies [44,46], which used the predicted mean vote (PMV) index and concluded that EC glazing increased thermal comfort when compared to clear glazing. The impact of EC glazing on indoor glare is investigated by some studies, mainly through the daylight glare index (DGI) [47–49] or the daylight glare probability (DGP) [49,50], which concluded that glare reduction is possible without compromising available daylight, increasing visual comfort. Since people spend a large amount of time inside buildings, the evaluation of the impact of building elements on indoor thermal and visual comfort through multiple metrics and standards is extremely important. Existing studies [44,46,47] that assess both the energy and comfort performance of EC glazing are scarce, focusing on specific standards and metrics, so the comfort performance of this smart glazing should be further investigated, along with its energy performance.

Table 1. Brief description and main findings of previous research studies on the performance of electrochromic glazing.

Ref.	Climate Group [1]	Case Study	Research Approach [2]		Performance Assessment			Main Findings
			Exp.	Sim.	Energy	Thermal Comfort	Visual Comfort	
[51]	B, C, D	Office building		✓	✓		✓	• Energy savings ≥ 45% compared to single glazing. • Peak load carbon emissions reduced by 35% in new construction and 50% in renovation scenario.
[52]	C	Office room		✓	✓	✓	✓	• Energy savings of 48% (no overhang) and 37% (overhang), along with a blind control algorithm. • Unobstructed view for 10 months, against a few days with venetian blinds.
[44]	A, C, D	Office building		✓	✓		✓	• Higher energy savings obtained for warmer climates with high solar radiation. • Higher positive impact on visual comfort than thermal comfort.
[47]	C, D	Office building		✓	✓			• Primary annual energy use decreased by 5–10% for large-area windows, but increased by 2–5% for moderate-area windows. • Average annual DGI levels were significantly reduced.
[53]	D	Office building		✓	✓			• Energies savings of 8%, against results for low-e glazing.
[54]	C	Office room		✓	✓			• Highest reduction of energy needs for west orientation (62%), but no advantage for south orientation, compared to conventional double glazing.
[45]	A, B, C, D	Office building/apartment		✓	✓			• Annual primary energy savings of 6–30 kWh/ft^2 of window area with a dual-band EC against static windows, and of 0–1.2 kWh/ft^2 against other EC.
[55]	A, B, D	Office building		✓	✓			• Annual reduction of cooling needs by up to 125–200 kWh/m^2 with EC coating on low-e double glazing south-oriented windows.
[56]	B, C	Office building		✓	✓		✓	• Savings of up to 39% of cooling demand and 35% of total energy demand with EC combined with integrated photovoltaic system and an energy management system.

Table 1. *Cont.*

Ref.	Climate Group [1]	Case Study	Research Approach [2]		Performance Assessment			Main Findings
			Exp.	Sim.	Energy	Thermal Comfort	Visual Comfort	
[43,57]	B, C	Office rom/building		✓	✓		✓	• Annual energy savings up to 25% against static glazing. • Nearly 83% of hours with useful illuminance levels.
[48,58–60]	C	Test-cell/family house	✓	✓	✓	✓	✓	• Cooling reduction benefits could be exceeded by the increase in lighting and heating needs for low-area windows in heating dominated climates.
[50]	C	Test-cell	✓	✓			✓	• Useful illuminance levels higher in May (40–48%) than in June (6–8%). • DGP values lower than 0.36 (comfortable) for 69% of occupancy time.
[49]	C	Test-room	✓			✓	✓	• EC glazing prevents disturbing glare for most users when the sun is close to the central field of view, but does not provide comfort.
[46,61]	A	Test-room	✓		✓	✓		• Reduction of about 80% of heat flux through the glazing and reduction of operative temperature up to 11 °C. • Total of 39% of daytime spent with visual comfort, without glare.
[62]	C	Office room	✓	✓	✓			• Annual energy consumption reduced by 39–48% and peak demand by 22–35%. • PPD reduced from 18% to 13–15%.
[63]	C	Test-room	✓		✓		✓	• Daily lighting energy savings of 8–59% against static glazing, for large-area, south-oriented windows.
[64]	C	Office room	✓		✓			• Energy efficiency and visual comfort may not be fulfilled with low solar angles. • Daily lighting energy use reduced by 3–24% against static glazing.
[65]	C	Test-room	✓		✓			• Cooling energy needs reduced by 80%, but heating increased 35%. • Payback period of 6 years, considering a residential apartment.

[1] Climate group: A—tropical, B—arid, C—temperate, D—continental; [2] research approach: Exp.—experimental, Sim.—dynamic simulation.

The studies on the performance of EC glazing existing in the literature tend to focus on energy performance analysis, usually not taking into account the energy use expended by the control of the glazing. Moreover, studies that assess the impact of this glazing on indoor comfort are in lower number, usually not considering different metrics. With the identification of these research gaps, this study aims to investigate the performance of an EC glazing (controlled by indoor glare or temperature), comprising a holistic analysis that consists of the evaluation of both the energy performance (climatization, artificial lighting, and glazing control) and the visual and thermal comfort in the presence of this smart glazing. An existing office room was used as a case study for a refurbishment scenario under the main European climates, using a calibrated dynamic simulation model. This is a follow-up study of the once conducted by Teixeira et al. [66], which evaluated the energy, thermal, and visual performance of static versus thermochromic (TC) double-glazing under the same European climate locations. While the case study and the calibration of the simulation model are retained, new features are introduced in this study, aiming at evaluating the impact of an EC glazing on building energy use and indoor comfort. In addition, a new analysis on the impact of solar orientation on the performance of the EC glazing and the other glazing solutions for solar control is introduced. The combination of an energy and comfort assessment in this study, as well as the consideration of different glazing solutions (both static and dynamic) and climates, aims at achieving more robust results that could help fill the research gaps identified in the literature.

2. Methodology

The methodology followed in the present work is shown in Figure 1.

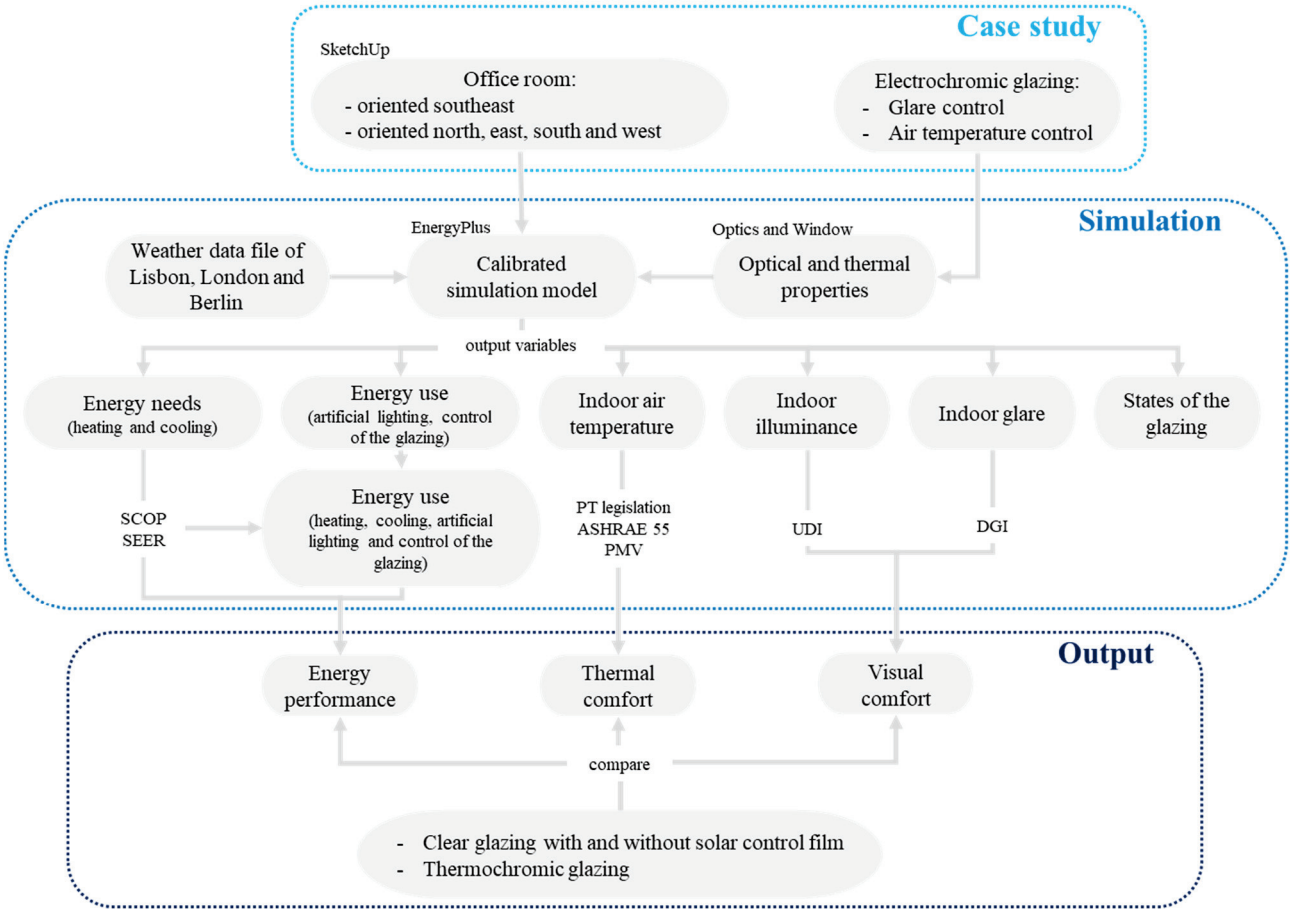


Figure 1. Methodology adopted.

An office room with an EC double-glazing, located in Lisbon, was used as a case study. The analyzed EC glazing was controlled by indoor air temperature or glare levels, with the aim of promoting indoor quality thermal and luminous conditions, while trying to achieve energy savings, similar to the methods of previous studies [27,39,43,45]. The thermal and optical properties of the EC glazing system were computed by Optics (version 6; Optics, Berkeley, CA, USA) [67] and Window (version 7.6; Berkeley Lab WINDOW, Berkeley, CA, USA) [68] software. A 3D model of the office room was constructed using SketchUp [69]. The energy performance and indoor comfort results were obtained through a dynamic simulation model in EnergyPlus [70], previously calibrated [66] with experimental data measured during an in situ experimental campaign under real occupancy conditions [66,71]. The synthetic weather data files [72] of the cities of Lisbon, London, and Berlin were associated to the dynamic simulation model to evaluate and compare the performance under the three European climates (hot-summer Mediterranean climate, temperate oceanic climate, and warm-summer humid continental climate, in accordance with the Köppen–Geiger climate classification [73]).

The annual energy needs (heating and cooling) and energy use (climatization, artificial lighting, and control of the dynamic glazing) were computed and analyzed to evaluate the energy performance of the glazing system. The indoor thermal comfort was evaluated through the percentage of annual working hours within the comfort ranges of the following standards: Portuguese legislation [74], ASHRAE 55 adaptive model [75], and PMV [76]. The indoor visual comfort was evaluated through the percentage of annual working hours within the comfort ranges of the following indexes: useful daylight index (UDI) [77,78] and DGI [79].

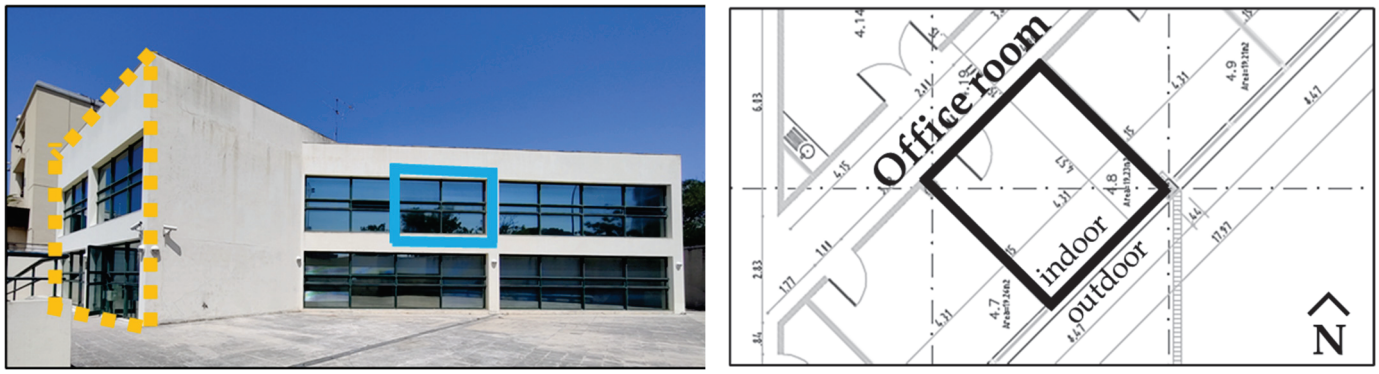
A comparative assessment on the performance of the EC glazing compared to other glazing solutions with different types and levels of solar control (clear glazing with a solar control film and a TC glazing) was also conducted, using a clear glazing as reference. These comparative glazing solutions, whose properties are shown in Table 6 of Section 4, correspond to the ones considered in the previous study conducted by Teixeira et al. [66], adopting the same case study and climate locations. The comparative analysis was carried out for the climates of the same European cities (Lisbon, London, and Berlin), and the impact of the solar orientation (north, east, south, and west) on the performance of different glazing systems was also addressed. It is expected that this comparison will yield additional insights regarding the potential of installing dynamic glazing solutions under these European climates.

2.1. Case Study

An individual office room (Figure 2a), located on the top floor of a university building of Instituto Superior Técnico, Lisbon, was used as a case study. A shading effect on the facade of the building, caused by a protruding wall (south facade), is usually noticed around 12 a.m. (summer) or 2 p.m. (winter).

The glazed facade is southeast oriented (Figure 2b). The original glazing system consisted of a conventional double-glazing unit of clear float glass, with an air gap, and a green aluminum frame (without a thermal break). Due to high solar heat gains through the glazing, a reflective solar control film was later installed on the interior surface of the glazing.

The indoor air temperature of the office can be controlled during working hours through an HVAC system, with an established setpoint of 22 $\pm$ 2 °C, which is within the thermal comfort temperature range for commercial buildings (20–25 °C), according to Portuguese legislation [74]. Table 2 shows a brief description of the case study. More information regarding the office room can be found in the study by Teixeira et al. [66].



(**a**) (**b**)

Figure 2. Case study: (**a**) location of the individual office room (contour in full blue) and the protruding south wall (contour in dotted orange) in the university building; (**b**) office room outline (contour in full black) and solar orientation of the glazed facade.

Table 2. Characterization of the office room.

Location	**38°44′14.1″ N 9°08′12.7″ W**
Solar orientation	Southeast
Geometry	4.31 m (width) × 4.57 m (depth) × 2.97 m (height)
Floor area	19 m^2
Glazing area	10.4 m^2
Window to wall ratio	81%
Shading system	Manual interior venetian blinds with metallic horizontal slats
Occupation	one person during working hours
Artificial lighting	LED lights
Electric equipment	Laptop and desktop computer
HVAC system	SCOP—4.43; SEER—7.98

Since the process behind electrochromism lies on the dual adjustment of electrons and ions, the transmission kinetics of the chosen electrolyte plays a key role in an EC device. There is a vast variety of EC materials that can be incorporated into EC devices, as reviewed by Ding et al. [80], with lithium-ion-based EC devices being the most common. EC thin films with vanadium pentoxide grown by spray pyrolysis [81,82] have proved to be a simple and cost-effective deposition method suitable for large areas, like building glazing. Figure 3 shows the different layers of the EC glazing system (7 + 12 + 4 mm) evaluated in this study that comprises an EC coating with tungsten oxide. This glazing can reversibly change its optical properties, shifting between clear and tinted states in response to applying a small electrical charge that transfers lithium ions between five layers of ceramic material coated onto a thin annealed glass pane, darkening the glass. By reversing the polarity, the glass returns to its clear state. The chromatic change can be manual or automatically controlled and aims at increasing energy efficiency and indoor comfort by modeling sunlight passing through the glazing and offering solar protection. The EC glazing can shift between five tinted states: a fully clear state, three intermediate states, and a fully tinted state.

As part of a previous research study that focused on the assessment of the thermal and luminous performance of solar control films [71], an extended field experimental campaign was conducted under real occupancy conditions in the office room. During a heating (11 March to 16 April) and a cooling (28 May to 28 June) period, the following data were simultaneously and continuously collected: indoor and outdoor solar radiation; indoor and outdoor illuminance; indoor and outdoor air temperature; surface temperature of the glazing system and shading system; indoor relative humidity; heat flux through the glazing. For more information regarding the methodology, equipment, and results of this experimental campaign, please refer to Teixeira et al. [71]. Some of the data collected during

this experimental campaign were used to calibrate the dynamic simulation model of the office room used in this work and described in the next subsection.

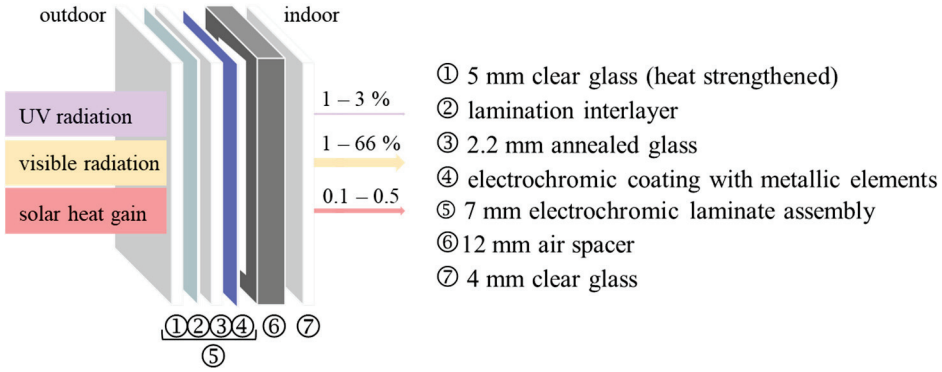


Figure 3. Layers of the electrochromic glazing system analyzed in this study, and respective UV transmittance (clear—3%, dark—1%), visible transmittance (clear—66%, dark—1%), and solar heat gain (clear—0.5, dark—0.1).

2.2. Dynamic Simulation

A 3D geometric model of the office room was created using SketchUp [69]. Apart from the exterior wall (U-value = 2.63 W/m·K) and the flat roof (U-value = 0.77 W/m^2·K), all other opaque elements of the facade were considered adiabatic in the simulation model. The thermal and optical properties of the existing static glazing with the solar control film were computed using Optics [67] and Window [68] software and were used to calibrate the dynamic simulation model.

The properties of the existing glazing system and the 3D model of the office room, together with the meteorological data gathered during the experimental campaign [71], were used as inputs in the EnergyPlus (version 9.5) [70] dynamic simulation model for the calibration procedure. The simulation model was calibrated by computing the NMBE and Cv (RMSE) statistical parameters to compare the simulated data with the experimental data previously collected [71]. After editing the input schedules and the airflow of the simulation model, the NMBE and Cv (RMSE) values of the selected calibration variables were within the limits for manually hourly calibration ($|\text{NMBE}| \leq 10\%$; Cv (RMSE) $\leq 30\%$ [83]); therefore, the simulation model was found suitable to accurately reproduce the office room. The calibration variables and respective NMBE and Cv (RMSE) for the heating (1 to 7 April) and cooling (6 to 12 July) periods are shown in Table 4. The calibration procedure is more deeply explained in the previously published study by Teixeira et al. [66].

The simulation model was used, after calibration, to evaluate the energy performance and the indoor comfort in the presence of the EC glazing. Two different controls were given to the EC glazing using the energy management system group in the EnergyPlus [70] software (Figure 4): the indoor glare levels and the indoor air temperature levels. These controls were selected with the aim of achieving energy efficiency, while providing good indoor thermal and visual conditions, similar to the methods used in previous studies [27,39,43,45]. The thermal and optical properties of the glazing system, computed with Optics [67] and Window [68] software, are shown in Table 3. Due to the low thermal transmittance and solar factor values of the EC glazing, a good thermal performance is expected. The EC glazing presents a large modulation range, with visible and solar transmittance values significantly lower than those of the clear glazing, even in the clear state. The EC glazing shows a higher solar absorption of the external pane, particularly for darker states that block excessive solar radiation gains through absorption. The EC glazing blocks 99% of the UV radiation incident on the glazing, having a positive impact on the duration and maintenance of furniture and on the occupant's health.

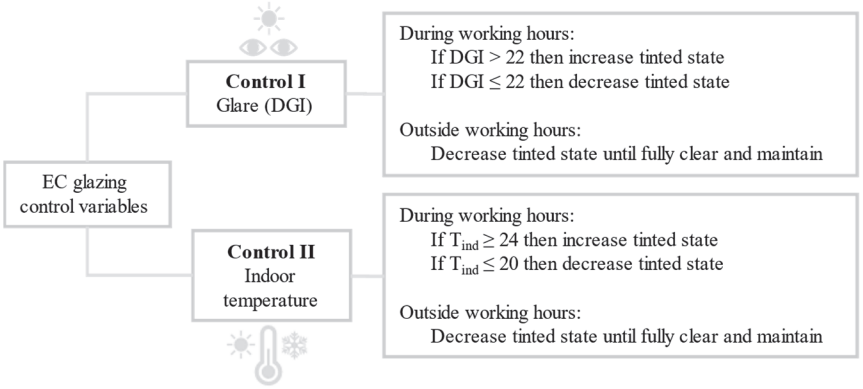


Figure 4. Controls of the electrochromic glazing considered in the simulation model.

Table 3. Thermal and optical properties of the electrochromic glazing system computed with Optics [67] and Window [68] software: thermal transmittance, U-value; solar factor, g; visible transmittance, τ_{vis}; visible front, ρ_{visF}, and back, ρ_{visB}, reflectance; solar transmittance, τ_{sol}; solar front, ρ_{solF}, and back, ρ_{solB}, reflectance; ultraviolet transmittance, τ_{UV}; absorptance of the external, α_1, and internal, α_2, glass panes.

Electrochromic Glazing States	U-Value [W/m^2·K]	g [-]	τ_{vis} [%]	ρ_{visF} [%]	ρ_{visB} [%]	τ_{sol} [%]	ρ_{solF} [%]	ρ_{solB} [%]	τ_{UV} [%]	α_1 [%]	α_2 [%]
Fully clear state	1.9	0.5	66	10	11	38	12	17	3	48	2
Intermediate state 1	1.9	0.2	18	6	9	7	7	16	1	85	0
Intermediate state 2	1.9	0.1	11	5	9	4	7	16	1	88	0
Intermediate state 3	1.9	0.1	6	5	9	2	7	15	1	91	0
Fully tinted state	1.9	0.1	1	5	9	0	8	16	0	92	0

Some of the parameters considered in the simulations of the energy performance and the indoor visual and thermal comfort are shown in Table 4. For a better understanding of the impact of the EC glazing on the performance of the office room, the existing venetian blinds were not considered in the simulation, making it possible to obtain results focused on the potential benefits of EC glazing installation in the considered case study, without the interference of a shading system. A "continuous off" type of control was assigned to the artificial lights in the simulation model, with a setpoint of 500 lx. The HVAC system was not considered in the simulations of the indoor thermal comfort under free-float conditions, except when computing the PMV [76] values (which require the operation of the HVAC system).

Table 4. Calibration variables, with respective NMBE and Cv (RMSE) for the heating and cooling period, and main parameters considered in the annual simulations of the energy performance and indoor comfort.

Calibration Variables	Indoor Temperature (T_{ind}) Interior (T_{si}) and Exterior (T_{se}) Surface Temperature of the Glazing
NMBE/Cv(RMSE)	Heating period: T_{ind}—0.49/4.60; T_{si}—−4.46/20.04; T_{se}—−11.15/22.60 Cooling period: T_{ind}—−1.84/4.41; T_{si}—−3.94/13.94; T_{se}—−8.23/13.89
Shading system	Not considered
Occupation	one person sitting at the desk during working hours (from 9 a.m. to 6 p.m. on weekdays)
Air changes per hour	1.0 h^{-1}
Artificial lighting	LED lights (110 W) on during working hours, if needed ("continuous off" control)
Electric equipment	Laptop computer (30 W) on during working hours, off otherwise Desktop computer (155 W) on during working hours, suspended otherwise
HVAC system	Available during working hours with deadband (20–24 °C)

To evaluate the energy performance in the presence of the EC glazing with the two implemented controls, both the energy needs and energy use of the office room were computed. Energy needs only include climatization needs, meaning heating and cooling. Energy use includes climatization (heating and cooling), artificial lighting, and control of the glazing. The energy use of the electric equipment (desktop and laptop computers) was not considered, since it is not affected by the type of glazing system. The energy needs were estimated using the simulation model, considering an ideal HVAC system. Knowing the seasonal energy efficiency values (SEER—7.98; SCOP—4.43) of the HVAC installed in the office room, the heating energy use was computed through the ratio between the heating energy needs and the SCOP value, and similarly, the cooling energy use was computed through the ratio between the cooling energy needs and the SEER value. The artificial lighting energy use was directly obtained from the simulation model. The energy consumed to control the EC glazing tinted states was calculated through the evolution of tinted states given by the simulation and the following energy consumption values of the control: clear state—0 W/m^2; change state—5 W/m^2; maintain state—1.4 W/m^2.

The visual comfort was evaluated based on the percentage of monthly and annual working hours with specific simulated illuminance levels at the center of the desk (Figure 5) and glare levels at eye level, with the occupant sitting at the desk facing the southwest wall (Figure 5). The UDI and the DGI were used to analyze the illuminance and glare values, respectively. The UDI metric [77,78] expresses the percentage of working hours with horizontal illuminance values at work plane that are within a specific range considered useful for occupants: from 0.1 klx to 3.0 klx. Illuminance values lower than 0.1 klx are considered insufficient to provide visual comfort, while illuminance values higher than 3.0 klx are associated with visual discomfort (high glare probability) [77,78]. The DGI metric [79] expresses glare values caused by daylight based on the following comfort ranges: DGI $\leq$ 16—imperceptible glare; 16 < DGI < 20—perceptible glare; 20 $\leq$ DGI < 24—uncomfortable glare; DGI $\geq$ 28—intolerable glare.

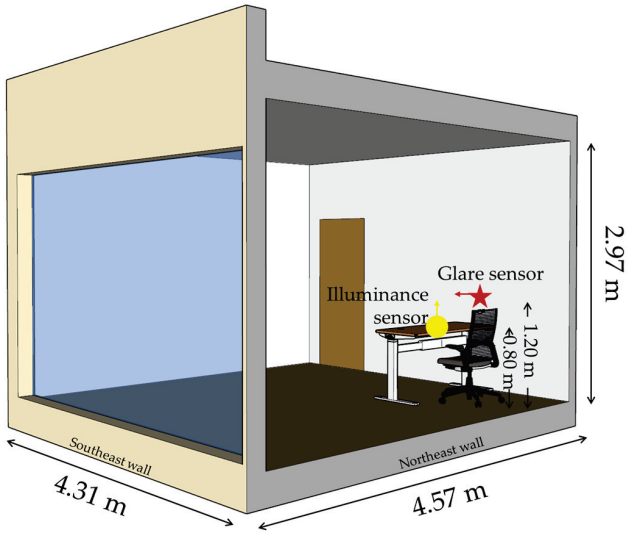


Figure 5. Location of the glare and illuminance sensors in the dynamic simulation.

The thermal comfort was evaluated at the sitting position at the desk (Figure 5), based on the monthly and annual percentage of working hours within the ranges of the following standards: Portuguese legislation [74]; ASHRAE 55 adaptive model (80% acceptability limit) [75]; PMV [76]. Following the Portuguese legislation [74], indoor air temperature values between 20 °C and 25 °C are considered comfortable for occupants of commercial buildings. No other parameters, like metabolic rate, clothing insulation, air speed, and relative humidity, are considered by this standard. The ASHRAE 55 adaptive model [75] defines the acceptable thermal conditions in spaces with natural ventilation controlled by occupants, relating acceptable temperature ranges to climatological parameters. This

standard is only applicable when spaces are occupied, and the average outdoor air dry-bulb temperature is between 10 °C and 33.5 °C over the last 7 days. The 80% acceptability limit [75] was considered in this study. The PMV index [76] predicts the mean value of votes of a group of occupants, through a thermal sensation scale, in an air-conditioned space. This index considers that when the internal heat production of the occupant equals its heat loss, the thermal equilibrium is achieved. The range ($-0.7 \leq \text{PMV} \leq 0.7$) for category III, in accordance with EN 16798 [84], was adopted in the present study. All of the energy produced by the occupant was assumed to being converted to heat. The dynamic predictive clothing insulation model, developed by Schiavon and Lee [85], was adopted, as well as an indoor air velocity of 0.2 m/s.

The typical meteorological year weather data of the three European cities of Lisbon, London, and Berlin were associated with the simulation model to evaluate the impact of the type of climate on the performance of the glazing systems. These three cities were selected to be representative of the main European climates: Lisbon—hot-summer Mediterranean climate; London—temperate oceanic climate; Berlin—warm-summer humid continental climate. Some geographic and climatic characteristics of the three cities are shown in Table 5. The assessment under different climates aims to enable the identify the impact of climatic conditions on the performance of the EC glazing. The results of the dynamic simulation of the energy performance and the thermal and visual comfort of the EC glazing, under the different climates, are shown and analyzed in the next section.

Table 5. Geographical and climatic characteristics of the cities of Lisbon, London, and Berlin.

		Lisbon (PT)	London (UK)	Berlin (DE)
Elevation [m]		71	44	147
Latitude [°]		38.73 N	51.15 N	52.47 N
Longitude [°]		9.15 W	0.18 W	13.4 E
Köppen–Geiger climate classification [73]		Csa	Cfb	Dfb
Monthly average outdoor air dry-bulb temperature [°C]	Minimum	10.6	3.9	0.3
	Average	16.3	10.2	9.8
	Maximum	22.6	17.3	19.1
Monthly average accumulated solar radiation incident on a south-facing vertical surface [kWh/m^2]	Minimum	76.1	28.6	17.4
	Average	102.0	68.0	64.9
	Maximum	120.8	93.4	96.3

3. Results

As previously mentioned, the tinted state of the EC glazing is controlled in the present study by the indoor glare (control I) or air temperature (control II) levels. Figure 6a shows the evolution of the solar factor and the transmittance of the EC glazing between tinted states. A significant decrease in the values of these properties can be noticed when the glazing alters from the fully tinted to the first intermediate state.

Figure 6b shows the percentage of working hours with specific tinted states of the EC glazing simulated throughout the year under the different climates. Since the operation of the HVAC system is expected to have an impact on the tinted states of the EC glazing with control II, and its operation is not considered in the computation of the thermal comfort in accordance with the Portuguese legislation [74] and the ASHRAE 55 adaptive model [75], both scenarios (with the HVAC system on and off) are shown. When considering control I (glare), for nearly the totality of working hours, the EC glazing is in the fully clear state for the three climates. This might be explained by the fact that the desk is located far away from the glazing, so there is limited need to tint the glazing when the control is indoor glare. Even though the accumulated vertical solar radiation levels are lower for the climates of London and Berlin (Table 5), the activation of the fully tinted state in these climates can be explained by the higher latitudes, when compared to the city of Lisbon, which result in lower solar angles and consequently, higher maximum values of indoor illuminance/glare. The EC glazing with control II (temperature) presents a similar dynamic behavior in both

HVAC on and off scenarios, under the climate of the city of Lisbon, with a higher percentage of working hours in the fully tinted state (HVAC on—83%; HVAC off—90%), followed by the climates of Berlin (HVAC on—29%; HVAC off—43%) and London (HVAC on—28%; HVAC off—41%). These results are in agreement with the temperature and solar radiation levels, previously shown in Table 5, which are higher for the city of Lisbon.

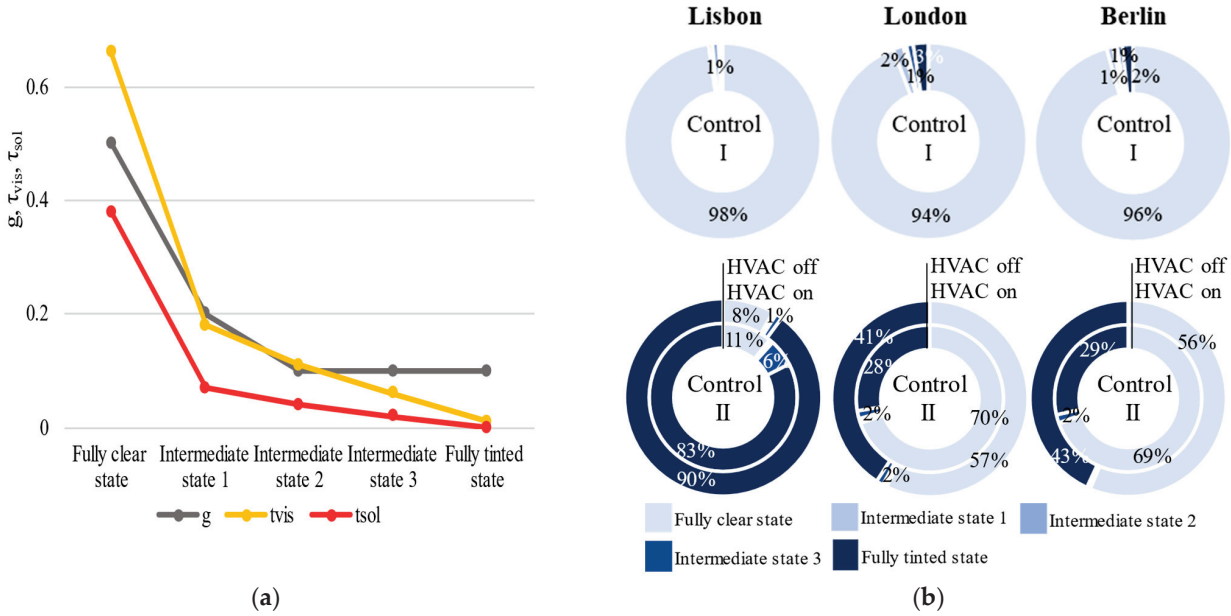


Figure 6. Dynamic behavior of the electrochromic glazing during the simulations: (**a**) evolution of the solar factor (g), the visible transmittance (τ_{vis}) and the solar transmittance (τ_{sol}) of the EC glazing depending on its tinted state; (**b**) percentage of working hours with specific tinted states of the glazing.

The following subsections present the results of the dynamic simulation for the energy performance and visual and thermal comfort of the office room in the presence of the EC glazing, under the different climates. The real solar orientation of the office room (southeast) was considered in this assessment.

3.1. Energy Performance

Both the energy needs and energy use are assessed in this subsection. As previously stated, energy needs only include climatization, and in addition, energy use includes artificial lighting and control of the glazing.

Figure 7a shows the (monthly and annual) energy needs, in kWh/m^2 of floor area, of the office room with the EC glazing (control I and II) under the three climates, as computed from the simulation. Due to the warmer climate and the higher solar radiation levels, the EC glazing showed higher cooling energy needs in Lisbon than in London and Berlin throughout the year. The dynamic behavior of the EC glazing made it possible to obtain practically null energy needs in some months, for all climates. The cooling energy needs were lower with control II, with reductions of approximately 30% when compared to control I for all climates. A small decrease in the heating energy needs (4–6%) was obtained, meaning the EC glazing also helped to increase solar heat when needed during cold months.

Figure 7b shows the (monthly and annual) energy use, in kWh/m^2 of floor area, of the office room with the EC glazing (control I and II) under the different climates, as obtained from the simulation. The significant difference between climatization energy needs and energy use is explained by the high efficiency of the HVAC system considered in the case study. Since the EC glazing spends more time in the fully tinted state with control II, the artificial lighting energy use suffered a significant increase throughout the year, for all

climates, but more strongly for the climate of Lisbon. The activation of the tinted states with control II led to an increase in the energy use to control the glazing. The type of control had a stronger impact on the energy use under the climate of Lisbon, with a difference of approximately 7 kWh/m^2 between the total energy use values of both control types. The highest total energy use was obtained with control II under the climate of Lisbon (27 kWh/m^2), closely followed by the same control type in Berlin (26 kWh/m^2). The lowest total energy use was achieved with control I in London (17 kWh/m^2).

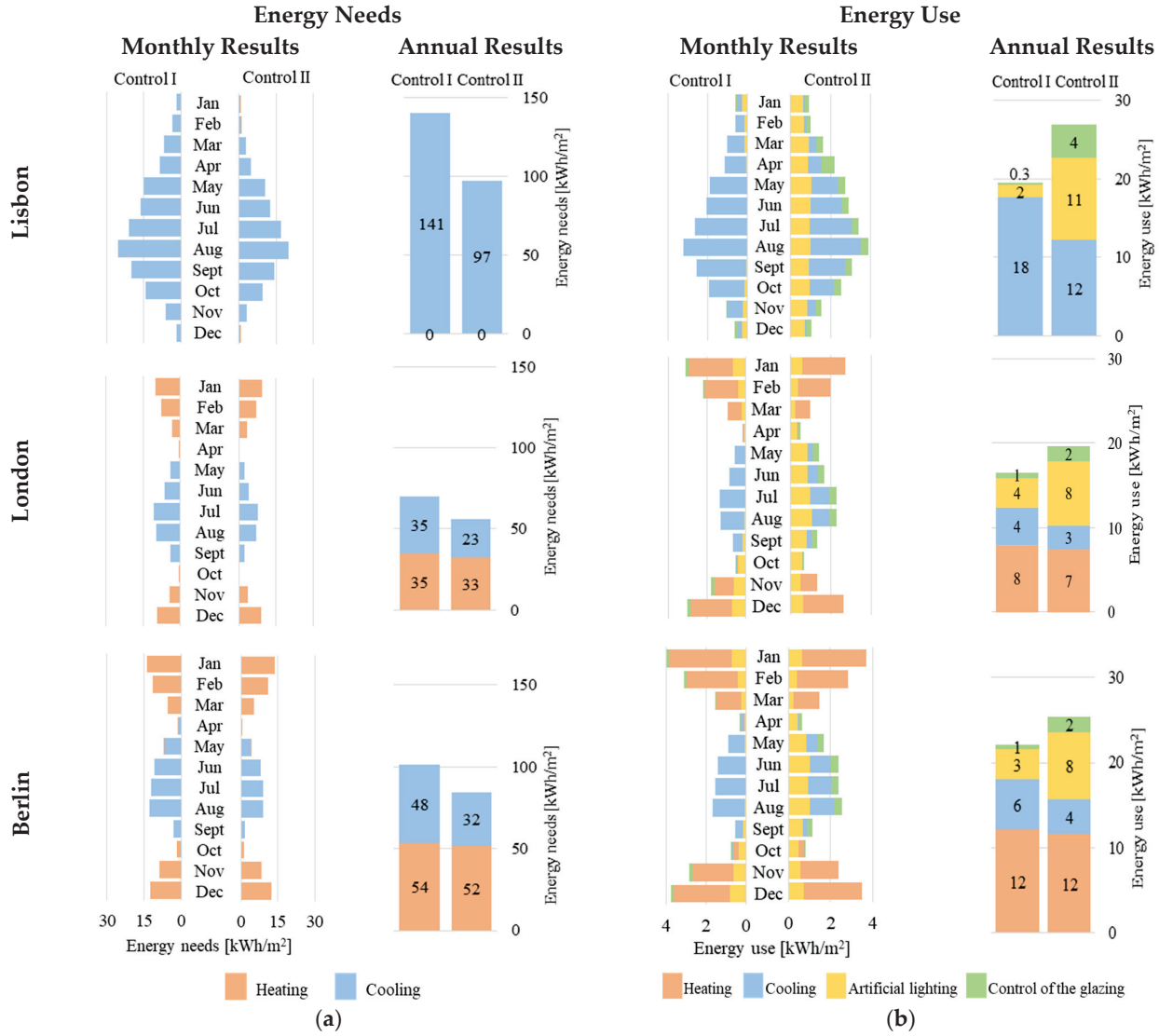


Figure 7. Energy performance of the electrochromic glazing, considering the two different controls (control I and II), under the climates of the cities of Lisbon, London, and Berlin: (**a**) simulated monthly and annual energy needs, in kWh/m^2, and (**b**) simulated monthly and annual energy use, in kWh/m^2.

3.2. Visual Comfort

Figure 8a shows the percentage of monthly and annual working hours with specific simulated indoor horizontal illuminance levels at the desk, in accordance with the UDI ranges [77,78], in the presence of the EC glazing (control I and II) under the different climates. When considering control I, higher percentages of working hours with exceeded illuminance levels were achieved throughout the year, particularly for the climate of Lisbon (20%). Control II shows a similar visual performance regarding illuminance levels under the climates of the cities of London and Berlin. The highest percentages of annual

working hours with useful illuminance levels were obtained with control I (Lisbon—75%; London—80%; Berlin—77%). The lowest percentage of annual working hours with useful illuminance levels was obtained with control II in Lisbon (16%), with the large majority of working hours (79%) showing insufficient illuminance levels.



Figure 8. Visual comfort in the presence of the electrochromic glazing, considering the two different controls (control I and II), under the climates of the cities of Lisbon, London, and Berlin: (**a**) percentage of monthly and annual working hours within specific UDI ranges at the desk center throughout the year, and (**b**) percentage of monthly and annual working hours within specific DGI ranges at eye level.

Figure 8b shows the percentage of monthly and annual working hours with specific simulated indoor glare levels at eye level, in accordance with the DGI metric ranges [79], with the EC glazing (control I and II) under the different climates. The highest percentages of working hours with imperceptible glare levels were obtained with control II during summer months because the high temperature values triggered the fully tinted state of the glazing. Uncomfortable and intolerable glare levels were obtained during winter months in the presence of the EC glazing with control II, for the climates of London and Berlin. The highest percentages of annual working hours with imperceptible glare (83–93%) were achieved with control II for all climates.

3.3. Thermal Comfort

The percentages of working hours within thermal comfort with each glazing control (control I and II), considering the comfort ranges defined by the Portuguese legislation, the adaptive model of ASHRAE 55, and PMV, are shown in Figure 9. The investigation of thermal comfort, taking into account these different approaches, makes it possible to assess the impact of the type of glazing control under a free-float regime (Portuguese legislation comfort range and ASHRAE 55 adaptive model comfort range) and with the operation of the HVAC system (PMV comfort range).

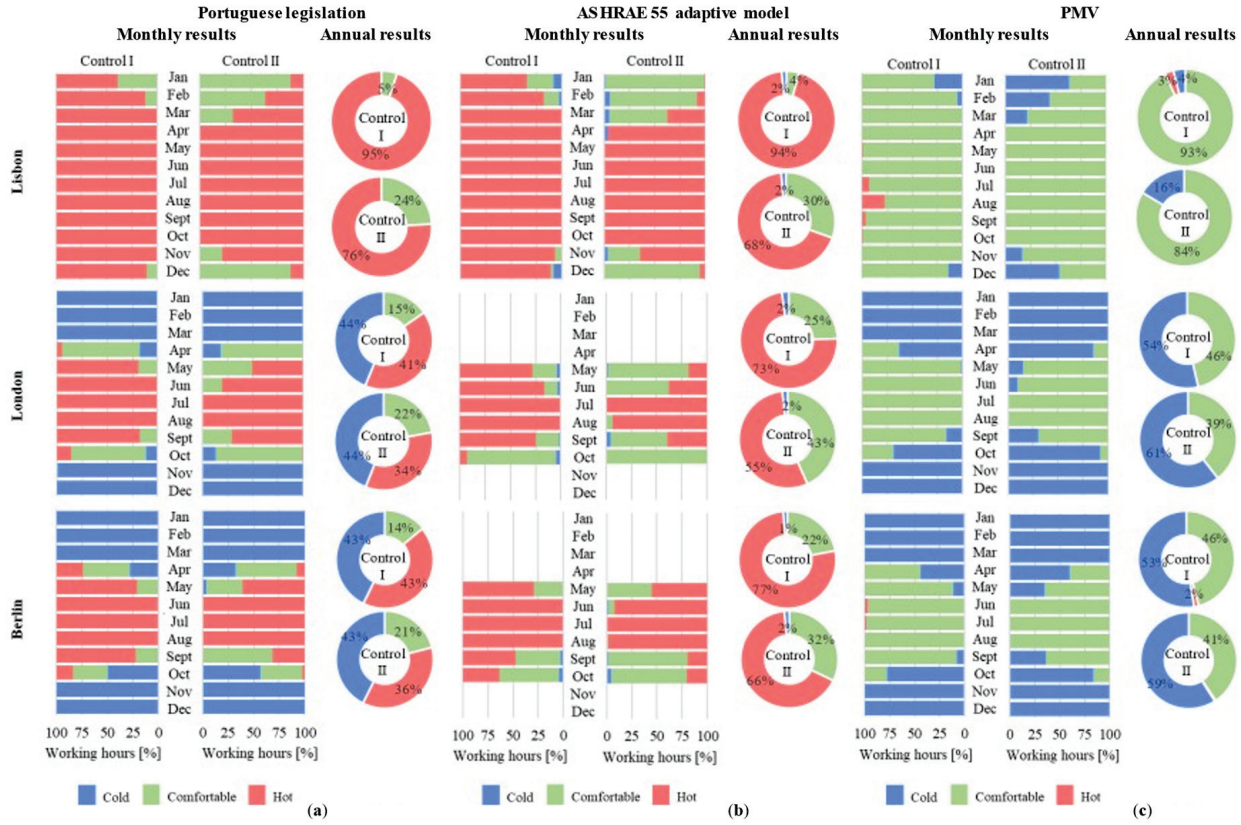


Figure 9. Thermal comfort in the presence of the electrochromic glazing (control I and II) under the climates of the cities of Lisbon, London, and Berlin: (**a**) percentage of monthly and annual working hours within the Portuguese legislation [43] thermal comfort ranges; (**b**) percentage of monthly and annual working hours within the ASHRAE 55 adaptive model [44] thermal comfort ranges (80% acceptability limit); (**c**). percentage of monthly and annual working hours within the predicted mean vote [45] thermal comfort ranges.

Figure 9a shows the percentage of monthly and annual working hours with specific indoor air temperature levels, in accordance with the Portuguese legislation [74], in the presence of the EC glazing (control I and II) under the different climates. Indoor air temperature levels higher than the comfort range were obtained during the large majority of working hours in the hot climate of Lisbon throughout the year. The results are similar for the cities of London and Berlin, with 100% of working hours with cold temperature levels during winter months. The highest percentages of annual working hours with too hot temperature levels were obtained for the city of Lisbon (control I—95%; control II—76%). Nevertheless, the highest percentage of annual working hours within thermal comfort (24%) was achieved with control II under the climate of the city of Lisbon. Control II made it possible to reduce too hot temperature levels and, in this way, increase the percentage of annual working hours within thermal comfort (London—22%; Berlin—21%), while

maintaining the percentage of working hours with too cold indoor temperature levels in the climates of London and Berlin.

Figure 9b shows the percentage of monthly and annual working hours within the thermal comfort ranges of ASHRAE 55 adaptive model (80% acceptability limit) [75], in the presence of the EC glazing (control I and II) under the three climates. For the climate of Lisbon, too hot temperature levels were obtained for practically 100% of monthly working hours between April and October, considering both control types. The highest percentages of annual working hours within thermal comfort were again obtained with control II (Lisbon—30%; London—43%; Berlin—32%). Control II made it possible to achieve reductions of the percentage of working hours with too hot temperature levels of up to 26%.

Figure 9c shows the percentage of monthly and annual working hours within the comfort ranges of the PMV index [45], in the presence of the EC glazing with both controls (control I and II), under the different climates. High percentages of working hours within thermal comfort were obtained throughout the year under the climate of Lisbon. Considering both control types, 100% of working hours showed too cold temperature levels during winter months under the climates of London and Berlin. The highest percentages of annual working hours within thermal comfort were obtained under the climate of Lisbon (control I—93%; control II—84%). The percentages of annual working hours within thermal comfort are very similar for the climates of London and Berlin. In contrast to what was observed in the previous results of the other two thermal comfort standards, control II did not increase the percentage of annual working hours within thermal comfort, compared to the results for control I, when computing thermal comfort with the PMV index.

As expected, thermal comfort results are improved with the operation of the HVAC system, making it possible to achieve high percentages of working hours within thermal comfort with both glazing controls. The reduction of the transmittance of solar gains with temperature control was beneficial under a free-float regime but had a negative impact considering climatization.

4. A Comparative Study of the Performance of Electrochromic Glazing and Other Glazing Technologies

In this section, a comparative study using the same office room is carried out regarding the performance of EC glazing compared to other glazing systems with different types and levels of solar control. This study aims to be comprehensive, meaning that it will be carried out in contexts of use that have a high impact on performance, such as climate variables and solar orientation.

Regarding the glazing systems used for comparison, the following solutions are considered: clear glazing, which is representative of the original glazing of the office room; clear glazing with a solar control film (SCF), which is representative of the existing glazing of the office room; and TC glazing, which increased the percentage of annual working hours with useful illuminance levels and within adaptive thermal comfort by up to 24% and 38%, respectively, and achieved energy savings of up to 50%, compared to the results for clear glazing, as noted by the authors in a previous publication [66]. These glazing options have different optical and solar characteristics and therefore, different levels of solar control. The first two work with constant values of these characteristics, representing a static solar control, while the TC works with variable values within a range, which represents a dynamic type of solar control.

To evaluate the influence of climate variables in this comparative study, the same climates of the three European cities used previously in the EC glazing study are again considered—Lisbon, London, and Berlin. Regarding the influence of solar orientation, the study is conducted assuming that the glazing facade can be exposed to north, east, south, west exposures, which are the directions between which the greatest contrasts in performance can be observed.

Table 6 shows the thermal and optical properties of the clear, with and without SCF, and TC glazing systems, computed using Optics [67] and Window [68] software. The clear

glazing without film exhibits high thermal, solar, and visible transmittance values, which can be linked to poor thermal and visual performance [66]. The clear glazing with an SCF provides high solar and visible reflectance values, blocking excessive solar radiation by reflection. The TC glazing, which reacts to a temperature stimulus, presents a dynamic behavior between 5 °C and 95 °C, altering its optical properties to modulate daylight and solar heat gains, reaching low visible and solar transmittance values in the darker states (higher temperature values). Similar to the EC glazing, the clear glazing with SCF and the TC glazing provide a UV protection of 99%. When comparing the EC (Table 3) and TC (Table 6) glazing systems in the fully clear state, the EC glazing exhibits higher visible and solar transmittance values.

Table 6. Main thermal and optical properties of the clear (with and without solar control film) and the thermochromic glazing systems computed with Optics [67] and Window [68] software: thermal transmittance, U-value; solar factor, g; visible transmittance, τ_{vis}; visible front, ρ_{visF}, and back, ρ_{visB}, reflectance; solar transmittance, τ_{sol}; solar front, ρ_{solF}, and back, ρ_{solB}, reflectance; ultraviolet transmittance, τ_{UV}; absorptance of the external, α_1, and internal, α_2, glass panes.

	U-Value [W/m^2·K]	g [-]	τ_{vis} [%]	ρ_{visF} [%]	ρ_{visB} [%]	τ_{sol} [%]	ρ_{solF} [%]	ρ_{solB} [%]	τ_{UV} [%]
Clear glazing without film	2.7	0.8	81	15	15	70	13	13	51
Clear glazing with film	2.6	0.4	27	43	44	17	35	42	1
TC glazing (clear state/dark state)	1.6	0.3/0.1	49/1	9/4	10/8	19/1	36/18	38/37	1/0

Given that solar radiation levels differ between the considered locations (Lisbon, London, and Berlin), the monthly average accumulated solar radiation incident on the facade when oriented north, east, south and west, during the winter and summer months, is presented in Table 7. The winter months comprise December, January, and February. The summer months comprise June, July, and August. For a specific climate, lower solar radiation levels were obtained for the north orientation, as expected. Solar radiation levels are higher during summer than winter months for each solar orientation under all climates, except for the case of the south orientation in Lisbon, with lower values during summer months, which can be explained by the higher solar altitude angle during this time of the year. The minimum, mean, and maximum solar radiation values for each solar orientation under the climate of Lisbon are higher than the ones observed for the other cities. The city of Berlin presents the lowest minimum and mean solar radiation levels for each solar orientation. The maximum solar radiation levels under the climate of London are lower than the ones observed for Berlin. The magnitude of incident solar radiation is directly related to solar gains. As a result, for climates and orientations with higher incident solar radiation, a greater impact of the solar gains on the performance is expected. The largest solar gains are expected to be associated with higher cooling needs and visual discomfort.

Table 7. Minimum, mean, and maximum monthly average accumulated solar radiation [kWh/m^2] incident on the office facade facing north (N), east (E), south (S) and west (W) during winter and summer months under the climates of the three European cities (Lisbon, London, and Berlin).

		Lisbon				London				Berlin			
		N	E	S	W	N	E	S	W	N	E	S	W
Winter months	Minimum	17.4	45.2	100.2	37.8	7.1	9.6	28.6	11.0	5.6	6.8	17.4	7.9
	Mean	19.2	52.1	104.6	40.1	9.2	15.1	40.1	16.0	8.3	12.5	28.9	12.9
	Maximum	22.2	62.7	109.6	42.7	12.3	22.0	47.8	21.3	12.0	21.0	46.8	20.4
Summer months	Minimum	46.1	128.2	74.9	95.2	41.5	74.6	79.4	79.9	42.4	78.1	83.1	79.0
	Mean	54.3	138.1	89.6	100.4	47.6	77.3	86.9	82.3	48.6	84.0	90.0	83.1
	Maximum	58.8	144.8	106.5	107.0	51.1	82.6	93.2	87.1	52.2	90.1	95.1	85.8

The side-by-side analysis of the impact of solar orientation on the performance of the different glazing systems, considering the clear glazing without film as reference, is presented in the next subsections.

4.1. Energy Performance

Figure 10 shows the annual energy savings (positive values—decreased energy consumption, resulting in energy savings; negative values—increased energy consumption) of the total energy use in the presence of each glazing system when compared to the results for the clear glazing for different solar orientations under the climate of the three cities. When assessing north solar orientation, the EC glazing controlled by glare showed the highest energy savings when compared to the other glazing solutions under the climates of Lisbon (9%) and London (2%). Still assessing north solar orientation, the EC glazing controlled by temperature showed a lower energy increase than the EC glazing controlled by glare and the clear glazing with film under the climate of Berlin, being surpassed by the TC glazing, which reached a neutral energy savings. The negative impact of the glazing systems with solar control, considering the north orientation, is more significant during winter months, when solar radiation levels are lower, and the reduction of solar heat gains and daylighting through the glazing are relatively higher, compared to their results during the summer months. When focusing on the results for the east solar orientation, the EC glazing with glare control presented similar energy savings (24%) to those for the clear glazing with film (26%) for the city of Lisbon, and the highest energy savings for the cities of London (6%) and Berlin (9%), along with the TC glazing (London—6%; Berlin—11%). The EC glazing with glare control showed the highest energy savings when compared to that of the EC glazing with temperature control and the clear glazing with film for a south orientation under the climates of the cities of London and Berlin. The EC glazing with glare control presented the highest energy savings (between 14% and 36%) when compared to the other glazing solutions for the west solar orientation, under all climates. Contrary to other glazing solutions, the EC glazing controlled by glare achieved positive energy savings for all solar orientations under the climates of Lisbon and London. Except for the south orientation under the climate of Lisbon, the EC glazing with temperature control showed negative energy savings.

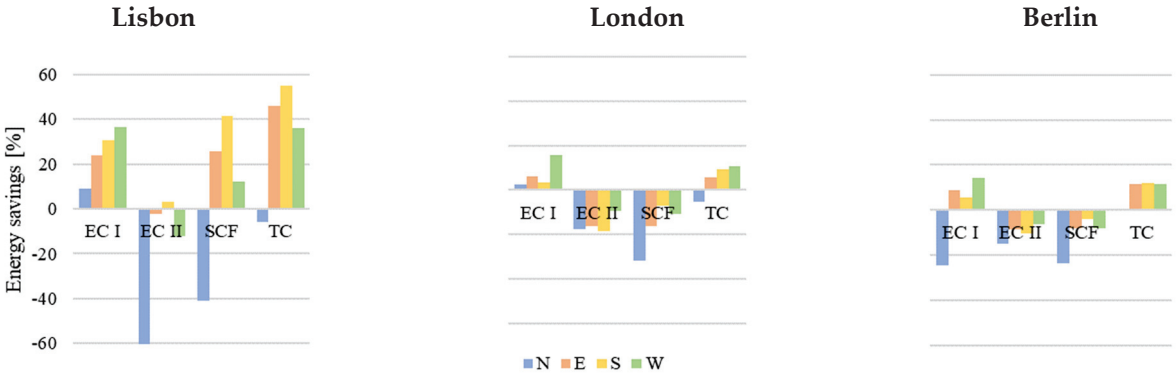


Figure 10. Annual energy savings, in % (positive values—decreased energy consumption, which resulted in energy savings; negative value—increased energy consumption), of the total energy use (climatization and artificial lighting) by the office room in the presence of each glazing system (electrochromic glazing with control I, electrochromic glazing with control II, clear glazing with film, thermochromic glazing) compared with the results for the clear glazing, for different solar orientations (N—north, E—east, S—south, W—west) under the three European climates.

4.2. Visual Comfort

Figure 11a shows the increase (positive percentage values) and decrease (negative percentage values) in annual working hours with useful illuminance levels (UDI metric [77,78]) in the presence of each glazing system when compared with the results for the clear glazing

for different solar orientations under the climate of the three cities. Positive percentage results are desirable, since they represent an increase in the indoor visual comfort. Focusing on the results for a north solar orientation, which is exposed to significantly low daylight levels, the EC glazing controlled by glare had the lowest decrease (between −1% and −2%) of working hours with useful illuminance levels for all climates, when compared to the other glazing systems because of the high visible transmittance of its clear state. For the east orientation, the EC glazing controlled by glare promoted an increase (5%) in working hours with useful illuminance in Lisbon (similar to the glazing with SCF—6%) that was surpassed by the TC glazing (10%); however, the EC showed the lowest decrease (up to 1%) in working hours with useful illuminance, comparing to the other glazing solutions, under the cold climates of London and Berlin. The EC glazing controlled by glare always showed an increase in working hours with useful illuminance when installed in a west-oriented façade, being surpassed by the TC glazing under all climates. The EC glazing controlled by temperature had a negative impact on illuminance levels for all solar orientations under the three climates, particularly in Lisbon.

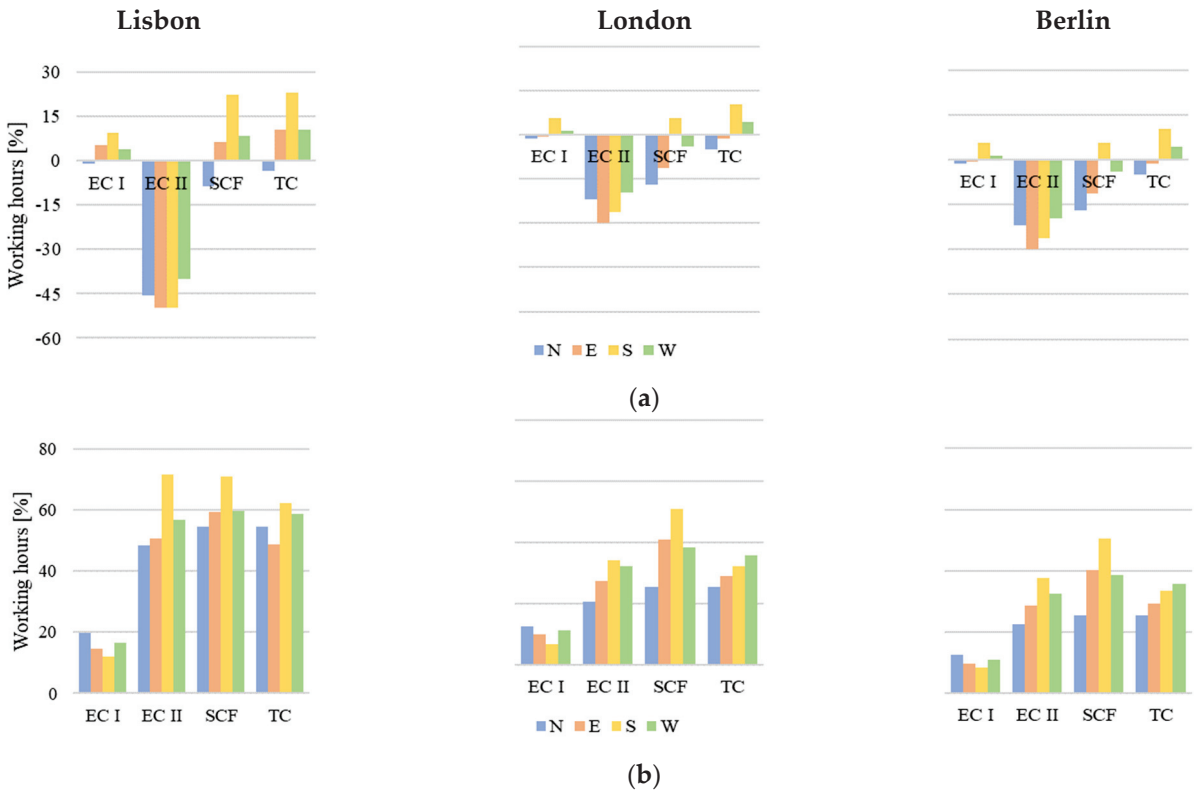


Figure 11. Increase (positive percentage values) and decrease (negative percentage values) in annual working hours with (**a**) useful illuminance levels and (**b**) imperceptible glare levels in the presence of each glazing system (electrochromic glazing with control I, electrochromic glazing with control II, clear glazing with film, thermochromic glazing) compared with the results for the clear glazing for different solar orientations (N—north, E—east, S—south, W—west) under the three European climates.

Figure 11b shows the increase (positive percentage values) and decrease (negative percentage values) in annual working hours, with imperceptible glare levels (DGI [79]), in the presence of each glazing system against the clear glazing for different solar orientations under the climate of the three cities. Positive percentage results are desirable, since they represent an increase in the indoor visual comfort. Due to the constant reduction of indoor illuminance levels in the presence of the EC glazing controlled by temperature, as previously stated, the percentage of working hours with imperceptible glare significantly increased with this glazing solution for all solar orientations under the different climates, particularly

in Lisbon. Focusing on east and west solar orientations, the EC glazing controlled by temperature showed a very similar performance to that of the TC glazing, under all climates. The EC glazing controlled by temperature promoted the highest glare reduction (72% of working hours with imperceptible glare) when oriented south, compared to the other glazing solutions, under the climate of Lisbon. For the cold climates of London and Berlin, the EC glazing controlled by temperature showed high percentages of working hours with imperceptible glare (London—34%; Berlin—38%) for the south solar orientations, being only surpassed by the clear glazing with SCF (London—51%; Berlin—51%).

4.3. Thermal Comfort

Figure 11a shows the increase (positive percentage values) and decrease (negative percentage values) in annual working hours within thermal comfort in accordance with the Portuguese legislation standards [59], in the presence of each glazing system compared with the clear glazing, for different solar orientations under the climate of the three cities. Positive percentage results are desirable, since they represent an increase in the indoor thermal comfort. Focusing on the east solar orientation, the EC glazing controlled by temperature showed the highest increases in working hours within thermal comfort (between 6% and 9%), under all climates, when compared with the remaining glazing solutions. The EC glazing controlled by temperature showed the best performance (between 9% and 17% of working hours within thermal comfort) for a south orientation, when comparing to the other glazing solutions, under all climates, being only surpassed by the TC glazing in Lisbon (22%). Under the climate of Lisbon, the EC glazing is the only glazing solution that made it possible to increase working hours within thermal comfort, helping to achieve an increase of 3%. Under the cold climates, the performance of this glazing system also surpassed the performance of the other glazing solutions when oriented west.

Figure 12b shows the increase (positive percentage values) and decrease (negative percentage values) in annual working hours within thermal comfort, in accordance with the ASHRAE 55 adaptive model [75], in the presence of each glazing system compared to the results for the clear glazing, for different solar orientations under the climate of the three cities. Positive percentage results are desirable, since they represent an increase in the indoor thermal comfort. The EC glazing controlled by temperature showed the highest increase in working hours within thermal comfort for the north (between 10% and 26%) and west (between 14% and 33%) solar orientations compared to the other glazing solutions, under all climates. Focusing on the south solar orientation, the EC glazing controlled by temperature made it possible to significantly increase (between 22% and 38%) the percentage of working hours within thermal comfort, under all climates, being only slightly surpassed by the TC glazing under the climates of Lisbon (26%) and London (40%).

Figure 12c shows the increase (positive percentage values) and decrease (negative percentage values) in annual working hours within thermal comfort in accordance with the PMV [76], in the presence of each glazing system compared with the results for the clear glazing, for different solar orientations under the climate of the three cities. Positive percentage results are desirable, since they represent an increase in the indoor thermal comfort. The EC glazing controlled by glare is the only glazing solution that increased the percentage of working hours within thermal comfort when assessing the south (9%) and west (2%) solar orientations, under the climate of Lisbon. The EC glazing controlled by temperature showed the highest increase when oriented east (12%), when compared to the other glazing solutions, under the climate of Lisbon. In accordance with this standard, all the glazing solutions decreased the percentage of working hours within thermal comfort for the different solar orientations under the cold climates of the cities of London and Berlin. For a specific solar orientation, this decrease was smaller in the presence of the EC glazing controlled by glare.



Figure 12. Increase (positive percentage values) and decrease (negative percentage values) in the annual percentage of working hours within thermal comfort, in accordance with (**a**) the Portuguese legislation [43], (**b**) the ASHRAE 55 adaptive model [44], and (**c**) the predicted mean vote [45] in the presence of each glazing system (electrochromic glazing with control I, electrochromic glazing with control II, clear glazing with film, thermochromic glazing) compared with the results for the clear glazing, for different solar orientations (N—north, E—east, S—south, W—west) under the three European climates.

5. Critical Discussion and Limitations

The added value of this study lies on the assessment of different performance aspects of an EC glazing, covering energy performance and indoor thermal and visual comfort, thus providing a holistic approach. The evaluation of the impact of climate and solar orientation on the performance of the glazing, comparing it with other glazing systems with different types and levels of solar control, are also key aspects of this study.

Even though the EC glazing controlled by temperature levels showed lower cooling and heating energy requirements, this glazing increased the artificial lighting energy use because of the low visible transmittance of its intermediate and fully tinted states, resulting in higher annual total energy use values.

The EC glazing controlled by glare showed high percentages regarding annual working hours (74–80%) with useful illuminance levels for all climates. In addition, uncom-

fortable and intolerable glare levels were reduced in the presence of this glazing system. The EC controlled by temperature significantly reduced indoor glare, achieving 80–93% of annual working hours with imperceptible glare; however, this control was less efficient in regards to blocking uncomfortable and intolerable glare levels. This can be explained by the fact that during the winter months, the solar altitude is lower, increasing indoor glare levels, but the temperature is insufficient to trigger the chromatic change to darken the EC glazing.

The thermal comfort assessment covering different standards made it possible to consider different requirements, parameters, and comfort conditions. Under free-float conditions, the EC glazing controlled by temperature showed higher percentages of working hours (up to 43%) within thermal comfort. Contrary to the results under free-float, this glazing did not show high percentages of working hours within thermal comfort when assessed using the PMV index. This could be due to the reduction of solar gains through the glazing, which increased the percentage of working hours with too cold temperature levels. As a result, the EC glazing controlled by glare showed a better thermal performance, when considering the operation of the HVAC system, with up to 93% of working hours within thermal comfort.

The comparative analysis of the performance of the EC glazing compared with that of the other glazing solutions (clear glazing with SCF and TC glazing), for different solar orientations, made it possible to better measure the evolution of the different performance aspects assessed and to evaluate the installation potential of the considered glazing solutions, using a clear glazing as the reference.

It was only possible to obtain energy savings for all solar orientations in the presence of the EC glazing controlled by glare under the climates of Lisbon (9–36%) and London (2–16%). The highest energy savings (14–36%) for a west solar orientation were also obtained with this glazing. Nevertheless, for east and south solar orientations, the energy savings obtained with the EC glazing controlled by glare were surpassed by the TC glazing. These finds are not in agreement with those obtained in the simulation study by Tällberg et al. [27], where energy consumption with the EC glazing was lower than with the TC glazing for south-oriented windows under temperate and continental climates, considering the real thermal and optical property values. This discrepancy of results can be explained by the lower WWR adopted by Tällberg et al. [27] and by the difference between the TC glazing properties used in the studies.

As expected, the percentage of annual working hours with useful illuminance levels, for a north orientation, suffered a negative impact in the presence of the glazing solutions with solar control (clear glazing with SCF, TC glazing, and EC glazing). However, it is worth mentioning that the EC glazing with glare control resulted in the lowest decrease in the useful illuminance levels (1–2%) for a north orientation. For south and west solar orientations, the TC glazing made it possible to achieve between 10–23% and 3–11% of annual working hours with useful illuminance levels, respectively. Even though the EC glazing controlled by temperature showed significant increases (34–72%) in annual working hours with imperceptible glare, considering the south solar orientation, its performance was surpassed by the clear glazing with SCF in London (51%) and Berlin (51%), which promoted a static/continuous type of solar control.

When assessing thermal comfort under a free-float regime, the EC glazing with temperature control presented the highest increases in annual working hours (6–33%) within thermal comfort, for a west orientation. With the HVAC system operating, all glazing systems were found to decrease the percentage of working hours within thermal comfort under the cold climates of the cities of London and Berlin.

It is noteworthy to mention that the findings that resulted from the methodology of this work (Section 2) were influenced by limitations that can act as constrains when generalizing the research findings, such as, specifically: office room and glazing system geometry; glazing solutions with characteristic thermal and optical properties; climates; specific occupation and equipment operation schedules; comfort conditions imposed; solar

orientation; type and energy efficiency of the climatization system; and software used. The same opaque elements of the envelope were adopted for the different locations/climates to allow a direct glazing performance comparison between the different climate conditions. However, it is important to note that this decision can negatively affect the glazing performance results under the cold climates of London and Berlin, since the regulatory requirements were not taken into account, and high heat exchanges are expected to occur due to low temperature levels. Even though EnergyPlus [70] is a well-established energy simulation program commonly used by engineers, architects and researchers, its ability to compute the visual performance of the assessed glazing systems can be considered limited because of its difficulty in solving for the internal reflectance of solar radiation, which results in an overestimation of the computed illuminance. A co-simulation strategy between EnergyPlus and Radiance could be more appropriate to assess the visual performance; nevertheless, for small square office rooms, such as the one used as the case study, the difference between the computed illuminance values of EnergyPlus and Radiance is less than 20% [86]. Still, regarding the visual performance assessment, the glare metric chosen (DGI) can act as a limitation, since it is based on the effect of contrast between adaptation luminance and a bright element in the field of view, and this metric is considered to have a less robust performance in daylight-dominated spaces [87,88].

6. Conclusions

This study comprises a multiple performance assessment of an EC glazing, controlled by indoor glare or temperature levels. Both energy performance and indoor (visual and thermal) comfort were evaluated under the main European climates, through a calibrated simulation model of an office room for a refurbishment scenario. The impact of solar orientation on the performance of the EC glazing was also assessed and compared to the performance of a clear glazing with a solar control film and a TC glazing, considering a clear glazing without film as the reference.

Regarding performance of the EC glazing oriented to the southeast, the following conclusions can be drawn:

- The EC glazing controlled by temperature levels reduced climatization needs. However, its negative impact on artificial lighting and higher control energy use resulted in higher annual total energy use. The lowest annual total energy use was achieved with glare control under the climate of London.
- Annual working hours (74–80%) with useful illuminance levels increased with glare control. Even though indoor glare levels were significantly reduced with temperature control, annual working hours with insufficient illuminance (48–79%) suffered a considerable increase.
- Even though temperature control showed a better performance (21–43%) under free-float, glare control showed a better performance (46–93%) when considering the operation of the HVAC system.

Regarding the comparative analysis of the impact of solar orientation on the performance of the different glazing solutions, the following conclusions can be drawn:

- The EC glazing controlled by glare was the only glazing solution that achieved energy savings for all solar orientations under the climates of Lisbon (9–36%) and London (2–16%). Even though it achieved the highest energy savings for a west orientation (up to 36%), it was surpassed by the TC glazing for the east (up to 46%) and south (up to 55%) orientations.
- The EC glazing with glare control had the lowest negative impact (−2%) on useful illuminance levels for a north orientation. The TC glazing was more efficient in regards to illuminance control for a south (10–33%) and west (3–12%) orientation. The EC glazing controlled by temperature significantly increased imperceptible glare levels when oriented south (34–72%), only being surpassed by the SCF glazing in London (51%) and Berlin (51%).

- Considering free-float regime, the EC glazing with temperature control was the most effective at promoting thermal comfort for a west orientation (3–33%). With the HVAC system operating, all glazing systems were found to decrease thermal comfort under cold climates.

This study has provided important insights regarding the potential for implementing EC glazing in largely glazed buildings for refurbishment scenarios, under different European climates. Further studies on the performance of EC glazing could be conducted to complement the research findings on the topic, such as: a parametric analysis to help understand the impact of construction aspects and glazing properties on performance; economic and environmental analyses; and comparing its performance with other dynamic glazing technologies, such as photochromic glazing.

Author Contributions: Conceptualization, M.G.G.; investigation, H.T., A.M.R., D.A. and M.G.G.; methodology, H.T., A.M.R., D.A. and M.G.G.; supervision, A.M.R., D.A. and M.G.G.; writing—original draft, H.T.; writing—review and editing, A.M.R., D.A. and M.G.G. All authors have read and agreed to the published version of the manuscript.

Funding: The first author wishes to acknowledge the support of Fundação para a Ciência e a Tecnologia (FCT) for funding her PhD Grant FCT PD/BD/150576/2020 (DOI: 10.5449/PD/BD/150576/2020). The authors thank FCT for funding the Civil Engineering Research and Innovation for Sustainability (CERIS) research unit through UIDB/04625/2020 (DOI: 10.54499/UIDB/04625/2020).

Data Availability Statement: The datasets are available on request from the authors.

Acknowledgments: The authors would like to thank the occupant of the office room (Department of Mechanical Engineering of Instituto Superior Técnico) for supporting the study. The authors also wish to express their gratitude to the IMPERSOL company for their technical support. The authors extend their gratitude to the CERIS research unit of the Associação do Instituto Superior Técnico para a Investigação e Desenvolvimento.

Conflicts of Interest: The authors declare no conflicts of interest. The funders had no role in the design of the study; in the collection, analyses, or interpretation of data; in the writing of the manuscript; or in the decision to publish the results.

Abbreviations

ASHRAE	American Society of Heating, Refrigerating, and Air-Conditioning Engineers
CO_2	carbon dioxide
Cv(RMSE)	coefficient of variation of the root mean square error
DGI	daylight glare index
DGP	daylight glare probability
EC	electrochromic
HVAC	heating, ventilation, and air conditioning
NMBE	normalized mean bias error
PMV	predicted mean vote
SCOP	seasonal coefficient of performance
SEER	seasonal energy efficiency ratio
TC	thermochromic
UDI	useful daylight illuminance

References

1. United Nations Environment Programme. *Global Status Report for Buildings and Construction: Beyond Foundations—Mainstreaming Sustainable Solutions to Cut Emissions from the Buildings Sector*; United Nations Environment Programme: Nairobi, Kenya, 2024. [CrossRef]
2. Sung, D. A New Look at Building Facades as Infrastructure. *Engineering* **2016**, *2*, 63–68. [CrossRef]
3. Nadoushani, Z.S.M.; Akbarnezhad, A.; Jornet, J.F.; Xiao, J. Multi-criteria selection of façade systems based on sustainability criteria. *Build. Environ.* **2017**, *121*, 67–78. [CrossRef]

4. Fernando, D.; Navaratnam, S.; Rajeev, P.; Sanjayan, J. Study of Technological Advancement and Challenges of Façade System for Sustainable Building: Current Design Practice. *Sustainability* **2023**, *15*, 14319. [CrossRef]
5. Hee, W.J.; Alghoul, M.A.; Bakhtyar, B.; Elayeb, O.; Shameri, M.A.; Alrubaih, M.S.; Sopian, K. The role of window glazing on daylighting and energy saving in buildings. *Renew. Sustain. Energy Rev.* **2015**, *42*, 323–343. [CrossRef]
6. De Masi, R.F.; Festa, V.; Gigante, A.; Ruggiero, S.; Vanoli, G.P. The role of windows on building performance under current and future weather conditions of European climates. *Energy Build.* **2023**, *292*, 113177. [CrossRef]
7. Amaral, A.R.; Rodrigues, E.; Gaspar, A.R.; Gomes, Á. A thermal performance parametric study of window type, orientation, size and shadowing effect. *Sustain. Cities Soc.* **2016**, *26*, 456–465. [CrossRef]
8. Gomes, M.G.; Santos, A.; Rodrigues, A.M. Solar and visible optical properties of glazing systems with venetian blinds: Numerical, experimental and blind control study. *J. Affect. Disord.* **2014**, *71*, 47–59. [CrossRef]
9. Karlsen, L.; Heiselberg, P.; Bryn, I.; Johra, H. Solar shading control strategy for office buildings in cold climate. *Energy Build.* **2016**, *118*, 316–328. [CrossRef]
10. Sghiouri, H.; Mezrhab, A.; Karkri, M.; Naji, H. Shading devices optimization to enhance thermal comfort and energy performance of a residential building in Morocco. *J. Build. Eng.* **2018**, *18*, 292–302. [CrossRef]
11. Moghaddam, S.A.; Mattsson, M.; Ameen, A.; Akander, J.; Da Silva, M.G.; Simões, N. Low-emissivity window films as an energy retrofit option for a historical stone building in cold climate. *Energies* **2021**, *14*, 7584. [CrossRef]
12. Teixeira, H.; Gomes, M.G.; Rodrigues, A.M.; Pereira, J. Thermal and visual comfort, energy use and environmental performance of glazing systems with solar control films. *J. Affect. Disord.* **2019**, *168*, 106474. [CrossRef]
13. Pereira, J.; Gomes, M.G.; Rodrigues, A.M.; Almeida, M. Thermal, luminous and energy performance of solar control films in single-glazed windows: Use of energy performance criteria to support decision making. *Energy Build.* **2019**, *198*, 431–443. [CrossRef]
14. Michael, M.; Favoino, F.; Jin, Q.; Luna-Navarro, A.; Overend, M. A Systematic Review and Classification of Glazing Technologies for Building Façades. *Energies* **2023**, *16*, 5357. [CrossRef]
15. Jaysawal, R.K.; Chakraborty, S.; Elangovan, D.; Padmanaban, S. Concept of net zero energy buildings (NZEB)—A literature review. *Clean. Eng. Technol.* **2022**, *11*, 100582. [CrossRef]
16. Favoino, F.; Loonen, R.C.G.M.; Doya, M.; Goia, F.; Bedon, C.; Babich, F. Building Performance Simulation and Characterisation of Adaptive Facades—Adaptive Facade Network. 2018. Available online: http://tu1403.eu/wp-content/uploads/Vol-3-2_for-web-Open-Access_9789463661119.pdf (accessed on 18 December 2019).
17. Baetens, R.; Jelle, B.P.; Gustavsen, A. Properties, requirements and possibilities of smart windows for dynamic daylight and solar energy control in buildings: A state-of-the-art review. *Sol. Energy Mater. Sol. Cells* **2010**, *94*, 87–105. [CrossRef]
18. Brzezicki, M. A systematic review of the most recent concepts in smart windows technologies with a focus on electrochromics. *Sustainability* **2021**, *13*, 9604. [CrossRef]
19. Casini, M. Active dynamic windows for buildings: A review. *Renew. Energy* **2018**, *119*, 923–934. [CrossRef]
20. Rezaei, S.D.; Shannigrahi, S.; Ramakrishna, S. A review of conventional, advanced, and smart glazing technologies and materials for improving indoor environment. *Sol. Energy Mater. Sol. Cells* **2017**, *159*, 26–51. [CrossRef]
21. Casini, M. Smart buildings: Advanced materials and nanotechnology to improve energy-efficiency and environmental performance. In *Woodhead Publishing Series in Civil and Structural Engineering*; Jones, G., Dean, M., Eds.; Woodhead Publishing: Sawston, UK, 2016.
22. Ke, Y.; Chen, J.; Lin, G.; Wang, S.; Zhou, Y.; Yin, J.; Lee, P.S.; Long, Y. Smart Windows: Smart Windows: Electro-, Thermo-, Mechano-, Photochromics, and Beyond. *Adv. Energy Mater.* **2019**, *9*, 1970153. [CrossRef]
23. Ke, Y.; Zhou, C.; Zhou, Y.; Wang, S.; Chan, S.H.; Long, Y. Emerging Thermal-Responsive Materials and Integrated Techniques Targeting the Energy-Efficient Smart Window Application. *Adv. Funct. Mater.* **2018**, *28*, 1800113. [CrossRef]
24. Leftheriotis, G.; Yianoulis, P. 3.10—Glazings and Coatings. In *Comprehensive Renewable Energy*; Elsevier: Amsterdam, The Netherlands, 2012. [CrossRef]
25. Cui, Y.; Ke, Y.; Liu, C.; Chen, Z.; Wang, N.; Zhang, L.; Zhou, Y.; Wang, S.; Gao, Y.; Long, Y. Thermochromic VO2 for Energy-Efficient Smart Windows. *Joule* **2018**, *2*, 1707–1746. [CrossRef]
26. Arnesano, M.; Pandarese, G.; Martarelli, M.; Naspi, F.; Gurunatha, K.L.; Sol, C.; Portnoi, M.; Ramirez, F.V.; Parkin, I.P.; Papakonstantinou, I.; et al. Optimization of the thermochromic glazing design for curtain wall buildings based on experimental measurements and dynamic simulation. *Sol. Energy* **2021**, *216*, 14–25. [CrossRef]
27. Tällberg, R.; Jelle, B.P.; Loonen, R.; Gao, T.; Hamdy, M. Comparison of the energy saving potential of adaptive and controllable smart windows: A state-of-the-art review and simulation studies of thermochromic, photochromic and electrochromic technologies. *Sol. Energy Mater. Sol. Cells* **2019**, *200*, 109828. [CrossRef]
28. Arnaoutakis, G.E.; Katsaprakakis, D.A. Energy Performance of Buildings with Thermochromic Windows in Mediterranean Climates. *Energies* **2021**, *14*, 6977. [CrossRef]
29. Yuxuan, Z.; Yunyun, Z.; Jianrong, Y.; Xiaoqiang, Z. Energy saving performance of thermochromic coatings with different colors for buildings. *Energy Build.* **2020**, *215*, 109920. [CrossRef]

30. Favoino, F.; Giovannini, L.; Pellegrino, A.; Serra, V. Building performance of thermochromic glazing. In *Eco-Efficient Materials for Reducing Cooling Needs in Buildings and Construction*; Elsevier Ltd.: Amsterdam, The Netherlands, 2021; pp. 401–437. [CrossRef]
31. Giovannini, L.; Favoino, F.; Pellegrino, A.; Verso, V.R.M.L.; Serra, V.; Zinzi, M. Thermochromic glazing performance: From component experimental characterisation to whole building performance evaluation. *Appl. Energy* **2019**, *251*, 113335. [CrossRef]
32. Costanzo, V.; Evola, G.; Marletta, L. Thermal and visual performance of real and theoretical thermochromic glazing solutions for office buildings. *Sol. Energy Mater. Sol. Cells* **2016**, *149*, 110–120. [CrossRef]
33. Ghosh, A.; Norton, B. Advances in switchable and highly insulating autonomous (self-powered) glazing systems for adaptive low energy buildings. *Renew. Energy* **2018**, *126*, 1003–1031. [CrossRef]
34. Ruggiero, S.; De Masi, R.F.; Assimakopoulos, M.-N.; Vanoli, G.P. Energy saving through building automation systems: Experimental and numerical study of a smart glass with liquid crystal and its control logics in summertime. *Energy Build.* **2022**, *273*, 112403. [CrossRef]
35. Mesloub, A.; Ghosh, A.; Kolsi, L.; Alshenaifi, M. Polymer-Dispersed Liquid Crystal (PDLC) smart switchable windows for less-energy hungry buildings and visual comfort in hot desert climate. *J. Build. Eng.* **2022**, *59*, 105101. [CrossRef]
36. Mesloub, A.; Ghosh, A.; Touahmia, M.; Albaqawy, G.A.; Alsolami, B.M.; Ahriz, A. Assessment of the overall energy performance of an SPD smart window in a hot desert climate. *Energy* **2022**, *252*, 124073. [CrossRef]
37. Oh, M.; Park, J. Evaluation of building energy and daylight performance according to applying electrochromic and pdcl (Polymer dispersed liquid crystal) to office building in South Korea. *Int. J. Sustain. Build. Technol. Urban Dev.* **2019**, *10*, 227–240. [CrossRef]
38. Cannavale, A.; Ayr, U.; Fiorito, F.; Martellotta, F. Smart electrochromic windows to enhance building energy efficiency and visual comfort. *Energies* **2020**, *13*, 1449. [CrossRef]
39. Lee, J.H.; Jeong, J.; Chae, Y.T. Optimal control parameter for electrochromic glazing operation in commercial buildings under different climatic conditions. *Appl. Energy* **2019**, *260*, 114338. [CrossRef]
40. Assimakopoulos, M.; Tsangrassoulis, A.; Santamouris, M.; Guarracino, G. Comparing the energy performance of an electrochromic window under various control strategies. *J. Affect. Disord.* **2007**, *42*, 2829–2834. [CrossRef]
41. Tavares, P.; Bernardo, H.; Gaspar, A.; Martins, A. Control criteria of electrochromic glasses for energy savings in mediterranean buildings refurbishment. *Sol. Energy* **2016**, *134*, 236–250. [CrossRef]
42. Gugliermetti, F.; Bisegna, F. Visual and energy management of electrochromic windows in Mediterranean climate. *J. Affect. Disord.* **2003**, *38*, 479–492. [CrossRef]
43. Cannavale, A.; Ayr, U.; Martellotta, F. Innovative electrochromic devices: Energy savings and visual comfort effects. *Energy Procedia* **2018**, *148*, 900–907. [CrossRef]
44. Dussault, J.-M.; Gosselin, L. Office buildings with electrochromic windows: A sensitivity analysis of design parameters on energy performance, and thermal and visual comfort. *Energy Build.* **2017**, *153*, 50–62. [CrossRef]
45. DeForest, N.; Shehabi, A.; Selkowitz, S.; Milliron, D.J. A comparative energy analysis of three electrochromic glazing technologies in commercial and residential buildings. *Appl. Energy* **2017**, *192*, 95–109. [CrossRef]
46. Li, Y.; Shah, K.W.; Li, W.; Xiong, T. Experimental investigation on indoor thermal environment improvement and energy-saving of electrochromic window under Singapore's tropical climate. *J. Build. Eng.* **2023**, *73*, 106779. [CrossRef]
47. Lee, E.; Tavil, A. Energy and visual comfort performance of electrochromic windows with overhangs. *J. Affect. Disord.* **2007**, *42*, 2439–2449. [CrossRef]
48. Piccolo, A.; Simone, F. Effect of switchable glazing on discomfort glare from windows. *J. Affect. Disord.* **2009**, *44*, 1171–1180. [CrossRef]
49. Jain, S.; Karmann, C.; Wienold, J. Behind electrochromic glazing: Assessing user's perception of glare from the sun in a controlled environment. *Energy Build.* **2021**, *256*, 111738. [CrossRef]
50. Ajaji, Y.; André, P. Thermal comfort and visual comfort in an office building equipped with smart electrochromic glazing: An experimental study. *Energy Procedia* **2015**, *78*, 2464–2469. [CrossRef]
51. Sbar, N.L.; Podbelski, L.; Yang, H.M.; Pease, B. Electrochromic dynamic windows for office buildings. *Int. J. Sustain. Built Environ.* **2012**, *1*, 125–139. [CrossRef]
52. Fernandes, L.; Lee, E.; Ward, G. Lighting energy savings potential of split-pane electrochromic windows controlled for daylighting with visual comfort. *Energy Build.* **2013**, *61*, 8–20. [CrossRef]
53. Park, B.R.; Hong, J.; Choi, E.J.; Choi, Y.J.; Lee, C.; Moon, J.W. Improvement in energy performance of building envelope incorporating electrochromic windows (ECWs). *Energies* **2019**, *12*, 1181. [CrossRef]
54. Tavares, P.; Gaspar, A.; Martins, A.; Frontini, F. Evaluation of electrochromic windows impact in the energy performance of buildings in mediterranean climates. *Energy Policy* **2013**, *67*, 68–81. [CrossRef]
55. Jonsson, A.; Roos, A. Evaluation of control strategies for different smart window combinations using computer simulations. *Sol. Energy* **2010**, *84*, 1–9. [CrossRef]
56. Fathi, S.; Kavoosi, A. Effect of electrochromic windows on energy consumption of high-rise office buildings in different climate regions of Iran. *Sol. Energy* **2021**, *223*, 132–149. [CrossRef]
57. Cannavale, A.; Martellotta, F.; Cossari, P.; Gigli, G.; Ayr, U. Energy savings due to building integration of innovative solid-state electrochromic devices. *Appl. Energy* **2018**, *225*, 975–985. [CrossRef]

58. Piccolo, A.; Pennisi, A.; Simone, F. Daylighting performance of an electrochromic window in a small scale test-cell. *Sol. Energy* **2009**, *83*, 832–844. [CrossRef]
59. Piccolo, A. Thermal performance of an electrochromic smart window tested in an environmental test cell. *Energy Build.* **2010**, *42*, 1409–1417. [CrossRef]
60. Piccolo, A.; Marino, C.; Nucara, A.; Pietrafesa, M. Energy performance of an electrochromic switchable glazing: Experimental and computational assessments. *Energy Build.* **2018**, *165*, 390–398. [CrossRef]
61. Li, W.; Shah, K.W.; Li, Y. Effects of Electrochromic Glass Window on Energy Efficiency, Thermal and Visual Performances Under Tropical Climate. *SSRN Electron. J.* **2023**, *76*, 4330893. [CrossRef]
62. Lee, E.; Claybaugh, E.; LaFrance, M. End user impacts of automated electrochromic windows in a pilot retrofit application. *Energy Build.* **2012**, *47*, 267–284. [CrossRef]
63. Lee, E.; DiBartolomeo, D.; Selkowitz, S. Daylighting control performance of a thin-film ceramic electrochromic window: Field study results. *Energy Build.* **2006**, *38*, 30–44. [CrossRef]
64. Lee, E.; DiBartolomeo, D. Application issues for large-area electrochromic windows in commercial buildings. *Sol. Energy Mater. Sol. Cells* **2002**, *71*, 465–491. [CrossRef]
65. Frattolillo, A.; Loddo, G.; Mastino, C.; Baccoli, R. Heating and cooling loads with electrochromic glazing in Mediterranean climate. *Energy Build.* **2019**, *201*, 174–182. [CrossRef]
66. Teixeira, H.; Gomes, M.G.; Rodrigues, A.M.; Aelenei, D. Assessment of the visual, thermal and energy performance of static vs thermochromic double-glazing under different European climates. *Build. Environ.* **2022**, *217*, 109115. [CrossRef]
67. Optics Software Downloads. Windows and Daylighting. Available online: https://windows.lbl.gov/tools/optics/software-download (accessed on 31 March 2022).
68. Curcija, C.; Vidanovic, S.; Hart, R.; Jonsson, J.; Mitchell, R. *WINDOW Technical Documentation*; Lawrence Berkeley National Laboratory: Berkeley, CA, USA, 2018.
69. Trimble Inc. Sketchup Pro. 2016. Available online: https://www.sketchup.com/ (accessed on 3 November 2016).
70. EnergyPlus Simulation Software. Available online: https://energyplus.net (accessed on 30 December 2018).
71. Teixeira, H.; Gomes, M.d.G.; Rodrigues, A.M.; Pereira, J. In-Service Thermal and Luminous Performance Monitoring of a Refurbished Building with Solar Control Films on the Glazing System. *Energies* **2021**, *14*, 1388. [CrossRef]
72. Weather Data by Location. EnergyPlus. Available online: https://energyplus.net/weather-location/europe_wmo_region_6/PRT//PRT_Lisboa.085360_INETI (accessed on 28 January 2021).
73. Beck, H.E.; Zimmermann, N.E.; McVicar, T.R.; Vergopolan, N.; Berg, A.; Wood, E.F. Present and future Köppen-Geiger climate classification maps at 1-km resolution. *Sci. Data* **2018**, *5*, 180214. [CrossRef] [PubMed]
74. Direção-Geral de Energia e Geologia and ADENE, Manual Técnico para a Avaliação do Desempenho Energético dos Edifícios. Available online: https://www.sce.pt/wp-content/uploads/2021/07/Manual-SCE.pdf (accessed on 25 April 2024).
75. *ASHRAE Standard 55-2017*; Thermal Environmental Conditions for Human Occupancy. The American Society of Heating, Refrigerating and Air-Conditioning Engineers: Atlanta, GA, USA, 2017.
76. *ISO Standard 7730*; Ergonomics of the Thermal Environment—Analytical Determination and Interpretation of Thermal Comfort Using Calculation of the PMV and PPD Indices and Local Thermal Comfort Criteria. International Organization for Standardization: Geneva, Switzerland, 2005.
77. Nabil, A.; Mardaljevic, J. Useful daylight illuminance: A new paradigm for assessing daylight in buildings. *Light. Res. Technol.* **2005**, *37*, 41–57. [CrossRef]
78. Mardaljevic, J.; Andersen, M.; Roy, N.; Christoffersen, J. Daylighting metrics: I there a relation between useful daylight illuminance and daylight glare probability? In Proceedings of the First Building Simulation and Optimization Conference, Loughborough, UK, 10–11 September 2012; pp. 189–196.
79. Hopkinson, R. Glare from daylighting in buildings. *Appl. Ergon.* **1972**, *3*, 206–215. [CrossRef] [PubMed]
80. Ding, Y.; Wang, M.; Mei, Z.; Diao, X. Different ion-based electrolytes for electrochromic devices: A review. *Sol. Energy Mater. Sol. Cells* **2022**, *248*, 112037. [CrossRef]
81. Romanitan, C.; Tudose, I.V.; Mouratis, K.; Popescu, M.C.; Pachiu, C.; Couris, S.; Koudoumas, E.; Suchea, M. Structural Investigations in Electrochromic Vanadium Pentoxide Thin Films. *Phys. Status Solidi (A) Appl. Mater. Sci.* **2021**, *219*, 2100431. [CrossRef]
82. Mouratis, K.; Tudose, V.; Romanitan, C.; Pachiu, C.; Tutunaru, O.; Suchea, M.; Couris, S.; Vernardou, D.; Emmanouel, K. Electrochromic performance of V_2O_5 thin films grown by spray pyrolysis. *Materials* **2020**, *13*, 3859. [CrossRef] [PubMed]
83. ANSI/ASHRAE. *ASHRAE Guideline 14-2002 Measurement of Energy and Demand Savings*; ASHRAE: Peachtree Corners, Georgia, 2002.
84. *BS EN 16798*; Energy Performance of Buildings. Ventilation for Buildings. BSI: London, UK, 2019.
85. Schiavon, S.; Lee, K.H. Dynamic predictive clothing insulation models based on outdoor air and indoor operative temperatures. *J. Affect. Disord.* **2013**, *59*, 250–260. [CrossRef]
86. Ramos, G.; Ghisi, E. Analysis of daylight calculated using the EnergyPlus programme. *Renew. Sustain. Energy Rev.* **2010**, *14*, 1948–1958. [CrossRef]

87. Wienold, J.; Iwata, T.; Khanie, M.S.; Erell, E.; Kaftan, E.; Rodriguez, R.; Garreton, J.Y.; Tzempelikos, T.; Konstantzos, I.; Christoffersen, J.; et al. Cross-validation and robustness of daylight glare metrics. *Light. Res. Technol.* **2018**, *51*, 983–1013. [CrossRef]
88. Quek, G.; Wienold, J.; Khanie, M.S.; Erell, E.; Kaftan, E.; Tzempelikos, A.; Konstantzos, I.; Christoffersen, J.; Kuhn, T.; Andersen, M. Comparing performance of discomfort glare metrics in high and low adaptation levels. *J. Affect. Disord.* **2021**, *206*, 108335. [CrossRef]

Disclaimer/Publisher's Note: The statements, opinions and data contained in all publications are solely those of the individual author(s) and contributor(s) and not of MDPI and/or the editor(s). MDPI and/or the editor(s) disclaim responsibility for any injury to people or property resulting from any ideas, methods, instructions or products referred to in the content.

energies

MDPI

Article

Exploring Multiple Benefits of Urban and Energy Regeneration Projects: A Stakeholder-Centred Methodological Approach

Irene Bertolami [1], Adriano Bisello [1,*], Marco Volpatti [1,2] and Marta Carla Bottero [2]

[1] Eurac Research, Institute for Renewable Energy, Viale Druso 1, 39100 Bolzano, Italy; irene.bertolami@eurac.edu (I.B.); marco.volpatti@polito.it (M.V.)
[2] Interuniversity Department of Urban and Regional Studies and Planning, Polytechnic of Turin, Viale Mattioli 39, 10125 Turin, Italy; marta.bottero@polito.it
* Correspondence: adriano.bisello@eurac.edu

Abstract: An effective way to promote energy transition while tackling climate change involves redefining cities from being part of the problem to integral parts of the solution. Positive energy districts and climate positive circular communities are excellent examples of how this is feasible. But how do we understand which are the multiple benefits that these projects can bring to the local territory and relative community? This article aims to answer this question by developing a specific engagement and evaluation methodology. Our approach involves consulting with project partners to explore the multiple benefits of each case study. Subsequently, it plans to engage the stakeholders through the submission of a questionnaire to gather information regarding the relative importance of different benefits as perceived by each stakeholder. The questionnaire is based on the best–worst scaling method, which is a survey technique for determining people's priorities. The preliminary findings of the study conducted on project partners of two European projects, ARV and ProLight, indicate a strong alignment with current European policy priorities. The involvement of other stakeholders in the study will serve to assess whether bottom-up priorities coincide with broader perspectives or whether adaptations to project strategies and dissemination approaches are needed.

Keywords: multiple benefits; positive energy district; climate positive circular community; smart city; stakeholders' consultation; best–worst scaling; non-financial impact; ESG criteria

1. Introduction

Climate change is unequivocally one of the most pressing worldwide dilemmas facing humanity in the 21st century. Cities carry a significant portion of responsibility for driving these changes [1]. Nevertheless, our focus should shift towards converting them from being perceived as problematic to being seen as opportunities [2]. Nowadays, the urban population constitutes over half of the global populace [3] and, given the projected escalation of this proportion in the years to come, it becomes fundamental to foster the development of environmentally conscious and sustainable urban areas. Particularly, buildings have a considerable impact on global resource consumption and the environment. Buildings use about 40% of the world's energy, 25% of its water, and 40% of global resources. Moreover, they produce approximately one third of all greenhouse gas emissions (GHG), contributing significantly to global warming [4]. However, by improving the built environment, we can achieve substantial GHG emission reductions, leading to environmental benefits and economic advantages through lower energy costs and a more sustainable infrastructure [5,6].

Nowadays, there are ongoing efforts to especially align with the objectives of the Paris Agreement [7]. Notable initiatives, such as the European Green Deal [8] and the Mission on Climate-neutral and Smart Cities [9], are taking significant steps in this direction. These

initiatives have established ambitious energy and climate targets within Europe, aimed at reducing greenhouse gas (GHG) emissions, enhancing energy security, and promoting greater reuse and recycling of materials [10]. Moreover, the New European Bauhaus initiative extends beyond these objectives, aiming to incorporate the vital principles of inclusivity and aesthetics as well [11].

Within these initiatives, projects are structured to translate ideologies into practical implementation. This involves the creation of sustainable pilot districts to serve as leading examples that inspire transformative change. The sustainable urban models currently considered successful are, for instance, smart cities, positive energy districts, and climate positive circular communities. However, an apparently trivial but crucial question arises: what are the concrete positive impacts of such models on local communities?

One key strategy to address this question is the analysis and assessment of the multiple benefits associated with urban and energy retrofitting projects. By following this approach, all the benefits should be considered without privileging any of them, since they all contribute to the improvement of the community and its territory. This method considers not just the technical enhancements of a project, like increased energy efficiency, but also its associated positive impacts, such as addressing energy poverty or making energy more accessible and affordable for vulnerable communities [12].

Moreover, the task of preparing our cities to effectively tackle the challenges posed by climate change demands active engagement from all individuals, from large corporations to ordinary citizens. A good way to guarantee success is to consider the needs of all the city users as well as to try to make everyone feel part of the community [13].

This article intends to present an innovative way of performing multiple benefit analysis in relation to urban and energy regeneration projects, outlining a precise methodology to be followed by decision makers. What sets this methodology apart is its emphasis on participation, as it actively engages a wide array of people from various backgrounds and interests. In particular, the approach seeks dialogue with stakeholders, who are individuals or groups of people who are or could be affected by organizations' actions [14] or, as in this case, by a project.

The methodological process begins with the identification of expected multiple benefits through a review of the scientific literature and an analysis of recent smart cities and positive energy districts projects. Subsequently, interactive workshops are organised with project partners, using in-person and/or remote interaction to compile a list of expected benefits tailored to each case study. Stakeholders are then invited to participate in a questionnaire based on the best–worst scaling technique, allowing them to identify the most significant benefits based on their professional or individual roles in the project. The workshops facilitate conversations with chosen stakeholders, offering a platform for targeted discussions. Meanwhile, the surveys contribute to a wider understanding by presenting expansive viewpoints and empirical data. This approach is designed to be adaptable and versatile, making it applicable to a range of urban development initiatives.

The methodology for studying multiple benefits, developed in the context of this research, is supported by initial findings from its implementation in two ongoing European urban innovation initiatives, namely ARV and ProLight. At the core of this approach is stakeholder interaction and discourse, facilitated by the use of the best–worst scaling method for assessing individual preferences. Our approach encourages close interaction with stakeholders, facilitating a deeper understanding of their perspectives and priorities within the project. This greater understanding can help stakeholders recognise the potential positive impacts of urban and energy redevelopment, while providing decision makers with an additional opportunity to listen to and consider the voices of those involved. Moreover, this methodology opens new opportunities for making investments in urban energy transition more advantageous, considering the overall impacts. It can be applied to a wide range of urban projects and policies, with tangible benefits in terms of environmental sustainability, social equity, and economic development.

2. Methodological Background

2.1. The "Multiple Benefits" Concept

The concept of multiple benefits refers to any positive impact that can result from a project when it is seen holistically, without assigning it a particular ranking [15].

At its core, the notion of multiple benefits implies that evaluating a project's success should not be limited to a single dimension of assessment. Instead, it encourages an exploration of the multifaceted ways in which the project can bring about positive change, including social, environmental, economic, and governance advantages. Multiple benefits include the following types of advantages:

1. Main goals (expected benefits): these are the positive outcomes that are typically planned for and anticipated during the project's inception and planning stages. They are often aligned with the project's primary objectives and can be usually quantified and measured using specific criteria [16]. Examples of expected benefits could include economic and energy savings, improved efficiency, or reduced fossil fuel dependency.
2. Co-benefits (unexpected and secondary benefits): these are the positive impacts that emerge unexpectedly or collaterally as a result of the project's implementation since they were not initially accounted for in the project's planning or evaluation [17]. These benefits often arise due to the complex interactions between various components of the project and its broader context. The notion of co-benefits is not restricted to any particular realm of society; it can encompass domains such as health and well-being, the environment, economics, and social aspects, among others [16]. Examples of unexpected benefits might include improved quality of life of the inhabitants, enhanced citizen engagement, and increased knowledge exchange. Many of these can be found within the conceptual categories of ESG criteria, which, nowadays, are particularly relevant for every business area.

In other words, multiple benefits are all the expected and unexpected benefits with a horizontal perspective [18], as no single benefit is considered more significant than others nor the main goals compared to the co-benefits [15].

The notion of multiple benefits is a progression from the more commonly recognised concept of co-benefits. Although the definition has experienced slight modifications over time, the notion of co-benefits dates back to the 1990s [19]. Nevertheless, the term gained more comprehensive attention from the Intergovernmental Panel on Climate Change (IPCC) in the third evaluation report of 2001 [4], wherein the concept is employed to signify the non-climatic advantages of policies aimed at mitigating greenhouse gas emissions. The concept of multiple benefits is more recent since it was introduced by the International Energy Agency (IEA) in 2014 [5] to fully harness the investment potential in building energy efficiency. IEA identified 15 multiple benefits, which may originate from the improvement of energy efficiency, and represented them in the so-called "multiple benefits' flower" diagram. The innovation lies in the fact that the identified positive impacts were not limited to the energy sector but extended to social, economic, environmental aspects, and more. Even though nearly a decade has passed since then, its practical implementation remains a challenge today, especially when evaluating complex urban contexts, such as entire neighbourhoods rather than an individual building.

Exploring a variety of benefits is key to maximising the potential of a project or policy. This comprehensive assessment not only aids in understanding the positive outcomes but also in sharing these impacts to increase awareness among investors, end users, and other stakeholders. Notably, Sareen et al. [20] propose that emerging impacts could incentivise stakeholder participation. Furthermore, a technical report by the Joint Research Centre released in 2020 [21] reported that integrating a multiple benefits analysis into the cost-optimality calculation process for an energy district positively influences community involvement. Recognising the significance of studying multiple benefits extends beyond attracting investors; it involves engaging the project's end users in decision making and aiding their comprehension of the project's advantages. Embracing this inclusive approach could gather broader support, acknowledging that stakeholders perceive different benefits

as more significant and engaging based on evolving perspectives while also enhancing the main goals of the project.

2.2. Overview of the Concepts of Smart City, Positive Energy District, and Climate Positive Circular Community

To gain a comprehensive understanding of the practical application of multiple benefits, it is essential to provide an overview of the concepts of smart cities, positive energy districts (PED), and climate positive circular communities (CPCC). These are just some city models, among the most cutting-edge at the moment; however, the methodology can be utilised for any type of urban project.

These concepts have evolved from the broader idea of sustainable and liveable urban settings and are in alignment with the United Nations' sustainable development goals [22]. They receive support and funding from the European Union and various other initiatives.

Smart cities integrate information and communication technologies (ICTs) with sustainability, aiming to enhance the quality of urban life through technology-driven solutions. For example, they may employ sensors to monitor air quality, traffic flow, and energy usage, allowing for real-time adjustments and improvements [23]. Moreover, smart cities are not just about technology but also involve active engagement with the community to create a more comfortable and sustainable urban environment [24].

Positive energy districts (PED) take the sustainability approach further, focusing on creating urban areas that generate more energy than they consume from renewable sources. This excess energy can be shared with other parts of the city, promoting energy efficiency and environmental sustainability [25]. Implementing PEDs may require adjustments to urban planning tools, such as creating variants to general master plans, to optimise mixed-use development while respecting territorial guidelines.

Climate positive circular communities (CPCC) expand on the PED concept, envisioning urban areas that not only produce surplus energy but also emphasise renewable resources, waste reduction, and circular economy principles. These communities aim to integrate social, economic, and environmental sustainability in a balanced way. Achieving a climate-positive status involves actively supporting environmental regeneration and restoration in addition to avoiding harmful environmental consequences. The possibility of generating climate positive circular communities was explored within the framework of the European project ARV.

Each concept mentioned above reflects a commitment to making urban areas more liveable, environmentally friendly, and resilient in the face of evolving challenges like climate change and resource scarcity considering different aspects.

2.3. Best–Worst Scaling

In order to enhance the effectiveness of the multiple benefits analysis and integrate stakeholders' perspectives, a questionnaire was distributed to all individuals directly or indirectly involved in the project. This initiative employed the best–worst scaling (BWS) method, chosen for its efficacy in capturing nuanced stakeholder viewpoints.

BWS, sometimes referred to as MaxDiff [26–28], was developed by Louviere and Woodworth in 1990 and its first application was published in 1992 [29]. This methodology evolved from the desire of creating user-friendly surveys. This methodical approach allows for a more focused and purposeful selection, ensuring the subsequent use and analysis of these benefits would be robust and effective. Its fundament is based on the notion that individuals find it easier to assess extremes rather than rank items, moving away from the approach suggested by other models [30]. Respondents are tasked with selecting the "best" and "worst" elements from a set of options.

BWS aligns with the Random Utility Theory (RUT), which states that people have preferences and make choices based on the utility associated with each alternative [31].

It categorises items into groups or tasks, each consisting of a minimum of three items. Respondents are supposed to identify the "best" and "worst" elements within each task.

Effective implementation of the methodology depends on striking a suitable balance between the number of tasks and the number of items per task.

Initially utilised in the food industry to examine the role of product safety in consumer purchasing decisions [29], this methodology has since then found application across diverse fields, including marketing [32], social sciences [33], and medicine [34].

BWS offers three variations for data collection and preference analysis: object case, profile case, and multi-profile case [35]. This study opted for the first case, known for its simplicity and familiarity. In this scenario, respondents rank items based on subjective scales, providing measures on a known scale [36]. Case 1 proves valuable when the focus is on understanding relative differences between objects rather than obtaining absolute measurements or ratings [37].

In the analysis of best–worst scaling, there are different methods available to calculate results. These methods can be broadly classified into two groups: count-based methods and model-based methods, as outlined by Chrzan et al. in 2019 [27]. The best–worst scaling score was calculated with the Analytical Best–Worst Scoring (ABW) proposed by Lipovetsky & Conklin [38], which follows Equation (1):

$$\mathrm{ABW} = \ln\left(\frac{1+\mathrm{NBW}}{1-\mathrm{NBW}}\right) \tag{1}$$

where NBW is the best–worst score normalised by the unit calculated according to Equation (2):

$$\mathrm{NBW} = \frac{\#\mathrm{Bests} - \#\mathrm{Worsts}}{\text{Total times shown}} \tag{2}$$

where the distinction between #Bests and #Worsts indicates how often an item is chosen as the best or worst option, respectively. The denominator reflects the total number of times the item is presented for selection.

The creation of the questionnaire was supported by the use of Sawtooth Software Discover® (sawtoothsoftware.com, accessed on 9 January 2023), which is designed to apply the best–worst scaling method.

3. Methodology: PHASES of Evaluation

The present methodology is an evolution of the approach used by Bisello [15] for the investigation of multiple benefits in a Smart and Sustainable Energy-District Project (SSEDP).

While versatile across contexts, this approach has been tested within the framework of the above concepts of smart cities, PEDs, and CPCCs, in particular, where applied to the ARV and ProLight projects.

The ARV project, which spans from 2022 to 2025 and is funded by the H2020 EU program, aims to obtain six pilot CPCCs across Europe. Through initiatives like energy renovation on existing or new buildings, it aims to safeguard threatened heritage while addressing energy poverty and promoting sustainability. In addition to showcasing exemplary models, it intends to create replicable, scalable solutions beyond showcasing exemplary models, fostering knowledge sharing, and best practices dissemination.

The ProLight Project, also funded by H2020 and initiated in late 2022, centres around the PED concept, focusing on small-scale building interventions for energy transition and local urban innovation ecosystems. In line with the principles of the New European Bauhaus, it aims to create sustainable living environments, integrating technologies such as photovoltaic panels and sensors into renovation actions in six case studies in Europe. It seeks to share excess energy across community networks and use innovative digital tools to monitor and address user concerns.

In this context, where projects consist of multiple localised demonstration cases across various European countries, the aim is focused on extracting unique outcomes tailored to each specific local case study within the project. These specific findings hold a pivotal role in executing the project comprehensively, adding significant value to its overall success.

Initially, an extensive literature review was conducted on various online repositories, including ScienceDirect, SCOPUS, Academia, and others. The aim was to delve into diverse topics such as multiple benefits, smart cities, positive energy districts, and best–worst scaling, totalling 122 publications. These readings were instrumental in developing an in-depth understanding of the concepts mentioned.

The procedure for conducting the multiple benefits analysis described in this article will be explained with references to the practical applications and has been subdivided into four steps (Figure 1).

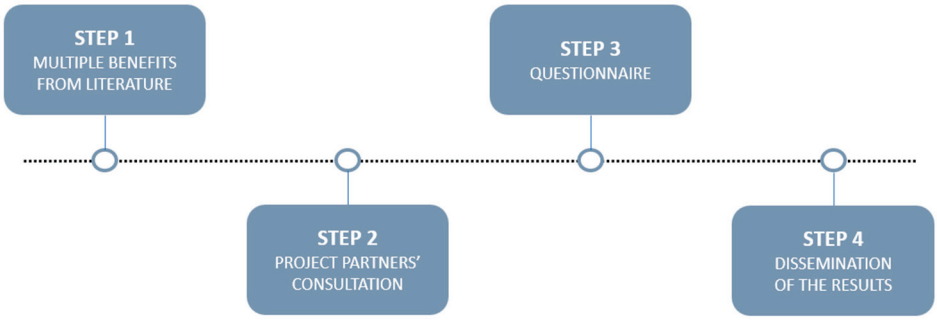


Figure 1. Scheme of the proposed methodology for multiple benefit analysis.

To initiate the multiple benefits analysis, an in-depth literature review of comparable projects to the one under analysis is undertaken (STEP 1). Subsequently, project partners collaborate to curate tailored lists of relevant multiple benefits at both the project and demonstration case levels (STEP 2). Following this, a comprehensive questionnaire is designed and circulated to capture stakeholders' perspectives on the selected multiple benefits' significance (STEP 3). Finally, the results of the questionnaire are disseminated to conclude the process (STEP 4).

3.1. STEP 1: Identify Key Multiple Benefits from the Literature Review

The literature review represents the base of the methodology. It is useful to gain insights into the most frequently cited benefits associated with energy and urban redevelopment projects. This effort is useful for understanding the potential effects and expected results of initiatives similar to the one being considered. The approach is inspired by the ones used by [16,39].

A thorough online screening has been conducted and sixteen projects and four scholarly articles were chosen as references (Table 1). Both theoretical publications and European initiatives (completed or in progress) in the field of city models, such as smart cities, positive energy districts, and climate positive circular communities, were brought into the analytical process. The selection of projects involved an exhaustive review of numerous deliverables and online resources spanning from November to December 2022. These projects have received funding from the European Union and are primarily geared toward introducing innovative solutions to enhance the quality of life for residents and promote environmental well-being. Additionally, we considered articles unrelated to specific projects to explore the concepts of smart cities and positive energy districts in a more theoretical context. This focus was motivated by the recognition that these urban models represent an encompassing and pioneering concept, supported by a substantial body of literature. It is worth noting that the CPCC model is even more recent, and its inception occurred exclusively within the ARV project, which remains ongoing. The analysis extended to include the documentation related to both the ARV and ProLight projects. This deeper examination aimed to fortify the available resources, enhancing the groundwork for subsequent discussions with project partners. The type of partners in these projects is very diverse, ranging from universities and research centres, companies of different sizes (from start-ups or small and medium-sized enterprises to large energy or real estate companies), municipalities and public bodies,

associations, or interest groups. A broad representation of the actors needed to trigger innovation as well was argued in the quadruple helix innovation model [40].

Table 1. Projects and scientific literature consulted to extrapolate multiple benefits.

No.	Title	Type	Urban Model	Description	Main Ref.
1	ARV	EU project	CPCC	ARV seeks to provide and implement appealing, durable, and practical solutions that greatly speed up extensive energy renovations.	[10]
2	SPARCS	EU project	PED	SPARCS aims to encourage the participation of residents in the energy market to transform urban areas into energy prosumers and involve the community. It seeks to introduce innovative solutions in buildings and mobility.	[41]
3	POCITYF	EU project	PEB and PED	POCITYF aims to demonstrate and replicate solutions for improving the energy system in buildings and districts, favouring renewable energies. It will support the transformation of historical cities into greener, smarter, and more liveable communities while maintaining their cultural heritage.	[42]
4	Triangulum	EU project	Smart City	Triangulum aims to show how technologies from the energy, buildings, mobility, and ICT sectors can be used in a single district to significantly reduce energy demand and local GHG emissions while also improving the quality of life and favouring economic growth.	[43]
5	+CityxChange	EU project	PEB and PED	+CityxChange creates positive energy block solutions that lead to positive energy districts and cities. It employs community engagement strategies and decision-support technologies to empower all community stakeholders to make well-informed decisions. It also implements reduction, flexibility, and energy efficiency measures.	[44,45]
6	SINFONIA	EU project	Smart City	SINFONIA aims to implement integrated and scalable energy solutions on a large scale. The target is mid-sized European cities.	[15,46]
7	ATELIER	EU project	PED	ATELIER aims to create and replicate positive energy districts (PEDs). Reducing obstacles to the adoption of clever solutions on a local level will boost the ecology of local innovation.	[47]

Table 1. *Cont.*

No.	Title	Type	Urban Model	Description	Main Ref.
8	SYN.IKIA	EU project	PED	SYN.IKIA aims to provide a model for sustainable plus-energy buildings and neighbourhoods. The goal is to achieve 100% energy savings, 90% of the energy produced from renewable sources, 100% GHG emission reduction, and 10% life cycle cost reduction, compared to Nearly Zero Energy Building (nZEB) levels.	[48]
9	Smart-BEEjS	EU project	PED	Smart-BEEjS aims to train Ph.D. students in policy making, planning, and business model innovation specialised in the energy and efficiency sectors.	[49]
10	MAtchUP	EU project	Smart City	MAtchUP aims to develop and use strategies that can convert urban issues into smart opportunities to create a more liveable urban environment for citizens.	[50,51]
11	GrowSmarter	EU project	Smart City	GrowSmarter aims to create smart city solutions that primarily target the issues of energy, infrastructure, and transportation. It is also intended to generate opportunities for replication in other contexts.	[52]
12	IRIS	EU project	Smart City	IRIS aims to provide energy and mobility systems creating cheaper, better accessible, reliable, and sustainable cities. The project seeks to incentivise citizens to become prosumers and improve their quality of life.	[53]
13	mySMARTLife	EU project	Smart City	mySMARTLife aims to increase the use of renewable sources, focusing on creating inclusive cities. The interventions also comprehend mobility and the use of ICT solutions.	[54,55]
14	smartENCity	EU project	Smart City	SmartEnCity seeks to develop sustainable, smart, and resource-efficient urban environments. Based on the implementation of measures for increasing energy efficiency and the renewable energy supply.	[56]
15	ProLight	EU project	PED	ProLight aims to lower energy consumption per capita and increase the proportion of renewable energy used in the housing sector. By following the European Bauhaus principles, the six demonstration districts should lead to a better quality of life for all targeted end users.	[57]

Table 1. *Cont.*

No.	Title	Type	Urban Model	Description	Main Ref.
16	CITYkeys	EU project	Smart City	CITYkeys seeks to create a set of indicators for the assessment of smart city initiatives. This approach is based on the needs of European cities and citizens and was developed with input from 40 other sustainable systems for smart urban performance.	[58]
17	Environmental sustainability approaches and positive energy districts: A literature review	Article	PED	Analysis of the scientific literature concerning the topic of positive energy district, with particular attention to the sphere of environmental sustainability.	[59]
18	Enabling Positive Energy Districts across Europe: energy efficiency couples renewable energy	Report	PED	Analysis of district-level energy performance objectives. It takes the idea of PEDs into account from a legal and economic perspective and confirms that the minimum energy performance standards on a district scale may be defined using the cost–benefit calculation technique of the EPBD.	[21]
19	Europe Towards Positive Energy Districts	Booklet	PED	Overview of different European projects based on the concept of the positive energy district model.	[60]
20	Positive Energy Districts Solution booklet	Booklet	PED	The booklet contains essential information for decision makers on how to create and manage a PED.	[61]

1. https://greendeal-arv.eu/ (accessed on 10 December 2022), 2. https://sparcs.info/en/ (accessed on 14 December 2022), 3. https://pocityf.eu/ (accessed on 12 December 2022), 4. https://triangulum.no/?lang=en (accessed on 12 December 2022), 5. https://cityxchange.eu/ (accessed on 12 December 2022), 6. http://www.sinfonia-smartcities.eu/en/project (accessed on 12 December 2022), 7. https://smartcity-atelier.eu/ (accessed on 14 December 2022), 8. https://www.synikia.eu/ (accessed on 12 December 2022), 9. https://smart-beejs.eu/ (accessed on 28 December 2022), 10. https://www.matchup-project.eu/ (accessed on 28 December 2022), 11. https://grow-smarter.eu/home/ (accessed on 14 December 2022), 12. https://irissmartcities.eu/ (accessed on 12 December 2022), 13. https://www.mysmartlife.eu/mysmartlife/ (accessed on 4 January 2023), 14. http://smartencitynetwork.eu/ (accessed on 12 December 2022), 15. https://www.prolight-project.eu/ (accessed on 8 February 2023), 16. https://cordis.europa.eu/project/id/646440 (accessed on 4 January 2023).

In the quest to identify multiple benefits, an evaluation of positive impacts was conducted within open-access operational documents through explicit and implicit forms and the examination of Key Performance Indicators (KPIs). The review of the scholarly literature revealed an absence of dedicated sections explicitly addressing multiple benefits. Consequently, the identification of benefits demanded a meticulous examination of the text itself, often requiring a diligent search throughout the material, as they were scattered throughout the documents. As the practice of analysing multiple benefits gains prominence, the expectation is for this information to become more accessible and systematically organised in future research endeavours.

In our case, the benefits derived from the articles were systematically categorised based on their respective articles and a list of 56 benefits has been obtained.

The list was reduced to 18 primary advantages by a careful selection procedure to capture only the most representative benefits. This curation process was guided by several discerning criteria. Firstly, the frequency of citations across multiple articles was considered, ensuring the selected benefits were supported by diverse sources. Secondly, a

preference was given to broader definitions over specific ones, aiming for inclusivity and relevance across varied contexts. Additionally, the perceived significance of each benefit was evaluated through an analytical review. This comprehensive evaluation ensured that the final list of 18 benefits encompassed a diverse range while also being pertinent and impactful.

The decision to settle on 18 benefits was strategic, aiming to strike a balance between comprehensiveness and manageability. This number was considered adequate to avoid overwhelming detail yet comprehensive enough to offer a holistic understanding. Furthermore, this specific count was chosen to facilitate the development of the questionnaires employing the best–worst scaling method.

Table 2 illustrates the multiple benefits selected through the described process. Each benefit is accompanied by a description provided by the authors that represents a broad definition derived from various definitions encountered in the references consulted.

Table 2. Most relevant multiple benefits derived from literature review and project screening.

No.	Multiple Benefits	Description	Ref.
1	Energy savings	Energy saving is given by the renewal of the district and by the use of sustainable actions that increase energy performance. This leads not only to savings from an economic point of view but also to a lower environmental impact. The implementation of measures that favour energy efficiency ensures less waste of energy and therefore a demand related to the real needs of the individual.	smartENCity, GrowSmarter, POCITYF, Triangulum, MAtchUP, mySMARTLife, IRIS, ATELIER, +CityxChange, SPARCS, Smart-BEEjS, ProLight
2	Overcoming energy poverty	By adopting sustainable energy solutions and helping citizens to decrease energy costs and consumption to an affordable level, it is possible to reduce the number of residents considered in an energy poverty situation. Consequently, also the number of deaths related to interior temperature shocks can be decreased.	SINFONIA, CITYkeys, POCITYF, ProLight, MAtchUP, IRIS, SCIS, Smart-BEEjS, SYN.IKIA, ARV
3	Increased energy efficiency	The project ensures an increase in energy efficiency at the district (and city) scale, maximising the share of renewable energies and their intelligent integration into the energy system.	MAtchUP, smartENCity, GrowSmarter, POCITYF, mySMARTLife, SPARCS, Smart-BEEjS, SYN.IKIA, +CityxChange, ProLight
4	Local labour market stimulated	Project-sponsored interventions and activities are expected to result in the creation of new employment and market opportunities, either directly with the initiative's solution providers and partners or indirectly through links with and inducement from the project.	GrowSmarter, CITYkeys, POCITYF, SINFONIA, MAtchUP, Triangulum, IRIS, smartENCity, SPARCS, Smart-BEEjS, +CityxChange, ARV
5	Innovation promotion	The innovations brought about are a benefit for the entire community, as they allow progress in building a more sustainable society. Furthermore, pioneering enterprises will also have a competitive advantage over other enterprises in the market. Innovative solutions may include technological, governance, and legislative improvements.	SINFONIA, smartENCity, MAtchUP, Triangulum, GrowSmarter, POCITYF, mySMARTLife, IRIS, SPARCS, [61]

Table 2. *Cont.*

No.	Multiple Benefits	Description	Ref.
6	Citizens involvement	End users' involvement in the decision-making process for the construction of their own community. Participating citizens will increase the likelihood that the outcome will be supported, and it will better meet the needs of the community.	Triangulum, smartENCity, MAtchUP, GrowSmarter, mySMARTLife, IRIS, CITYkeys, SPARCS, Smart-BEEjS, SYN.IKIA, ProLight, POCITYF, +CityxChange, ARV, [59]
7	Overcoming policy/regulatory barriers	The adoption of new solutions results in the identification of governmental barriers, legal issues, and security/data protection concerns. Therefore, it presents a chance to make useful recommendations for how to overcome them.	smartENCity, IRIS, ATELIER, POCITYF, SPARCS, +CityxChange
8	Knowledge creation and exchange	The collaboration of researchers and experts in the field leads to a fruitful exchange of knowledge, which also favours future developments. It also incentivises capacity-building, training, and awareness-raising opportunities.	Triangulum, smartENCity, MAtchUP, SPARCS, Smart-BEEjS, ATELIER, ARV, ProLight
9	Increased awareness on environmental and energy issues	The introduction of energy-efficiency solutions, combined with an explanation of how to promote energy sustainability, raises user awareness, which may lead to behavioural changes. Greater information is considered to benefit not only the inhabitants of the project's impacted areas but the community as a whole.	SINFONIA, smartENCity, GrowSmarter, Triangulum, MAtchUP, mySMARTLife, IRIS, POCITYF, ATELIER, Smart-BEEjS, SYN.IKIA, +CityxChange, ARV, ProLight, [61]
10	Improved quality of life of the inhabitants	The living and psychological conditions of inhabitants can be improved by greater quality of the buildings, indoor thermal comfort, and reduction in environmental, acoustic, and olfactory pollution.	CITYkeys, martENCity, SINFONIA, Triangulum, MAtchUP, GrowSmarter, mySMARTLife, ATELIER, ARV, SPARCS, SYN.IKIA, POCITYF, ProLight, [59]
11	Improved indoor comfort	A good energy efficiency system leads to the improvement of thermal, humidity, and living comfort.	GrowSmarter, smartENCity, IRIS, Smart-BEEjS, SYN.IKIA, POCITYF, ATELIER, ProLight, [59]
12	Territorial quality and attractiveness increased	An area that is an example of smart and sustainable development might attract tourists who are environmentally conscious as well as institutions, professionals, and researchers.	SINFONIA, MAtchUP, GrowSmarter, POCITYF, SPARCS, [60]
13	Local air quality improved	Utilising renewable energy sources for energy production and consumption instead of fossil fuels will have a lot of significant positive effects on society and the environment. For instance, it will contribute to reducing the amount of pollutants in the air and the urban heat island effect and, as a consequence, the air quality will increase.	SINFONIA, GrowSmarter, Triangulum, MAtchUP, SPARCS, POCITYF, SYN.IKIA, +CityxChange, ARV
14	Reduced fossil fuel dependency and import	Utilising renewable energy sources for energy production and consumption reduces fossil fuel dependency, contributing to increasing the security of the energy supply.	smartENCity, GrowSmarter, SPARCS, Smart-BEEjS, [61]

Table 2. *Cont.*

No.	Multiple Benefits	Description	Ref.
15	Increase in property value	Buildings with attractive and innovative features that are also high performing in terms of energy have a property value premium that is greater than the estimated economic benefit of the energy savings.	SINFONIA, SPARCS, [59]
16	Increased investment prospects and investor confidence	The vision of a project that brings benefits to society, also in economic terms, fosters the confidence of investors who will be more inclined to finance future similar interventions; this will create new economic incentives for promoting energy-efficient districts and sustainable mobility actions.	smartENCity, MAtchUP, SPARCS, Smart-BEEjS, POCITYF, +CityxChange
17	Economic saving	The redevelopment of the area with more cutting-edge and sustainable solutions makes it possible to reduce the prices for energy and heating buildings. The advantages are found in the reduced initial costs, maintenance, and in general of the entire life cycle of the buildings (in fact, proper management of large-scale interventions allows economies of scale). Moreover, the stakeholders and inhabitants can benefit from the increased economic value of real estate, higher performances, and additional revenue from delivering specific energy services.	SINFONIA, CITYkeys, smartENCity, MAtchUP, IRIS, Smart-BEEjS GrowSmarter, Triangulum, MAtchUP, SPARCS, POCITYF, SYN.IKIA, +CityxChange, ARV, ProLight, [61]
18	Increased neighbourhood safety	Thanks to the redevelopment of the place in many aspects, it is expected that the neighbourhood will become safer for citizens.	MAtchUP, CITYkeys, GrowSmarter, SPARCS, ARV

The benefits were then categorised into four broad categories, each encompassing distinct aspects of society: social, governance, environmental, and economic. In turn, there is an almost perfect correspondence between ESG (nonfinancial) and economic criteria.

- Social refers to the impact on individuals and communities, encompassing aspects such as well-being, equity, and social cohesion.
- Governance concerns structures and processes of decision making and regulation within society, including elements such as transparency, collaboration between different levels of government, and long-term planning frameworks.
- Environmental involves the effects on the natural world, including conservation, sustainability, and the preservation of ecosystems and biodiversity.
- Economic relates to the financial implications and prosperity within society, covering factors such as employment, income distribution, and overall economic growth.

As illustrated in Figure 2, numerous identified multiple benefits intersect across multiple categories. This observation is significant as it underscores the interconnected nature of these benefits and emphasises their potential to yield positive impacts across society as a whole. This reveals that improving one area, like the environment, can positively affect others, such as social well-being or economic prosperity. This knowledge is essential for accurate and integrated decision making, since it emphasises the necessity of considering the wider effects and possible synergies that may result from initiatives or projects.

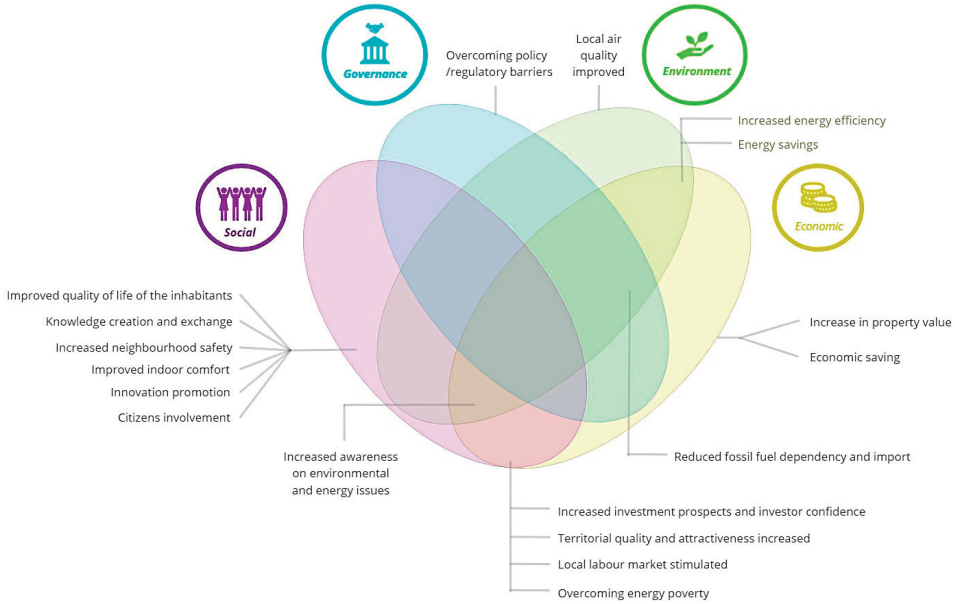


Figure 2. Multiple benefits classified by categories.

3.2. STEP 2: Collaborative Sessions with Project Partners

In this phase, the consultation process involved engaging with project partners closely associated with the targeted initiatives (ARV and ProLight).

Project partners serve as the foundation of project consortia, since they drive the development of the project's implementation. They generally come from a variety of countries particularly those included in the case studies, and they are representative of various sectors. They include research institutes, industrial players, companies, municipalities, and governmental bodies. In addition, the network of partners extends beyond conventional boundaries to include clusters, funding agencies, consulting firms, and professional associations.

Project partners work together to contribute their expertise, resources, and networks to achieve the objectives outlined in the project proposal. Each partner brings a unique set of skills and perspectives to the project, facilitating multidisciplinary collaboration and maximising the project's impact. The main purpose of consulting with them is to comprehensively capture the multiple benefits that could result from implementing such projects within specific areas or contexts.

This stage should be conducted with thoroughness, encompassing two levels of detail to capture a deeper understanding. The initial level focuses on a broad overview, outlining the general benefits and potential impacts of the project. Subsequently, a deeper examination should be carried out, focusing on the single case studies for each project. Although each of the two projects has a general framework, each of their individual case studies undergoes a unique implementation process. Their unique contexts, diverse in cultural, legal, climatic, and geographical aspects, play a significant role in shaping the specific benefits expected from the proposed changes within their respective areas.

The insights and outcomes generated during these workshops would be instrumental in refining the survey materials and aligning them with the perspectives and priorities of the project stakeholders.

3.2.1. Collaborative Sessions with All Project Partners

A dedicated workshop should be conducted for each project, aimed at gathering insights and discussions from project partners. The purpose of this initial phase is to serve as a preliminary step to understand the multiple benefits of the entire projects before engaging separately local partners in the survey process to tailor the list of positive impacts. Through this collaborative approach, knowledge exchange can be fostered, allowing for the identification of both shared and unique benefits. This can significantly contribute to a more

comprehensive understanding of the varied advantages resulting from the implementation of these projects.

For both the ARV and ProLight projects, workshop participants, approximately 30 per project, were instructed to utilise the collaborative online platform known as Miro (https://miro.com/it/, accessed on 10 March 2023). This platform served as a virtual workspace for conducting workshop activities seamlessly. Miro was chosen for its ability to accommodate multiple users at the same time, facilitating continuous interaction and simultaneous online viewing. Once accessed, participants encountered a workshop-tailored board on the platform, ensuring parity in brainstorming and engagement for both in-person and remote attendees. The Miro board also incorporated findings from the literature review, serving as a reference and inspiration for participants to identify and document the benefits linked to implementing each analysed project.

The participants actively contributed by sharing their insights during a joint brainstorming session. Each person listed at least 10 benefits from the project considered, even if these were mentioned before, ensuring all advantages were captured. This emphasis on inclusivity aimed to compile a concise and comprehensive final list based on both individual significance and the frequency of occurrence noted by participants. To embrace the various dimensions through which the project's multiple benefits might manifest, workshop participants were asked to classify these advantages using a four-set Venn diagram. This diagram integrated the four principal categories: Social, Governance, Economic, and Environmental, offering a holistic representation of the potential scopes of project benefits. This approach facilitated a visual representation illustrating how the benefits intersected and converged within different categories.

Once the participants contributed to filling out the diagram during the workshop, similar-meaning benefits were grouped to prevent redundancy. Subsequently, a selection of 18 elements was made to create a finalised list, which underwent review and agreement by the participants. This selection process considered the perceived importance and impact of the multiple benefits, as well as the frequency of repetition for each concept.

3.2.2. Collaborative Sessions with Local Partners

Once the general multiple benefits of the project have been identified, the next step involves examining the specific benefits that each case study can offer to its respective area. This phase necessitates collaboration with local-level case study partners. As the benefits may differ slightly from those of the entire project, it is crucial to conduct separate sessions for each case study. Furthermore, this approach aims to prevent the influence of different case study partners on each other's benefit choices.

Given the likely smaller number of local partners participating in these workshops, usually two or three at a time, the recommended brainstorming method involves presenting a range of multiple benefits from similar projects (see Section 3.1), previous workshops involving all partners (see Section 3.2.1), and existing preliminary studies and project deliverables related to the specific case studies. Participants are then tasked with selecting the most pertinent multiple benefits for their case study and suggesting additional ones as needed. This process can be facilitated through the Miro online platform. Participants are not only encouraged to write down the benefits but are also asked to actively participate in discussions regarding the pertinence of each identified benefit concerning the specific case study.

The workshop's tangible outcome comprises once more an inventory of 18 multiple benefits. These lists are crucial in formulating a questionnaire intended for circulation among stakeholders engaged in each project's case study, as detailed in the following section.

3.3. STEP 3: Questionnaire on the Most Relevant Multiple Benefits

At this point, project stakeholders are invited to complete a questionnaire that aims to identify the most significant benefits associated with each project's case study. Participants are asked to rank these benefits based on their respective roles in the project. The goal

is to establish a priority ranking of the most relevant benefits, providing insights into the preferences of different stakeholder groups. This process helps in comprehending the objectives of each demonstration case and contributes to implementing changes that align with the needs and aspirations of its residents. Additionally, it facilitates the phase of communication of improvements resulting from the project's implementation. The analysis can thus clarify the different perceptions, which arise from the different needs of the various stakeholder groups. Understanding that an element may be perceived as a significant benefit by one stakeholder group but less beneficial by another underlines the importance of assessing perspectives comprehensively.

Since the intention is to study the multiple benefits as a result of project implementation on the territory, a questionnaire has to be created for each case study. In the case of both ProLight and ARV, six questionnaires should be created. The use of the best–worst scaling technique in this questionnaire ensures reliable outcomes with minimal effort required from the respondents. In alignment with the theory outlined in Section 2.3, the questionnaire is designed to force respondents to select a benefit they consider most relevant and one they consider less relevant from a set of six items. In the examples of ARV and ProLight, 18 previously chosen elements are considered, necessitating the repetition of this process nine times. In the end, each benefit will have been presented to the respondent three times, in comparison with different benefits (Table 3).

Table 3. Examples of task sets used in the BWS survey addressed to ARV project partners.

The Most Relevant	**Task 1**	**The Least Relevant**
○	Increased energy efficiency	○
○	Reduced energy fossil fuels	○
○	Increased in property value	○
○	Citizen involvement	○
○	Improved quality of life of the inhabitants	○
○	Climate change awareness	○
The Most Relevant	**Task 3**	**The Least Relevant**
○	Respect of human rights	○
○	Increased energy efficiency	○
○	Citizen involvement	○
○	Innovation in governance processes	○
○	Energy costs reduction	○
○	Energy poverty reduction	○
The Most Relevant	**Task 9**	**The Least Relevant**
○	Territorial quality and attractiveness	○
○	Increase in property value	○
○	Increased comfort levels	○
○	Climate change awareness	○
○	Economic savings	○
○	Fostering technological innovation	○

To refine the study of multiple benefits, the questionnaire was enriched with questions related to gender, age, and participants' role in the project case study. Additionally, a

question was introduced asking participants to express their opinion on the aspect that should be given the highest consideration in an urban redevelopment project, choosing from economic, social, environmental, or governance aspects. Including the latter question in the survey seeks to identify respondents' primary sensitivity among these categories and validate the consistency of their responses. This is crucial, because each benefit could align with one or more of these categories and, therefore, it could be noticed if there was a consistency or otherwise between the final ranking of multiple benefits and the importance attributed to each category in the separate question.

The questionnaire proposes a list of possible roles of each respondent within the case study defined based on a preliminary stakeholder mapping study, which generally is already conducted within the framework of these kinds of projects.

Therefore, this question was constructed to be slightly different for diverse case studies, since the stakeholders who have implications in practice are not always the same. An example of stakeholders' categories may be the following: Cultural Promoter (neighbourhood committee, student association, and cultural foundation), Non-resident urban user (commuter, tourist, and co-worker), Financial Actor (Chamber of Commerce, construction sector association, and Confindustria), Local Authority (district, municipality, and province), Citizen (owner and-tenant), Researcher (research-institutes and-universities).

Due to the variety of stakeholders, methods of reaching potential respondents are diverse. They encompass participation in local events, direct engagement based on existing connections, and outreach through online platforms and websites. To be more effective, the questionnaires should be translated into the local language.

3.4. STEP 4: Elaboration and Dissemination of the Results

Effective dissemination of the results is crucial, especially to comprehensively analyse the multiple benefits that contribute to the success of the project. Dissemination takes place through various means, including project results, articles published in journals, and the organisation of local public events. These events serve as platforms to present and learn more about the specific project, promoting broader understanding and engagement with the community. This proactive approach enhances the overall impact and success of the initiative, ensuring that the project results and benefits are communicated widely and transparently.

4. Preliminary Results

Although the application of the methodology on the ARV and ProLight projects has not yet been fully concluded, it is possible to outline some preliminary observations and results.

Despite differing methods in multiple benefits identification, the study revealed a significant overlap between the benefits identified in workshops and those found in the literature review (Figure 3). These shared benefits underscore the consistent positive impacts achievable through these models of urban and energy requalification projects.

The social category emerged as highly significant in both initiatives, indicating its massive importance. Moreover, it is essential to highlight the numerous connections identified within these categories, suggesting that the benefits identified during the workshops could positively influence various societal aspects beyond the social domain alone. Participants' recognition of these interconnections emphasises their comprehensive understanding and consideration of the broader societal implications of the projects.

The activity of disseminating questionnaires and collecting data at the local level is still ongoing, but the procedure was initially tested on project partners, considering the multiple benefits of the entire project. Following the scheduled workshops, the questionnaires were distributed and completed; 20 replies were obtained for ProLight and 21 for ARV. Although the responses to the questionnaire may seem limited, they are in line with expectations, considering that the target group is the project partners, who represent a relatively small group.

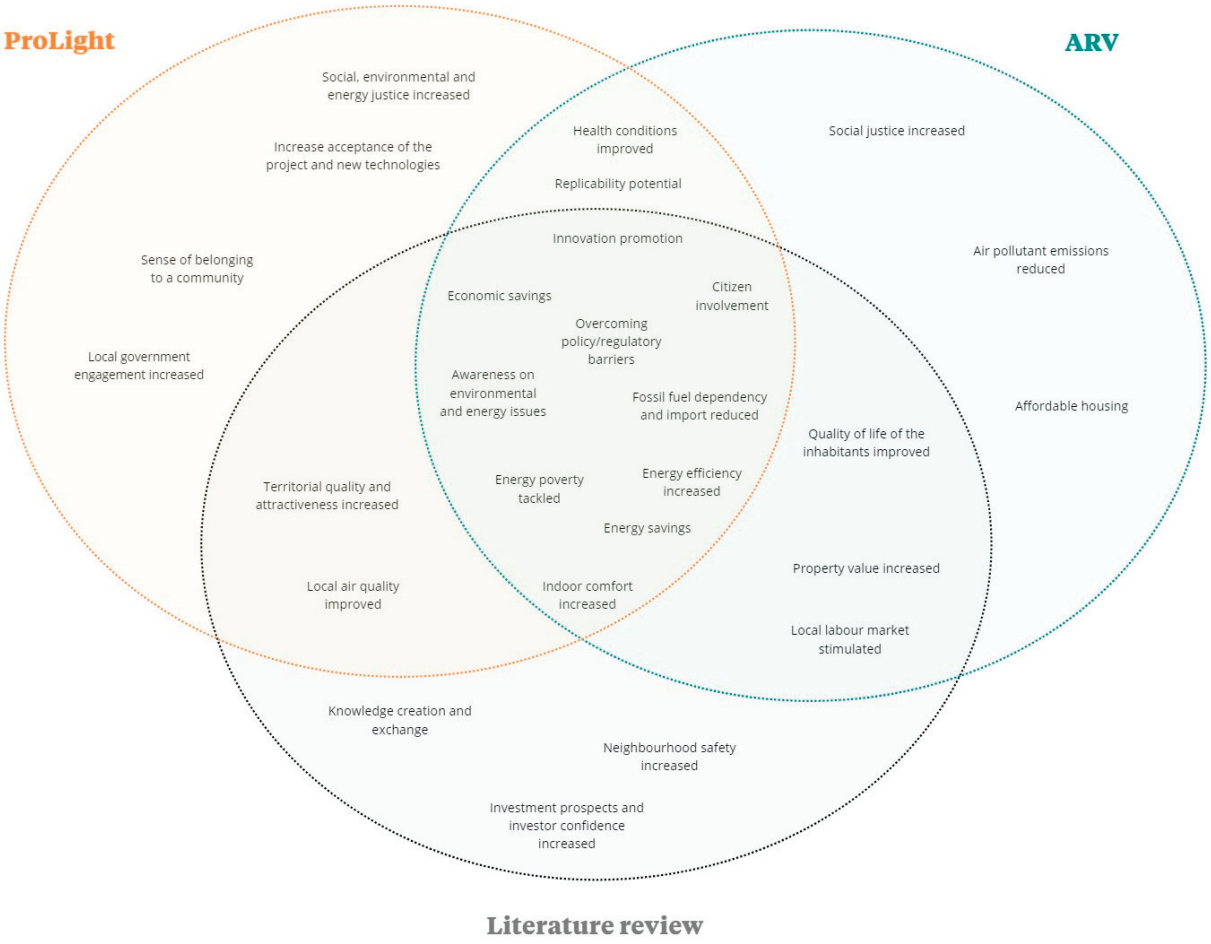


Figure 3. Linkages of multiple benefits between the two projects and the literature review.

Similar trends have been observed across different projects (Table 4).

Table 4. Ranking of multiple benefits according to the perception of ARV and ProLight project partners.

Predominant Category	Multiple Benefits	ARV	ProLight
Environmental	Increased energy efficiency	1	1
Environmental	Reduced energy fossil fuels	4	/
Environmental	Reduced air pollutants	15	/
Environmental	Energy savings	/	4
Environmental	Reduce CO_2 emissions	/	6
Environmental	Local air quality improved	/	16
Social	Improved quality of life of the inhabitants	2	/
Social	Energy and environmental consciousness	3	/
Social	Citizen involvement	5	9
Social	Energy poverty reduction	6	5
Social	Territorial quality and attractiveness increased	9	15
Social	Climate change awareness	11	/
Social	Increased comfort levels	12	/
Social	Respect of human rights	14	/
Social	Investing in architectural training	16	/

Table 4. *Cont.*

Predominant Category	Multiple Benefits	ARV	ProLight
Social	Increased awareness on environmental and energy issues	/	2
Social	Adaptation of personal behaviours for limiting climate change	/	3
Social	Energy and social justice	/	7
Social	Creation of energy communities	/	8
Social	Social cohesion	/	10
Social	Improved indoor comfort	/	11
Social	Sense of belonging	/	17
Economic	Energy cost reduction	8	/
Economic	Economic savings	10	/
Economic	Off-site construction market improved	13	/
Economic	Increased in property value	17	/
Economic	Resilience to energy price fluctuation	/	13
Governance	Fostering technological innovation	7	/
Governance	Innovation in governance processes	18	/
Governance	Local governance improved	/	12
Governance	Overcoming policy/regulatory barriers	/	14
Governance	Innovation promotion	/	18

The aspect deemed most important in both projects is the focus on increasing energy efficiency, followed by benefits related to raising awareness of environmental issues. Although the lists of benefits were customised for each project by different individuals, the significance of the environmental issue and its educational aspect is recognised as a priority over other benefits by the project partners. This aligns perfectly with the priorities outlined in recent guidelines, such as those of the New European Bauhaus. Another similarity lies in the positioning of economic benefits, which are predominantly ranked in the second half of the list. This suggests that economic aspects, although important, are considered less pivotal than other benefits by the samples of project partners in the context of urban and energy redevelopment. A similar observation can be extended to the governance category. Upon reviewing the two rankings, it becomes evident that the project partners of ARV and ProLight are closely aligned.

Interestingly, despite respondents not having access to benefit lists compiled by other project partners, the lists from different cases showed similar percentages of benefits within each macro-category across the list of multiple benefits of the projects, with a predominance of the social and environmental categories (Table 5). This observation is relevant because it denotes further confirmation of the consolidation of a common direction, and thus of the main benefits, in current urban and energy regeneration projects.

Table 5. Occurrence in the percentage of multiple benefits by their prevalent category in ARV and ProLight projects.

Category	ARV	ProLight
Economic	16.67%	5.56%
Social	55.56%	61.11%
Environmental	22.22%	22.22%
Governance	5.56%	11.11%

Since the questionnaire testing phase was conducted within the project consortium, the sample is very different from the one that we could obtain delivering the questionnaire to the overall stakeholders of each demonstration case. The background and the perspectives of the sample of the project partners are expected to be more homogeneous than the one of the stakeholders. In any case, this test provided valuable insights into the perspectives of

the project partners. Through this process, a deeper understanding of their perspectives was gained, which informed decision-making and collaboration strategies for the future.

For what concerns the local level, the distribution of the questionnaire is ongoing to expand its reach through dissemination at community meetings, various remote communication platforms, and personal contacts. This strategy aims to foster broad involvement and participation.

During the interactive sessions with demo leaders, which lasted approximately half an hour each, various discussion points and pertinent details regarding the demos emerged. This moment provided a valuable opportunity to assess the current status of the projects, clarify the direction of each demo, and identify both strengths and areas for improvement.

Although still in progress, the questionnaire began to be disseminated in Trento, starting with an event open to the citizenship, where the project's progress was discussed. On this occasion, the multiple benefits of the project were presented, which were useful to make all the positive impacts of the project understood, especially by the citizenship.

5. Discussion

To successfully promote energy transition, it is essential to adopt more sustainable territorial planning, transforming urban spaces into smart neighbourhoods and cities. The analysis and communication of the advantages arising from such projects constitute an effective approach to garnering support from communities, often resistant to change, and from investors.

This article introduces an innovative methodology for the multiple benefits analysis in relation to urban and energy redevelopment projects, emphasising stakeholder involvement and employing the Best–Worst Scaling method for constructing questionnaires. This approach enhances decision-making procedures and guarantees conformity with community requirements, helping to redefine strategies for a greater urban energy transition.

In addition to theoretical explanation, the discourse is enriched with practical insights from European projects, namely ARV and ProLight, to demonstrate the methodology's efficacy and its potential to capture the broad range of perspectives of different stakeholders that these initiatives can provide. The results of both projects emphasise a common emphasis on environmental improvements and greater citizen involvement. Comparing these findings with a 2020 study on SINFONIA's co-benefits [15], a change in priorities emerges, with SINFONIA emphasising economic and individual health co-benefits. This discrepancy may be an indication, together with variations in stakeholder sensitivity and contextual differences, of potential changes in societal values and trends. The approach described in the article aims to capture the diverse perspectives of stakeholders, suggesting its applicability in different cultural contexts and indicating whether perceived benefits are universal or specific.

The study's engagement with stakeholders via the best–worst scaling methodology revealed both strengths and weaknesses. While the approach facilitated stakeholder involvement, concerns arose regarding its length and potential for stakeholder fatigue. Future research could mitigate these issues by streamlining the selection process and incorporating open-ended questions to capture additional stakeholder perspectives.

Another next development is to integrate multiple benefits with key performance indicators (KPIs) and quantify them in a more objective and quantitative way. This facilitates the association of benefits with corresponding KPIs and economic value, improving the rigor of the evaluation process and providing a structured framework for understanding economic impact. In fact, this method heavily relies on stakeholders' perceptions rather than quantitative data, which can be limiting. Therefore, further analysis quantifying aspects such as willingness to pay would enhance the significance of this study and allow decision makers to prioritise and allocate resources effectively, maximising the positive outcomes of urban projects.

Moreover, further research could explore proactive strategies to mitigate potential negative impacts and examine the applicability of the methodology outside European contexts.

Author Contributions: Conceptualization, I.B. and A.B.; Methodology, I.B. and A.B.; Software, I.B.; Validation, A.B. and M.C.B.; Formal analysis, I.B.; Investigation, I.B. and M.V.; Data curation, I.B.; Writing—original draft, I.B.; Writing—review and editing, A.B., M.V. and M.C.B.; Supervision, A.B. and M.C.B.; Project administration, A.B.; Funding acquisition, A.B. All authors have read and agreed to the published version of the manuscript.

Funding: This work has been developed within the context of ProLight (https://www.prolight-project.eu/) and ARV (https://greendeal-arv.eu/) projects. ARV has received funding from the European Union's Horizon 2020 program under grant agreement no. 101036723. ProLight has received funding from the European Union's Horizon Europe program under grant agreement no. 101079902. The European Union is not liable for any use that may be made of the information contained in this document, which merely represents the authors' view.

Data Availability Statement: The data presented in this study are available on request from the corresponding author.

Acknowledgments: The authors thank colleagues at Eurac Research, as well as all the partners involved in the ProLight and ARV projects, for their valuable contributions during the workshops. The methodology presented in the paper is a re-elaboration of the Master Thesis of Irene Bertolami titled "The multiple benefits approach in energy requalification projects.", Master Degree Programme in Urban and Regional Planning, Politecnico di Torino, a.y 2022/2023, supervisors: Marta Carla Bottero and Adriano Bisello. This work has been developed within the context of the International Energy Agency (IEA) Energy in Buildings and Construction (EBC) Annex 83 working group on "Positive Energy Districts".

Conflicts of Interest: The author declares no conflicts of interest.

References

1. Ren21. *Renewables 2021: Global Status Report*; REN21 Secretariat: Paris, France, 2021; ISBN 978-3-948393-03-8. Available online: https://www.unep.org/resources/report/renewables-2021-global-status-report (accessed on 5 May 2023).
2. European Commission Communication from the Commission to the European Parliament, the Council, the European Economic and Social Committee and the Committee of the Regions. The Urban Dimension of EU Policies—Key Features of an EU Urban Agenda. Available online: https://eur-lex.europa.eu/legal-content/EN/ALL/?uri=CELEX:52014DC0490 (accessed on 5 May 2023).
3. Short, J.R.; Farmer, A. Cities and Climate Change. *Earth* **2021**, *2*, 1038–1045. [CrossRef]
4. Zhivov, A. *Energy Master Planning toward Net Zero Energy Resilient Public Communities Guide*; Springer International Publishing: Cham, Switzerland, 2022; ISBN 978-3-030-95832-9.
5. UNEP. *UNEP Annual Report: 2015*; UNEP: Nairobi, Kenya, 2016; ISBN 978-92-807-3518-5.
6. United Nations Environment Programme. *District Energy in Cities: Unlocking the Potential of Energy Efficiency and Renewable Energy*; United Nations Environment Programme (UNEP): Paris, France, 2015. Available online: https://www.unep.org/resources/report/district-energy-cities-unlocking-potential-energy-efficiency-and-renewable-energy (accessed on 10 May 2023).
7. Delbeke, J.; Runge-Metzger, A.; Slingenberg, Y.; Werksman, J. The Paris Agreement. *Clim.-Neutral Eur.* **2019**, 24–45. [CrossRef]
8. European Commission. The European Green Deal. Available online: https://ec.europa.eu/info/strategy/priorities-2019-2024/european-green-deal_en (accessed on 10 May 2023).
9. EU Mission: Climate-Neutral and Smart Cities. Available online: https://research-and-innovation.ec.europa.eu/funding/funding-opportunities/funding-programmes-and-open-calls/horizon-europe/eu-missions-horizon-europe/climate-neutral-and-smart-cities_en (accessed on 11 May 2023).
10. Salom, J.; Maskova, I.; Grazieschi, G.; Woods, R.; Schneider-Marin, P. ARV: D2.1 Assessment Framework for CPCC. 2022. Available online: https://app.cristin.no/results/show.jsf?id=2219703 (accessed on 10 December 2022).
11. European Commission. Report from the Commission to the European Parliament, the Council, the European Economic and Social Committee and the Committee of the Regions: New European Bauhaus Progress Report. Available online: https://eur-lex.europa.eu/legal-content/EN/TXT/?uri=CELEX:52023DC0024 (accessed on 14 May 2023).
12. Bisello, A.; Vettorato, D. Multiple Benefits of Smart Urban Energy Transition. In *Urban Energy Transition*; Elsevier: Amsterdam, The Netherlands, 2018; pp. 467–490, ISBN 978-0-08-102074-6.
13. Bossi, S.; Gollner, C.; Theierling, S. Towards 100 Positive Energy Districts in Europe: Preliminary Data Analysis of 61 European Cases. *Energies* **2020**, *13*, 6083. [CrossRef]
14. Eskerod, P. A Stakeholder Perspective: Origins and Core Concepts. In *Oxford Research Encyclopedia of Business and Management*; Oxford University Press: Oxford, UK, 2020; ISBN 978-0-19-022485-1.
15. Bisello, A. Assessing Multiple Benefits of Housing Regeneration and Smart City Development: The European Project SINFONIA. *Sustainability* **2020**, *12*, 8038. [CrossRef]

16. Bisello, A.; Grilli, G.; Balest, J.; Stellin, G.; Ciolli, M. Co-Benefits of Smart and Sustainable Energy District Projects: An Overview of Economic Assessment Methodologies. In *Smart and Sustainable Planning for Cities and Regions*; Bisello, A., Vettorato, D., Stephens, R., Elisei, P., Eds.; Green Energy and Technology; Springer International Publishing: Cham, Switzerland, 2017; pp. 127–164, ISBN 978-3-319-44898-5.
17. Ürge-Vorsatz, D.; Herrero, S.T.; Dubash, N.K.; Lecocq, F. Measuring the Co-Benefits of Climate Change Mitigation. *Annu. Rev. Environ. Resour.* **2014**, *39*, 549–582. [CrossRef]
18. Zilio, S.; Borsari, A.; Bisello, A.; Segata, A.; Alonzo, V.D.; Croce, S. VARCITIES. D3.4: Report on Multiple Benefits Expected from Visionary Solutions. 2022. Available online: https://varcities.eu/resources/deliverables/d3-4-report-on-multiple-benefits-expected-from-visionary-solutions/ (accessed on 3 January 2023).
19. OECD. *Ancillary Benefits and Costs of Greenhouse Gas Mitigation*; OECD: Paris France, 2000; ISBN 978-92-64-18542-5.
20. Sareen, S.; Albert-Seifried, V.; Aelenei, L.; Reda, F.; Etminan, G.; Andreucci, M.-B.; Kuzmic, M.; Maas, N.; Seco, O.; Civiero, P.; et al. Ten Questions Concerning Positive Energy Districts. *Build. Environ.* **2022**, *216*, 109017. [CrossRef]
21. European Commission; Joint Research Centre. *Enabling Positive Energy Districts across Europe: Energy Efficiency Couples Renewable Energy*; Publications Office: Luxemburg, 2020.
22. United Nations Department of Economic and Social Affairs. *The Sustainable Development Goals Report 2023: Special Edition*; The Sustainable Development Goals Report; United Nations: New York, NY, USA, 2023; ISBN 978-92-1-002491-4.
23. Nam, T.; Pardo, T.A. Conceptualizing Smart City with Dimensions of Technology, People, and Institutions. In Proceedings of the 12th Annual International Digital Government Research Conference: Digital Government Innovation in Challenging Times, College Park, MD, USA, 12–15 June 2011; pp. 282–291. Available online: https://www.scirp.org/reference/referencespapers?referenceid=3161790 (accessed on 15 April 2023).
24. Kourtzanidis, K.; Angelakoglou, K.; Apostolopoulos, V.; Giourka, P.; Nikolopoulos, N. Assessing Impact, Performance and Sustainability Potential of Smart City Projects: Towards a Case Agnostic Evaluation Framework. *Sustainability* **2021**, *13*, 7395. [CrossRef]
25. Gabaldón Moreno, A.; Vélez, F.; Alpagut, B.; Hernández, P.; Sanz Montalvillo, C. How to Achieve Positive Energy Districts for Sustainable Cities: A Proposed Calculation Methodology. *Sustainability* **2021**, *13*, 710. [CrossRef]
26. Goodman, S.; Lockshin, L.; Cohen, E. Best-Worst Scaling: A Simple Method to Determine Drinks and Wine Style Preferences. In Proceedings of the 2nd International Wine Marketing Symposium, Sonoma, CA, USA, 9 July 2005. Available online: https://digital.library.adelaide.edu.au/dspace/bitstream/2440/33743/1/hdl_33743.pdf (accessed on 6 March 2023).
27. Chrzan, K.; Peitz, M. Best-Worst Scaling with Many Items. *J. Choice Model.* **2019**, *30*, 61–72. [CrossRef]
28. Schuster, A.L.R.; Crossnohere, N.L.; Campoamor, N.B.; Hollin, I.L.; Bridges, J.F.P. The Rise of Best-Worst Scaling for Prioritization: A Transdisciplinary Literature Review. *J. Choice Model.* **2024**, *50*, 100466. [CrossRef]
29. Finn, A.; Louviere, J.J. Determining the Appropriate Response to Evidence of Public Concern: The Case of Food Safety. *J. Public Policy Mark.* **1992**, *11*, 12–25. [CrossRef]
30. Bottero, M.; Bravi, M.; Caprioli, C.; Dell'Anna, F.; Dell'Ovo, M.; Oppio, A. New Housing Preferences in the COVID-19 Era: A Best-to-Worst Scaling Experiment. In *Computational Science and Its Applications—ICCSA 2021*; Lecture Notes in Computer Science; Springer International Publishing: Cham, Switzerland, 2021; Volume 12954, pp. 120–129, ISBN 978-3-030-86978-6.
31. Cascetta, E. Random Utility Theory. In *Transportation Systems Analysis*; Springer Optimization and Its Applications; Springer: Boston, MA, USA, 2009; Volume 29, pp. 89–167, ISBN 978-0-387-75856-5.
32. Parvin, S. Review of Best-Worst Scaling Method: A New Method over Other Scales in Marketing Research. *J. Bus. Stud.* **2016**, *37*, 13. Available online: https://api.semanticscholar.org/CorpusID:215925635 (accessed on 15 January 2023).
33. Colbourn, T.E. Investigating the Benefits of Women's Groups in Malawi: Adapted Quality of Life Measurement, Best-Worst Scaling Choice-Experiments and Contingent Valuation. Doctoral Dissertation, University College London, London, UK, 2012.
34. Mühlbacher, A.C.; Kaczynski, A.; Zweifel, P.; Johnson, F.R. Experimental Measurement of Preferences in Health and Healthcare Using Best-Worst Scaling: An Overview. *Health Econ. Rev.* **2016**, *6*, 5. [CrossRef] [PubMed]
35. Flynn, T.N.; Marley, A.A.J. Best-Worst Scaling: Theory and Methods. In *Handbook of Choice Modelling*; Hess, S., Daly, A., Eds.; Edward Elgar Publishing: Cheltenham, UK, 2014; ISBN 978-1-78100-315-2.
36. Marley, A.A.J.; Louviere, J.J. Some Probabilistic Models of Best, Worst, and Best–Worst Choices. *J. Math. Psychol.* **2005**, *49*, 464–480. [CrossRef]
37. Louviere, J.; Lings, I.; Islam, T.; Gudergan, S.; Flynn, T. An Introduction to the Application of (Case 1) Best–Worst Scaling in Marketing Research. *Int. J. Res. Mark.* **2013**, *30*, 292–303. [CrossRef]
38. Lipovetsky, S.; Conklin, M. Best-Worst Scaling in Analytical Closed-Form Solution. *J. Choice Model.* **2014**, *10*, 60–68. [CrossRef]
39. Martin, C.J.; Taylor, P.G.; Upham, P.; Ghiasi, G.; Bale, C.S.E.; James, H.; Owen, A.; Gale, W.F.; Slack, R.J.; Helmer, S. Energy in Low Carbon Cities and Social Learning: A Process for Defining Priority Research Questions with UK Stakeholders. *Sustain. Cities Soc.* **2014**, *10*, 149–160. [CrossRef]
40. Carayannis, E.G.; Campbell, D.F.J. Triple Helix, Quadruple Helix and Quintuple Helix and How Do Knowledge, Innovation and the Environment Relate To Each Other?: A Proposed Framework for a Trans-Disciplinary Analysis of Sustainable Development and Social Ecology. *Int. J. Soc. Ecol. Sustain. Dev.* **2010**, *1*, 41–69. [CrossRef]
41. Zarrin, F. SPARCS. In D1.8 Strategy for Developing Interoperability and Ecosystems for Positive Energy Districts. 2020. Available online: https://sparcs.info/en/deliverables/d1-08-strategy-for-developing-interoperability-and-ecosystems-for-positive-energy-districts/ (accessed on 14 December 2022).

42. Kourtzanidis, K.; Angelakoglou, K.; Giourka, P.; Tsarchopoulos, P.; Nikolopoulos, N.; Ioannidis, D.; Kantorovitch, J.; Formiga, J.; Verbeek, K.; de Vries, M.; et al. POCITYF. D11.7: Technical and Innovation Management Plans. 2020. Available online: https://www.pocityf.eu/wp-content/uploads/2020/09/POCITYF-864400_D11.7_Technical-and-Innovation-Management-Plans_compressed.pdf (accessed on 12 December 2022).
43. Watson, K.; Rees, J.; Watson, K.; Evans, J. Triangulum. D2.6 Final Impact Report M60. 2020. Available online: https://triangulum-project.eu/wp-content/uploads/2020/08/D2.6-Final-Report-M60v2.pdf (accessed on 12 December 2022).
44. Wyckmans, A.; Karatzoudi, K.; Brigg, D.; Ahlers, D. +CityxChange: D9.5 Report on Attendance at Events Held by Other SCC-01 Co-Ordinators 2. 2019. Available online: https://cityxchange.eu/wp-content/uploads/2019/11/D9.5_Report-on-Attendance-at-events-held-by-other-SCC-01-co-ordinators2.pdf (accessed on 12 December 2022).
45. Hynes, W.; Sweeney, J.; Lynch, S.; Rood, D. +CityxChange: D7.1 Approach and Methodology for Monitoring and Evaluation. 2020. Available online: https://cityxchange.eu/wp-content/uploads/2019/08/D7.1-Approach-and-Methodology-for-Monitoring-and-Evaluation-v2.0.pdf (accessed on 12 December 2022).
46. Brito, M.; Palha, G. SiNfONiA. D6.2 Dissemination Kit. 2017. Available online: https://www.sisal-pilot.eu/documents/d6-2-dissemination-kit-1st-version/ (accessed on 12 December 2022).
47. University of Deusto; Amsterdam University of Applied Science; Paul Scherrer Institute. ATELIER Monitoring and Evaluation Framework. D9.1 Repository of Definitions of Terms, Key Characteristics Archetypes, and a Set of KPIs. 2020. Available online: https://smartcity-atelier.eu/outcomes/deliverables/d9-1/ (accessed on 14 December 2022).
48. Salom, J.; Tamm, M. Syn.Ikia. WP3 Technology Integration in Smart Managed Plus Energy Buildings and Neighbourhoods. D3.1 Methodology Framework for Plus Energy Buildings and Neighbourhoods. 2020. Available online: https://www.synikia.eu/wp-content/uploads/2024/04/syn.ikia-D3.5-Analysis-of-shared-infrastructures-in-plus-energy-neighbourhoods-v2.pdf (accessed on 12 December 2022).
49. Dallara, L.; Lujan, M. Human-Centric Energy Districts: Smart Value Generation by Building Efficiency and Energy Justice for Sustainable Living. Available online: https://cordis.europa.eu/project/id/812730/results (accessed on 6 February 2023).
50. Croci, E.; Molteni, T.; Huovila, A.; Kuusisto, J.; Tuominen, P.; Akyürek, Ö.; Alpagut, B.; Faubel, E.; Arnhold, L.; Wolter, S. MAtchUP. D5.2: Economic Evaluation Framework. 2020. Available online: https://www.matchup-project.eu/wp-content/uploads/2021/10/MATCHUP_D5.2_Economic_evaluation_framework_FINAL.pdf (accessed on 28 December 2022).
51. Branchini, B.; Folco, G.; Huovila, A.; Kuusisto, J.; Arnhold, L.; Erdem, A. MAtchUP. In D5.3: Social Evaluation Framework. 2020. Available online: https://www.matchup-project.eu/wp-content/uploads/2020/11/D5.3-Social-evaluation-framework_FINAL.pdf (accessed on 28 December 2022).
52. Rolando, D.; Palm, B.; Claesson, J.; Nilsson, A.; Robért, M.; Shahrokni, H. GrowSmarter. In D5.4 Final Report on Results of Technical and Social Validation. 2019. Available online: https://grow-smarter.eu/fileadmin/editor-upload/Reports/GrowSmarter_Validation.pdf (accessed on 14 December 2022).
53. Tsarchopoulos, P. IRIS. D1.1: Report on the List of Selected KPIs for Each Transition Track. 2018. Available online: https://irissmartcities.eu/wp-content/uploads/2022/01/d1.1_report_on_the_list_of_selected_kpis_for_each_transition_track.pdf (accessed on 12 December 2022).
54. Kaiser, G.; Rutanen, E.; Vuorinen, M.; Buron, M. mySMARTLife. D1.2 Key Issues for Social Awareness and Acceptance. WP1, Task 1.1 Transition of EU Cities towards a New Concept of Smart Life and Economy. 2019. Available online: https://www.mysmartlife.eu/fileadmin/user_upload/Deliverables/D1.2_Key_issues_for_social_awareness_and_acceptance_01.pdf (accessed on 4 January 2023).
55. Peschel, H.; Cuvelier, B.; Gillion, S. mySMARTLife. D1.1 Social Acceptance Campaign at Local and District Level WP1, Task 1.1. Transition of EU Cities towards a New Concept of Smart Life and Economy. 2017. Available online: https://www.mysmartlife.eu/fileadmin/user_upload/Deliverables/D1.1_Social_acceptance_campaign_at_local_and_district_level.pdf (accessed on 4 January 2023).
56. Quijano, A.; Vicente, J.; Gomis Paya, I.; Urrutia Azcona, K. SmartENCity. D7.4 City Impact Evaluation Procedure. WP7, Task 7.1. 2017. Available online: https://smartencity.eu/outcomes/public-papers/ (accessed on 12 December 2022).
57. ProLight Project. Available online: https://www.prolight-project.eu/ (accessed on 8 February 2023).
58. Bosch, P.; Jongeneel, S.; Rovers, V.; Neumann, H.-M.; Airaksinen, M.; Huovila, A. CITYkeys Indicators for Smart City Projects and Smart Cities. 2017. Available online: https://www.researchgate.net/publication/326266723_CITYkeys_indicators_for_smart_city_projects_and_smart_cities (accessed on 18 January 2023). [CrossRef]
59. Marotta, I.; Guarino, F.; Longo, S.; Cellura, M. Environmental Sustainability Approaches and Positive Energy Districts: A Literature Review. *Sustainability* **2021**, *13*, 13063. [CrossRef]
60. JPI Urban Europe. Europe towards Positive Energy Districts: A Compilation of Projects towards Sustainable Urbanization and the Energy Transition. 2020. Available online: https://setis.ec.europa.eu/document/download/f0614eb5-c352-4872-9a28-5674a7111d9d_en?filename=PED-Booklet-Update-Feb-2020_2.pdf (accessed on 3 December 2022).
61. Vandevyvere, H.; Ahlers, D.; Alpagut, B.; Cerna, V.; Cimini, V.; Haxhija, S.; Hukkalainen, M.; Kuzmic, M.; Livik, K.; Padilla, M.; et al. *Positive Energy Districts Solution Booklet*; SCIS Smart Cities Information System: Brussels, Belgium, 2020.

Disclaimer/Publisher's Note: The statements, opinions and data contained in all publications are solely those of the individual author(s) and contributor(s) and not of MDPI and/or the editor(s). MDPI and/or the editor(s) disclaim responsibility for any injury to people or property resulting from any ideas, methods, instructions or products referred to in the content.

energies

MDPI

Systematic Review

Status, Challenges and Future Directions in the Evaluation of Net-Zero Energy Building Retrofits: A Bibliometrics-Based Systematic Review

Qin Xiaoxiang [1,2], Yin Junjia [1,*], Nuzul Azam Haron [1], Aidi Hizami Alias [1], Teik Hua Law [1] and Nabilah Abu Bakar [1]

[1] Department of Civil Engineering, Faculty of Engineering, Universiti Putra Malaysia, Serdang 43300, Selangor, Malaysia; gs65302@student.upm.edu.my (Q.X.); nuzul@upm.edu.my (N.A.H.); aidihizami@upm.edu.my (A.H.A.); lawteik@upm.edu.my (T.H.L.); nabilah@upm.edu.my (N.A.B.)
[2] School of Architectural Engineering, Nanning Vocational and Technical University, Nanning 530008, China
* Correspondence: gs64764@student.upm.edu.my; Tel.: +86-18908453651

Abstract: Net-zero energy building (NZEB), an initiative to address energy conservation and emission reduction, has received widespread attention worldwide. This study aims to systematically explore recent challenges in NZEB retrofit research through a mixed-method approach and provide recommendations and future directions. A review of 106 documents (2020–2024) retrieved from the Web of Science and Scopus databases found that the globalization of NZEB retrofit research is unstoppable. Assessment methods are diverse, ranging from modeling energy efficiency (using different software such as DesignBuilder 7.0, PVsyst 7.4, EnergyPlus 24.1.0, etc.) to multi-attribute decision-making methods (e.g., DEMATEL-AHP/ANP-VIKOR) and comparative analysis. Current assessment metrics are dominated by economic benefits (e.g., net present value, dynamic payback period, and total operating cost) and energy consumption (e.g., electricity consumption and generation), with less consideration of environmental impacts (e.g., carbon reduction), as well as comfort (e.g., thermal comfort and indoor comfort). The study found that current challenges mainly include "Low economic feasibility of retrofitting", "Building retrofit energy code irrationality", and "Insufficient understanding, communication, and trust between stakeholders". To overcome these challenges, the study also proposes a framework of strategies to address them, including (1) maximizing natural space, (2) introducing a tenant equity system, (3) upgrading waste management, (4) strengthening energy monitoring, (5) establishing complete life cycle mechanisms, (6) providing systemic solutions; (7) promoting the use of low-carbon building materials, and (8) increasing policy support.

Keywords: systematic review; net zero energy building; Web of Science; Scopus; bibliometric analysis; retrofit challenges; renewable energy; sustainability; applied science

1. Introduction

A net-zero energy building, also known as a zero-energy building or a zero-carbon building, is a building that has zero or near-zero net energy consumption, i.e., a balance between the amount of energy it produces and the amount of energy it consumes over a year, through the use of advanced energy efficiency measures and renewable energy technologies in its design, construction, and operation [1]. The concept originated in the 1970s because of the energy crisis. Still, it was not until the beginning of the 21st century that "net zero" became an explicit goal in building design and sustainability [2]. It has also been argued that meeting the annual balance alone is insufficient to adequately describe a net-zero energy building and that the interaction between the building and the energy grid needs to be addressed [3]. Decarbonizing the construction sector, which accounts for 40% of global energy consumption and 36% of total greenhouse gas emissions, is critical to mitigate climate change [4]. With increased environmental awareness and technological

advances, net-zero energy buildings are being widely promoted and applied worldwide. The American Society of Heating, Refrigerating, and Air Conditioning Engineers (ASHRAE) has set a goal of NZEB marketability by 2030 [5]. As early as September 2016, the China Construction Association (CCA) drafted "Best Practice Cases of Ultra-Low/Near-Zero Energy Buildings in China" under the guidance of the Ministry of Housing and Urban–Rural Development [6]. The revised version of the EU Energy Efficiency in Buildings Directive introduces the concept of "near-zero energy buildings", which is required for all new and existing buildings needing major retrofitting from 2021 onwards [7]. Malaysia plans to have all new public and private buildings (on average) in the zero-energy building category by 2030 [8]. A classic example is the "SURIA 16" strategic partnership project between Universiti Putra Malaysia (UPM) and Tenaga Nasional Berhad (TNB) for installing solar photovoltaic systems [9]. As depicted in Figure 1, through the New Energy Supply Agreement (SARE), GSPARX installed solar systems at 12 locations, including various buildings such as mosques, parking lots, and a floating solar project called SURIA Floating & Walkway @ Eng UPM. This mega project is geared to deliver 16.18 MWp in capacity. It benefits UPM by reducing electricity by RM 114 million over 25 years, with an installation cost of RM 45 million funded by TNB [10]. It can also reduce CO_2 emission by 15,655 metric tons per year, equivalent to minimizing the greenhouse gas emission from 3187 vehicles per year or carbon absorption by 242,320 tree seedlings planted over ten years [11].



Figure 1. "SURIA 16" project.

As the subject has caught fire and research has increased, some scholars have begun to conduct literature reviews on it. Most of the reviews were limited to conceptual clarification and policy analysis [2]. For example, the Australian study by Louise et al. argues that the NZEB concept may apply to new and existing buildings to have a tangible impact on overarching issues such as greenhouse gas emissions, sustainability, and consumer protection from electricity price increases [12]. Satola et al. reviewed the policy frameworks for net-zero buildings in Norway, the United Kingdom, the United States, and Singapore. They found an urgent need for harmonized and transparent international and national standards to ensure consistency in the life cycle assessment of buildings [13]. Christopher et al.'s study, on the other hand, conducted a literature review from the perspective of renewable energy technologies (RETs) and found that most RETs are usually unstable and intermittent, fluctuating widely over hours or days [14]. Brown et al.'s literature review, on the other hand, found that in addition to government policy factors, a lack of knowledge,

climate issues, and cost issues were identified as the main barriers encountered by the Australian NZEB industry [15]. The review by Li et al. discusses strategies for applying net-zero energy (NZE) building technologies (i.e., achieving net-zero non-renewable energy consumption on-site) to poultry houses, arguing that any modifications to existing technologies should be based on a careful consideration of the physiological needs of poultry (e.g., ambient temperatures, air quality, availability of feed and water, etc.) [16]. Falana's review categorized the impediments solely due to crucial stakeholder engagement and the relationship with a complete life cycle of net-zero carbon building development [17]. Noh et al.'s study, also from a renewable energy perspective, found that the evaluation of NZEB practices should include an assessment of the building's energy balance, occupant comfort, and interaction with the energy grid [18]. The application of Building Integrated Photovoltaics (BIPV) in NZEB has also received attention, with studies finding that the building envelope size, height, glazing material, light transmission, etc., have significant impacts on meeting NZEB standards and that it is important not to focus solely on roof-integrated PV [19]. A multi-case review in China identified significant advantages and room for incremental development in promoting BIPV in China [20]. Unfortunately, there are currently no studies that have focused the review theme on a retrofit evaluation. This study aims to fill this gap by combining bibliometrics with a systematic review to provide a comprehensive picture of the status, challenges, and future directions in NZEB retrofit and evaluation.

The rest of the paper unfolds as follows: Section 2 provides detailed information on the methodology of this study; Section 3 presents the results of this study; Section 4 discusses the current challenges encountered in NEZB retrofitting and strategies to deal with them; and Section 5 summarizes the research and points out limitations.

2. Materials and Methods

PRISMA, known as Preferred Reporting Items for Systematic Reviews and Meta-Analyses, is a set of standardized specifications for the quality of research in systematic reviews [21]. It applies to published literature reviews containing primary data sources [22]. This study builds on the guidelines provided by the PRISMA on transparency and the quality of systematic review reporting [23]. It aims to improve systematic reviews' scientific validity and comparability [24,25]. Referring to previous classical studies, Figure 2 illustrates the steps of conducting a systematic literature review using the PRISMA protocol and quantitative analysis through bibliometric analysis to achieve the research objectives [14,26].

The Scopus and Web of Science databases were selected as the most extensive proprietary databases for searching the extant literature. They are particularly well suited for searching the literature based on architecture and building disciplines [27]. This combination of databases has been used to explore "Zero Energy Building Technology Options and Strategies for Climate Change Mitigation", "Life Cycle Energy Analysis of Buildings", and "Dynamic Facades in Buildings". It has shown an excellent fit [28–30]. Combining these two databases results in a more complete search of the available scientific literature. The selection with energy efficiency goals was based on the most recent research on net-zero energy buildings to ensure the use of established terminology. In reference to previous studies [31,32], search terms included (1) emission reduction targets, (2) energy as a metric, (3) diverse project sizes and types, and (4) types of upgrades, as shown in Table 1.

Table 1. Search terms applied in Scopus and Web of Science.

Abatement Goal	Unit	Scale and Typology	Upgrading Type
Nearly zero	Energy	Dwelling	Retrofitting
Net zero		House	Refurbishment
Zero		Building	Modernization
Low		Office	Renovation

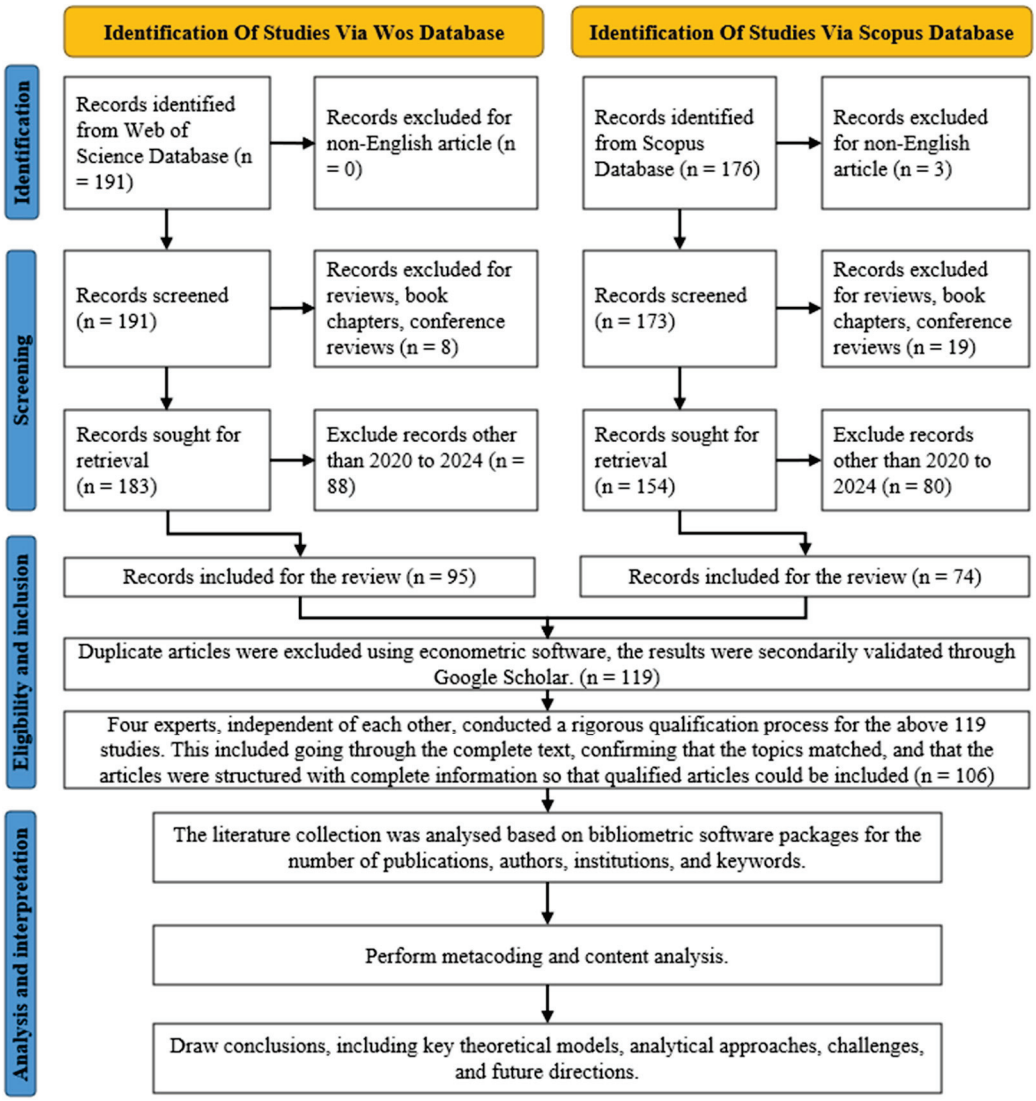


Figure 2. Research process.

As indicated in Table 2, the established search terms were combined into a single search query for each database using its specific search syntax, which also allowed Boolean and proximity operators. Document titles, abstracts, and keywords were searched in Scopus, while titles, abstracts, and author keywords were searched in Web of Science. Both databases consider British and American spelling variations. Concerning previous research [33,34] in the field and to ensure that the research is cutting edge and that the information required for the content analysis is complete, the eligibility criteria for literature inclusion were as follows: (1) publication year—between 2020 and 2024; (2) language—English; (3) type of article—research article; (4) topic—retrofitting of existing buildings; and (5) study content—a clear description of the location of the study, methodology, evaluation metrics, and limitations.

Table 2. Retrieve code applied in Scopus and Web of Science.

Databases	Retrieve Code
Scopus	TITLE-ABS-KEY ((“low” OR “nearly zero” OR “net zero” OR “zero”) PRE/2 (energy) AND (“dwelling” OR “house” OR “building” OR “office”) AND (“retrofitting” OR “refurbishment” OR “modernization” OR “renovation”) AND (“evaluation”))
Web of Science	TS = (((low OR “nearly zero” OR “net zero” OR zero) NEAR/2 (energy)) AND (dwelling OR house OR building OR office) AND (retrofitting OR refurbishment OR modernization OR renovation) AND (evaluation))

The search was conducted on 1 July 2024 and found 74 documents in Scopus and 95 in Web of Science. RStudio 3.6's Bibliometrix® package was used to remove 50 papers (as they were either duplicates or inaccessible), leaving 119 documents. The results were secondarily validated using Google Scholar. In the end, the 119 papers were qualified by four independent experts who browsed through the full texts. The 106 documents remaining after screening were analyzed and reviewed in two steps. The first step was to examine their metadata using Biblioshiny® to select bibliometric charts representing the annual scientific output, thematic evolution, most represented countries, and keywords. This analysis used the bibliometric metadata fields included in the search results, such as the title, keywords, authors and country of publication, and year of publication. The purpose of a bibliometric study is to provide an overview of the field of study. The second step of the literature review (36 strongly related articles) was to manually analyze the full text of the publications. These 36 studies are the result of a comprehensive selection based on four main principles: (1) fresher articles (date of publication), (2) highly cited articles, (3) high-impact factor articles, and (4) accessibility. The following themes were extracted for this review: (1) research location, (2) evaluation methods, (3) evaluation indicators, and (4) research limitations.

3. Results

3.1. Results of the Bibliometric Analysis

3.1.1. Annual Issuance of Significant Publications

Figure 3 shows the articles published in major journals on the topics reviewed in this study between 2020 and 2024. The journals include *Energies*, *Energy and Buildings*, *Applied Energy*, *Sustainability*, *Building Simulation*, *Buildings*, and *Journal of Cleaner Production*. Overall, the number of articles published increased year by year over this period, with the journal *Energy and Buildings* publishing the most significant number of articles in 2022 and the following years, remaining at around 8 articles, while the number of articles published in the journal *Energies* gradually increased from 0 in 2020 to 9 in 2024, showing a significant growth trend. Other journals such as *Applied Energy*, *Sustainability*, *Building Simulation*, and *Buildings* also show a year-on-year increase. This indicates that this topic is receiving more and more attention from scholars and reflects the significance of this study.

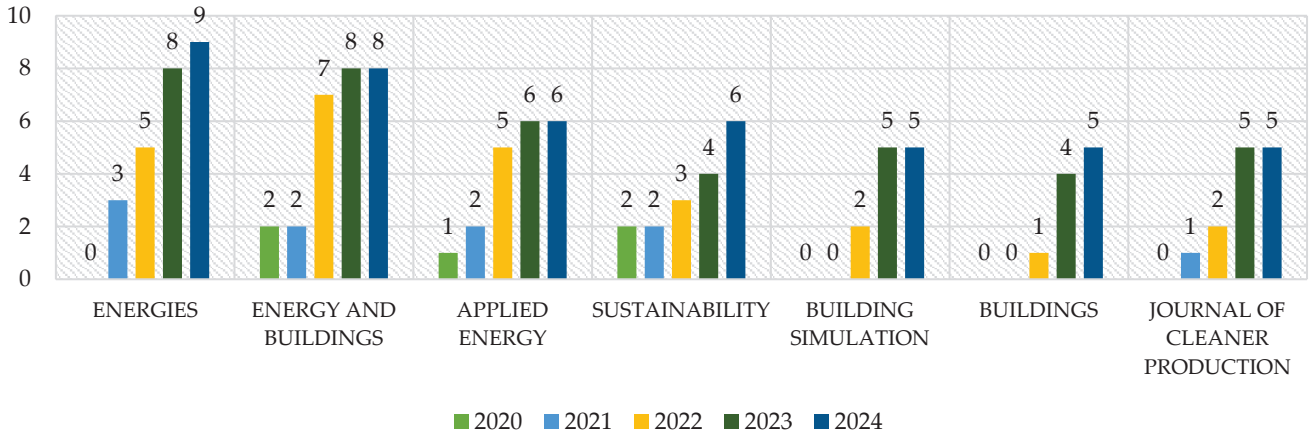


Figure 3. Annual issuance of significant publications.

3.1.2. Top Ten Highly Cited Articles

In academia, the number of citations is regarded as one of the indicators of research quality and impact [35]. Table 3 summarizes the top ten highly cited articles on this theme. The highly cited literature usually contains essential theories, methods, or findings [36]. Identifying this literature helps to disseminate this knowledge to the broader academic community, thereby influencing more researchers and practitioners. Second, it reflects current hotspots and trends in the research field. By analyzing this literature, researchers

can understand which issues are receiving widespread attention and where research is heading in the future. It is worth noting that the top ten highly cited articles in the literature are from 2020 to 2022, which means that more influential articles have not appeared in the last two years and expresses the urgent need to find breakthroughs under the topic.

Table 3. The top 10 highly cited articles.

Paper	DOI	Total Citations	TC per Year	Normalized TC
Zhao et al. (2021) [37]	10.1155/2021/6638897	39	9.75	2.82
Hong et al. (2021) [38]	10.1007/s12273-021-0778-7	39	9.75	2.82
Opher et al. (2021) [39]	10.1016/j.jclepro.2020.123819	38	9.50	2.75
Figueroa-Lopez et al. (2021) [40]	10.1016/j.jobe.2021.102607	35	8.75	2.53
Hong et al. (2020) [41]	10.1016/j.enbuild.2020.109959	30	6.00	2.00
Rabani et al. (2021) [42]	10.1016/j.buildenv.2021.108159	29	7.25	2.10
Albatayneh et al. (2021) [43]	10.3390/en14102946	23	5.75	1.66
Mitchell et al. (2020) [44]	10.1016/j.enbuild.2020.110240	22	4.40	1.47
Colclough et al. (2022) [45]	10.1016/j.enbuild.2021.111563	21	7.00	2.57
Apostolopoulos et al. (2022) [46]	10.1016/j.scs.2022.103921	20	6.67	2.45

3.1.3. Keyword Co-Occurrence Network

A keyword co-occurrence bibliometric analysis is a method of analysis that examines the phenomenon of co-occurrence between feature items in the literature [47]. The strength of the association between keywords is measured by counting the co-occurrences between them, thus revealing the association of information in the literature [48]. In this study, a network diagram was generated using Bibliometrix® to provide insights into the data selected for the eligibility phase of the PRISMA protocol and to show the crucial keywords in the data. The Walktrap algorithm was chosen for this study as a method for community discovery based on the idea of random wandering. Its key idea is to use random walks on the graph to determine the distance metric between vertices and between communities. It is considered to surpass previous methods in terms of the quality of community structure and is one of the best methods in terms of runtime [49]. The steps of the Walktrap algorithm are as follows [50]: First, the similarity between vertices is computed by random wandering. Then, hierarchical clustering is performed using these similarities to merge neighboring communities. Finally, the division with the largest modularity is selected as the best community structure.

Regarding similarity computation, the Walktrap algorithm uses a random wandering probability matrix to compute node similarity. The similarity between nodes i and j is calculated by Euclidean distance as follows:

$$r_{ij} = \parallel D^{-1}P_i^t - D^{-1}P_j^t \parallel \quad (1)$$

where D is the degree diagonal matrix of the node and P_i^t is the probability of going from vertex i to vertex j in the tth step.

Referring to previous studies, in this study, the number of nodes was set to 50, the minimum number of edges was set to 2, and the rest were default parameters. As depicted in Figure 4, differences in the brightness and transparency of the keyword colors shown in the visualization indicate keyword interconnections. At the same time, the nodes' sizes highlight the keywords' prominence in the literature. The larger the node of the item, the higher the weight in the network [51]. The distance between the circles also represents the relevance between the keywords, emphasizing co-occurring links [52]. Thus, if two keywords are located close, their link is more robust. Since "performance", "optimization", "design", and "consumption" have the most prominent circles on the network diagram, they have the highest weight in the literature. This also indicates that these keywords are hot research topics within the evaluation field. "Residential buildings" is also a recurring keyword, suggesting that most of the evaluations on retrofitting are related to residential

buildings on a global scale. Another noteworthy point from the network diagram is the range of keywords related to potential solutions for evaluation. Keywords such as "education", "decision-making", "sensitivity analysis", "multi-objective", "life cycle assessment", and "cost" all have significant weights. They are interlinked with the evaluation clusters, suggesting that these elements are frequently discussed.

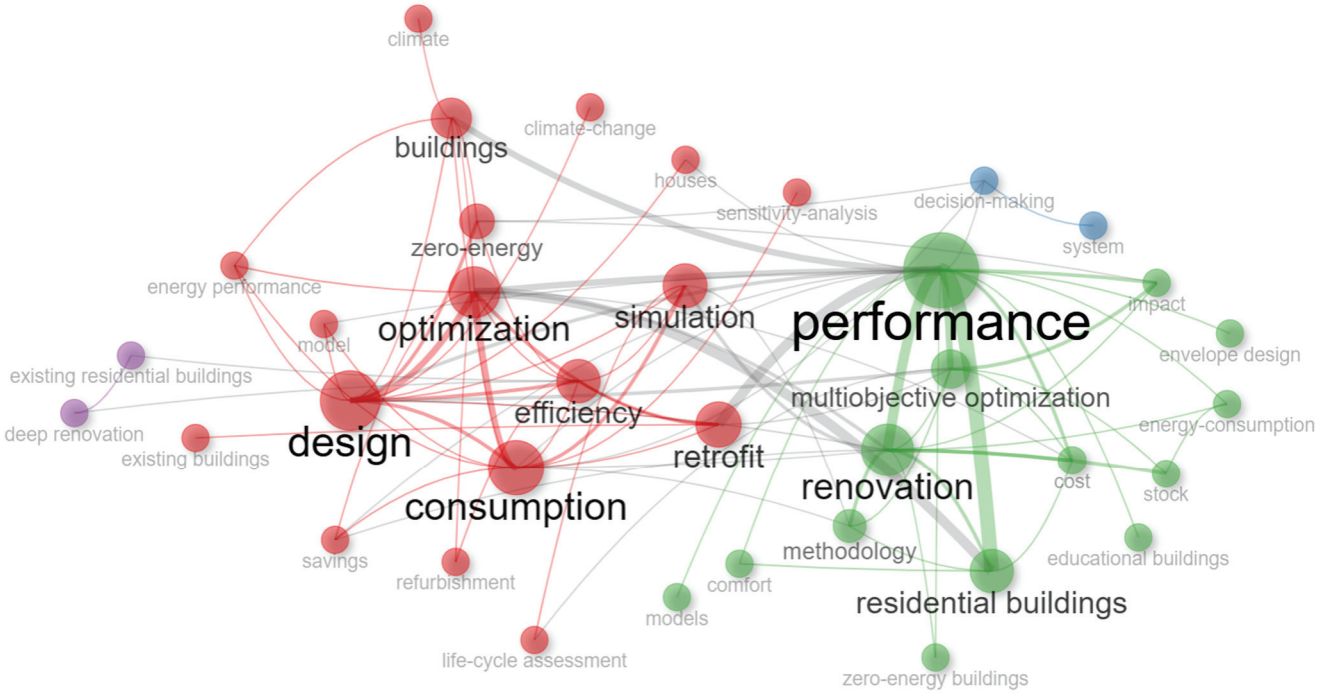


Figure 4. Keyword co-occurring network.

3.2. Results of the Content Analysis

Table 4 compiles various methodologies used to evaluate the retrofit of Nearly Zero Energy Buildings (NZEBs) across different regions. Each entry in the table details each study's source, location, method, evaluation indicators, and limitations. The current research covers several world regions, including Turkey, China, Poland, Sweden, UAE, USA, Japan, MENA, Europe, South Korea, Pakistan, Italy, Lithuania, and Portugal, demonstrating the globalization of NZEB retrofit studies. Evaluation methods are also diverse, ranging from modeling energy efficiency analysis (using different software such as DesignBuilder, PVsyst, EnergyPlus, etc.) to multi-attribute decision-making methods (e.g., DEMATEL-AHP/ANP-VIKOR) and case studies. Scholars have tried to assess the effectiveness of NZEB retrofit from multiple perspectives using different strategies. The assessment indicators cover economic benefits (e.g., net present value, dynamic payback period, and total operating cost), energy consumption (e.g., electricity consumption and generation), environmental impacts (e.g., carbon reduction), and comfort (e.g., thermal comfort and indoor comfort). The diversity of indicators also represents that there is currently no industry consensus or standard paradigm for evaluation systems. Many studies have specific limitations, such as only considering cost effectiveness, only applying to PV retrofit projects, only targeting cold regions, small sample sizes, and not considering the building life cycle. In addition, most of the studies were conducted for specific application scenarios, such as hospital buildings, multi-story wood-frame buildings, brick-frame dwellings, and wall-mounted PV systems, which led to different evaluation methods and indicators for various application scenarios.

Table 4. NZEB retrofit evaluation methodology.

Source	Location	Method	Evaluation Indicators	Limitations
[53]	Turkey	Modeling energy performance (DesignBuilder)	Payback period (NPV)	Only cost effectiveness was considered.
[54]	China	Modeling energy performance (PVsyst 7.2)	Dynamic payback period (NPV)	Only for photovoltaic retrofit projects
[55]	China	Modeling energy performance (Dest-C)	Net present value (NPV) ratio	Only for cold regions
[56]	China	Modelling energy performance (EnergyPlus)	Economic and carbon reduction benefits	Only for a colored radiant cooling wall retrofit
[57]	China	Logic-AHP-TOPSIS method	Upfront investment, payback period, heating cost savings	Only available in Lanzhou, China.
[58]	Poland	DEMATEL-AHP/ANP-VIKOR method, modelling energy performance (ArCADia-TERMOCAD)	Total operating costs, compliance with air quality parameters, the impacts of the building and its facilities on the surrounding environment, total building completion time, etc.	The choice of decision criteria needs to be tailored to the specifics of the decision maker's preferences.
[59]	Sweden	Modeling energy performance (Grasshopper/Rhinoceros 3D/EnergyPlus)	Thermal performance of buildings	Small sample size
[60]	United Arab Emirates	Case study	Reduction in cooling load	Only for energy-saving retrofits with high solar reflectance index (SRI) coatings
[61]	China, USA, Europe	Multiple case studies	Benefits, costs, heat sources, and technology	Small sample size
[62]	Japan	Modeling energy performance (BEST)	Heat, power generation	The impact of the amount of hot water obtained from the HFCs on reducing the building's energy consumption cannot yet be determined.
[63]	Middle East and North Africa (MENA) region	Modelling energy performance	Orientation, window location and size, glazing type, wall and roof insulation levels, lighting fixtures, appliances, and the efficiency of heating and cooling systems	Building envelope insulation needs to vary by climate.
[64]	European	Comparative analysis (actual data)	Energy, the function of the house, and its internal comfort	The local competition and the described concept of post-competition use influenced the energy efficiency assessment.
[65]	China	Parameter reverse identification and load forward calculation	Internal heat gain	Only for integrated building envelopes
[66]	United State	Comparative analysis (actual data)	Electricity consumption and generation	Historical average data, such as weather conditions, usually do not match actual operating conditions.
[67]	Singapore	Modeling energy performance (RNSYS 17)	Energy savings and annual cost (NPV)	The setting of economic parameters has a considerable impact.

Table 4. *Cont.*

Source	Location	Method	Evaluation Indicators	Limitations
[68]	China	Modeling energy performance (TRNSYS)	Building energy use and renewable energy generations, economic cost, load matching, and grid interaction	A simplified battery model did not consider the battery's energy loss during charging, storage, and discharging.
[69]	United State	Modeling energy performance (ASHRAE Inverse Modeling Toolkit (IMT))	Measured data on building energy consumption and photovoltaic power output	The effects of the building orientation, envelope improvements, and HVAC system upgrades using calibrated simulation models were not considered.
[70]	Iraq	Modeling energy performance (TRNSYS/TRNBuild)	Energy consumption rate and cost	Failure to consider the impact of passive structures
[71]	European	Modelling energy performance (SketchUp/Open Studio/EnergyPlus)	Electricity and primary energy consumption	The ability to use energy building modeling to describe the hourly heat demand of a building is not possible.
[72]	European	Differential sensitivity analysis (DSA), elementary effects method	Interest rates, building and equipment maintenance costs, structural element costs, and electricity prices	Small sample size
[73]	South Korea	Comparative analysis (actual data)	Operational energy consumption and total environmental costs	Energy measurement masks the complexity of building energy flows and ignores the large-scale thermodynamics (economic, cultural, informational, etc.) surrounding the building.
[74]	Pakistan	Modelling energy performance (HOMER Pro)	Solar radiation potential, operating costs, initial capital costs, energy generated by PV, payback period, and NPV costs	Only for hospital buildings
[75]	Italy	Modeling energy performance (FATA-e®)	Electricity demand (sum of HVAC, hot water, and artificial lighting), PV generation, electricity absorbed from the grid, and PV surplus exported to the grid	Only for multi-story timber buildings
[76]	China	Sensitivity analysis	Building geometry, building envelope thermal performance, equipment energy efficiency, and internal heat sources	The range of applications is limited by geography and building type.
[77]	China	Modeling energy performance (TRNSYS/RETScreen)	Tilt angle, orientation, volumetric ratio, PV conversion efficiency, location, and power generation	The difference between the simulated and calculated results is about 10%.
[78]	South Korea	Modeling energy performance (TRNSYS)	Passive element S/V ratio (surface-to-volume ratio) for the building type, building orientation, final energy consumption, and investment costs for active elements (building-integrated PV)	Failure to consider the life cycle of a net-zero energy building

Table 4. *Cont.*

Source	Location	Method	Evaluation Indicators	Limitations
[79]	Italy	Preferred method of sorting organization	Energy consumption, life cycle costs, carbon emissions, property values, and indoor comfort standards	Assumed spatial changes in appreciation of NZEB buildings in the property market
[80]	Lithuanian	Multi-Attribute Decision Making Methods for Optimal Solutions (MADM-opt)	Heat exchange, relative air humidity, air temperature, air flow rate, surface area-to-volume ratio, noise insulation, and annual heat demand	For brick dwellings only
[81]	Lithuanian	Primary energy consumption formula	Average power generation, wind speed, wind turbine capacity, conversion efficiency, and turbine power consumption	For wind turbines only
[82]	China	Modelling energy performance (EnergyPlus)	Baseline cooling demand, typical incident solar radiation, direct solar transmittance, and percentage of solar energy savings from exterior shading blinds	The external shading devices were not quantified only for external louver sunshade shading performance and geometric (e.g., slat width and shape) and physical (e.g., front and rear side slat solar reflectance) parameters.
[83]	Portugal	Primary energy consumption formula	Renewable energy ratio (RER) and onsite energy fraction (OEF)	Options for exporting energy carriers (e.g., electricity) are always better than options for self-consumption energy generated on-site.
[84]	Italy	Modeling energy performance (HOMER Pro\PV Sol)	User well-being, energy and greenhouse gas savings, and cost optimization	Only for photovoltaic power plant projects
[85]	Japan	Comparative analysis (actual data)	Spectral variation, solar radiation, electricity generation	For wall-mounted PV systems only
[86]	Italy	Comparative analysis (actual data)	Building load, photovoltaic power generation, indoor comfort	Only for typical Mediterranean climates
[87]	Belgium	Comparative analysis (actual data)	Thermal comfort and energy parameters	No post-occupancy qualitative assessment was considered regarding thermal comfort.
[88]	China	Energy efficiency assessment method based on time-series current simulations	Proportion of energy storage capacity, annual electricity use, yearly electricity consumption, energy efficiency, and stakeholder income	System costs do not include the cost of losses from poor power quality.

4. Discussion

4.1. Challenges of NZEB Retrofit

Table 5 details the technical, economic, social, and policy challenges in assessing NZEB retrofits. First, there are the technical challenges. For example, most cities need higher coverage and more data related to older buildings. However, collecting and analyzing building energy efficiency data on a large scale are complex and time-consuming and require multiple resources [89]. Factors such as the structural load-bearing capacity or layout of older buildings also limit integration with many large installations. Indeed, current modeling methods cannot capture all the geometric features in the category represented by the prototype [90]. There is also a lack of real-time optimization models for carbon reduction at the building design stage,

limiting our ability to accurately estimate and optimize carbon emissions. Digital and intelligent technologies are crucial for zero-energy building retrofits, while data privacy and systems integration are also topics worthy of in-depth research. The next challenge is economic. For example, net-zero energy retrofits typically require significant capital investment in technology upgrades, engineering and construction, and materials procurement [91]. This can be burdensome for many homeowners, especially if returns are difficult to obtain in the short term. For example, in China, most energy efficiency retrofits are generated by policy guidance and government subsidy incentives [92]. However, owners' enthusiasm for energy efficiency retrofits inevitably fades as incentives end or are scaled back. The third is the social challenge, where mutual understanding is too romantic for citizens or potential partners (e.g., developers, distributors, engineers, and space planners) who are less familiar with modern approaches in the energy sector [93]. The fourth is the policy challenge. For example, building codes and guidelines vary widely across climatic regions and countries, as do the amounts of incentives [94].

Table 5. Challenges of NZEB retrofit.

Categorization	ID	Challenge	Validation Reference
Technology	T1	Mechanisms of solar cell aesthetics and carrier transport layers and interfaces	[95]
	T2	Air source heat pumps are prone to failure in cold climates.	[96]
	T3	Failure to consider operational and occupant behavioral changes	[97]
	T4	PV systems are prone to module ruptures, inverter failures, performance degradation, and other failures.	[98]
	T5	High initial construction costs	[99]
	T6	Energy simulation does not provide the best results because many potential system configurations are untested.	[100]
	T7	Failure to consider the aging of the power generation system	[101]
	T8	Implicit carbon in the life cycle of a building is not considered.	[102]
	T9	Insufficient use of new technologies, such as digital twins and artificial intelligence algorithms	[103]
	T10	Modeling methods cannot capture all the geometric features in the category represented by the prototype.	[104]
Economics	E1	The payback period is about 10 years.	[105]
	E2	Dynamic electricity and oil prices hinder the accuracy of cost measurements.	[106]
	E3	Financing mechanisms and incentives	[107]
	E4	Uncertainty in energy supply markets makes people pessimistic and reluctant to make decisions.	[108]
	E5	Life Cycle Cost Analysis (LCCA) indicators are not comprehensive.	[109]
	E6	Using energy storage systems (electrical and thermal) increases losses, increasing the energy demand and electricity bills.	[110]
	E7	Lack of standardized value assessments for sustainable buildings	[111]
Society	S1	Most communities have not yet published up-to-date measurements of NZEB's success, and no data on its energy performance exist.	[112]
	S2	Limited information on climate change data	[113]
	S3	Insufficient understanding, communication, and trust between stakeholders	[114]
	S4	The currently applied NZEB retrofit technologies are dominated by solar photovoltaics, with a small share of other energy sources such as wind, biomass, and micro-hydro.	[115]
	S5	Lack of platforms to integrate data, including city castle maps, building information, building models and projects, and energy networks	[116]
	S6	Public awareness of NZEB remains low.	[117]
	S7	The immaturity of innovative city systems, smart grids, smart meters, and local energy trading platforms	[118]
	S8	The complex impact of urban density on costs	[119]
	S9	Lack of NZEB building professionals such as owners, facility managers, building design engineers, and builders	[120]
	S10	Conflict of interest with traditional electricity suppliers	[121]
	S11	Regional differences in types of renewable energy	[122]
	S12	Instability and variations in regional climate and local weather conditions	[123]
	S13	Fewer members of the public, businesses, or NGOs are involved and on board in realizing zero-energy buildings.	[124]
Policy	P1	Localization of standards and requirements, such as source and supply requirements, timescales, emission sources, and grid connections	[125]
	P2	Decarbonization strategies and mechanisms are not in place in lagging countries.	[126]
	P3	The region does not have a policy for excess electricity to be recovered by the national grid.	[127]
	P4	Incentive policies such as subsidies and tax breaks are not provided.	[128]
	P5	Lack of consensus on the definition and calculation of NZEB	[129]
	P6	Delays in the NZEB approval process	[130]

Note: The above challenges are derived from [53–88] and are secondarily validated by the validation references.

4.2. Strategies for Promoting Net-Zero Energy Building Retrofits

This study develops eight strategies to promote retrofitting older buildings with zero-carbon emissions to address these challenges, as illustrated in Figure 5. Not only does it contribute to urban regeneration to combat climate change and improve energy efficiency but it also promotes technological innovation, improves indoor environmental quality, and creates employment opportunities, which are vital for sustainable development.

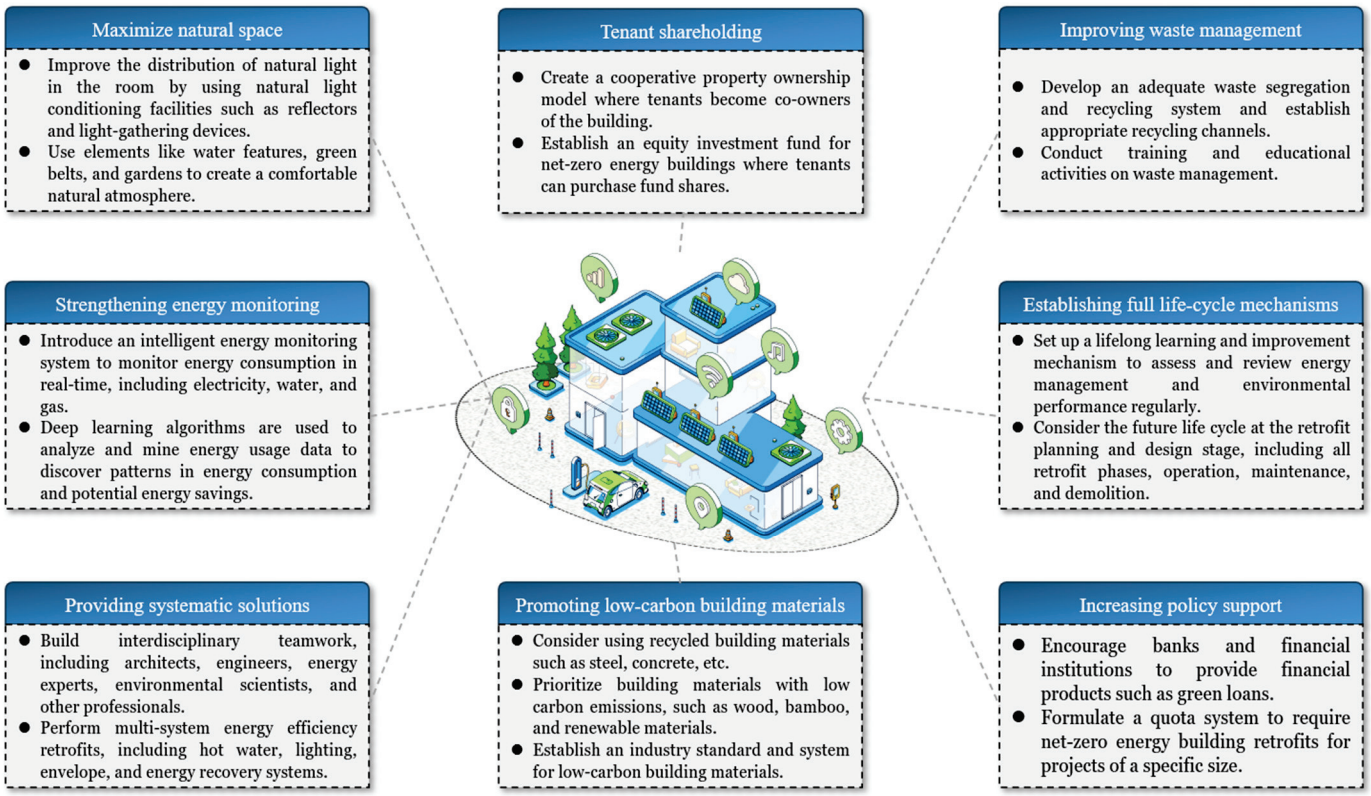


Figure 5. Strategies for promoting net-zero energy building retrofits.

4.2.1. Maximizing Natural Space

Maximizing natural space in net-zero energy building retrofits contributes to the environmental quality and comfort of the building. There are various ways to maximize natural space in a net-zero energy building retrofit. The first is redesigning the building layout to maximize natural light and ventilation. For example, by installing insulation on the interior or renovating or installing new windows, the theoretical energy consumption could still be reduced by 68% compared to the original building [131]. Second, green space should be added around or inside the building, such as gardens, lawns, and plant walls. This can provide more natural landscaping and recreational space. It is also good to introduce natural elements into the design, such as water features, green walls, and waterfalls, which can enhance the natural feel of the space [132]. We also suggest transforming older buildings with more outdoor spaces, such as terraces, balconies, and courtyards, and considering the balance of ecosystems, such as birds, insects, and plants, which can be protected and promoted through rational design. It is worth noting that the building orientation, energy-efficient windows, and vegetation types require retrofit strategies tailored to local climatic and environmental conditions, such as tropical and humid climates [133].

4.2.2. Introducing a Tenant Equity System

Introducing a tenant equity system can enhance tenant participation and responsibility in net-zero-energy building retrofit projects, thereby contributing to the sustainable development and long-term operation of buildings. It is a collection of innovative approaches

designed to incentivize tenants to participate more actively. The first model establishes co-operative property ownership, where tenants become co-owners of the building. They can purchase an equity stake in the building, participate in decision-making and management as owners, and monitor the building's energy use and environmental performance [134]. The second model is a rent discount or incentive program. For example, tenants who adopt energy-saving measures or participate in environmental protection activities are given a certain percentage of rent discounts, or environmental bonuses are offered as incentives [135]. The third model is to establish an equity investment fund for net-zero energy buildings. Tenants can buy a share of the fund as one of the investors in the retrofit project and share in the benefits of the building. We also recommend linking tenant equity to voting and decision-making rights, allowing tenants to participate in decision-making on important matters, such as energy management and facility maintenance. At the same time, to ensure that tenants have complete transparency on the operations and financial status of the retrofit project, the construction company should provide relevant information and reports. In addition, this study recommends enhancing tenants' access to low-cost or free retrofit options, coupled with tenant protection mechanisms, and proactively exploring mechanisms that enable landlords to recoup the cost of retrofits while ensuring that tenants benefit from energy savings to address the issue of decentralized incentives between landlords and tenants [136].

4.2.3. Upgrading Waste Management

The importance of upgrading waste management in net-zero energy building retrofits cannot be overstated, as it reduces the negative impact of waste on the environment and maximizes the use of waste resources. First, an effective waste classification and recycling system should be established to categorize waste into different categories, such as recyclable, organic, and hazardous, and to develop corresponding recycling channels. In the case of Thailand, Malaysia, and Indonesia, for example, it must be considered that the occupants can decide to set lower values to balance the outdoor overheating so that the management strategy can be chosen according to their preferences [137]. Tenants should be actively encouraged and guided to segregate waste and promote waste resource utilization. Secondly, measures should also be taken during the remodeling construction phase to reduce the generation of construction waste. For example, the range of baseline conditions and constraints imposed by heritage values in historic buildings is a crucial factor strictly intertwined with the energy (and carbon) saving potential of the measures investigated [138]. Finally, the concept of the circular economy is advocated to focus on reusing and recycling waste resources in building renovation. For example, it can be used to reprocess waste materials for building materials or compost organic waste for landscaping. This includes developing building materials from agricultural and non-agricultural wastes [139].

4.2.4. Strengthening Energy Monitoring

Most studies do not consider real-time energy-related information [140]. Strengthening energy monitoring aims to enhance energy monitoring in NZEB retrofits to achieve comprehensive monitoring and management of energy use, thereby improving buildings' energy efficiency and sustainability. First, advanced intelligent energy monitoring systems are introduced to monitor building energy consumption in real time using energy sources such as electricity, water, and gas [18]. These systems can provide real-time data and reports to help managers promptly identify energy wastage and anomalies. For instance, by leveraging advanced digital twin solutions such as DanRETwin, building owners, facility managers, consultants, and urban planners can benefit from improved energy efficiency, enhanced comfort, systematic recommissioning, data-driven decision-making, and scalable tools for evaluating retrofit options [141]. Second, each region should establish clear energy consumption targets and goals. For example, indicators such as the energy consumption intensity and energy utilization rate should be established based on the building type and

size to better measure the energy performance of buildings. On the other hand, energy efficiency analyses by Park et al. [142] show that combining photovoltaic panels, high-efficiency HVAC systems, airtight film, and LED light technology is efficient. Third, deep learning algorithms analyze energy usage data to discover energy consumption patterns and potential energy savings and identify the causes of energy waste. It has been shown that combining DL algorithms with building information modelling (BIM) technology and Internet of Things (IoT) systems enables a wide range of monitoring and sensing mechanisms within a building complex, facilitating real-time energy consumption management and indoor climate sustainability [143]. Finally, regular energy reviews and assessments are conducted to inspect and commission the building's energy systems and equipment to ensure proper operation and efficient utilization. Establishing a specialized energy management team, including energy experts, engineers, and technicians, is also necessary.

4.2.5. Establishing Complete Life Cycle Mechanisms

Net-zero energy building retrofits require an integrated consideration of all life cycle stages, from material selection to energy use and waste disposal, to achieve carbon neutrality and net-zero energy goals [144]. Multi-objective optimization models for a lifecycle cost analysis and retrofit planning can enhance decision-making by considering factors such as production, economy, and sustainability [145]. Integrating building information modeling (BIM) technology can simplify the retrofit process by providing solutions for quality control, energy analysis, costs, and life cycle assessments. First, during the design phase of the retrofit scheme, the CO_2 emission characteristics of different materials should be understood to optimize the amount of building materials used. Choosing to use local materials reduces carbon emissions during the transportation of materials. Prefabricated assembly buildings are used to improve construction efficiency and reduce raw material and energy consumption. Second, reducing energy demand and avoiding installing traditional HVAC systems are prioritized through passive designs such as internal and external sun shading, natural ventilation, and natural lighting during construction. Third, in the operation phase, energy-saving lamps and lanterns should be used to improve energy efficiency, and renewable energy sources such as solar, wind, and geothermal energy should be used to replace fossil energy sources. Energy consumption is also reduced through the automatic regulation of equipment systems. Finally, waste doors, windows, steel structures, etc., should be actively recycled and reused during the demolition and clean-up. Furthermore, Loveday et al. [146] argue that an entire life cycle mechanism should consider material and energy flows and social impacts, such as well-being and equity.

4.2.6. Providing Systemic Solutions

Creating a systematic solution is crucial. First, an in-depth understanding of energy consumption is needed. A plan to create an all-electric facility is developed to identify energy needs and plan for on-site or on-grid renewable energy to meet those needs, including electricity use, heat demand, seismic defenses, etc. Fichera et al. [147] investigated an innovative technology that simultaneously considers seismic, energy, and building retrofit in framed buildings, i.e., combining the seismic performance provided by steel trusses and the thermal performance of man-made panels, both of which are applied to the building envelope. Then, an energy consumption standard is developed for the space, the amount of electricity the space will generate every week is calculated, and a clear energy budget for achieving a net-zero energy building is created. Finally, energy systems are optimized. Efficient energy systems, such as high-efficiency split air conditioners, LED lighting, etc., are selected and an intelligent building energy management system (BEMS) is used to monitor and optimize energy use, including energy supply, energy use, energy storage, and energy scheduling. Typical designs according to different retrofit measures are also important because the solar water heater's length and the working fluid's flow rate impact the working fluid's outlet temperature and the solar water heater's overall performance. They are considered the king of cost effectiveness, while biomass boilers offer the lowest cost savings

at around 53%. One study found that photovoltaic panels (24,000 kWh/year) produced more energy than wind turbines (20,000 kWh/year) in renewable energy technologies [148]. We also emphasize a tailor-made approach for specific types. For example, university buildings seem closer to office buildings regarding their typological characteristics and usage patterns than primary and secondary school buildings [149].

4.2.7. Promoting the Use of Low-Carbon Building Materials

Promoting low-carbon building materials is one of the critical steps towards achieving the zero-carbon goal. First, one should look for building materials with environmental certifications, such as LEED, BREEAM, and other certification standards. These certifications ensure that the materials meet sustainability and environmental requirements. Second, the use of recycled building materials, such as steel and concrete, should be prioritized, which helps reduce the production of new materials and carbon emissions. Using bio-based materials in refurbishment is also a key strategy because of their low global warming potential, cost-effectiveness, and recycling potential [150]. A carbon footprint assessment should be conducted during material selection to understand different materials' life cycle carbon emissions. Third, awareness of low-carbon building materials should be raised among construction practitioners and the public. This includes organizing seminars and training courses to share the latest information on low-carbon building materials or using media and social media platforms to publicize the advantages and feasibility of low-carbon building materials. Finally, we have also established an industry chain cooperation mechanism for low-carbon building materials to promote the synergistic development of the upstream and downstream of the industry chain. The cooperation among material suppliers, architects, construction units, etc., should be strengthened to jointly promote the R&D, production, and application of low-carbon building materials.

4.2.8. Increasing Policy Support

China, the United States, and Malaysia have all adopted policy measures to promote NEZB building retrofits. The Chinese government has set targets for carbon peaking (by 2030) and carbon neutrality (by 2060). In addition, China has promoted green building certification standards, such as three-star, gold, and diamond green building standards, to encourage low-carbon, efficient building design and construction [151]. State and federal governments in the United States have adopted various policies to promote NZEB retrofits. For example, the federal infrastructure bill includes measures such as clean energy transmission grants. It has also promoted green building certification standards such as LEED (Leadership in Energy and Environmental Design) to encourage sustainable building design and operation. The Malaysian government encourages green building development and promotes sustainable buildings through green building guidelines and certification standards. It has energy efficiency codes that require builders to use energy-efficient technologies and materials. However, some policies focus only on incentives in one area, neglecting support and promotion in other areas. Even with good policies, there are deficiencies at the implementation level, resulting in ineffective policies, including lax regulation, weak enforcement, and inadequate supervision. Many policies need long-term stability and sustainability, and frequent changes or policy uncertainties make it difficult for building owners and developers to formulate long-term plans and investments. An example is optimizing government subsidy strategies for energy retrofit of building stock [152]. Therefore, we first suggest providing long-term loan interest rate concessions for net-zero energy building retrofit projects to reduce financing costs and attract more capital. Second, an incentive mechanism for net-zero energy building retrofits should be established to reward projects with outstanding performance and significant results. Third, it is worth noting that whether policy should support large-scale solar PV self-generation depends on the economic trade-off between energy savings and seasonal costs. In the case of New Zealand, for example, where local renewable electricity costs for various alternative energy sources are low, large-scale adoption of solar NZEB is not favorable [153]. Finally,

tax breaks for net-zero energy building retrofit projects, such as tax breaks for VAT and corporate income tax, should be provided to reduce the tax pressure on the projects. In northern China, Liu et al. [154] show that retrofitting heat sources and outdoor heating networks is cost-effective, while building envelope retrofitting is not, mainly due to high energy prices without government subsidies. In Ireland, where VAT on building materials and labor is currently 13.5%, only shallow retrofitting of houses is economically viable without grant incentives [155]. It has also been argued that it is impossible to estimate the number of incentives because it is not feasible to calculate the investment cost of each transformation program in each province [156]. Therefore, the policy of providing more universally applicable indicators (energy saving rate and energy savings) and more cutting-edge and accurate algorithms may be a breakthrough in solving this problem [157].

5. Conclusions

This study reviews the current state of the art in evaluating net-zero energy building (NZEB) retrofits by combining bibliometric and systematic review methods. It is found that current evaluation methods are dominated by models of energy efficiency (using different software such as DesignBuilder, PVsyst, EnergyPlus, etc.). In contrast, other methods, such as multi-attribute decision-making methods (e.g., DEMATEL-AHP/ANP-VIKOR), also play an essential role. The main evaluation metrics used cover economic benefits (e.g., NPV, dynamic payback period, and total operating costs), energy consumption (e.g., electricity consumption and generation), environmental impacts (e.g., carbon emission reduction), and comfort (e.g., thermal comfort and indoor comfort). However, the NZEB retrofit faces several challenges, including technical, economic, social, and policy challenges:

(1) Technical challenges—Restrictions are more prevalent in existing buildings than new ones. Retrofitting existing buildings to meet near-zero energy building (NZEB) standards requires overcoming technical barriers related to energy efficiency measures, renewable energy integration, and the optimization of building systems. The main issues include imperfections in the appearance of solar cells and interfacial mechanisms in the transmission layer, the susceptibility of air source heat pumps to failure in cold climates, and module breakage and performance degradation of photovoltaic (PV) systems.

(2) Economic challenges—High initial construction costs, long payback periods, poor financing mechanisms, and dynamic tariffs that affect the accuracy of cost measurements are significant barriers. Assessing the economic viability of retrofit projects involves analyzing factors such as a discounted payback period, internal rate of return, and total return on investment. This is because of the significant upfront investment costs required to implement energy efficiency measures, renewable energy technologies, and building system optimization. Such initial costs create financial barriers to retrofit projects, and feasibility often depends on the ability to recoup these investments through energy savings over time. Balancing the costs and benefits of zero-energy building retrofits in the face of uncertainty and variability in project costs is the challenge to be addressed.

(3) Cultural challenges—Insufficient public awareness of NZEB, lack of relevant data and information platforms, and insufficient communication and trust among stakeholders have hindered the advancement of NZEB retrofits. Furthermore, balancing energy performance and heritage preservation when retrofitting heritage buildings is crucial. Retrofitting heritage buildings to near-zero energy standards requires a careful consideration of preserving cultural values while improving energy efficiency, which can create conflicting priorities and challenges. In other words, combining high energy performance and renewable energy with heritage buildings poses a dilemma for retrofit practices due to the need to maintain architectural integrity and cultural significance.

(4) Policy challenges—Inadequate policy support, such as the localization of standards and requirements, lack of incentives, and delays in the approval process, have signif-

icantly affected the implementation of NZEB retrofits. Good policy change should support energy retrofit projects and empower local authorities to scale up retrofit programs across the region, often including challenges to the retail energy market and empowering local authorities and their partners. Current policies in most areas do not create opportunities for households vulnerable to energy poverty to access low-cost or free retrofit options.

In the future, net-zero energy building retrofits must be improved and developed in the following directions. First, at the technological level, research and application of new technologies, such as digital twins and cutting-edge algorithms (including the Go-Explore algorithm and the Transform reinforcement learning algorithm), should be strengthened to improve energy modeling accuracy and system operation stability. Second, better financing mechanisms and incentive policies (e.g., green credit, green bonds, government subsidy and incentive programs, and energy service company (ESCO) models) should be established at the economic level to promote investor motivation. A standardized sustainable building value assessment system should be developed. In addition, at the social level, there is a need to strengthen public education and publicity to increase awareness and understanding of NZEB and establish a comprehensive data and information platform to promote communication and cooperation among stakeholders. The data platform collects data on building energy consumption, material use, and the indoor environment and integrates data from different sources, including sensors, monitoring systems, and building management software. Finally, at the policy level, countries should introduce and improve regulations and standards related to net-zero energy buildings as soon as possible and provide policy incentives, such as subsidies and tax incentives, to promote the full implementation of NZEB retrofits. Regional climates should prepare the specification, clearly defining and identifying assessment criteria and performance indicators, such as green building certification standards, energy efficiency, and indoor air quality.

Although this study contributes to the body of knowledge in the field, there are some limitations. Firstly, the articles included in this study were mainly sourced from the Web of Science and Scopus databases, which may not cover all current research. Future reviews could expand the range of databases, including, but not limited to, well-known databases such as China Knowledge (CNKI) and IEEE Xplore.

Author Contributions: Conceptualization, Q.X. and Y.J.; methodology, Q.X. and Y.J.; software, Q.X. and Y.J.; validation, A.H.A., N.A.H., T.H.L. and N.A.B.; formal analysis, Q.X. and Y.J.; investigation, Q.X. and Y.J.; resources, Q.X. and Y.J.; data curation, Q.X. and Y.J.; writing—original draft preparation, Q.X. and Y.J.; writing—review and editing, Q.X. and Y.J.; visualization, Q.X. and Y.J.; supervision, A.H.A., N.A.H., T.H.L. and N.A.B.; project administration, Q.X. and Y.J. All authors have read and agreed to the published version of the manuscript.

Funding: This research received no external funding.

Data Availability Statement: Data are contained within the article.

Acknowledgments: The authors thank all the anonymous reviewers and editors for their honest advice on this paper.

Conflicts of Interest: The authors declare no conflicts of interest.

References

1. Lin, Y.; Zhong, S.; Yang, W.; Hao, X.; Li, C.-Q. Towards Zero-Energy Buildings in China: A Systematic Literature Review. *J. Clean. Prod.* **2020**, *276*, 123297. [CrossRef]
2. Jaysawal, R.K.; Chakraborty, S.; Elangovan, D.; Padmanaban, S. Concept of Net Zero Energy Buildings (NZEB)—A Literature Review. *Clean. Eng. Technol.* **2022**, *11*, 100582. [CrossRef]
3. Sartori, I.; Napolitano, A.; Voss, K. Net Zero Energy Buildings: A Consistent Definition Framework. *Energy Build.* **2012**, *48*, 220–232. [CrossRef]
4. Ahmed, A.; Ge, T.; Peng, J.; Yan, W.-C.; Tee, B.T.; You, S. Assessment of the Renewable Energy Generation towards Net-Zero Energy Buildings: A Review. *Energy Build.* **2022**, *256*, 111755. [CrossRef]

5. Wu, W.; Skye, H.M. Residential Net-Zero Energy Buildings: Review and Perspective. *Renew. Sustain. Energy Rev.* **2021**, *142*, 110859. [CrossRef]
6. Yang, X.; Zhang, S.; Xu, W. Impact of Zero Energy Buildings on Medium-To-Long Term Building Energy Consumption in China. *Energy Policy* **2019**, *129*, 574–586. [CrossRef]
7. Ferreira, M.; Almeida, M.; Rodrigues, A.; Silva, S.M. Comparing Cost-Optimal and Net-Zero Energy Targets in Building Retrofit. *Build. Res. Inf.* **2014**, *44*, 188–201. [CrossRef]
8. Sustainable Energy Development Authority of Malaysia (SEDA). Zero Energy Building (ZEB) Facilitation Program. Available online: https://www.seda.gov.my/energy-demand-management-edm/zeb-renovation-for-existing-buildings/ (accessed on 4 July 2024).
9. Faculty of Engineering UPM. [Montage Video] Rooftop Solar PV UPM Project. Available online: https://www.youtube.com/watch?v=ywGuW4l7wAI (accessed on 4 July 2024).
10. Juferi, N.E. UPM-TNB-GSPARX Sdn. Bhd. Collaborate on Rooftop Solar Photovoltaic Project. Available online: https://cirnet.upm.edu.my/berita/upm_tnb_gsparx_sdn_bhd_jalin_kerjasama_bagi_projek_rooftop_solar_photovoltaic-65196 (accessed on 4 July 2024).
11. Faculty of Engineering UPM. UPM'S Energy Transition Initiative. Available online: https://eng.upm.edu.my/upload/dokumen/20240119090250Floating_Solar_and_Walkway_compressed.pdf (accessed on 4 July 2024).
12. Wells, L.; Rismanchi, B.; Aye, L. A Review of Net Zero Energy Buildings with Reflections on the Australian Context. *Energy Build.* **2018**, *158*, 616–628. [CrossRef]
13. Satola, D.; Wiberg, A.H.; Singh, M.; Babu, S.; James, B.; Dixit, M.; Sharston, R.; Grynberg, Y.; Gustavsen, A. Comparative Review of International Approaches to Net-Zero Buildings: Knowledge-Sharing Initiative to Develop Design Strategies for Greenhouse Gas Emissions Reduction. *Energy Sustain. Dev.* **2022**, *71*, 291–306. [CrossRef]
14. Christopher, S.; Vikram, M.P.; Bakli, C.; Thakur, A.K.; Ma, Y.; Ma, Z.; Xu, H.; Cuce, P.M.; Cuce, E.; Singh, P. Renewable Energy Potential towards Attainment of Net-Zero Energy Buildings Status—A Critical Review. *J. Clean. Prod.* **2023**, *405*, 136942. [CrossRef]
15. Brown, D.; Tokede, O.; Li, H.X.; Edwards, D. A Systematic Review of Barriers to Implementing Net Zero Energy Buildings in Australia. *J. Clean. Prod.* **2024**, *467*, 142910. [CrossRef]
16. Li, Y.; Arulnathan, V.; Heidari, M.D.; Pelletier, N. Design Considerations for Net Zero Energy Buildings for Intensive, Confined Poultry Production: A Review of Current Insights, Knowledge Gaps, and Future Directions. *Renew. Sustain. Energy Rev.* **2022**, *154*, 111874. [CrossRef]
17. Falana, J.; Osei-Kyei, R.; Tam, V.W. Towards Achieving a Net Zero Carbon Building: A Review of Key Stakeholders and Their Roles in Net Zero Carbon Building Whole Life Cycle. *J. Build. Eng.* **2023**, *82*, 108223. [CrossRef]
18. Noh, Y.; Jafarinejad, S.; Anand, P. A Review on Harnessing Renewable Energy Synergies for Achieving Urban Net-Zero Energy Buildings: Technologies, Performance Evaluation, Policies, Challenges, and Future Direction. *Sustainability* **2024**, *16*, 3444. [CrossRef]
19. Kong, J.; Dong, Y.; Poshnath, A.; Rismanchi, B.; Yap, P.-S. Application of Building Integrated Photovoltaic (BIPV) in Net-Zero Energy Buildings (NZEBs). *Energies* **2023**, *16*, 6401. [CrossRef]
20. Li, Y.; Mao, Y.; Wang, W.; Wu, N. Net-Zero Energy Consumption Building in China: An Overview of Building-Integrated Photovoltaic Case and Initiative toward Sustainable Future Development. *Buildings* **2023**, *13*, 2024. [CrossRef]
21. Welch, V.; Petticrew, M.; Petkovic, J.; Moher, D.; Waters, E.; White, H.; Tugwell, P.; the PRISMA-Equity Bellagio Group. Extending the PRISMA Statement to Equity-Focused Systematic Reviews (PRISMA-E 2012): Explanation and Elaboration. *J. Dev. Eff.* **2016**, *8*, 287–324. [CrossRef]
22. Hutton, B.; Catalá-López, F.; Moher, D. The PRISMA Statement Extension for Systematic Reviews Incorporating Network Meta-Analysis: PRISMA-NMA. *Med. ClíNica* **2016**, *147*, 262–266. [CrossRef]
23. Moher, D.; Liberati, A.; Tetzlaff, J.; Altman, D.G. Preferred Reporting Items for Systematic Reviews and Meta-Analyses: The PRISMA Statement. *PLoS Med.* **2009**, *6*, e1000097. [CrossRef]
24. Junjia, Y.; Alias, A.H.; Haron, N.A.; Bakar, N.A. A Bibliometric Review on Safety Risk Assessment of Construction Based on CiteSpace Software and WoS Database. *Sustainability* **2023**, *15*, 11803. [CrossRef]
25. Junjia, Y.; Alias, A.H.; Haron, N.A.; Abu Bakar, N. A Bibliometrics-Based Systematic Review of Safety Risk Assessment for IBS Hoisting Construction. *Buildings* **2023**, *13*, 1853. [CrossRef]
26. Bjelland, D.; Brozovsky, J.; Hrynyszyn, B.D. Systematic Review: Upscaling Energy Retrofitting to the Multi-Building Level. *Renew. Sustain. Energy Rev.* **2024**, *198*, 114402. [CrossRef]
27. Paul, J.; Jacob, J.; Pandey, A.K.; Vaka, M.; Samykano, M.; Kadirgama, K.; Abd Rahim, N.; Selvaraj, J. Meta Data Analysis on Building Thermal Management Using Phase Change Materials. *J. Energy Storage* **2024**, *76*, 109760. [CrossRef]
28. Cabeza, L.F.; Chàfer, M. Technological Options and Strategies towards Zero Energy Buildings Contributing to Climate Change Mitigation: A Systematic Review. *Energy Build.* **2020**, *219*, 110009. [CrossRef]
29. Dahiya, D.; Laishram, B. Life Cycle Energy Analysis of Buildings: A Systematic Review. *Build. Environ.* **2024**, *252*, 111160. [CrossRef]
30. Gonçalves, M.; Figueiredo, A.; Almeida, R.M.S.F.; Vicente, R. Dynamic Façades in Buildings: A Systematic Review across Thermal Comfort, Energy Efficiency and Daylight Performance. *Renew. Sustain. Energy Rev.* **2024**, *199*, 114474. [CrossRef]

31. Hawks, M.A.; Cho, S. Review and Analysis of Current Solutions and Trends for Zero Energy Building (ZEB) Thermal Systems. *Renew. Sustain. Energy Rev.* **2024**, *189*, 114028. [CrossRef]
32. Kang, Y.; Xu, W.; Wu, J.; Li, H.; Liu, R.; Lu, S.; Rong, X.; Xu, X.; Pang, F. Study on Comprehensive Whole Life Carbon Emission Reduction Potential and Economic Feasibility Impact Based on Progressive Energy-Saving Targets: A Typical Renovated Ultra-Low Energy Office. *J. Build. Eng.* **2022**, *58*, 105029. [CrossRef]
33. Wu, Z.; Jin, Y.; Huang, L.; Zhang, N.; Luo, X.; Wang, X. Appraisal of Indoor Environment Quality (IEQ) in Nearly Zero Energy Building (NZEB): A Literature Review. *Sci. Technol. Built Environ.* **2023**, *29*, 251–267. [CrossRef]
34. Chung-Camargo, K.; González, J.; Austin, M.C.; Carpino, C.; Mora, D.; Arcuri, N. Advances in Retrofitting Strategies for Energy Efficiency in Tropical Climates: A Systematic Review and Analysis. *Buildings* **2024**, *14*, 1633. [CrossRef]
35. Antonakis, J.; Bastardoz, N.; Liu, Y.; Schriesheim, C.A. What Makes Articles Highly Cited? *Leadersh. Q.* **2014**, *25*, 152–179. [CrossRef]
36. Aksnes, D.W. Characteristics of Highly Cited Papers. *Res. Eval.* **2003**, *12*, 159–170. [CrossRef]
37. Zhao, L.; Zhang, H.; Wang, Q.; Wang, H. Digital-Twin-Based Evaluation of Nearly Zero-Energy Building for Existing Buildings Based on Scan-To-BIM. *Adv. Civ. Eng.* **2021**, *2021*, 6638897. [CrossRef]
38. Hong, X.; Shi, F.; Wang, S.; Yang, X.; Yang, Y. Multi-Objective Optimization of Thermochromic Glazing Based on Daylight and Energy Performance Evaluation. *Build. Simul.* **2021**, *14*, 1685–1695. [CrossRef]
39. Opher, T.; Duhamel, M.; Posen, I.D.; Panesar, D.K.; Brugmann, R.; Roy, A.; Zizzo, R.; Sequeira, L.; Anvari, A.; MacLean, H.L. Life Cycle GHG Assessment of a Building Restoration: Case Study of a Heritage Industrial Building in Toronto, Canada. *J. Clean. Prod.* **2021**, *279*, 123819. [CrossRef]
40. Figueroa-Lopez, A.; Arias, A.; Oregi, X.; Rodríguez, I. Evaluation of Passive Strategies, Natural Ventilation and Shading Systems, to Reduce Overheating Risk in a Passive House Tower in the North of Spain during the Warm Season. *J. Build. Eng.* **2021**, *43*, 102607. [CrossRef]
41. Hong, Y.; Ezeh, C.I.; Deng, W.; Hong, S.-H.; Peng, Z.; Tang, Y. Correlation between Building Characteristics and Associated Energy Consumption: Prototyping Low-Rise Office Buildings in Shanghai. *Energy Build.* **2020**, *217*, 109959. [CrossRef]
42. Rabani, M.; Madessa, H.B.; Ljungström, M.; Aamodt, L.; Løvvold, S.; Nord, N. Life Cycle Analysis of GHG Emissions from the Building Retrofitting: The Case of a Norwegian Office Building. *Build. Environ.* **2021**, *204*, 108159. [CrossRef]
43. Albatayneh, A.; Jaradat, M.; AlKhatib, M.B.; Abdallah, R.; Juaidi, A.; Manzano-Agugliaro, F. The Significance of the Adaptive Thermal Comfort Practice over the Structure Retrofits to Sustain Indoor Thermal Comfort. *Energies* **2021**, *14*, 2946. [CrossRef]
44. Mitchell, R.; Natarajan, S. UK Passivhaus and the Energy Performance Gap. *Energy Build.* **2020**, *224*, 110240. [CrossRef]
45. Colclough, S.; Hegarty, R.O.; Murray, M.; Lennon, D.; Rieux, E.; Colclough, M.; Kinnane, O. Post Occupancy Evaluation of 12 Retrofit NZEB Dwellings the Impact of High In-Use Interior Temperatures on the Predictive Accuracy of the NZEB Energy Standard. *Energy Build.* **2021**, *254*, 111563. [CrossRef]
46. Apostolopoulos, V.; Giourka, P.; Martinopoulos, G.; Angelakoglou, K.; Kourtzanidis, K.; Nikolopoulos, N. Smart Readiness Indicator Evaluation and Cost Estimation of Smart Retrofitting Scenarios—A Comparative Case-Study in European Residential Buildings. *Sustain. Cities Soc.* **2022**, *82*, 103921. [CrossRef]
47. Radhakrishnan, S.; Erbis, S.; Isaacs, J.A.; Kamarthi, S. Novel Keyword Co-Occurrence Network-Based Methods to Foster Systematic Reviews of Scientific Literature. *PLoS ONE* **2017**, *12*, e0172778. [CrossRef]
48. Yuan, C.; Li, G.; Kamarthi, S.; Jin, X.; Moghaddam, M. Trends in Intelligent Manufacturing Research: A Keyword Co-Occurrence Network Based Review. *J. Intell. Manuf.* **2022**, *33*, 425–439. [CrossRef]
49. Brusco, M.; Steinley, D.; Watts, A.L. A Comparison of Spectral Clustering and the Walktrap Algorithm for Community Detection in Network Psychometrics. *Psychol. Methods* **2022**, *ahead of print*. [CrossRef] [PubMed]
50. Toth, C.; Helic, D.; Geiger, B.C. Synwalk: Community Detection via Random Walk Modelling. *Data Min. Knowl. Discov.* **2022**, *36*, 739–780. [CrossRef]
51. Grames, E.M.; Stillman, A.N.; Tingley, M.W.; Elphick, C.S. An Automated Approach to Identifying Search Terms for Systematic Reviews Using Keyword Co-Occurrence Networks. *Methods Ecol. Evol.* **2019**, *10*, 1645–1654. [CrossRef]
52. Bornmann, L.; Haunschild, R.; Hug, S.E. Visualizing the Context of Citations Referencing Papers Published by Eugene Garfield: A New Type of Keyword Co-Occurrence Analysis. *Scientometrics* **2017**, *114*, 427–437. [CrossRef] [PubMed]
53. Senturk, A.; Ozcan, M. Nearly Zero Energy Building Design and Optimization: A Residential Building Transformation in Türkiye. *Energy Explor. Exploit.* **2023**, *42*, 997–1026. [CrossRef]
54. Wang, C.; Zhang, X.; Chen, W.; Jiang, F.; Zhao, X. Multivariate Evaluation of Photovoltaic Utilization Potential of Primary and Secondary School Buildings: A Case Study in Hainan Province, China. *Buildings* **2024**, *14*, 810. [CrossRef]
55. Kang, Z.; Wang, Y.; Wang, T.; Yin, N.; Xu, Z. Research on Ultra-Low Energy Consumption Renovation of Teaching Buildings in Severe Cold Areas under EPC Mode. *E3S Web Conf.* **2024**, *490*, 02004. [CrossRef]
56. Chen, J.; Lu, L.; Jia, L.; Gong, Q. Performance Evaluation of High-Rise Buildings Integrated with Colored Radiative Cooling Walls in a Hot and Humid Region. *Sustainability* **2023**, *15*, 12607. [CrossRef]
57. Han, T.; Liu, P.; Niu, C.; Li, Q. Evaluation of Energy-Saving Retrofit Projects of Existing Rural Residential Envelope Structures from the Perspective of Rural Residents: The Chinese Case. *Environ. Dev. Sustain.* **2022**, *25*, 8419–8446. [CrossRef] [PubMed]
58. Radomski, B.; Mróz, T. Application of the Hybrid MCDM Method for Energy Modernisation of an Existing Public Building—A Case Study. *Energies* **2023**, *16*, 3475. [CrossRef]

59. Campamà Pizarro, R.; Bernardo, R.; Wall, M. Streamlining Building Energy Modelling Using Open Access Databases—A Methodology towards Decarbonisation of Residential Buildings in Sweden. *Sustainability* **2023**, *15*, 3887. [CrossRef]
60. Nutakki, T.U.K.; Kazim, W.U.; Alamara, K.; Salameh, T.; Abdelkareem, M.A. Experimental Investigation on Aging and Energy Savings Evaluation of High Solar Reflective Index (SRI) Paints: A Case Study on Residential Households in the GCC Region. *Buildings* **2023**, *13*, 419. [CrossRef]
61. Wang, R.; Feng, W.; Wang, L.; Lu, S. A Comprehensive Evaluation of Zero Energy Buildings in Cold Regions: Actual Performance and Key Technologies of Cases from China, the US, and the European Union. *Energy* **2021**, *215*, 118992. [CrossRef]
62. Kuwahara, R.; Kim, H.; Sato, H. Evaluation of Zero-Energy Building and Use of Renewable Energy in Renovated Buildings: A Case Study in Japan. *Buildings* **2022**, *12*, 561. [CrossRef]
63. Krarti, M.; Ihm, P. Evaluation of Net-Zero Energy Residential Buildings in the MENA Region. *Sustain. Cities Soc.* **2016**, *22*, 116–125. [CrossRef]
64. Rodriguez-Ubinas, E.; Rodriguez, S.; Voss, K.; Todorovic, M.S. Energy Efficiency Evaluation of Zero Energy Houses. *Energy Build.* **2014**, *83*, 23–35. [CrossRef]
65. Li, H.; Li, Y.; Wang, Z.; Shao, S.; Deng, G.; Xue, H.; Xu, Z.; Yang, Y. Integrated Building Envelope Performance Evaluation Method towards Nearly Zero Energy Buildings Based on Operation Data. *Energy Build.* **2022**, *268*, 112219. [CrossRef]
66. Lin, B.; Chen, Z. Net Zero Energy Building Evaluation, Validation and Reflection—A Successful Project Application. *Energy Build.* **2022**, *261*, 111946. [CrossRef]
67. Li, X.; Lin, A.; Young, C.-H.; Dai, Y.; Wang, C.-H. Energetic and Economic Evaluation of Hybrid Solar Energy Systems in a Residential Net-Zero Energy Building. *Appl. Energy* **2019**, *254*, 113709. [CrossRef]
68. Sun, Y.; Huang, G.; Xu, X.; Lai, A.C.-K. Building-Group-Level Performance Evaluations of Net Zero Energy Buildings with Non-Collaborative Controls. *Appl. Energy* **2018**, *212*, 565–576. [CrossRef]
69. Shin, M.; Baltazar, J.-C.; Haberl, J.S.; Frazier, E.; Lynn, B. Evaluation of the Energy Performance of a Net Zero Energy Building in a Hot and Humid Climate. *Energy Build.* **2019**, *204*, 109531. [CrossRef]
70. Abdul-Zahra, A.S.; Al Jubori, A.M. Potential Evaluation and Analysis of Near-To-Net Zero Energy Building in Hot and Dry Climate. *Energy Convers. Manag. X* **2021**, *12*, 100146. [CrossRef]
71. Kampelis, N.; Gobakis, K.; Vagias, V.; Kolokotsa, D.; Standardi, L.; Isidori, D.; Cristalli, C.; Montagnino, F.M.; Paredes, F.; Muratore, P.; et al. Evaluation of the Performance Gap in Industrial, Residential & Tertiary Near-Zero Energy Buildings. *Energy Build.* **2017**, *148*, 58–73. [CrossRef]
72. Pernetti, R.; Garzia, F.; Filippi Oberegger, U. Sensitivity Analysis as Support for Reliable Life Cycle Cost Evaluation Applied to Eleven Nearly Zero-Energy Buildings in Europe. *Sustain. Cities Soc.* **2021**, *74*, 103139. [CrossRef]
73. Yi, H.; Srinivasan, R.S.; Braham, W.W.; Tilley, D.R. An Ecological Understanding of Net-Zero Energy Building: Evaluation of Sustainability Based on Emergy Theory. *J. Clean. Prod.* **2017**, *143*, 654–671. [CrossRef]
74. Arif, S.; Taweekun, J.; Ali, H.M.; Theppaya, T. Techno Economic Evaluation and Feasibility Analysis of a Hybrid Net Zero Energy Building in Pakistan: A Case Study of Hospital. *Front. Energy Res.* **2021**, *9*, 668908. [CrossRef]
75. Bruno, R.; Bevilacqua, P.; Cuconati, T.; Arcuri, N. Energy Evaluations of an Innovative Multi-Storey Wooden near Zero Energy Building Designed for Mediterranean Areas. *Appl. Energy* **2019**, *238*, 929–941. [CrossRef]
76. Chen, S.; Zhao, L.; Zheng, L.; Bi, G. A Rapid Evaluation Method for Design Strategies of High-Rise Office Buildings Achieving Nearly Zero Energy in Guangzhou. *J. Build. Eng.* **2021**, *44*, 103297. [CrossRef]
77. Liu, C.; Xu, W.; Li, A.; Sun, D.; Huo, H. Energy Balance Evaluation and Optimization of Photovoltaic Systems for Zero Energy Residential Buildings in Different Climate Zones of China. *J. Clean. Prod.* **2019**, *235*, 1202–1215. [CrossRef]
78. Lee, S.; Park, S. A Study on Economic Evaluation of Design Elements of Zero-Energy Buildings according to Energy Consumption and Production. *Appl. Sci.* **2023**, *13*, 7309. [CrossRef]
79. Dell'Anna, F.; Bottero, M.; Becchio, C.; Corgnati, S.P.; Mondini, G. Designing a Decision Support System to Evaluate the Environmental and Extra-Economic Performances of a Nearly Zero-Energy Building. *Smart Sustain. Built Environ.* **2020**, *9*, 413–442. [CrossRef]
80. Zavadskas, E.K.; Antucheviciene, J.; Kalibatas, D.; Kalibatiene, D. Achieving Nearly Zero-Energy Buildings by Applying Multi-Attribute Assessment. *Energy Build.* **2017**, *143*, 162–172. [CrossRef]
81. Tamašauskas, R.; Šadauskienė, J.; Bruzgevičius, P.; Krawczyk, D.A. Investigation and Evaluation of Primary Energy from Wind Turbines for a Nearly Zero Energy Building (NZEB). *Energies* **2019**, *12*, 2145. [CrossRef]
82. Huo, H.; Xu, W.; Li, A.; Wu, J.; Guo, J. A Simple Evaluation Method of External Venetian Blind Shading Performance for Nearly Zero Energy Buildings. *Renew. Energy* **2023**, *218*, 119260. [CrossRef]
83. Oliveira Panão, M.J.N. The Overall Renewable Energy Fraction: An Alternative Performance Indicator for Evaluating Net Zero Energy Buildings. *Energy Build.* **2016**, *127*, 736–747. [CrossRef]
84. Marino, C.; Nucara, A.; Panzera, M.F.; Pietrafesa, M. Towards the Nearly Zero and the plus Energy Building: Primary Energy Balances and Economic Evaluations. *Therm. Sci. Eng. Prog.* **2019**, *13*, 100400. [CrossRef]
85. Nagaoka, A.; Ota, Y.; Sakai, K.; Araki, K.; Matsuo, H.; Kadota, N.; Maeda, K.; Nakajima, A.; Nishioka, K. Performance Evaluation and Spectrum-Based Analysis of a Wall-Mounted Photovoltaic System for Zero-Energy Building. *Renew. Energy* **2021**, *174*, 147–156. [CrossRef]

86. Ascione, F.; Borrelli, M.; De Masi, R.F.; Vanoli, G.P. Hourly Operational Assessment of HVAC Systems in Mediterranean Nearly Zero-Energy Buildings: Experimental Evaluation of the Potential of Ground Cooling of Ventilation Air. *Renew. Energy* **2020**, *155*, 950–968. [CrossRef]
87. Amaripadath, D.; Velickovic, M.; Attia, S. Performance Evaluation of a Nearly Zero-Energy Office Building in Temperate Oceanic Climate Based on Field Measurements. *Energies* **2022**, *15*, 6755. [CrossRef]
88. Jiang, K.; Li, H.; Ye, X.; Lei, Y.; Lao, K.-W.; Zhang, S.; Hu, X. Energy Efficiency Evaluation and Revenue Distribution of DC Power Distribution Systems in Nearly Zero Energy Buildings. *Energies* **2022**, *15*, 5726. [CrossRef]
89. Zhang, Y.; Lu, Y.; Wang, C.; Huang, Z.; Lv, T. Reward–Penalty Mechanism Based on Daily Energy Consumption for Net-Zero Energy Buildings. *Sustainability* **2021**, *13*, 12838. [CrossRef]
90. Jin, B.; Bae, Y. Prospective Research Trend Analysis on Zero-Energy Building (ZEB): An Artificial Intelligence Approach. *Sustainability* **2023**, *15*, 13577. [CrossRef]
91. Khakian, R.; Karimimoshaver, M.; Aram, F.; Zoroufchi Benis, S.; Mosavi, A.; Varkonyi-Koczy, A.R. Modeling Nearly Zero Energy Buildings for Sustainable Development in Rural Areas. *Energies* **2020**, *13*, 2593. [CrossRef]
92. Wang, Y.; Yang, X.; Hou, Q.; Tao, J.; Dong, J. Quantitative Study on the Life-Cycle Carbon Emissions of a Nearly Zero Energy Building in the Severe Cold Zones of China. *Sustainability* **2022**, *14*, 1448. [CrossRef]
93. Famiglietti, J.; Aprile, M.; Spirito, G.; Motta, M. Net-Zero Climate Emissions Districts: Potentials and Constraints for Social Housing in Milan. *Energies* **2023**, *16*, 1504. [CrossRef]
94. Gaeta, M.; Nsangwe Businge, C.; Gelmini, A. Achieving Net Zero Emissions in Italy by 2050: Challenges and Opportunities. *Energies* **2021**, *15*, 46. [CrossRef]
95. Basher, M.K.; Nur-E-Alam, M.; Rahman, M.M.; Alameh, K.; Hinckley, S. Aesthetically Appealing Building Integrated Photovoltaic Systems for Net-Zero Energy Buildings. Current Status, Challenges, and Future Developments—A Review. *Buildings* **2023**, *13*, 863. [CrossRef]
96. D'Agostino, D.; Mele, L.; Minichiello, F.; Renno, C. The Use of Ground Source Heat Pump to Achieve a Net Zero Energy Building. *Energies* **2020**, *13*, 3450. [CrossRef]
97. Attia, S. Spatial and Behavioral Thermal Adaptation in Net Zero Energy Buildings: An Exploratory Investigation. *Sustainability* **2020**, *12*, 7961. [CrossRef]
98. Hong, J.; Park, J.; Kim, S.; Lim, C.; Kong, M. Energy Analysis of a Net-Zero Energy Building Based on Long-Term Measured Data: A Case Study in South Korea. *Buildings* **2023**, *13*, 3134. [CrossRef]
99. Tirelli, D.; Besana, D. Moving toward Net Zero Carbon Buildings to Face Global Warming: A Narrative Review. *Buildings* **2023**, *13*, 684. [CrossRef]
100. Hirvonen, J.; Kosonen, R. Waste Incineration Heat and Seasonal Thermal Energy Storage for Promoting Economically Optimal Net-Zero Energy Districts in Finland. *Buildings* **2020**, *10*, 205. [CrossRef]
101. Lu, Y.; Alghassab, M.; Alvarez-Alvarado, M.S.; Gunduz, H.; Khan, Z.A.; Imran, M. Optimal Distribution of Renewable Energy Systems Considering Aging and Long-Term Weather Effect in Net-Zero Energy Building Design. *Sustainability* **2020**, *12*, 5570. [CrossRef]
102. Lou, H.-L.; Hsieh, S.-H. Towards Zero: A Review on Strategies in Achieving Net-Zero-Energy and Net-Zero-Carbon Buildings. *Sustainability* **2024**, *16*, 4735. [CrossRef]
103. Shen, K.; Ding, L.; Wang, C.C. Development of a Framework to Support Whole-Life-Cycle Net-Zero-Carbon Buildings through Integration of Building Information Modelling and Digital Twins. *Buildings* **2022**, *12*, 1747. [CrossRef]
104. Tuyet, T.; Delinchant, B.; Phan, A.T.; Bui, V.C.; Nguyen, D.-Q. A Practical Approach to Launch the Low-Cost Monitoring Platforms for Nearly Net-Zero Energy Buildings in Vietnam. *Energies* **2022**, *15*, 4924. [CrossRef]
105. Lim, H.-W.; Kim, J.-H.; Lee, H.-S.; Shin, U.-C. Case Study of Load Matching and Energy Cost for Net-Zero Energy Houses in Korea. *Energies* **2021**, *14*, 6407. [CrossRef]
106. Lv, T.; Lu, Y.; Zhou, Y.; Liu, X.; Wang, C.; Zhang, Y.; Huang, Z.; Sun, Y. Optimal Control of Energy Systems in Net-Zero Energy Buildings Considering Dynamic Costs: A Case Study of Zero Carbon Building in Hong Kong. *Sustainability* **2022**, *14*, 3136. [CrossRef]
107. Mohammed, B.U.; Wiysahnyuy, Y.S.; Ashraf, N.; Mempouo, B.; Mengata, G.M. Pathways for Efficient Transition into Net Zero Energy Buildings (NZEB) in Sub-Sahara Africa. Case Study: Cameroon, Senegal, and Côte D'Ivoire. *Energy Build.* **2023**, *296*, 113422. [CrossRef]
108. Szymańska, E.J.; Kubacka, M.; Woźniak, J.; Polaszczyk, J. Analysis of Residential Buildings in Poland for Potential Energy Renovation toward Zero-Emission Construction. *Energies* **2022**, *15*, 9327. [CrossRef]
109. Kotarela, F.; Kyritsis, A.; Papanikolaou, N. On the Implementation of the Nearly Zero Energy Building Concept for Jointly Acting Renewables Self-Consumers in Mediterranean Climate Conditions. *Energies* **2020**, *13*, 1032. [CrossRef]
110. Richter, M.; Lombardi, P.; Arendarski, B.; Naumann, A.; Hoepfner, A.; Komarnicki, P.; Pantaleo, A. A Vision for Energy Decarbonization: Planning Sustainable Tertiary Sites as Net-Zero Energy Systems. *Energies* **2021**, *14*, 5577. [CrossRef]
111. Hamzah, A.H.; Go, Y.I. Design and Assessment of Building Integrated PV (BIPV) System towards Net Zero Energy Building for Tropical Climate. *E-Prime—Adv. Electr. Eng. Electron. Energy* **2023**, *3*, 100105. [CrossRef]
112. Moghaddasi, H.; Culp, C.; Vanegas, J. Net Zero Energy Communities: Integrated Power System, Building and Transport Sectors. *Energies* **2021**, *14*, 7065. [CrossRef]

113. Kim, D.; Cho, H.; Mago, P.J.; Yoon, J.; Lee, H. Impact on Renewable Design Requirements of Net-Zero Carbon Buildings under Potential Future Climate Scenarios. *Climate* **2021**, *9*, 17. [CrossRef]
114. Alghamdi, H.; Meza, A. A Novel Strategy for Converting Conventional Structures into Net-Zero-Energy Buildings without Destruction. *Sustainability* **2023**, *15*, 11229. [CrossRef]
115. Souza, R.; Lima, J.; Giovani, E.; Sampaio, R.R.; Nascimento, S.; Saba, H. Renewable Energy Generation Technologies for Decarbonizing Urban Vertical Buildings: A Path towards Net Zero. *Sustainability* **2023**, *15*, 13030. [CrossRef]
116. Li, Y.; Feng, H. GIS for the Potential Application of Renewable Energy in Buildings towards Net Zero: A Perspective. *Buildings* **2023**, *13*, 1205. [CrossRef]
117. Makvandia, G.; Safiuddin, M. Obstacles to Developing Net-Zero Energy (NZE) Homes in Greater Toronto Area. *Buildings* **2021**, *11*, 95. [CrossRef]
118. Komninos, N. Net Zero Energy Districts: Connected Intelligence for Carbon-Neutral Cities. *Land* **2022**, *11*, 210. [CrossRef]
119. Isaac, S.; Shubin, S.; Rabinowitz, G. Cost-Optimal Net Zero Energy Communities. *Sustainability* **2020**, *12*, 2432. [CrossRef]
120. Alam, S.; Airaksinen, M.; Lahdelma, R. Attitudes and Approaches of Finnish Retrofit Industry Stakeholders toward Achieving Nearly Zero-Energy Buildings. *Sustainability* **2021**, *13*, 7359. [CrossRef]
121. Wang, S.; Tae, S.; Jang, H. Prediction of the Energy Self-Sufficiency Rate of Major New Renewable Energy Types Based on Zero-Energy Building Certification Cases in South Korea. *Sustainability* **2021**, *13*, 11552. [CrossRef]
122. Mancò, G.; Guelpa, E.; Colangelo, A.; Virtuani, A.; Morbiato, T.; Verda, V. Innovative Renewable Technology Integration for Nearly Zero-Energy Buildings within the Re-COGNITION Project. *Sustainability* **2021**, *13*, 1938. [CrossRef]
123. Wei, J.; Li, J.; Zhao, J.; Wang, X. Hot Topics and Trends in Zero-Energy Building Research—A Bibliometrical Analysis Based on CiteSpace. *Buildings* **2023**, *13*, 479. [CrossRef]
124. Mahmoodi, M.; Rasheed, E.; Le, A. Systematic Review on the Barriers and Challenges of Organisations in Delivering New Net Zero Emissions Buildings. *Buildings* **2024**, *14*, 1829. [CrossRef]
125. Moghaddasi, H.; Culp, C.; Vanegas, J.; Ehsani, M. Net Zero Energy Buildings: Variations, Clarifications, and Requirements in Response to the Paris Agreement. *Energies* **2021**, *14*, 3760. [CrossRef]
126. Le, A.; Rodrigo, N.; Domingo, N.; Senaratne, S. Policy Mapping for Net-Zero-Carbon Buildings: Insights from Leading Countries. *Buildings* **2023**, *13*, 2766. [CrossRef]
127. Jin, Y.; Li, J.; Wu, W. I-Yard 2.0: Integration of Sustainability into a Net-Zero Energy House. *Appl. Sci.* **2020**, *10*, 3541. [CrossRef]
128. Azam, U.; Farooq, M.; Munir, M.A.; Riaz, F.; Sultan, M.; Rehman, A.U.; Imran, M. Modelling Framework for Reducing Energy Loads to Achieve Net-Zero Energy Building in Semi-Arid Climate: A Case Study. *Buildings* **2023**, *13*, 2695. [CrossRef]
129. Zhang, S.; Wang, K.; Xu, W.; Iyer-Raniga, U.; Athienitis, A.; Ge, H.; Cho, D.W.; Feng, W.; Okumiya, M.; Yoon, G.; et al. Policy Recommendations for the Zero Energy Building Promotion towards Carbon Neutral in Asia-Pacific Region. *Energy Policy* **2021**, *159*, 112661. [CrossRef]
130. Alaifan, B.; Azar, E. Potential for Net-Zero Energy Communities in Kuwait: An Empirical Techno-Economic Modeling and Optimization Approach. *Buildings* **2023**, *13*, 2096. [CrossRef]
131. Morelli, M.; Rønby, L.; Mikkelsen, S.E.; Minzari, M.G.; Kildemoes, T.; Tommerup, H.M. Energy Retrofitting of a Typical Old Danish Multi-Family Building to a "Nearly-Zero" Energy Building Based on Experiences from a Test Apartment. *Energy Build.* **2012**, *54*, 395–406. [CrossRef]
132. Dong, J.; Schwartz, Y.; Korolija, I.; Mumovic, D. Unintended Consequences of English School Stock Energy-Efficient Retrofit on Cognitive Performance of Children under Climate Change. *Build. Environ.* **2024**, *249*, 111107. [CrossRef]
133. Chung-Camargo, K.; González, J.; Solano, T.; Yuil, O.; Velarde, V.; Austin, M.C. *Energy-Efficiency Measures to Achieve Zero Energy Buildings in Tropical and Humid Climates*; IntechOpen: London, UK, 2023. [CrossRef]
134. Garcia-Teruel, R.M. Overcoming the "Tenant-Owner Dilemma" to Foster Energy Efficiency in Residential Private Rented Housing. *J. Prop. Plan. Environ. Law* **2023**, *ahead-of-print*. [CrossRef]
135. Jansson-Boyd, C.V.; Robison, R.A.V.; Cloherty, R.; Jimenez-Bescos, C. Complementing Retrofit with Engagement: Exploring Energy Consumption with Social Housing Tenants. *Int. J. Energy Res.* **2016**, *41*, 1150–1163. [CrossRef]
136. Tozer, L.; MacRae, H.; Smit, E. Achieving Deep-Energy Retrofits for Households in Energy Poverty. *Build. Cities* **2023**, *4*, 258–273. [CrossRef]
137. Gigante, A.; Papadaki, D.; Mazzoli, C.; Ntouros, V.; De Masi, R.F.; Assimakopoulos, M.-N.; Ferrante, A. Indoor Quality-Oriented Approach for the Performance Evaluation of Building Retrofit with Façade Transformation: Case Study of Student Dormitory in Mediterranean Climate. *Energy Build.* **2024**, *312*, 114227. [CrossRef]
138. Menconi, M.; Painting, N.; Piroozfar, P. Modelling and Simulation of Low-Risk Energy Retrofit Measures for Traditional Listed Dwellings in the UK. *J. Build. Eng.* **2024**, *82*, 108346. [CrossRef]
139. Jannat, N.; Hussien, A.; Abdullah, B.; Cotgrave, A. Application of Agro and Non-Agro Waste Materials for Unfired Earth Blocks Construction: A Review. *Constr. Build. Mater.* **2020**, *254*, 119346. [CrossRef]
140. Oh, J.; Hong, T.; Kim, H.; An, J.; Jeong, K.; Koo, C. Advanced Strategies for Net-Zero Energy Building: Focused on the Early Phase and Usage Phase of a Building's Life Cycle. *Sustainability* **2017**, *9*, 2272. [CrossRef]
141. Jradi, M.; Madsen, B.E.; Kaiser, J.H. DanRETwin: A Digital Twin Solution for Optimal Energy Retrofit Decision-Making and Decarbonization of the Danish Building Stock. *Appl. Sci.* **2023**, *13*, 9778. [CrossRef]

142. Park, H.; Park, J.; Kim, S.; Chang, S.J. Energy Retrofit Technology for Modern and Contemporary Educational Historical Buildings Considering Preservation and Utilization Aspects. *Energy Rep.* **2024**, *11*, 3995–4007. [CrossRef]
143. Dzulkifly, S.; Aris, H.; Jorgensen, B.N.; Santos, A.Q. Methodology for a Large Scale Building Internet of Things Retrofit. In Proceedings of the University of Southern Denmark Research Portal (University of Southern Denmark), Selangor, Malaysia, 24 August 2020; pp. 62–67.
144. Thomas, A.; Menassa, C.C.; Kamat, V.R. A Systems Simulation Framework to Realize Net-Zero Building Energy Retrofits. *Sustain. Cities Soc.* **2018**, *41*, 405–420. [CrossRef]
145. Ma'bdeh, S.N.; Ali, H.H.; Al-Momani, M. Life Cycle Assessment of Energy Retrofit Measures in Existing Healthcare Facility Buildings: The Case of Developing Countries. *Int. J. Energy Econ. Policy* **2022**, *12*, 418–431. [CrossRef]
146. Loveday, J.; Morrison, G.M.; Martin, D.A. Identifying Knowledge and Process Gaps from a Systematic Literature Review of Net-Zero Definitions. *Sustainability* **2022**, *14*, 3057. [CrossRef]
147. Fichera, G.; Guardo, V.; Margani, G.; Tardo, C. Application of a Retrofit System to Improve the Seismic and Energy Performances of RC Framed Buildings. *Procedia Struct. Integr.* **2024**, *55*, 193–200. [CrossRef]
148. Pyloudi, E.; Papantoniou, S.; Kolokotsa, D. Retrofitting an Office Building towards a Net Zero Energy Building. *Adv. Build. Energy Res.* **2014**, *9*, 20–33. [CrossRef]
149. Irulegi, O.; Ruiz-Pardo, A.; Serra, A.; Salmerón, J.M.; Vega, R. Retrofit Strategies towards Net Zero Energy Educational Buildings: A Case Study at the University of the Basque Country. *Energy Build.* **2017**, *144*, 387–400. [CrossRef]
150. Gajić, D.; Peulić, S.; Mavrič, T.; Sandak, A.; Tavzes, Č.; Malešević, M.; Slijepčević, M. Energy Retrofitting Opportunities Using Renewable Materials—Comparative Analysis of the Current Frameworks in Bosnia-Herzegovina and Slovenia. *Sustainability* **2021**, *13*, 603. [CrossRef]
151. Zhou, Z.; Zhang, S.; Wang, C.; Zuo, J.; He, Q.; Rameezdeen, R. Achieving Energy Efficient Buildings via Retrofitting of Existing Buildings: A Case Study. *J. Clean. Prod.* **2016**, *112*, 3605–3615. [CrossRef]
152. Prada, A.; Cappelletti, F.; Gasparella, A. Optimization of Government Subsidization Strategies for Building Stock Energy Refurbishment. In Proceedings of the International Building Physics Conference 2018, Syracuse, NY, USA, 26 September 2018. [CrossRef]
153. Jack, M.W.; Konings, H.B. Seasonal Variation in Electricity Demand of Solar-Powered Net-Zero Energy Housing in Temperate Climates. *Energy Build.* **2024**, *303*, 113826. [CrossRef]
154. Liu, Y.; Liu, T.; Ye, S.; Liu, Y. Cost-Benefit Analysis for Energy Efficiency Retrofit of Existing Buildings: A Case Study in China. *J. Clean. Prod.* **2018**, *177*, 493–506. [CrossRef]
155. Moran, P.; O'Connell, J.; Goggins, J. Sustainable Energy Efficiency Retrofits as Residenial Buildings Move towards Nearly Zero Energy Building (NZEB) Standards. *Energy Build.* **2020**, *211*, 109816. [CrossRef]
156. Asaee, S.R.; Ugursal, V.I.; Beausoleil-Morrison, I. Development and Analysis of Strategies to Facilitate the Conversion of Canadian Houses into Net Zero Energy Buildings. *Energy Policy* **2019**, *126*, 118–130. [CrossRef]
157. Junjia, Y.; Alias, A.H.; Haron, N.A.; Bakar, N.A. Machine Learning Algorithms for Safer Construction Sites: Critical Review. *Build. Eng.* **2024**, *2*, 544. [CrossRef]

Disclaimer/Publisher's Note: The statements, opinions and data contained in all publications are solely those of the individual author(s) and contributor(s) and not of MDPI and/or the editor(s). MDPI and/or the editor(s) disclaim responsibility for any injury to people or property resulting from any ideas, methods, instructions or products referred to in the content.

energies

MDPI

Article

Simulation of Malfunctions in Home Appliances' Power Consumption

Alexios Papaioannou [1,2,*], Asimina Dimara [1,3], Christoforos Papaioannou [2], Ioannis Papaioannou [1], Stelios Krinidis [1,2], Christos-Nikolaos Anagnostopoulos [3,*], Christos Korkas [1], Elias Kosmatopoulos [1], Dimosthenis Ioannidis [1] and Dimitrios Tzovaras [1]

[1] Centre for Research and Technology Hellas, Information Technologies Institute, 57001 Thessaloniki, Greece; adimara@iti.gr (A.D.); johnpap@iti.gr (I.P.); krinidis@mst.ihu.gr (S.K.); chriskorkas@iti.gr (C.K.); kosmatop@iti.gr (E.K.); djoannid@iti.gr (D.I.); dimitrios.tzovaras@iti.gr (D.T.)
[2] Management Science and Technology Department, Democritus University of Thrace (DUTh), 65404 Kavala, Greece
[3] Intelligent Systems Lab, Department of Cultural Technology and Communication, University of the Aegean, 81100 Mytilene, Greece
* Correspondence: alexiopa@iti.gr (A.P.); canag@aegean.gr (C.-N.A.)

Abstract: Predicting errors in home appliances is crucial for maintaining the reliability and efficiency of smart homes. However, there is a significant lack of such data on appliance malfunctions that can be used in developing effective anomaly detection models. This research paper presents a novel approach for simulating errors of heterogeneous home appliance power consumption patterns. The proposed model takes normal consumption patterns as input and employs advanced algorithms to produce labeled anomalies, categorizing them based on the severity of malfunctions. One of the main objectives of this research involves developing models that can accurately reproduce anomaly power consumption patterns, highlighting anomalies related to major, minor, and specific malfunctions. The resulting dataset may serve as a valuable resource for training algorithms specifically tailored to detect and diagnose these errors in real-world scenarios. The outcomes of this research contribute significantly to the field of anomaly detection in smart home environments. The simulated datasets facilitate the development of predictive maintenance strategies, allowing for early detection and mitigation of appliance malfunctions. This proactive approach not only improves the reliability and lifespan of home appliances but also enhances energy efficiency, thereby reducing operational costs and environmental impact.

Keywords: error simulation; malfunction prediction; home appliance power consumption; anomaly detection; smart homes

1. Introduction

A significant proportion of residential energy consumption is spent on activities such as cooking, washing clothes, and heating water. Specifically, space heating represents about 65% of the total energy consumption in households, while water heating accounts for approximately 14%, and cooking for approximately 6%. Other household activities and appliances consume another 13% [1]. However, residents do not realize the degree to which the actual energy consumption of their home appliances contributes to the total energy consumption. As a result, this lack of awareness can lead to an increase in energy usage by up to a third [2]. Furthermore, malfunctions in home appliances can result in a significant increase in energy consumption while remaining unnoticed by residents, as the home appliance continues to operate "normally" [3]. These unnoticed errors can lead to an increase in energy usage of up to 75% in certain cases, significantly affecting overall energy efficiency and costs [4]. Implementing effective anomaly detection systems can

help identify these inefficiencies and malfunctions early, reducing unnecessary energy consumption while improving overall energy management in households.

Anomaly detection techniques can identify potential errors or anomalies in home appliance energy usage patterns, indicating a possible malfunction. When accurate, such methods can also be used for predictive maintenance. These anomaly detection techniques detect either anomaly points or patterns. As an example, support vector machines (SVM), may be employed to distinguish normal and abnormal usage patterns in data related to energy consumption [5]. Moreover, deep learning (DL) models are effective in recognizing intricate patterns from large datasets, making neural networks useful for identifying small variations in energy consumption over time [6]. The k-Nearest Neighbors (kNN) algorithm analyzes an appliance's consumption compared to that of its closest neighbors to recognize outliers in datasets [7]. Likewise, time-series analysis is used to observe trends in energy use over time and identify variations that demonstrate problems [8]. By recreating incoming data and comparing it to the original, autoencoders are used to learn a compressed representation of typical energy usage patterns and spot abnormalities [9]. By identifying and mitigating malfunctions before they occur, adopting these strategies can significantly improve the reliability and effectiveness of household appliances.

However, implementing these techniques in real-time and real-world scenarios is challenging. Home appliance energy usage patterns are numerous and diverse, even for the same appliance's model, due to varying climates and/or usage habits. Moreover, for most of the methods, there is a critical need for historical consumption data to accurately identify the anomalies. In addition, labeled data with anomalies or specific malfunctions is necessary to effectively monitor and detect errors. Numerous other challenges exist in applying these techniques, such as data variability, the need for large datasets, and the complexity of real-time processing. The wide range of home appliances and potential malfunctions complicate the detection of errors and anomalies. Furthermore, there is limited availability of public datasets to train supervised models, which limits the development of accurate anomaly detection systems. This lack of data is a significant barrier, as supervised models rely on large, labeled datasets to learn the difference between normal and abnormal behavior. Therefore, addressing these challenges requires substantial effort in data collection, labeling, and the development of robust models capable of handling diverse and dynamic patterns of appliance usage.

Within this context, this paper suggests a method for simulating errors for common home appliances such as fridges, washing machines, dryers, dishwashers, and water heaters. This method is designed to be general, allowing it to be applied to all types of appliances and patterns. It can simulate and produce relevant errors, including minor, major, and specific faults. This simulation method is crucial for training and testing anomaly detection methods, as well as for applying predictive maintenance techniques. By simulating such a wide range of errors, this approach provides comprehensive datasets that can be used to enhance the accuracy and robustness of anomaly detection systems. It allows the creation of realistic scenarios in which appliances fail in various ways while preparing detection algorithms to recognize and respond to actual malfunctions effectively. Additionally, the ability to simulate different types of errors supports the development of predictive maintenance strategies, which can significantly improve the reliability and lifespan of home appliances.

In general, this method contributes significantly to enhancing the overall energy efficiency of households, ensuring that home appliances function correctly and sustainably. The main novelties are:

- Novel and adaptable method for simulating errors across a wide range of home appliances. This method can be applied to various appliances and usage patterns, generating comprehensive datasets for anomaly detection while being generally applied (cross-appliance applicability).

- Simulation of a broad spectrum of errors, including minor, major, and specific malfunctions. This provides detailed and realistic scenarios crucial for the development and testing of robust anomaly detection and predictive maintenance algorithms.
- Facilitation of efficient training and testing of anomaly detection technologies and predictive maintenance strategies by providing comprehensive datasets that reflect realistic appliance usage and error patterns.
- Integration of anomalies seamlessly into normal consumption patterns, ensuring the resulting data is realistic and representative of actual malfunctions, thereby improving the reliability of detection algorithms.

The remainder of this paper is structured as follows: Section 2 presents the current methodologies and applications of simulations in the energy sector and the techniques used to detect anomalies in the power consumption patterns of home appliances. Section 3 includes an extensive analysis of the energy usage patterns of home appliances as well as the algorithms and techniques used to simulate error patterns in the power consumption data. Simulated datasets and the analyses of real and anomalous patterns for each home appliance are presented in Section 4. Finally, in the last section, Section 5, the paper summarizes the key findings of the research.

2. Literature Review

In this section, the most recent literature related to this research topic is addressed. A search on Google Scholar including the keywords "simulation, errors, home appliance, consumption" reveals nearly 32,000 publications. Despite this number of publications, only the top two results are directly relevant to this paper: "Closing the Gap Between Simulation and Measured Energy Use in Home Archetypes" [10] and "A Scalable Real-Time Non-Intrusive Load Monitoring System for the Estimation of Household Appliance Power Consumption" [11]. However, these papers discuss the simulation of energy consumption and not the simulation of error anomalies. To broaden the research scope, a more general search using "Simulation energy" yielded approximately 6,690,000 publications. The differences in results indicate that while there is a plethora of research for the energy sector, there are far fewer tailored simulations. Specifically, it is observed that there is a significant gap in the literature concerning techniques specifically designed for simulating home appliance errors. Moreover, to the best of the authors' knowledge, and the Google search, there are no published papers on the simulation of anomalies in energy consumption of home appliance errors. Based on this criterion, the literature review is divided into two sections: Section 2.1 presents existing models for simulations in the energy sector, providing a detailed analysis of methodologies and applications. Following that, Section 2.2 covers the techniques for anomaly detection, highlighting the current methodologies specifically used for detecting anomalies in the power consumption patterns of home appliances.

2.1. Existing Models for Simulation in the Energy Sector

Existing models for simulating consumption patterns often employ statistical distributions to predict power usage with high accuracy. For example, methodologies using the Kolmogorov–Smirnov test and Pearson's X2 test have forecasted power consumption of household appliances with maximum errors as low as 3.9% for fridges and 4.27% for lighting, and even lower for washing machines, dishwashers (less than 1%), and dryers (about 1.17%) [12]. Despite their accuracy, these models are often limited to specific home environments and cannot replicate abnormalities across diverse settings. As there are different types of home appliances, more adaptable modeling techniques are needed to accommodate different household configurations. Additionally, predictive models using machine learning techniques such as multiple linear regression, random forest regressor, and support vector machines have been developed to enhance the accuracy of energy consumption forecasts, demonstrating significant potential in improving residential energy management systems [13]. Another approach involves modeling energy consumption profiles of smart home appliances, tailored to specific environmental conditions.

Et-Tolba et al., developed models for Moroccan conditions that consider user preferences and environmental factors to enhance energy efficiency and reduce consumption costs [14]. These models are often created and simulated using platforms like Matlab/Simulink (2023b) [15]. Similarly, Sánchez-Cervantes et al. introduced a Big-Data-and-machine-learning-based smart home energy management system (HEMS-IoT) designed to learn user behaviors and energy consumption patterns. This system employs the J48 machine learning algorithm to classify energy consumption and generate energy-saving recommendations based on user preferences, contributing to home comfort, safety, and energy efficiency [16]. The significant impact of consumer behavior and ambient factors on energy consumption is evident in these simulations, offering valuable insights into customizing energy consumption profiles to reflect actual usage scenarios and user needs.

L. Diao et al., examine the simulation of energy consumption in residential buildings with a focus on occupant behavior and its impact on energy usage [17]. Using data from the American Time Use Survey (ATUS), the authors applied k-means clustering methods to identify and classify occupant behavior patterns. The proposed model integrates these behaviors into a bottom-up simulation model to estimate energy consumption. It is highlighted that the proposed model offers more accurate and reliable predictions compared to the standardized schedules of the American Society of Heating, Refrigerating, and Air-Conditioning Engineers (ASHRAE), indicating the need for personalized simulation models that take into account actual occupant behaviors. Similarly, Chen et al., (2021) developed a stochastic simulator integrated with a building stock model to more accurately predict residential energy loads. This model uses clustering techniques and Markov chain simulations to reflect the heterogeneity of occupant behavior, enhancing the reliability of energy consumption forecasts for the community on national scales [18].

Another relevant work in this context by A. Dimara et al., discusses the application of simulation in building energy systems, encompassing computational, mathematical, and machine learning models to represent a building's physical characteristics and operational strategies [19]. This technique supports various tasks throughout the renovation life cycle, such as decision-making integration, design scenario evaluation, real-time monitoring and diagnostics for energy management, and the incorporation of virtual reality for digital design and operation experiences. Despite its established role in building performance, significant challenges remain, particularly in integrating data from fragmented systems and modeling human–building interactions. This work defines the domain of building performance simulation, highlighting key use cases, prevalent simulation tools, and implementation challenges. Finally, Zhao et al., develop a practical data-mining approach using office appliance power consumption data to model occupant behavior and schedules for building energy simulations [20]. The study demonstrates that accurately predicting occupant behavior can significantly impact HVAC energy consumption in buildings, especially in different climate zones. This approach emphasizes the importance of integrating occupant behavior modeling into energy simulations to enhance building performance and energy efficiency. Similarly, Azar and Menassa present a comprehensive framework that combines data-mining techniques with building information modeling to predict occupant behavior and energy use in commercial buildings. Their approach highlights the role of detailed occupant behavior modeling in improving the accuracy of energy simulations and optimizing building performance [21].

2.2. Techniques for Anomaly Detection

In the context of detecting anomalies in the power consumption of home appliances, researchers focus on identifying unusual patterns that may indicate potential appliance failures or inefficient energy use. One notable approach is the ensemble anomaly detection (EAD) and collective contextual anomaly detection using sliding window (CCAD-SW) frameworks developed by Araya et al., (2017) [22]. The CCAD-SW framework enhances detection performance by identifying abnormal consumption patterns through the use of overlapping sliding windows, thereby recognizing collective contextual anomalies. Addi-

tionally, the EAD framework employs majority voting to merge different anomaly detection classifiers, which improves sensitivity and reduces false alarm rates. Compared to individual classifiers, the EAD framework significantly enhances anomaly detection performance.

Furthermore, closely related to this paper, another approach was introduced by Qian et al. (2024) [23]. Using the DBSCAN method, a gray-relation-projection-based clustering learning strategy was developed to detect abnormal patterns in power use. By grouping users with comparable consumption habits and detecting anomalies within these groups, this technique makes it possible to spot unusual usage patterns that might point to appliance problems. This technique is very accurate and resilient, as shown by PR-AUC values of 0.96 and AUC values of 0.911, which make it a useful tool for simulating and spotting possible problems in home appliances. Additionally, Pan et al., (2022) propose a high-dimensional energy consumption anomaly detection method based on deep learning. This method utilizes high-dimensional energy data to predict and detect abnormal electricity usage in real-time, demonstrating its effectiveness in reducing energy waste and improving energy efficiency in buildings [24].

Priyadarshini et al., (2022) proposed a reliable approach for evaluating time series data from smart meters using several machine learning algorithms, including ARIMA, SARIMA, LSTM, Prophet, LightGBM, and VAR [25]. Their method uses the ChangeFinder algorithm, which recognizes shifts in consumption trends, to identify unusual usage patterns that can point to appliance issues. The outstanding MAE, MSE, and RMSE values of the ARIMA model demonstrate its great performance, highlighting its dependability in forecasting and simulating home appliance problems. This thorough process ensures that potential issues are quickly found and fixed, preserving the reliability of smart home systems. Similarly, Zamani et al. present a deep-learning approach using autoencoders with 1D-CNN and TCN backbones for time-series anomaly detection in smart homes. Their method effectively differentiates between normal and abnormal energy consumption patterns, particularly in dishwashers and refrigeration units, enhancing the ability to identify and address unusual consumption behaviors [26].

2.3. Contribution of This Paper

Despite the existing research on simulating energy consumption and the comparatively underexamined topic of simulating home appliance errors, there is still a significant gap in developing models that can simulate errors in home appliances with heterogeneous patterns. This paper addresses this gap by presenting a novel approach for simulating errors in home appliance power consumption patterns. Unlike existing studies, which primarily concentrate on modeling normal consumption patterns or detecting anomalies using supervised algorithms, our research introduces a novel unsupervised method capable of producing a wide range of error patterns in home appliances. Specifically, this method allows for the simulation of errors without requiring ground-truth or predefined anomaly data, making it highly applicable to real-world and real-time scenarios. As a result, the simulated anomaly patterns may be used for developing robust anomaly detection systems and predictive maintenance strategies in smart homes, where the diversity of error patterns can vary significantly based on usage habits and environmental conditions. By providing diverse error patterns, our method enhances the reliability and efficiency of smart home systems. This innovative contribution marks a substantial advancement in the field of anomaly detection, offering a valuable resource for mitigating appliance malfunctions in real-world scenarios.

3. Methodology

In this section, different types of home appliance anomalies are presented. Additionally, an extensive analysis of the datasets used, including types of home appliances and data preprocessing steps, is illustrated. Finally, the algorithms and techniques used to simulate error patterns in the power consumption data are presented.

3.1. Overview of Anomalies in Home Appliance Power Consumption Patterns

Anomalies in home appliance power consumption patterns refer to deviations from normal operational consumption patterns. These deviations can indicate various issues, from minor inefficiencies to major malfunctions [6]. Traditional methods for detecting anomalies often rely on predefined thresholds or supervised learning algorithms that require labeled datasets that indicate normal and faulty states [27]. However, these approaches have limitations and also require extensive labeled data [9]. Moreover, they have difficulty generalizing across different types of appliances and usage patterns [28]. Moreover, typically types of anomalies are referred to as:

i Point Anomalies, as Figure 1 shows, refers to single data points that deviate significantly from the rest of the data (e.g., a sudden spike in power consumption) [29].

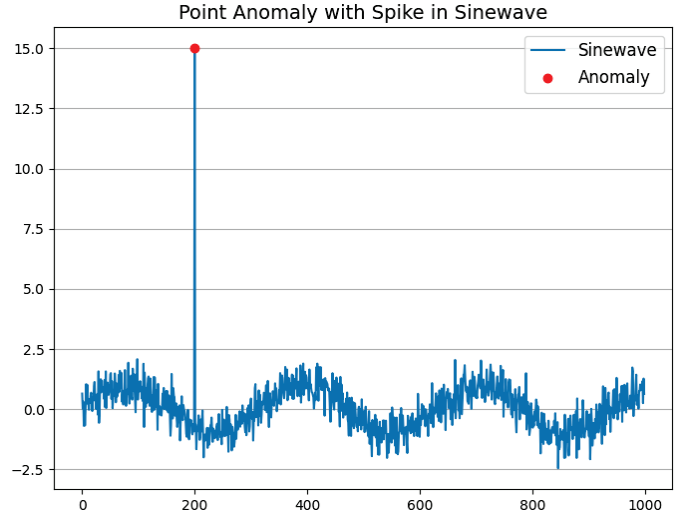


Figure 1. Point Anomalies.

However, this spike may be misleading as it could also be a normal pattern such as a fridge compressor starting or a sensor reading error (Figure 2) [30]. When a fridge compressor kicks in, it can cause a temporary surge in power usage that may appear as an anomaly but is actually part of normal operation [31]. Additionally, such spikes can also be caused by sensor reading errors, leading to false positives in anomaly detection [32]. Consequently, while point anomalies are widely used, they should be approached with caution or carefully calibrated to avoid false positives.

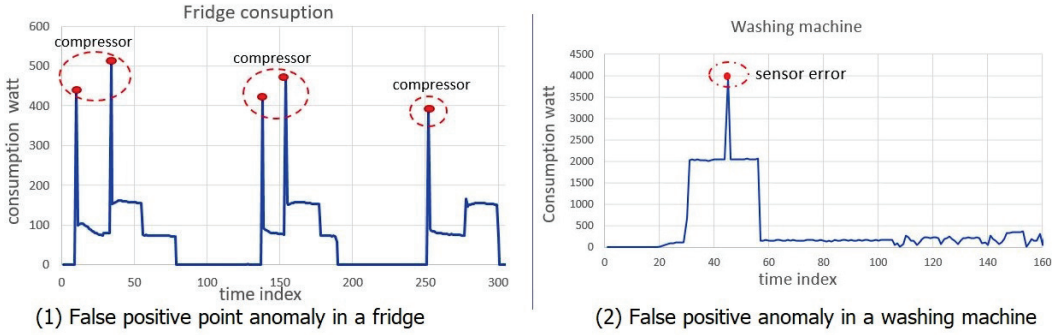


Figure 2. False positive point anomaly detection.

ii Contextual Anomalies (Figure 3) refers to data points that are considered anomalies within a specific context (e.g., high power consumption during an idle phase) [33].

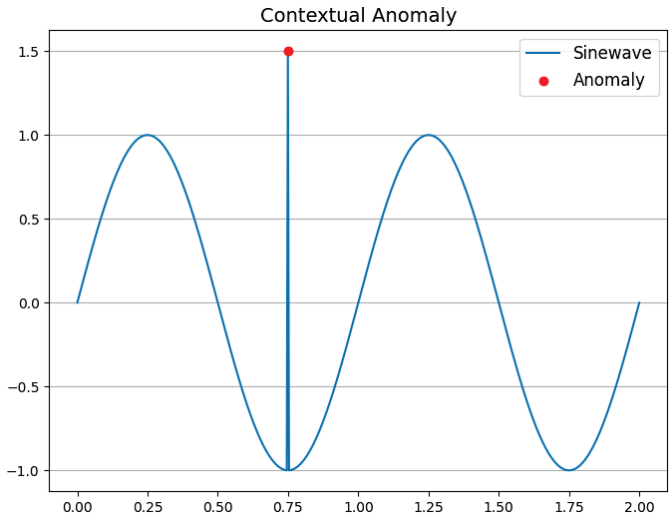


Figure 3. Contextual Anomalies.

High power consumption during an idle phase of a dishwasher might be flagged as an anomaly. However, this could be misleading as it might reflect legitimate operational variations, such as the dishwasher entering a self-cleaning cycle or handling a particularly heavy load [34]. Additionally, sensor errors (Figure 4) or variations in water pressure can also cause temporary spikes in power consumption that appear anomalous but are actually within normal operating parameters [35], while contextual anomalies are useful, they should be carefully analyzed and calibrated to avoid false positives.

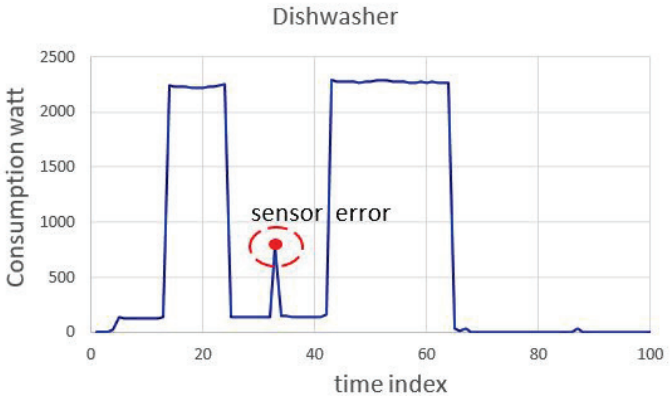


Figure 4. False positive contextual anomaly detection.

Due to two main reasons, namely, the lack of labeled anomaly data to run supervised anomaly detection and the false positives arising from detecting anomaly patterns (whether point or contextual), a different method is employed in this paper. Traditional anomaly detection often relies on labeled datasets, which are challenging to obtain and can lead to inaccurate results due to false positives from normal operational patterns. In this paper, we use an unsupervised method that does not rely on detecting individual anomaly points.

Instead, after carefully examining patterns in home appliances, the method is based on the increase in power consumption caused by malfunctions, which translates to the prolonged duration of operational cycles [3,4]. Minor or major malfunctions typically result in increased power consumption, which is detected in the home appliance usage pattern as a prolonged operational cycle (time duration) compared to a normal cycle. For instance, a malfunctioning dishwasher may take significantly longer to complete a cycle due to issues like clogged filters or faulty sensors, leading to extended power usage beyond normal operational parameters. By focusing on these prolonged consumption patterns rather than

isolated spikes or contextual anomalies, our method provides a more reliable and practical solution for real-time anomaly detection in smart home environments.

In developing our simulation model, various potential sources of error, including the assumptions underlying the model, the impact of missing data, and the effects of different types of anomalies on the simulation's accuracy are considered. One key factor is that in appliance malfunctions leading to prolonged operational cycles, the extension to the operational cycle needs to be sufficiently long to be detected; if the prolonged cycle is less than one minute longer, this may be lost in the data. Additionally, the presence of missing data can significantly affect the model's performance. Our analysis indicates that if more than 30% of the data are missing, the accuracy of the simulation decreases substantially. Otherwise, the data are cured to maintain its integrity. It is important to note that errors in the simulation model will not occur due to the robust design of our methodology, which incorporates real-time data adaptability.

As a result, in this paper, the total simulated anomaly patterns refer to a comprehensive set of prolonged operational cycles that reflect various types of malfunctions in home appliances as depicted in Figure 5. An anomaly is determined to be present in each of the patterns due to the existence of a prolonged operational cycle. These patterns are generated without relying on predefined labels or ground truth, making them applicable for developing robust anomaly detection systems. By simulating the extended duration of operational cycles indicative of different malfunction scenarios, this approach creates realistic anomalies while enhancing the reliability and efficiency of smart home systems. By focusing on prolonged consumption patterns rather than isolated spikes or contextual anomalies, the suggested method provides a more reliable and practical solution for real-time anomaly detection in smart home environments.

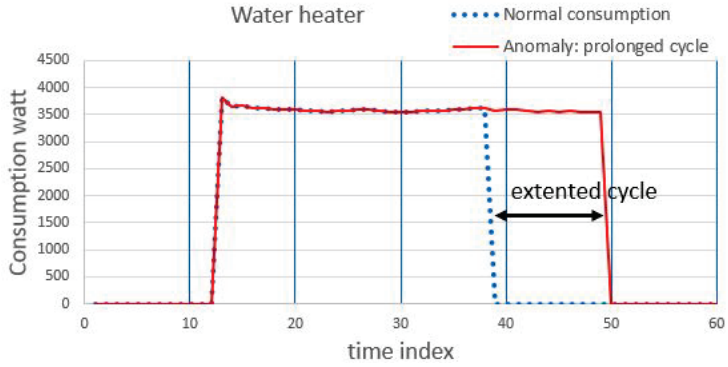


Figure 5. Example of an anomaly pattern with a prolonged cycle.

3.2. Types of Anomalies by Severity

The devices that are either widely owned (e.g., fridges [36]) or have high energy consumption (e.g., water heaters [36]), making them crucial for mitigating energy consumption due to overconsumption and errors, were selected for the suggested methodology. There is an additional important category not studied here: appliances focused on space heating and cooling. These were not included in the analysis due to the variety of systems available, such as air conditioners (AC), HVAC systems, heat pumps, electric radiators, gas heaters, and more. The lack of public data for all these systems, and the challenge of accurately measuring their consumption in integrated central systems, further complicated their inclusion. In future work, there is a plan to extend our analysis to include these heating and cooling appliances to further enhance our understanding of energy consumption and anomaly detection in these systems.

Specifically, according to the U.S. Department of Energy, water heating typically accounts for 13% to 17% of a household's energy usage, making it one of the most significant energy expenses after heating and cooling [37]. Fridges and freezers, which are in almost every residence [38], also contribute to substantial energy use. As a result, the common or wasteful home appliances selected for analysis include fridges and freezers, washing

machines, dishwashers, dryers, and water heaters. These appliances were selected as they are prevalent in most households while having significant energy demands. Fridges and freezers operate continuously, making them major contributors to household energy consumption [39]. Moreover, washing machines and dishwashers are used frequently and involve a water-heating phase, which increases the energy they consume [40]. Dryers are also known for their high power consumption, especially during drying cycles [41]. Finally, water heaters also represent substantial energy use in homes [42]. Therefore, these are the devices whose errors should be simulated to understand and mitigate their impact on overall energy consumption.

All home appliances may experience minor or major errors/malfunctions while continuing to operate, with these errors often remaining unnoticed by the homeowner. They continue to operate, but the consumption of the home appliance increases as the operation cycles are prolonged [3,4,43]. The duration of the prolongation depends on the type of malfunction. Minor errors are typically small malfunctions that do not immediately affect the appliance's ability to perform its primary function but can cause it to operate less efficiently. Examples include slightly worn door seals on fridges or partially clogged lint filters in dryers. These minor issues lead to increased energy consumption but the appliance still appears to operate normally [3]. Conversely, major errors significantly impact an appliance's performance and will eventually lead to complete failure [4]. These errors often remain unnoticed until the home appliance breaks. Examples include a faulty compressor in a fridge or a broken heating element in a water heater. These errors not only increase energy consumption substantially but also cause the appliance to underperform or stop working altogether.

Figure 6 provides an overview of the percentage of minor and major errors for each home appliance [43], as well as the percentage increase in energy consumption associated with specific malfunctions [43]. For instance, faulty thermostats in fridges can increase energy use by 23% [3,44]. Similarly, water heater major malfunctions can raise energy consumption by up to 35% [45]. Dishwashers with heating element issues can see a 15% increase in energy usage [46]. Additionally, inefficient heating elements in dryers can lead to a 25% increase in energy consumption [47].

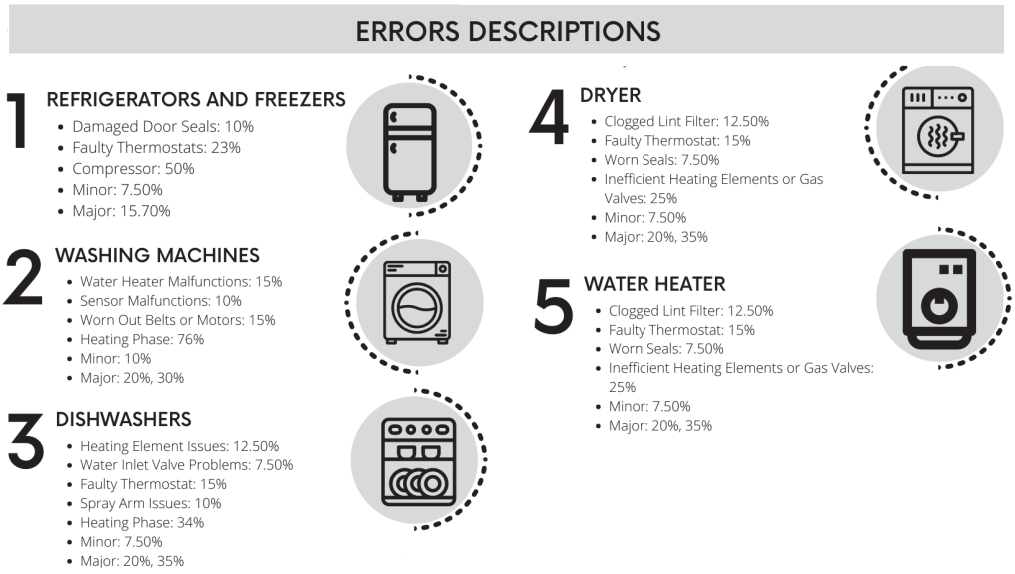


Figure 6. Error description per selected home appliance.

3.3. Home Appliance Consumption Pattern Analysis

Understanding the power consumption patterns of home appliances is crucial for creating accurate simulated anomaly patterns. Each appliance has unique consumption characteristics influenced by its function, usage frequency, and operational cycles. This

section provides a detailed analysis of the power consumption patterns for five common home appliances: fridge, washing machine, dishwasher, dryer, and water heater. This section also addresses the importance of granularity in real-time applications, emphasizing the need for high-resolution data to accurately detect anomalies and optimize appliance recognition.

3.3.1. Granularity and Its Importance in Real-Time Applications

When considering methods, especially for real-time and real-world applications, granularity is critical, particularly in energy consumption analysis. High-time resolution data are essential because they preserve the detailed patterns necessary for accurate analysis. Specifically, for methods such as Non-Intrusive Load Monitoring (NILM), a resolution smaller than 1 min, typically around 1 s, is often required [48]. These high-resolution data allow for the detection of subtle and rapid changes in power consumption that are crucial for recognizing anomalies and appliance-specific usage. However, for tasks such as load prediction, PV prediction, anomaly detection, and predictive maintenance in energy consumption, a 1 min resolution has been found to offer a good balance [49–51]. This maintains sufficient detail to detect anomalies and predict load changes accurately while managing data volume effectively.

Overall, in real-time applications, a balance must be struck between data management and pattern efficacy. For example, storing 1 s resolution data results in 86,400 data points per day, equating to approximately 31.5 million data points per year. In contrast, 1 min resolution data results in 1440 data points per day, or around 525,600 data points per year. This significant reduction in data volume (approximately 98.3% less) is crucial for practical data storage and processing in real-world applications. For long-term applications, such as smart home energy management, the implications of data storage are even more pronounced. Continuously storing 1 s resolution data can quickly lead to memory exhaustion and increased costs for data storage infrastructure. This can be particularly wasteful for applications that need to operate over many years. In contrast, 1 min resolution data provide a more manageable data volume that balances the need for detailed consumption patterns with the practicalities of long-term data storage.

As a result, the proposed solution is tested and recommended for use with a 1 min resolution as this provides the perfect balance between data richness and data management, while it can be adapted for resolutions of less than 1 min, its efficacy diminishes significantly when applied to resolutions greater than 5 min. Beyond this threshold, prolonged patterns might be misclassified as normal patterns, reducing the accuracy of anomaly detection and appliance recognition. Due to the prolonged patterns being subsumed within normal patterns, the anomaly patterns will become unrecognizable. Therefore, a 1 min resolution is optimal for maintaining a detailed yet manageable dataset, ensuring effective anomaly detection and appliance recognition.

3.3.2. Fridge

Fridges show a relatively stable power consumption pattern with periodic peaks. The power consumption pattern is composed of two phases: the cooling phase and the idle phase. During the active cooling phase, the compressor runs to cool the interior of the fridge. The power consumption in this phase is at its highest level as both the compressor motor and fans are operating. The duration of this phase depends on the efficiency of the fridge, as well as the internal and external temperatures, and may last from a few minutes to hours.

In the idle phase, the power consumption drops significantly, as only the sensors, lights, and display panels are active. The compressor is turned off when the set temperature has been achieved. The fridge remains in this phase until the temperature inside exceeds a certain set point. Figure 7 presents the power consumption pattern of a fridge.

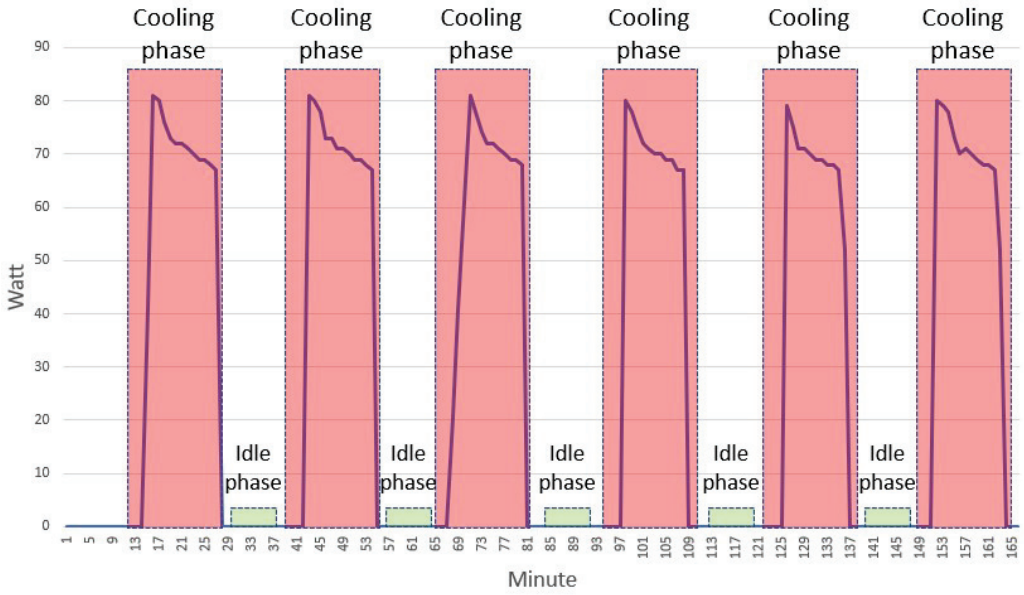


Figure 7. Example of power consumption of a fridge.

3.3.3. Washing Machine

Washing machines are a commonly used home appliance that greatly contributes to the convenience of daily life. These devices come in various types, such as top-loading and front-loading machines, each with its unique operational characteristics. In this work, data from front-loading washing machines was utilized.

All types of washing machines exhibit cyclical power consumption patterns characterized by distinct phases: heating, washing, and spinning. The heating phase is the most power-consuming, with power consumption peaks due to the activation of the heating elements. This phase is important for raising the water temperature to the desired level, which is necessary for the selected washing program. There is another phase before the heating phase called the pre-washing phase, but this appears only in specific washing programs with a pre-washing process.

Figure 8 presents the pattern of a washing cycle without a pre-washing phase. As can be observed, the heating phase is the most power-consuming, accounting for almost 90% of the total power consumption. The washing and spinning phases have lower power consumption, and the duration of these phases depends on the operation program selected by the user.

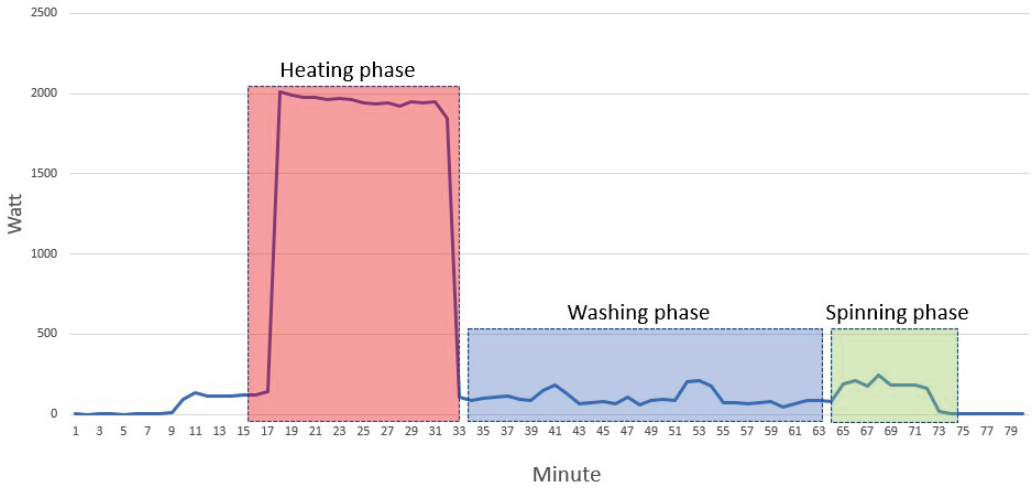


Figure 8. Example of power consumption of a washing machine.

3.3.4. Dishwasher

Dishwashers have a multi-phase power consumption pattern, similar to washing machines. The phases consist of the pre-wash, wash, rinse, and dry phases. The different phases are presented in Figure 9.

The initial phase is the pre-washing phase. During this phase, a brief period of power consumption occurs as the machine prepares for the main washing phase. This involves pumping in water and slightly heating it. The next phase is the washing phase, in which a significant increase in power consumption is observed. The heating element works to maintain the water temperature at an optimal level, while the motor drives the spray arms to distribute water and detergent. The power peaks in this phase can be substantial, reflecting the combined energy demands of heating and mechanical action.

The rinsing phase includes the removal of water from the machine. The power consumption decreases compared to the washing phase. The motor continues to operate, and in some models, additional heating elements are activated to ensure the water is at the right temperature for effective rinsing. The last phase includes the drying process involving passive air drying or active heat drying. In models with heat drying, the power consumption peaks again as the heating element works to dry the dishes. This phase can show varied power usage depending on the drying method and settings used.

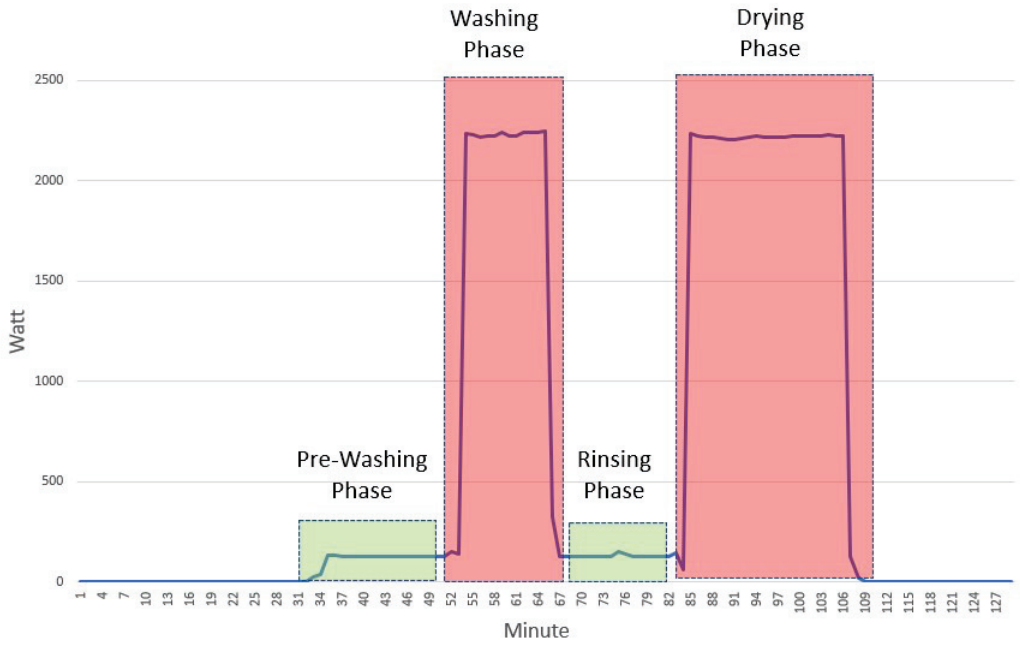


Figure 9. Example of power consumption of a dishwasher.

3.3.5. Dryer

Dryer power consumption patterns depend on the selected program and the main feature of all programs is the high power consumption due to the heating elements. The power usage is relatively consistent throughout the drying cycle, with minor variations depending on the cycle's intensity and the load size. The primary phases are the warming-up, heating, and cooling-down phases and are presented in Figure 10.

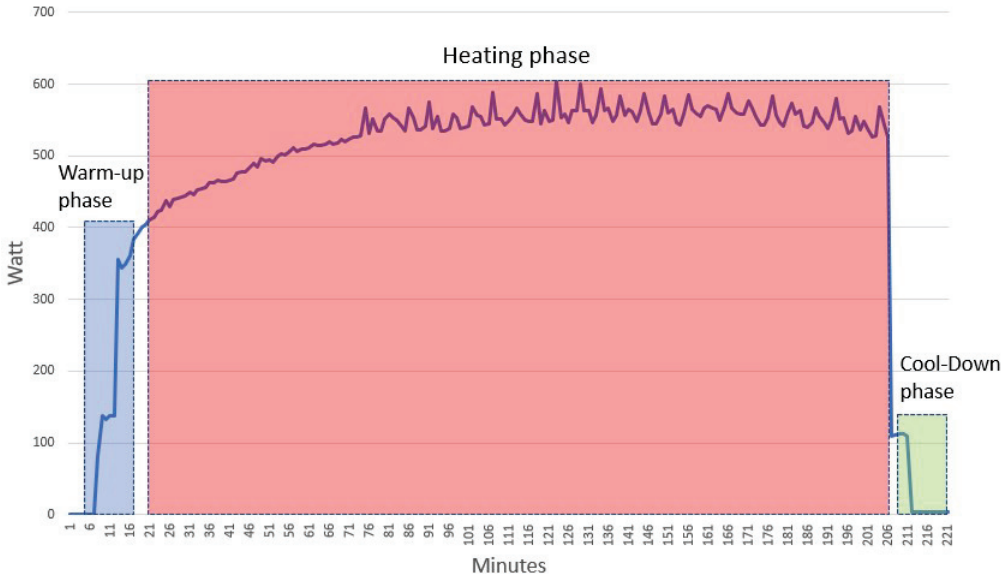


Figure 10. Example of power consumption of a dryer.

In the warm-up phase, the dryer begins to heat up, and power consumption rises as the heating elements engage. This phase is relatively short. During the heating phase, the dryer operates at a high power level. The heating elements operate continuously or intermittently to maintain a high temperature, while the motor keeps the drum rotating. Despite minor fluctuations based on the drying cycle's intensity, power consumption stays high and relatively stable. The cool-down phase is the final stage of the dryer power consumption pattern. In this phase, the dryer enters a cool-down period where the heating elements turn off, and the drum continues to rotate to cool the clothes. Power consumption drops significantly during this phase.

3.3.6. Water Heater

Water heater power consumption typically exhibits a relatively constant pattern, with high power usage during heating periods and negligible consumption during idle periods. The thermostat settings and hot water usage frequency influence the consumption pattern.

The power consumption pattern of a water heater is shown in Figure 11. It is constantly high during active heating, which indicates the energy needed to heat the water. The consumption reduces significantly once the target temperature is attained and stays low during standby periods. In some models, occasional power spikes may occur due to reheating cycles to maintain the water temperature.

The power consumption patterns of the aforementioned home appliances have distinctive characteristics that are important for developing simulated anomaly situations. The fridge shows stable patterns with periodic peaks, the washing machine displays cyclical patterns with three main phases, the dishwasher displays multiple peaks corresponding to their operational phases, the dryer has relatively consistent high consumption, and the water heater shows high consumption during heating periods.

Table 1 presents the values for six statistical features. For the mean value, "Low" represents a value lower than 100 watts, "Moderate" shows a value between 100 and 500 watts, and "High" represents values above 500 watts. For peak power consumption values, "Moderate" includes values between 500 and 1500 watts, and "High" represents values above 1500 watts.

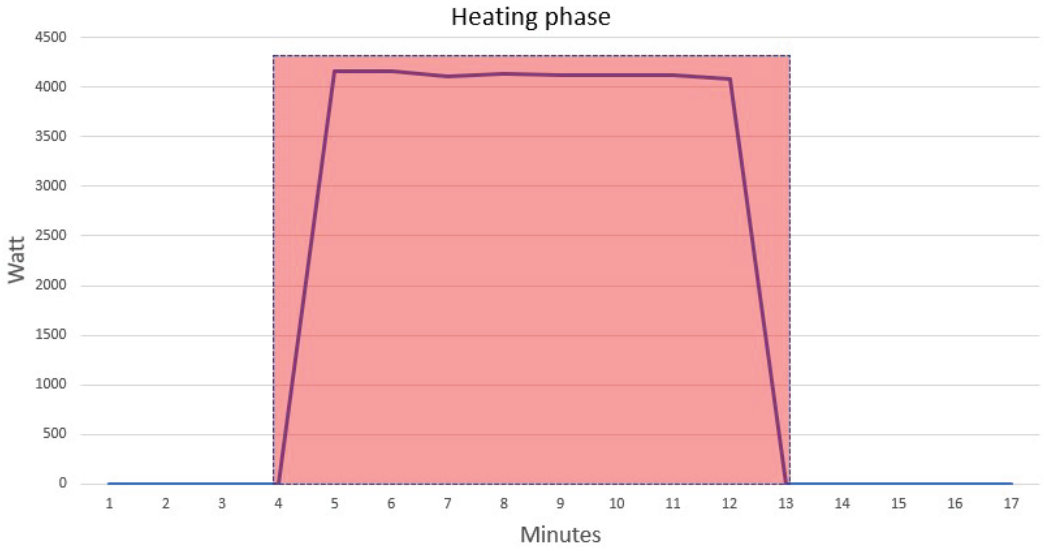


Figure 11. Example of power consumption of a water heater.

For cycle duration, "Continuous" means that the appliance operates consistently without defined cycles, while "Varies" indicates that the duration of the appliance's operating cycle can change significantly based on usage patterns and settings. The frequency of peaks characterizes whether a consumption pattern is consistent or periodic. "Low" indicates stable power usage, "Moderate" reflects periodic increases in power consumption, and "High" indicates regular significant power usage fluctuations.

Finally, the values of power consumption variance indicate that "Low" corresponds to a relatively stable pattern with minimal fluctuations, "Moderate" reflects variations in power consumption due to changes in operating states, and "High" reflects significant fluctuations in power consumption, often due to different operational phases or cycles. This detailed analysis serves as a foundation for generating simulated data that can be used to train and validate advanced anomaly detection algorithms.

Table 1. Statistical Features of Power Consumption for Various Home Appliances.

Appliance	Mean Power Consumption	Peak Power Consumption	Cycle Duration (Avg)	Frequency of Peaks	Power Consumption Variance
Fridge	Low	Moderate (Compressor, Defrost)	Continuous	Moderate (Periodic Peaks)	Low
Washing Machine	Moderate	High (Heating, Spinning)	1–3 h	High (Cyclical Peaks)	High
Dishwasher	Moderate	High (Wash, Dry Phases)	1–2 h	High (Multiple Phases)	High
Dryer	High	High	1–1.5 h	Low (Consistent)	Moderate
Water Heater	Low (Idle)/ High (Heating)	High	Varies	Low (Heating Spikes)	High

3.4. Simulation Techniques

In this section, the simulation techniques used to generate the simulated anomaly datasets are presented. These techniques involve algorithms designed to identify sequences of normal power consumption, introduce simulated errors, and create a comprehensive dataset of power consumption anomaly patterns.

Different workloads can influence the operational efficiency and power consumption patterns of appliances, such as washing machines and dishwashers, leading to different

power consumption patterns as well as anomaly patterns. Varying usage scenarios, including differences in load sizes, fabric types, and settings, result in changes in energy consumption and operational behavior. To address these variations, different workload scenarios in the analysis and simulation algorithms should be used.

3.4.1. Methodology Overview and Application to Diverse Appliance Types

The proposed methodology for simulating anomaly patterns in home appliance power consumption involves several key steps, as depicted in Figure 12, which provides a comprehensive flow chart of the process. This methodology is designed to be applicable across a wide range of home appliances, each with unique power consumption characteristics.

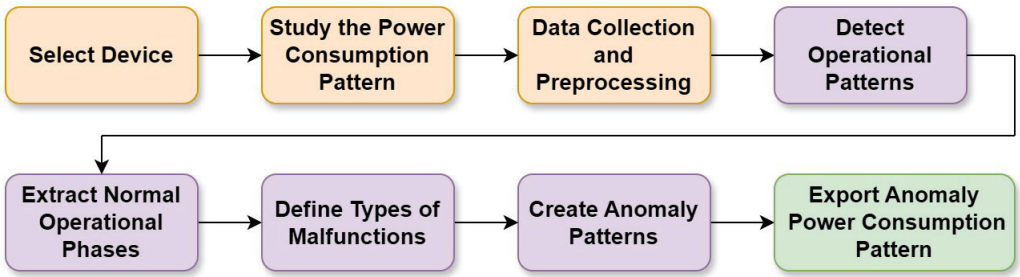


Figure 12. Flow chart of the proposed methodology for simulating anomaly patterns.

Select Device and Study the Power Consumption Pattern: The process begins with selecting a specific device, followed by a detailed study of its power consumption pattern. This step is crucial for understanding the normal operational behavior of the appliance, which varies significantly between different types of devices. For example, refrigerators display consistent patterns with regular cycles of high power consumption when the compressor is running, while washing machines exhibit distinct peaks during specific intervals of a washing cycle. This stage ensures that the model is not limited to a specific set of home appliances, allowing the approach to be generalized to other types of devices, ensuring that the model has sufficient scope.

Data Collection and Preprocessing: A key aspect of the methodology is the collection and preprocessing of time-series power consumption data. This step involves cleaning the data to remove outliers, filling in missing values, and ensuring consistency in data granularity, typically set at a one-minute interval. This preprocessing step is essential for managing the data's variability and noise, which are common in real-world environments. Importantly, this process is conducted offline, meaning that the data preprocessing is performed locally rather than in real-time. This approach allows for more thorough and robust data handling, free from the constraints of real-time processing. Consequently, the preprocessed data, once cleaned and structured, can then be utilized effectively in real-time applications. By implementing these robust preprocessing techniques, the model's ability to handle diverse and noisy data is significantly enhanced, making it well-suited for practical, real-time applications.

Detection of Operational Power Consumption Pattern: After preprocessing the data, the next step is to detect the operational power consumption pattern of each appliance. This involves analyzing the power consumption data and dividing the data into distinct subsequences that correspond to the various operational patterns of the device. For example, refrigerators typically exhibit a consistent daily pattern due to their regular cooling cycles, while washing machines show power consumption only during specific intervals when a washing program is running.

Extraction of Normal Operational Phases: After identifying the operational cycles, the normal operational phases are extracted. This step focuses on segmenting the power consumption data into distinct sub-sequences that represent the different phases of an appliance's operation, such as the heating, washing, and drying phases of a washing machine.

Definition of Malfunction Types: In this step, different types of malfunctions are defined based on their impact on the appliance's operational phases. Malfunctions are categorized into minor and major types, with each category reflecting a different level of deviation from normal operation. This categorization is crucial for the subsequent simulation of anomaly patterns and allows the model to be applied without the use of labeled data. The specific percentages of energy increase associated with minor and major malfunctions, as well as the percentage increase related to specific types of malfunctions, are derived from the study of the power consumption data in the previous step. This data-driven approach ensures that the model accurately reflects the real-world impact of different malfunctions on energy consumption, thereby enhancing the reliability and applicability of the simulated anomaly patterns.

Creation of Anomaly Patterns: Using the defined malfunction types, anomaly patterns are created by altering the duration and intensity of specific operational phases. For instance, in a washing machine, the heating phase might be extended to simulate a faulty heating element. These simulated anomalies are integrated into the normal consumption patterns to produce a dataset that reflects both normal and faulty operation scenarios.

Export of Anomaly Power Consumption Patterns: The final step involves exporting the simulated anomaly patterns, which can be used for training and testing anomaly detection models.

Overall, This approach addresses the challenge of the limited availability of labeled data by generating a comprehensive set of simulated data that can be used to improve the accuracy and robustness of anomaly detection systems. The proposed methodology can be used for a wide range of home appliances. In this paper, five of the most commonly used home appliances were used to create simulated anomaly datasets.

3.4.2. Fridge

The procedure for simulating anomaly patterns in fridges involves two steps. The first step is identifying each sub-sequence within the total power consumption. A sub-sequence is defined as the duration of power consumption from the moment the compressor is enabled until it is disabled. The detailed procedure is provided in Algorithm 1. The algorithm takes as input the power consumption data organized in a time series. A threshold T is then defined to detect when the compressor is off. This threshold is crucial for accurately identifying the compressor's operational cycles and it was empirically set at 20 watts. This value was chosen based on typical power consumption patterns of fridges, where the power consumption drops significantly below 20 watts during idle phases when the compressor is off. This threshold ensures that only periods of active compressor operation are selected.

Algorithm 1 Detect Sub-Sequences

1: **Input:** Power consumption data y
2: **Output:** List of sub-sequences with power consumption, last positions
3: Define threshold T
4: Identify indices where power consumption y is below threshold T for k consecutive points

$$indices = \{i \mid \forall j \in [i, i+k-1],\, y_j < T\}$$

5: Split data into sub-sequences based on identified indices

$$sub_sequences = \{\text{data}[i:j] \mid i, j \in \text{indices}\}$$

6: Select sub-sequences longer than 5 min

$$selected_sequences = \{s \mid s \in \text{sub_sequences and length}(s) > 5\,\text{minutes}\}$$

7: **Return:** List of sub-sequences with power consumption, last positions

In the next step, the indices in which the power consumption is below T for k consecutive time intervals are identified. The value of k was defined as 2 min. This means that if the power consumption is below the threshold T for more than 2 min, this indicates that the compressor is off, as there is no power consumption attributed to the compressor's operation. The following equation describes the procedure:

$$\text{indices} = \{i \mid \forall j \in [i, i+k-1],\, y_j < T\}, \tag{1}$$

where y is the power consumption data, i is the starting index of the sub-sequence, j is the index within the range of consecutive points, and k is the number of consecutive points below the threshold T.

Subsequently, the power consumption data are split into sub-sequences based on these indices, and only sub-sequences with durations exceeding 5 min are selected. The minimum size of the sub-sequences was set to 5 min. According to [3], the operation cycle of the refrigerator is typically longer than 5 min. Therefore, sub-sequences shorter than 5 min are removed. The following equations describe the procedure:

$$\text{sub_sequences} = \{\text{data}[i:j] \mid i, j \in \text{indices}\}, \tag{2}$$

where $\text{data}[i:j]$ represents a sub-sequence of power consumption data from index i to j.

$$\text{selected_sequences} = \{s \mid s \in \text{sub_sequences and length}(s) > 5\,\text{minutes}\}, \tag{3}$$

where s represents a sub-sequence from the set of sub-sequences. This selection is based on the assumption that the compressor requires more than 5 min of operation to maintain the fridge's temperature as mentioned before.

The outputs are a list of sequences representing continuous power consumption periods below the specified threshold T as well as the last position j of each sub-sequence relative to the input dataset.

The second step involves the simulation of anomaly patterns. In this step, power consumption anomaly patterns are generated. According to [3], most of the total power consumption is consumed when the compressor is enabled. Thus, anomaly patterns are generated during periods when the compressor is enabled. The complete procedure is described in Algorithm 2. The outputs from Algorithm 1 and the user-defined error percentage serve as inputs. For each final position value j, the size of the extension is calculated based on the size of the sub-sequences and the error percentage (e). To calculate the extension, the weighted mean of the last three instances is used, with weights proportional to their values. The following formula was used to calculate the extension values: Given the last n instances of power consumption values $\{x_{p-n}, x_{p-(n-1)}, \ldots, x_{p-2}, x_{p-1}\}$, the weighted mean is calculated as:

$$\text{weighted_mean_last_n} = \frac{\sum_{i=1}^{n} i \cdot x_{p-n+i-1}}{\sum_{i=1}^{n} i}, \tag{4}$$

where n is the number of instances for calculating the weighted mean, $(x_{p-n}, x_{p-(n-1)}, \ldots, x_{p-2}, x_{p-1})$ is the power consumption values at the last n positions in the sequence, and x_{p-k} represents the power consumption value at position $p-k$. In the final step, a random value is added on each weighted_mean_last_n and the output is the anomaly power consumption pattern for each sub-sequence.

Algorithm 2 Simulated Error

1: **Input:** Power consumption data y, last positions P, error percentage e
2: **Output:** Power consumption anomaly patterns
3: **for** each position $p \in P$ **do**
4: Calculate the size of the extension E based on the size of the sequences and the error percentage e

$$E = \text{length of the sequence} \times e$$

5: Calculate the weighted mean of the last three instances with weights proportional to their values to create anomaly patterns

$$weighted_mean_last_n = \frac{\sum_{i=1}^{n} i \cdot x_{p-n+i-1}}{\sum_{i=1}^{n} i}$$

6: Add the anomaly patterns to the sequence at the specific position p

$$y_p = \text{weighted_mean_last_n} \times (1 + \text{random.uniform}(0.001, 0.009))$$

7: **end for**
8: **Return:** Power consumption anomaly patterns for each sub-sequence

3.4.3. Washing Machine, Dishwasher, and Dryer

Algorithms 3 and 4 describe the procedure for creating anomaly patterns in the existing power consumption patterns of washing machines, dishwashers, and dryers. The procedure consists of two steps. The first step is responsible for extracting the heating phases of the consumption pattern, and the second step is responsible for extending the consumption pattern based on the category of malfunctions selected by the user.

Algorithm 3 Extract Heating Phases of a Washing Machine

1: **Input:** Power consumption data y over time x
2: **Output:** Segments with the heating phases
3: Fit a mathematical equation to the power consumption pattern: $f(x)$
4: Calculate the first derivative to find the slopes: $f'(x) = \frac{d}{dx} f(x)$
5: Set a threshold T to keep only the high changes in the pattern:

$$High_Changes = \{x_i \mid y_i > T \text{ and } |f'(x_i)| > 0.5 \times \max(|f'(x)|)\}$$

6: **if** len(High_Changes) $\mod 2 \neq 0$ **then**
7: Recalculate High Changes with reduced threshold:

$$High_Changes = \{x_i \mid y_i > T \text{ and } |f'(x_i)| > 0.2 \times \max(|f'(x)|)\}$$

8: **end if**
9: Filter out indices based on the final threshold
10: **Return:** Segments with the heating phases

Specifically, the input for Algorithm 3 is the power consumption data and the output includes segments with the detected heating phases. Initially, the algorithm fits a mathematical Equation ($f(x)$) to the power consumption pattern. The next step involves identifying the portion of the data that corresponds to the heating phase by calculating the first derivative of the fitted equation, $f'(x) = \frac{d}{dx} f(x)$. Examples of the calculation of the first derivative for a washing machine, dishwasher, and dryer are presented in Figure 13. As can be observed, calculating the first derivative makes it easy to detect when the heating phases start. The starting point of the heating phase is when a big change in the first derivative is observed.

Algorithm 4 Extend Heating Phase

1: **Input:** Heating phase segments, power consumption data, percentage anomaly
2: **Output:** Extended pattern
3: Find the end of the heating phase
4: Calculate the extension based on the percentage anomaly:

$$extension = \text{length of heating phase segments} \times \text{percentage anomaly}$$

5: Extend pattern with random adjustment:
6: **for** each value in the extended segment **do**

7: $adjustment = \text{random.uniform}(0.001, 0.009)$
8: $new_value = \text{last value of the heating phase} \times (1 + adjustment)$

9: **end for**
10: Append the extended segment with the random adjustments to the original dataset

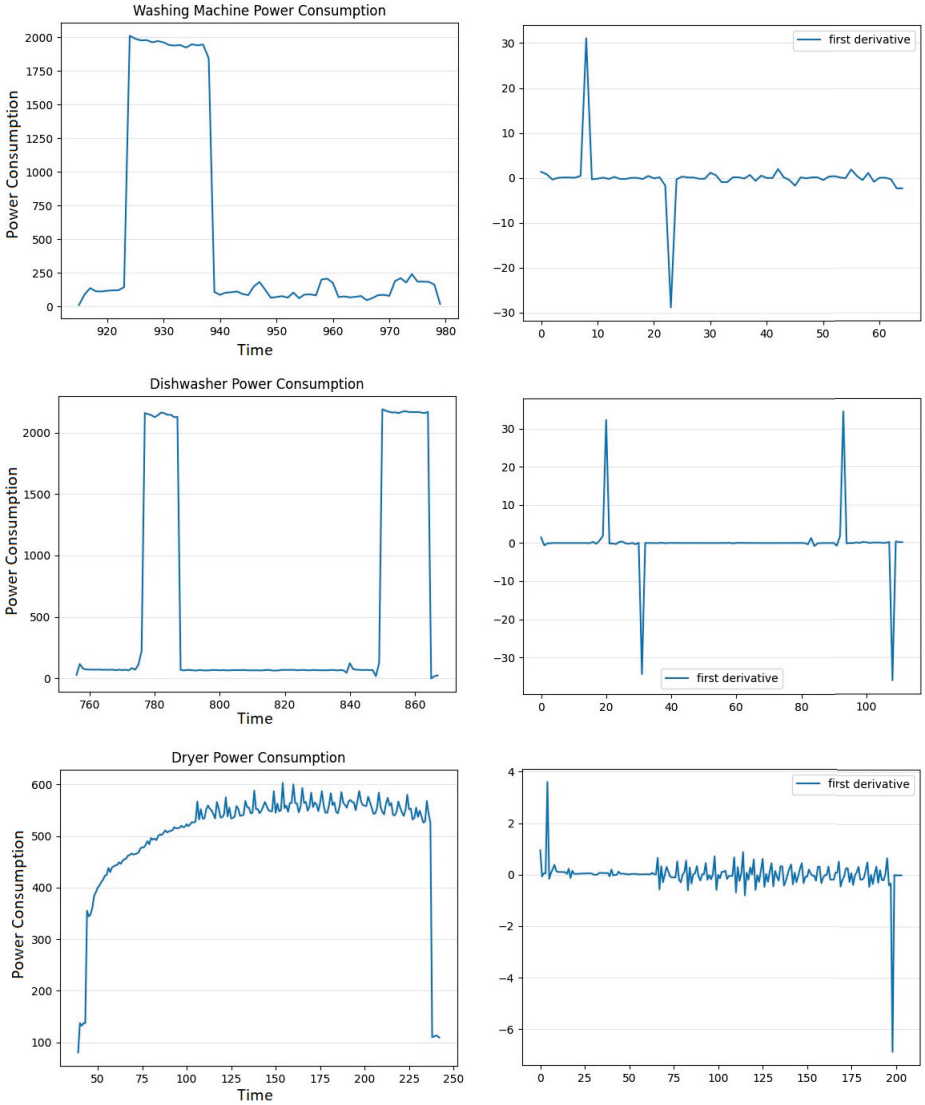


Figure 13. Power consumption and first derivatives of a washing machine, dishwasher, and dryer.

The results of the first derivative analysis are used in the next step to detect when the heating phase starts. A threshold T is set to identify significant changes in the power consumption pattern. For the washing machine and dishwasher, where the high values of

power consumption are very close, the same threshold value of 10 was selected. This value was chosen based on typical power consumption patterns, in which significant power spikes occur during the heating phase. Conversely, for the dryer, where the changes in power consumption values are smaller, a threshold value of 2 was selected. The algorithm then identifies points where the power consumption y_i exceeds the threshold T and where the absolute value of the first derivative $|f'(x_i)|$ is greater than 50% of the maximum absolute value of the first derivative. The following equation describes the threshold:

$$\text{High_Changes} = \{x_i \,|\, y_i > T \text{ and } |f'(x_i)| > 0.5 \times \max(|f'(x)|)\}, \tag{5}$$

where y_i is the power consumption value at time x_i. If the number of identified high-change points is odd, the threshold is recalculated with a reduced value (20% of the maximum absolute value of the first derivative) to ensure an even number of high-change points. It is not possible to have an odd number of high-change points as the heating phase must have both a starting point (enable) and an ending point (disable). Finally, the algorithm filters out indices based on the recalibrated or final threshold to accurately identify the segments of the heating phases.

Algorithm 4 takes as input the segments with the heating phase from the previous algorithm, and the output is an extended consumption pattern that includes the anomaly pattern. The first step involves identifying the endpoint of the heating phase within the power consumption data. Based on the user's input (percentage anomaly), the extension of the existing consumption pattern is then calculated. To determine the values for the new extended values (anomaly pattern), a small random adjustment is applied. Finally, the extended segment, with random adjustments, is appended to the original dataset to form the extended heating phase pattern.

3.4.4. Water Heater

The procedure for simulating anomaly patterns in the water heater focuses on detecting the heating phase, which can be identified using a pre-defined threshold. Unlike other appliances with multiple phases, the water heater primarily has a single heating phase in all patterns. For water heaters, the threshold T was set at 1000 watts. This threshold was chosen because water heaters typically consume a large amount of power during their heating phase, and setting a high threshold ensures that only significant power consumption periods are detected. The process starts by identifying the heating phase within the power consumption data. To identify the heating phase, Algorithm 1 is used.

As input data, the device's power consumption is used, organized in a time series. A threshold T is defined to detect when the heater is in operation. The next step includes identifying indices where the power consumption exceeds the threshold T for consecutive time intervals of 2 min. This means that if the power consumption is above the threshold T for more than 2 min, this indicates that the resistance is on, and the water heater is enabled. Then, the power consumption data is split into sub-sequences based on the identified indices, and only those sub-sequences where the duration exceeds a minimum operational time of 3 min are selected. Only sub-sequences longer than 3 min are selected to ensure that short, insignificant spikes in power consumption are not considered. This duration was chosen based on the typical operational characteristics of water heaters and other home appliances.

The extracted sub-sequences are used as input in Algorithm 4. First, the algorithm identifies the end point of each heating phase within the power consumption data. Then, it calculates the extension size based on the length of the heating phase segments and the specified percentage anomaly selected by the user, determining how much longer the heating phase will be extended to simulate anomalies. Finally, the algorithm extends the pattern by applying a small random adjustment to each value in the extended segment, ensuring the anomalies appear realistic and append the anomaly patterns to the original dataset, forming an extended heating phase pattern that includes the simulated anomaly patterns.

3.5. Time Complexity of the Proposed Methodology

Time complexity is a measure of the amount of computational time that an algorithm requires as a function of the size of the input data [52]. It is a crucial metric for evaluating the efficiency of an algorithm, particularly for real-time applications where rapid processing and quick response times are essential. Estimating the time complexity helps in understanding how the performance of the algorithm scales with increasing data sizes, ensuring that it can handle large datasets efficiently without significant delays.

The time complexity of the proposed methodology can be estimated based on the main steps involved in the simulation of anomaly patterns. An outline of the steps and their respective time complexities is as follows:

I Step 1. Data Preprocessing:
- Removing outliers involves scanning the dataset once, so this step has a time complexity of $O(n)$, where n is the number of data points.
- Filling missing values also requires scanning the dataset, hence $O(n)$.

II Step 2. Identifying Sub-Sequences (Algorithm 1):
- This step involves scanning the power consumption data to identify points below a threshold, which is $O(n)$.
- Splitting data into sub-sequences and selecting those longer than 5 min also requires a single pass through the data, resulting in $O(n)$.

III Step 3. Simulating Anomaly Patterns (Algorithm 2):
- For each sub-sequence identified, calculating the extension size and applying a weighted mean calculation involves constant time operations for each sub-sequence, leading to $O(k)$, where k is the number of sub-sequences.
- Since $k \leq n$, this step can be approximated as $O(n)$.

IV Step 4. Extracting Heating Phases (Algorithm 3):
- Fitting a mathematical equation to the power consumption pattern and calculating the first derivative are operations that depend on the complexity of the fitting algorithm. Assuming a linear or polynomial fitting, this can be carried out in $O(n)$.
- Identifying high-change points and recalculating thresholds involves scanning the data and applying conditions, resulting in $O(n)$.

V Step 5. Extending Heating Phase (Algorithm 4):
- extending the pattern and applying random adjustments involve a single pass through the segments, giving a complexity of $O(m)$, where m is the length of the heating phase segments.
- Since, $m \leq n$, this step is also $O(n)$.

Combining all these steps, the overall time complexity of the proposed methodology can be estimated as $O(n)$, where n is the number of data points in the power consumption dataset. This linear time complexity indicates that the suggested method is efficient and scalable for large datasets. Furthermore implementing optimizations, like parallel processing and efficient data structures, will further enhance performance, ensuring the suggested approach can handle scenarios involving large datasets effectively.

4. Simulation Results and Analysis

In this section, the datasets used for the simulation of anomaly patterns are presented. Specifically, for each device in the experiment set-up, the normal consumption pattern of the device is compared to the simulated anomaly pattern to illustrate the results clearly. In addition, results on the simulation data for each device, along with a statistical analysis, are presented in this section. The analysis includes examining the distribution, frequency, and impact of the simulated anomalies on the overall power consumption patterns. This com-

prehensive evaluation helps in understanding the effectiveness of the anomaly simulation techniques and their applicability in real-world scenarios.

4.1. Dataset

The datasets used for the simulations were collected from various household appliances, namely, fridges, washing machines, dishwashers, dryers, and water heaters. For each home appliance, different setups and workloads were used. Table 2 presents the different parameters used. For the washing machines, a normal washing cycle was selected with three different loads (below half-load, half-load, and full-load). For the dishwasher, the normal program with a water temperature of 50 °C was selected with two load sizes (half-load and full-load). For the fridge, a scenario with an ambient temperature between 18 and 28 °C and an internal temperature between 2 and 4 °C was used. For the dryer, the normal program was selected with a temperature of 60 °C and three different load sizes (below half-load, half-load, and full-load). Finally, for the water heater, three scenarios were selected with three usage frequencies and two different selected temperatures (40 °C and 50 °C).

Table 2. Experimental setup and selected parameters for each appliance.

Appliance	Load Size	Program Settings	Conditions
Washing Machine	Bellow half-load	Normal	Water Temperature: 40 °C
	Half-load	Normal	Water Temperature: 40 °C
	Full-load	Normal	Water Temperature: 40 °C
Dishwasher	Half-load	Normal	Water Temperature: 50 °C
	Full load	Normal	Water Temperature: 50 °C
Fridge	N/A	N/A	Door Opening: Low Ambient Temp: 18–28 °C Internal Temp: 2–4°C
Dryer	Bellow half-load	Normal	Temperature: 60 °C
	Half-load	Normal	Temperature: 60 °C
	Full load	Normal	Temperature: 60 °C
Water Heater	N/A	N/A	Usage Frequency: Low Thermostat: 40 °C
	N/A	N/A	Usage Frequency: Medium Thermostat: 50 °C
	N/A	N/A	Usage Frequency: High Thermostat: 50 °C

Each dataset consists of time-series power consumption data recorded at one-minute intervals. Z-Wave smart plugs (FIBARO Wall Plug (FGWPF-102 ZW5)) were used to collect the power consumption data for each device. Data from nine different houses were collected. The duration of the collected data was 1.5 years and the total number of collected data points for an operational cycle of each fridge, washing machine, dishwasher, and water heater was 43.200, while for each dryer, it was 28.800. Table 3 presents an overview of the experimental datasets. The last row of the table describes the total number of the simulated anomaly patterns derived from Figure 6. Moreover, the datasets were preprocessed to remove outliers, fill missing values, and ensure consistency in data granularity.

Table 3. Overview of the experimental datasets.

Pilots	Fridge	Washing Machine	Dishwasher	Dryer	Water Heater
House 1	✓	✓	✓		✓
House 2	✓	✓			✓
House 3	✓		✓	✓	
House 4	✓	✓	✓		✓
House 5	✓	✓		✓	
House 6	✓	✓		✓	✓
House 7	✓	✓			
House 8	✓		✓		✓
House 9	✓	✓			
Total different Simulated Anomaly Patterns	8	7	8	7	6

4.2. Fridge

Figure 14 illustrates the power consumption of normal and abnormal operations with minor and major errors for the fridge. Minor errors, such as a partially malfunctioning compressor, result in a slight increase in power consumption, with anomalies contributing to a 7.5% increase in mean power consumption. In contrast, major errors, such as a faulty thermostat, lead to a significant increase in power consumption, with anomalies causing a 15.7% rise. The simulation was made for the duration of the cycle, ensuring that the anomalies are realistically integrated into the normal consumption patterns.

Table 4 presents an overview of the data for the fridge. As observed, the mean power consumption during minor error scenarios increased from 38.815 W (normal) to 39.765 W, indicating that minor malfunctions cause a noticeable but relatively small increase in energy usage. The standard deviation and variance in power consumption slightly decreased, indicating that minor errors introduce consistent, low-level increases in energy consumption without causing large fluctuations. Finally, the skewness and kurtosis remained relatively stable, indicating that the distribution of power consumption values did not change significantly, even with the presence of minor errors. In the case of major errors, the mean power consumption increased to 40.707 W, the standard deviation and variance decreased further compared to minor errors, and the skewness and kurtosis remained almost at the same values with minor changes.

Table 4. Overview of the experimental datasets for the fridge.

Statistic	Normal Data	Anomaly Data (Minor)	Anomaly Data (Major)
Mean (W)	38.815	39.765	40.707
Median (W)	0	0	0
Standard Deviation (W)	59.472	58.668	57.881
Variance (W^2)	3537.032	3442.019	3350.252
Skewness	2.860	2.832	2.804
Kurtosis	11.012	11.105	11.193

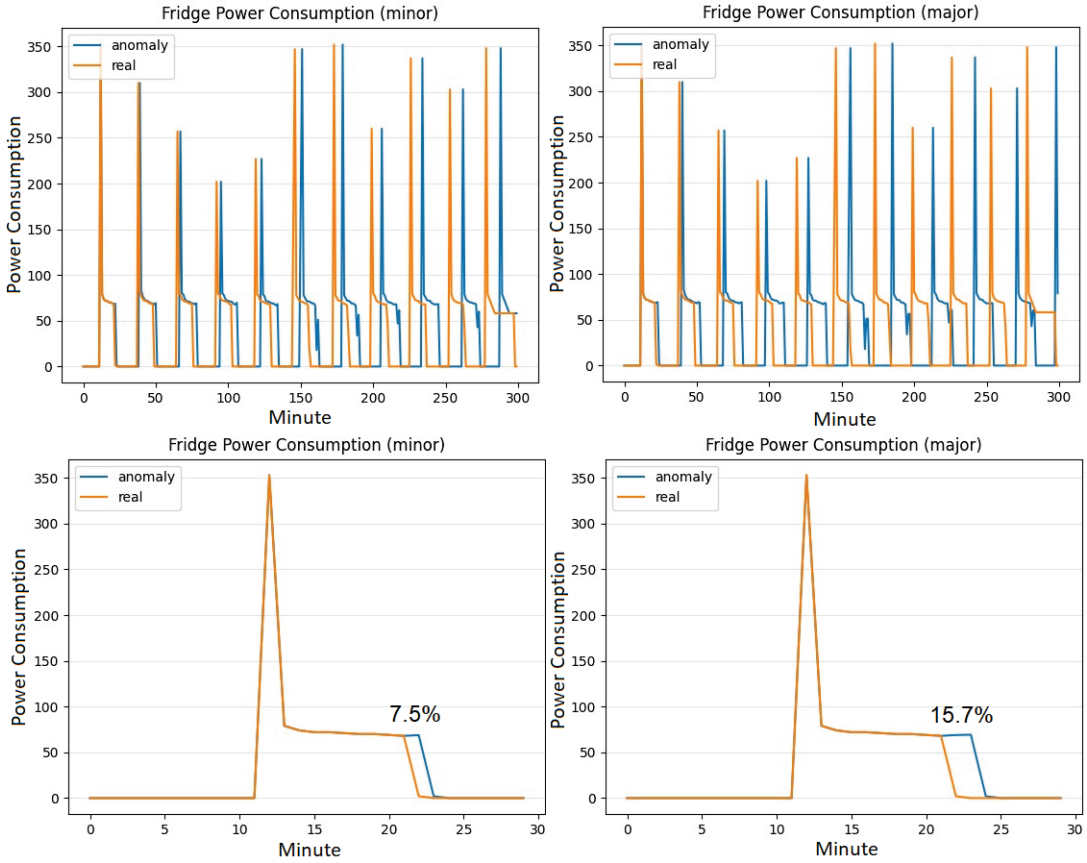


Figure 14. Power consumption of a fridge with minor errors (7.5%) and major errors (15.7%).

To ensure the reliability of the model and the collected experimental data, a series of statistical tests were conducted, including Levene's test for equality of variances and the Shapiro–Wilk test to assess whether the power consumption data follows a normal distribution under different conditions. For Levene's test, comparisons between the variances under normal and minor error conditions, as well as between minor and major error conditions were made. For the comparison between normal and minor error conditions, the null hypothesis (H_0) posits that the variances are equal, while the alternative hypothesis (H_a) suggests that the variances are different. Similarly, the equality of variances between minor and major error conditions was evaluated. The results of Levene's test indicated that there were no significant differences in variances ($p > 0.05$) across these conditions (normal and minor errors $F_{static} = 1.128$, $p = 0.288$, normal and major errors $F_{static} = 0.0662$, $p = 0.912$), supporting the assumption of homogeneity of variances.

For the Shapiro–Wilk test, the null hypothesis (H_0) posits that the data are normally distributed. The tests were conducted for normal operation and minor error, as well as major error conditions. The results of the Shapiro–Wilk test for normal operation ($F_{static} = 0.999$, $p = 0.771$), minor error ($F_{static} = 0.998$, $p = 0.608$), and major error ($F_{static} = 0.998$, $p = 0.612$) conditions indicated that the data follow a normal distribution ($p > 0.05$), justifying the normality of the data distributions.

4.3. Washing Machine

Figure 15 presents the power consumption of a washing machine during normal operation and under conditions with minor errors (10%) and major errors (30%). It can be seen that errors primarily affect the heating phase, which represents nearly 90% of the total power consumption. Minor errors cause a slight increase in power consumption during this phase, while major errors result in a more significant increase.

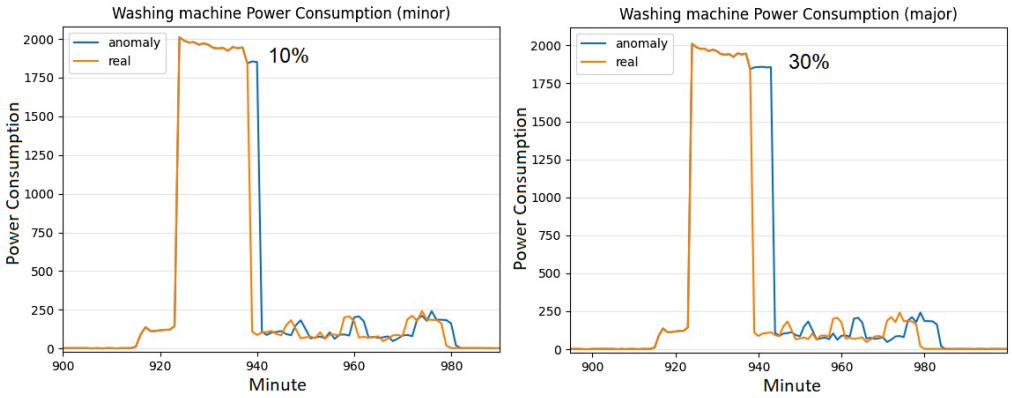


Figure 15. Power consumption of a washing machine with minor errors (10%) and major errors (30%).

Table 5 summarizes the statistical features from data derived from a washing machine. As can be observed, the average power consumption while a minor error occurs increased from 45.805 W to 49.6499 W, indicating that even minor malfunctions result in a considerable rise in energy consumption. The standard deviation and variance in power consumption slightly increased, which means that the presence of minor errors causes some form of variability in energy consumption. The Skewness and kurtosis values decreased slightly, indicating a minor shift in the distribution of power consumption values. For major errors, the mean power consumption increased to 59.940 W, and both the standard deviation and variance increased significantly compared to minor errors. The Skewness and kurtosis values further decreased, reflecting a more substantial shift in the distribution due to major errors.

Table 5. Overview of the experimental dataset for a washing machine.

Statistic	Normal Data	Anomaly Data (Minor)	Anomaly Data (Major)
Mean (W)	45.805	49.649	59.940
Median (W)	2	2	2
Standard Deviation (W)	271.440	283.963	315.162
Variance (W^2)	73,680.04	80,635.217	99,327.303
Skewness	6.936	6.583	5.842
Kurtosis	46.9309	42.029	32.599

To ensure the reliability of the washing machine data, Levene's test for equality of variances, and the Shapiro–Wilk test for normality were conducted. For Levene's test of the comparison between normal and minor errors, the results were $F_{static} = 1.077$ and $p = 0.299$, suggesting no significant difference in variances. However, for the comparison between normal and major error, the test yielded $F_{static} = 27.75$ and $p = 1.47 * e^{-7}$ indicating a significant difference in variances ($p < 0.05$). When Levene's test indicates a significant difference in variances, this suggests that the variability in power consumption is not consistent across different error conditions. This can be due to the different nature and impact of errors on the appliance's operation.

For the Shapiro–Wilk tests, the results for normal operation ($F_{static} = 0.999$, $p = 0.761$), minor errors ($F_{static} = 0.991$, $p = 0.612$), and major errors ($F_{static} = 0.989$, $p = 0.601$) indicated that the data is normally distributed as $p > 0.05$ in all cases.

4.4. Dishwasher

Figure 16 presents the power consumption of a dishwasher with minor (7.5%) and major (35%) errors. Similar to the washing machine, the power consumption increases noticeably with the presence of errors. Minor errors result in a modest increase in power usage during different phases, whereas major errors lead to a higher rise in overall consumption.

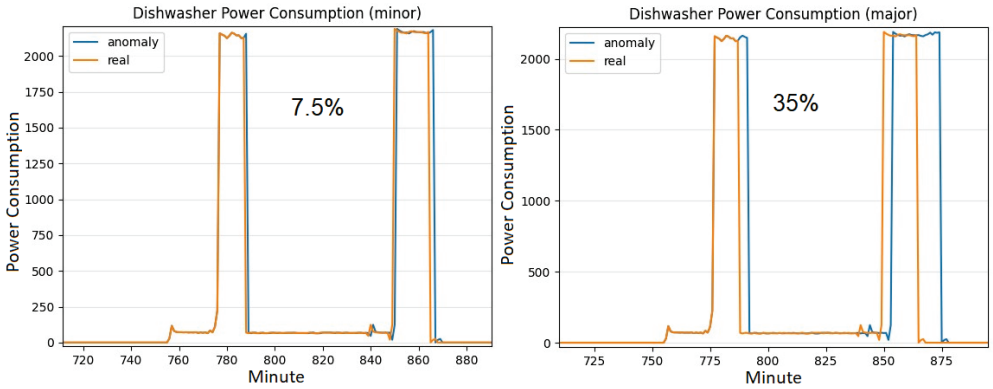


Figure 16. Power consumption of a dishwasher with minor errors (7.5%) and major errors (35%).

Table 6 provides a comprehensive summary of the statistics related to the dishwasher. When minor errors occur, the mean power consumption rises from 43.196 W (normal) to 46.13 W, indicating a moderate increase in energy consumption. This suggests that minor malfunctions result in a noticeable yet relatively small escalation in power usage. Similarly, the standard deviation and variance in power consumption also increase, as some variability is added to the energy consumption pattern with minor errors. A decrease in skewness and kurtosis values indicates a slight alteration in the distribution of power consumption values, indicating a minor shift in the data distribution due to these errors. Conversely, for major errors, a significant increase in the mean is observed, as well as in the standard deviation and variance, indicating a considerable rise in consumption variability. The skewness and kurtosis values decrease further, illustrating a more pronounced change in the distribution of power consumption values due to major errors. These changes underscore the critical effect of major errors, leading to higher energy consumption and greater fluctuations in power usage.

Table 6. Overview of the experimental dataset for a dishwasher.

Statistic	Normal Data	Anomaly Data (Minor)	Anomaly Data (Major)
Mean (W)	43.196	46.13	76.616
Median (W)	0	0	0
Standard Deviation (W)	287.393	297.860	388.938
Variance (W^2)	82,594.825	88,721.146	151,273.000
Skewness	7.205	6.936	5.175
Kurtosis	50.191	46.348	24.874

Levene's test for equality of variances and the Shapiro–Wilk test for normality were conducted for the dishwasher normal, minor error, and major error dataset. For Levene's test and the comparison between normal and minor errors, the results were $F_{static} = 1.605$ and $p = 0.205$, suggesting no significant difference in variances. However, for the comparison between normal and major error, the test yielded $F_{static} = 110.766$ and $p = 1.91 * e^{-10}$ indicating a significant difference in variances ($p < 0.05$). Similar to the previous dataset

of a washing machine, the results of Levene's test suggest that the variability in power consumption is not consistent across different error conditions.

For the Shapiro–Wilk tests, the results for normal operation (F_{static} = 0.999, p = 0.771), minor error (F_{static} = 0.998, p = 0.608), and major errors (F_{static} = 0.998, p = 0.611) indicated that the data are normally distributed as $p > 0.05$ in all cases.

4.5. Dryer

The real and simulated data for minor (7.5%) and major (35%) are presented in Figure 17. The error in this device is detected during the heating phase, which is almost 100% of the total power consumption of a dryer cycle.

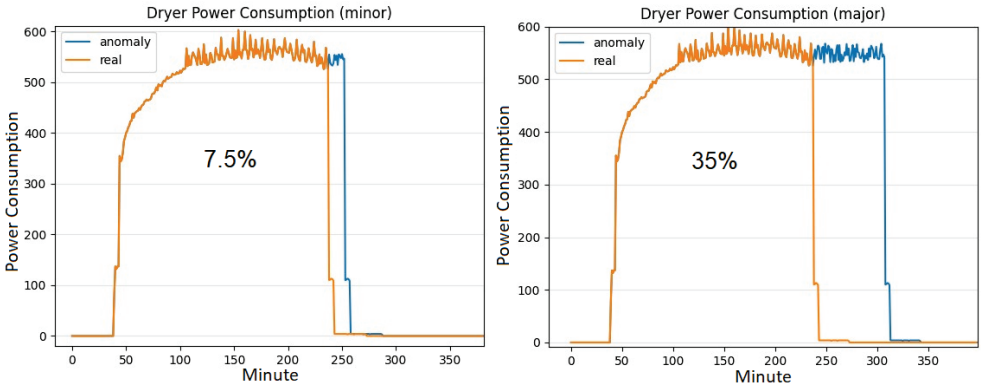


Figure 17. Power consumption of a dryer with minor errors (7.5%) and major errors (35%).

Table 7 presents an overview of the extracted statistical features of an operated cycle of a dryer. For minor errors, the mean power consumption increases from 71.949 W (normal) to 76.910 W, suggesting that minor malfunctions cause a noticeable but modest rise in energy usage. In addition, the standard deviation and variance also increase, indicating variability in the power consumption when minor errors occur. The skewness and kurtosis values decrease slightly, suggesting a minor shift in the distribution of power consumption values. For major errors, a higher increase in power consumption is observed, highlighting the severe impact of these errors on energy usage. The standard deviation and variance show considerable increases, reflecting a greater variability in power consumption. Finally, the skewness and kurtosis values further decrease, indicating a more substantial shift in the distribution.

Table 7. Overview of the experimental dataset for a dryer.

Statistic	Normal Data	Anomaly Data (Minor)	Anomaly Data (Major)
Mean (W)	71.949	76.910	94.032
Median (W)	0	0	0
Standard Deviation (W)	181.005	186.521	203.193
Variance (W²)	32,763.064	34,790.350	41,287.73
Skewness	2.172	2.062	1.736
Kurtosis	2.803	2.329	1.065

As with the other home appliances, to ensure the reliability of the analysis, Levene's test and the Shapiro–Wilk test were applied. Levene's test indicated a significant difference in variances between normal and major error conditions (F_{static} = 16.702 and $p = 4.492 * e^{-5}$). This suggests that the variability in power consumption differs significantly between these

conditions. Conversely, for the comparison between normal and minor errors, Levene's test indicated F_{static} = 1.1315 and p = 0.287, suggesting no significant difference in variances.

The Shapiro–Wilk test results for normal operation (F_{static} = 0.994 p = 0.698), minor error (F_{static} = 0.981, p = 0.178), and major error (W = 0.994, p = 0.612) conditions showed that the data follow a normal distribution ($p > 0.05$).

4.6. Water Heater

Figure 18 shows the power consumption of a water heater under normal conditions and with minor (7.5%) and major (35%) errors. The water heater's power consumption pattern is influenced by its heating phase, where errors cause substantial increases in energy usage.

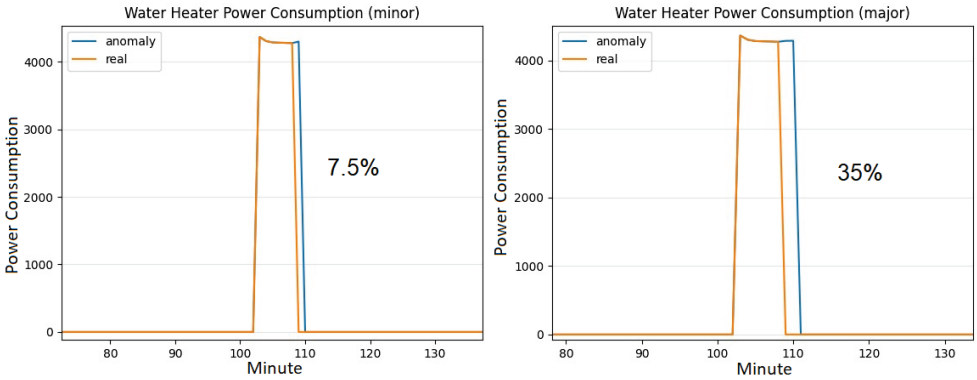


Figure 18. Power consumption of a water heater with minor errors (7.5%) and major errors (35%).

Table 8 presents the statistical features extracted from the 24-h usage of a water heater. With minor errors, the mean power consumption increases from 253.893 W (normal) to 267.699 W. The standard deviation and variance also increase, indicating a moderate rise in energy usage due to these errors. The skewness and kurtosis values decrease slightly, indicating a minor change in the distribution of power consumption patterns. For major errors, the mean power consumption increases significantly to 332.963 W. The standard deviation and variance also increase further. The skewness and kurtosis values further decrease, reflecting a more pronounced shift in the distribution.

Table 8. Overview of the experimental dataset for a water heater.

Statistic	Normal Data	Anomaly Data (Minor)	Anomaly Data (Major)
Mean (W)	253.893	267.699	332.963
Median (W)	0	0	0
Standard Deviation (W)	1007.974	1033.175	1143.125
Variance (W²)	1,016,012.6176	1,067,451.803	1,306,737.0230
Skewness	3.725364	3.60718	3.1474
Kurtosis	11.909	11.0402	7.9272

For the water heater, Levene's test and the Shapiro–Wilk test were conducted to ensure the reliability of the analysis. Levene's test for the water heater showed no significant differences in variances between normal and minor error conditions (F_{static} = 0.765, p = 0.3815) and significant differences in variances between normal and major error conditions (F_{static} = 19.755, $p = 9.131 * e^{-6}$). These results indicate that the variability in power consumption is not consistent across these conditions. The Shapiro–Wilk test results for normal operation (F_{static} = 0.991, p = 0.771), minor error (F_{static} = 0.993, p = 0.609), and major

error (F_{static} = 0.979, p = 0.612) conditions confirmed that the data are normally distributed ($p > 0.05$).

The exported dataset for the presented home appliances, namely, fridge, washing machine, dishwasher, dryer, and water heater, as well as for the minor, major, and specific errors, is available in the GitHub repository https://github.com/AlexisPapaioannou/Power-Consumption-Anomaly-Dataset. The data is organized in csv format files, with comprehensive labels provided for the anomaly power consumption patterns. This dataset serves as a valuable resource for researchers and practitioners in the field, facilitating the development and testing of robust anomaly detection algorithms and predictive maintenance strategies [53].

5. Conclusions

This paper introduced a novel method for simulating error patterns in the power consumption of various home appliances to be used as ground truth for anomaly detection methods. Different home appliances were used, namely, fridges, washing machines, dishwashers, dryers, and water heaters. For each home appliance, an extensive analysis of the different phases that occur during an operational cycle was presented. Different algorithms were developed to create simulated anomaly data for each different type of error for each device. Additionally, an extensive analysis of detected anomaly patterns for each home appliance was presented.

The analysis of the simulated results indicates that the proposed method can accurately replicate the impact of different types of malfunctions on power consumption patterns. This capability is crucial for developing predictive maintenance strategies that can detect and address potential issues before they escalate, thereby improving the reliability and efficiency of home appliances. The statistical analysis of the simulated data highlights the significant shifts in power consumption patterns caused by various error types, underscoring the importance of effective anomaly detection systems in smart home environments.

Regarding future work, more home appliances and more specific errors will be added to cover an even broader spectrum of appliances and error types. Additionally, the challenging task of enhancing the granularity of the simulation to capture more detailed consumption patterns and anomalies will be attempted.

Author Contributions: Conceptualization, A.P., A.D. and S.K.; Data curation, A.P., I.P., A.D. and C.-N.A.; Formal analysis, C.P. and S.K.; Investigation, A.P., A.D., S.K. and C.-N.A.; Methodology, A.P., A.D., C.P., I.P. and C.-N.A.; Software, A.P., A.D., C.P., C.K., E.K., D.I. and D.T.; Supervision, S.K., C.-N.A., C.K. and E.K.; Validation, A.P., A.D., C.P., I.P., S.K., C.K., D.I. and D.T.; Visualization, A.P., A.D., C.P. and I.P.; Writing—original draft, A.P., A.D., C.P. and I.P.; Writing—review and editing, A.P., A.D., I.P., S.K., C.-N.A., C.K., E.K., D.I. and D.T. All authors have read and agreed to the published version of the manuscript.

Funding: This work is partially supported by the HARMONISE project funded by the European Union's Horizon 2020 under Grant Agreement No. 101138595.

Data Availability Statement: The datasets generated and analyzed during the current study are available in the GitHub repository: https://github.com/AlexisPapaioannou/Power-Consumption-Anomaly-Dataset. The repository contains all the necessary files to replicate the analyses presented in this paper.

Conflicts of Interest: The authors declare no conflicts of interest.

References

1. Energy Consumption in Households—Ec.europa.eu. Available online: https://ec.europa.eu/eurostat/statistics-explained/index.php?title=Energy_consumption_in_households (accessed on 4 June 2024).
2. Dimara, A.; Krinidis, S.; Tzovaras, D. activin: A novel non-intrusive activity inference tool. In Proceedings of the 2020 International Conferences on Internet of Things (iThings) and IEEE Green Computing and Communications (GreenCom) and IEEE Cyber, Physical and Social Computing (CPSCom) and IEEE Smart Data (SmartData) and IEEE Congress on Cybermatics (Cybermatics), Rhodes, Greece, 2–6 November 2020; IEEE: New York, NY, USA , 2020; pp. 372–378.

3. Papaioannou, A.; Dimara, A.; Krinidis, S.; Tzitziou, G.; Papaioannou, I.; Michailidis, I.; Anagnostopoulos, C.N.; Ioannidis, D.; Kosmatopoulos, E.; Tzovaras, D. A novel AI-powered method for robust identification of operational phases in refrigerators. *Sustain. Energy Grids Netw.* **2024**, *39*, 101405. [CrossRef]
4. Papaioannou, A.; Dimara, A.; Krinidis, S.; Anagnostopoulos, C.N.; Ioannidis, D.; Tzovaras, D. Advanced proactive anomaly detection in multi-pattern home appliances for energy optimization. *Internet Things* **2024**, *26*, 101175. [CrossRef]
5. Himeur, Y.; Ghanem, K.; Alsalemi, A.; Bensaali, F.; Amira, A. Artificial intelligence based anomaly detection of energy consumption in buildings: A review, current trends and new perspectives. *Appl. Energy* **2021**, *287*, 116601. [CrossRef]
6. Himeur, Y.; Alsalemi, A.; Bensaali, F.; Amira, A. A novel approach for detecting anomalous energy consumption based on micro-moments and deep neural networks. *Cogn. Comput.* **2020**, *12*, 1381–1401. [CrossRef]
7. Himeur, Y.; Alsalemi, A.; Bensaali, F.; Amira, A. Smart power consumption abnormality detection in buildings using micromoments and improved K-nearest neighbors. *Int. J. Intell. Syst.* **2021**, *36*, 2865–2894. [CrossRef]
8. Schmidl, S.; Wenig, P.; Papenbrock, T. Anomaly detection in time series: A comprehensive evaluation. *Proc. VLDB Endow.* **2022**, *15*, 1779–1797. [CrossRef]
9. Himeur, Y.; Alsalemi, A.; Bensaali, F.; Amira, A. Detection of appliance-level abnormal energy consumption in buildings using autoencoders and micro-moments. In *Proceedings of the International Conference On Big Data and Internet of Things*; Springer: Cham, Switzerland, 2021; pp. 179–193.
10. Beagon, P.; Boland, F.; Saffari, M. Closing the gap between simulation and measured energy use in home archetypes. *Energy Build.* **2020**, *224*, 110244. [CrossRef]
11. Athanasiadis, C.; Doukas, D.; Papadopoulos, T.; Chrysopoulos, A. A scalable real-time non-intrusive load monitoring system for the estimation of household appliance power consumption. *Energies* **2021**, *14*, 767. [CrossRef]
12. Villanueva, D.; San-Facundo, D.; Miguez-García, E.; Fernández-Otero, A. Modeling and simulation of household appliances power consumption. *Appl. Sci.* **2022**, *12*, 3689. [CrossRef]
13. Pawar, S.; Mole, P.; Phadtare, S.; Aghor, D.; Vadtile, P. Electricity Forecasting Using Machine Learning: A Review. In *Machine Learning and Information Processing: Proceedings of ICMLIP 2020*; Springer: Singapore, 2021; pp. 127–134.
14. Ouassaid, M.; Maaroufi, M. Smart home appliances modeling and simulation for energy consumption profile development: Application to Moroccan real environment case study. In Proceedings of the 2016 International Renewable and Sustainable Energy Conference (IRSEC), Marrakech, Morocco, 14–17 November 2016; IEEE: New York, NY, USA , 2016; pp. 1050–1055.
15. MathWorks. *MATLAB and Simulink*; 2023b ed.; MathWorks: Natick, MA, USA, 2023.
16. Machorro-Cano, I.; Alor-Hernández, G.; Paredes-Valverde, M.A.; Rodríguez-Mazahua, L.; Sánchez-Cervantes, J.L.; Olmedo-Aguirre, J.O. HEMS-IoT: A big data and machine learning-based smart home system for energy saving. *Energies* **2020**, *13*, 1097. [CrossRef]
17. Diao, L.; Sun, Y.; Chen, Z.; Chen, J. Modeling energy consumption in residential buildings: A bottom-up analysis based on occupant behavior pattern clustering and stochastic simulation. *Energy Build.* **2017**, *147*, 47–66. [CrossRef]
18. Chen, J.; Adhikari, R.; Wilson, E.; Robertson, J.; Fontanini, A.; Polly, B.; Olawale, O. Stochastic simulation of residential building occupant-driven energy use in a bottom-up model of the US housing stock. *arXiv* **2021**, arXiv:2111.01881.
19. Dimara, A.; Krinidis, S.; Ioannidis, D.; Tzovaras, D. Building Performance Simulation. In *Disrupting Buildings: Digitalisation and the Transformation of Deep Renovation*; Springer International Publishing: Cham, Switzerland, 2023; pp. 53–67.
20. Zhao, J.; Lasternas, B.; Lam, K.P.; Yun, R.; Loftness, V. Occupant behavior and schedule modeling for building energy simulation through office appliance power consumption data mining. *Energy Build.* **2014**, *82*, 341–355. [CrossRef]
21. Azar, E.; Menassa, C.C. A comprehensive framework to quantify energy savings potential from improved operations of commercial building stocks. *Energy Policy* **2014**, *67*, 459–472. [CrossRef]
22. Araya, D.B.; Grolinger, K.; ElYamany, H.F.; Capretz, M.A.; Bitsuamlak, G. An ensemble learning framework for anomaly detection in building energy consumption. *Energy Build.* **2017**, *144*, 191–206. [CrossRef]
23. Qian, Y.; Wang, Y.; Shao, J. Enhancing power utilization analysis: detecting aberrant patterns of electricity consumption. *Electr. Eng.* **2024**, 1–16. [CrossRef]
24. Pan, H.; Yin, Z.; Jiang, X. High-dimensional energy consumption anomaly detection: a deep learning-based method for detecting anomalies. *Energies* **2022**, *15*, 6139. [CrossRef]
25. Priyadarshini, I.; Alkhayyat, A.; Gehlot, A.; Kumar, R. Time series analysis and anomaly detection for trustworthy smart homes. *Comput. Electr. Eng.* **2022**, *102*, 108193. [CrossRef]
26. Zamani, S.; Talebi, H.; Stevens, G. Time Series Anomaly Detection in Smart Homes: A Deep Learning Approach. *arXiv* **2023**, arXiv:2302.14781.
27. Pang, G.; Shen, C.; Cao, L.; Hengel, A.V.D. Deep learning for anomaly detection: A review. *ACM Comput. Surv. (CSUR)* **2021**, *54*, 1–38. [CrossRef]
28. Blázquez-García, A.; Conde, A.; Mori, U.; Lozano, J.A. A review on outlier/anomaly detection in time series data. *ACM Comput. Surv. (CSUR)* **2021**, *54*, 1–33. [CrossRef]
29. Jose, E.; Chemmanam, A.J.; Jose, B.A.; Mooppan, A. Detecting Anomalies in Power Consumption of an Internet of Things Network Using Statistical Techniques. In *Artificial Intelligence Driven Circuits and Systems: Select Proceedings of ISED 2021*; Springer: Singapore , 2022; pp. 153–164.

30. Hosseini, S.S.; Agbossou, K.; Kelouwani, S.; Cardenas, A.; Henao, N. A practical approach to residential appliances on-line anomaly detection: A case study of standard and smart refrigerators. *IEEE Access* **2020**, *8*, 57905–57922. [CrossRef]
31. Murthy, A.A.; Subiantoro, A.; Norris, S.; Fukuta, M. A review on expanders and their performance in vapour compression refrigeration systems. *Int. J. Refrig.* **2019**, *106*, 427–446. [CrossRef]
32. Teh, H.Y.; Kempa-Liehr, A.W.; Wang, K.I.K. Sensor data quality: A systematic review. *J. Big Data* **2020**, *7*, 11. [CrossRef]
33. Shaukat, K.; Alam, T.M.; Luo, S.; Shabbir, S.; Hameed, I.A.; Li, J.; Abbas, S.K.; Javed, U. A review of time-series anomaly detection techniques: A step to future perspectives. In *Advances in Information and Communication: Proceedings of the 2021 Future of Information and Communication Conference (FICC)*; Springer: Cham, Switzerland , 2021; Volume 1, pp. 865–877.
34. Sun, Q.; Ke, J.; Dunham, C.; Sim, J.H.; Chen, Y. Using Field-Metered Data to Characterize Consumer Usage Patterns of Residential Dishwashers. *Lawrence Berkeley Natl. Lab.* **2023** .
35. Nieto, F.J.; Aguilera, U.; López-de Ipiña, D. Analyzing particularities of sensor datasets for supporting data understanding and preparation. *Sensors* **2021**, *21*, 6063. [CrossRef]
36. Park, J.; Yun, S.J. Social comparison of home appliance ownership and use and heterogeneous impact on electricity consumption: A case of apartment households in Korea. *Energy Effic.* **2024**, *17*, 44. [CrossRef]
37. Porter, W.A.; Lee, H.J.; Ruppert, K.C.; Cantrell, R.A. Energy efficient homes: Water heaters. *EDIS* **2011**, *2011*. [CrossRef]
38. Topic: Refrigerators—Statista.com. Available online: https://www.statista.com/topics/2182/refrigerators-and-freezers/#topicOverview (accessed on 11 June 2024).
39. Gürel, A.E.; Ağbulut, Ü.; Ergün, A.; Ceylan, I. Environmental and economic assessment of a low energy consumption household refrigerator. *Eng. Sci. Technol. Int. J.* **2020**, *23*, 365–372. [CrossRef]
40. Aloise-Young, P.A.; Lurbe, S.; Isley, S.; Kadavil, R.; Suryanarayanan, S.; Christensen, D. Dirty dishes or dirty laundry? Comparing two methods for quantifying American consumers' preferences for load management in a smart home. *Energy Res. Soc. Sci.* **2021**, *71*, 101781. [CrossRef]
41. Huang, X.M.; Xiong, L.S.; Zheng, Y.W.; Liu, H.Q.; Xu, Y.Z.; Li, Y.C. Comparative investigation of performance of gas dryer and two other types of domestic clothes dryers. *Int. J. Low-Carbon Technol.* **2021**, *16*, 294–304. [CrossRef]
42. Ritchie, M.J.; Engelbrecht, J.A.; Booysen, M.J. Practically-achievable energy savings with the optimal control of stratified water heaters with predicted usage. *Energies* **2021**, *14*, 1963. [CrossRef]
43. Papaioannou, A.; Dimara, A.; Papaioannou, I.; Stefanopoulou, A.; Georgios, L.; Michailidis, I.; Korkas, C.; Anagnostopoulos, C.N.; Kosmatopoulos, E.; Krinidis, S.; et al. An Innovative Methodology for Revealing Home Appliances' Consumption Patterns to Transform Energy Management and Maintenance Strategies. In Proceedings of the IFIP International Conference on Artificial Intelligence Applications and Innovations, Corfu, Greece, 27–30 June 2024; Springer: Cham, Switzerland , 2024; pp. 377–390.
44. Ballestas-Ortega, O.; Villa, J. Failures identification in refrigeration equipment. In Proceedings of the 2020 IX International Congress of Mechatronics Engineering and Automation (CIIMA), Cartagena, Colombia, 4–6 November 2020; IEEE: New York, NY, USA , 2020; pp. 1–6.
45. Purnomoadi, A.; Priambodo, N.; Surya, A.; Tambunan, H.; Jintaka, D.; Tofani, K.; Ridwan, M. Safety for Electric Shower Water Heater installation in Indonesia. In *IOP Conference Series: Materials Science and Engineering*; IOP Publishing: Bristol, UK , 2021; Volume 1098, p. 042047.
46. Tecchio, P.; Ardente, F.; Mathieux, F. Understanding lifetimes and failure modes of defective washing machines and dishwashers. *J. Clean. Prod.* **2019**, *215*, 1112–1122. [CrossRef] [PubMed]
47. Mathias, J.A.; Juenger, K.M.; Horton, J.J. Advances in the energy efficiency of residential appliances in the US: A review. *Energy Effic.* **2023**, *16*, 34. [CrossRef]
48. Angelis, G.F.; Timplalexis, C.; Krinidis, S.; Ioannidis, D.; Tzovaras, D. NILM applications: Literature review of learning approaches, recent developments and challenges. *Energy Build.* **2022**, *261*, 111951. [CrossRef]
49. Yazici, I.; Beyca, O.F.; Delen, D. Deep-learning-based short-term electricity load forecasting: A real case application. *Eng. Appl. Artif. Intell.* **2022**, *109*, 104645. [CrossRef]
50. Kaddour, S.M.; Lehsaini, M. Electricity consumption data analysis using various outlier detection methods. *Int. J. Softw. Sci. Comput. Intell. (IJSSCI)* **2021**, *13*, 12–27. [CrossRef]
51. Atassi, R.; Alhosban, F. Predictive Maintenance in IoT: Early Fault Detection and Failure Prediction in Industrial Equipment. *J. Intell. Syst. Internet Things* **2023**, *9*. [CrossRef]
52. Dutta, A.; Harshith, J.; Soni, Y.; Gupta, A.; Gupta, V.K.; Gupta, A. Computational time complexity for sorting algorithm amalgamated with quantum search. In Proceedings of the 2023 International Conference for Advancement in Technology (ICONAT), Goa, India, 24–26 January 2023; IEEE: New York, NY, USA , 2023; pp. 1–6.
53. Papaioannou, A.; Papaioannou, C. *AlexisPapaioannou/Power-Consumption-Anomaly-Dataset: DOI Version*; Zenodo: Honolulu, HI, USA, 2024. [CrossRef]

Disclaimer/Publisher's Note: The statements, opinions and data contained in all publications are solely those of the individual author(s) and contributor(s) and not of MDPI and/or the editor(s). MDPI and/or the editor(s) disclaim responsibility for any injury to people or property resulting from any ideas, methods, instructions or products referred to in the content.

energies

MDPI

Article

A Comprehensive Approach to Nearly Zero Energy Buildings and Districts: Analysis of a Region Undergoing Energy Transition

Georgios Martinopoulos [1,2,*], Alexandros Tsimpoukis [1], Vasileios Sougkakis [1], Petros Dallas [1], Komninos Angelakoglou [1], Paraskevi Giourka [1] and Nikolaos Nikolopoulos [1]

[1] Chemical Process and Energy Resources Institute, Center for Research and Technology Hellas, Thermi, GR-57001 Thessalonik, Greece; a.tsimpoukis@certh.gr (A.T.); sougakis@certh.gr (V.S.); dallas@certh.gr (P.D.); angelakoglou@certh.gr (K.A.); giourka@certh.gr (P.G.); n.nikolopoulos@certh.gr (N.N.)
[2] Merchant Marine Academy of Macedonia, Néa Michanióna, GR-57004 Thessaloniki, Greece
* Correspondence: g.martinopoulos@certh.gr

Abstract: This paper explores the development of positive energy communities using Eordaia, Greece, as a case study. The approach combines building and district-level energy analysis to achieve nearly zero energy performance through retrofitting, district-level storage systems, and renewable energy technologies. A parametric analysis utilizing RETSCREEN Expert and EnergyPlan software determines the optimal mix of technologies based on technical and financial parameters, with Eordaia, a region in energy transition and part of the RESPONSE Horizon project, illustrating the practical benefits. It includes a neighborhood of 105 mixed-use properties and two municipal buildings where a range of renewable energy sources and energy efficiency measures are applied. Insulation, photovoltaic systems, LED lighting, predictive thermostats, and windows coated with nanotechnology are some of the key interventions considered. The findings show considerable reductions in CO_2 emissions and energy use, with payback periods ranging from 8.7 to 9.6 years. This study underscores the value of district-level strategies over individual building retrofits, highlighting cost savings and improved energy performance. These findings offer valuable insights for urban planners and policymakers aiming to transform urban areas into sustainable, positive energy districts, supporting the EU's 2050 net-zero emissions goals.

Keywords: positive energy; energy efficiency; smart and green buildings and districts; urban development; sustainability; retrofitting; renewable energy

1. Introduction

The ambitious goal of the European Union is to reach net-zero greenhouse gas (GHG) emissions by 2050. As of 2023 [1], the EU revised goals for 2030 aim to raise the share of renewables in the EU's final energy consumption to 42.5% and set an ambitious energy efficiency target of reducing final energy consumption by at least 11.7% [1] compared to the projected energy use for 2030 (based on the 2020 reference scenario). The building sector, responsible for over 35% [2] of GHG emissions, will play a crucial role in achieving these goals.

Although there is a continuous emphasis on increasing energy efficiency at the building level, there is a growing recognition of the importance of improving energy performance at the community level. Urban regions play a critical role in achieving emissions targets, as they are responsible for 70% of GHG emissions and two-thirds of energy consumption [3]. Furthermore, cities accommodate approximately 75% of the EU's population, a figure projected to increase to 80% by 2050 [4].

Near Zero Energy Districts (NZED) have emerged as a promising approach to reducing energy consumption and carbon emissions at the district scale. Several studies have explored various aspects of NZED, including the impact of urban morphology on building energy performance [5], the use of urban sustainability simulations and building energy

modeling [6], and the assessment of district-scale energy modeling tools [7] and certification schemes [8].

Synnefa et al. [9] examined four Net Zero Energy (NZE) settlements located in Cyprus, France, Italy, and the UK, revealing that these settlements were cost-effective and achieved both energy use and renewable energy production targets. Hachem [10] investigated how design elements can affect the performance of solar communities and successfully reduce GHG emissions. In Hachem-Vermette et al. [11], solar thermal, borehole energy storage, and photovoltaic technology were explored to produce energy in excess of consumption within a neighborhood in Canada. The financial implications associated with NZE settlements were also investigated by Isaac et al. [12], who developed a model for optimizing renewable technologies. This study revealed that although urban density had a complicated effect on costs, larger communities could still demonstrate energy savings. In evaluating retrofit techniques for enhancing the performance of NZEB, Paduos and Corrado [13] identified substantial cost savings alongside significant reductions in non-renewable energy consumption.

District-level energy system planning often requires optimization and iterative calculation methods. Evins [14] and Allegrini et al. [15] emphasized the importance of tools that facilitate decision-making in district energy modeling during the initial phases of planning. To assess the energy positivity of neighborhoods in Finland and France, Ala-Juusela et al. [16] employed a decision support tool defining positive energy communities as ones having an annual energy consumption that is less than the locally produced renewable energy. Rehman et al. [17] created a positive energy community model optimized for life-cycle cost and electricity import, integrating district heating, wind turbines, photovoltaic cells, and electric vehicles tailored to the Nordic environment. Angelakoglou et al. [5] proposed a model to assess the feasibility of the transition of districts to Nearly Zero Energy Districts (NZEDs), based on locally produced RES, identifying thresholds in terms of climate, population density, and solar efficiency, among other factors. Saarlos et al. [18] provided a techno-economic assessment applying NZED design principles to the National Western Center in Denver, USA, emphasizing strategies for maximizing solar potential and renewable thermal energy utilization. Iturriaga et al. [19] on the other hand, presented an optimization methodology for drafting renovation strategies at the district level, utilizing the Mixed Integer Linear Programming (MILP) model. Sougkakis et al. [20] investigated the feasibility of near-zero and positive energy communities in the Greek context providing a methodology grounded on technical and economic criteria.

The EU's shift to a carbon-neutral economy depends heavily on cities since they serve as hubs for innovation and present opportunities for systemic local transformation despite the inherent challenges this entails. The European Strategic Energy Technology Plan encourages the use of positive energy blocks and smart cities, utilizing building synergies to provide energy-efficient lighting, heating, and cooling [21].

This paper provides a holistic framework that goes beyond individual building retrofits, examining district-wide energy interventions. This district-level focus allows for optimization across multiple buildings, which is often more efficient and cost-effective than isolated building retrofits.

It presents the application of a comprehensive methodology originally developed by Sougkakis et al. [20] for evaluating and recommending various interventions to improve energy efficiency at various scales ranging from single buildings to entire districts within the Municipality of Eordaia, Greece, a Fellow City in the RESPONSE Horizon project [22].

By applying parametric analysis, this study identifies the optimal combination of energy technologies tailored to both technical performance and financial feasibility. This approach ensures that the proposed interventions are not only energy-efficient but also economically viable, which is crucial for wider adoption in real-world applications.

Eordaia serves as a case study to demonstrate and discuss the applicability and usefulness of the proposed methodology. By quantifying the CO_2 reductions and payback periods, the paper provides practical insights for policymakers and investors, aligning the findings with financial and environmental sustainability goals. This evidence-based

approach helps justify initial investments by demonstrating the long-term cost savings and emissions reductions achievable.

The methodology incorporates data-driven modeling and Key Performance Indicators (KPI) to identify and replicate effective energy solutions, providing urban planners and city officials with a tool to evaluate different strategies to improve energy performance, taking also into consideration the Smart Readiness Indicator of the buildings.

Overall, this study provides a robust template for PED development, offering insights and data that can guide the implementation of similar projects across the EU and beyond, making it a valuable addition to both academic and practical efforts in sustainable urban development.

2. Methodology

The methodology encompasses two distinct levels of analysis: the first at the building level aimed at achieving Positive Energy Buildings (PEB) and the second at the district level aiming at achieving Positive Energy Districts (PEDs). Each level follows a systematic step-by-step process that includes data collection and the identification of the most appropriate retrofit solutions.

2.1. Methods of Retrofitting Analysis and Selected Software Tools

The process for assessing energy upgrades is outlined in the following steps and in Figure 1. Steps 1 to 5, referring to the building level analysis, should be repeated for different typologies of buildings within the examined district:

1. **Data Collection.** Data related to the building's envelope and electromechanical systems are collected through an in situ inspection to ensure understanding of existing conditions, such as:
   - The building's location, occupancy schedule, thermostat settings, and the fuel types that are consumed by the building during its use (e.g., natural gas, electricity, etc.)
   - Specifications of the heating and cooling systems installed in the building, i.e., heat pumps, boilers, district heating system, etc.
   - The end-uses, which consume energy and/or result in heat gains in the building. This involves information on the building envelope (walls, floors, roofs, windows, etc.) infiltration rates and ventilation losses, lighting gains, equipment gains, etc.
   - Specifications for any renewable systems installed in the building.
2. **Baseline Condition.** The baseline energy condition of the building is required and is determined through energy simulations. A suitable software, RETScreen Expert v.9 [23–25], is selected for the simulations at the building level, combining ease of use and the capacity to model a wide range of building technologies. This tool has been utilized in many studies focusing on the assessment of the energy performance of buildings, effectively accounting for the performance of various RES and energy efficiency technologies [20,26,27]. Due to its ease of use, RETScreen Expert can also be employed by non-experts, such as municipal officials.
3. **Smart Readiness Indicator (SRI) Calculation.** The Smart Readiness Indicator (SRI) is calculated for the buildings based on the available energy systems. The SRI evaluates the smart readiness of buildings by assessing their capability to perform three key functionalities: optimize energy efficiency, adapt operations to meet occupant needs, and respond to signals from the grid [28].
4. **Identification of RES technologies.** Innovative energy efficiency and renewable energy sources (RES) technologies are identified for potential installation in the buildings. The selection of the retrofitting measure includes both conventional and innovative technologies drawn from a curated pool of options demonstrated by the RESPONSE project [29].
5. **Performance Simulation Post-Retrofit.** Following the calibration of the model and identification of the applicable technologies, the performance of the building after the energy retrofit is simulated. The calibration of the model was concluded by comparing the results of the simulation for the initial state of the buildings with their energy

consumption (based on the energy bills) from the previous 2 years. The time step of the analysis was on a monthly basis. Then, the SRI is recalculated, taking into consideration the technologies to be integrated into the buildings.

6. **Estimation of District Energy Requirements.** The energy requirements for the entire district are estimated by aggregating the energy needs of residential, commercial, and other buildings within the designated area.
7. **EnergyPLAN Analysis.** The total annual district energy demand, expressed in terms of heating, cooling, and electricity obtained from the previous step, serves as the input for conducting the analysis using the EnergyPLAN software v16.22 [30]. This tool is specifically designed for conducting district energy analyses and can create detailed energy models at national or regional levels, offering a user-friendly interface that facilitates these processes.
8. **Key Performance Indicators (KPI) Calculation.** Finally, key performance indicators (KPI) are calculated to evaluate PEDs performance before and after the energy retrofit, providing a quantifiable measure of the improvements achieved through the implemented retrofit measures. The analysis of the KPIs provides valuable insights into the effectiveness of the various technologies and helps identify those that can contribute to the development of PEDs, leading to informed decision-making at the district scale.

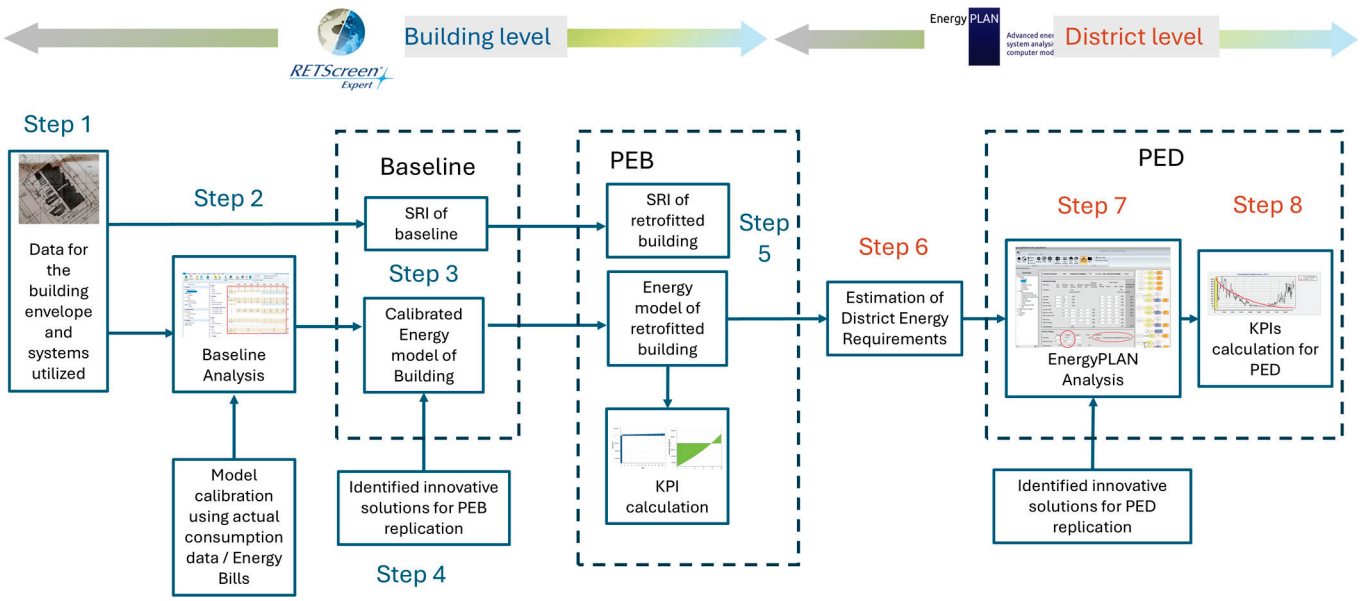


Figure 1. Flow chart of methodology for energy analysis at both the building and district levels.

2.2. Techno-Economic Assessment

Following the building and district-level processes aimed at achieving PEB and PEDs, respectively, a simplified techno-economic assessment is performed to evaluate the performance of the retrofit measures. The assessment incorporates three key indicators: the degree of energetic self-supply (DE) from renewable energy systems (RES), the payback period, and the reduction of CO_2 emissions. The degree of energetic self-supply through RES is measured by the ratio of on-site energy production from RES to the total energy consumption over a defined period [31].

$$DE_E = LPE_E / EE_C, \quad (1)$$

where

LPE_E = locally produced electrical energy (kWh/year),
EE_C = electrical energy consumption (kWh/month or kWh/year).

Following this, the static payback period (EPP) is defined as the energy-related investment cost over the difference between the total annual costs (TAC) after the energy-related investment (TAC_{after}) and the total annual costs before the investment (TAC_{before}).

$$EPP = ERI/m, \quad (2)$$

where

ERI = energy-related investment (EUR)

$m = TAC_{after} - TAC_{before}$ (EUR/year)

TAC_{after} = total annual costs (or revenues) after the energy-related investment (EUR/year). In the case of revenues, when energy exports exceed energy imports, the TAC_{after} receives a negative sign.

TAC_{before} = total annual costs before the energy-related investment (EUR/year).

The total annual cost is calculated by summing costs associated with heating, cooling, and electricity. These costs are calculated by multiplying each type of energy consumption by its corresponding energy vector price.

Finally, emissions reduction is defined as the difference between the amount of CO_2 emitted after the implementation of energy efficiency measures and the CO_2 emitted in the baseline scenario. The emissions are calculated by multiplying the energy consumption by national coefficients of carbon dioxide emissions per unit of energy, which can vary by country [32]. In this paper, the relevant coefficients for the Greek energy mix utilized are 0.347 kg CO_2 per kWh of thermal energy delivered by the district heating network and 0.989 kg CO_2 of electrical energy supplied from the grid [33].

3. Case Study in the Municipality of Eordaia

This section provides a detailed description of the application of the above methodology for the case study of the Municipality of Eordaia. The Municipality of Eordaia, located at the center of the lignite basin of Western Macedonia, has a population of 42,515 people (according to the 2021 census) [34]. Eordaia was the first municipality of Greece to join the Covenant of Mayors in 2008, and it approved its Sustainable Energy Action Plan (SEAP) in 2016. A recent revision, now termed Sustainable Energy and Climate Action Plan (SECAP), has been prepared to incorporate climate change adaptation measures. As one of four pilot projects under the Platform on Coal Regions in Transition, Western Macedonia is focusing on initiatives to facilitate a gradual transition to the meta-lignite era. The region has a continental climate, characterized by cold winters and hot summers, with an average annual air temperature of 12 °C. Additionally, a district heating network is operated within the municipality.

In the Municipality of Eordaia, several renovation measures were evaluated at the building and district levels. The municipality identified ten municipal buildings to assess the feasibility of implementing deep-energy renovations aimed at achieving nearly Zero Energy Building performance levels, two of which are included in the current study. In addition, a neighborhood in the city center was selected for achieving PED status by applying and evaluating energy upgrade measures. The selected municipal buildings and the PED area are illustrated in Figure 2.

3.1. Overview of the District's Building Characteristics

The selected PED area is in the city center and comprises 105 mixed-use privately owned (non-municipal) buildings, including residential and non-residential structures, as well as two municipal buildings: the Commercial Polycenter and the Municipal Library. An in situ inspection assessed the key characteristics of the non-residential building, including usage, useful area, number of floors, geometry, and age, to determine the energy requirements of the neighborhood in its baseline condition prior to any renovation measures examined.



Figure 2. Aerial view of Eordaia where the identified residential neighborhood (yellow box) with the two municipal buildings is presented.

Among the non-municipal buildings, eighty-eight are classified as residential, twelve as commercial (including shops and supermarkets), three as offices, one as a bank, and one as a hotel. Most buildings (60%) have three or more floors, while the rest have one to two floors. The total gross area of the PED was 68,617 m^2, which includes 46,284 m^2 of residential space, 15,913 m^2 for shops, 680 m^2 for supermarkets, 2592 m^2 for offices, 364 m^2 for the bank, and 1136 m^2 for the hotel. In addition, non-heated buildings, including abandoned structures, parking, and storage spaces, accounted for 2328 m^2.

Residential buildings were clustered into four groups, based on their year of construction, with a representative building selected from each group. These four representative buildings of each group align with typical building typologies for the region (Climatic Zone D) as defined by the TABULA Web Tool [35]. According to TABULA, buildings in Greece are grouped into four main categories based on the year of construction: (1) buildings constructed until 1980, (2) buildings from 1981 to 2000, (3) buildings from 2001 to 2010, and finally buildings constructed after 2011. The selected representative buildings from the PED are Building 27 (Tabula MFH-04), Building 57 (Tabula SFH-01), Building 59 (Tabula MFH-02), and Building 69 (Tabula MFH-03). The main characteristics of these buildings and the corresponding TABULA typologies are presented in Table 1. Data required for the simulations, including materials thermal transmittance, infiltration rate, typical shading coefficients, building element areas, and more, were obtained from the TABULA database.

Table 1. Main characteristics of the selected buildings in each group and corresponding typologies from the TABULA Webtool.

Group	Building	Type	Construction Year	Floors	Floor Area (m^2)	TABULA Building ID
Pre-1980	57	Single-family	1972	2	118	SFH.01
1981–2000	59	Multi-family	1995	5	212	MFH.02
2001–2010	69	Multi-family	2005	5	211	MFH.03
2011–	27	Multi-family	2020	4	118	MFH.04

The municipal buildings included in the assessment are as follows:

- Municipal Library (1953): This building has a total heated area of 288 m^2;
- Commercial Polycenter: A one-story building complex with a roof terrace and a total heated area of 872 m^2;

It is important to note that the assumptions used in the analysis were derived from the relevant national Technical Directive (TOTEE 20701-1:2017 [33]), with the exception of lighting gains, which in some cases were determined through a detailed inventory. In buildings where indoor access was not possible, reference data for the lighting gains were obtained from the Technical Directive. For residential buildings, the occupancy schedule is assumed to be 18 h per day, with internal gains at 4 W/m^2, lighting gains at 6.4 W/m^2, and appliance gains at 2 W/m^2. Lights operate for an average of 4 h per day (yearly average), while domestic hot water is supplied by district heating in winter and by an electric heater in summer, with consumption based on the number of bedrooms in each building at a rate of 27.38 m^3/year/bedroom [33].

Heating in the buildings is supplied by the district heating network of Eordaia, while cooling is provided through split-type air conditioning units. The thermostat settings are maintained at 20 °C during the heating season and 26 °C during the cooling season for all zones, except for corridors where the heating temperature is set to 18 °C.

By inserting all the data in the RETscreen, the consumption levels for electricity and thermal energy are calculated. In order to increase confidence in the simulations, results of the analysis of the two municipal buildings in RETScreen were compared against actual consumption data collected from the energy bills (Table 2). Deviations between the simulation and the actual consumption data for the Municipal Library were from 0.4% for the thermal and 21% for the electrical loads, while the respective deviations in the Municipal Commercial Polycenter were 9.9% and 18.8%, respectively. Such deviations are considered normal as it is common to encounter discrepancies between simulation models and actual building energy performance due to the use of standardized climatic data rather than actual conditions, assumptions regarding occupants, and approximations used in the simulations related to the building envelope and the HVAC systems [36]. A deviation of ±20% in the fuel and electricity consumption is considered a reasonable threshold for confirming that the model is calibrated and suitable for incorporating the innovative solutions discussed in the subsequent sections. Regarding the residential building typologies, due to the lack of actual monitored data, results from the RETScreen analysis were compared to the relevant calculation sheets obtained from the TABULA website [35]. Since the TABULA calculations estimated only the heating load of the buildings, the comparison of the results was based only on this parameter.

Table 2. Energy consumption from bills and simulation results from RETsrceen.

Building	Energy Consumption from Bills and TABULA (kWh/Year)		Simulation Results (kWh/Year)	
	Heat (District Heating)	Electricity	Heat (District Heating)	Electricity
Municipal Commercial Polycenter	365,914	43,308	329,734	51,444
Municipal Library	42,920	16,886	42,761	13,362
Building 27 (Tabula MFH-04)	32,742	-	25,745	-
Building 57 (Tabula SFH-01)	58,141	-	67,124	-
Building 59 (Tabula MFH-02)	143,670	-	147,929	-
Building 69 (Tabula MFH-03)	52,579	-	52,386	-

The baseline scenario is completed by calculating the Smart Readiness Indicator (SRI) for both municipal and residential buildings. SRI [37] is an EU scheme for rating the smart readiness of buildings. It is a key policy tool that will help the evaluation of the impacts of building smartification as well as support the decision-making and action planning as the EU building stock is modernized and becomes more sustainable and smarter. The SRI assesses the ability of a building to operate in such a way as to optimize its energy efficiency and overall performance, its ability to adapt to signals from the grid (energy flexibility), and respond to the needs of the building occupants [38]. The calculation of SRI as well as the methodology is described in detail in [39,40].

In the present analysis, the SRI estimations have been conducted by utilizing the SRI assessment package provided by the European Commission [41]. Method B, Expert SRI assessment, is chosen here for the non-residential municipal buildings as well as the residential buildings of the district. The SRI is calculated for the baseline scenario, i.e., the status of municipal buildings, using the default weighting factors for multicriteria evaluation.

Table 3 presents the total SRI scores for the baseline scenario of all categories of PED buildings. All buildings fall into the "lower than 20%" classification, with SRI scores ranging from 6 to 12%. Notably, the highest SRI score is found at the TABULA building 27, which is the most recently constructed residential building, while the lowest score is assigned to the Municipal Library. Buildings equipped with cooling devices generally exhibit higher SRI scores compared to those lacking such equipment. Overall, the buildings share similar characteristics leading to comparable low SRI results, with the notable exception being the presence of cooling systems, which influences significantly the total SRI score. Consequently, retrofit scenarios are necessary to improve the SRI score of all buildings, including newer ones, since despite having adequate thermal insulation and better heating systems, they still do not meet the criteria to be classified as smart buildings.

Table 3. Total SRI scores for the baseline scenario.

Building	Total SRI Score (%) and SRI Class
Municipal Commercial Polycenter	9.2 (<20%)
Municipal Library	5.5 (<20%)
Building 27 (Tabula MFH-04)	10.5 (<20%)
Building 57 (Tabula SFH-01)	6.3 (<20%)
Building 59 (Tabula MFH-02)	7.3 (<20%)
Building 69 (Tabula MFH-03)	8.3 (<20%)

The next step involves utilizing the previous analysis to facilitate the selection of the most appropriate retrofit scenarios for implementation, tailored to the specific requirements of each building. The following list presents selected retrofitting solutions for the analyzed buildings; however, users of this methodology are encouraged to select options that align with the individual requirements of the buildings under study.

1. **Pergola with bi-facial PVs and conventional rooftop PVs:** Bi-facial photovoltaic (PVs) panels integrated into pergolas, along with conventional rooftop PVs, are proposed as an alternative when exterior space is limited. The BIPV pergolas utilize double-laminated glass with embedded bi-facial cell technology, which helps to minimize roof load and reduce shading on the PV arrays.
2. **Predictive Thermostats:** Predictive thermostats incorporate advanced capabilities featuring a display interface and a data platform [29]. They collect energy data to perform daily consumption calculations using machine learning techniques, allowing for predictive estimates for the remainder of the year. This type of thermostat is estimated to reduce annual heating energy consumption by 7–25% and cooling demand by 15–40% [42]. For the purposes of this analysis, it is conservatively assumed that energy requirements for heating and cooling will be reduced by 15% and 25%, respectively.
3. **Nano-coated four-glazing windows**: Nano-coated four-glazing windows offer exceptional energy efficiency with performance levels 75% better than existing windows. The four-glazing modern nanocoatings on the windowpanes block the radiative heat transfer from the clear sky, with technical specifications that include a U-value of 0.55 W/m^2K and an infiltration rate of 0.5 $m^3/h\ m^2$ according to the Greek Building Code.
4. **LED lights:** Replacing traditional light bulbs with LED lights is a common yet critical retrofit measure that significantly impacts the energy efficiency of buildings.
5. **Conventional retrofit:** A typical yet important intervention is the conventional retrofit, which includes adding insulation to walls, roofs, and floors. Furthermore, older windows are replaced with newer double-glazed windows featuring more insulated frames.

The costs associated with these interventions are presented in Section 3.3.

3.2. Calculating the Baseline Energy Consumption of the District

The energy consumption of the district under study encompasses the aggregated energy consumption of both the municipal and the non-municipal buildings. Energy consumption for non-municipal buildings was estimated separately for residential and non-residential buildings.

The analysis to estimate the energy requirements of each building, including space heating (district heating demand), electricity for cooling, lighting, appliances, and district heating demand for domestic hot water (DHW), was conducted using RETScreen following the methodology outlined in Section 2. The results are presented in Table 4 in terms of specific heat (kWh/m^2) and were subsequently multiplied by the total area of the buildings in each group to calculate the total consumption for the 88 residential buildings (Table 5).

Table 4. Specific energy demand of the four building typologies.

Building	District Heating (Space Heating) (kWh/m^2)	Electricity (Cooling) (kWh/m^2)	Electricity (Appliances/Lights) (kWh/m^2)	District Heating (DHW) (kWh/m^2)	Electricity (DHW) (kWh/m^2)	Total Area (m^2)
57	567.6	20.1	22.5	9.9	3.9	29,755
59	237.1	18.7	22.5	14.2	5.6	11,316
69	127.5	11.2	22.5	21.5	8.4	4859
27	57.2	11.6	22.5	15.7	6.2	354

Table 5. Total energy demand of the residential buildings.

Building	Total District Heating Demand (kWh)	Total Electricity Demand (kWh)
57	17,183,301	1,381,161
59	2,842,673	529,023
69	724,020	204,802
27	25,800	14,241
Total	20,775,794	2,129,227

The calculation of the energy required for non-residential buildings followed a different methodology due to the absence of typical building typologies for comparison (as utilized for residential buildings with TABULA data). Instead, the specific energy demand for each type of use was derived from statistical data obtained from Energy Performance Certificates issued in the city for the period 2011 to 2023 [43]. The following assumptions relevant to Eordaia were applied to convert these values to final energy:

- 100% of space heating demand is covered by the District Heating network.
- 100% of cooling demand is met by Air-Source Heat Pumps.
- The District Heating Network Cover Domestic Hot Water needs from October to May, while electrical heaters cover the remaining DHW demand in the summer. It is assumed that the DH network provides 75% of the annual DHW demand, while the remaining 25% is covered by electrical heaters.
- The primary energy conversion factors were 0.7 for the district heating network and 2.9 for electricity [33].

The resulting final energy demand per category, i.e., heating, cooling, lighting, and DHW is presented in Table 6.

Table 6. Specific final energy demand for the non-residential building uses.

	Final Energy Demand (kWh/m^2/Year)			
Building Use	**Heating**	**Cooling**	**Lighting**	**DHW**
Shops	340.31	23.41	55.31	3.58
Super Markets	143.51	29.04	62.47	0.35
Offices	192.89	15.68	54.37	3.82
Bank	154.71	12.45	48.03	13.44
Hotel	145.57	28.29	97.07	16.68

The final energy consumption for the non-residential buildings, based on the above assumptions and the total area for each building use, is provided in Table 7.

Table 7. Total final energy demand of the non-residential buildings.

	Final Energy Demand (kWh/Year)				
Building Use	**District Heating (Space Heating)**	**Electricity (Cooling)**	**Electricity (Appliances/Lighting)**	**District Heating (DHW)**	**Electricity (DHW)**
Shops	5,184,007	356,609	927,944	40,946	13,648
Super Markets	97,589	19,745	48,884	179	59
Offices	499,959	40,649	171,586	7418	2472
Bank	56,316	4531	17,941	3669	1223
Hotel	165,369	32,141	125,197	14,211	4737
TOTAL	**6,003,242**	**453,677**	**1,291,554**	**66,424**	**22,141**

The total final energy consumption of the district is calculated as the sum of the demands for space heating, cooling, electricity for appliances lighting, and DHW for the 105 neighborhood buildings, comprising both residential (Table 5) and non-residential structures (Table 7), as well as the two municipal buildings (Table 2). The total energy demand of the PED area was determined at 27,217,955 kWh of thermal energy supplied by the district heating network (covering space heating and DHW) and 3,961,409 kWh of electricity (for cooling, lighting, appliances, and DHW).

3.3. Results

This section presents the results of the retrofitting measures for the individual buildings and the overall district. The renovation measures for each building, as well as those within the district, were selected based on their technical suitability and cost-effectiveness. A parametric analysis was performed to identify the most economically viable solutions for each building. Each renovation measure was assessed in isolation, allowing the calculation of the resulting thermal energy savings (from heating and DHW supplied from the district heating network) and electricity savings, along with the associated annual cost savings and payback period for each solution. A summary of the results is presented in Table 8. To estimate the payback period of the technologies examined, the following assumptions were made regarding the cost of the renovation measures and the energy prices:

- **Insulation costs:** Estimated at EUR 50–55/m^2 for the external walls, roofs, and floors based on information provided by installers
- **Window replacement costs:** Set at EUR 250/m^2 (based on information provided by installers)
- **Cost of nano-coated four-glazing windows:** Estimated at EUR 380/m^2 based on manufacturer's data
- **Photovoltaic (PV) system Cost:** Estimated at EUR 1100/kW (a conservative value for Greece) for conventional systems [44,45], and at EUR 1250/kW for the bi-facial PVs installed in pergolas/canopies [46]
- **Cost of LED lights:** Priced at EUR 3 per 10 W lightbulb, based on market data
- **Cost of predictive thermostats:** Ranging from EUR 4000 to EUR 40,000, depending on the size of the building and based on market data

- **Cost of thermal energy:** EUR 0.04/kWh [47]
- **Cost of electricity purchase:** EUR 0.18/kWh, according to billing

Table 8. Payback period (years) of each renovation measure when examined individually in each building.

Building	Conventional Retrofit	LED Lights	Nano Coated 4-Glazed Windows	Predictive Thermostats	PV Canopies	Rooftop PV
Commercial Polycenter	42.3	5.4	65.0	5.1	7.1	-
Municipal Library	21.3	2.7	39.3	15.2	-	4.4
Building 27 (Tabula MFH-04)	50.6	3.8	47.2	8.8	-	4.2
Building 57 (Tabula SFH-01)	10.2	4.2	22.7	5.4	-	4.2
Building 59 (Tabula MFH-02)	17.4	4.1	28.3	8	-	4.2
Building 69 (Tabula MFH-03)	31.6	4.2	28.4	20.5	-	4.2

Based on the results presented in Table 8, the most cost-effective solutions were selected for each building examined for each renovation scenario. In some cases, additional technologies were also selected from the pool of the RESPONSE Innovative Solutions (IS) (even though they were not the most financially attractive) for alternative purposes, such as exploring innovative solutions or due to their suitability when conventional technologies were not technically feasible for installation. A summary of the selected measures applied to each building is provided in Table 9.

Table 9. Selection of measures considered for the renovation in each building ("X" indicates the technology has been implemented to the building, whereas "-" indicates that it has not).

Building	Conventional Retrofit	LED Lights	Nano Coated Four-Glazed Windows	Predictive Thermostats	PV Canopies	Rooftop PV
Commercial Polycenter	-	X	-	X	X	-
Municipal Library	X	X	-	X	-	X
Building 27 (Tabula MFH-04)	-	X	-	-	-	X
Building 57 (Tabula SFH-01)	X	X	-	X	-	X
Building 59 (Tabula MFH-02)	X	X	-	X	-	X
Building 69 (Tabula MFH-03)	X	X	-	-	-	X

The amount of savings in thermal energy and electricity varies considerably depending on the selected measures at each building. The two municipal buildings incorporated photovoltaic (PV) systems, either conventional rooftop panels (Library) or those installed on pergolas/canopies (Commercial Polycenter), to meet all electricity needs. Consequently, the buildings achieved electricity savings of over 100%, resulting in a positive electricity balance where the electricity produced exceeded the net electricity demand on an annual basis (considering net metering). Savings in district heating consumption ranged from modest to substantial, with a reduction from 15% in the Municipal Commercial Polycenter to over 90% in the Municipal Library, depending on the baseline condition and the measures implemented. The thermal and electrical consumption of the two municipal buildings and the four typical buildings (when examined individually) prior to and post renovation are illustrated in Figure 3 below.

A summary of the technical and economic KPIs for all PED building typologies is presented in Table 10.

The smart readiness indicator (SRI) for all the examined buildings was recalculated following the methodology outlined in Section 2. The renovation Scenario aims to retrofit the building towards the Nearly Zero Energy Building (NZEB) standard [48], as introduced by the Energy Performance of Buildings Directive (EPBD). The interventions include the installation of a photovoltaic (PV) system (BAPV/BIPV) and a building management system (BMS) for controlling HVAC systems, lighting, and renewable electricity loads in

all residential and municipal buildings. The cost of the BMS is estimated at 25–80 EUR/m^2. Additionally, a solar thermal system is installed in the residential buildings SFH.01 (57), MFH.02 (59), and MFH.03 (69), with costs ranging from EUR 150 to EUR 500 per person depending on the installation location. The renovation scenario primarily emphasizes the smartification of the buildings rather than an extensive retrofit of the energy systems. Given that there is district heating utilized in Eordaia, significant changes to the heating system are not feasible, except for minor HVAC automation such as occupant detection sensors.

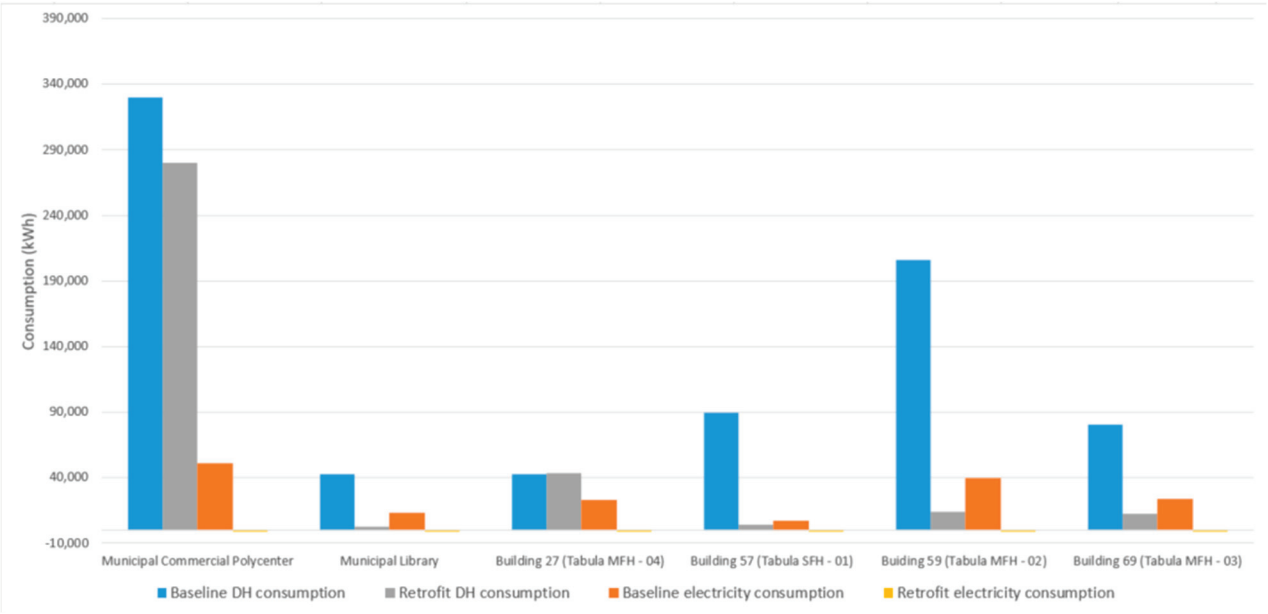


Figure 3. Reduction in thermal and electrical energy consumption in the two municipal buildings and the four residential building typologies.

Table 10. Summary of the technical and economic KPIs.

Building	Total Cost of Measures (EUR)	Total Emission Savings (kg CO_2)	Annual Savings (EUR)	Payback Period (Years)	DE_E
Commercial Polycenter	71,926	68,154	11,259	6.4	100.28%
Municipal Library	48,788	27,892	4147	11.8	106.73%
Building 27 (Tabula MFH-04)	17,932	23,483	4293	4.2	102.20%
Building 57 (Tabula SFH-01)	39,204	37,180	4783	8.2	101.83%
Building 59 (Tabula MFH-02)	161,326	106,171	12,069	13.4	100.50%
Building 69 (Tabula MFH-03)	98,022	47,768	2766	35.4	101.08%

Results for the SRI calculation for municipal and residential buildings are presented in Table 11, including the total SRI score (%), achieved SRI improvement (%), total intervention cost (in EUR), and relative SRI improvement (%) per EUR 5000 invested. Overall, the application of the SRI methodology across the 10 different buildings indicates that all buildings achieve similar SRI scores after the interventions, regardless of their initial status, with scores ranging from 25.7 to 30.8%.

The highest performance in terms of cost-effectiveness is observed in residential buildings 27, 59, 69, and the Municipal Library, which have smaller floor areas and therefore achieve higher value increases from the renovation scenario interventions. Conversely, larger buildings exhibit lower SRI improvements (%) per EUR 5000 invested. The remaining differences among buildings can be attributed to the presence of cooling systems and their associated higher baseline scores.

Table 11. SRI score, class, and cost analysis for renovation scenario.

Building	Scenario (%) and SRI Class	SRI Improvement (%)	SRI Improvement (%/5000 EUR Invested)
Commercial Polycenter	27.1 (between 20% and 35%)	17.9	1.3
Municipal Library	27.1 (between 20% and 35%)	21.6	7
Building 27 (Tabula MFH-04)	30.8 (between 20% and 35%)	20.3	2.3
Building 57 (Tabula SFH-01)	27.4 (between 20% and 35%)	21.1	9.8
Building 59 (Tabula MFH-02)	30.8 (between 20% and 35%)	23.5	1.4
Building 69 (Tabula MFH-03)	30.8 (between 20% and 35%)	22.5	1.5

The investigation into the development of a Near Zero/Positive Energy District involved a parametric analysis that explored various cases that involved different configurations for a range of potential renovation measures. Some of these measures were assessed in individual buildings, while additional measures were also considered to collectively reduce energy consumption in the neighborhood. In total, eight different cases were examined. The specific configurations of these technologies for each case (Cases 1–8) are presented in Table 12 below. The measures evaluated include the following:

- Insulation of the building envelope
- Replacement of old inefficient windows with more efficient options
- Upgrading old inefficient lights with LED lighting
- Installation of rooftop photovoltaic (PV) systems for the generation of renewable electricity
- Implementation of solar thermal systems to produce domestic hot water (DHW), thereby decreasing electrical loads for DHW during the summer months
- Integration of battery energy storage systems, including both conventional and second-life batteries

Table 12. Summary of cases examined in the PED.

Case	Conventional Retrofit	PV (kWp)	BESS (kWh)	Solar Thermal (Units)
Case 1	Building envelope insulation—windows replacement—LED lights	957.35 (30% of available roof area)	0	144
Case 2		1500.19 (45% of available roof area)	0	144
Case 3		2043.03 (60% of available roof area)	0	144
Case 4		2043.03 (60% of available roof area)	1000	144
Case 5		2043.03 (60% of available roof area)	2000	144
Case 6		1137.34 (45% of available roof area)	0	552
Case 7		1680.18 (60% of available roof area)	1000	552
Case 8		1680.18 (60% of available roof area)	2000	552

Conventional retrofit measures, including insulation, window replacement, and the installation of LED lighting to replace the old inefficient lightbulbs, were considered in all cases. In contrast, the capacity of the photovoltaic (PV) systems, the amount of installed solar thermal systems, and the capacity of the battery varied among the different scenarios. The assumptions made to determine the system configuration for each case include:

- Solar thermal systems are already installed in 26% of the neighborhood apartments; the total number of neighborhood apartments is estimated at approximately 552 apartments based on an average dwelling size of 84 m^2 [49] in Greece, with 144 of them already having a solar thermal system installed. Cases 1 to 5 focus only on existing solar thermal system installations, while Cases 6 to 8 include new solar thermal systems. The solar thermal

system has a flat plate glazed collector with an area of 2.5 m^2 and a 160-liter storage capacity, typical for Greek dwellings [50]. In all cases, solar thermal systems were covering all thermal needs of the DHW during the mid-May to mid-October period when the district heating network was not operating. Dwellings with no solar thermal systems were using electrical heaters for the provision of DHW during the summer months. During autumn-winter, the DHW was covered solely by the district heating network.

- In certain cases, collective battery systems were implemented to enhance electrical self-consumption. Collective battery energy storage systems (BESS) with a total capacity of 1000 kWh were considered in Cases 4 and 7, while a capacity of 2000 kWh was evaluated in Cases 5 and 8.
- The total available roof space of the neighborhood's buildings, excluding the area occupied by existing solar thermal systems, is 20,338 m^2. To account for factors such as roof orientations and required spacing to avoid self-shading, the maximum area suitable for installing photovoltaic (PV) panels and/or additional solar thermal systems is limited to 60% of the total available space. Additional PV capacities were examined, with 30% of the available free space considered in Case 1 and 45% in Cases 2 and 6. In scenarios with solar thermal systems (Cases 6–8), the total available roof area was adjusted accordingly, maintaining the 60% limit for PV installation while accounting for the space taken by new solar thermal systems. A standard monocrystalline PV panel, approximately 2.3 m^2 in size with a nominal capacity of 410 Wp, was used as a reference for these PV systems.

The district heating demand for the neighborhood, which includes both space heating and DHW, was estimated at 1,674,064 kWh, while the total electricity consumption amounted to 3,623,677 kWh for Cases 1–5. In Cases 6–8, which included additional solar thermal systems, the DHW demand in the summer months decreased, resulting in a reduction of overall electricity demand to 3,431,053 kWh. These collective thermal energy and electricity demands were then used as inputs in the EnergyPlan software to derive the annual energy balance of the district on an hourly basis. After determining the annual energy balances for the various cases, the technical and economic KPIs were calculated and are presented in Table 13. To estimate the basic economic indicators, additional assumptions were made regarding the costs of renovation measures and electricity prices, including the following:

- Battery system cost: EUR 800/kWh based on information provided from installers
- Solar thermal system cost: EUR 800/unit, based on market data
- Selling price of electricity: EUR 0.06887/kWh [51]

Table 13. Main technical and economic indicators for the cases examined.

Case	Cost (EUR)	Total Cost Savings (EUR/Year)	Payback Period (Years)	CO_2 Reduction (Tons CO_2)	DEE (%)
Case 1	12,389,365	1,383,429	9.0	11,373	30.3%
Case 2	12,932,205	1,470,251	8.8	12,253	36.6%
Case 3	13,475,045	1,544,934	8.7	13,133	39.9%
Case 4	14,275,045	1,573,569	9.1	13,054	48.2%
Case 5	15,075,045	1,598,746	9.4	12,994	55.4%
Case 6	12,895,755	1,443,567	8.9	11,857	33.4%
Case 7	14,238,595	1,551,196	9.2	12,668	46.8%
Case 8	15,038,595	1,573,873	9.6	12,609	53.5%

In all scenarios, the payback periods are notably similar, ranging from 8.7 to 9.6 years, indicating that no case stands out significantly from a financial perspective. In terms of CO_2 emissions reduction, Cases 3–5 demonstrate the most significant reductions, totaling approximately 13,000 tonnes of CO_2 per year, followed by cases 7 and 8. Additionally, cases 5 and 8 exhibit the highest degree of energetic self-supply, achieving 55.4% and 53.5%, respectively.

It is important to note that since all thermal energy is supplied by the Eordaia district heating network, the Degree of Energetic Delf-Supply Thermal (DE_T) is 0% across all cases. To increase DE_T and achieve near-zero energy performance for the district, RES needs to be integrated into the network. A photovoltaic (PV) system providing the required electricity to the boilers has been proposed. With an assumed boiler efficiency of 99% efficiency [52], the estimated annual electricity demand that needs to be met by the PV systems totals 1,809,358 kWh. A 1.3 MW PV power plant is considered sufficient to meet this demand when connected to the grid (utilizing virtual net metering) with a total cost of approximately EUR 1,300,000.

4. Discussion

This study's detailed analysis of renovation measures across individual buildings and the entire Eordaia district underscores the potential of PED strategies, offering a systematic approach to achieve NZED standards. The renovation measures for each building were selected based on their technical suitability and cost-effectiveness, aligning with a broader district-level strategy that emphasizes not only thermal and energy efficiency but also financial viability. The analysis conducted enabled the identification of economically viable solutions for individual buildings by isolating each renovation measure to calculate respective thermal and electrical energy savings, annual cost savings, and payback periods. Such an approach illustrates the importance of evaluating solutions on a per-building basis to achieve optimal outcomes across varied building conditions within a district.

Key findings reveal that the most cost-effective measures were achieved through conventional retrofits, such as insulation upgrades, window replacement, and LED lighting installation, alongside renewable technologies like PV systems. Notably, two municipal buildings achieved electricity savings exceeding 100% due to PV installations, with systems like rooftop panels at the library and PV pergolas at the Commercial Polycenter allowing these structures to achieve a positive energy balance. This demonstrates the effectiveness of renewable integration in urban settings, supporting broader PED goals by showcasing substantial savings and a positive electricity surplus.

Thermal energy savings varied significantly across buildings depending on the existing baseline conditions and renovation measures implemented. For example, district heating savings ranged from modest reductions of 15% in the Commercial Polycenter to over 90% in the library, highlighting how baseline thermal efficiency and targeted retrofits affect energy savings. To capture the added benefits of modernization, this study recalculated the SRI for each building, revealing SRI scores ranging from 25.7% to 30.8% following the interventions. Smaller residential buildings exhibited the highest cost-effectiveness in SRI improvements per investment unit, indicating that floor area plays a crucial role in maximizing SRI value in smaller structures compared to larger buildings.

The case analysis for eight different renovation scenarios within the district revealed that conventional retrofitting measures, such as insulation and efficient lighting, were consistently effective across cases, while the capacity and configuration of PV systems, solar thermal units, and battery storage varied. Collective battery storage was introduced in certain cases to increase self-consumption, achieving a degree of energetic self-supply of over 55% in Cases 5 and 8, which maximized the district's energy independence. Despite similar payback periods across cases (8.7 to 9.6 years), significant differences were observed in CO_2 emissions reduction, with Cases 3–5 showing the highest impact at roughly 13,000 tonnes per year. These findings highlight that while financial feasibility may be consistent, environmental benefits vary substantially depending on technology configuration.

This study also points to district-level limitations, particularly in the degree of energetic self-supply thermal, which remained at 0% across cases due to the district's reliance on an external heating network. This finding suggests that for districts like Eordaia to attain near-zero energy performance, further integration of RES within the district's heating infrastructure is essential. As a proposed solution, a 1.3 MW PV power plant connected through virtual net metering would provide sufficient electricity to offset boiler demands,

thus supporting the district's heating needs sustainably. The feasibility of this measure, estimated at approximately EUR 1,300,000, could provide a model for integrating renewables into urban district heating networks in similar European regions, aiding in achieving broader EU sustainability goals.

Overall, this study emphasizes that district-level energy strategies, combined with building-specific parametric analyses, offer valuable insights into optimizing PED designs, suggesting that such frameworks can effectively guide urban planners and policymakers in achieving financially viable, energy-efficient districts. Future research should expand this framework to diverse urban and rural environments, particularly in varying climatic regions, to assess the transferability of these results across the EU and beyond.

5. Conclusions

This study offers a valuable blueprint for urban planners and policymakers working toward the EU's 2050 net-zero emissions target by developing a replicable framework for PEDs. The results demonstrate the economic and environmental benefits of district-wide energy interventions, including advanced insulation, renewable energy sources, and predictive energy management systems.

The analysis shows that, with payback periods of 8.7 to 9.6 years, these interventions present a financially viable path toward sustainability. Moreover, achieving a degree of energetic self-supply above 55% in optimal scenarios highlights the potential for positive energy communities to enhance urban energy resilience and independence.

While the Eordaia case provides a practical benchmark for transitioning urban areas, future studies should explore the adaptability of these findings in various climates, building typologies, and policy contexts. Expanding the framework to include a range of urban and rural settings as well as diverse economic conditions would provide a more comprehensive understanding of the feasibility of positive energy communities across Europe.

Longitudinal studies examining the long-term effectiveness and adaptability of these energy strategies under evolving technological, economic, and policy conditions would further refine this approach. By advancing district-level strategies for Positive Energy Districts, this research supports sustainable urban development and provides a critical pathway toward meeting ambitious climate goals.

Author Contributions: Conceptualization, V.S., A.T. and G.M.; methodology, V.S. and G.M.; software, V.S. and A.T.; validation, V.S. and A.T.; formal analysis, V.S., G.M. and A.T.; investigation, P.D.; resources, V.S. and P.D.; data curation, V.S. and P.D.; writing—original draft preparation G.M., A.T., V.S. and P.D.; writing—review and editing, V.S., G.M., A.T., K.A. and P.G.; visualization, V.S. and A.T.; supervision, G.M. and N.N.; project administration, G.M. and N.N.; funding acquisition, N.N. All authors have read and agreed to the published version of the manuscript.

Funding: This research was funded by the European Union's H2020 program as part of the RESPONSE project (integRatEd Solutions for POsitive eNergy and reSilient CitiEs), Grant Agreement ID 957751.

Data Availability Statement: Data are available upon request.

Conflicts of Interest: The authors declare no conflicts of interest. The funders had no role in the design of this study; in the collection, analyses, or interpretation of data; in the writing of the manuscript; or in the decision to publish the results.

References

1. Renewable Energy Targets—European Commission. Available online: https://energy.ec.europa.eu/topics/renewable-energy/renewable-energy-directive-targets-and-rules/renewable-energy-targets_en (accessed on 29 August 2024).
2. Greenhouse Gas Emissions from Energy Use in Buildings in Europe | European Environment Agency's Home Page. Available online: https://www.eea.europa.eu/en/analysis/indicators/greenhouse-gas-emissions-from-energy (accessed on 29 August 2024).
3. Luqman, M.; Rayner, P.J.; Gurney, K.R. On the Impact of Urbanisation on CO_2 Emissions. *NPJ Urban Sustain.* **2023**, *3*, 6. [CrossRef]
4. European Commission; Directorate-General for Research and Innovation. *The Human-Centred City: Opportunities for Citizens Through Research and Innovation*; Publications Office of the European Union: Berlin/Heidelberg, Germany, 2019.
5. Komninos, N. Net Zero Energy Districts: Connected Intelligence for Carbon-Neutral Cities. *Land* **2022**, *11*, 210. [CrossRef]

6. Delmastro, C.; Gargiulo, M. Capturing the Long-Term Interdependencies Between Building Thermal Energy Supply and Demand in Urban Planning Strategies. *Appl. Energy* **2020**, *268*, 114774. [CrossRef]
7. Murray, P.; Marquant, J.; Niffeler, M.; Mavromatidis, G.; Orehounig, K. Optimal Transformation Strategies for Buildings, Neighbourhoods and Districts to Reach CO_2 Emission Reduction Targets. *Energy Build.* **2020**, *207*, 109569. [CrossRef]
8. Becchio, C.; Bottero, M.C.; Corgnati, S.P.; Dell'Anna, F. Decision Making for Sustainable Urban Energy Planning: An Integrated Evaluation Framework of Alternative Solutions for a NZED (Net Zero-Energy District) in Turin. *Land Use Policy* **2018**, *78*, 803–817. [CrossRef]
9. Synnefa, A.; Laskari, M.; Gupta, R.; Pisello, A.L.; Santamouris, M. Development of Net Zero Energy Settlements Using Advanced Energy Technologies. *Procedia Eng.* **2017**, *180*, 1388–1401. [CrossRef]
10. Hachem, C. Impact of Neighborhood Design on Energy Performance and GHG Emissions. *Appl. Energy* **2016**, *177*, 422–434. [CrossRef]
11. Hachem-Vermette, C.; Grewal, K.S. Investigation of the Impact of Residential Mixture on Energy and Environmental Performance of Mixed Use Neighborhoods. *Appl. Energy* **2019**, *241*, 362–379. [CrossRef]
12. Isaac, S.; Shubin, S.; Rabinowitz, G. Cost-Optimal Net Zero Energy Communities. *Sustainability* **2020**, *12*, 2432. [CrossRef]
13. Paduos, S.; Corrado, V. Cost-Optimal Approach to Transform the Public Buildings into NZEBs: An European Cross-Country Comparison. *Energy Procedia* **2017**, *140*, 314–324. [CrossRef]
14. Evins, R. A Review of Computational Optimisation Methods Applied to Sustainable Building Design. *Renew. Sustain. Energy Rev.* **2013**, *22*, 230–245. [CrossRef]
15. Allegrini, J.; Orehounig, K.; Mavromatidis, G.; Ruesch, F.; Dorer, V.; Evins, R. A Review of Modelling Approaches and Tools for the Simulation of District-Scale Energy Systems. *Renew. Sustain. Energy Rev.* **2015**, *52*, 1391–1404. [CrossRef]
16. Ala-Juusela, M.; Crosbie, T.; Hukkalainen, M. Defining and Operationalising the Concept of an Energy Positive Neighbourhood. *Energy Convers. Manag.* **2016**, *125*, 133–140. [CrossRef]
17. Rehman, H.u.; Reda, F.; Paiho, S.; Hasan, A. Towards Positive Energy Communities at High Latitudes. *Energy Convers. Manag.* **2019**, *196*, 175–195. [CrossRef]
18. Saarloos, B.A.; Quinn, J.C. Net-Zero Energy Districts and the Grid: An Energy-Economic Feasibility Case-Study of the National Western Center in Denver, CO, USA. *Buildings* **2021**, *11*, 638. [CrossRef]
19. Iturriaga, E.; Campos-Celador, Á.; Terés-Zubiaga, J.; Aldasoro, U.; Álvarez-Sanz, M. A MILP Optimization Method for Energy Renovation of Residential Urban Areas: Towards Zero Energy Districts. *Sustain. Cities Soc.* **2021**, *68*, 102787. [CrossRef]
20. Sougkakis, V.; Lymperopoulos, K.; Nikolopoulos, N.; Margaritis, N.; Giourka, P.; Angelakoglou, K. An Investigation on the Feasibility of Near-Zero and Positive Energy Communities in the Greek Context. *Smart Cities* **2020**, *3*, 362–384. [CrossRef]
21. Communication from the Commission to the European Parliament, the Council, the European Economic and Social Committee and the Committee of the Regions on the Revision of the Strategic Energy Technology (SET) Plan. Available online: https://eur-lex.europa.eu/legal-content/EN/TXT/?uri=CELEX:52023DC0634 (accessed on 4 November 2024).
22. RESPONSE—IntegRatEd Solutions for POsitive ENergy and ReSilient CitiEs. Available online: https://h2020response.eu/ (accessed on 29 August 2024).
23. Owolabi, A.B.; Emmanuel Kigha Nsafon, B.; Wook Roh, J.; Suh, D.; Huh, J.S. Measurement and Verification Analysis on the Energy Performance of a Retrofit Residential Building after Energy Efficiency Measures Using RETScreen Expert. *Alex. Eng. J.* **2020**, *59*, 4643–4657. [CrossRef]
24. Natural Resources Canada RETScreen Software Online User Manual. Available online: https://publications.gc.ca/collections/Collection/M39-114-2005E.pdf (accessed on 1 November 2024).
25. Psomopoulos, C.S.; Ioannidis, G.C.; Kaminaris, S.D.; Mardikis, K.D.; Katsikas, N.G. A Comparative Evaluation of Photovoltaic Electricity Production Assessment Software (PVGIS, PVWatts and RETScreen). *Environ. Process.* **2015**, *2*, S175–S189. [CrossRef]
26. Mukhtar, M.; Ameyaw, B.; Yimen, N.; Zhang, Q.; Bamisile, O.; Adun, H.; Dagbasi, M. Building Retrofit and Energy Conservation/Efficiency Review: A Techno-Environ-Economic Assessment of Heat Pump System Retrofit in Housing Stock. *Sustainability* **2021**, *13*, 983. [CrossRef]
27. Augustowski, Ł.; Kułyk, P. The Economic Profitability of Photovoltaic Installations in Households in Poland from a New Policy Perspective. *Energies* **2023**, *16*, 7595. [CrossRef]
28. Smart Readiness Indicator—European Commission. Available online: https://energy.ec.europa.eu/topics/energy-efficiency/energy-efficient-buildings/smart-readiness-indicator_en (accessed on 29 August 2024).
29. Shemeikka, J. D1.3 "Master City Plans for TA#1 Positive Energy Building Systems" 2021. pp. 1–131. Available online: https://h2020response.eu/wp-content/uploads/2022/05/D1.3-Master-City-Plans-for-TA1-Positive-Energy-Building-Systems.pdf (accessed on 29 August 2024).
30. Lund, H.; Thellufsen, J.Z.; Østergaard, P.A.; Sorknæs, P.; Skov, I.R.; Mathiesen, B.V. EnergyPLAN—Advanced Analysis of Smart Energy Systems. *Smart Energy* **2021**, *1*, 100007. [CrossRef]
31. Tryferidis, A.; Pramangioulis, D.; Kakaras, E.; Tsarchopoulos, P.; Nikolopoulos, N.; Salanova, J.M.; Chrysostomou, K.; Nooij, T.; Crombie, D. D1.1-"Report on the List of Selected KPIs for Each Transition Track". Project Deliverable IRIS. 2018. Available online: https://irissmartcities.eu/wp-content/uploads/2022/01/d1.1_report_on_the_list_of_selected_kpis_for_each_transition_track.pdf (accessed on 29 August 2024).
32. Ministry of Finance, Ministry of Environment Energy and Climate Change Regulation for the Energy Efficiency in Buildings. *Greek Off. Gov. Gaz.* **2017**, *B2367*, 23905–23924. Available online: https://ypen.gov.gr/wp-content/uploads/2020/11/KENAK_FEK_B2367_2017.pdf (accessed on 29 August 2024). (In Greek).

33. Technical Chamber of Greece Technical Directive 20701-1/2017—Analytical National Specifications of Parameters for the Calculation of the Energy Efficiency of Building and the Issuance of Energy Efficiency Certificate, 1st Ed. Available online: https://web.tee.gr/wp-content/uploads/%CE%95%CE%93%CE%9A%CE%A1%CE%99%CE%A3%CE%97-TOTEE-1.pdf (accessed on 29 August 2024). (In Greek).
34. Hellenic Statistical Authority, Census Results of Population and Housing; 2023. Available online: https://www.statistics.gr/documents/20181/18019778/census_results_2022_en.pdf/7c52ff55-9de3-d0d0-d9ea-73d6e908468b?version=1.0&t=1679057363566&download=true (accessed on 29 August 2024).
35. Loga, T.; Stein, B.; Diefenbach, N. TABULA Building Typologies in 20 European Countries—Making Energy-Related Features of Residential Building Stocks Comparable. *Energy Build.* **2016**, *132*, 4–12. [CrossRef]
36. Hensen, J.L.M.; Radošević, M. Teaching Building Performance Simulation—Some Quality Assurance Issues and Experiences. In Proceedings of the 21th Conference on Passive and Low Energy Architecture, Eindhoven, The Netherlands, 19 September 2004; pp. 19–22.
37. Directive-2018/844-EN-EUR-Lex. Available online: https://eur-lex.europa.eu/eli/dir/2018/844/oj (accessed on 29 August 2024).
38. European Commission Smart Readiness Indicator (SRI). Training Slide Deck; Version 2.0; European Commission Smart Readiness Indicator (SRI). Available online: https://energy.ec.europa.eu/topics/energy-efficiency/energy-efficient-buildings/smart-readiness-indicator/implementation-tools_en (accessed on 29 August 2024).
39. Directorate-General for Energy; Verbeke, S.; Aerts, D.; Reynders, G.; Ma, Y.; Waide, P. *Final Report on the Technical Support to the Development of a Smart Readiness Indicator for Buildings—Final Report*; Publications Office of the European Union: Berlin/Heidelberg, Germany, 2020.
40. Apostolopoulos, V.; Giourka, P.; Martinopoulos, G.; Angelakoglou, K.; Kourtzanidis, K.; Nikolopoulos, N. Smart Readiness Indicator Evaluation and Cost Estimation of Smart Retrofitting Scenarios—A Comparative Case-Study in European Residential Buildings. *Sustain. Cities Soc.* **2022**, *82*, 103921. [CrossRef]
41. SRI. Implementation Tools. Available online: https://energy.ec.europa.eu/topics/energy-efficiency/energy-efficient-buildings/smart-readiness-indicator/implementation-tools_en (accessed on 29 August 2024).
42. Luo, M.; Zheng, Q.; Zhao, Y.; Zhao, F.; Zhou, X. Developing Occupant-Centric Smart Home Thermostats with Energy-Saving and Comfort-Improving Goals. *Energy Build.* **2023**, *299*, 113579. [CrossRef]
43. Ministry for the Environment and Energy. Statistical Results for the Energy Efficiency of Buildings in the Residential, Tertiary and Public Sector. Available online: https://bpes.ypeka.gr/?page_id=21&stat=222 (accessed on 29 August 2024). (In Greek).
44. Hyperion Energy Community. The First Solar Energy Community in Greece, Powered by Citizens. Available online: https://2022.prizes.new-european-bauhaus.eu/sites/default/files/uploaded-reports/_Hyperion%20Summary%20Report%20Members%20(3).pdf (accessed on 29 August 2024).
45. Bellos, E.; Iliadis, P.; Papalexis, C.; Rotas, R.; Mamounakis, I.; Sougkakis, V.; Nikolopoulos, N.; Kosmatopoulos, E. Holistic Renovation of a Multi-Family Building in Greece Based on Dynamic Simulation Analysis. *J. Clean. Prod.* **2022**, *381*, 135202. [CrossRef]
46. A Guide to Bifacial Solar Panels. Available online: https://www.marketwatch.com/guides/solar/bifacial-solar-panels/ (accessed on 23 April 2024).
47. District Heating Municipal Company of Ptolemaida Pricelist. Available online: https://tpt.gr/%CE%98%CE%95%CE%9C%CE%91%CE%A4%CE%91-%CE%9A%CE%91%CE%A4%CE%91%CE%9D%CE%91%CE%9B%CE%A9%CE%A4%CE%A9%CE%9D/%CE%A0%CE%9B%CE%97%CE%A1%CE%9F%CE%A6%CE%9F%CE%A1%CE%99%CE%95%CE%A3-%CE%A4%CE%99%CE%9C%CE%9F%CE%9B%CE%9F%CE%93%CE%99%CE%91-%CE%A3%CE%A5%CE%9D%CE%94%CE%95%CE%A3%CE%97%CE%A3-%CE%9A%CE%91%CE%99-%CE%9A (accessed on 21 November 2023).
48. BPIE—Buildings Performance Institute Europe. Principles for Nearly Zero-Energy Buildings. Available online: https://www.bpie.eu/publication/principles-for-nearly-zero-energy-buildings/# (accessed on 24 April 2024).
49. Average Size of Dwelling. Available online: https://entranze.enerdata.net/average-size-of-dwelling.html (accessed on 29 August 2024).
50. Tsilingiridis, G.; Martinopoulos, G. Thirty Years of Domestic Solar Hot Water Systems Use in Greece—Energy and Environmental Benefits—Future Perspectives. *Renew. Energy* **2010**, *35*, 490–497. [CrossRef]
51. Guide to PV Investment | Solarway. Available online: https://solarway.gr/guides/odigos-stin-ependysi-fwtovoltaikwn/ (accessed on 24 April 2024).
52. Schoeneberger, C.; Zhang, J.; McMillan, C.; Dunn, J.B.; Masanet, E. Electrification Potential of U.S. Industrial Boilers and Assessment of the GHG Emissions Impact. *Adv. Appl. Energy* **2022**, *5*, 100089. [CrossRef]

Disclaimer/Publisher's Note: The statements, opinions and data contained in all publications are solely those of the individual author(s) and contributor(s) and not of MDPI and/or the editor(s). MDPI and/or the editor(s) disclaim responsibility for any injury to people or property resulting from any ideas, methods, instructions or products referred to in the content.

energies

MDPI

Article

Application and Performance Evaluation of Key Technologies in Green Buildings

Ran Wang [1,2], Zijian He [2], Xue Zhai [2] and Shilei Lu [2,*]

[1] State Key Laboratory of Building Safety and Built Environment, Beijing 100013, China; wang_ran@tju.edu.cn
[2] School of Environmental Science and Engineering, Tianjin University, Tianjin 300072, China; hezijian@tju.edu.cn (Z.H.); zhaixue@tju.edu.cn (X.Z.)
* Correspondence: lvshilei@tju.edu.cn

Abstract: To ensure the high-quality development of green buildings, a lot of attention has been paid to the post-evaluation of the actual operational performance of green buildings. Post-evaluation is a method to evaluate the effect of green buildings after putting them into use. It objectively expresses the actual implementation of green technologies, reflects occupants' experience, and scientifically guides the project operation through questionnaires, field visits, data analysis, etc. Since most post-evaluation studies only focus on the overall performance of green buildings, this study carried out a systematic post-evaluation of six typical technologies of green buildings based on more than 50 green cases in China. The overall performance of green buildings mainly considers the energy performance and building satisfaction. The six typical technologies include cold source systems, air conditioning terminal systems, energy-saving lighting technology, air heat recovery, the natural lighting technique, and roof greening technologies. The application form and frequency of each technology are studied by investigation, and the actual effect of each technology is evaluated by practical tests and questionnaires. The results show that although the overall performance of case green buildings, including the energy efficiency and staff satisfaction, can basically meet the standard requirements, the application effect of energy-saving and environmental protection technology is difficult to meet the expectations. The overall performance of green buildings can be further improved by improving the application effect of individual energy-saving and environmental protection technologies.

Keywords: green building; post-evaluation; technology application; case study; questionnaire survey; field visits

1. Introduction

The construction industry significantly impacts the environment, economy, and society [1]. The world oil crisis in the 1960s brought increasing attention to energy costs and drove the construction industry's transformation to energy efficiency [2]. Until 1990, when the first green building standard was published in the UK, "green building" gradually became a mainstream trend. Green building is growing rapidly and remains a research hotspot today, as evidenced by the number of papers published over the past three decades.

Different countries and regions have different definitions and standards for the topic of "what is a green building" at different times [3]. The BREEAM (Building Research Establishment Environmental Assessment Method) [4] released in the UK, as the earliest green building evaluation standard, has 14 versions, and more than 2 million buildings around the world are rated as BREEAM buildings. The LEED (Leadership in Energy and Environmental Design) [5] in the United States is one of the most widely recognized green building rating standards, with LEED-certified buildings in 182 countries worldwide. Due to the rating summation method of the LEED, there may be a problem of the ineffective stacking of green building technologies to obtain high scores [6]. The CASBEE (Comprehensive Assessment System for Built Environment Efficiency) [7] in Japan proposes

a new concept of "built environment efficiency", where the architectural boundary is a hypothetical enclosed space that contains the building itself [8]. With the industrialization, informatization, and intelligence of China's buildings, the ASGB (Assessment Standard for Green Building) [9] encourages the industrialized design of green buildings and the adoption of BIM technology and intelligent service systems. Green building evaluation standards in different regions are generally not fully compatible, but are broadly similar in structure. And, green buildings embody the core of saving resources, protecting the environment, and creating a good indoor environment [3].

A large number of scholars have conducted research on the overall performance of green buildings, mainly in terms of the indoor environment and energy conservation. It is generally accepted that green buildings can improve energy efficiency and slow down the process of energy scarcity [10]. For example, a study by Su, et al. [11] showed that a three-star green building in Dalian, China, was able to save 44.14 kWh/m^2·a in electricity consumption and water consumption compared to a traditional building. Vosoughkhosravi, et al. [12] investigated 11 university buildings. Limited by the sample size, the results are not statistically significant, but it is clear from the preliminary statistics that the highest electricity and heating energy consumption is always in non-LEED buildings and the lowest in LEED buildings. Similar conclusions were reached by Chokor, et al. [13] and Alborz and Berardi [14] in their studies of college buildings. Turner [15], Baylon [16], Jeong [17], and Scofield [18] et al. found that green buildings have an estimated 10–20% energy saving potential through the research and analysis of the energy use intensity (EUI) of hundreds of buildings in the United States, Chicago, and Korea. And thanks to the development of various building simulation platforms, simulation studies of green buildings are more convenient and feasible [19]. For example, Pan et al. [20] conducted a green building design for an office building with a data center in Shanghai and achieved energy savings of approximately 27% compared to Chinese code buildings through EnergyPlus simulations.

While the above studies illustrate the energy-saving advantages of green buildings, the subjective perception of occupants has been gradually gaining attention. For example, Pastore et al. [21] found that the environmental parameters of the green buildings studied were generally in compliance with the standards, but occupant satisfaction was not as high as expected, with the temperature and air quality being the most important factors. Pei, et al. [22] combined objective measurements and subjective evaluations of the indoor environmental parameters of office buildings in China and concluded that green building satisfaction was higher than that of non-green buildings. Khoshbakht, et al. [23] concluded that there was no significant difference between occupant satisfaction in green and non-green buildings in British and American countries, while in eastern countries, green building satisfaction was significantly higher than that of non-green buildings. To sum up, green buildings may have a better energy performance in general, while there is more potential for development in the creation of indoor environments.

Some other scholars have conducted studies around the application of green building technologies to provide references for the promotion of green building technologies according to local conditions. Shum et al. reviewed the application of smart solar shading systems in cold climate regions [24]. Su et al. [11] investigated the use of green building technologies in energy, land, water, and materials conservation in residential and public buildings in Dalian, China, respectively, and found that energy-efficient lighting and equipment [25] and efficient heating equipment are commonly used in public buildings, while residential buildings pay more attention to the thermal performance of the envelope and the greening rate of the landscape, and both types of buildings use ready-mixed concrete to reduce the material loss and on-site pollution [26]. Ge, et al. [27] found that intelligent lighting, energy-efficient elevators, air-source heat pumps, and solar hot water systems are the most commonly used and highly applicable green building technologies in Zhejiang, China. Lai, et al. [28] studied the green building technologies commonly used in southeast Asia, where the hot and humid climate characteristics impose moisture and thermal insulation performance requirements on the building envelope. Due to the

climate characteristics of southeast Asia, the development of phase change materials has certain advantages [28]. Meanwhile, natural ventilation [29], evaporative cooling technology [30], solar energy systems, and roof gardens [31] also have good application prospects. In summary, energy-saving technologies with a high frequency of application in green buildings include high-performance envelopes, energy-efficient lighting and equipment, high-efficiency HVAC (heating, ventilation, and air conditioning) systems, solar energy systems, natural ventilation, and green roofs, which have the potential to save resources while improving the indoor environment.

Based on the above analysis, a large number of scholars have conducted post-evaluation studies mainly from the aspects of the overall building operation energy consumption and the subjective perception of occupants, and some scholars have also investigated the type and frequency of technology application in green buildings. However, it is necessary to clarify the actual operation effect of each key technology in green buildings to improve the overall building performance. Therefore, this paper mainly explores the practical application effect of typical energy-saving and environmental protection technology in green buildings by using the post-evaluation method. Based on more than 50 green building cases in China, the green building performance is analyzed from two dimensions of the overall performance and the application effect of energy-saving and environmental protection technology. In terms of the overall building performance, the energy performance and occupant satisfaction in different climate zones are studied by using field surveys and questionnaire surveys. In terms of the energy-saving and environmental protection technology application, the application type and application frequency in different climate zones are analyzed through interviews and surveys. Further, six typical energy-saving and environmental protection technologies with a high application frequency or significant impact on the overall energy consumption of buildings are selected, and their application effects are analyzed in detail by a continuous testing method.

2. Materials and Methods

This study mainly carries out a post-evaluation of green buildings in China, including the overall performance of green buildings and the application performance of energy-saving technology in green buildings. The data types involved in the research mainly include design information and actual operation data. The basic information and design information of green building cases were obtained by collecting self-assessment reports of different green building cases, and the actual operation data were obtained by a questionnaire survey, interview survey, and test calculation. Figure 1 shows the research framework.

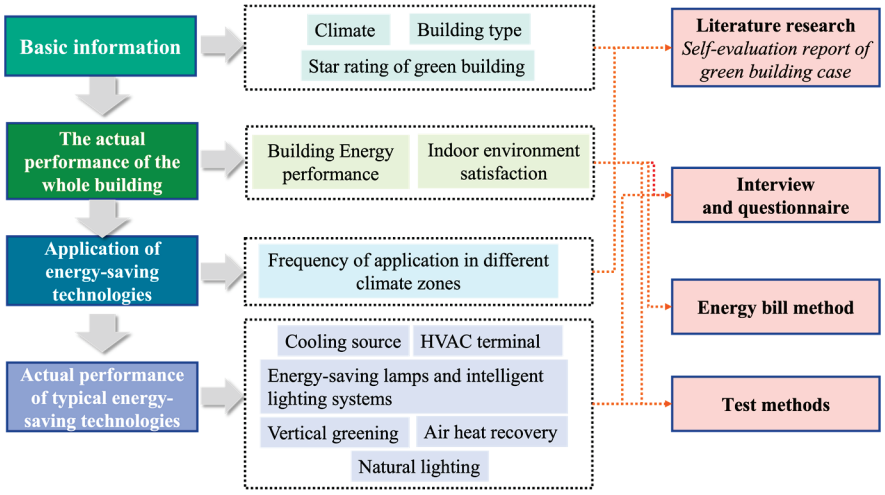


Figure 1. The research framework.

2.1. Case Information

Figure 2 shows the basic information on green building cases involved in this study. These green building cases are mainly distributed in four climate zones: the severe cold climate, the cold climate, the hot summer and the cold winter climate (HSCW), and the hot summer and warm winter climate (HSWW). The building types are mainly office buildings (accounting for 58%), and most of the cases have obtained three-star green building identifiers (accounting for 55%).

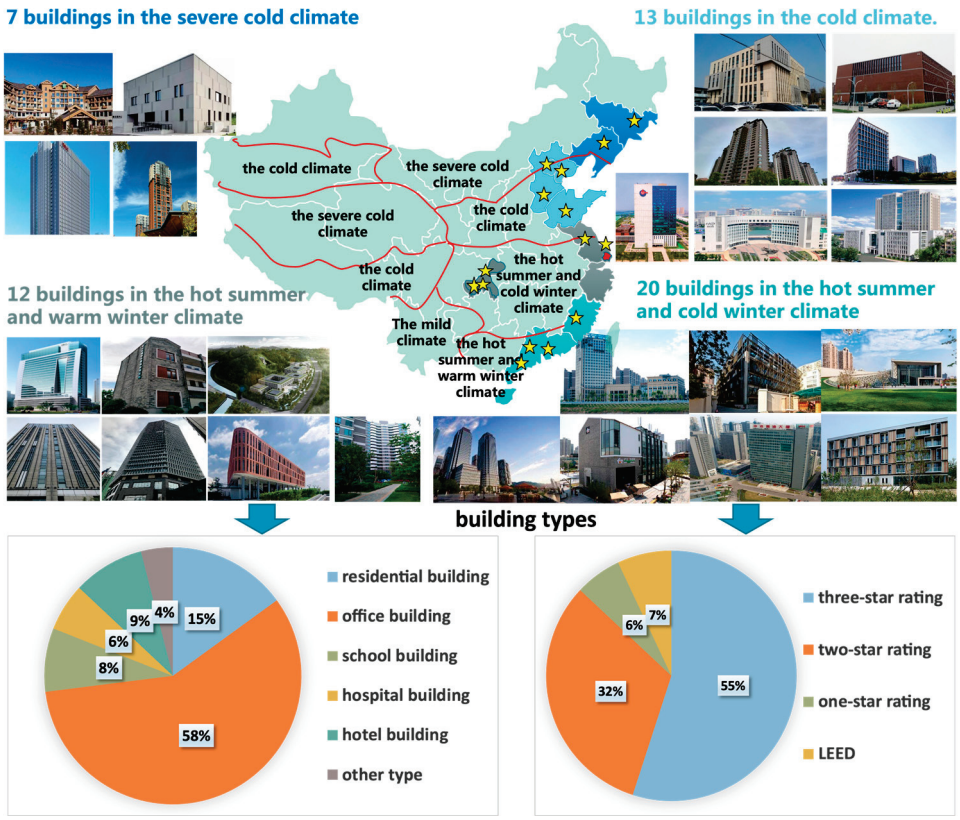


Figure 2. Case climate zone, building type, and star rating.

Note that not all building cases contain complete information. Therefore, in the subsequent detailed analysis of each part, there will be differences in the building cases each is based upon.

2.2. Bill Analysis Method

To reduce the difficulty of the data collection, the energy bill analysis method is preferred for the information related to the operational energy consumption of the whole building and energy-saving technology. The overall energy consumption of the building can be converted by the energy bill provided by the energy company, and the operating energy consumption of the energy-using equipment (system) can be obtained according to the itemized measurement.

2.3. Questionnaire Inquiry

This study carried out some questionnaire surveys on the overall indoor environmental satisfaction and subjective perception of the thermal environment. The overall indoor environment satisfaction survey includes five items: the thermal environment, light environment, air quality, sound environment, and overall indoor environment satisfaction. A subjective perception survey for the thermal environment is mainly used to evaluate the performance of the air conditioning terminal to maintain the indoor thermal environment. It mainly investigates the occupancies' subjective perception of the

indoor thermal environment, wet environment, and air-drying sensation as well as their satisfaction with the overall thermal environment. The survey used a seven-level rating scale, with a satisfaction score of 1 representing very dissatisfied and 7 representing very satisfied. Tables 1 and 2, respectively, show the questionnaire information on the overall indoor environment satisfaction and subjective feeling about the thermal environment.

Table 1. Basic information of questionnaire about the overall satisfaction of the green building environment.

Climate Zone	Severe Cold	Cold	HSCW	HSWW	Total
Cases	2	11	10	5	28
Valid questionnaires	60	1470	341	152	2023

Table 2. Basic information of questionnaire about subjective feelings of the indoor thermal environment.

Climate Zone	Cold	HSWW	Total
Cases	8	5	13
Valid questionnaires	808	592	1400

2.4. Test and Calculation Methods

2.4.1. The Cold Source System

The cold source system is the refrigeration system in the air conditioning system. It is a group of equipment combinations connected in a certain order and able to produce a refrigeration effect. It provides a cold capacity for the air conditioning system in the building and thus realizes indoor temperature control. The cold source system includes two parts: the cold source unit and the distribution system. The performance of the cold source system refers to the thermal performance. The *COP* (coefficient of performance, kW/kW) is the most commonly used performance parameter, which represents the ratio of the cooling capacity to power under a certain working condition.

$$COP = \frac{Q_e}{N} = \frac{cm(t_{in} - t_{out})}{N} \quad (1)$$

where Q_e is the cooling capacity, kW; N is the power, kW; c is the specific heat capacity of the refrigerant, kJ/(kg·°C); m is the flow rate of the refrigerant, kg/s; and t_{in} and t_{out}, respectively, represent the temperature of the refrigerant entering and exiting the unit, °C.

According to Formula (1), to evaluate the *COP* of a cold source system, parameters that need to be continuously tested include the flow rate, inlet and outlet temperature of chilled water, inlet and outlet temperature of cooling water, and power consumption. The test instruments include an ultrasonic flowmeter, dual-probe attached temperature recorder, and power quality analyzer, and the relevant parameters are shown in Table 3. The ultrasonic flowmeter is arranged on the vertical main pipe of the chilled water supply, and the probe is installed by the V method. The probe of the temperature recorder is, respectively, placed in the insulation layer of the supply and return pipe of frozen water. The power quality analyzer is installed in the distribution box of the unit, respectively, connected with a three-phase voltage and three-phase current. The frequency of the automatic data collection is 1 h, and the test period is from May to August.

Table 3. Monitoring instrument and accuracy.

Name (Type)	Measured Parameters	Measured Accuracy	Measured Range
Portable ultrasonic flowmeter (Fluke TDS-100P, Everett, WA, USA)	Velocity	±1%	——
Dual probe (Fluke TR004, Everett, WA, USA)	Water temperature	±0.5 °C	−30~125 °C
Power quality analyzer (Fluke 435 II, Everett, WA, USA)	Power	±1%	0~6000 MW

2.4.2. HVAC Terminal

(1) Objective thermal environment parameter monitoring

In this study, 13 green buildings in cold areas (8 buildings) and hot summer and warm winter areas (5 buildings) were selected to carry out the long-term monitoring of indoor thermal environment objective parameters (including the indoor air temperature and indoor air relative humidity) throughout the cooling/heating season. The relevant parameters of the test instrument are shown in Table 4. The automatic recording interval is 15 min. The measurement points are selected in typical functional areas of each building, such as open office areas, private offices, conference rooms, etc. The location of the measuring point is more than 1 m away from the window to avoid the interference of solar radiation and cold air penetration. The height of the measuring point is 1.1 m, which is the standard height for the sitting office.

Table 4. Basic information about indoor temperature and humidity measuring instruments.

Production Type	Parameter	Precision	Measuring Range
Onset-U30, Bourne, MA, USA	Temperature	±0.2 °C	−40–75 °C
	Relative humidity	±2.5%	0–100%

(2) Thermal environment satisfaction evaluation

Thermal Comfort refers to the subjective satisfaction of occupants with the surrounding thermal environment. The Thermal Comfort Zone refers to the range of the thermal environment restricted by the air temperature, average radiation temperature, and air relative humidity at a specific air velocity, human metabolic rate, and clothing thermal resistance [32]. In this study, the Predicted Mean Vote (PMV) and Actual Mean Vote (AMV) were selected as the main evaluation indexes of indoor thermal comfort. PMV adopts 7 grades (see Table 5), which represent the thermal sensation of the vast majority of occupants in the same environment. It is the most authoritative and widely used thermal comfort evaluation index worldwide [33]. PMV contains six main factors affecting human thermal comfort (including the air temperature, radiation temperature, relative humidity, wind speed, clothing thermal resistance, and human metabolic rate), which can calculate and predict the thermal sensation of humans in different thermal environments [34]. The AMV index is directly obtained from the questionnaire survey results of occupants, and its value is the same as that of PMV. AMV and PMV are considered to be the actual and predicted perceived values of occupants in the same thermal environment, respectively.

Table 5. Thermal sensation scale of PMV.

Thermal Sensation	Hot	Warm	Slightly Warm	Moderation	Slightly Cool	Cool	Cold
PMV value	+3	+2	+1	0	−1	−2	−3

2.4.3. Energy-Saving Lamps and Intelligent Lighting System

Energy-saving lamps and intelligent lighting systems are the most widely used energy-saving lighting technologies in green buildings. In the field of building energy conservation, energy-saving lamps generally refer to alternative lamps with higher energy efficiency and longer service life than traditional incandescent lamps and fluorescent lamps. The intelligent lighting system refers to the fine control of lighting according to the room function, period, and human traffic. The Assessment Standard for Green Building GB/T50378-2019 [9] put forward requirements for energy-saving lighting technologies in terms of the lighting power density and intelligent control, as shown in Table 6. In this study, the types of luminaires and lighting control systems used in green building cases and their practical application effects were investigated. The practical application effect is mainly evaluated from the energy-saving performance and comfort.

Table 6. Requirements for energy-saving technologies related to lighting in Green Assessment Standard for Green Building GB/T 50378-2019.

Items	Chapter	Detailed Requirements
Energy-saving lamps	7.1.4	The lighting power density value of each room or place shall not be higher than the current value specified in the current national Standard for Lighting Design of Buildings GB50034-2013 [35].
	7.2.7	The lighting power density of the main function room meets the requirement of the target value and can be scored 5 points.
Intelligent lighting system	7.1.4	The lighting system in the public area should adopt zoning, timing, induction, and other energy-saving controls, and the lighting control in the daylighting area should be independent of the lighting control in other areas.
	7.2.7	When the artificial lighting in the daylighting area can be automatically adjusted with the change in natural illumination, the evaluation score is 2 points.
	6.2.9	An intelligent service system with a lighting control function can give a corresponding score.

(1) Energy-saving performance

At present, China, the United States, Japan, Russia, and other countries have adopted the lighting power density (*LPD*) as the evaluation index for building lighting energy conservation. According to the Standard for Lighting Design of Buildings GB50034-2013, the calculation formula of *LPD* is as follows:

$$LPD = \frac{\sum P_i}{S} \quad (2)$$

LPD: the actual lighting power consumed per unit area (including the light source, ballast, and transformer), w/m^2.

P_i: the input power of the *i*-th lamp in the lighting place to be measured, W.

S: the area of the lighting place measured, m^2.

(2) Light environment comfort

The Standard for Lighting Design of Buildings GB50034-2013 gives clear regulations on the evaluation indexes of the light environment comfort of common functional rooms in common types of buildings, mainly including illuminance, illuminance uniformity, the color temperature, and the color rendering index. For office areas, illuminance should be greater than 300 lx, the uniform glare value should be less than 19, illuminance uniformity should be no less than 0.6, the color rendering index should be no less than 80, and the recommended color temperature between 3300 and 5300 K. In addition, considering that the intelligent lighting system should realize a personalized service for different occupants, occupant satisfaction should be evaluated by a questionnaire survey in terms of a comfort evaluation.

(3) Test method

According to Measurement Methods for Lighting GB/T5700-2008 [36] and the Standard for Energy Efficiency Test of Public Buildings JGJ/T177-2009 [37], the test value of the evaluation index should be the average value of different measuring points. The selection of measuring points adopts the center layout method, that is, the measuring area is divided into an equal rectangular grid, the central position of the rectangular grid is taken as the measuring point, and the spacing of measuring points is generally 0.5~10 m. Lighting tests should be conducted in the absence of natural light and other non-measured light sources.

2.4.4. Natural Lighting

This study investigates the application forms and actual effects of natural lighting in different green building cases. The actual effect of natural lighting technology is mainly

evaluated by illuminance. The illuminance and test plane requirements of different functional rooms refer to the Standard for Lighting Design of Buildings GB50034-2013. The following requirements shall be met when performing illuminance tests: All artificial lighting shall be ensured to be extinguished. The test time should be between 10 a.m. and 2 p.m. local time. The measuring range of the illuminometer should meet 0.1 lx~105 lx. The central distribution method described in list (3) in Section 2.4.3 was adopted for the selection of the measuring points, and the number of measuring points was not less than 4.

2.4.5. Air Heat Recovery Technology

In this study, the application of air heat recovery technology in green building cases was investigated and the practical application effect was tested. The incremental cost and maintenance cost were obtained mainly by collecting self-assessment reports of green building cases. The heat recovery efficiency was used as the evaluation index for the practical application effect.

In general, the volume of fresh air and exhaust air is equal, and the heat recovery efficiency can be simplified as:

$$\varepsilon_T = \frac{T_1 - T_2}{T_1 - T_3} \tag{3}$$

$$\varepsilon_h = \frac{h_1 - h_2}{h_1 - h_3} \tag{4}$$

where ε_T and ε_h are the sensible heat and the total heat exchange efficiency, respectively, T_1 and h_1 are the temperature and enthalpy of outdoor fresh air, T_2 and h_2 are the temperature and enthalpy of pretreated fresh air, and T_3 and h_3 are the temperature and enthalpy of indoor exhaust air.

2.4.6. Roof Greening

The adaptability of roof greening in green buildings was studied by the literature research and field research. First, the characteristics of the economy are analyzed based on the literature research. Secondly, based on the field research, the adaptability analysis of the climate zone and building types is carried out. In addition, to quantify the contribution of roof greening technology to the green building cooling load, typical cases are selected for actual operation data tests, and the test parameters include the roof internal and external surface temperature and the surface temperature of different greening types. Table 7 shows the principles followed for the placement of the measuring points.

Table 7. Layout principles of measuring points for roof greening performance.

Area (m^2)	<16	>16, and <30	>30, and <60	>60, and <100	>100
The number of measuring points	1	2	3	5	For every increase of 20~50 m^2, add 1~2 measuring points.

3. Results and Discussion

3.1. Energy Performance and Indoor Environment Satisfaction

Building energy consumption indicators are expressed in terms of the annual energy consumption per unit area (kWh/m^2·a). The constraint value of the energy consumption indicator corresponding to the case in the Standard for Energy Consumption of Building GB/T51161-2016 [38] is used as the evaluation criteria. Since it is relatively difficult to collect annual energy consumption data for residential buildings, the analysis here is mainly for public buildings. Figure 3 shows the building energy consumption indicators and their constraint values for 22 green building cases located in three climate zones. When the point is above the balance line, it means that the actual energy consumption of the building meets the constraint requirements. The measured energy consumption indicators in most cases

have reached the constraint value, especially in the hot summer and cold winter climate zone, where most of the cases are below 70% of the constraint value.

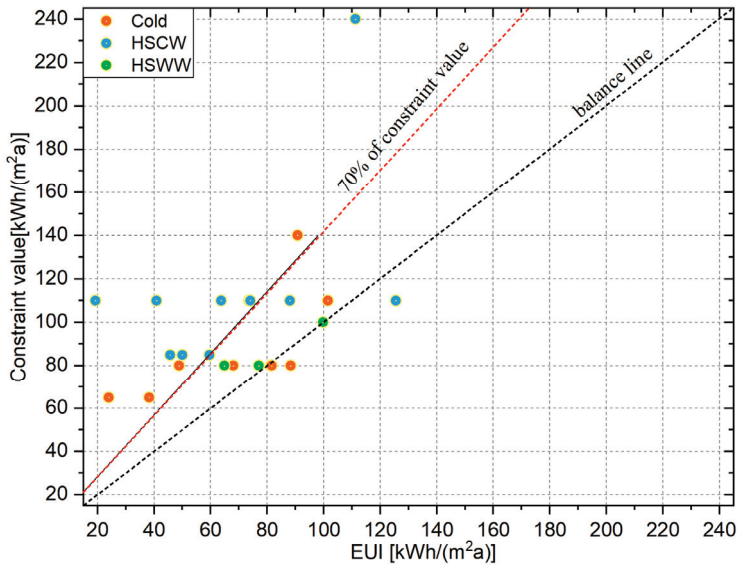


Figure 3. The building energy consumption indicators and their constraint values for 22 green building cases.

The occupant satisfaction is evaluated utilizing the questionnaire survey, which mainly covers thermal comfort, lighting quality, air quality, acoustic quality, and the whole indoor environment. The questionnaire survey involved 29 cases located in four climate zones and a total of 2030 valid questionnaires. Figure 4 shows the survey results of occupant satisfaction in different climate zones. Except for the air quality in hot summer and cold winter climate zones, the satisfaction of sub-items and whole ones has reached more than 80%. The whole indoor satisfaction in the hot summer and warm winter climate zone is higher than that in other climate zones, with an average satisfaction rate of 90%. The difference in thermal comfort satisfaction among the four climate zones is relatively small, with the average satisfaction rate being 80.8–86.5%. The thermal comfort satisfaction in the severe cold climate zone is the highest, with an average satisfaction rate of 86.5%.

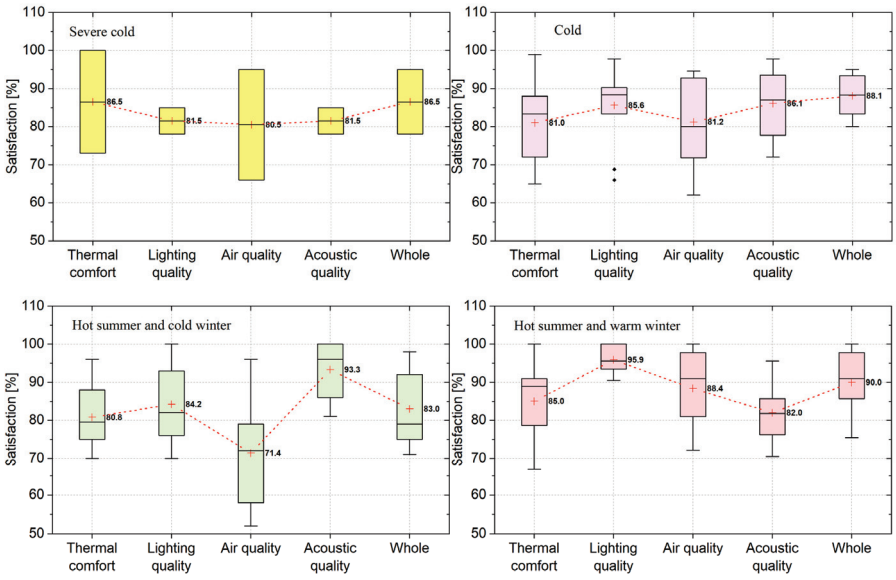


Figure 4. The survey results of occupant satisfaction in different climate zones.

3.2. Technology Application

This study investigated the application of energy-saving technology in 43 green building cases. The investigated cases were mainly distributed in the cold climate zone, the hot summer and cold winter climate zone, and the hot summer and warm winter climate zone, and the number of cases were 15, 18, and 10, respectively. Figure 5 shows the types and application frequencies of energy-saving technologies in green building cases. As the application conditions are not significantly different in the building type and climate zone, the high-performance envelope, energy-saving lamps, and intelligent lighting system are the most frequently applied technologies, with an application frequency of up to 100%. Natural ventilation optimization and air heat recovery are also widely used, with application frequencies of 86.1% and 79.1%, respectively. Among them, the natural ventilation optimization technology mainly involves the simulation prediction and optimization of the indoor ventilation effect by using professional software in the building design stage to enhance the indoor natural ventilation effect and improve the indoor environment. The building energy-subentry measure has not been fully popularized in green buildings, and the application frequency is only 65.1%. In addition, the application frequency of building automation systems is 69.8%. The application frequency of natural lighting technology is about 67.4%, which mainly refers to introducing more natural light through other passive means based on a conventional architectural design, including light guide tubes, skylights, and so on. The application frequency of external shading is 55.8%, mainly including horizontal shading and vertical shading, to reduce solar heat in summer. In some cases, the angle and length of the visor will be accurately calculated according to the local solar altitude angle on the winter solstice and summer solstice, to achieve the design goal of summer shading without affecting winter heating, and ultimately achieve the highest shading efficiency. The adjustable fresh air ratio technology mainly refers to the fact that the fresh air ratio of the whole air system can be adjusted on demand, and the application ratio reaches 34.9%. The technology can be operated with fresh air in the transition season to improve the indoor environment and reduce energy consumption. In some offices with high indoor air quality requirements, frequency conversion fans are linked with CO_2 concentration sensors, which can automatically adjust the air volume according to the increase or decrease in the CO_2 concentration. The applications of temperature and humidity-independent control air conditioning systems and double-layer breathing curtain walls are relatively less, accounting for 14.0% and 9.3%, respectively. External breathing curtain wall systems can effectively discharge the hot air in the cavity in the cooling season, and reduce the heat transfer of the envelope. In the case study, it is mainly used in the hot summer and cold winter and the hot summer and warm winter climate.

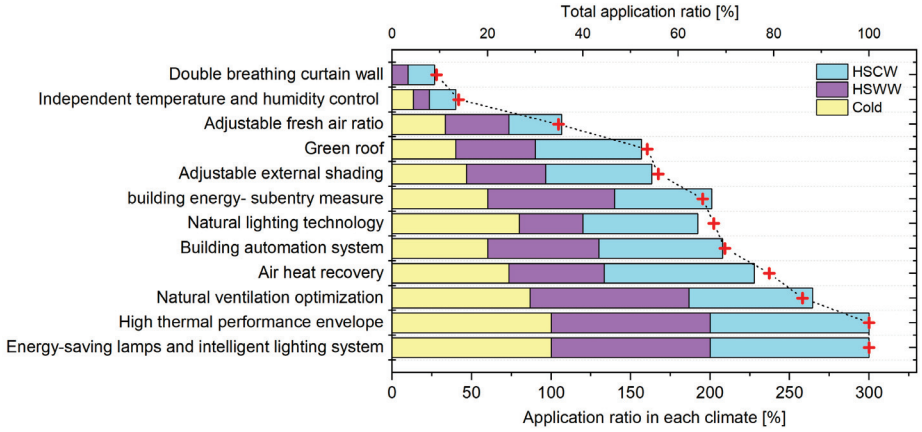


Figure 5. Application of typical energy-saving technology.

3.3. Cooling Source System

Figure 6 shows the application types and frequencies of cold source systems in different climatic zones. Water cooling units and VRV (variable refrigerant volume) units are widely used in all three climate zones, and GSHP (ground source heat pump) is mainly used in the HSCW and the cold climate zones. New techniques have also been tried, albeit less frequently. For example, a cold source system with heat recovery can provide a free domestic hot water supply in summer. In the investigation case, there are mainly two forms: a chiller with heat recovery and a ground source heat pump unit with heat recovery. For example, in a hospital green building located in a hot summer and warm winter climate zone, the cold-water room is equipped with a water-cooled screw chiller with a heat recovery capacity of 908 kW and a heat recovery capacity of 26 kW, which can realize a free hot water supply in summer. In another example of a green building in the climate zone, a ground source heat pump system with heat recovery is used to provide domestic hot water for the efficient use of energy. In summer, the system uses the waste heat of the condenser to heat domestic hot water and pumps it to each water point through the hot water circulation. The waste heat can meet part of the domestic hot water demand of the project. In winter, domestic hot water is provided directly by the ground source heat pump. An office park located in the hot summer and warm winter climate has a large area of electronic information room. The information room has the characteristics of a high calorific value, stable cooling load, and year-round operation. Therefore, in this project, the information room is equipped with a water-cooled centrifugal unit with heat recovery, and the supply and return water temperature of waste heat recovery is 45 °C/40 °C. The waste heat recovered from the information room can be used as a free heat source to preheat the hot water system in summer and can be used as a free heat source to preheat both the air conditioning heating system and the hot water system in winter. The configuration scheme of the cold source system not only meets the heat demand, but also improves the comprehensive utilization efficiency of energy.

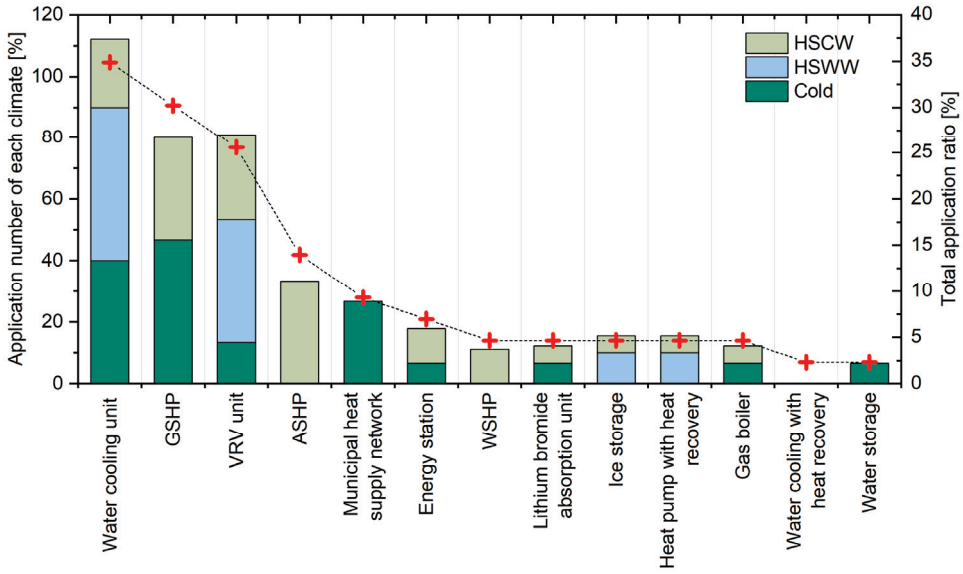


Figure 6. The application type and ratio of cold source.

The Assessment Standard for Green Building GB/T50378-2019 provides that, compared with the Design Standard for Energy Efficiency of Public Buildings GB50189-2015 [39], if the energy efficiency improvement of cold source units reaches 6%, the building will receive a green building score of 5 points, and if the energy efficiency improvement reaches 12%, the score will be 10 points. Figure 7 shows the rated energy efficiency of the four main types of cold sources (ASHP (air source heat pump), VRV, GSHP, and chiller) in the green building case, and their increase relative to GB50189. It can be seen that the lifting

range of the four types of cold source units reached 6%, except for the VRV which reached 12%. But in actual operation, it is difficult for the energy efficiency of the unit to reach the rated value.

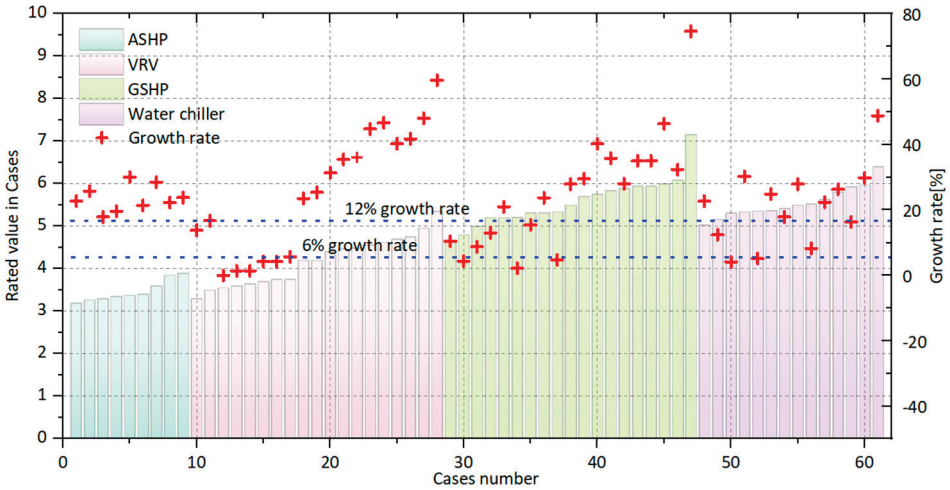


Figure 7. The rated value in cases and its growth rate compared to the base value.

Furthermore, the long-term operation data of seven GSHP cases and five chiller cases were collected. As shown in Figure 8, the actual operational energy efficiency in all cases was generally below its rating, with an average hourly COP of about 50–100% of the rating. The main reason is that the configuration of cold source units generally has the problem of too large a capacity, which causes the unit to operate under a low load in most working conditions in actual operation, and the average load rate of 11 units is 64.7%. Therefore, the cold source that receives the green building score through the rated energy efficiency index cannot guarantee that it meets the requirements of the standard in actual operation.

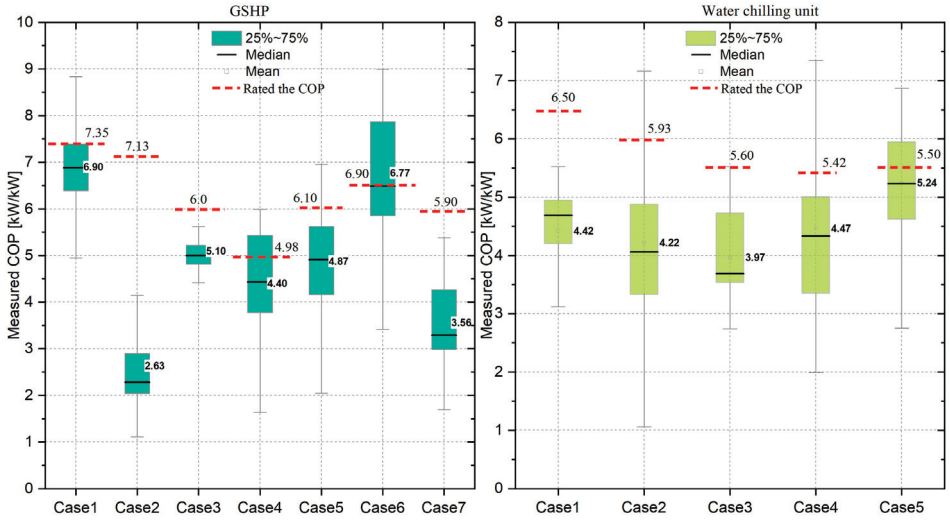


Figure 8. Measured COP of two main cold source types.

3.4. HVAC Terminal System

In recent years, new types of air conditioning terminals emerge endlessly. The purpose of green buildings is to provide the occupant with a healthy, comfortable, and efficient use of space, so some designers intentionally tend to use new types of air conditioning terminal products when designing green buildings. However, through a field survey (Figure 9), it is found that most practical cases still use the traditional terminal form, such as floor radiant heating, fan-coil-coupled fresh air system, whole air system, etc. There are also

cases where new-type end-products are used, such as capillary radiation cooling, a constant temperature and humidity air conditioning system, underfloor air distribution system and chilling panels, etc.

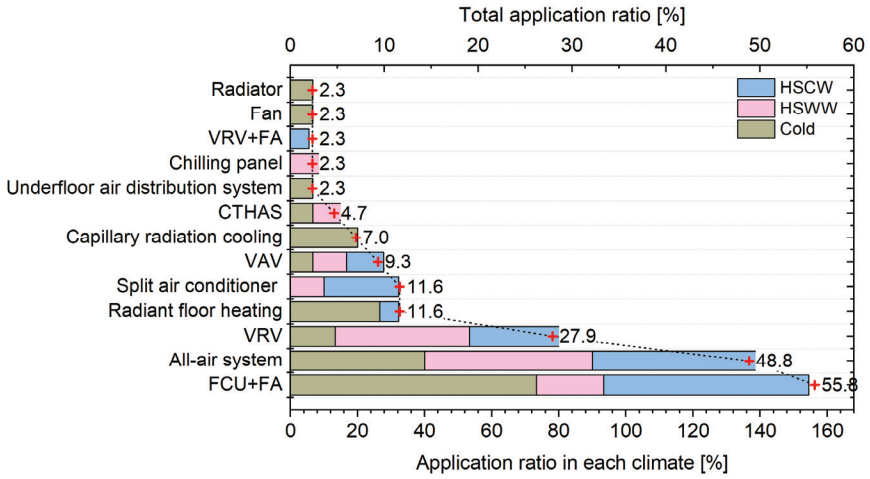


Figure 9. The application type and ratio of the HVAC terminal system.

To investigate the actual operating performance of air conditioning terminals in green buildings, this study collected the indoor environmental parameters of eight three-star green buildings located in cold areas and five three-star green buildings located in hot summer and warm winter areas. In addition, the collected thermal environment data are evaluated by taking indoor thermal comfort level II as the limit of the Design Code for Heating Ventilation and Air Conditioning of Civil Buildings GB50736-2012 [40]. The thermal comfort range is as follows: the indoor air temperature in summer is 24 °C~28 °C and the relative humidity is 40~70%; in winter, the indoor air temperature is 18 °C~24 °C, and the indoor air relative humidity is less than 60%. According to Figure 10, the overall rate of reaching the standard in the research cases is not high. The maximum rate of reaching the standard in winter is 95%, the minimum is 18%, and the average is 62%; the maximum rate of reaching the standard in summer is 93%, the minimum is 0%, and the average is 52%. It is found that the rate of reaching the standard is mainly affected by the relative humidity. In cold regions, the outdoor air relative humidity is low in winter, so the measured indoor air relative humidity is generally low in winter, which is about 15% most of the time. In hot summer and warm winter areas, the outdoor air relative humidity in summer is larger so the collected indoor temperature and humidity parameters have a wider distribution range and are more concentrated in high-humidity areas.

Furthermore, the AMV and PMV are used to comprehensively evaluate the thermal environment comfort of green building cases. PMV is mainly calculated based on objective monitoring data, which can reflect objective thermal comfort. AMV is obtained based on a questionnaire survey, reflecting the occupants' subjective feelings towards the thermal environment. According to the results of the questionnaire survey, the thermal resistance of the clothing is 1.0 clo in winter and 0.5 clo in summer. The indoor activities are sitting and working, so the metabolic rate is 1 met, and the measured wind speed is 0.1 m/s when filling in the questionnaire. According to Figure 11, the fitting results of AMV and PMV show that there are certain differences in subjective and objective satisfaction. By comparing the AMV and PMV, the subjective thermal sensation correction model (AMV = d × PMV) of the green building air conditioning environment in our country is obtained. The correction factor *d* is introduced, and *d* is calculated to be 0.44 in the hot summer and warm winter area and 0.66 in the cold area.

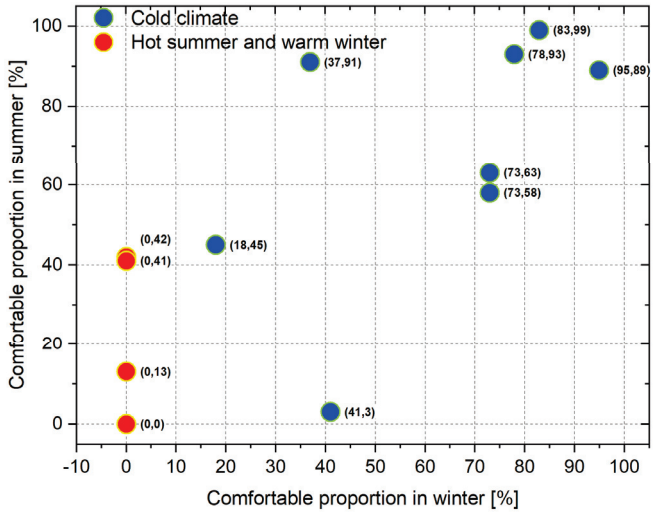


Figure 10. Indoor thermal environment evaluation results of green building cases based on GB50736 standard.

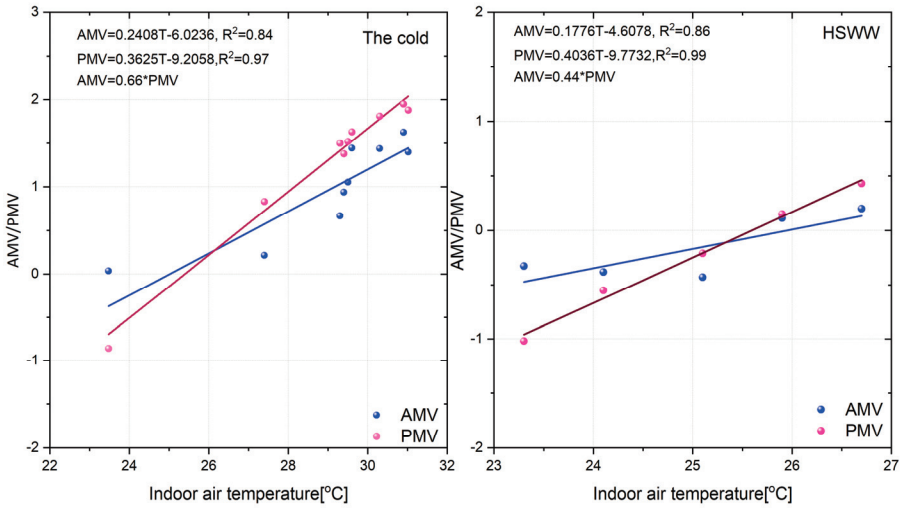


Figure 11. Fitting results of AMV and PMV in the cold region and the hot summer and warm winter region.

3.5. Energy-Saving Lamps and Intelligent Lighting Systems

This study selected 33 green building cases (residential buildings accounted for 30.3%, public buildings accounted for 69.7%, and three-star green buildings accounted for 63.6%) and conducted research and tests on the detailed application of energy-saving lamps and intelligent lighting systems. As shown in Figure 12, the fluorescent lamp (CFL), followed by the LED lamp (light emitting diode), was the most used energy-saving method in the research cases, with application frequencies of 56.9% and 27.5%, respectively. But, LED lighting is more widely used in new green buildings. In the research cases, the intelligent lighting system with a high application frequency is mainly infrared induction and sound–light time-delay control, with an application ratio of 24.1% and 20.7%, respectively. The public areas of residential buildings are mostly controlled by sound–light time-delay control. Combined with specific architectural functions, public buildings mainly adopt centralized and local control modes in the main functional space, and adopt infrared induction, motion induction, light induction, scene control, and so on in the public area. Some new green buildings and special function areas have more complex intelligent lighting control system applications.

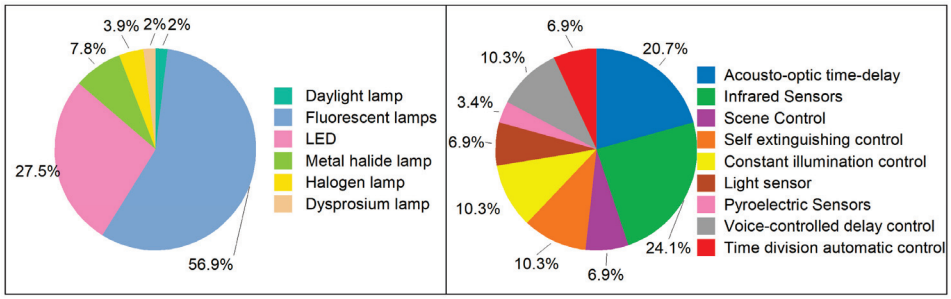


Figure 12. The application proportion of energy-saving lamps and intelligent lighting systems in the case.

In terms of the energy-saving performance, the LPD of 25 different types of areas in green building cases was investigated, and the current value and target value of LPD stipulated in the Standard for Lighting Design of Buildings GB50034-2013 was used to evaluate the survey results. The current value is formulated after comprehensive consideration, based on the research results of the current situation of the lighting energy consumption of all kinds of buildings in China, the existing level of lighting products, and the relevant lighting energy saving standards at home and abroad. The target value is the prediction of future LPD considering the progress of lighting science and the improvement of the energy efficiency level of lighting products. The target value is about 10%~20% lower than the current value. As shown in Figure 13, the actual LPD of about 36% of green building cases exceeds the current value. By comparison, the areas exceeding the current value are mainly restaurants, meeting rooms, and guest rooms. Moreover, the illuminance test results of these areas show that the illuminance is much higher than the standard requirement value. It can be seen that the lighting design of these areas in the early stage is not reasonable, and there are problems with high lighting equipment configuration.

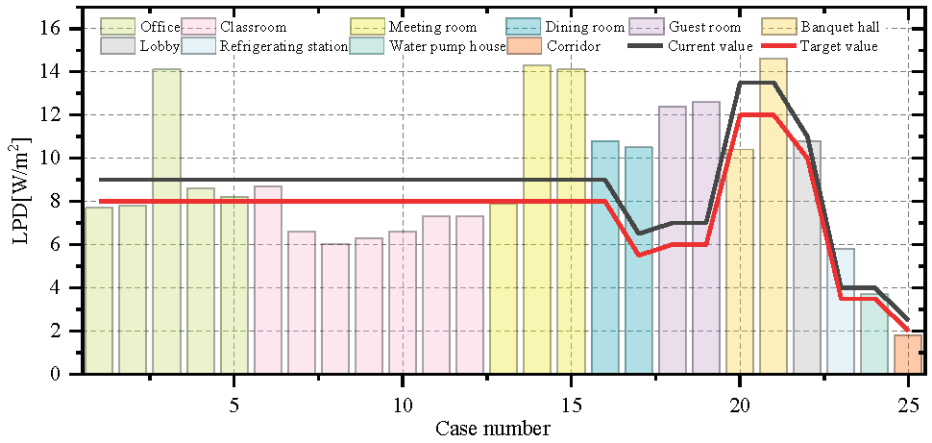


Figure 13. Survey results of lighting power density in green building cases.

In terms of light environment comfort, the illuminance, color temperature, and color rendering index were tested, respectively. Figure 14 shows the average illumination of rooms with different functions compared to the baseline required in the standard. The results show that the illuminance of most test samples can meet the standard requirements. According to the Standard for Lighting Design of Buildings GB50034-2013 on the color representation of the light source and applicable places, the color temperature of the office should be 3300~5300 K, and the color index of the lighting source should not be less than 80. Figure 15 shows the test results of the color temperature and color rendering index of different office areas. It can be seen that the overall color temperature is slightly cold and the color rendering index is slightly low. This indicates that in the selection of energy-saving lamps, more attention is paid to illuminance and power, but not enough attention to the

color temperature and color rendering index of lamps. In addition, 200 questionnaires were distributed to investigate the occupants' satisfaction with the indoor light environment comfort and their main concern factors, as shown in Figure 16. The results show that occupants have high satisfaction with the artificial lighting environment of green buildings. Most occupants think that the illumination and adjustability of lamps have the greatest impact on the comfort level and pay less attention to the energy-saving performance, the true degree of color, and the intelligence of lamps.

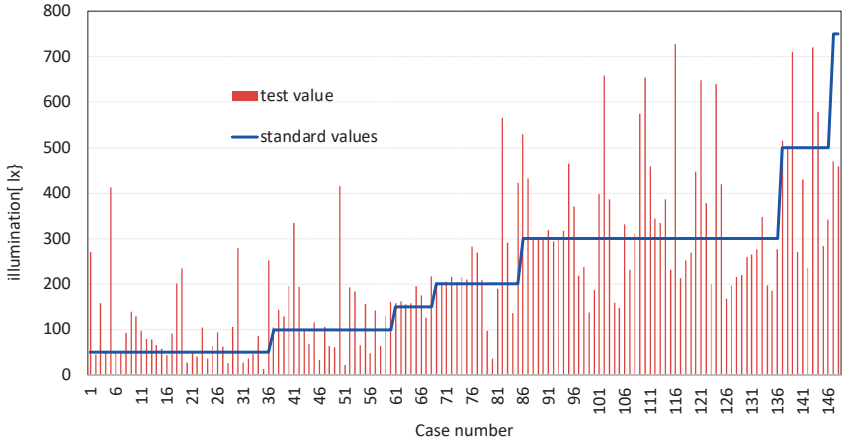


Figure 14. The average illumination of some room cases with different functions compared to the baseline required in the standard.

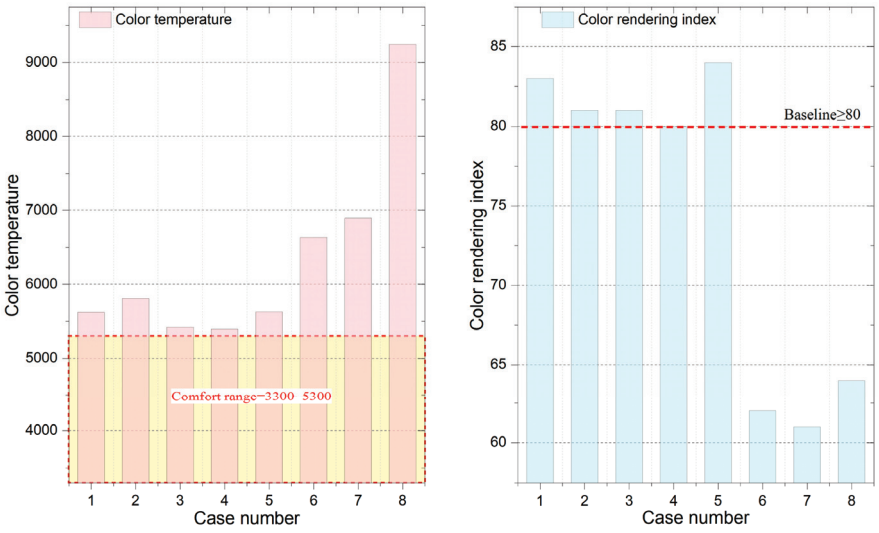
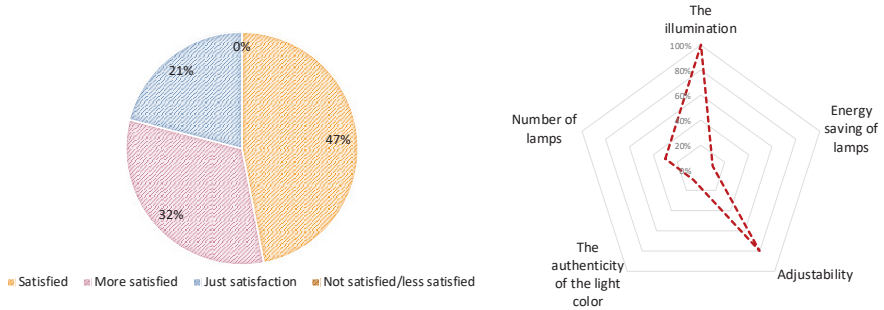


Figure 15. Test results of color temperature and color rendering index.



(**a**) Satisfaction (**b**) Attention to relevant factors

Figure 16. Results of the questionnaire survey on occupant satisfaction with artificial lighting.

3.6. Air Heat Recovery Technology

According to the technical post-evaluation, field measurement, and maintenance personnel feedback, the application status of air heat recovery technology in green buildings was summarized, including the main application sites, application types, and actual heat recovery efficiency. The utilization rate of air heat recovery technology in green public buildings reaches 70%, which is specifically applied in offices, hotels, exhibitions, hospitals (partial), and shopping malls. Air heat recovery technology is not suitable for school buildings. In a three-star university teaching building located in a cold climate area, sensible heat recovery in winter is 65%, and recovery energy accounts for 71.48% of the fresh air load. However, according to the survey, due to the special use time of university buildings, heat recovery is only used in winter and stopped during holidays. Therefore, the economy of the air heat recovery technology is not outstanding in such university buildings with a low operating frequency. In different forms of heat recovery, total heat recovery is the highest application frequency, accounting for more than 60%.

To evaluate the gap between the actual heat recovery efficiency and the rated value, field tests were conducted on ten cases with the application of the total heat recovery technology, and the results are shown in Figure 17. The actual performance of the heat recovery technology is much lower than the rated value, and the actual heat recovery efficiency of different cases is between 0.42 and 0.54. Moreover, the heat recovery efficiency of the cooling condition is lower than that of the heating condition. Figure 18 shows the energy-saving rate and the corresponding incremental costs of air heat recovery devices in different cases. It can be seen that there is no significant positive correlation between the energy-saving rate and the corresponding incremental cost of heat recovery technology, with the coefficient of the determination being lower than 0.1. The distribution range of the incremental cost of the initial investment is 0–20 CNY/m^2, and that of the incremental cost of maintenance is 0–2.0 CNY/m^2.

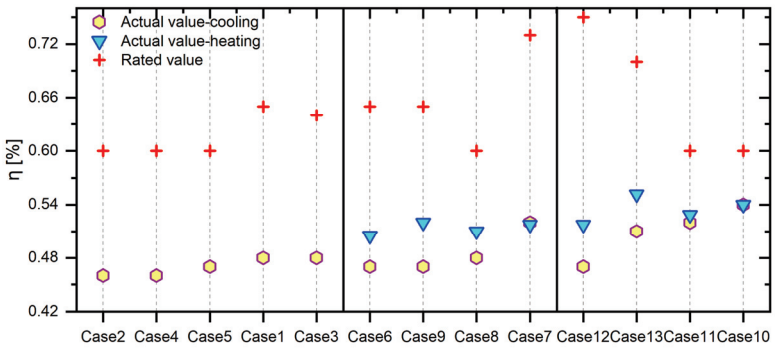


Figure 17. Heat recovery efficiency of the research case.

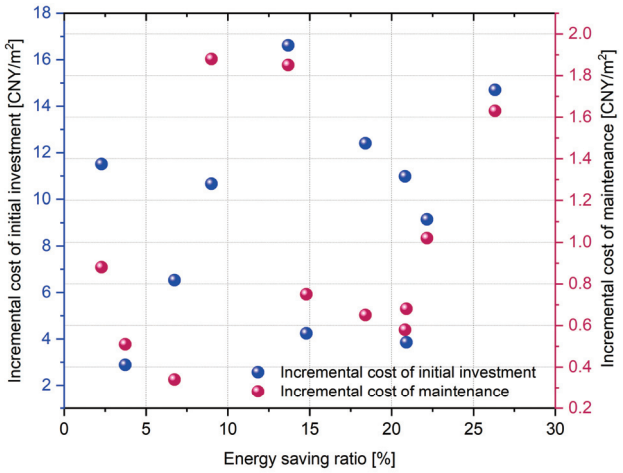


Figure 18. Incremental cost of the initial investment and the maintenance for air heat recovery technology.

3.7. Natural Lighting Technology

Figure 19 shows the application types and frequencies of natural lighting technology in green buildings, and they are the light guide tube, skylight, atrium, light well, sunken courtyard, and light guide louvers in descending order of frequency. Among them, skylights, atriums, and light guide louvers are mainly used to enhance the natural lighting in above-ground spaces; light wells and sunken courtyards are mainly used to enhance the natural lighting in underground spaces; and light guide tubes can be used to enhance the natural lighting in above-ground and underground spaces. Light guide tubes, skylights, and atriums are commonly used in three climate zones, lighting wells are only used in the cold climate, and sunken courtyards and light guide louvers are only used in HSCW.

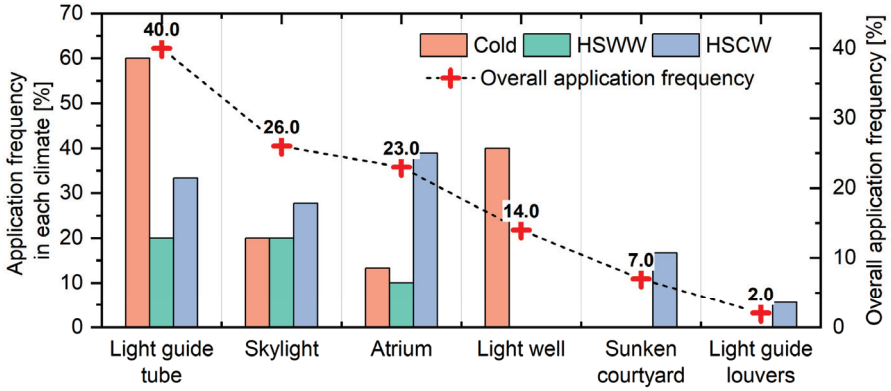


Figure 19. Application types and frequencies of natural lighting technology.

The application places of light guide tubes in green buildings generally include office and public places. The actual application effect of the light guide tube in seven cases was tested. The test index is the illuminance of the reference surface. The test index is the illuminance of the reference surface. The reference planes of offices and public places are 0.75 m and 0 m planes from the ground, respectively. On the reference plane, the light guide tube is taken as the center and the measurement is carried out sequentially at intervals of 0d, 2d, 4d, and 6d, where d is the diameter of the light guide tube. The test period is a typical week, and the test period is from 11:00 to 14:00 local time.

Figure 20 shows the illuminance test results of seven light pipe cases, where the illuminance value of each measuring point is the average value at 10–14 h in a typical week. The application purpose of the light guide tube is to introduce more natural light in the room during the day to reduce the energy consumption of artificial lighting. However, the actual application has not achieved the expected results. The application place of cases 1 and 2 is the office, and the reference surface is 0.75 m. According to the Standard for Lighting Design of Buildings GB50034-2013, the illuminance of the office work surface cannot be lower than 300 lx, and the illuminance of the walkway and public garage cannot be lower than 50 lux. For the office, the test results show that the effective service area (meeting the illuminance requirements) of the light guide tube is very limited. As shown in Figure 20, only the direct area (0d) of illumination generally meets the normal work requirements. In addition, the illuminance of the light guide tube in both the horizontal and vertical directions attenuates quickly, and the illuminance is unstable over time, which easily causes glare and even reduces the work efficiency. In the process of field investigation, it was found that although some offices have installed adjustable-angle light guides, glare still exists. Therefore, the light guides are closed for a long-time during building operations. According to Figure 5, the effective service area of the light guide tube used in public areas such as underground garages and walkways (case 3–4) has reached 6d, with illumination above 50 lux. Although only the light guide tube can meet the illuminance requirements during the test, it is found that the artificial lighting general is still on in this case. Therefore, for light guide tubes used in public spaces, the adjustment and management of artificial

lighting by relevant management personnel is the key to determining whether the light guide tube can achieve the purpose of energy saving.

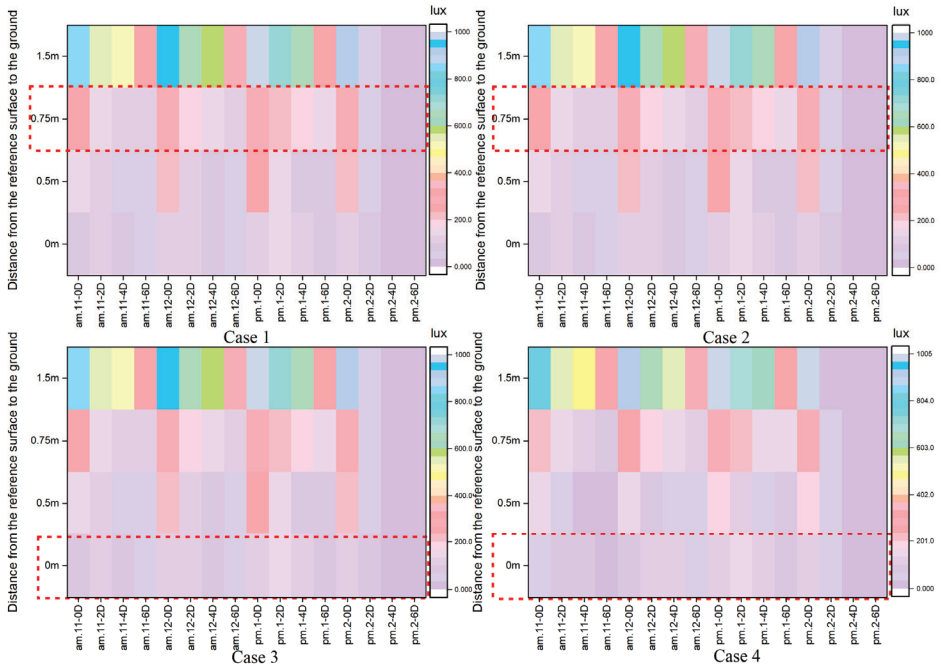


Figure 20. Test results of the illuminance of light guide tubes in 4 building cases.

3.8. Roof Greening Technology

According to the site visit and field measurement, the application suitability of roof greening technology can be evaluated from the suitability of the climate zone. First of all, the survival of plants is a problem in the cold climate and the severe cold climate. In winter, the temperature is low and the rainfall is low. When the soil temperature is below 0 °C, the frozen soil layer appears, which may cause a change in soil thermophysical properties. The hot summer and warm winter climate zones have longer summers without winter. In these areas, the annual and daily temperature ranges are small and the rainfall is sufficient. Therefore, it is more suitable to adopt roof greening technology, but it needs to pay attention to the influence of typhoon weather. In the hot summer and cold winter climate area, summer is sultry and winter is wet and cold, and the daily temperature difference is small, so it is also more suitable for roof greening technology.

To further quantify the improvement effect of roof greening technology on the surrounding environment and building roof insulation, this study conducted operational effect tests on three cases located in hot summer and cold winter areas. Figure 21 shows the effect of roof greening on the surrounding ambient temperature. In Case 1, the green cover contains six different plants; the rests are wood planks and pebbles. In Case 2, the green cover also contains six different plants, while the rest is brick. As can be seen from the figure, greening has a significant effect on the surrounding environment. The average temperature around the greening part is significantly lower than that of the non-greening part, which is about 16.7 °C and 12.9 °C lower in the two cases, respectively. Figure 22 shows the mean temperature difference between the inner and outer surfaces of the green part and the non-greening part of the building roof in case 3. The results show that the inner surface temperature of the green part is significantly lower than that of the non-green part, about 2–6 °C lower. The temperature difference between the inner and outer surfaces of the green part is about 9–14 °C lower than that of the non-green part. Therefore, roof greening can significantly improve the thermal performance and reduce the cooling load. In addition, the cooling effect varies on the vegetation type. The temperature difference between the inside and outside of the roof with the surface of the flower bed is about 7 °C, while that of the roof with the surface of the lawn is about 12 °C.

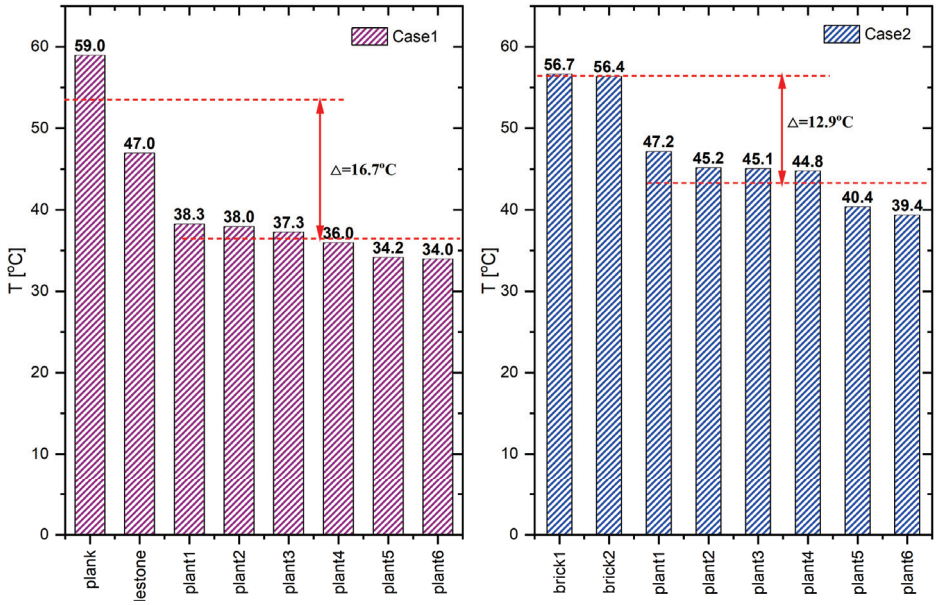


Figure 21. Improvement effect of roof greening on the surrounding thermal environment.

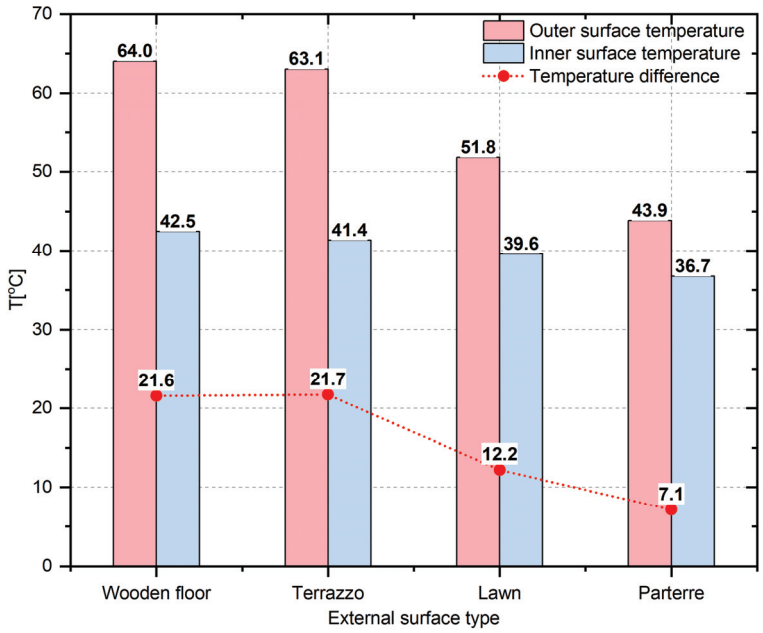


Figure 22. Temperature difference between the inner and outer surfaces of the roof greening.

4. Conclusions

Based on more than 50 actual green building cases in China, this paper evaluated the actual building's whole performance and the applicability of energy-saving technologies used in these cases. Firstly, the overall performance of green buildings is evaluated mainly from two dimensions of energy performance and overall occupants' satisfaction. Secondly, the application of energy-saving technology in green building cases is analyzed, including the type and frequency of application. Furthermore, the actual operating performance of each main energy-saving technology is further analyzed such as the cold source system, the air conditioning terminal system, the lighting energy-saving technology, the natural lighting technology, the air heat recovery technology, and the roof greening technology. Moreover, the adaptability of these energy-saving technologies is analyzed from the dimensions of climate characteristics, building types, and use places. The relevant data on green buildings used in this study are mainly obtained through each case's green building identification self-

assessment report, visit survey, questionnaire survey, and field test. The main conclusions are as follows:

(1) The overall energy consumption and occupant satisfaction of case green buildings basically meet the standard requirements. The measured energy consumption indicators in most cases have reached the constraint value, especially in the hot summer and cold winter climate zone, and most of the cases are below 70% of the constraint value. Except for the air quality in hot summer and cold winter climate zones, the satisfaction of the sub-items and whole has reached more than 80%. The whole indoor satisfaction in the hot summer and warm winter climate zone is higher than that in other climate zones, with an average satisfaction rate of 90%. The difference in thermal comfort satisfaction among the four climate zones is relatively small, with the average satisfaction rate being 80.8–86.5%. The thermal comfort satisfaction in the severe cold climate zone is the highest, with an average satisfaction rate of 86.5%.

(2) The practical application effect of energy-saving and environmental protection technology is basically difficult to meet the expectations. For the cooling source system, the actual operational energy efficiency in all cases was generally below its rating, with an average hourly COP of about 50–100% of the rating. For the HVAC terminal system, the overall rate of reaching the standard in the research cases is not high. The average rate of reaching the standard in winter and summer are 62% and 52%, respectively. For artificial lighting, the actual LPD of about 36% of green building cases exceeds the current value. In addition, in the selection of energy-saving lamps, more attention is paid to illuminance and power, but not enough attention to the color temperature and color rendering index of lamps. For air heat recovery, the actual performance of the heat recovery technology is much lower than the rated value, and the actual heat recovery efficiency of different cases is between 0.42 and 0.54. For a light guide tube, the illuminance in both the horizontal and vertical directions attenuates quickly, and the illuminance is unstable over time, which easily causes glare and even reduces the work efficiency.

Author Contributions: Conceptualization, R.W. and S.L.; methodology, R.W.; the origin mapping software, Z.H.; validation, Z.H. and X.Z.; investigation, R.W. and X.Z.; resources, R.W. and X.Z.; data curation, R.W. and Z.H.; writing—original draft preparation, R.W., Z.H. and X.Z.; writing—review and editing, R.W. and S.L.; supervision, S.L.; project administration, R.W.; funding acquisition, R.W. All authors have read and agreed to the published version of the manuscript.

Funding: Supported by the Opening Funds of the State Key Laboratory of Building Safety and the Built Environment and the National Engineering Research Center of Building Technology, grant number BSBE2023-02.

Data Availability Statement: The original contributions presented in this study are included in the article. Further inquiries can be directed to the corresponding author.

Conflicts of Interest: The authors declare that they have no known competing financial interests or personal relationships that could have appeared to influence the work reported in this paper.

Nomenclature

AMV	Actual mean vote
ASGB	Assessment Standard for Green Building
ASHP	Air source heat pump
BREEAM	Building Research Establishment Environmental Assessment Method
CASBEE	Comprehensive Assessment System for Built Environment Efficiency
CFL	Compact fluorescent lamp
COP	Coefficient of performance (kW/kW)
EUI	Energy use intensity (kWh/m^2·a)
GSHP	Ground source heat pump
HSCW	Hot summer and cold winter climate
HSWW	Hot summer and warm winter climate

HVAC	Heating, ventilation, and air conditioning
LED	Light-emitting diode
LEED	Leadership in Energy and Environmental Design
LPD	Lighting power density
PMV	Predicted mean vote
VRV	Variable refrigerant volume

References

1. Chuai, X.; Lu, Q.; Huang, X.; Gao, R.; Zhao, R. China's construction industry-linked economy-resources environment flow in international trade. *J. Clean. Prod.* **2021**, *278*, 123990. [CrossRef]
2. Economidou, M.; Todeschi, V.; Bertoldi, P.; D'Agostino, D.; Zangheri, P.; Castellazzi, L. Review of 50 years of EU energy efficiency policies for buildings. *Energy Build.* **2020**, *225*, 110322. [CrossRef]
3. Zuo, J.; Zhao, Z.-Y. Green building research-current status and future agenda: A review. *Renew. Sustain. Energy Rev.* **2014**, *30*, 271–281. [CrossRef]
4. Building Research Establishment. BREEAM—The World's Leading Science-Based Suite of Validation and Certification Systems for a Sustainable Built Environment. Available online: https://bregroup.com/products/breeam/ (accessed on 25 February 2024).
5. U.S. Green Building Council. How LEED Works. Available online: https://www.usgbc.org/leed (accessed on 25 February 2024).
6. Schwartz, Y.; Raslan, R. Variations in results of building energy simulation tools, and their impact on BREEAM and LEED ratings: A case study. *Energy Build.* **2013**, *62*, 350–359. [CrossRef]
7. Japan Sustainable Building Consortium. CASBEE Certification System. Available online: https://www.ibec.or.jp/CASBEE/english/certificationE.htm (accessed on 25 February 2024).
8. Ferrari, S.; Zoghi, M.; Blázquez, T.; Dall'O, G. New Level(s) framework: Assessing the affinity between the main international Green Building Rating Systems and the european scheme. *Renew. Sustain. Energy Rev.* **2022**, *155*, 111924. [CrossRef]
9. *GB/T50378-2019*; Assessment Standard for Green Building. Ministry of Housing and Urban-Rural Development of the People's Republic of China: Beijing, China, 2019.
10. Zhang, Y.; Wang, W.; Wang, Z.; Gao, M.; Zhu, L.; Song, J. Green building design based on solar energy utilization: Take a kindergarten competition design as an example. *Energy Rep.* **2021**, *7*, 1297–1307. [CrossRef]
11. Su, Y.; Wang, L.; Feng, W.; Zhou, N.; Wang, L. Analysis of green building performance in cold coastal climates: An in-depth evaluation of green buildings in Dalian, China. *Renew. Sustain. Energy Rev.* **2021**, *146*, 111149. [CrossRef]
12. Vosoughkhosravi, S.; Dixon-Grasso, L.; Jafari, A. The impact of LEED certification on energy performance and occupant satisfaction: A case study of residential college buildings. *J. Build. Eng.* **2022**, *59*, 105097. [CrossRef]
13. Chokor, A.; El Asmar, M.; Tilton, C.; Srour, I. Dual assessment framework to evaluate LEED-certified facilities' occupant satisfaction and energy performance: Macro and micro approaches. *J. Archit. Eng.* **2016**, *22*, A4015003. [CrossRef]
14. Alborz, N.; Berardi, U. A post occupancy evaluation framework for LEED certified US higher education residence halls. *Procedia Eng.* **2015**, *118*, 19–27. [CrossRef]
15. Turner, C.; Frankel, M.; Council, U. Energy performance of LEED for new construction buildings. *New Build. Inst.* **2008**, *4*, 1–42.
16. Baylon, D.; Storm, P. *Comparison of Commercial LEED Buildings and Non-LEED Buildings Within the 2002–2004 Pacific Northwest Commercial Building Stock*; ACEEE Summer Study on Energy Efficiency of Buildings; American Council for an Energy-Efficient Economy: Washington DC, USA, 2008; pp. 4-1–4-12.
17. Jeong, J.; Hong, T.; Ji, C.; Kim, J.; Lee, M.; Jeong, K. Development of an evaluation process for green and non-green buildings focused on energy performance of G-SEED and LEED. *Build. Environ.* **2016**, *105*, 172–184. [CrossRef]
18. Scofield, J.H.; Doane, J. Energy performance of LEED-certified buildings from 2015 Chicago benchmarking data. *Energy Build.* **2018**, *174*, 402–413. [CrossRef]
19. Zhang, G.; Ge, Y.; Pan, X.; Afsharzadeh, M.S.; Ghalandari, M. Optimization of energy consumption of a green building using PSO-SVM algorithm. *Sustain. Energy Technol. Assess.* **2022**, *53*, 102667. [CrossRef]
20. Pan, Y.; Yin, R.; Huang, Z. Energy modeling of two office buildings with data center for green building design. *Energy Build.* **2008**, *40*, 1145–1152. [CrossRef]
21. Pastore, L.; Andersen, M. Building energy certification versus user satisfaction with the indoor environment: Findings from a multi-site post-occupancy evaluation (POE) in Switzerland. *Build. Environ.* **2019**, *150*, 60–74. [CrossRef]
22. Pei, Z.; Lin, B.; Liu, Y.; Zhu, Y. Comparative study on the indoor environment quality of green office buildings in China with a long-term field measurement and investigation. *Build. Environ.* **2015**, *84*, 80–88. [CrossRef]
23. Khoshbakht, M.; Gou, Z.; Lu, Y.; Xie, X.; Zhang, J. Are green buildings more satisfactory? A review of global evidence. *Habitat Int.* **2018**, *74*, 57–65. [CrossRef]
24. Shum, C.; Zhong, L. A review of smart solar shading systems and their applications: Opportunities in cold climate zones. *J. Build. Eng.* **2023**, *64*, 105583. [CrossRef]
25. Kwong, Q.J. Light level, visual comfort and lighting energy savings potential in a green-certified high-rise building. *J. Build. Eng.* **2020**, *29*, 101198. [CrossRef]
26. Kumanayake, R.; Luo, H. A tool for assessing life cycle CO_2 emissions of buildings in Sri Lanka. *Build. Environ.* **2018**, *128*, 272–286. [CrossRef]

27. Ge, J.; Zhao, Y.; Luo, X.; Lin, M. Study on the suitability of green building technology for affordable housing: A case study on Zhejiang Province, China. *J. Clean. Prod.* **2020**, *275*, 122685. [CrossRef]
28. Lai, F.; Zhou, J.; Lu, L.; Hasanuzzaman, M.; Yuan, Y. Green building technologies in Southeast Asia: A review. *Sustain. Energy Technol. Assess.* **2023**, *55*, 102946. [CrossRef]
29. Aviv, D.; Chen, K.W.; Teitelbaum, E.; Sheppard, D.; Pantelic, J.; Rysanek, A.; Meggers, F. A fresh (air) look at ventilation for COVID-19: Estimating the global energy savings potential of coupling natural ventilation with novel radiant cooling strategies. *Appl. Energy* **2021**, *292*, 116848. [CrossRef]
30. Abdullah, S.; Zubir, M.N.B.M.; Bin Muhamad, M.R.; Newaz, K.M.S.; Oztop, H.F.; Alam, M.S.; Shaikh, K. Technological development of evaporative cooling systems and its integration with air dehumidification processes: A review. *Energy Build.* **2023**, *283*, 112805. [CrossRef]
31. Nasr, Y.; El Zakhem, H.; Hamami, A.E.A.; El Bachawati, M.; Belarbi, R. Comprehensive Assessment of the Impact of Green Roofs and Walls on Building Energy Performance: A Scientific Review. *Energies* **2024**, *17*, 5160. [CrossRef]
32. Wang, R.; Lu, S.; Feng, W. Impact of adjustment strategies on building design process in different climates oriented by multiple performance. *Appl. Energy* **2020**, *266*, 114822. [CrossRef]
33. Wang, R.; Lu, S.; Feng, W. A three-stage optimization methodology for envelope design of passive house considering energy demand, thermal comfort and cost. *Energy* **2020**, *192*, 116723. [CrossRef]
34. Fanger, P.O. *Thermal Comfort-Analysis and Applications in Environmental Engineering*; R.E. Krieger Publishing Company: Malabar, FL, USA, 1982.
35. *GB50034-2013*; Standard for Lighting Design of Buildings. Ministry of Housing and Urban-Rural Development of the People's Republic of China: Beijing, China, 2013.
36. *GB/T5700-2008*; Measurement Methods for Lighting. General Administration of Quality Supervision, Inspection and Quarantine of the People's Republic of China: Beijing, China, 2008.
37. *JGJ/T177-2009*; Standard for Energy Efficiency Test of Public Buildings. Ministry of Housing and Urban-Rural Development of the People's Republic of China: Beijing, China, 2009.
38. *GB/T51161-2016*; Standard for Energy Consumption of Building. Ministry of Housing and Urban-Rural Development of the People's Republic of China: Beijing, China, 2016.
39. *GB50189-2015*; Design Standard for Energy Efficiency of Public Buildings. Ministry of Housing and Urban-Rural Development of the People's Republic of China: Beijing, China, 2015.
40. *GB50736-2012*; Design Code for Heating Ventilation and Air Conditioning of Civil Buildings. Ministry of Housing and Urban-Rural Development of the People's Republic of China: Beijing, China, 2012.

Disclaimer/Publisher's Note: The statements, opinions and data contained in all publications are solely those of the individual author(s) and contributor(s) and not of MDPI and/or the editor(s). MDPI and/or the editor(s) disclaim responsibility for any injury to people or property resulting from any ideas, methods, instructions or products referred to in the content.

energies

MDPI

Article

Design and Implementation of a Wireless Power Transfer System Using LCL Coupling Network with Inherent Constant-Current and Constant-Voltage Output for Battery Charging

Pengqiang Nie, Song Xu , Zhenlin Wang, Seiji Hashimoto *, Linfeng Sun and Takahiro Kawaguchi

Division of Electronics and Informatics, Gunma University, Kiryu 376-8515, Japan; npq97111@gmail.com (P.N.); songxu@just.edu.cn (S.X.); zhenlinwang8689@gmail.com (Z.W.); felicityslf@outlook.com (L.S.); kawaguchi@gunma-u.ac.jp (T.K.)

* Correspondence: hashimotos@gunma-u.ac.jp

Abstract: The constant current followed by constant voltage (CC-CV) charging method is commonly employed for battery charging, effectively extending battery life and reducing charging time. However, as charging progresses, the battery's internal resistance increases, complicating the charging circuit. This paper designs a wireless power transfer system utilizing an LCL coupling network for battery charging. The system employs frequency modulation (FM) to manage its CC and CV output characteristics at two fixed frequency points. The influence of the LCL coupling network parameters on system output characteristics was investigated using MATLAB. A simulation model was developed in the PSIM environment to validate the CC and CV output characteristics. The simulation results show that the system has load-independent constant-current and constant-voltage characteristics at two different frequency points. In order to verify the theoretical analysis, an experimental platform was also established. Experimental results demonstrate that the proposed system operates effectively in CC mode, maintaining constant output current across various loads, while in CV mode, it effectively regulates output voltage for different loads. The designed frequency modulation controller ensures a rapid response to sudden changes in load resistance, regardless of operating in CC or CV modes.

Keywords: LCL coupling network; constant current; constant voltage; frequency modulation

1. Introduction

With the rapid development of renewable energy and the increasing popularity of electric vehicles, batteries have become widely used as efficient energy storage devices across various fields [1–3], due to their advantages of high energy density and good cycle stability. The constant current followed by constant voltage (CC-CV) charging method has been widely adopted in battery-charging processes [4,5], as shown in Figure 1.

It can be seen that the battery-charging process can be divided into two stages. Stage 1: CC charging mode: the battery voltage increases rapidly while the charging current remains constant. Stage 2: CV charging mode: the battery current declines rapidly while the voltage remains stable. Additionally, the equivalent internal resistance of the battery increases during the whole charging process, which brings huge challenges to the constant-current or constant-voltage charging of batteries. Various control strategies have been investigated to provide the required output current or output voltage for time-variable loads against different charging stages. One common approach involves using a DC-DC converter on either the primary or secondary side to regulate the output voltage or current, which has

been widely adopted in battery-charging processes [6,7]. In reference [6], a buck converter was adopted on the secondary side to regulate the system's output voltage and current, enabling constant-voltage or constant-current charging of the battery. In order to track the optimal load and improve the system's efficiency, a DC-DC converter was used in a wireless power transfer system that utilized an S-S-type resonant network to transfer energy in [7]. However, this method leads to additional power losses and high system costs, and necessitates extra space for the installation of the DC-DC converter [8].

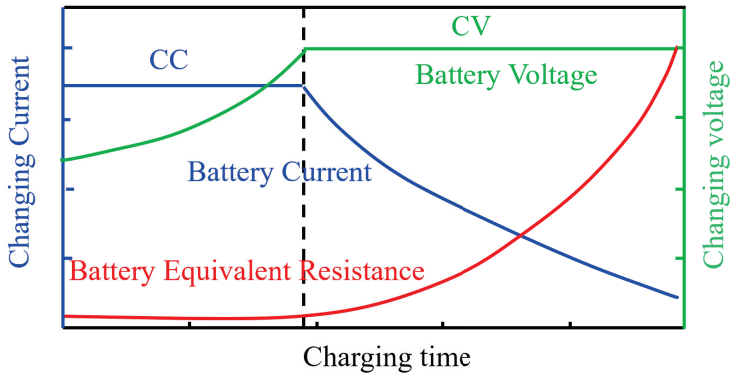


Figure 1. The battery-charging process.

Magnetic coupling wireless power transfer (MCWPT) systems enable efficient, convenient, and safe energy transfer through electromagnetic fields, making them particularly suitable for applications such as smartphones, electric vehicles, and medical devices [9–11]. One of the most important parts of these MCWPT systems is the resonant compensation network, which significantly enhances system efficiency and minimizes reactive power [12–14]. This resonant compensation network demonstrates excellent output characteristics, providing either constant voltage or constant current [15]. Specifically, the series–series (S-S)-type compensation network delivers a load-independent constant-current output in [16], whereas the LCL-S-type compensation network ensures a load-independent constant-voltage output in [17].

Therefore, some researchers have proposed using a hybrid topology design to adjust the connected resonant compensation network through switch switching, thereby achieving constant-current or constant-voltage mode control. In [18], a dual-topology WPT system was proposed, which achieves both CC and CV outputs by switching between S-S and series–parallel (S-P) topologies with different compensation parameters. However, the proposed circuit is quite complex, incorporating a center-tapped loosely coupled transformer and four switches. Reference [19] presents a novel topology that combines LLC and LCL-T resonant tanks to facilitate the CC and CV charging of lithium batteries, significantly reducing the operational switching frequency range compared to traditional LLC converters. This system utilizes switching to adjust the resonant compensation network connected to the secondary side, enabling control in either constant-current or -voltage mode. In [20], series and parallel compensation circuits are thoroughly discussed, leading to the development of a hybrid topology that delivers both load-independent output current and load-independent output voltage. A hybrid topology-based charging strategy for electric bicycles (EBs) using a single high-frequency inverter (HFI) to provide configurable constant-current (CC) and constant-voltage (CV) outputs was proposed in [21]. The system utilizes two AC switches to achieve CC and CV outputs without the need for complex control schemes or wireless communication. The above structures employ additional switches to facilitate the transition between constant-current and constant-voltage modes, resulting in higher system costs and increased control complexity. Reference [22] introduced a

primary-side control technique employing phase-shift modulation for series–series (SS) and series–parallel (SP) compensated wireless power transfer (WPT) systems, enabling CV and CV charging. However, phase-shift control exhibits limitations such as sensitivity to parameter variations affecting regulation and stability, and heightened design complexity under varying load conditions, which collectively reduce efficiency and scalability in WPT systems.

To reduce system costs, eliminate additional switches for mode switching, and further enhance system compactness, some researchers have explored higher-order resonant compensation networks, which enable the system to achieve CC or CV charging at different operating frequencies. Reference [23] proposed a WPT system to achieve CC and CV output characteristics by utilizing two additional intermediate coils with resonant capacitors to achieve CC and CV output at two fixed frequencies. A novel three-coil WPT system was proposed to achieve CC and CV charging. A novel three-coil WPT system to address the limitations of achieving CC and CV charging modes was introduced in [24]. The addition of extra coils to achieve CC or CV output results in increased system complexity, higher costs, and larger system volume. Additionally, the mutual coupling between the coils complicates the theoretical modeling of the system and introduces greater challenges in system control. Reference [25] presents a design method for achieving CC and CV charging in an inductive power transfer (IPT) system with minimal frequency variation using a double-sided LCC compensation network at two resonant frequencies. The use of three resonant compensation components on both the primary and secondary sides provides the system with greater design flexibility, but also increases its cost and size.

This paper presents a wireless charging system based on an LCL coupling network, designed for battery-charging applications. By carefully optimizing the parameters of the LCL resonant network, the system inherently provides load-independent constant-current and constant-voltage output without any additional switches, which simplifies the system structure and reduces system costs. The system can achieve load-independent constant-current or constant-voltage output characteristics at two different operating frequencies. Thus, by implementing FM around these two resonant frequency points, only slight frequency adjustments are needed to maintain the desired constant-voltage or constant-current output characteristics.

The remainder of the manuscript is arranged as follows: The LCL equivalent coupling model is built and the control system is designed in Section 2. Section 3 analyzes the influence of LCL resonant network parameters on system output characteristics in detail and verifies the load-independent CC and CV characteristics of the system. The system characteristic scanning and dynamic response test experiments are conducted in Section 4. Finally, a brief conclusion is given in Section 5.

2. System Analysis and Control System Design

2.1. Topology of the Designed System Using LCL Resonant Network

The topology of the proposed system is shown in Figure 2, where an input voltage source and a battery are integrated. The double-sided LCL resonant network, comprising a pair of coupled coils L_p, L_s and their corresponding resonant compensation components (C_p, C_s, L_1, L_2), serves to transfer energy from the primary side to the secondary side while also being used as an isolation device. U_{in} and U_b are the input voltage and battery voltage, respectively. The high-frequency full-bridge inverter, comprising four switches $Q_1 \sim Q_4$, converts DC power into high-frequency AC power U_{AB}, which serves as the input of the LCL resonant coupling network. Furthermore, the full-bridge rectifier composed of four diodes $D_1 \sim D_4$ rectifies the received AC power from the LCL resonant network into DC power for the battery. In addition, M is the mutual inductance between the primary

resonant coil L_p and the secondary resonant coil L_s. Additionally, the input voltage source and battery port are equipped with voltage-stabilizing capacitors C_{in} and C_o to maintain the stability of their respective port voltages.

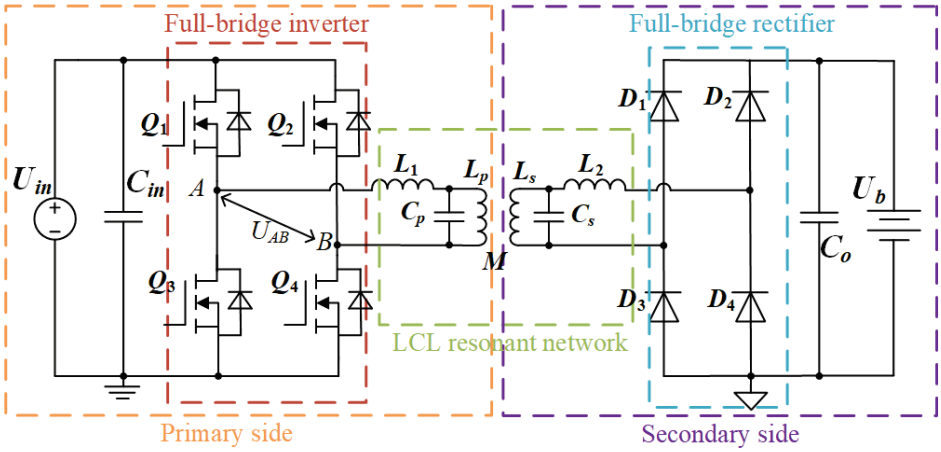


Figure 2. Topology of the designed system using the LCL resonant network.

2.2. Analysis of LCL Coupling Equivalent Model

Figure 3 shows the simplified LCL coupling model, ignoring the internal resistance of the coils where the primary LCL resonant network's input and output currents are denoted as I_1 and I_P, respectively. I_S and I_2 are the secondary LCL resonant network's input and output currents. Z_1 and Z_2 represent the total system impedance and the secondary LCL resonant network impedance, respectively.

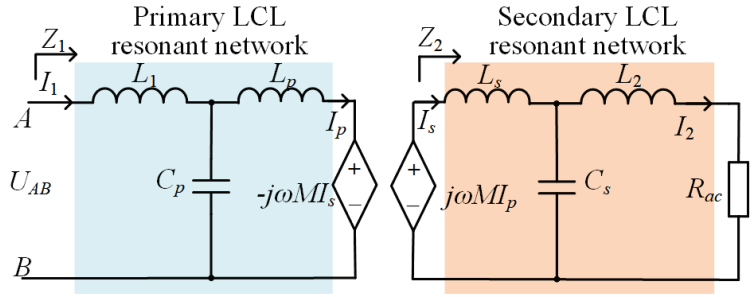


Figure 3. The simplified LCL coupling model.

U_{AB} stands for the inverter output voltage, which also serves as the input for the LCL network and can be expressed as follows.

$$U_{AB} = \frac{2\sqrt{2}}{\pi} U_{in} \tag{1}$$

The rectifier and its subsequent resistance can be equivalent to R_{ac} shown in Equation (2), while the battery's equivalent internal resistance is R.

$$R_{ac} = \frac{8}{\pi^2} R \tag{2}$$

Thus, a two-port network of the primary-side LCL resonant network can be established as follows.

$$\begin{bmatrix} 1 & 0 & 0 & 0 \\ 1 & 0 & -Z_{11} & -Z_{12} \\ 0 & 1 & -Z_{21} & -Z_{22} \\ 0 & 1 & 0 & Z_{\mathrm{eq}} \end{bmatrix} \begin{bmatrix} U_{\mathrm{in}} \\ U_{\mathrm{p}} \\ I_1 \\ I_{\mathrm{p}} \end{bmatrix} = \begin{bmatrix} U_{\mathrm{in}} \\ 0 \\ 0 \\ 0 \end{bmatrix} \tag{3}$$

where Z_{11}, Z_{12}, Z_{21}, and Z_{22} are the Z-parameters of the two-port network of the primary side; Z_{eq} is the equivalent impedance of the secondary LCL resonant to the primary LCL resonant network. Additionally, ω is the switching angular frequency.

$$Z_{eq} = \frac{M\omega^2}{Z_2} \tag{4}$$

From the two-port network model, it can be deduced that the primary LCL coupling network's input current I_1, output voltage U_p, and system impedance Z_1 are as follows. Here, $A = 1 - \omega^2 C_p L_p$, $B = \omega C_p Z_{eq}$.

$$I_p = \frac{U_{in}}{Z_{eq}(1 - C_p L_1 \omega^2) - j(C_p L_p L_1 \omega^3 - L_1\omega - L_p\omega)} \tag{5}$$

$$U_p = \frac{jZ_{eq}U_{in}}{jZ_{eq}(1 - C_p L_1 \omega^2) + (C_p L_p L_1 \omega^3 - L_1\omega - L_p\omega)} \tag{6}$$

$$Z_1 = \frac{Z_{eq} + j\omega(L_p A - C_p Z_{eq}^2 + L_1 A^2 + L_1 B^2)}{A^2 + B^2} \tag{7}$$

Similarly, the two-port network of the secondary LCL resonant network can be established as shown below, where Z'_{11}, Z'_{12}, Z'_{21} are the secondary LCL two-port Z parameters.

$$\begin{bmatrix} 1 & 0 & 0 & 0 \\ 1 & 0 & -Z'_{11} & -Z'_{12} \\ 0 & 1 & -Z'_{21} & -Z'_{22} \\ 0 & 1 & 0 & R_{ac} \end{bmatrix} \begin{bmatrix} U_s \\ U_{out} \\ -I_s \\ I_{out} \end{bmatrix} = \begin{bmatrix} U_s \\ 0 \\ 0 \\ 0 \end{bmatrix} \tag{8}$$

According to coupling theory, U_s is affected by I_p and the mutual inductance M between coils L_p and L_s, which can be expressed as follows.

$$U_s = j\omega M I_p \tag{9}$$

According to Equation (8), the output current I_o, the output voltage U_o, and the secondary LCL resonant impedance Z_1 can be obtained, where $C = 1 - \omega^2 C_s L_2$, $D = \omega C_s R_{ac}$.

$$I_o = \frac{U_s}{R_{ac}(1 - C_s L_s \omega^2) - j(C_s L_2 L_s \omega^3 - L_s\omega - L_2\omega)} \tag{10}$$

$$U_{out} = \frac{R_{ac}U_s}{R_{ac}(1 - C_s L_s \omega^2) - j(C_s L_2 L_s \omega^3 - L_s\omega - L_2\omega)} \tag{11}$$

$$Z_2 = \frac{R_{ac} + j\omega(L_2 C - C_s R_{ac}^2 + L_s C^2 + L_s D^2)}{C^2 + D^2} \tag{12}$$

It is evident that the imaginary part of Equation (10) must be set to zero to realize the secondary LCL resonant network constant-current characteristic. Then, the derivation of the resonance condition and the output current of the secondary LCL resonant network are illustrated in Equations (13) and (14), respectively.

$$\omega_s = \frac{1}{\sqrt{C_s L_s}} \tag{13}$$

$$I_o = \frac{U_s}{j\omega L_s} \tag{14}$$

It can be derived from Equations (9) and (14) that I_o is relevant to I_p. To ensure the stability of the output current, the primary side current must be subjected to further

control measures. Specifically, by setting the real part in Equation (3) to zero, the resonance condition of the primary side LCL coupling network can be obtained.

$$\omega_c = \omega_p = \frac{1}{\sqrt{C_p L_1}} \tag{15}$$

Given that $L_1 = n_1 L_p$, $L_2 = n_2 L_s$, I_o can finally be expressed as

$$I_o = \frac{k U_{in}}{j\omega_c \sqrt{L_p L_s} n_1} \tag{16}$$

where both the primary and secondary LCL resonant networks are in resonance, satisfying $\omega_c = \omega_p = \omega_s$. It can be seen from Equation (16) that I_o is affected by the coupling coefficient k, input voltage U_{in}, coil size, and coefficient n_1, but has a constant-current output characteristic under different loads.

Similarly, in order to achieve a constant-voltage output from the secondary LCL coupling network, it is evident from Equation (11) that the secondary resonant network must fulfill the following equation:

$$\omega_v = \frac{\sqrt{1 + \frac{1}{n_2}}}{\sqrt{C_s L_s}} \tag{17}$$

Thus, the following equations can be obtained:

$$Z_2 = \frac{R_{\mathrm{ac}} + \mathrm{j}\omega_v \frac{1}{n_2} C_{\mathrm{s}} R_{\mathrm{ac}}^2}{n_2^2 + (1 + \frac{1}{n_2}) \frac{C_{\mathrm{s}}}{L_{\mathrm{s}}} R_{\mathrm{ac}}^2} \tag{18}$$

$$Z_{\mathrm{eq}} = \frac{(\omega_v M n_2)^2}{R_{\mathrm{ac}}} - \mathrm{j} n_2 \omega_v^3 M^2 C_{\mathrm{s}} \tag{19}$$

$$U_{out} = \frac{j\omega_v M U_{in}}{j\frac{1}{n_2^2}\left[(n_1 - \frac{1}{n_2})L_p + \frac{k^2 L_s (1+1/n_2)}{n_1 C_p}\right] - \frac{k^2 L_s (1+1/n_2)}{n_1 C_p R_{ac}}} \tag{20}$$

It can be seen from Equation (20) that the secondary LCL resonant network can achieve a constant-voltage output approximately when R_{ac} is far larger than n_1. From the above analysis, it can be concluded that by properly configuring the parameters of the LCL resonant network, a constant-current output can be achieved under light load conditions, and a constant-voltage output can be achieved under heavy load conditions, which allows the LCL resonant network to be utilized in battery-charging applications.

2.3. Parameter Design of the Proposed System

Based on the above analysis, the system achieves load-independent CC and CV outputs at two resonant frequency points by appropriately configuring the parameters of the LCL coupling network. The flowchart for the system parameter design process is shown in Figure 4. The design process begins with determining the operating frequency for the constant-current output mode, along with the desired output current and other system parameters. In this design, the input power supply is set to 30 V, and the output current is specified as 1.5 A. Subsequently, the size and turns of the coils can be determined. And the inductance of the primary and secondary coils, as well as the mutual inductance between the coils, are measured. Using these values, the related resonant compensation network parameters are calculated to ensure the desired performance of the system.

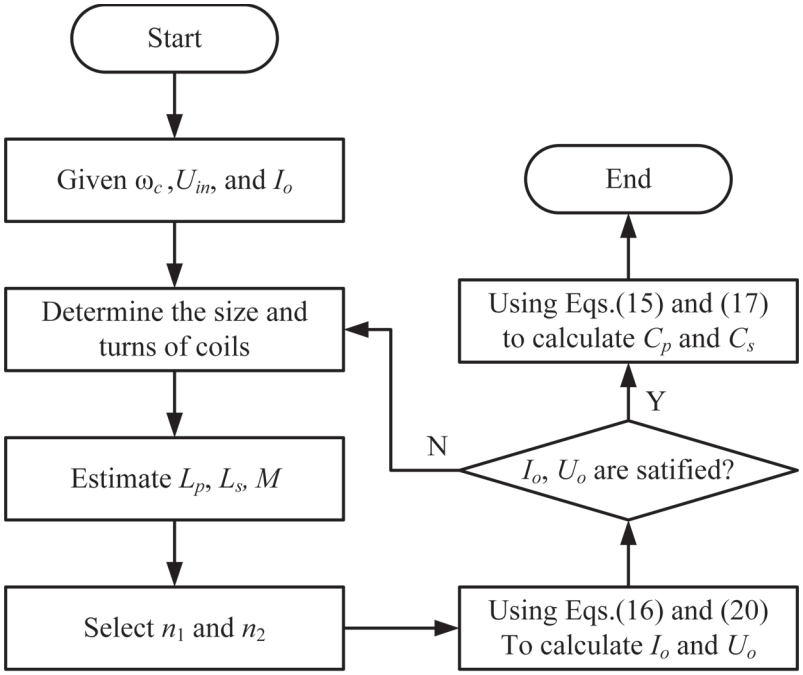


Figure 4. The flowchart for the system parameter design process.

2.4. Control System Design

From the above analysis, it can be seen that by properly configuring the LCL coupling network parameters, the system's load-independent constant-current and constant-voltage output can be achieved at two different frequency points, which can be used for battery charging. Thus, the control system can be designed as shown in Figure 5. The designed system operates in two modes: constant-current mode and constant-voltage mode, which can be switched by mode selection. The battery-charging current I_o and voltage V_o are measured using current and voltage sensors, which are then compared to the reference charging values I_{oref} and V_{oref}, respectively. The errors between the measured and reference currents, as well as the differences between the measured and reference voltages, serve as inputs for FM controllers. The output of the FM controller, after being processed through a limiter, determines the operating frequency f of the system.

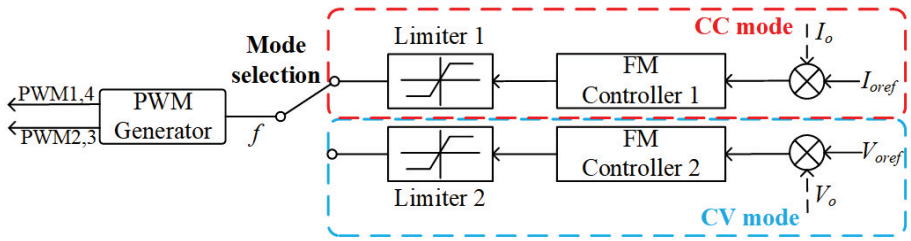


Figure 5. The designed control system.

3. The LCL Resonant Network Parameter Design and Simulation Verification

To verify the correctness of the theoretical analysis, the appropriate LCL coupling network is designed to provide constant-current output under light-load conditions and constant-voltage output under heavy-load conditions.

3.1. Parameter Scanning Simulation

The parameter scanning simulation was carried out in MATLAB2023 to explore the influence of ω, coefficients n_1 and n_2, and the coupling coils' inductance L_p and L_s on the LCL resonant network output. And part of the simulation parameters are listed in Table 1.

Table 1. Part of the scanning simulation parameters in MATLAB.

Parameter	Values
Input voltage U_{in}	24 V
Normalized switching angular frequency ω_n	0.5~2
Equivalent load R_{ac}	10~90 ohms
Primary resonant inductance L_p	8.5 u
Primary resonant capacitor C_p	0.4 u
Secondary resonant inductance L_s	17.5 u
Secondary resonant capacitor C_s	0.2 u
coefficient n_1, n_2	0.5~2
Coupling coefficient k	0.3

Figure 6 shows the variation curve of I_{out} with normalized angular frequency ω_n under different loads, where $n_1 = n_2 = 1$, $\omega_n = \omega/\omega_c$. Under different loads, the output current increases first and then decreases as ω_n increases. In addition, when $\omega_n = 1$, the LCL coupling network has a load-independent constant-current characteristic output.

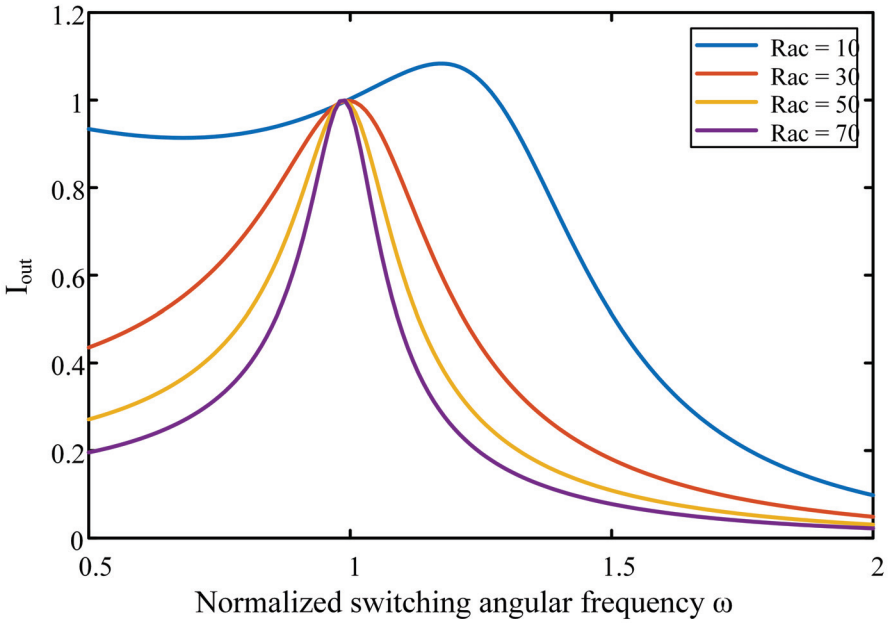


Figure 6. The influence of ω_n on I_{out} under different loads.

Figure 7 shows that the LCL resonant network output voltage varies with the normalized angular frequency under different loads, where $n_1 = n_2 = 1$, and $\omega_n = \omega/\omega_v$. It can be seen that U_{out} initially rises before gradually decreasing when ω_n increases from 0.5 to 2. Notably, within a wide frequency range of ω_n from 0.9 to 2, U_{out} almost remains unaffected by the changes in R_{ac}, which demonstrates that the LCL resonant network has a constant output voltage under the condition that $\omega_n > 0.9$.

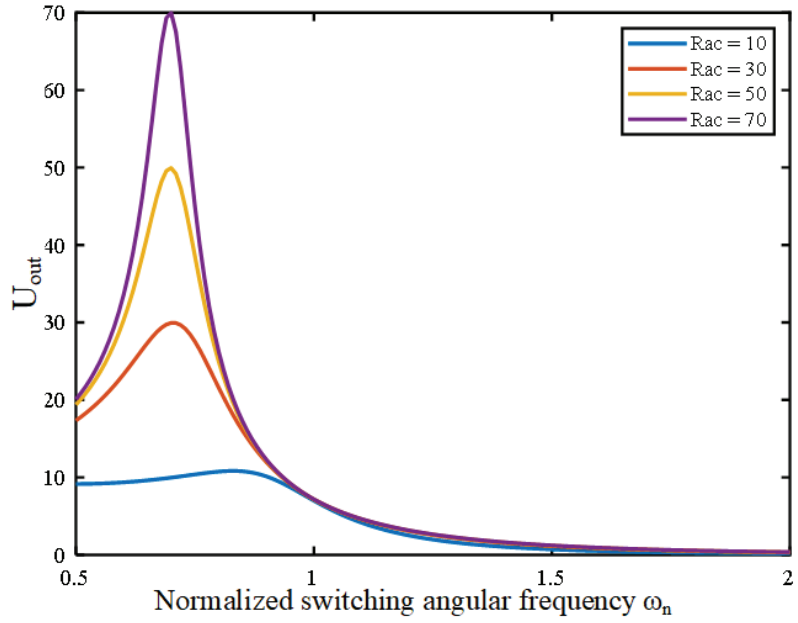


Figure 7. The influence of ω_n on U_{out} under different loads.

In order to investigate the influence of different coefficients on the system output current, the output current of the LCL resonant network was obtained under a load of 20 ohms for various combinations of coefficients n_1 and n_2, as shown in Figure 8. It can be observed that as ω_n increases, I_{out} initially rises and then decreases. Furthermore, when n_1 is fixed, the system has a constant-current output characteristic at $\omega_n = 1$ under different values of n_2. Notably, as n_2 increases, I_{out} varies with ω_n quickly. Additionally, the output of the LCL resonant network approximates a constant voltage, displaying load-independent characteristics for different combinations of n_1 and n_2 when $\omega_n > 1.3$.

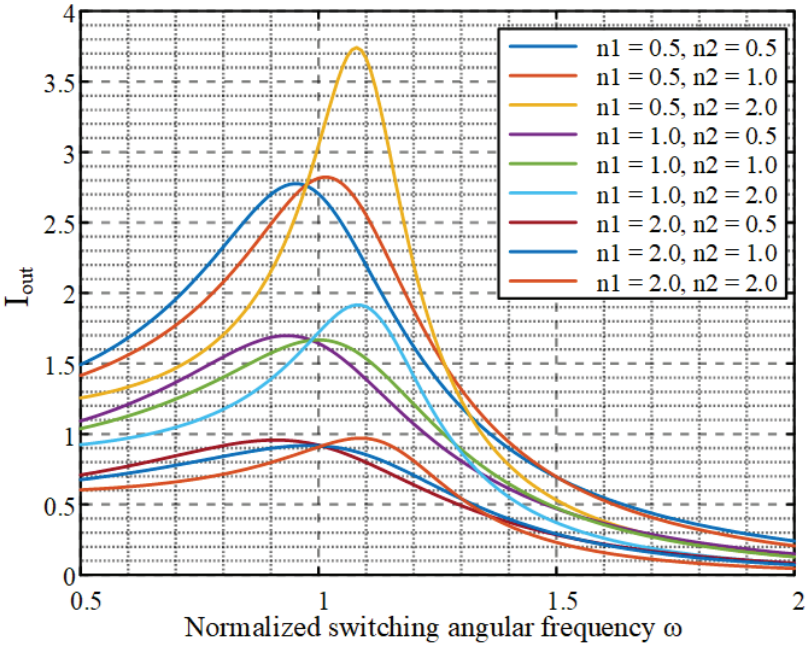
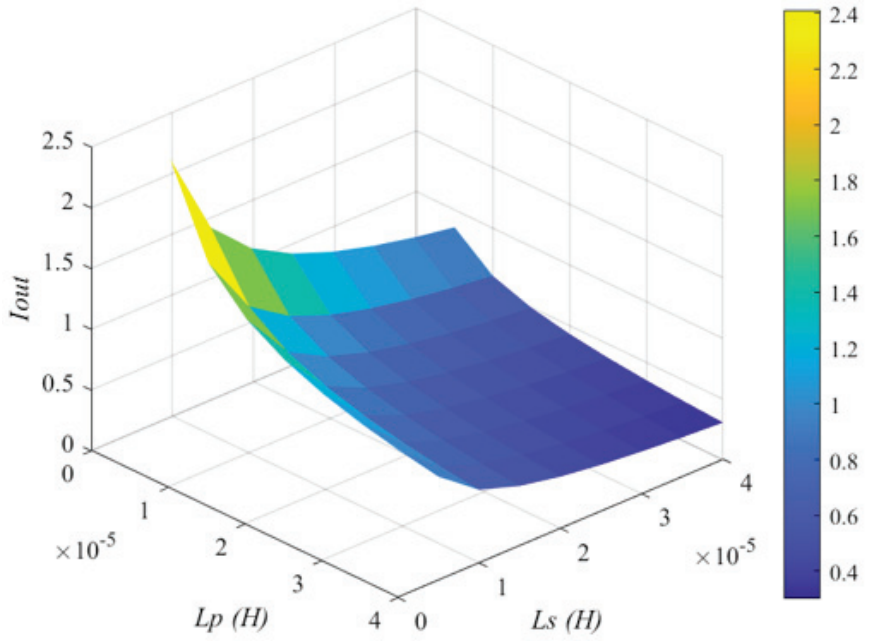


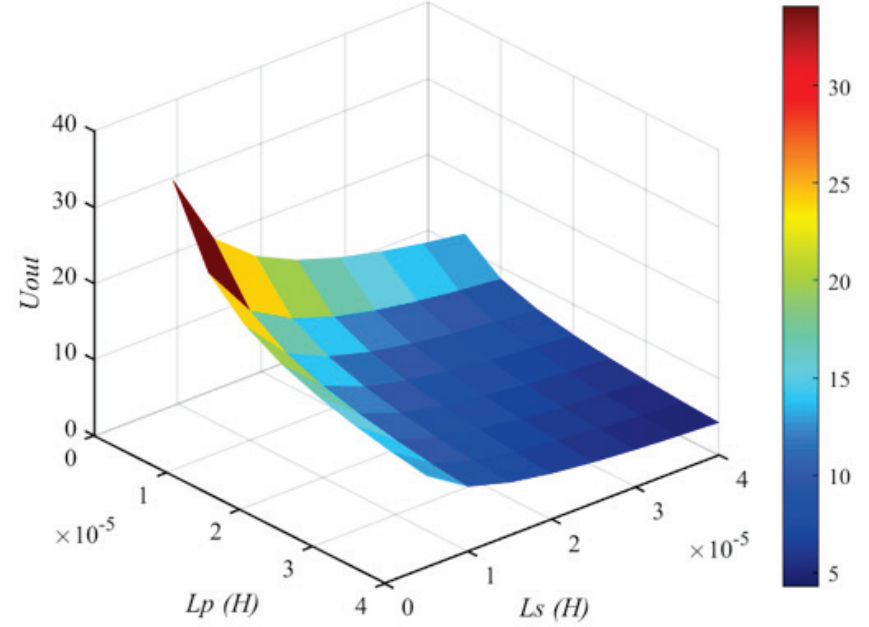
Figure 8. The influence of coefficients n_1 and n_2 on system output current I_{out}.

Figure 9 presents a 3D plot illustrating the output current and voltage of the LCL resonant network as functions of L_p and L_s when the system operates at frequencies ω_c and ω_v, respectively, with a load of 20 ohms and $n_1 = n_2 = 1$. It can be seen that

both the maximum output current and maximum output voltage decrease as L_p and L_s increase. Therefore, smaller values of L_p and L_s are preferable to achieve higher current and voltage gains.



(**a**) The influence of L_p and L_s on I_{out} ($\omega = \omega_c$).



(**b**) The influence of L_p and L_s on U_{out} ($\omega = \omega_v$).

Figure 9. The output characteristics of the LCL resonant network vs. L_P and L_s at two different frequency points ω_c and ω_v. (**a**) Influence on output current I_{out} at $\omega = \omega_c$; (**b**) influence on output voltage U_{out} at $\omega = \omega_v$.

The parameter scanning simulation results show the influence of coefficients n_1, n_2, ω, L_p, and L_s on the input characteristics of the LCL resonant network. It can be seen that by appropriately configuring the LCL resonant network parameters, the constant-current or constant-voltage output of the system can be achieved, independent of the load conditions.

3.2. Simulation Verification in PSIM

As illustrated in Figure 5, two PI controllers are employed to regulate the system in either constant-current (CC) or constant-voltage (CV) operation modes. Each controller introduces small perturbations around the fixed frequency corresponding to the selected operation mode, enabling the system to maintain stable output in either constant-current or constant-voltage conditions. To validate the effectiveness of the designed controllers, the AC sweep function in PSIM was utilized to analyze the system's frequency response.

Figures 10 and 11 show the Bode diagrams of the system under different loads in constant-current mode and constant-voltage mode, respectively. As illustrated in Figure 10, the system operates in constant-voltage mode with a crossover frequency of 10.2 kHz and a phase margin of 52.3°. In contrast, as depicted in Figure 11, the system operates in constant-current mode with a crossover frequency of 5.76 kHz and a significantly higher phase margin of 122.2°. These results confirm that the system remains stable under both CC and CV modes.

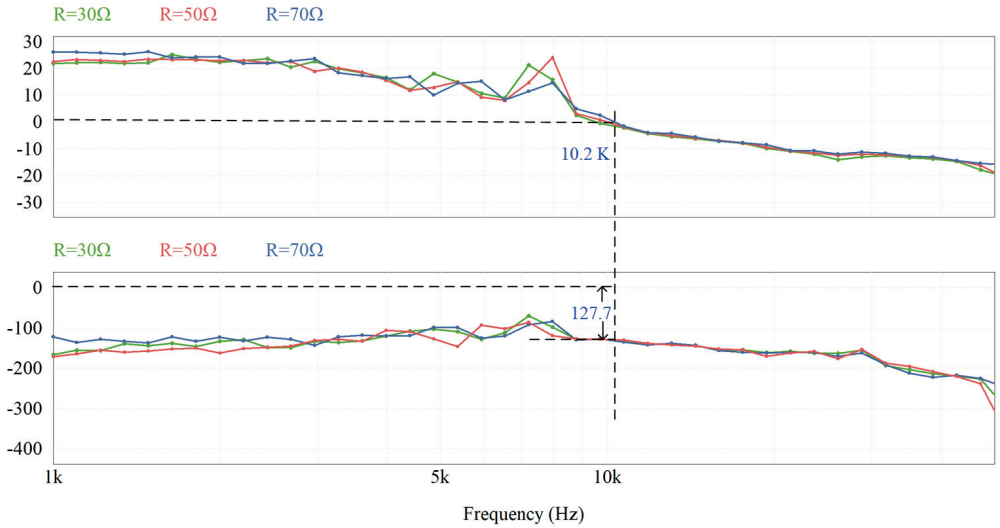


Figure 10. Bode plots of the designed system at different loads in CV mode.

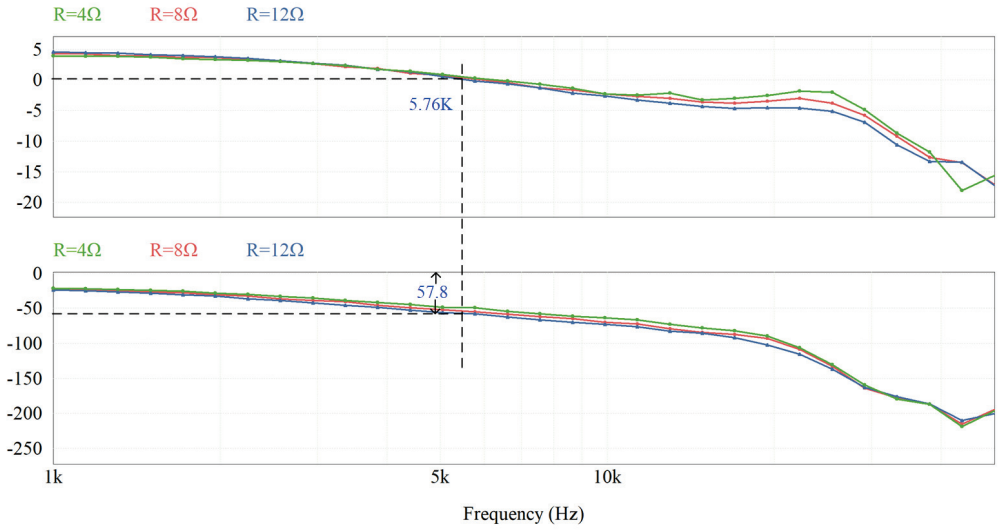


Figure 11. Bode plots of the designed system at different loads in CC mode.

4. Experimental Platform Verification

An experimental platform has been built to verify system efficiency as displayed in Figure 12, where the electronic load is used to simulate the resistance of the battery during

charging. The detailed experiment parameters are depicted in Table 2. In addition, the two switches on each half-bridge inverter are in a complementary state with a duty cycle of 0.5.

Table 2. The system parameters.

Parameter	Values
Primary inductance L_1	8.5 u
Secondary inductance L_s	17.5 u
Primary resonant inductance L_p	8.5 u
Primary resonant capacitor C_p	0.4 u
Secondary resonant inductance L_s	17.5 u
Secondary resonant capacitor C_s	0.2 u
DSP controller	dsPIC33FJ64GS606
Voltage sensor	HVS-AS3.3
Current sensor	CHCS-PS3.3-15A

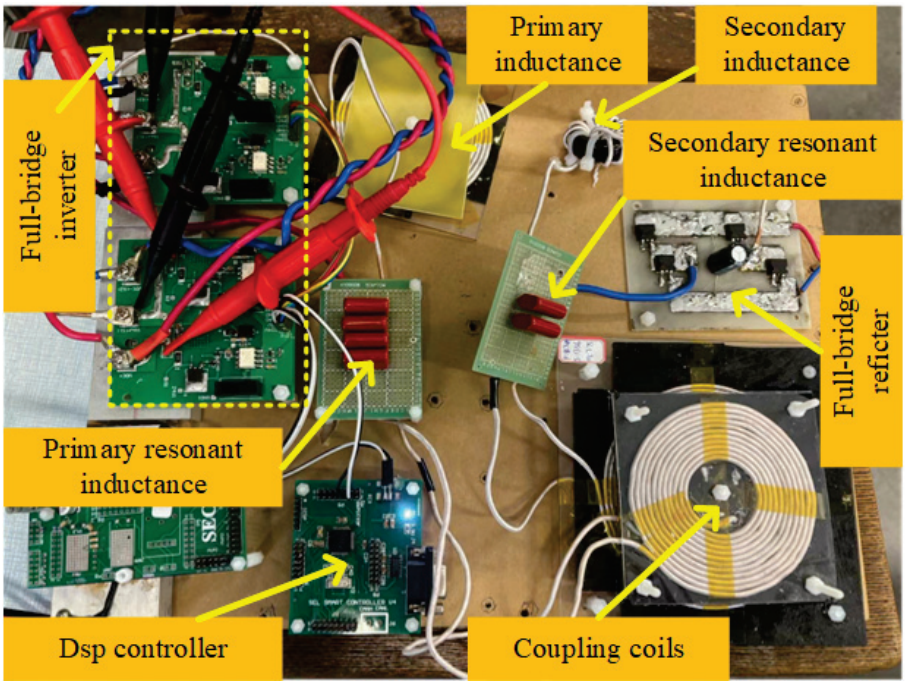


Figure 12. The experimental platform.

4.1. System Characteristic Scanning

The system characteristic scanning experiment aims to verify the relationship between system output and switching frequency across various load conditions, where a 12 V voltage source is used as the system input. Figures 13 and 14 present the curves illustrating the variations in system output current and voltage as the switching frequency changes from 80 kHz to 130 kHz under different loads. In addition, ω_c and ω_v can be calculated as 85 K and 120.2 K, respectively, by Equations (15) and (17).

Figure 13 shows that the load current varies with switching frequency under different loads (R = 4 Ω, 8 Ω, 12 Ω). It can be seen that the load current shows a trend of first increasing and then decreasing with an increase in switching frequency. So, FM can be used to adjust the load current. Moreover, the load-independent constant-voltage characteristic of the system can be obtained approximately when the switching frequency is near ω_c.

Figure 14 shows the load voltage curve with the switching frequency under different loads (R = 30 Ω, 50 Ω, 70 Ω). As the switching frequency f increases from 80 K to 130 K, the load voltage shows a trend of first increasing and then decreasing, so the load volt-

age can be adjusted by the PF control. In addition, the system has a constant-voltage characteristic independent of the load when the switching frequency is near ω_v.

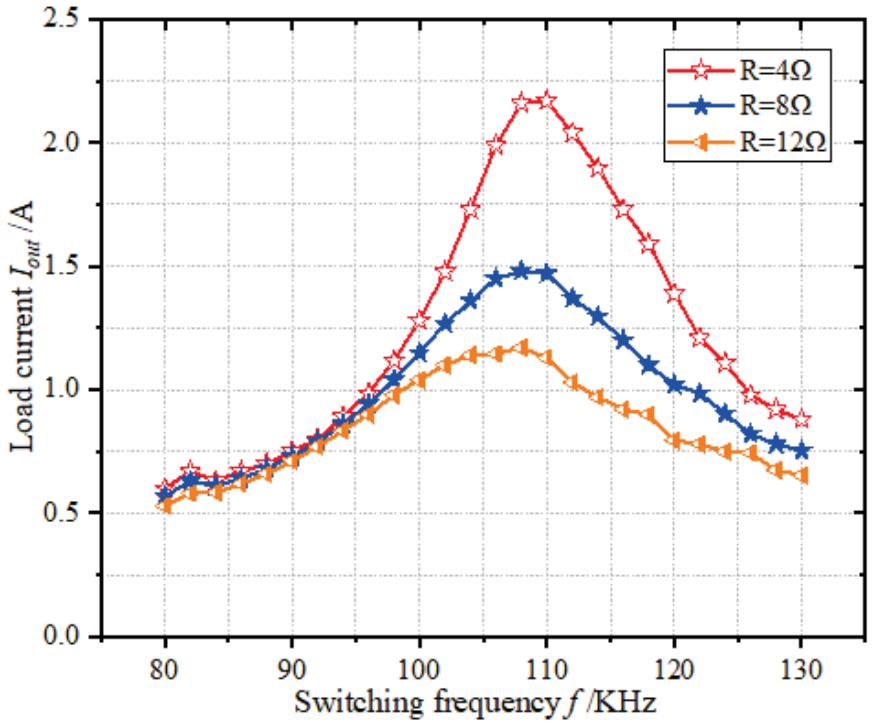


Figure 13. Load current *VS* switching frequency under different loads (U_{in} = 12 V).

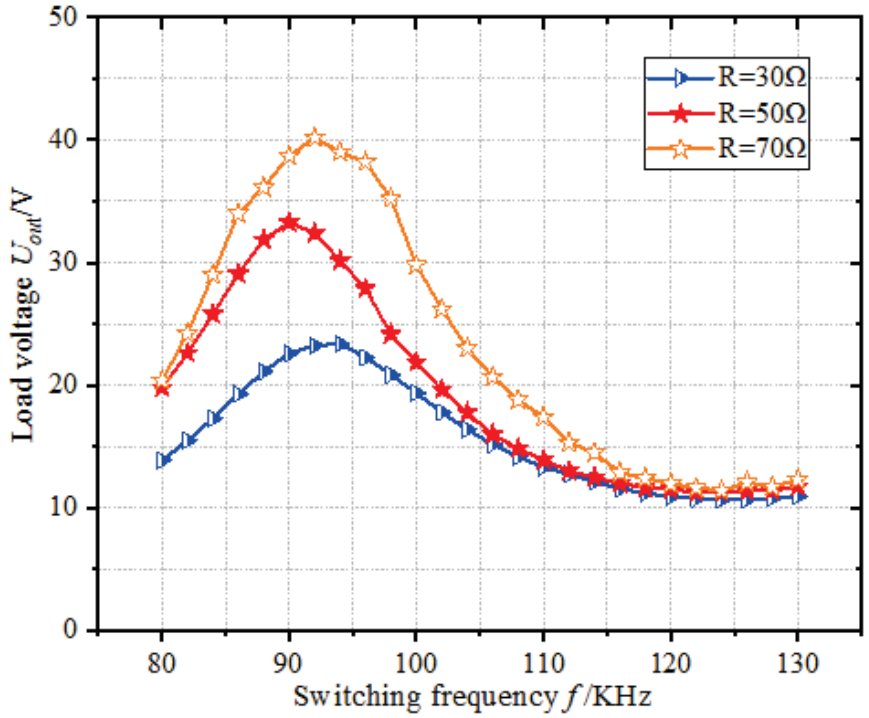


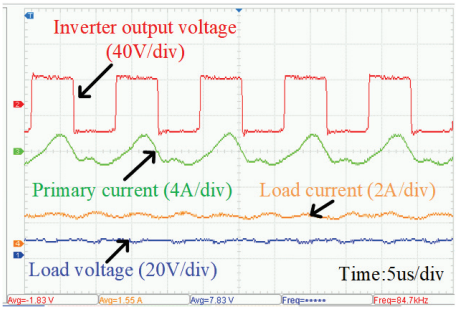
Figure 14. Load voltage *VS* switching frequency under different loads (U_{in} = 12 V).

4.2. System Dynamic Response Test

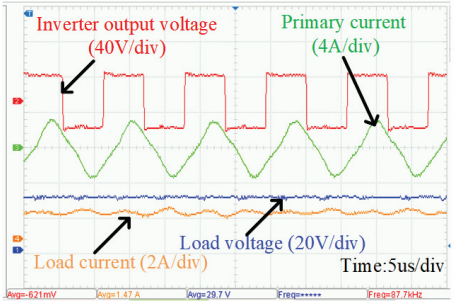
The system dynamic response experiment aims to verify the effectiveness of the designed controller, which can be divided into two phases: phase 1: the system's dynamic response to sudden load changes in CC mode; phase 2: the system's response to sudden load changes in CV mode. In addition, a 30 V voltage source is used as the system input

and an electronic load is used to simulate the change in load resistance during battery charging. Moreover, when the system operates in CC mode, the load current is set to 1.5 A, while in CV mode, the load voltage is set to 33 V.

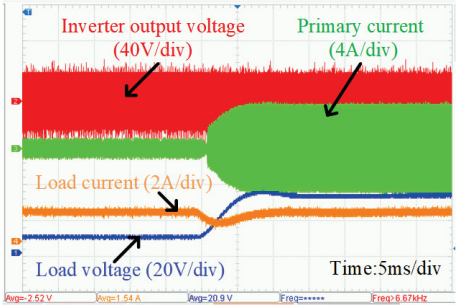
Figure 15 illustrates the dynamic response of the system when the load suddenly changes from 5 ohms to 20 ohms in CC mode, with the system output current set to 1.5 A. It can be seen that Figure 15a illustrates the system's operation in CC mode under a load resistance of 5 ohms, achieving a load current of 1.55 A with an efficiency of 80.6%. Figure 15b demonstrates the system operating in CC mode with a load resistance of 20 ohms, delivering a load current of 1.47 A and achieving an efficiency of 83.9%. It is evident from these figures that the output current is effectively maintained at the desired value. Figure 15c depicts the dynamic response characteristics of the system during the sudden load change from 5 ohms to 20 ohms. The results show that after the load change, the load current quickly stabilizes at the set value within 8 ms, indicating that the designed controller effectively manages sudden load changes while operating in CC mode.



(**a**) Steady-state waveform when R = 5 ohms.



(**b**) Steady-state waveform when R = 20 ohms.



(**c**) System dynamic response to sudden load changes in CC mode

Figure 15. System dynamic response to sudden load changes from 5 ohms to 20 ohms in CC mode. (**a**) Steady-state waveform when R = 5 ohms, (**b**) steady-state waveform when R = 20 ohms, (**c**) system dynamic response to sudden load changes from 5 ohms to 20 ohms.

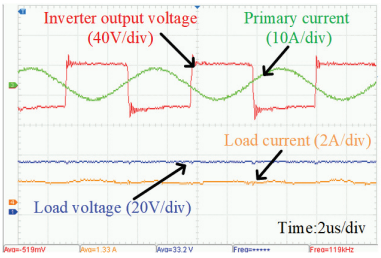
In order to show the advantages of the proposed system compared to related works, a detailed comparison is presented in Table 3. As shown in Table 3, the proposed system requires fewer resonance compensation components and eliminates the need for additional

switches. These features significantly contribute to reducing system cost and simplifying the control strategy, demonstrating the system's practicality.

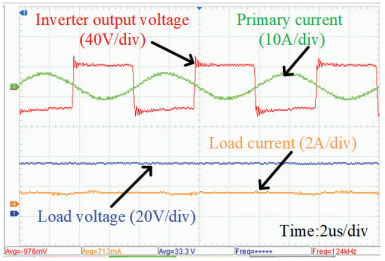
Figure 16 shows the system dynamic response waveform and the system steady-state waveform when the system is in CC mode and the load resistance suddenly changes from 25 to 50 ohms, where the system output voltage is set as 33V. Figure 16a,b are the steady-state waveforms of the system when the load resistance is 25 ohms and 50 ohms, respectively, showing that the designed controller can control the system output voltage to the designed value under different loads. As shown in Figure 16a, the system achieves a load current of 1.33 A, a load voltage of 33.2 V, and an efficiency of 82.1%. Similarly, Figure 16b illustrates the system operating with a load voltage of 33.3 V, a load current of 0.713 A, and an efficiency of 79.5%. Figure 16c is the dynamic response of the system to load changes. It can be seen that after the load change, the load current reaches a new steady state after a short drop of 10 ms. During this process, the load voltage remains stable at 33 V, indicating that the designed controller can cope with the change in load resistance in CV mode and maintain the stability of the system output voltage.

Table 3. Comparison results between proposed system and previous related work.

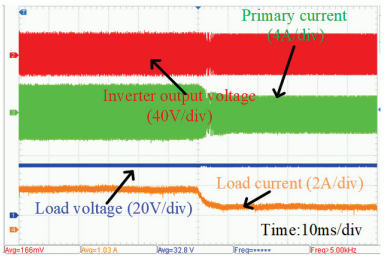
Proposed in	Ref. [21]	Ref. [22]	Ref. [23]	Ref. [25]	This Work
Modulation	Switches	PSM	FM	FM	FM
Additional switches	YES	NO	NO	NO	NO
Additional coils	NO	NO	YES	NO	NO
Compensation components	7	2	6	6	4



(**a**) Steady-state waveform when R = 25 ohms.



(**b**) Steady-state waveform when R = 50 ohms.



(**c**) System dynamic response to sudden load changes in CV mode

Figure 16. System dynamic response to sudden load changes from 25 ohms to 50 ohms in CV mode. (**a**) Steady-state waveform when R = 25 ohms, (**b**) steady-state waveform when R = 50 ohms, (**c**) system dynamic response to sudden load changes from 25 ohms to 50 ohms.

5. Conclusions

This paper proposes a novel wireless power transfer system based on an LCL coupling network with a load-independent CC or CV output for battery charging. FM control has been applied to adjust the CC or CV output characteristic of the system, providing flexibility and reliability during the charging process. The impact of LCL coupling network parameters on system output characteristics was assessed in a MATLAB environment. A PSIM simulation model was built to verify the correctness of the theoretical analysis. The simulation results show that the system can achieve load-independent constant-current or -voltage output characteristics at two different frequency points. Finally, an experimental platform based on the dsPIC33FJ64GS606 digital controller was built to verify the system's robustness during sudden load resistance changes when the system operates in CC or CV mode. The experimental results show that when the load resistance experiences a significant change from 5 ohms to 20 ohms, representing a 300% increase in load, the system has an excellent dynamic performance by quickly responding and stabilizing within 8 ms with the desired load current of 1.5 A. The system also has an excellent dynamic response during sudden load changes from 25 ohms to 50 ohms with a desired voltage of 33 V. Thus, the designed controller can respond quickly to sudden load changes and maintain the output current or voltage at the desired value regardless of whether the system is in CC or CV mode.

Author Contributions: Conceptualization, S.X. and S.H.; methodology, S.H.; software, P.N.; validation, L.S. and Z.W.; formal analysis, P.N.; investigation, S.X.; resources, P.N.; data curation, T.K.; writing—original draft preparation, P.N.; writing—review and editing, S.X.; visualization, S.X.; supervision, S.H.; project administration, S.X.; funding acquisition, S.H. All authors have read and agreed to the published version of the manuscript.

Funding: This research received no external funding.

Data Availability Statement: Data are contained within the article.

Conflicts of Interest: The authors declare no conflicts of interest.

References

1. Devassy, S.; Singh, B. Performance analysis of solar PV array and battery integrated unified power quality conditioner for microgrid systems. *IEEE Trans. Ind. Electron.* **2020**, *68*, 4027–4035. [CrossRef]
2. Fathabadi, H. Improving the power efficiency of a PV power generation system using a proposed electrochemical heat engine embedded in the system. *IEEE Trans. Power Electron.* **2018**, *34*, 8626–8633. [CrossRef]
3. Xiao, J.; Jiang, C.; Wang, B. A review on dynamic recycling of electric vehicle battery: Disassembly and echelon utilization. *Batteries* **2023**, *9*, 57. [CrossRef]
4. Komiyama, Y.; Komanaka, A.; Zhu, W.; Konishi, A.; Nguyen, K.; Sekiya, H. Analysis and Design of Load-Independent Series Resonant Power Amplifier with Constant Current Output and Its Application for WPT System. *IEEE Trans. Power Electron.* **2024**, *39*, 6515–6525. [CrossRef]
5. [CrossRef] Chen, W.; Liu, Z.; Liu, J.; Su, H. Analysis and Design of Wireless Charging Systems Without Extra Components for Load-Independent Constant Current and Voltage Battery Charging. *IEEE J. Emerg. Sel. Top. Power Electron.* **2024**, *12*, 3200–3210. [CrossRef]
6. Li, Z.; Zhu, C.; Jiang, J.; Song, K.; Wei, G. A 3-kW wireless power transfer system for sightseeing car supercapacitor charge. *IEEE Trans. Power Electron.* **2016**, *32*, 3301–3316. [CrossRef]
7. Li, H.; Li, J.; Wang, K.; Chen, W.; Yang, X. A Maximum Efficiency Point Tracking Control Scheme for Wireless Power Transfer Systems Using Magnetic Resonant Coupling. *IEEE Trans. Power Electron.* **2015**, *30*, 3998–4008. [CrossRef]
8. Vu, H.N.; Choi, W. A novel dual full-bridge LLC resonant converter for CC and CV charges of batteries for electric vehicles. *IEEE Trans. Ind. Electron.* **2017**, *65*, 2212–2225. [CrossRef]
9. Regensburger, B.; Sinha, S.; Kumar, A.; Maji, S.; Afridi, K.K. High-performance multi-MHz capacitive wireless power transfer system for EV charging utilizing interleaved-foil coupled inductors. *IEEE J. Emerg. Sel. Top. Power Electron.* **2020**, *10*, 35–51. [CrossRef]

10. Tan, L.; Guo, J.; Huang, X.; Liu, H.; Wang, W.; Yan, C.; Zhang, M. Coordinated source control for output power stabilization and efficiency optimization in WPT systems. *IEEE Trans. Power Electron.* **2017**, *33*, 3613–3621. [CrossRef]
11. Chittoor, P.K.; Chokkalingam, B.; Mihet-Popa, L. A review on UAV wireless charging: Fundamentals, applications, charging techniques and standards. *IEEE Access* **2021**, *9*, 69235–69266. [CrossRef]
12. Zhang, W.; Mi, C.C. Compensation topologies of high-power wireless power transfer systems. *IEEE Trans. Veh. Technol.* **2015**, *65*, 4768–4778. [CrossRef]
13. Wu, S.-T.; Han, C.-H. Design and implementation of a full-bridge LLC converter with wireless power transfer for dual mode output load. *IEEE Access* **2021**, *9*, 120392–120406. [CrossRef]
14. Jia, Y.; Zhao, L.; Wang, Z.; Tang, C.; Chen, F.; Feng, H. Integrated LCC-LCC Topology for WPT System with CC Output Regarding Air Gap and Load Variations. *IEEE Trans. Power Electron.* **2024**, *39*, 11904–11915. [CrossRef]
15. Yao, Y.; Wang, Y.; Liu, X.; Lin, F.; Xu, D. A novel parameter tuning method for a double-sided LCL compensated WPT system with better comprehensive performance. *IEEE Trans. Power Electron.* **2017**, *33*, 8525–8536. [CrossRef]
16. Yang, L.; Ren, L.; Shi, Y.; Wang, M.; Geng, Z. Analysis and design of an S/S/P-compensated three-coil structure WPT system with constant current and constant voltage output. *IEEE J. Emerg. Sel. Top. Power Electron.* **2022**, *11*, 2487–2500. [CrossRef]
17. Li, K.; Gong, Z.; Liu, Q.; Zheng, S.; Liu, J.; Wang, S. A MCR-WPT system based on LCL-S/P hybrid compensation network with CC/CV and maximum power optimization suiting for battery charging. *IET Power Electron.* **2024**, *17*, 351–363. [CrossRef]
18. Auvigne, C.; Germano, P.; Ladas, D.; Perriard, Y. A dual-topology ICPT applied to an electric vehicle battery charger. In Proceedings of the International Conference on Electrical Machines, Marseille, France, 2–5 September 2012; pp. 2287–2292.
19. Wei, Y.; Luo, Q.; Mantooth, H.A. An LLC and LCL-T resonant tanks based topology for battery charger application. *CPSS Trans. Power Electron. Appl.* **2021**, *6*, 263–275. [CrossRef]
20. Qu, X.; Han, H.; Wong, S.C.; Tse, C.K.; Chen, W. Hybrid IPT topologies with constant current or constant voltage output for battery charging applications. *IEEE Trans. Power Electron.* **2015**, *30*, 6329–6337. [CrossRef]
21. Chen, Y.; Kou, Z.; Zhang, Y.; He, Z.; Mai, R.; Cao, G. Hybrid topology with configurable charge current and charge voltage output-based WPT charger for massive electric bicycles. *IEEE J. Emerg. Sel. Top. Power Electron.* **2017**, *6*, 1581–1594. [CrossRef]
22. Song, K.; Li, Z.; Jiang, J.; Zhu, C. Constant current/voltage charging operation for series-series and series-parallel compensated wireless power transfer systems employing primary-side controller. *IEEE Trans. Power Electron.* **2018**, *33*, 8065–8080. [CrossRef]
23. Tran, D.H.; Vu, V.B.; Choi, W. Design of a high-efficiency wireless power transfer system with intermediate coils for the on-board chargers of electric vehicles. *IEEE Trans. Power Electron.* **2017**, *33*, 175–187. [CrossRef]
24. Yang, L.; Li, X.; Liu, S.; Xu, Z.; Cai, C.; Guo, P. Analysis and design of three-coil structure WPT system with constant output current and voltage for battery charging applications. *IEEE Access* **2019**, *7*, 87334–87344. [CrossRef]
25. Vu, V.-B.; Tran, D.-H.; Choi, W. Implementation of the constant current and constant voltage charge of inductive power transfer systems with the double-sided LCC compensation topology for electric vehicle battery charge applications. *IEEE Trans. Power Electron.* **2017**, *33*, 7398–7410. [CrossRef]

Disclaimer/Publisher's Note: The statements, opinions and data contained in all publications are solely those of the individual author(s) and contributor(s) and not of MDPI and/or the editor(s). MDPI and/or the editor(s) disclaim responsibility for any injury to people or property resulting from any ideas, methods, instructions or products referred to in the content.

energies

MDPI

Article

Leveraging Positive Energy Districts Surplus for the Achievement of the Sustainable Development Goals

Maurizio Cellura [1,2], Alberto Fichera [3], Francesco Guarino [2] and Rosaria Volpe [3,*]

[1] Centre for Sustainability and Ecological Transition, University of Palermo, Piazza Marina 61, 90133 Palermo, Italy; maurizio.cellura@unipa.it
[2] Department of Engineering, University of Palermo, Viale Delle Scienze, Building 9, 90133 Palermo, Italy; francesco.guarino@unipa.it
[3] Department of Electrical, Electronics and Computer Engineering, University of Catania, Via Santa Sofia 64, 95125 Catania, Italy; alberto.fichera@unict.it
* Correspondence: rosaria.volpe@unict.it

Abstract: This study explores the role of Positive Energy Districts (PEDs) in promoting sustainable urban development. PEDs, defined as urban areas that achieve net-zero energy import and CO_2 emissions while producing a surplus of renewable energy, have gained attention as a promising solution to the challenges of urban sustainability. This research presents a comprehensive methodology for assessing the impact of PEDs on key United Nations' Sustainable Development Goals (SDGs), such as energy accessibility (SDG 7), sustainable cities (SDG 11), and climate action (SDG 13). By examining a case study of a potential PED in Southern Italy, this study demonstrates that PEDs can not only produce sufficient energy to meet their electrical demands, but also support up to 30 low-income households through surplus redistribution, offering an estimated annual economic savings of EUR 1145 per household. Thus, this surplus energy redistribution highlights the practical potential of PEDs to alleviate energy poverty, enhance social equity, and foster community solidarity, thereby extending their impact beyond energy sustainability. Additionally, the correlation between self-consumption and virtual distribution is equal to 0.83, suggesting that PEDs with high self-consumption are also actively involved in virtual distribution, posing the condition for efficient energy use.

Keywords: performance indicators; environmental; economic; social; urban areas; buildings

1. Introduction

The built environment is energy intensive, using more than the 60% of the energy consumption worldwide [1] and, as cities are hubs of economic activity and population density, they are central to steering the trajectory of sustainable development. In this framework, the energy demands of the built environment in urban areas make cities key players in the transition to more sustainable energy systems. Central to this transformation is the emergence of Positive Energy Districts (PEDs), which represent an example of how urban habitats can evolve to meet the diverse objectives related to environmental sustainability and energy efficiency.

The European Union, recognizing the criticality of this evolution, includes the PEDs through its "Positive Energy Districts for Sustainable Urban Transformation" initiative, nestled within the broader SET-Plan's "Smart Cities and Communities" directive [2]. According to the definition, a Positive Energy District (PED) can be considered as a "district with annual net zero energy import and net zero CO_2 emissions, working towards an

annual local surplus production of renewable energy" [3]. The interests in PEDs can be traced back to the European Union's "Clean Energy for All" package, which also brought the formation of energy communities, another example of cooperative urban energy structures [4].

PEDs are characterized by their positive energy surplus [5] and their ability to address environmental, economic, and social sustainability targets [6]. The literature highlights the potential of localized energy production in enhancing district resilience and achieving sustainability goals through collaborative approaches [7]. Incorporating storage systems further reduces grid dependency, enabling community-centric energy-sharing configurations [8]. Key technological and operational features include redistribution within and between districts [9], intelligent building-to-building interactions [10], and energy trading with larger grids [11]. Advanced models have also been developed to assess PED performance. For example, Derkenbaeva et al. employed an agent-based model to evaluate the impact of human-centric behavior on PED pathways, examining energy efficiency and CO_2 emissions reduction [12]. In another study, the integration of agent-based models and fuzzy-logic has been used to evaluate PED contribution toward European sustainability targets for 2020, 2030, and 2050 [13]. Other studies have proposed strategies to improve underperforming buildings [14] and implement energy renovation strategies necessary to achieve the PED status [15].

A consistent amount of literature is debating the constraint of having a net-positive surplus. Gabaldon Moreno et al. introduced a model to measure energy balance within a specific district [16]. They defined the district's perimeter, followed by assessing energy requirements, consumption, and localized generation to assess the final energy balance. The need to have clear and well-defined boundaries also emerge from the surveys and interviews involving engineers, communication experts, and environmental scientists [17]. Apart from retrofitted residential buildings [18], positive balances have been assessed for university campuses [19], non-residential buildings with a bioclimatic design [20], and social housing [21]. The importance of a quantitative energy balance is evident, constituting it as an essential element needed to allow the certification and standardization process [22].

Therefore, as emerging from the cited literature, PEDs are conceived as an urban form able to impact on the environmental, economic, and social dimensions. To this scope, the concept of sustainable PEDs seeks for innovative procedures to balance the pillars of sustainability without having one of the before-mentioned dimensions prevailing on the others [23]. Any technological and operational improvement should be measurable and performances should be quantified to allow for cross comparisons [24]. In addition, the challenge, and also the potential, resides in coherently channeling the positive surplus of PEDs in order to contribute to the aforementioned sustainability of urban areas [25]. In this direction, the Sustainable Development Goals (SDGs) Framework comes to the aid. In fact, SDGs may be helpful to define a structured approach useful to strengthen the beneficial impacts of PEDs in terms of urban sustainability.

The United Nations' Sustainable Development Goals (SDGs) outline a comprehensive framework of 17 goals, 169 targets, and 232 indicators within the "2030 Agenda for Sustainable Development" [26–28]. Among these, SDG 7 focuses on affordable, reliable, and sustainable energy, and holds particular relevance to PEDs. Achieving SDG 7 not only advances energy efficiency and accessibility but also positively impacts health, economic development, and community inclusion. The framework's flexibility enables its integration into specific contexts, such as PEDs, which contribute directly to SDG 7 and intersect with other goals, including SDG 11 (sustainable cities and communities) and SDG 13 (climate action). As underscored in [29], in urban areas, PEDs represent a practical pathway to address these interconnected goals by leveraging renewable energy, improving energy

efficiency, and fostering collaborative energy-sharing systems. By aligning PED objectives with relevant SDGs, such as energy accessibility and climate action, PEDs can serve as catalysts for urban sustainability and societal progress.

Despite the aforementioned models and implementation strategies, comprehensive guidelines on surplus energy utilization to enhance district energy performance and promote sustainable evolution remain relatively uncharted. The transition towards sustainable urban areas needs a holistic vision that delves deep into the impact that PEDs can have in terms of the achievement of environmental, economic, and social targets envisioned by the SDGs. In this direction, this study aims at directing PEDs planning in alignment with SDGs, especially those that are directly linked to PEDs. In more detail, the objectives of this study are the following:

- To propose a procedure to demonstrate how PEDs can directly contribute to the sustainable development of urban areas and to the achievement of pertaining SDGs;
- To evaluate how the energy surplus originating from the renewable production can be sustainably leveraged to target other SDGs;
- To develop tailored indicators to measure the PED's impact in terms of SDGs achievement.

With respect to the above-listed objectives, this paper aims to develop a procedural framework outlining step by step how PEDs can be planned, implemented, and managed in order to achieve specific SDGs. In this perspective, it is of utmost importance to establish the identification of the sources of energy production, the quantification of the energy flows within the district, and the amount available for additional uses. This quantitative analysis is strategic to leverage surplus energy by assessing environmental, economic, and social impacts. This can be achieved by developing tailored indicators for measuring progress towards SDGs that are relevant for PEDs. These indicators are inspired by the SDGs' indicators and then customized to reflect the specific context of PEDs.

Results from a candidate PED area previously derived in [30] and are discussed here. The proposed modeling procedure and the defined indicators are not country-specific, thus permitting them to easily replicate their quantification for different case studies and allowing for cross-comparison among PEDs of different countries.

The remainder of this paper is structured as follows. The Section 2 introduces a four-step procedure to delve into the evaluation of the energy surplus of PEDs and how to allocate it in a sustainable way. Subsequently, the case study selected for the analysis is presented in Section 3 and, in Section 4, the results of the modelling procedure and the redistribution of energy surplus in the area to achieve specific goals is discussed. Finally, limitations and implications of this study are discussed and the conclusion is drawn.

2. Materials and Methods

The implementation of PEDs in urban areas may be considered as a way to foster the sustainable transition advocated by the United Nations. To assess how effectively the implementation of PEDs contributes to achieving one or more SDGs, and concurrently gauge the impact of the positive surplus generated by the installation of renewable energy-based production systems, this research proposes the iterative procedure reported in Figure 1.

2.1. Step 1: PED Implementation and Positive Surplus Evaluation

The first step of the elaborated approach consists in the PED's definition and positive surplus evaluation. The term "positive" in PEDs emphasizes, indeed, that these districts produce more energy than they consume. Therefore, evaluating the positive surplus involves calculating the net energy output after considering the energy consumption of the district. Although being a simple balance between the energy produced by renewable

sources and the energy consumed at the district level, the calculation of the energy surplus at the district level requires a wide set of data, ranging from spatial data (urban scale, geographical boundaries of the districts) to technological data (energy production technology, energy sources—solar, wind, geothermal, etc.—configurations and efficiencies), and including information on the number of buildings, as well as physical and geometrical parameters as the number of floors, height, surface, volume, and available rooftop areas, number of occupants, and eventual energy-trading mechanisms.

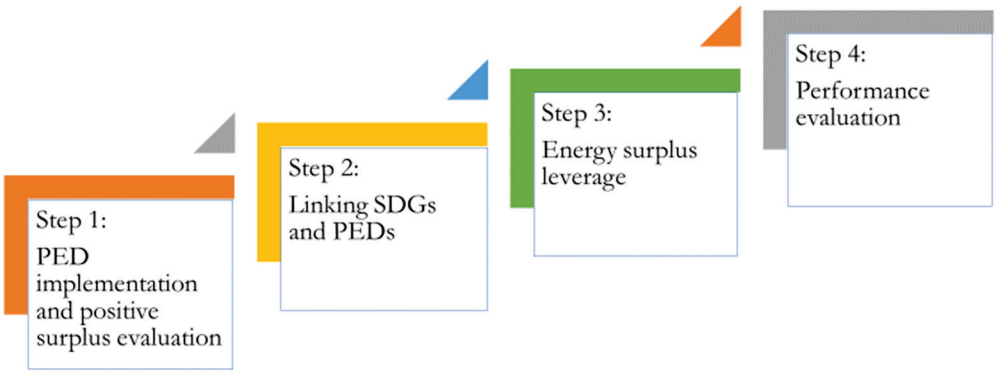


Figure 1. Procedure for performance evaluation of PEDs based on the SDGs.

As said, this surplus is not only a measure of the district's efficiency, but also its potential contribution to the achievement of the SDGs. To perform such an analysis, a tailored modeling approach is needed. By applying the model developed in previous research by the authors [30], the foremost goal of this study is to evaluate how the achieved positive surplus can be converted into a concrete contribution towards the achievement of related SDGs. Each building j within the PED has its own energy demand $E_{dem,j}$ and potentially its own energy production $E_{prod,j}$ from renewable sources. The goal of the model is to optimize the distribution of this energy to achieve the highest level of self-sufficiency, minimizing the reliance on external power grids. To this scope, the objective function can be expressed as

$$\min \sum_{j=1}^{n} E_{g,j} \quad (1)$$

In Equation (1), $E_{g,j}$ is the net imported energy from the grid and n is the total number of buildings in the PED. The model includes the following constraints to ensure that the energy needs of each building are met and that the energy flows are physically feasible. The first constraint refers to the demand and, in particular, the sum of energy produced $E_{prod,j}$ and energy imported from the grid $E_{g,j}$ must be greater or equal to the energy demand for each building:

$$E_{prod,j} + E_{g,j} \geq E_{dem,j}, \forall j \quad (2)$$

In addition, the energy imported from the grid should be non-negative for each building:

$$E_{g,i} \geq 0, \forall j \quad (3)$$

This mathematical formulation permits it to gain awareness on the different energy flows within the PED. In particular, beyond the energy demand and energy production of the area, it is also possible to calculate the amount of energy that is self-consumed from buildings, i.e., in terms of energy that is immediately consumed from renewable production, the energy that is distributed within the district, and the virtual balances within the PED for distribution and with the main grid. Indeed, in this first stage, it is supposed that the PED still maintains its reliance to the grid, to fulfill the demand in case of insufficiency or

to serve as a reservoir to account for the mismatch between production and demand. With this specification, the model can be extended not only to PEDs, but also to existing areas in their transition towards the PED paradigm.

2.2. Step 2: Linking SDGs and PEDs

With a clear understanding of the energy flows within the PED, the next step is to establish a connection between the PEDs and the SDGs. This involves mapping how the various components and energy assets of PEDs align with the broader objectives of SDGs. SDG 7, "Ensure access to affordable, reliable, sustainable and modern energy for all", is probably the most relevant goal to be analyzed for the performance evaluation of PEDs. Indeed, the renewable energy aspect of PEDs directly contributes to SDG 7 (affordable clean energy), while the decentralization and community-focused design of PEDs can be linked to SDG 11 (sustainable cities and communities). These connections are immediate, due to the intrinsic essence of PEDs. However, PEDs also contribute to SDG 12 (responsible consumption and production) and to SDG 13 (climate action). Table 1 reports the list of SDGs, targets, and chosen indicators.

Table 1. Some examples of PED-related SDGs.

SDG	Target	Indicator	SDG	Target	Indicator
SDG 7 	7.1	7.1.1	SDG 11 	11.1	11.1.1
		7.1.2		11.2	11.2.1
	7.2	7.2.1		11.3	11.3.1
	7.3	7.3.1		11.6	11.6.2
	7.b	7.b.1		11.a	11.a.1
SDG 12 	12.7	12.7.1	SDG 13 	13.2	13.2.2
	12.a	12.a.1			

Among the different targets and indicators of SDG 7, the most representative ones chosen in this study are the following:

Target 7.1: "*By 2030, ensure universal access to affordable, reliable, and modern energy services*". This target is measured by two indicators, 7.1.1 and 7.1.2, referring to the access to electricity and primary reliance on clean technologies, respectively. The indicator 7.1.1 is expressed as a percentage by the UN and, usually, data mostly cover the developing countries [31]. The indicator 7.1.2 refers to "clean" technologies, i.e., related to the emission rate targets against fossil fuels [32].

Target 7.2: "*By 2030, increase substantially the share of renewable energy in the global energy mix*", here measured by the indicator 7.2.1 expressed as the percentage of final consumption of energy deriving from renewable sources [33]. More particularly, this indicator considers the amount of renewable energy effectively consumed and not the installed renewable capacity. According to this formulation, it is possible to exclude bias and distortions deriving from intermittency of renewable sources (difficult to take into consideration) and energy losses along the entire energy production and distribution chain [33].

Target 7.3: "*By 2030, double the global rate of improvement in energy efficiency*", for which the indicator 7.3.1 on the dependence of the energy intensity with economic outputs has

been formulated. The UN defines the energy intensity as the amount of energy used to produce one unit of economic output and expressed in terms of GDP [34].

Target 7.b: "*By 2030, expand infrastructure and upgrade technology for supplying modern and sustainable energy services for all in developing countries, in particular least developed countries, small island developing States and landlocked developing countries, in accordance with their respective programmes of support*", measured by indicator 7.b.1 on the installed renewable energy per capita. This indicator refers to developing countries, and has significant impacts in the environmental, economic, and social dimensions [35]. Tracking progress for this indicator will also result in the enhancement of Target 7.1 indicators.

The diffusion of PEDs can also realize the SDG 11: "Make cities and human settlements inclusive, safe, resilient and sustainable". The targets and indicators here included are the following:

Target 11.1: "*By 2030, ensure access for all to adequate, safe and affordable housing and basic services and upgrade slums*", measured by indicator 11.1.1 on the proportion of population living in inadequate housing, as, for example, in case of overcrowding, poor structural quality, or durability of dwellings [36].

Target 11.2: "*By 2030, provide access to safe, affordable, accessible and sustainable transport systems for all, improving road safety, notably by expanding public transport, with special attention to the needs of those in vulnerable situations, women, children, persons with disabilities and older persons*". Here, the indicator 11.2.1 measures the proportion of population with convenient access to the public transport sector. The access is considered "convenient" if the distance from a reference point to the station is achievable with a 500 m walk (in case of buses) or 1 km (in case of trains, metro), as defined by the UN guidelines [37].

Target 11.3: "*By 2030, enhance inclusive and sustainable urbanization and capacity for participatory, integrated and sustainable human settlement planning and management in all countries*". The indicator 11.3.1 could be helpful to highlight the impact of PEDs on land use.

Target 11.6: "*By 2030, reduce the adverse per capita environmental impact of cities, including by paying special attention to air quality and municipal and other waste management*". Among the different indicators that underlie the achievement of this target, here the 11.6.2 has been selected as particularly relevant for PEDs' performance evaluation, which refers to the annual levels of particulate matter in urban settlements and, therefore, directly correlates to air pollution [38].

Target 11.a: "*Support positive economic, social and environmental links between urban, peri-urban and rural areas by strengthening national and regional development planning*". The indicator 11.a.1 counts the number of countries with dedicated development plans at both the regional and territorial level. Any progress achieved in this direction emphasizes a global progress in terms of sustainable transition in urban settlements [39]. Therefore, national policies focusing on PED implementation may be recognized as a significant step towards more sustainable urban areas.

PEDs represent an innovative urban form producing more energy than they consume, therefore also aligning with SDG 12: "Ensure sustainable consumption and production patterns". For this goal, the following targets can be considered as crucial for PED-related contexts:

Target 12.7: "*Promote public procurement practices that are sustainable, in accordance with national policies and priorities*" fits for the sustainable performance evaluation of PEDs, in particular, by calculating the indicator 12.7.1 referring to the number of countries implementing sustainable action plans in public organizations.

Target 12.a: "*Support developing countries to strengthen their scientific and technological capacity to move towards more sustainable patterns of consumption and production*". The indicator

12.a.1 is also used as 7.b.1 [40], therefore, although listed among the relevant targets and indicators, will not be included in the analysis due to overlapping issues.

In the context of urgent climate action demanded by SDG 13, "Take urgent action to combat climate change and its impacts", PEDs actively contribute to mitigating GHGs, also considering that they encapsulate this feature in their definition. For this goal, target 13.2, "*Integrate climate change measures into national policies, strategies and planning*", is highly relevant in the case of PED evaluation and can be measured by indicator 13.2.2, accounting for the total greenhouse gas emissions per year and calculated using the Global Warming Potentials as the common weighting factor [32]. This indicator is based on national inventory reports; a complete repository and time series are available from the United Nations Framework Convention on Climate Change (UNFCCC) website [33].

To facilitate the implementation of the SDGs' framework, the Inter-Agency and Expert-Group on SDGs IAEG-SDGs introduced three tiers to group the indicators on grounds of the data availability and methodological advancement [34]. The classification criteria are defined as Tier I (clear definition of the indicator and relevant data availability at the national level), Tier II (clear definition of the indicator and data availability not regular at the national level), and Tier III (unclear definition of the indicator). In this study, all indicators belong to Tier I, except for 11.2.1 and 12.7.1, classified as Tier II. For these last two indicators, it is convenient to refer to case-specific data for PEDs to facilitate calculation or evaluation.

As mentioned, the indicators should be tailored to capture the essential aspects of PEDs, i.e., measuring the amount of renewable energy produced by a PED in a year or the reduction in greenhouse gas emissions due to PED implementation. The indicator 7.1.1 can be calculated as the proportion of population with access to electricity PP_{EA} and indicator 7.1.2 as the proportion of population with primary reliance on renewable-based production technologies PP_{REN}, as reported below:

SDG 7
$$PP_{EA} = \frac{\text{PED occupants with access to electrical services}}{\text{Total PED occupantsoccupants}} \quad (4)$$

SDG 7
$$PP_{REN} = \frac{\text{PED occupants with primary reliance on renewables}}{\text{Total PED occupants}} \quad (5)$$

The indicator PP_{EA} could be considered as immediately satisfied, being the access to electricity granted for occupants of PEDs. To provide a useful analysis, especially for developed countries, this indicator can be referred to as the district before its identification as a PED or to similar districts not yet defined as PEDs. This, however, may not apply to slums or poor areas. The indicator PP_{REN} is evaluated here considering the proportion of population with installed renewable technologies on or in proximity to their houses. To calculate this indicator, it has to be distinguished between the proportion of population living in buildings or houses in which renewable production technologies have been effectively installed and the population belonging to the PED but not actively contributing to the renewable production, such as those occupants that do not have PV installed on their rooftops.

The indicator 7.2.1 refers to the percentage of renewable energy in the total final energy consumption of the PED. Therefore, it can be calculated by considering the total renewable production from installed technologies in each building j and the energy demand of each building j of the district, as reported in Equation (4):

SDG 7
$$REN_{share} = \frac{\sum_{j=1}^{N} E_{prod}}{\sum_{j=1}^{N} E_{dem}} \cdot 100 \quad (6)$$

Referring to indicator 7.3.1, it can be useful to correlate the energy production with the economic sphere in terms of GDP:

$$\text{SDG 7} \qquad \text{EnEc} = \frac{\sum_{j=1}^{N} E_{prod}}{\text{Total GDP}} \tag{7}$$

The indicators for SDG 11 are translated into the PED concept as follows. The indicator 11.1.1 refers to the population living in inadequate housing. Again, PEDs ensure adequate, safe, and energy-efficient buildings. Therefore, the analysis of this indicator may help in comparing PEDs to the regional or national reference values or to similar districts not yet recognized as PEDs. It can be expressed as

$$\text{SDG 11} \qquad PP_{housing} = \frac{\text{Occupants with inadequate housing}}{\text{Total occupants}} \tag{8}$$

This indicator may be useful for urban planners and developers as it helps to identify areas where housing conditions are below acceptable standards, thus allowing for targeted interventions and, consequently, resource allocation. In addition, from the social viewpoint, it can also highlight disparities in housing quality and being a starting point for tailored policies focusing on social inclusiveness. The indicator 11.2.1 measures the access to public transport services, here specified as $PP_{transport}$ for the case of PEDs:

$$\text{SDG 11} \qquad PP_{transport} = \frac{\text{PED occupants with access to public transport services}}{\text{Total PED occupants}} \tag{9}$$

The indicator 11.3.1 measures the impact on land use, here calculated as a measure of urban footprint and related to the metropolitan areas for which indicators are derived:

$$\text{SDG 11} \qquad PL_{use} = \frac{\text{urban area covered by PEDs}}{\text{Total urban area of the municipality}} \tag{10}$$

This indicator can be used with a comparative function across municipalities, i.e., to assess the recorded progress in expanding PEDs and replicate the experience in other areas. The environmental dimension for SDG 11 is calculated from the indicator 11.6.2, expressed as the concentration of particulate matter per capita, and here formulated as in PM_{urban} in Equation (9):

$$\text{SDG 11} \qquad PM_{urban} = \frac{\text{Air quality (PM 2.5 concentration)}}{\text{Total PED occupants}} \tag{11}$$

The indicator 11.a.1 refers to the development and implementation of action plans and the PED implementation can be considered as progress for the achievement of the goal.

Finally, the indicator 13.2.2 accounts for the percentage of avoided total greenhouse gas emissions per year compared with a traditional supply from centralized fossil sources GHG_{trad}:

$$\text{SDG 13} \qquad GHG_{y} = \text{Tons of greenhouse gases per occupants} \tag{12}$$

The calculation of the aforementioned indicators allows us to evaluate the role of PEDs in achieving SDGs closely linked to sustainable urban transition. Yet, solely relying on these indicators might not provide a comprehensive assessment of the potential impact of PEDs on urban regions and their alignment with sustainability goals. It is crucial to also understand how the positive energy surplus might be applied in this context.

2.3. Step 3: Energy Surplus Leverage

Having established the link between PEDs and those SDGs to which they directly contribute, the next step is to develop specific indicators that measure the impact of PEDs' surplus to other relevant SDGs. Indeed, assessing indirect connections or, generally, achievement of specific goals due to the impact that the surplus energy or the net-zero balance may have on the territory, is pivotal. Establishing these links provides a comprehensive framework for understanding how PEDs can drive sustainable development on a global scale. These correlations as well as the indicator formulation and description are presented in Table 2.

Table 2. Second-stage indicators for energy surplus allocation.

SDGs Impacts	Indicator Formulation	Description	Correlations	
SDG 1 SDG 10	$\frac{H_{aff,energy}}{H_{region}}$	Number of households in underserved areas or in energy poverty conditions gaining access to affordable energy through PEDs	SDG 7 SDG 11	(13)
SDG 1 SDG 10	$\frac{EC_{trad} - EC_{PED}}{EC_{trad}}$	Economic savings for marginalized groups due to PED savings and sustainable redistribution in the area	SDG 7 SDG 11	(14)
SDG 12	$\frac{\sum_{j=1}^{N} E_{cons,j}}{\sum_{j=1}^{N} E_{prod,j}}$	Energy consumption efficiency due to PEDs	SDG 7 SDG 11 SDG 13	(15)

Indicator (13) measures the number of households in underserved areas or in energy poverty conditions that gain access to affordable energy through PEDs. This indicator is primarily linked to SDG 7 and SDG 11, as it relates to energy access and urban sustainability. Equation (14) presents an indicator that calculates the economic savings within PEDs. It

reflects the difference between energy costs of the supply from centralized power grids, EC_{trad}, and those within PEDs, EC_{PED}, showing the economic benefit to marginalized communities. Like the previous indicators, this also correlates with SDG 7 and SDG 11, highlighting the financial benefits of sustainable energy practices within PEDs for low-income families. Finally, the indicator in Equation (15) represents the energy consumption efficiency within PEDs. It is calculated by dividing the total energy consumed, E_{cons}, by the total energy produced, E_{prod}, across all users within the PED. This indicator is related to SDG 7, SDG 11, and SDG 13, as it touches on energy efficiency, urban sustainability, and climate impact through efficient energy use.

In addition to the abovementioned metrics, the indicator 12.7.1 may become relevant for PEDs' impact assessment in the case of active enrollment in the district of public organizations or public administrations, such as municipalities [41]. In the case of public procurement inside the PED, it can be considered achieved.

2.4. Step 4: Performance Evaluation

The final step involves using the developed indicators to evaluate the performance of PEDs in real-life contexts. This step encompasses several activities, including collecting data, detailed analyses, and drawing conclusions about the effectiveness of PEDs in achieving the SDGs. Performance evaluation not only provides insights into the current state of PEDs' contribution to SDGs but also offers guidance for future improvements and diffusion. To properly evaluate the impact of the positive surplus of PEDs, annual national or regional values may serve as the baseline.

In addition, it is also important to define if the values of energy produced, self-consumed, and distributed within the PED are correlated and to what extent. To pursue this analysis, the Pearson correlation coefficient formula can be used. By employing this calculation, it is possible to quantitatively evaluate the degree of association between these variables. Therefore, this analysis is useful to evaluate the operational synergies within PEDs but also provides valuable information that can guide strategic decisions aimed at optimizing energy distribution and consumption patterns within these districts.

These indicators are independent to allow the consideration of specific challenges and opportunities within PEDs. Using independent indicators is important as it enhances transparency in the evaluation process, making it easier to justify any decisions. They also permit to identify areas for improvement and support any informed decision-making process aiming to lead to more efficient and sustainable urban energy solutions. Lastly, the independence of the indicators ensures that the evaluation framework is both scalable and adaptable to PEDs of varying sizes and in different urban contexts, such allowing for replication.

3. Case Study

A specific district in Catania, Southern Italy, falling under climate zone B, consists of two dozen buildings. Primarily designed for residential purposes, these buildings are illustrated in Figure 2. The district supports a population of approximately 407 residents and is a workplace for 45 individuals. The chosen area is not yet a PED, but may be considered as a viable candidate, with it working to the constitution of a renewable energy community, according to the normative, technological, and operational constraints of the European Directive 2018/2001 [35] and the Italian transposition, Law 199/2022 [36]. A detailed explanation of the case study can be found in [30]. In detail, the area consists of twenty buildings, predominantly used for residential purposes. Most of these residential buildings are similar in terms of area, with living spaces being around 250 m^2. These are typically buildings with three floors. A couple of houses are smaller, with one being

under 100 m^2 and another around 130 m^2, with inhabitants from three to nine people. The area also comprises two larger residential buildings, each with a total floor area of approximately 480 m^2 and 64 inhabitants in each. On the commercial front, there are three buildings: one at around 143 m^2 and the other two spanning over 640 m^2.

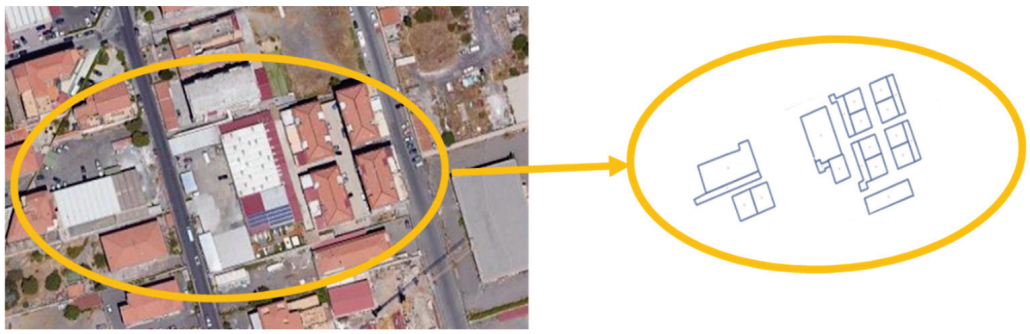


Figure 2. Case study area.

Energy-related data were sourced from property owners and commercial establishments that are part of the district. Aggregate electrical consumption data were provided, necessitating estimated breakdowns for each structure. The electrical demand was inferred by combining this data with insights from a prior survey of a similar district. This led to an annual electrical demand estimation for the district at approximately 374.89 MWh_{el}. Photovoltaic (PV) electrical output was determined using the area's global irradiance and a 65% conversion factor for net electricity generation, as proposed by Huld [37]. Monthly direct normal irradiation values were sourced from the Global Solar Atlas [38]. PV panel setups are included in the study accounting for technical limitations, rooftop space, maintenance and cabling areas, roof type, tilt, and potential shading. The model simulates the ideal electrical balance for varying geographical boundaries to understand the inter-building electricity flow dynamics under the PED concept.

4. Results and Discussion

The optimized results for the candidate PED are detailed and discussed herein. Electrical demand, production, and self-consumption from PV, as well as exceeding electricity, for each building is plotted in Figure 3. Indeed, buildings contribute to the SDGs' achievement either through self-consumption, providing excess energy, or participating in virtual distribution. Self-consumption indicates the energy used directly from production, contributing to SDG7 and SDG 11; the exceeding production reflects surplus energy that could be stored or shared, supporting SDG 7 and, potentially, SDG 11 and SDG 13, by proper allocation. Virtual distribution shows the energy distributed within the PED, again contributing to SDG 7 and SDG 11.

Electrical output from the panels differs due to the aforementioned constraints. As can be observed, for 10 buildings out of 20, PV output predominantly meets the electrical demands. Some buildings, such as 18, 19, and 20, possess expansive PV installation space, resulting in PV production exceeding 50 MWh/y in some instances. Other buildings produce electricity that exceeds their consumption, making it available for contributing to the net-positive balance of the area.

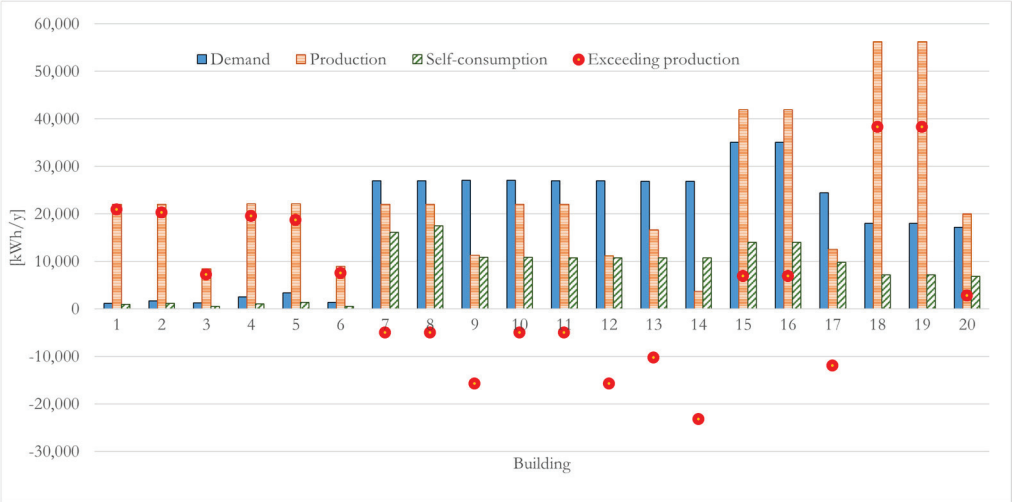


Figure 3. Electrical balances in the PED.

As emerging from Figure 3, a substantial electricity amount is exported to the grid, representing the portion of exceeding production. This surplus electricity offers multiple options for the PED: it can be stored in batteries to counteract the inherent intermittency of renewable sources like solar, promote electric mobility, or be redirected to assist underserved and low-income households, in line with the United Nations' Agenda 2030 and Sustainable Development Goals recommendations.

Before deepening how the exceeding electrical surplus can be allocated, the PED capabilities in terms of achievement of the SDGs indicated in Table 1 should be evaluated. To this scope, the indicators from Equations (4)–(12) have been calculated, taking into consideration baseline values.

The first target of SDG 7 can be measured by two indicators, 7.1.1 and 7.1.2, indicating the proportion of population with access to electricity and with primary reliance on renewables, respectively; in the context of PEDs, they can be calculated as in Equations (4) and (5). Regarding the first indicator, PP_{EA}, it is the proportion of PED occupants with access to electrical services with respect to the total number of PED occupants. In this case, given that access to electricity is granted for occupants of PEDs (especially for developed countries), this indicator can be considered as immediately satisfied, with values at 1 or 100%. The indicator PP_{REN} is the proportion of PED occupants with primary reliance on renewables. At rigor, PEDs are urban forms in which energy should be produced by renewable sources; still, this aspect is not explicit in the actual available definition, and, therefore, it is common to refer to a net-zero balance. To calculate this index, the number of PED occupants with installed renewables technologies (as in this case, PVs) with respect to the total number of occupants should be calculated. In this study, given the heterogeneity of the PED's population, both occupants and workers are included in the analysis. Target 7.2 refers to the percentage of final consumption of energy deriving from renewable sources. The indicator refers to the renewable energy produced and used for self-consumption or distribution within the PED, and is not indicated in terms of installed power size: in the case of PED implementation, it is described by the indicator REN_{share}, particularized from the UN indications. Having a value higher than the unity indicates a positive surplus from the balance of demand and production. Target 7.3 correlates the dependence of the energy intensity with the economic sphere, here with the declination in GDP. For the context of a PED, calculating the GDP would be unconventional since GDP is typically associated with countries or larger economic regions, not specific districts. However, for this study, it can be assumed as the mean Sicilian value, which was around EUR 87 billion for 2022 [40].

For the realization of SDG 11, four indicators are calculated as reported in Table 3. It has been chosen to report the national values. It is worth noting that these data may be easily reproduced for any country from the consultation of national statistics and reports or from the UN website [26]. For the general indicator 11.1.1 on the proportion of population living in inadequate housing, here specified for PED occupants, $PP_{housing}$, the value is again approximated to 1, from the definition of PED itself. In this sense, it can be immediately stated that the diffusion of PEDs in urban areas contributes to the achievement of target 1.1. of SDG 11. Regarding indicator $PP_{transport}$, representative of the target 11.2, data of the simulated scenarios do not permit to infer appropriate conclusions and is, therefore, not possible to calculate in this study. Still, it is maintained in the proposed evaluation procedure to account for general applications. The indicator PL_{use}, useful to refer to the target 11.3 on sustainable urbanization, can be considered as a measure of the urban footprint, i.e., the impact on land use. It can be calculated, as per Equation (8), that is considering the urban area covered by PEDs and compared with the area of the municipality in which the PED is going to be implemented. The simulated area is part of a small municipality in Catania; therefore, the value of the covered territory from PED is significantly high. Target 11.6 refers to the annual particulate matter per capita. In this case, the reference value is calculated by making the hypothesis for which the average levels of the PM concentration remain comparable to the case with and without PED. Finally, in the context of SDG 13, even in this case it can be supposed that the average percentage of avoided GHG emissions is equal to 100%, given that PEDs are urban areas with a net-zero emissions balance.

Table 3. Comparison of the baseline values for the selected SDG indicators in Italy [39] with the simulated outputs for the examined case study area.

SDG	Target	Indicator	Baseline Value (Italy)	Simulated Value
SDG 7 	7.1	PP_{EA}	0.92	1
		PP_{REN}	0.88	0.67
	7.2	REN_{share}	0.351	1.62
	7.3	EnEc	0.93	N.A.
SDG 11 	11.1	$PP_{housing}$	0.834	1
	11.2	$PP_{transport}$	0.693	N.A.
	11.3	PL_{use}	-	0.57
	11.6	PM_{urban}	0.717	0.717
SDG 13 	13.2	GHG_y	7 ton/inhab	Net-zero

At this point, it is of crucial importance to define the impact of PED surplus on the other identified SDGs, as reported in Table 2. The exceeding electricity, indeed, could be used to contribute to SDG 1 on energy poverty, SDG 10 about the need of reducing inequalities, and SDG 12 focusing on responsible production and consumption. SDG 1 and SDG 10 are influenced by SDG 7 and SDG 11 and their achievement can be measured by the indicators in Equations (13) and (14), referring to the number of households in underserved areas or in energy poverty conditions gaining access to affordable energy produced within the PED and to the economic savings for marginalized groups arising from the energetic

supply from PED, respectively. Basically, the two indicators give insights into how families in energy poverty conditions can be supported from the PED production, both energetically and economically. These calculations can be pursued by considering the average energy consumption of a family in Italy of around 2300–3200 kWh/year [41]. In this case, from the obtained electrical balance of the PED, around 28–30 families can be supported, with a net economic savings of 1145 EUR/y per family, related to the specific cost of energy [41]. Thus, as has emerged from these initial results, PEDs not only bring benefits in terms of energy efficiency and emission reduction, but also have a significant impact on social dynamics and long-term urban development. The redistribution of the energy surplus to households in energy poverty conditions, as calculated here, improves living conditions, fosters the communitarian sense of solidarity and, therefore, yields a greater social cohesion within the PED. And, not to be considered as a separate topic from energy efficiency, energy production, and energy distribution, responsible energy consumption models can also bring long-term benefits, such as collaboration among citizens, attraction for local businesses, and close activity with municipal institutions. Having this new way of conceiving the district, and also the city, brings a new way of thinking for urban spaces, promoting investments in sustainable mobility, secure infrastructure, and greener areas.

Beyond renewable production, another important feature of PEDs is energy efficiency and its relationship with the values of self-sufficiency. Energy efficiency can be defined as the ratio of self-consumption and demand, as in Equation (15). From the optimized energy flows and the graph of Figure 3, it can be observed that buildings with higher energy efficiency tend to have higher energy self-sufficiency, indicating a positive relationship between efficient use of energy and the ability to meet demand with production. In this sense, they contribute to the achievement of SDG 7, SDG 11, and SDG 13. Some buildings stand out with particularly high self-sufficiency, suggesting that they produce significantly more energy than they consume. Conversely, buildings with lower efficiency and self-sufficiency indicate potential areas for improvement. In terms of energy performance evaluation, a correlation analysis between the different energy flows (such as energy production, self-consumption, etc.) and their impact on SDGs is pursued. This helps in identifying which factors are the most strongly associated with achieving specific goals.

The heat map of Figure 4 is a matrix that showcases the correlation coefficients between the different energy flows calculated as output from the optimization, i.e., the self-consumption, exceeding production and virtual distribution, along with the aggregated values of the demand and production. The colors typically represent the strength and direction of the correlation. A color gradient from green (positive correlation) to red (negative correlation) is used. The numbers within the cells represent the correlation coefficients between each pair of variables (indicated in the corresponding row and column). A value of 1 indicates a perfect positive correlation, meaning that as one variable increases, the other also increases. A value of -1 indicates a perfect negative correlation, meaning that as one variable increases, the other decreases. A value of 0 suggests no correlation between the variables. It directly emerges from the explanation that the diagonal shows perfect correlations, i.e., with values of 1, as it represents the relationship of each variable with itself. Correlation matrices are symmetric across the diagonal, meaning that the correlation between any variables A and B is the same as the correlation between variable B and variable A. These indications are important since they can provide insights into how different aspects of energy usage and distribution are related to each other and can help in understanding the dynamics within PEDs. The sparkline graphs on the right of Figure 4 present this dataset in a compact and simple way and helps in identifying the highest and lowest values in the data series of the correlations.

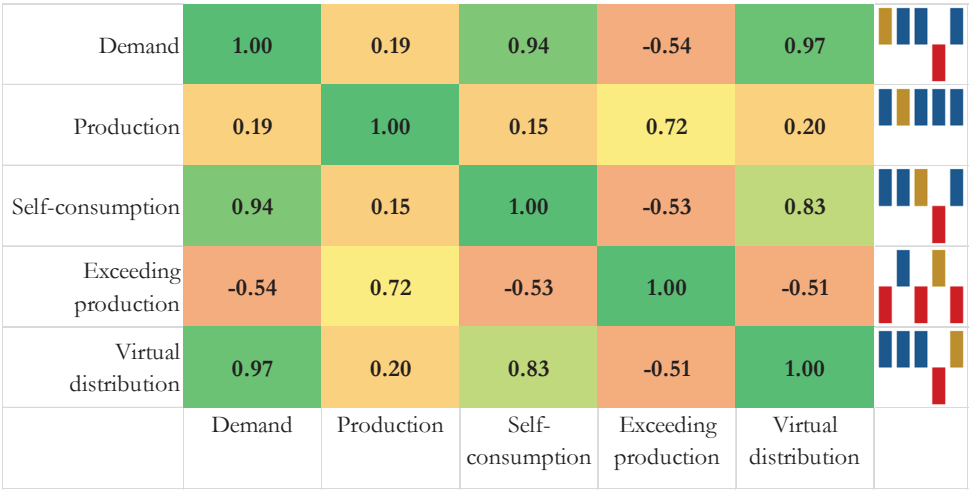


Figure 4. Heat map of electrical flows in the PED and sparkline graph.

In more detail, demand and production share a value of 0.19, indicating a weak positive correlation between energy demand and production. It suggests that an increase in energy demand within the PED does not strongly correlate with an increase in energy production. This implies that energy production capacity is likely not dynamically adjusted based on demand within the PED, possibly due to the nature of renewable energy sources such as solar and wind, which have fixed production profiles that do not respond immediately to changes in consumption patterns. There is a strong positive correlation between demand and self-consumption, at 0.94, therefore implying that as the energy demand in buildings increases, their self-consumption of energy also significantly increases. This indicates that buildings with higher energy demand are effectively utilizing the energy they produce on site, optimizing their internal consumption and reducing the need for external energy supply. The demand and exceeding production show a moderate negative correlation, with a value of—0.54, suggesting that buildings with higher energy demands are less likely to produce excess energy. This could be explained by the fact that energy-intensive buildings may consume almost all of the energy they generate, leaving little or no surplus for storage or redistribution. Demand and virtual distribution have a strong positive correlation (0.97), revealing that buildings with higher energy demands are significantly involved in the virtual distribution network within the PED. This high correlation suggests that energy-sharing mechanisms are effectively utilized in the district, as buildings with greater demand play a major role in both receiving and distributing energy, thereby enhancing grid stability within the PED.

Production and self-consumption have a weak positive correlation of 0.15. This suggests that an increase in energy production is only slightly associated with an increase in self-consumption. This could imply that buildings with higher production capacity may not always use their energy but might be channeling it into the PED's shared network. A moderate positive correlation of 0.72 can be observed between production and exceeding production. This suggests that these buildings have sufficient production capacity to meet their own needs and still produce surplus energy, which can be shared, stored, or exported. This surplus could be utilized for energy storage, shared within the PED, or exported to the grid. The weak positive correlation of 0.2 between production and virtual distribution suggests that increased energy production in buildings has a slight relationship with their involvement in virtual distribution. Other factors such as the energy demand profiles or local energy policies might be influencing the actual distribution decisions. While buildings with higher production are part of the network, their contribution or receipt of energy is not strongly determined by their production capacity.

Self-consumption exhibits a moderate negative correlation of—0.53 with the exceeding production, indicating that buildings with higher self-consumption tend not to have much excess energy. This implies that when buildings are efficiently using the energy they produce, there is limited surplus left for sharing or storage, highlighting a potential conflict between maximizing self-use and generating excess for the community network. The correlation between self-consumption and virtual distribution is 0.83. This strong positive correlation suggests that buildings with higher self-consumption are also actively involved in virtual distribution. This could indicate a balance between efficient self-use and participation in the energy-sharing network.

Finally, the moderate negative correlation between exceeding production and virtual distribution, i.e., -0.51, suggests that buildings with more excess production are less involved in virtual distribution, potentially due to a lack of local energy demand at that moment. This could indicate that buildings having surplus energy might be exporting it to the grid, rather than engaging in the PED's internal energy distribution. This observation can lead towards optimizing energy distribution systems within the PEDs, thus achieving a more efficient local distribution of energy surplus and reducing the need for external energy export.

While the correlations observed in this study refer to the dynamics of energy production, consumption, and distribution, it is also crucial to consider the potential for direct or indirect rebound effects, i.e., when energy savings lead to higher energy demand or where cost savings are spent on goods and services that also require energy. For PEDs, the direct rebound effect might occur when buildings increase their energy use after receiving a benefit in terms of energy surplus or energy bill reduction. This behavior could partly offset the environmental and economic benefits initially achieved through energy savings, ultimately reducing the anticipated positive impact of PEDs on energy consumption and emissions. For the indirect rebound effect, significant considerations can refer to socio-economic aspects, with energy savings potentially increasing new investments in goods or services with a high energy footprint, again diminishing the net environmental benefits of PEDs. To mitigate these effects, it is important to have a prior planning of PED implementation, with strategies including behavioral changes, energy storages, or demand-side systems that can ensure that surplus energy is used efficiently.

5. Policy Implications and Applicability

The PED model presented in this study highlights its potential to drive sustainable urban development and contribute significantly to various SDGs. The findings point to the importance of optimizing energy production and consumption and of dealing with surplus energy allocation to address energy poverty and reduce inequalities. However, the path from theory to practice needs dedicated resources and recommendations. As a first and very important aspect to be considered, there is a clear call for action to develop standardized policy frameworks. The importance of having policy indications lies not only in the need of having clear guidance and regulatory support for urban and energy planners, but also in incentives and financial support that can help the development of PEDs, especially for the case of existing neighborhoods. As an example, subsidies or tax incentives can be devoted to urban projects that meet PED criteria and ensure a sustainable redistribution of the energy surplus among the underserved population to contrast energy poverty. At the same time, the policies should adopt a multi-stakeholder approach, favoring collaboration among local governments, energy providers, building owners, architects and engineers, and urban planners.

At the same time, to properly streamline the process for energy sharing and trading, national governments should also provide regulatory reforms permitting an effective operation of PEDs.

Beyond the regulatory support and proactive policy actions, public engagement and education remain important aspects to be considered when planning any PED development. As a matter of fact, PEDs are made by people, who should be aware of the impact of their choices and of how they contribute to the energy saving and social impact.

Regarding the applicability and broader geographical extension, while this research focuses on a single district in Southern Italy, the methods and findings presented are designed to be adaptable and applicable to a diverse urban context, with the premise of having national available data. The same consideration applies to the model, as it refers to renewable production estimation and surplus distribution, concepts that can be tailored to different geographic, climatic, and socio-economic conditions.

6. Conclusions

The PED model delineated through this research not only showcases the feasibility of energy self-sufficient urban districts but also acts as a beacon for sustainable urban development. By intricately weaving the threads of renewable energy production, energy efficiency, and community engagement, PEDs stand as exemplars for cities of the future. Buildings that produce more energy than they consume could not only serve their own needs but also support their surrounding infrastructures and communities. Moreover, the surplus energy from PEDs, as suggested by the results of this study, holds the potential to tackle energy poverty and reduce inequalities, and promote responsible consumption and production. Among all aspects, energy poverty remains a pressing issue, even in developed nations. By redirecting the surplus energy from PEDs, underserved communities and households can gain access to affordable and sustainable energy. This not only aligns with SDG 1, which targets poverty alleviation, but also resonates with SDG 10, in which the objective is to reduce inequalities. The provision of surplus energy from PEDs to energy-poor households can significantly improve their living conditions, providing them with not only lighting and heating but also the opportunity for social and economic upliftment. Furthermore, the economic savings generated from the PED's surplus energy can empower marginalized groups by reducing their utility expenses. This can lead to improved educational outcomes, better health conditions, and enhanced opportunities for economic development, thereby also contributing to other SDGs, beyond the achievement of SDG 1 and SDG 10. However, it is also essential to consider the rebound effect, where savings on energy expenses could lead to increased energy consumption. The actualization of beneficial outcomes grounds on the capacity to effectively channel the economic savings into areas that are capable of yielding positive social and environmental impacts.

The PED concept emerges as a pivotal paradigm in the transition towards sustainable urbanization. The case study of the district in Southern Italy highlights how the implementation of PEDs can substantially contribute to the achievement of various SDGs, notably SDG 7, 11, and 13. Practically, optimizing energy production and consumption within the framework of a PED not only enhances energy efficiency and reduces the reliance on external power grids but also promotes urban resilience and the quality of life for residents. Theoretically, PEDs reinforce the notion that the integration of renewable technologies and sustainable practices at the district level can lead to positive transformations in terms of energy accessibility, inequality reduction, and climate change mitigation. The model proposed in the present study offers a replicable methodology for assessing the impact of PEDs on SDGs, paving the way for future research and applications in diverse urban contexts. PEDs inherently encourage responsible production and consumption, in line with

SDG 12. The surplus energy is redirected to serve the greater community good. The notion of self-sufficiency within PEDs, where buildings produce more energy than they consume, demonstrates that urban areas can be not just consumers of resources, but also producers, contributing to a sustainable urban ecosystem. Furthermore, the relationship between energy efficiency and self-sufficiency within PEDs confirms the potential of integrated urban energy systems; buildings with higher energy efficiency tend to have higher self-sufficiency levels, indicating a positive correlation between the efficient use of energy and the ability to meet energy demands with internal production.

The findings of this study underscore the importance of policies supporting the development of PEDs as a substantial way to contribute to reducing energy inequalities, improving access to sustainable energy services, and promoting environmental justice. From the social viewpoint, PEDs can also act as catalysts for greater community cohesion, encouraging citizen participation in sustainability initiatives and raising awareness about the importance of energy efficiency and the use of renewable energy. However, some limitations arise as certain SDG indicators were not assessed due to data unavailability. In addition, despite the promising outcomes, this study focuses on a single district in Italy considered as a potential PED candidate, which, however, does not restrict the generalizability of the findings, given that baseline values have been derived from national data.

The results from the case study, however, also point towards opportunities for improvement. Buildings with lower efficiency and self-sufficiency highlight the need for targeted interventions, such as retrofitting or the adoption of more efficient appliances and systems. By addressing these areas, urban areas can further enhance their contribution to the SDGs.

Further research directions could involve applying the model to a broader range of urban contexts, both in developed and developing countries. Further studies might also explore the interaction between PEDs and other SDGs not considered in this study, as well as analyze the long-term impact of PEDs on urban and social dynamics.

Author Contributions: Conceptualization, M.C., A.F., F.G. and R.V.; Methodology, M.C., A.F., F.G. and R.V.; Software, M.C., A.F., F.G. and R.V.; Validation, M.C., A.F., F.G. and R.V.; Formal analysis, M.C., A.F., F.G. and R.V.; Investigation, M.C., A.F., F.G. and R.V.; Resources, M.C., A.F., F.G. and R.V.; Data curation, M.C., A.F., F.G. and R.V.; Writing—original draft, M.C., A.F., F.G. and R.V.; Visualization, M.C., A.F., F.G. and R.V.; Supervision, M.C. and A.F.; Funding acquisition, F.G. and R.V. All authors have read and agreed to the published version of the manuscript.

Funding: All authors acknowledge the funding received by the National Recovery and Resilience Plan (NRRP), Mission 4, Component 2, Investment 1.1, Call for tender No. 1409 published on 14.9.2022 by the Italian Ministry of University and Research (MUR), funded by the European Union—NextGenerationEU– NETPLUS—Neighborhood Energy Transition: towards Positive energy baLance and carbon neUtral diStricts—CUP D53D23018330001—Grant Assignment Decree No. P2022LLYAF adopted on 01/09/2023 by the Italian Ministry of Ministry of University and Research (MUR). Rosaria Volpe also acknowledge the financial support of the Starting Grant under the ENACT project, Piano di Incentivi per la Ricerca di Ateneo 2020/2022, PIA.CE.RI., project number: 61722102158.

Data Availability Statement: The raw data supporting the conclusions of this article will be made available by the authors on request.

Acknowledgments: This work was developed within the context of the International Energy Agency (IEA) Energy in Buildings and Construction (EBC), Annex 83 Workgroup on "Positive Energy Districts".

Conflicts of Interest: The authors declare no conflicts of interest.

References

1. IPCC. *2022: Climate Change 2022: Impacts, Adaptation, and Vulnerability. Contribution of Working Group II to the Sixth Assessment Report of the Intergovernmental Panel on Climate Change*; Pörtner, H.-O., Roberts, D.C., Tignor, M., Poloczanska, E.S., Mintenbeck, K., Alegría, A., Craig, M., Langsdorf, S., Löschke, S., Möller, V., et al., Eds.; Cambridge University Press: Cambridge, UK; New York, NY, USA, 2022; 3056p. [CrossRef]
2. SET-Plan ACTION n. 3.2 Implementation Plan, Europe to Become a Global Role Model in Integrated, Innovative Solutions for the Planning, Deployment, and Replication of Positive Energy Districts. June 2018. Available online: https://jpi-urbaneurope.eu/wp-content/uploads/2021/10/setplan_smartcities_implementationplan-2.pdf (accessed on 25 April 2024).
3. JPI Urban Europe. White Paper on "Reference Framework for Positive Energy Districts and Neighbourhoods. Key Lessons from national consultations". March 2020. Available online: https://jpi-urbaneurope.eu/wp-content/uploads/2020/04/White-Paper-PED-Framework-Definition-2020323-final.pdf (accessed on 25 April 2024).
4. Clean Energy for All Europeans Package. Available online: https://energy.ec.europa.eu/topics/energy-strategy/clean-energy-all-europeans-package_en (accessed on 25 April 2024).
5. Gouveia, J.; Seixas, J.; Palma, P.; Duarte, H.; Luz, H.; Cavadini, G. Positive Energy District: A model for Historic Districts to Address Energy Poverty. *Front. Sustain. Cities* **2021**, *3*, 648473. [CrossRef]
6. Cellura, M.; Campanella, L.; Ciulla, G.; Guarino, F.; Brano, V.L.; Cesarini, D.N.; Orioli, A. The redesign of an Italian building to reach net zero energy performances: A case study of the SHC Task 40—ECBCS Annex 52. *ASHRAE Trans.* **2011**, *117*, 331–339.
7. Ulpiani, G.; Vetters, N.; Maduta, C. Towards (net) zero emissions in the stationary energy sector: A city perspective. *Sustain. Cities Soc.* **2023**, *97*, 104750. [CrossRef]
8. Fichera, A.; Frasca, M.; Volpe, R. The centralized energy supply in a network of distributed energy systems: A cost-based mathematical approach. *Int. J. Heat Technol.* **2017**, *35*, S191–S195. [CrossRef]
9. Leprince, J.; Schledorn, A.; Guericke, D.; Dominkovic, D.F.; Madsen, H.; Zeiler, W. Can occupant behaviors affect urban energy planning? Distributed stochastic optimization for energy communitites. *Appl. Energy* **2023**, *348*, 121589. [CrossRef]
10. Fichera, A.; Pluchino, A.; Volpe, R. Modelling energy distribution in residential areas: A case study including energy storage systems in Catania, Southern Italy. *Energies* **2020**, *13*, 3715. [CrossRef]
11. Castellini, M.; Menoncin, F.; Moretto, M.; Vergalli, S. Photovoltaic Smart Grids in the prosumers investment decisions: A real option model. *J. Econ. Dyn. Control* **2021**, *126*, 103988. [CrossRef]
12. Derkenbaeva, E.; Hofstede, G.J.; van Leeuwen, E.; Vega, S.H. Simulating households' energy transition in Amsterdam: An agent-based modeling approach. *Energy Convers. Manag.* **2023**, *294*, 117566. [CrossRef]
13. Castillo-Calzadilla, T.; Garay-Martinez, R.; Andonegui, C.-M. Holistic fuzzy logic methodology to assess positive energy district (PathPED). *Sustain. Cities Soc.* **2023**, *89*, 104375. [CrossRef]
14. Cellura, M.; Fichera, A.; Guarino, F.; Volpe, R. Sustainable Development Goals and Performance Measurement of Positive Energy District: A Methodological Approach. In *Sustainability in Energy and Buildings 2021. Smart Innovation, Systems and Technologies*; Littlewood, J.R., Howlett, R.J., Jain, L.C., Eds.; Springer: Singapore, 2021; Volume 263. [CrossRef]
15. Guarino, F.; Rincione, R.; Mateu, C.; Teixido, M.; Cabeza, L.F.; Cellura, M. Renovation assessment of building districts: Case studies and implications to the positive energy districts definition. *Energy Build.* **2023**, *296*, 113414. [CrossRef]
16. Moreno, A.G.; Vèlez, F.; Alpagut, B.; Hernàndez, P.; Montalvillo, C.S. How to Achieve Positive Energy Districts for Sustainable Cities: A Proposed Calculation Methodology. *Sustainability* **2021**, *13*, 710. [CrossRef]
17. Mattsson, M.; Olofsson, T.; Lundberg, L.; Korda, O.; Nair, G. An Exploratory Study on Swedish Stakeholders' Experiences with Positive Energy Districts. *Energies* **2023**, *16*, 4790. [CrossRef]
18. Bruck, A.; Diaz-Ruano, S.; Auer, H. Values and implications of building envelope retrofitting for residential Positive Energy Districts. *Energy Build.* **2022**, *275*, 112493. [CrossRef]
19. Neziric, E.; Spago, D.; Saric, M.; Sunje, E.; Beca, M. University Campus as a Positive Energy Districts—A Case Study. In *Advanced Technologies, Systems, and Applications VIII, Proceedings of the International Symposium on Innovative and Interdisciplinary Applications of Advanced Technologies (IAT 2023), Tuzla, Bosnia and Herzegovina, 1–4 June 2023*; Lecture Notes in Networks and Systems, 644; Springer: Cham, Switzerland, 2023. [CrossRef]
20. Barrutieta, X.; Gainza, J.; Irulegi, O.; Hernandez, R. The zero building: An exemplary nearly zero energy office building (NZEB) and its potential to become a positive energy building (PEB). *Archit. Sci. Rev.* **2021**, *66*, 214–225. [CrossRef]
21. Famiglietti, J.; Aprile, M.; Spirito, G.; Motta, M. Net-Zero Climate Emissions Districts: Potentials and Constraints for Social Housing in Milan. *Energies* **2023**, *16*, 1504. [CrossRef]
22. Schneider, S.; Zelger, T.; Sengl, D.; Baptista, J. A Quantitative Positive Energy District Definition with Contextual Targets. *Buildings* **2023**, *13*, 1210. [CrossRef]
23. Cellura, M.; Guarino, F.; Longo, S.; Mistretta, M. Modeling the energy and environmental life-cycle of buildings: A co-simulation approach. *Renew. Sustain. Energy Rev.* **2017**, *80*, 733–742. [CrossRef]

24. Casamassima, L.; Bottecchia, L.; Bruck, A.; Kranzl, L.; Haas, R. Economic, social, and environmental aspects of Positive Energy Districts—A review. *Wiley Interdiscip. Rev.* **2022**, *11*, e452. [CrossRef]
25. Tuttolomondo, A.; Ferrari, A.; Laloui, L. Pore-pressure coefficients for unsaturated soils: Generalized effective stress approach. *Can. Geotech. J.* **2023**, *60*, 11. [CrossRef]
26. United Nations. Department of Economic and Social Affairs. Available online: https://sdgs.un.org/2030agenda (accessed on 25 April 2024).
27. United Nations. Global indicator framework for the Sustainable Development Goals and target of the 2030 Agenda for Sustainable Development. Available online: https://unstats.un.org/sdgs/indicators/Global%20Indicator%20Framework%20after%2020 23%20refinement_Eng.pdf (accessed on 25 April 2024).
28. United Nations. General Assembly. Work of the Statistical Commission Pertaining to the 2030 Agenda for Sustainable Development. Available online: https://digitallibrary.un.org/record/1291226?ln=en&v=pdf (accessed on 25 April 2024).
29. Nerini, F.F.; Tomei, J.; To, L.S.; Bisaga, I.; Parikh, P.; Black, M.; Bor-rion, A.; Spataru, C.; Broto, V.C.; Anandarajah, G.; et al. Mapping synergies and trade-offs between energy and the Sustainable Development Goals. *Nat. Energy Perspect.* **2018**, *3*, 10–15. [CrossRef]
30. Volpe, R.; Gonzalez-Alriols, M.; Schmalbach, N.M.; Fichera, A. Optimal design and operation of distributed electrical generation for Italian positive energy districts with biomass district heating. *Energy Convers. Manag.* **2022**, *267*, 115937. [CrossRef]
31. SDG Indicatorsmetadata. Available online: https://unstats.un.org/sdgs/metadata/files/ (accessed on 25 April 2024).
32. United Nations. Climate Change. GHG Data from UNFCCC. Available online: https://unfccc.int/topics/mitigation/resources/registry-and-data/ghg-data-from-unfccc (accessed on 25 April 2024).
33. IEAG-SDGs Tier Classification for Global SDG Indicators. Available online: https://unstats.un.org/sdgs/iaeg-sdgs/tier-classification/ (accessed on 25 April 2024).
34. Directive (EU) 2018/2001 of the European Parliament and of the Council of 11 December 2018 on the Promotion of the Use of Energy from Renewable Sources. Available online: https://eur-lex.europa.eu/legal-content/EN/TXT/PDF/?uri=CELEX:32018L2001 (accessed on 25 April 2024).
35. Legislativo, D. 2021, n. 199 Attuazione della Direttiva (UE) 2018/2001 del Parlamento Europeo e del Consiglio, dell'11 Dicembre 2018, Sulla Promozione dell'uso Dell'energia da Fonti Rinnovabili. (21G00214) (GU Serie Generale n.285 del 30-11-2021-Suppl. Ordinario n. 42). Available online: https://www.gazzettaufficiale.it/eli/id/2021/11/30/21G00214/sg (accessed on 25 April 2024). (In Italian).
36. Huld, T. Estimating Solar Radiation and Photovoltaic System Performance, the PVGIS Approach. In Proceedings of the AFRETEP 1st Regional Workshop 2011, Kampala, Uganda, 2011. Available online: https://www.scribd.com/document/469217173/a6 (accessed on 25 April 2024).
37. Global Solar Atlas. Available online: https://globalsolaratlas.info/map (accessed on 25 April 2024).
38. Istat, Istituto Nazionale di Statistica, Rapporto SDGs 2023. Informazioni Statistiche per l'agenda 2030 in Italia. Available online: https://www.istat.it/storage/rapporti-tematici/sdgs/2023/Rapporto-SDGs-2023.pdf (accessed on 25 April 2024). (In Italian)
39. Istat. Istituto Nazionale di Statistica, Gross Domestic Product, Sicily. Available online: http://dati.istat.it/Index.aspx?QueryId=11455&lang=en (accessed on 25 April 2024).
40. Istat. Istituto Nazionale di Statistica. Available online: https://www.istat.it/it/files//2014/12/StatReport_Consumi_energetici.pdf (accessed on 25 April 2024).
41. Istat. Istituto Nazionale di Statistica. Consumi Energetici delle Famiglie, Anni 2020 e 2021. Available online: https://www.istat.it/it/files/2022/12/Consumi-energetici-famiglie-2020-2021-.pdf (accessed on 25 April 2024).

Disclaimer/Publisher's Note: The statements, opinions and data contained in all publications are solely those of the individual author(s) and contributor(s) and not of MDPI and/or the editor(s). MDPI and/or the editor(s) disclaim responsibility for any injury to people or property resulting from any ideas, methods, instructions or products referred to in the content.

energies

MDPI

Article

Lessons Learned from Four Real-Life Case Studies: Energy Balance Calculations for Implementing Positive Energy Districts

Helmut Bruckner [1,*], Svitlana Alyokhina [2], Simon Schneider [2], Manuela Binder [1], Zain Ul Abdin [3], Rudi Santbergen [3], Maarten Verkou [4], Miro Zeman [3,4], Olindo Isabella [3,4], Marco Pagliarini [5], Cristiana Botta [5] and Ana Streche [6]

[1] Sonnenplatz Großschönau GmbH, 3922 Großschönau, Austria
[2] University of Applied Sciences Technikum Wien, Renewable Energy Systems, 1200 Wien, Austria
[3] Delft University of Technology, PMVD, 2628 CD Delft, The Netherlands
[4] PV Works, 2628 CD Delft, The Netherlands
[5] LINKS Foundation, 10138 Torino, Italy
[6] Denkstatt Romania SRL, 300425 Timişoara, Romania
* Correspondence: h.bruckner@sonnenplatz.at

Abstract: Positive Energy Districts (PEDs) are integral to achieving sustainable urban development by enhancing energy self-sufficiency and reducing carbon emissions. This paper explores energy balance calculations in four diverse case study districts within different climatic conditions—Fiat Village in Settimo Torinese (Italy), Großschönau (Austria), Beursplain in Amsterdam (Netherlands), and Lunca Pomostului in Reşiţa (Romania)—as part of the SIMPLY Positive project. Each district faces unique challenges, such as outdated infrastructure or heritage protection, which we address through tailored strategies including building renovations and the integration of renewable energy systems. Additionally, we employ advanced simulation methodologies to assess energy performance. Simulation results highlight the significance of innovative technologies like photovoltaic-thermal (PVT) systems, application of demand-side actions, and flexible grid usage. Furthermore, mobility assessments and resident-driven initiatives demonstrate the critical role of community engagement in reducing carbon footprints. This study underscores the adaptability of PED frameworks across varied urban contexts and provides actionable insights for scaling similar strategies globally, supporting net-zero energy targets.

Keywords: positive energy district; energy balance; photovoltaic-thermal system; mobility; demand-side actions; sustainable development

1. Introduction

The global transition toward sustainable urban development has become a critical priority, motivated by the urgent need to combat climate change and achieve climate neutrality in line with international frameworks such as the Paris Agreement. Positive Energy Districts (PEDs) embody a transformative concept within this transition, focusing on empowering urban areas to generate more renewable energy than they consume. A PED is seen as a district with annual net-zero energy import and net-zero CO2 emissions, working towards an annual local surplus production of renewable energy [1]. They are seen as a tool for achieving climate-neutral cities, embedded in integrated urban strategies providing liveable, sustainable, and inclusive urban neighbourhoods. By leveraging energy-efficient buildings, smart grids, and innovative renewable energy technologies, PEDs significantly contribute to net-zero carbon goals while enhancing urban resilience. A PED Programme

has been aligned with the Driving Urban Transition (DUT) Partnership and has become one of the three DUT Pathways. The programme will continue to expand its activities, with the aim of initiating 100 PEDs in Europe by 2025. [2]

However, implementing PEDs, particularly in established urban locales, presents numerous challenges. These challenges include the lack of universally accepted methodologies for assessing energy balances, the complexities of integrating renewable energy systems into dense and often outdated urban infrastructures, and the pressing need for multi-stakeholder collaboration to secure local acceptance and ensure equitable development processes [3,4].

This paper highlights findings from the research project "Supporting Innovative and Ambitious Cities and Municipalities on Their Pathway to Positive Energy Districts through Easy, Clear, and Understandable Guidelines, Targets, and Strategies" (SIMPLY Positive) [5]. Its main goal is to provide a practical overview and outline possible strategies for energy balance calculation within the focus district, which is a key aspect of implementing PEDs.

2. Materials and Methods

2.1. Focus Districts Description

The project considers four focus districts: Fiat Village in Settimo Torinese (Italy), Großschönau (Austria), Beursplain in the centre of Amsterdam (Netherlands), and Lunca Pomostului in Reşiţa (Romania).

The main parameters of focus districts are presented in Table 1.

Table 1. Focus district parameters.

Parameter	Unit	IT, Fiat Village, Settimo Torinese	AT, Großschönau	NL, Beursplain, Amsterdam	RO, Lunca Pomostului Reşiţa
District Area	ha	19.0	705.0	3.0	47.0
Population	-	3200	450	300 [6]	9900
Gross Floor Area	m^2 GFA	213,937	401,060	98,941	130,700
District Buildable Plot Area	m^2 PA	146,000	391,000	30,035	420,859
Floor Area Ratio (FAR)	-	1.47	0.15	3.29	0.31
Site Coverage Ratio (SCR)	%	26	7	78	18
Net to Gross Floor Area Ratio	%	80	70	80	80
Building Storeys (avg)	-	5.6	1.5	4.2	4.9
Residential Usage	%	98.4	82.2	19.1	76.5
Commercial Usage	%	0.2	11.7	29.0	3.9
Primary School Usage	%	0.0	5.0	0.0	0.0
Secondary School Usage	%	0.0	0.0	0.0	9.8
Others (Retail) Usage	%	1.4	1.1	51.9	9.8
Heating Setpoint	°C	22	22	22	22
Heating COP Heat Pump (Flex)	-	3.5 (4.5)	3.5 (4.5)	3.5 (4.5)	3.5 (4.5)
Heating Degree Days	°C·d	4786.0	3483.1	3917.9	3877.8
Cooling Setpoint	°C	26	26	26	26
Cooling COP Heat Pump (Flex)	-	2.5 (5.0)	2.5 (5.0)	2.5 (5.0)	2.5 (5.0)
Cooling Degree Days	°C·d	0.4	6.9	1.1	16.4
Primary Energy Conversion Factors	Source	[7]	[8]	[9]	[10,11]

In Settimo Torinese, the district Fiat Village is primarily residential, with most buildings over 50 years old, requiring extensive renovations to enhance energy performance. Goals include establishing a Renewable Energy Community to facilitate local energy production and consumption and implementing energy management systems to optimize energy use across both public and private sectors.

Großschönau, a small rural municipality in Austria, is committed to sustainability and known for its long-standing environmental initiatives. Plans are in place to attain the Positive Energy Municipality status by 2030, focusing on energy self-sufficiency and innovative projects, including small-scale wind turbines and a centralized biomass heating network.

The selected area Beursplain in Amsterdam is characterized by old buildings under heritage protection. Some buildings already feature photovoltaic (PV) systems, with the primary goal being to achieve a positive energy balance.

In Reşiţa, the focus Lunca Pomostului district combines residential, commercial, and institutional spaces, although much of its infrastructure is outdated. Efforts in this district aim to reduce emissions by 20% compared to 1990 levels. Current initiatives focus on urban redevelopment, including the modernization of public spaces, the addition of green infrastructure, and improved mobility options such as cycling lanes and pedestrian pathways.

These four districts represent diverse climatic conditions and energy challenges. For instance, Reşiţa experiences a temperate climate with Mediterranean influences, while Settimo Torinese and Amsterdam share moderate climates with varying precipitation patterns. Großschönau has a relatively dry climate with cold winters. Despite these differences, all districts prioritize the integration of renewable energy systems, with Amsterdam and Settimo Torinese emphasizing centralized heating solutions, and Großschönau showcasing leadership in decentralized renewable energy projects.

2.2. Methodology Description

The core of the definition of Positive Energy Districts (PEDs) lies in establishing a clear rationale behind their design, which articulates the objectives they aim to achieve. This design approach [12] begins by defining specific goals and subsequently deriving criteria for their operationalization based on these objectives.

System boundaries are established from spatial, temporal, and functional perspectives, in line with the principles outlined in the fundamentals of PED energy modelling [13]:

1. Spatial boundaries: these refer to the geographical limits enclosing included energy services and supplies;
2. Temporal boundaries: these represent the balancing period, typically defined as one operational year;
3. Functional boundaries: these identify specific energy functions, uses, or demands that are included or excluded based on their purpose rather than proximity.

The functional boundaries and included energy services can be categorized into three main areas:

1. Operational energy and user electricity;
2. Mobility aspects;
3. Embodied energy and emissions.

This approach defines three variants or layers of PEDs:

- PED operation (innermost level): focuses solely on operational energy;
- PED mobility: expands to include private daily mobility;
- Climate-neutral PED (outermost layer): incorporates embodied energy related to district construction, maintenance, repair, and mobility.

Each layer adds complexity and introduces uncertainty compared to the previous one. Access to adequate data is critical for simulation and verification, and these system boundaries are visually represented in Figure 1.

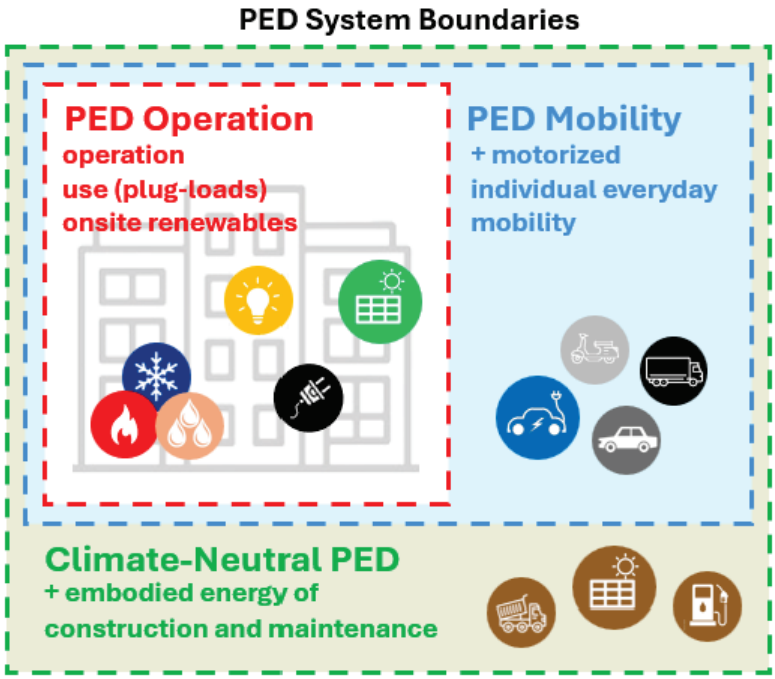


Figure 1. Three expanding functional system boundaries of PED: from operation and use (red) to including everyday individual motorized mobility (blue) to also include energy and emissions from construction and maintenance (green).

Under the SIMPLY Positive project, the first step in defining PEDs involved determining the type of each focus district along with its respective system boundaries. The spatial boundaries for each focus district align with the geographical borders of the selected regions. The sizes of these districts vary from the large city of Amsterdam to the small village of Großschönau. Despite these differences, nearly all self-set district goals include energy-related key performance indicators (KPIs).

The Romanian focus district set itself the goal of reducing CO_2 emissions. This can be reframed as increasing the share of renewable energy, which contributes directly to lowering CO_2 emissions and aligns it with the objectives of other districts. In the Italian focus district, two of the three self-set goals are socially oriented, making them more challenging to quantify; these can be classified as supportive objectives.

Temporal boundaries for all focus districts are set at one operational year, as there are no additional local or project-specific requirements. The functional boundary type of each focus district categorizes them primarily as residential areas with a minor proportion of social buildings (e.g., schools and offices).

The energy simulation was carried out to obtain the annual primary energy balance KPI and utilizes a simplified model of a single-zone thermal building and is calculated as follows:

$$PEB = CF + \sum_i \sum_j f_{ij} E_{ij}$$

with E_{ij} the energy flow j at hour i over the system boundary (outwards positive) weighed with f_{ij} the time-dependant primary energy conversion factor of that energy flow and CF representing "Context Factors", which are virtual balance components derived from top-down model parametrization described in [12]. The context factors depend on district density, expressed as the Floor Area Ratio (FAR) between the district's gross floor area (GFA) and the underlying buildable plot area (PA):

$$FAR = \frac{GFA}{PA}$$

The context factors used for analysis were operationalized according to the following [13]:

$$CFD = Min\left(2\left(\frac{61.94}{FAR + 0.15}\right) - 53.79\right), 125 \left[\frac{kWh_{PE}}{m^2_{GFA}}\right]$$

$$CFR = 15 \left[\frac{kWh_{PE}}{m^2_{GFA}}\right]$$

$$CFR + D = CFD + CFR$$

The functional system boundary of the energy balance includes building use of operation and plug-loads (BUB). A second boundary only includes building operation (BOB) and is calculated by subtraction of user electricity and plug-loads (UE) from the use balance:

$$BOB = BUB - UE$$

Electrical power needs are primarily met by a photovoltaic (PV) system. Any surplus energy generated can either be redirected to domestic hot water systems as part of demand-side management (DSM) strategies or fed back into the grid to offset overall energy consumption, with the inverted conversion factor for grid electricity at that time. Unmet energy demands are supplemented by grid-supporting sources, such as wind peak shaving from nearby wind farms, which are modelled by the use of external wind availability data (>40% of installed capacity) at which point the primary energy conversion is set to zero, effectively discounting grid use during these hours. The effect of these measures is separately shown as "Flexibility Measures".

Thermal energy demand is defined by the target temperature settings for heating, cooling, and domestic hot water (DHW) systems. This demand can be satisfied through electrical solutions, such as heat pumps, or other methods like district heating and natural gas boilers. Each energy system is evaluated using specific primary energy conversion factors, which may be obtained from national or regional standards, measurement data, or projections for future energy systems.

Any excess energy generated through demand-side management can be stored in the building's thermal mass, which helps to reduce peak load demands, particularly during winter nights. The simulation method is illustrated schematically in Figure 2 and described in more detail in [14].

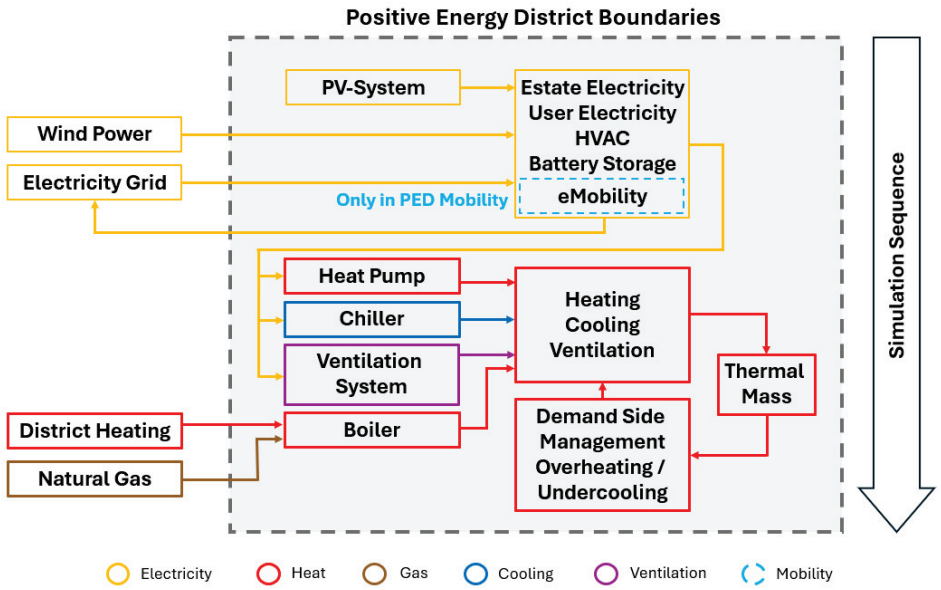


Figure 2. Applied simulation components of the PED establishment.

3. Energy Balance Calculation Results

For all the focus districts (FDs) considered, the development scenarios aimed at achieving Positive Energy Districts (PEDs) emphasize two primary strategies: building renovations (including insulating walls, roofs, and basements, as well as replacing windows) and the installation of photovoltaic (PV) panels. In regions with relatively cold climates, such renovations are crucial for minimizing heat loss during winter months. Conversely, in southern regions with high solar irradiation, PV installations are particularly effective, although these areas typically face increased energy demands for cooling during hotter months.

The most effective development scenarios combine a variety of available strategies, such as flexible grid usage and the integration of renewable energy technologies. Since primary energy is a critical factor in assessing PEDs, the effectiveness of these scenarios can be illustrated through a comparison of primary energy demand and supply, as shown in Figure 3.

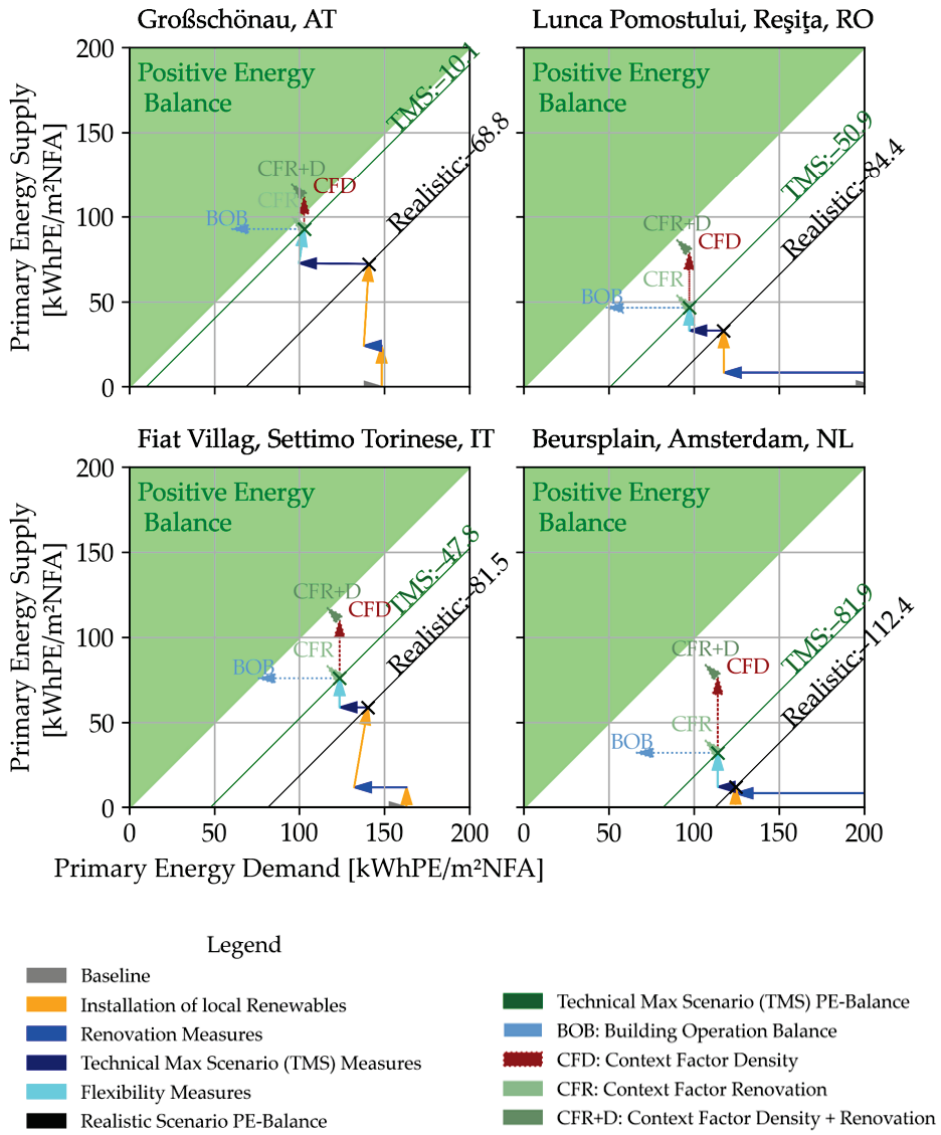


Figure 3. Primary energy in focus districts: demand vs. supply with and without accounting for contexts. BOB (blue): building operation balance; CFR (light green): context factor renovation; CFD (red): context factor density; CFR+D (green): combination of CFD and CFR. District scenarios with a final primary energy balance in the green shaded area are considered PEDs in Operation.

The dashed grey line in Figure 3 indicates the balance point, where energy demand equals supply—this represents the baseline requirement in the conventional definition of PEDs.

However, achieving a comprehensive understanding of PEDs also necessitates considering contextual factors [12].

In Figure 3, the blue line depicts PED pathways that do not account for these contextual factors, while the orange line illustrates pathways that include such considerations. The scenarios progress from the current state (represented by the rightmost points) through various stages, including the following

- Building renovation: initial energy efficiency improvements;
- Renovation with PV installation: increasing the integration of PV systems within districts;
- Implementation of flexible grid systems: enhancing management and distribution of energy.
- Adoption of all measures: combining renovations, PV installations, flexible grid systems, and more efficient energy equipment in the focus districts (represented by the leftmost points).

By considering these development scenarios, we can better understand the pathways toward achieving PEDs in diverse urban contexts.

4. Discussion on Further Improvement Areas of FDs Towards PEDs

In this research, focus districts were considered at the PED level of building operation and used to minimize complexity and uncertainty related to initial data. Several potential improvements could enhance the study's outcomes, including the following:

- Integrating a photovoltaic-thermal (PVT) simulation model to better align district goals with PED standards;
- Elevating the focus of the study to PED Mobility levels;
- Evaluating demand-side actions by residents to reduce energy consumption and carbon footprints within the districts.

4.1. Improvement of Simulation Results by Integrating PV/PVT Model in PED

One way to enhance the energy balance calculation within the focus districts is to utilize a more detailed model that accounts for various scenarios incorporating photovoltaic (PV) systems. In this work, we specifically compare photovoltaic-thermal (PVT) systems with conventional photovoltaic (PV) and solar thermal (ST) systems. While a PV module generates electricity, an ST module produces heat. In contrast, a PVT system integrates both PV and ST functionalities into a single unit, allowing for the simultaneous production of electricity and heat.

The modelling of these systems is grounded in energy conservation principles and considers heat exchanges—conductive, convective, and radiative—across each collector component. Several assumptions are made, including neglecting pressure losses, edge losses, dust, and partial shading. Additionally, we assume uniform temperature across components, with the thermo-physical properties of materials treated as temperature independent. Each collector area is approximately 2 m^2. To simplify annual simulations across the district, we apply a rapid and efficient reduced temperature T_{red} approach [15], obtaining unique coefficients by solving ordinary differential equations (ODEs), and these highly detailed models are integrated into the PVMD Toolbox [16]:

$$T_{red} = \frac{T_{in} - T_{am}}{G}, \quad (1)$$

This approach characterizes the thermal and electrical performance of the system as functions of operational conditions, which include fluid inlet temperature (T_{in}), ambient

temperature (T_{am}), and solar radiation (G). The reduced temperature also influences the efficiency of photovoltaic (PV) systems, as cell temperature is dependent on operating conditions; however, this impact on overall PV performance is minimal. The thermal efficiency of the solar thermal (ST) collector, considering unique coefficients, can be expressed as follows:

$$\eta_{th} = 0.75 - 3.67\ T_{red} \quad (2)$$

Similarly, the electrical and thermal efficiencies of the photovoltaic-thermal (PVT) collector are based on the PVMD Toolbox [16] calculated as follows:

$$\eta_{el} = 0.195 - 0.33\ \mathrm{T}_{red}, \quad (3)$$

$$\eta_{th} = 0.47 - 10\ \mathrm{T}_{red} \quad (4)$$

These equations define the efficiencies of the solar collectors, considering several operational parameters, including baseline efficiency and temperature-dependent loss coefficients. Both electrical and thermal efficiencies are calculated on an hourly basis, which allows us to estimate the electrical and thermal yield of each collector type effectively.

To evaluate the potential for large-scale implementation of PVT systems, we applied this modelling approach to the Dutch focus district, the city centre of Amsterdam. We utilized openly available height data [17], processed as a rasterized digital elevation model (DEM) with a resolution of 0.5 metres. The footprint data from the cadastre [18] were used to clip the data points corresponding to each building within their respective polygon shapes.

Subsequently, we employed the Random Sample Consensus (RANSAC) algorithm [19] to detect suitable planar surfaces of at least 10 m². The layout of modules on these surfaces was optimized using a heuristic algorithm designed to fit them in rectangular formations on sloped rooftops [20], utilizing both portrait and landscape orientations. For flat rooftops, a maximum fit strategy was used, along with a simple economic model that determined whether an east–west or south-facing layout was more beneficial. If a building hosted at least four modules, our skyline-based approach [21] was implemented to estimate solar irradiance as an hourly profile spanning an average year. The required climate data were procured from the Royal Netherlands Meteorological Institute (KNMI) [22] over the past ten years.

4.1.1. Key Results

- Buildings and footprint: There are a total of 16,452 buildings in the focus district, encompassing a combined footprint area of 2.76 km^2. This area is further divided into the following:
  - 1.09 km^2 detected as flat surfaces;
  - 1.17 km^2 categorized as sloped rooftops.
- Module installation potential: on these surfaces, it is feasible to install 333,145 modules across 11,300 separate systems.

Furthermore, Table 2 presents the results of the geospatial mapping of PV, PVT, and ST modules throughout the focus district.

4.1.2. Energy Yield Comparison

- Photovoltaic modules: yield only electricity, with no thermal yield;
- Solar thermal modules: yield only heat, with no electrical yield;
- PVT systems: achieve a combined total yield of 359.4 GWh/year, translating to 130 kWh/year/m^2 when divided by the building footprint area.

While the thermal yield of PVT systems is lower than that of ST systems, which generate a specific yield of 164 kWh/year/m^2, PVT systems are often the most efficient approach for roofs in terms of energy generation.

Table 2. Results of the geospatial mapping of PV, PVT and ST modules on the focus district.

	Module Count	Nominal Power (MW)	Electric Energy (GWh/yr)	Thermal Energy (GWh/yr)	Total Energy (GWh/yr)
PV	333,145	123.3	117.3	0	117.3
ST	333,145	123.3	0	452.6	452.6
PVT	333,145	123.3	121.9	237.5	359.4

4.2. Assessing Mobility in PED

To assess the electricity demand for private e-mobility within the Positive Energy District (PED), we developed a simulation model based on the parking-based approach described in the Horizon Europe INCIT-EV Project [23]. This model estimates both the overall annual energy demand and the temporal distribution of energy requests throughout the year [24].

The parking-based approach focuses on understanding drivers' habits and behaviours, particularly the timing and duration of parking. Notably, this method does not require knowledge of the origin-destination trip matrix; instead, it emphasizes modelling parking and charging patterns to determine energy demand.

4.2.1. Model Inputs

The model utilizes three main categories of inputs:

1. Car fleet characteristics:
    - Average number of electric vehicles (EVs) travelling within the PED (internal), originating from the PED (outgoing), and heading into the PED (incoming) each day;
    - Typical daily travel distances.
2. Driver behaviour:
    - Preferred times and locations for charging;
    - State of charge (SOC) thresholds that trigger a charging event (initial SOC) and stop the charging operation (final SOC);
    - These behaviours are represented in the model using probability distributions.
3. Charging infrastructure:
    - Number and power of charging points available within the district;
    - Temperature data can also be incorporated to account for variations in energy consumption due to seasonal temperature changes, which affect battery efficiency.

Once the inputs are defined, the model runs an hourly simulation for one entire year, processing each vehicle sequentially. Daily average values are used for all days of the year. It evaluates charging decisions based on the vehicle's current SOC, its travel or parked status, and the availability of charging stations. When all charging requirements are met, the vehicle's status changes to "charging," and its energy demand is added to the current timestep and cumulative annual demand.

4.2.2. Model Outputs

The outputs of the model include the following:

- Maximum power demand: the peak power demand on the local electricity grid and the specific time it occurs;
- Total annual energy demand: this provides essential insights regarding the additional energy supply requirements needed to meet district-wide demand;
- The model also tracks disservice events where charging requests cannot be fulfilled due to all stations being occupied.

As an example, we present the results of the simulation conducted for the focus district in Settimo Torinese (Italy), illustrated in Figure 4. The results are shown monthly to highlight potential annual patterns in energy demand.

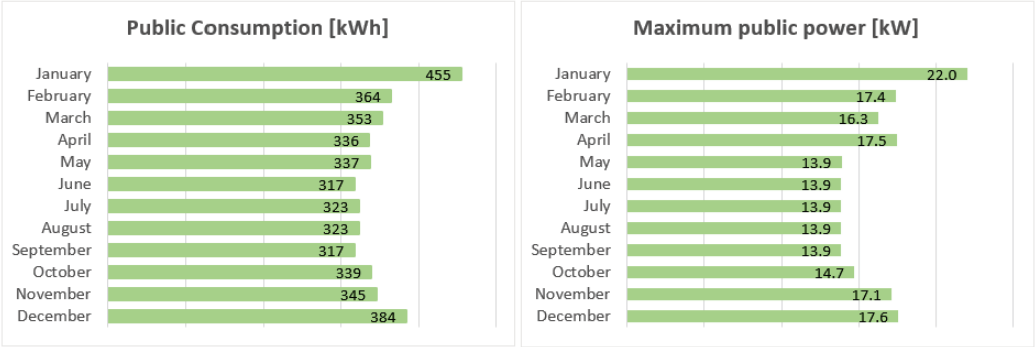


Figure 4. Annual public consumption and maximum public power in Fiat Village, Settimo Torinese.

4.2.3. Findings

- Seasonal trends: Winter months exhibit higher consumption due to reduced battery efficiency in cold temperatures. On average, the energy required monthly is approximately 400 kWh, comparable to the consumption of two average Italian-sized families [25].
- Maximum power: The maximum power requested from the grid is 22 kW, which the current infrastructure can easily accommodate. No disservice events were recorded, indicating that the existing charging infrastructure meets demand effectively.

These results were instrumental in completing the energy balance for the focus district of Settimo Torinese, providing a more comprehensive overview of total energy consumption.

4.3. Demand-Side Actions of Residents

Demand-side actions by residents—such as behavioural changes and the adoption of sustainable technologies—are essential components in the transition towards a PED. A study conducted in the SIMPLY Positive project evaluates the potential for energy and greenhouse gas (GHG) reductions through resident-driven actions within the Focus District of Großschönau, Austria [26].

Utilizing both qualitative and quantitative methods, the study identified and ranked scalable actions that contribute to district-wide energy reduction and provide insights for urban energy planning. Data on energy usage patterns were collected through household interviews, examining factors such as heating methods, appliance usage, and mobility practices. Subsequently, energy consumption data and GHG emission metrics were analyzed, and buildings were sorted based on Austrian typology [27], to quantify the saving potential.

The following Table 3 ranks best-practice examples by replication potential, which were identified as the most effective ones, considering the district-wide energy-saving potential.

Table 3. Most effective identified demand-side actions by replication potential.

Demand-Side Actions	Energy Saving Potential for the Whole Focus District [kWh]	GHG Saving Potential Depending on Energy Mix [kg CO_2-Equivalents]
(A) *Simple to replicate for everyone and associated with low costs*		
Energy consultations in residential buildings	135,660	n/a
Regular ventilation of radiators	129,430	n/a
Adapting the room temperature to the usage and daytime	74,053	3566
Reduction in the room temperature by 1 °C	68,304	2139
Conversion to LED technology	55,200	683–15,710
(B) *Possible under certain circumstances and/or low investment required*		
Switch to e-bikes for going to work	346,090	112,020
Carpooling with at least 2 persons	341,360	110,940
Conversion of street lighting to LED	268,755	n/a
Correct ventilation of windows and shadowing instead of an air conditioner	196,890	1970–45,280
Conversion from combustion cars to public transport	78,000	24,540
(C) *Costly and/or complex technical adaptation required*		
Renovate private buildings to passive house standard	4,060,720	n/a
Thermal renovation as performed in reality	3,401,460	n/a
Renovate public buildings to passive house standard	529,132	95,240
Conversion from combustion cars to electric cars	421,231	143,900–173,900
Conversion from oil heater to heat pumps	247,823	11,357–17,232

4.3.1. Key Findings

The analysis reveals that significant district-wide energy reductions can be achieved through several key measures, including the following:

1. Thermal renovation: Upgrading building insulation and installing energy-efficient windows and doors can dramatically reduce heating and cooling needs. For instance, a thermal renovation case in Großschönau has been shown to decrease energy consumption by over 50%, reducing the energy index from 119 kWh/m^2a to 56 kWh/m^2a. With approximately 111 buildings identified as suitable candidates for renovation, district-wide implementation could result in annual savings of up to 3400 MWh [28];
2. Transition to electric vehicles: Replacing combustion-engine vehicles with electric cars is one of the most effective strategies for reducing GHG emissions in the transportation sector. The study found that a typical household could save about 7 MWh and 3 tons of CO_2 equivalents per year by switching to an electric vehicle powered by renewable energy. Scaling this across all inhabitants in Großschönau could yield annual savings of about 420 MWh and 174 tons of CO_2 equivalents;
3. E-bike and carpooling initiatives: Encouraging residents to shift from personal vehicles to e-bikes or carpooling can significantly reduce energy consumption and emissions. For example, regular carpooling can save around 6 MWh annually, while covering a daily commute of 16 km on an e-bike instead of using a combustion vehicle could save approximately 350 MWh and 110 tons of CO_2 equivalents per year [29,30].

These actions not only support environmental goals but also provide health benefits and reduced transportation costs for residents.

4.3.2. Best-Practice Examples

The following measures were identified as having the highest potential for replication and impact on district-wide energy savings (see Table 3 for details):

1. Thermal renovations;
2. Conversion from combustible cars to electric cars;
3. Conversion to e-bikes and carpooling.

A final ranking provides a roadmap for scalable and impactful strategies that balance environmental gains with ease of implementation. Some actions, which require minimal technical intervention, can be readily adopted by most residents and still significantly impact the district's energy balance. By increasing awareness of energy usage and identifying inefficient appliances or consumption patterns, residents can make sustainable choices without substantial financial burden [30].

These findings provide a replicable framework for other districts aiming to achieve PED status, serving as a decision-support tool for public incentives and awareness-raising measures.

4.4. Integrating the SECAP Methodology to Trigger PEDs Within a City

Given the complexity surrounding the development of Positive Energy Districts (PEDs), we developed a guideline offering a framework for potential developers, including municipalities and private sector entities, focused on leveraging the Sustainable Energy and Climate Action Plan (SECAP) methodology [31]. The guideline emphasizes synergies and interoperability between the two processes, concentrating on shared principles, compatible frameworks, common data management, and specific integration points.

The guideline was developed by identifying SECAP steps that facilitate the operationalization of PEDs during the creation of the SECAP within the focus district in Reşiţa, Romania. Key elements common to both SECAP and PED processes were determined for effective planning and monitoring of PEDs, aligned with the PED framework and key performance indicators.

A fundamental premise of these guidelines is that an SECAP should be initiated prior to PED development, as PEDs typically represent neighbourhoods within cities where the spatial boundaries of SECAPs may extend beyond those of individual PEDs.

As PED development does not lend itself to a rigid standardized approach, these guidelines provide users with a structured framework that can serve as a foundation for personalized PED development and operationalization. The framework is presented in four main phases:

1. Initiation phase
    a. Political commitment: securing the backing of political leaders to foster support for PED initiatives;
    b. Mobilizing relevant stakeholders: engaging all key players, including residents, businesses, and civic organizations, to ensure comprehensive participation;
    c. Building support: gaining momentum and endorsement from stakeholders to facilitate the project.
2. Planning phase
    a. Framework setting: establishing the context and guidelines for PED operationalization;
    b. Documenting policy synergies: identifying and aligning existing policies that complement PED objectives;

c. Elaboration of a PED action plan: developing a detailed strategy to implement and achieve PED goals.

3. Implementation phase

This phase integrates all planning efforts into actionable steps, ensuring that strategies are executed effectively.

4. Monitoring phase

Implementing monitoring processes to track progress toward objectives and assess the effectiveness of implemented actions.

Although some SECAP elements may not apply directly to the development and establishment of PEDs, the maturity of the SECAP methodology has effectively supported municipal decarbonization planning throughout Europe for over a decade. Furthermore, these guidelines reference the SIMPLY Positive deliverables, which offer practical approaches for defining PEDs, operational scenarios, energy balances, key performance indicators, and project monitoring.

By synthesizing the SECAP methodology, as applied in the focus district in Reşiţa, and the insights from the SIMPLY Positive project, the "Guidelines on How to Use the SECAP Methodology to Trigger Flagship Positive Energy Districts Within a City" are expected to significantly aid developers in their PED operationalization processes.

5. Conclusions

This study underscores the critical role of Positive Energy Districts (PEDs) in fostering sustainable urban environments. Through an analysis of energy balance calculations across four diverse case studies—Settimo Torinese, Großschönau, Amsterdam, and Reşiţa—this research highlights the adaptability and efficacy of tailored strategies across various urban and climatic contexts. Key findings include the following:

- Significant potential for positive energy balances: despite variations in infrastructure age, climate, and urban density, all focus districts demonstrated substantial potential to achieve positive energy balances through targeted interventions, including the integration of renewable energy sources;
- Scalable methodologies: The structured framework—with three expanding functional system boundaries—provides a scalable approach to addressing increasing complexities, from operational energy management to embodied emissions. This framework ensures that solutions remain feasible and impactful over the long term.
- Innovative technologies: innovative solutions such as photovoltaic-thermal (PVT) systems have shown effectiveness in optimizing rooftop utilization by producing both electrical and thermal energy, thus meeting diverse energy needs.
- Community engagement: active community involvement and enhancements in e-mobility contribute significantly to energy efficiency and emissions reduction, highlighting the essential role of resident engagement and behavioural change in the success of PEDs.

The findings also emphasize the replicability of the proposed methodologies, presenting a robust framework for other cities aspiring to establish their own PEDs. Comprehensive energy simulations, collaborative planning, and adaptive measures are crucial to the successful implementation of these districts.

This research can serve as a valuable resource for policymakers, urban planners, and stakeholders focused on developing sustainable, resilient, and energy-positive communities. Future work should prioritize the integration of emerging technologies and advanced simulation techniques to refine the design and functionality of PEDs.

6. Future Work

Future research should focus on the integration of emerging technologies and advanced simulation techniques to enhance the design and functionality of Positive Energy Districts (PEDs). This includes exploring the potential of smart grid technology to optimize energy distribution and consumption, as well as incorporating energy storage solutions to manage supply and demand fluctuations effectively. Additionally, investigating the role of advanced data analytics and machine learning can provide deeper insights into resident behaviours and energy usage patterns, leading to more personalized and effective demand-side management strategies. Expanding the scope of case studies to include a wider range of urban contexts and geographical settings will also allow for a comprehensive understanding of how different factors—such as socio-economic conditions and local policies—impact the implementation and success of PEDs. By focusing on these areas, future work can build a more resilient framework for urban energy planning and foster broader adoption of sustainable practices in cities worldwide.

Author Contributions: Conceptualization, H.B. and S.A.; methodology of energy balance calculation, S.S.; methodology of PV/PVT calculation, Z.U.A., R.S., M.V., M.Z. and O.I.; methodology mobility calculation M.P. and C.B.; methodology of demand-side evaluation, H.B. and M.B.; methodology SECAP applying, A.S.; investigation of PED energy balance, S.A. and S.S.; investigation of PV/PVT, Z.U.A., R.S., M.V., M.Z. and O.I.; investigation of mobility, M.P. and C.B.; investigation of demand-side actions, H.B. and M.B.; writing—original draft preparation, S.A.; writing—review and editing, H.B., S.S., M.B., Z.U.A., R.S., M.V., M.Z., O.I., A.S., M.P. and C.B; project administration, H.B. All authors have read and agreed to the published version of the manuscript.

Funding: This project has been developed in the framework of the PED Program, which is implemented by the Joint Programming Initiative Urban Europe and SET Plan Action 3.2. The Austrian part is supported by the Austrian Ministry of Climate Action, Environment, Energy, Mobility, Innovation, and Technology (BMK); the Romanian part is supported by a grant of the Ministry of Research, Innovation and Digitization CNCS/CCCDI—UEFISCDI, project number PED-JPI-SIMPLY POSITIVE, contracts number 325/2022 and 326/2022, within PNCDI III; the Dutch part is supported by the RVO (the Netherlands Enterprise Agency), reference number ERANETPED-02767306; and the Italian part is supported by a grant of the Ministry of Education and Merit—Department for Higher Education and Research, project number PED_00042, from the Fund for Investment in Scientific and Technological Research (FIRST/FAR) and/or Special Accounting Account no. 5944.

Data Availability Statement: The original contributions presented in this study are included in the article. Further inquiries can be directed to the corresponding author.

Conflicts of Interest: Author Mr.Helmut Bruckner was employed by the company Sonnenplatz Großschönau GmbH, 3922 Großschönau, Austria. The remaining authors declare that the research was conducted in the absence of any commercial or financial relationships that could be construed as a potential conflict of interest.

References

1. SETIS. p. I: SET-Plan ACTION n°3.2 Implementation Plan. Europe to Become a Global Role Model in Integrated, Innovative Solutions for the Planning, Deployment, and Replication of Positive Energy Districts. June 2018. Available online: https://setis.ec.europa.eu/system/files/2021-04/setplan_smartcities_implementationplan.pdf (accessed on 22 November 2024).
2. SET Plan. p 71ff: SET Plan Progress Report 2024, Scaling up Research, Innovation and Competitiveness in Clean Energy Technologies, Implementing Positive Energy Districts. 2024. Available online: https://setis.ec.europa.eu/set-plan-progress-report-2024_en (accessed on 10 January 2025).
3. Khalid, M. Smart grids and renewable energy systems: Perspectives and grid integration challenges. *Energy Strat. Rev.* **2024**, *51*, 101299. [CrossRef]

4. Kataray, T.; Nitesh, B.; Yarram, B.; Sinha, S.; Cuce, E.; Shaik, S.; Vigneshwaran, P.; Roy, A. Integration of smart grid with renewable energy sources: Opportunities and challenges—A comprehensive review. *Sustain. Energy Technol. Assess.* **2023**, *58*, 103363. [CrossRef]
5. SIMPLY Positive, 2023–2024, International Research Project, Developed in the Framework of the PED Program, Which Is Implemented by the Joint Programming Initiative Urban Europe and SET Plan Action 3.2. Available online: http://simplypositive.eu/ (accessed on 12 December 2024).
6. Ayaz, M. No Gas All Local: Developing a Renewable-Based and Decentralised Energy System for the Historic Centre of Amsterdam, Wageningen University & Research—Library. 2022. Available online: https://edepot.wur.nl/633721 (accessed on 10 January 2025).
7. SET Plan. *Increase the Resilience and Security of the Energy System—Implementation Plan*; European Commission: Brussels, Belgium, 2018.
8. Sareen, S.; Albert-Seifried, V.; Aelenei, L.; Reda, F.; Etminan, G.; Andreucci, M.-B.; Kuzmic, M.; Maas, N.; Seco, O.; Civiero, P.; et al. Ten questions concerning positive energy districts. *Build. Environ.* **2022**, *216*, 109017. [CrossRef]
9. Vandevyvere, H.; Ahlers, D.; Wyckmans, A. The Sense and Non-Sense of PEDs—Feeding Back Practical Experiences of Positive Energy District Demonstrators into the European PED Framework Definition Development Process. *Energies* **2022**, *15*, 4491. [CrossRef]
10. Zhang, X.; Penaka, S.R.; Giriraj, S.; Sánchez, M.N.; Civiero, P.; Vandevyvere, H. Characterizing Positive Energy District (PED) through a Preliminary Review of 60 Existing Projects in Europe. *Buildings* **2021**, *11*, 318. [CrossRef]
11. Lindholm, O.; Rehman, H.U.; Reda, F. Positioning Positive Energy Districts in European Cities. *Buildings* **2021**, *11*, 19. [CrossRef]
12. Schneider, S.; Zelger, T.; Sengl, D.; Baptista, J. A Quantitative Positive Energy District Definition with Contextual Targets. *Buildings* **2023**, *13*, 1210. [CrossRef]
13. Albert-Seifried, V.; Murauskaite, L.; Massa, G.; Aelenei, L.; Baer, D.; Krangsås, S.G.; Alpagut, B.; Mutule, A.; Pokorny, N.; Vandevyvere, H. Definitions of Positive Energy Districts: A Review of the Status Quo and Challenges. In Proceedings of the Sustainability in Energy and Buildings 2021, Split, Croatia, 14–16 September 2022; Springer Nature: Singapore, 2022; pp. 493–506.
14. Schneider, S.; Drexel, R.; Zelger, T.; Baptista, J. PEExcel: A fast one-stop-shop Assessment and Simulation framework for Positive Energy Districts. In Proceedings of the BauSim Conference 2024, Vienna, Austria, 23–26 September 2024; IBPSA-Germany and Austria; Volume 10, pp. 80–88. [CrossRef]
15. Ul-Abdin, Z.; Zeman, M.; Isabella, O.; Santbergen, R. Investigating the annual performance of air-based collectors and novel bi-fluid based PV-thermal system. *Sol. Energy* **2024**, *276*, 112687. [CrossRef]
16. Vogt, M.; Tobon, C.R.; Alcañiz, A.; Procel, P.; Blom, Y.; El Din, A.N.; Stark, T.; Wang, Z.; Goma, E.G.; Etxebarria, J.; et al. Introducing a comprehensive physics-based modelling framework for tandem and other PV systems. *Sol. Energy Mater. Sol. Cells* **2022**, *247*, 111944. [CrossRef]
17. Height Data Retrieved from Algemeen Hoogtebestand Nederland. Available online: https://www.ahn.nl/open-data (accessed on 16 October 2024).
18. Bag Cadaster Data from Bag Viewer. Available online: https://bagviewer.kadaster.nl/lvbag/bag-viewer/ (accessed on 24 October 2024).
19. Torr, P.H.S.; Zisserman, A. MLESAC: A New Robust Estimator with Application to Estimating Image Geometry. *Comput. Vis. Image Underst.* **2000**, *78*, 138–156. [CrossRef]
20. De Vries, T.N.; Bronkhorst, J.; Vermeer, M.; Donker, J.C.; Briels, S.A.; Ziar, H.; Zeman, M.; Isabella, O. A quick-scan method to assess photovoltaic rooftop potential based on aerial imagery and LiDAR. *Sol. Energy* **2020**, *209*, 96–107. [CrossRef]
21. Calcabrini, A.; Ziar, H.; Isabella, O.; Zeman, M. A simplified skyline-based method for estimating the annual solar energy potential in urban environments. *Nat. Energy* **2019**, *4*, 206–215. [CrossRef]
22. Climate Data Procured from the Koninklijk Nederlands Meteorologisch Instituut, Ministerie van Infrastructuur en Waterstaat. Available online: https://daggegevens.knmi.nl/klimatologie/uurgegevens (accessed on 15 October 2024).
23. INCIT-EV Website | Electric Charging Solutions for Electric Vehicles. Available online: https://www.incit-ev.eu/ (accessed on 22 November 2024).
24. Macaluso, P.; Carboni, A.; Botta, C.; Lazzeroni, P.; Deflorio, F.; Arnone, M. Estimating charging demand by modelling EV drivers' parking patterns and habits. *Eur. Transp.\Trasp. Eur.* **2023**, *90*, 1–14. [CrossRef]
25. Italian Regulatory Authority for Energy. Networks and Environment (ARERA). 2023. Available online: https://www.arera.it/en/comunicati-stampa/dettaglio/elettricita-bolletta-in-tutela-186-nel-quarto-trimestre-contributo-straordinario-per-i-titolari-di-bonus (accessed on 4 November 2024).
26. Binder, M.; Bruckner, H. D4.4 Demand Side Actions of Residents to Reduce Districts. Available online: http://simplypositive.eu/wp-content/uploads/2024/12/D4.4-Demand-side-actions-of-residents-to-reduce-energy-consumption-and-carbon-footprint-in-focus-districts_final.pdf (accessed on 28 October 2024).
27. TABULA WebTool. Available online: https://webtool.building-typology.eu/#bm (accessed on 11 July 2024).

28. Brennwert. Available online: https://www.geothermie.de/bibliothek/lexikon-der-geothermie/b/brennwert (accessed on 1 August 2024).
29. Berechnung von Treibhausgas (THG)-Emissionen Verschiedener Energieträger. Available online: https://secure.umweltbundesamt.at/co2mon/co2mon.html (accessed on 15 July 2024).
30. Verordnung des Vorstands der E-Control Über die Voraussetzungen an die Fachliche Qualifizierung und Requalifizierung von Energiedienstleisterinnen und Energiedienstleistern (Energieeffizienz-Qualifikationsbewertungs-Verordnung—EEff-QBV)—BGBI.II Nr. 264/2023. Available online: https://www.ris.bka.gv.at/eli/bgbl/II/2023/264/20230908 (accessed on 19 July 2024).
31. European Commission: Joint Research Centre; Rivas, S.; Bertoldi, P.; Melica, G.; Dallemand, J.; Palermo, V. *Guidebook 'How to Develop a Sustainable Energy and Climate Action Plan (SECAP)'. Part 1, The SECAP Process, Step-by-Step Towards Low Carbon and Climate Resilient Cities by 2030*; Bertoldi, P., Ed.; Publications Office: Luxembourg, 2018; Available online: https://data.europa.eu/doi/10.2760/223399 (accessed on 23 January 2025).

Disclaimer/Publisher's Note: The statements, opinions and data contained in all publications are solely those of the individual author(s) and contributor(s) and not of MDPI and/or the editor(s). MDPI and/or the editor(s) disclaim responsibility for any injury to people or property resulting from any ideas, methods, instructions or products referred to in the content.

energies

MDPI

Article

Short-Term Building Electrical Load Prediction by Peak Data Clustering and Transfer Learning Strategy

Kangji Li *, Shiyi Zhou, Mengtao Zhao and Borui Wei

School of Electrical and Information Engineering, Jiangsu University, Zhenjiang 212013, China; 2222207051@stmail.ujs.edu.cn (S.Z.); 2222307027@stmail.ujs.edu.cn (M.Z.); 2212107028@stmail.ujs.edu.cn (B.W.)

* Correspondence: likangji@ujs.edu.cn; Tel.: +86-511-8879-1245

Abstract: With the gradual penetration of new energy generation and storage to the building side, the short-term prediction of building power demand plays an increasingly important role in peak demand response and energy supply/demand balance. The low occurring frequency of peak electrical loads in buildings leads to insufficient data sampling for model training, which is currently an important factor affecting the performance of short-term electrical load prediction. To address this issue, by using peak data clustering and knowledge transfer from similar buildings, a short-term electrical load forecasting method is proposed. First, a building's electrical peak loads are clustered through peak/valley data analysis and K-nearest neighbors categorization method, thereby addressing the challenge of data clustering in data-sparse scenarios. Second, for peak/valley data clusters, an instance-based transfer learning (IBTL) strategy is used to transfer similar data from multi-source domains to enhance the target prediction's accuracy. During the process, a two-stage similar data selection strategy is applied based on Wasserstein distance and locality sensitive hashing. An IBTL strategy, iTrAdaboost-Elman, is designed to construct the predictive model. The performance of proposed method is validated on a public dataset. Results show that the data clustering and transfer learning method reduces the error by 49.22% (MAE) compared to the Elman model. Compared to the same transfer learning model without data clustering, the proposed approach also achieves higher prediction accuracy (1.96% vs. 2.63%, MAPE). The proposed method is also applied to forecast hourly/daily power demands of two real campus buildings in the USA and China, respectively. The effects of data clustering and knowledge transfer are both analyzed and compared in detail.

Keywords: peak data clustering; instance-based transfer learning; Wasserstein distance; LSH; iTrAdaboost-Elman

1. Introduction

In recent years, along with the increased building electrification, the proportion of electricity used in buildings has grown rapidly. In building-intensive cities such as Hong Kong and Shanghai in China, the proportion of building electricity consumption in total social electricity consumption has exceeded 90% [1]. With the gradual penetration of new energy generation and storage to the building side, the fluctuation and randomness of power generation/consumption also brought new challenges to the stability and optimal operation of the power grid. Accurately predicting a building's short-term electricity consumption plays an increasingly important role in peak demand response and energy supply/demand balance. For load prediction tasks with plenty of historical data, data-driven approaches

are believed to be more convenient and accurate than mechanism models. Various types of machine learning and deep learning models have been widely used in the field of building energy prediction [2–4]. The related research continues to make progress with respect to data analysis [5,6], model construction [7,8], and algorithm design [9]. However, when buildings lack sufficient high-quality historic data, or the sampled data distribution is unbalanced, traditional data-driven models no longer guarantee prediction accuracy. In the face of such data scarcity or imbalance problems, transfer learning of knowledge is an important direction.

1.1. Related Work

Transfer learning utilizes knowledge from source domain(s) to assist in accomplishing the target task. This approach relaxes two basic requirements of the data-driven models: the distributions of the training and testing sets could be different; the model could guarantee high performance even if the available training data from target domain are limited. The primary mission in transfer learning is to identify source domain data similar to the target domain, which are suitable for auxiliary training of target model. Currently, there are various similarity judgment methods, and the commonly used ones include maximum mean discrepancy (MMD) [10], Wasserstein distance (WD) [11], and maximal information coefficient (MIC) [12]. MMD maps the original variables to the reproducing kernel Hilbert space (RKHS) [13] and then calculates the distance between the two distributions to determine the similarity. Li et al. [14] selected two educational buildings with the highest similarity from more than 1000 buildings by using MMD and performed load prediction through transfer learning. If the single source domain and the target domain do not overlap at all or the overlap is very small, the WD method is more appropriate for similarity judgment [11]. In addition, by measuring the correlation between samples from different distributions (MIC method), the data similarity could also be determined [12]. Lu et al. [15] measured the similarity of time series data from the target and source domains by introducing the MIC method and used transfer learning to improve the accuracy of load prediction with scarce historical data. Wei et al. [16] combined WD and MIC methods to find the source domain with high similarity, and knowledge was transferred to improve the accuracy and robustness of the target predictive model. Similar studies are also reported in the literature [17,18].

From the perspective of transfer models, the currently used models mainly belong to model-based transfer learning (MBTL). The common practice is: pre-training the learning model using building datasets from similar regions or types (schools, residences, etc.), then fine-tuning parameters of the pre-trained model with small amounts of target-domain data to improve the prediction accuracy. For example, Li et al. [19] interpolated the missing data from the target sensor using bidirectional LSTM and transfer learning, which improved the robustness and prediction accuracy. Gao et al. [20] proposed a transfer learning-based multilayer perceptron (TL-MLP) to improve the prediction performance of buildings without sufficient labeled data. Similar studies can be found in [21–23]. Pinto et al. [24] summarized most of the current transfer learning strategies for building energy prediction. In the survey, 57 of the 77 papers on transfer learning used the MBTL method. However, when the training data are relatively sparse in the target domain, the instance-based transfer learning (IBTL) is more effective, because IBTL is able to select suitable samples directly from the source domain and assigns weights to the samples according to the prediction errors, which would help obtain training data of higher quality. Zeng et al. [25] integrated the advantages of weighted support vector regression (WSVR) and transfer learning based on TrAdaboost to improve the prediction accuracy. Li et al. [26] compared methods such as MBTL and IBTL in predicting the cross-building energy consumption of office buildings

and academic buildings. Results showed that the IBTL strategy was more stable. Similarly, Li et al. [27] found by comparison that instance-based boosting-type transfer learning methods were able to obtain more complete features of the target domain data, thus could further improve the prediction accuracy.

When the data distribution between single source and target domain differ significantly, similar data searching could expand to multiple source domains [28]. Lu et al. [29] introduced a multi-source IBTL building load prediction combining LSTM and multi kernel MMD domain adaptation. It is noted that as the number of source domains increases, so does the amount of redundant data. In 2024, Li et al. [30] investigated the impact of the quantity of source domain buildings on prediction accuracy of IBTL. Table 1 summarizes the researches on IBTL based building energy prediction in the last three years. The source domain number, similarity judgment method, and predicted time scale are all listed.

Table 1. Related papers on building energy prediction using IBTL method, since 2022.

Literature	Source Domain	Similarity Judgment Method	Predictive Model	Building Type
Li et al. (2022) [26]	Single source	MMD	DANN-LSTM	Office/Education
Li et al. (2022) [14]	Single source	MMD	iTrAdaboost-BP	Education
Lu et al. (2022) [15]	Single source	MIC	LSTM	Residence
Yuan et al. (2023) [17]	Single source	MMD	Attention-CNN-LSTM	Commerce
Lu et al. (2023) [29]	Multi-source	DTW	MK-MMD-LSTM	Railway building
Qian et al. (2024) [31]	Multi-source	DTW	iTrAdaboost-LSTM	Office/Education
Li et al. (2024) [30]	Multi-source	WD	NNS-iTrAdaboost-LSTM	Education

According to the literature review on transfer learning, the current models mainly treat target domain datasets as a whole. However, for the short-term building electrical load prediction, the main error actually comes from the error of peak loads' prediction. The sampled data during the peak times are relatively insufficient due to their low occurring frequency, even though the data in other periods may be redundant. These inherent data distribution's imbalance particularly affects the performance of short-term load prediction. To this end, peak data's recognition and IBTL based transfer learning may be a more targeted and efficient prediction method. The classification of peak data from target domain needs an available data clustering method. The unsupervised K-means or fuzzy C-mean clustering (FCM) methods could be used for such clustered prediction problems [32,33]. However, such data clustering requires sufficient labeled data to identify the intrinsic pattern, which are not available in data-sparse scenarios. A proper data clustering approach is still needed for peak loads classification. Based on this, a more efficient transfer learning strategy for short-term building electrical load prediction is explored in this study.

1.2. Main Contribution of This Work

To address the above issues, using peak data clustering and knowledge transfer from similar buildings, a building's short-term electrical load forecasting method based on clustered transfer learning strategy is proposed. The main contributions of this paper include:

(1) By analyzing the error source of short-term building electrical load prediction, the historical peak load data are clustered according to timestamp and extreme search. Based on the obtained data clusters, the supervised KNN algorithm is then used for testing data classification. Addressing the scarcity of clustered peak data, a transfer learning strategy is designed to enhance the training procedure so as to improve the whole prediction accuracy.

(2) A multi-source instance-based transfer learning strategy is designed. The Wasserstein distance is used to filter multiple buildings similar to the target one as the source

domains, from which the most helpful data samples are further selected by locality sensitive hashing (LSH) for auxiliary model training. An improved TrAdaboost (iTrAdaboost) algorithm is combined with Elman networks for a transfer learning type's model construction.

(3) Three different case studies are carried out for performance validation. A benchmark dataset from ASHRAE is used to verify and compare the accuracy of the proposed model with other methods. On this basis, two campus buildings in the USA and China are selected as practical cases to further verify the performance at the respective different predictive time scales (hourly and daily) and knowledge transfer scopes.

1.3. Paper Organization

The second section describes the framework of transfer learning and the related data clustering method. In the third section, the proposed model is applied to perform load prediction on the public dataset and two actual buildings, respectively. The results are analyzed in detail. The last section gives a brief conclusion.

2. Principles and Methods

2.1. Instance-Based Transfer Learning

IBTL reuses labeled data from source domains to help train a model for the target task more accurately. Because there are differences between target and source domains, data samples from source domains do not necessarily improve the model performance [34]. An effective boosting-style approach involves adjusting the weights of source domain instances based on prediction errors, identifying misleading data, and iteratively training the target domain model, which leads to better results for the trained classifiers/predictors.

One of the boosting style methods, TrAdaboost [35], is chosen in this study. By increasing the weights of the samples that are favorable to the target task and decreasing the weights that are unfavorable to the target task, the model accuracy is improved [35]. The original TrAdaboost is used for classification, but building load prediction is considered a regression problem. Appropriate modifications are made on the basis of original TrAdaboost algorithm, which include:

(1) The weight update parameter of traditional TrAdaboost is

$$\beta_t = \frac{\varepsilon_t}{1-\varepsilon_t}. \tag{1}$$

For binary classification, the error rate ε_t of the original TrAdaBoost algorithm is less than 0.5. In the improved TrAdaBoost algorithm, when the error rate is greater than 0.5, it is reset to 0.5, which ensures the stability and effectiveness of the algorithm for forecasting tasks.

(2) The threshold (γ) of TrAdaboost is fixed for the classification problem. In regression prediction, it is updated by a function

$$\Delta\gamma_t = -\eta\frac{\partial E_t}{\partial y_t}. \tag{2}$$

Thus, the threshold γ will be dynamically changed according to the prediction error rate.

The Elman Network [36] is chosen as the sub-learners in the iTrAdaboost algorithm. This is because a building energy system usually has complex nonlinear relationships, which is what the Elman model is good at capturing. At the same time, the Elman model has the advantages of a simple structure, computational efficiency, and consideration of temporal information. Details of the transfer learning model (called iTrAdaboost-Elman) are given in Figure 1, where ω_N is the initial weight vector of the training set, and h_N is the base prediction in the target domain. The expressions x and y are the input features and energy consumption values of the training set, respectively; n and m are the number of data samples from source and target domain, respectively.

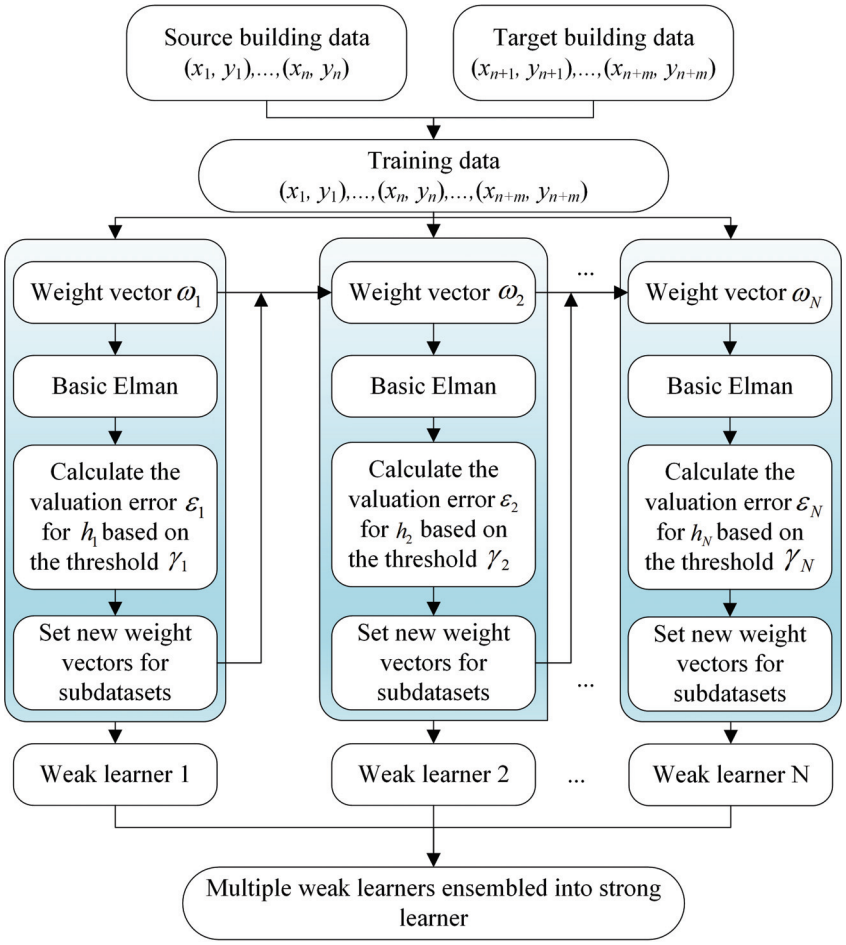


Figure 1. Schematic of the iTrAdaboost-Elman model.

2.2. Data Clustering Method

By analyzing the error source of short-term building electrical load prediction, the errors from peak loads seriously affect the whole prediction performance. Data clustering helps in finding the underlying patterns and characteristics within data samples, and it plays a key role in prediction and analysis tasks. As reviewed in the Introduction, various data clustering methods (such as K-means and FCM) have been applied for building energy clustering and prediction. However, data's transfer learning task in a data scarcity scenario naturally prevents the application of such traditional clustering methods, because the required sufficient labeled data can hardly be obtained.

To identify peak loads in limited historical data, the timestamp and extreme search method is used in this study. First, the dataset combined with timestamp is sorted by time series and the energy usage cycle is identified (24 hours a day, 7 days each week, etc.). In every energy usage cycle, the extreme values (maximum/minimum) are searched as peak and valley points. Then, based on the amplitude of each energy usage cycle (the difference between the maximum and minimum loads), a amplitude proportion ap (say, 15%) is determined to classify peak and valley data clusters. In this way, m_i data samples around the peak point are clustered as the peak data, and n_i data samples around the valley point are clustered as the valley data. The rest of the data are clustered as the others. The specific values of m_i and n_i are depended on the proportion ap.

It should be pointed out that only historical data can be clustered using the above method. For unknown data of the future (as validation/testing sets), such extreme searching is not feasible. We classify datasets for validation/testing according to the distances to the obtained three clusters (peak/valley/others). The K-nearest neighbors (KNN) [37] is

utilized, and by setting key parameter K, the nearest data points are clustered. The specific flowchart of the data clustering is shown in Figure 2.

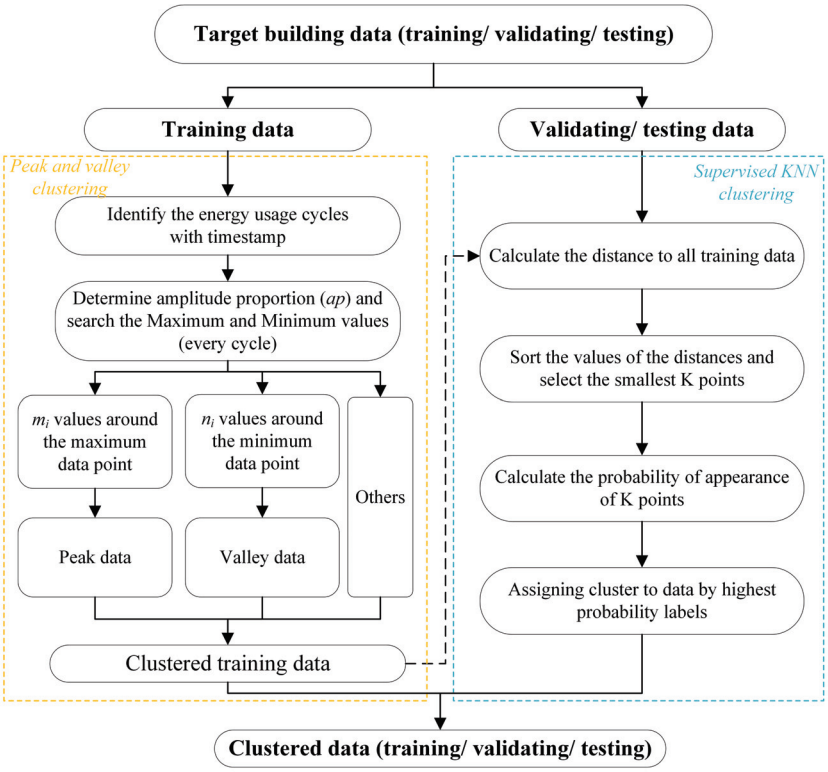


Figure 2. Peak and valley clustering and supervised KNN clustering method.

2.3. Two-Stage Selection of Similarity Data

This study uses a two-stage method for similar data selection from source domains. First, multiple source domain buildings are selected based on WD. Then, the LSH method is introduced to select similar data from them, so as to reduce the impact of redundant data in the source domain dataset on transfer learning.

2.3.1. Similar Buildings Recognition

By measuring the distance between two distributions, the similarity between them can be determined. For the commonly used MMD method, when two distributions (buildings) do not overlap or overlap very little, the results will be close to zero or do not reflect the true distance of the distributions. In contrast, WD directly calculates the minimum cost of converting one distribution to another, which could reflect the similarity more effectively. The Wasserstein distance can be defined as

$$W_p(\mu,\nu) = \left(\inf_{\pi\in\Gamma(\mu,\nu)} \int d(m,n)^p d\pi(m,n)\right)^{1/p}, \quad (3)$$

where $d(m,n)$ denotes the distance between points m and n, e.g., the Euclidean distance; $\Gamma(\mu,\nu)$ is the set of all joint probability distributions whose marginals are distributed as μ and ν; p is the order between μ and ν. More details can be found in [11]. By calculating the WDs, similar source domain buildings are selected.

Further, an optimal indicator is set for determining the number of source domains [38]. Considering optimal prediction accuracy and a small number of source domains, the function is defined as

$$\min_p f(p) = \lambda \times \frac{p}{q} + (1-\lambda) \times MAPE(p,q) \quad (4)$$

where p and q are the amount of selected source buildings and candidate source buildings, respectively. The $MAPE(p, q)$ is the error of the predictive model using p source domains to predict and obtain the model parameters; λ is the weighting coefficient to balance the two terms. In practice, it is difficult to find the exact λ. For this study, the λ is roughly adjusted to 0.8 according to expert experience. The optimal number of source domains p is determined through these two steps: First, minimize the number of source domains to reduce computational load while ensuring model performance; then, select as many source domains as possible to enhance model performance.

2.3.2. Similar Data Selection

In the field of electric load prediction, nearest neighbor search (NNS) has been used to find similar data from source domain buildings [30]. Different from NNS, LSH achieves approximate nearest neighbor search (ANNS) [39] by mapping high-dimensional data points to a low-dimensional hash space such that similar data points have a high probability of being mapped to the same hash bucket [40]. LSH is able to efficiently perform ANNS in high-dimensional spaces and usually has faster speed and smaller storage requirements than NNS, making it more suitable for finding similar high-dimensional data from source domains.

The specific searching procedure is as follows:

S1. Map the data to a lower dimensional space to reduce computational complexity and the impact of dimensionality curse.

S2. By constructing a hash table through one or more hash functions, similar data points have a higher probability of being mapped into the same hash bucket. The Minhash function is chosen in this study.

S3. Map data points into corresponding hash buckets according to the chosen hash function. Each hash bucket contains a set of similar data points, possibly the most neighboring ones.

S4. According to the query data points, by using the same hash function, the query points are mapped to the corresponding hash buckets, then the set of nearest neighbor candidate points are searched from the hash buckets.

S5. The set of candidate points is further filtered and sorted to identify the nearest neighbor data points. Euclidean distance, cosine similarity, or other similarity measurements are generally used to calculate and rank the closest neighboring points. The Euclidean distance is chosen for this study.

The primary used parameters are the similarity threshold σ (0 to 1) and the number of hash functions η. A higher σ results in selecting fewer similar data points. For this study, σ is set to 0.4, meaning only data with the similarity of 0.4 or greater will be selected. The larger the number of hash functions η, the more accurate the estimated similarity. But it also requires calculating and storing more hash values, which will increase the computation time to some extent. For this study, the value of η is set to 128.

2.4. The Proposed Predictive Model Framework

In this study, data clustering is combined with knowledge transfer learning for efficient short-term building electrical load prediction. The overall procedure of the prediction framework includes three parts.

First, data clustering is performed to pick out building's peak/valley loads. Concretely, building's historical electrical loads are clustered into three categories (peak/valley/others) through energy usage cycle identification and extreme value searching. Then, based on the recognized data clusters, the data from validating and testing sets are classified by KNN method. Second, similar data from source domains are selected for transfer learning

by a two-stage method. Specifically, the similar buildings are selected by calculating the WD metric; then, by the LSH method, most helpful data samples from the above similar buildings are picked to construct an auxiliary dataset for transfer learning. It is noted that only peak/valley data from source domains are identified and picked by this two-stage method. Third, the Elman network is constructed and iteratively trained as sub-learners with the proposed iTrAdaboost algorithm. The transfer learning procedure is carried out only for the peak/valley data that are insufficient for model training. For the data cluster of "others", the Elman model is directly used for prediction. In the following section, three case studies investigate the performance of the proposed method. Figure 3 summarizes the overall structure of this study.

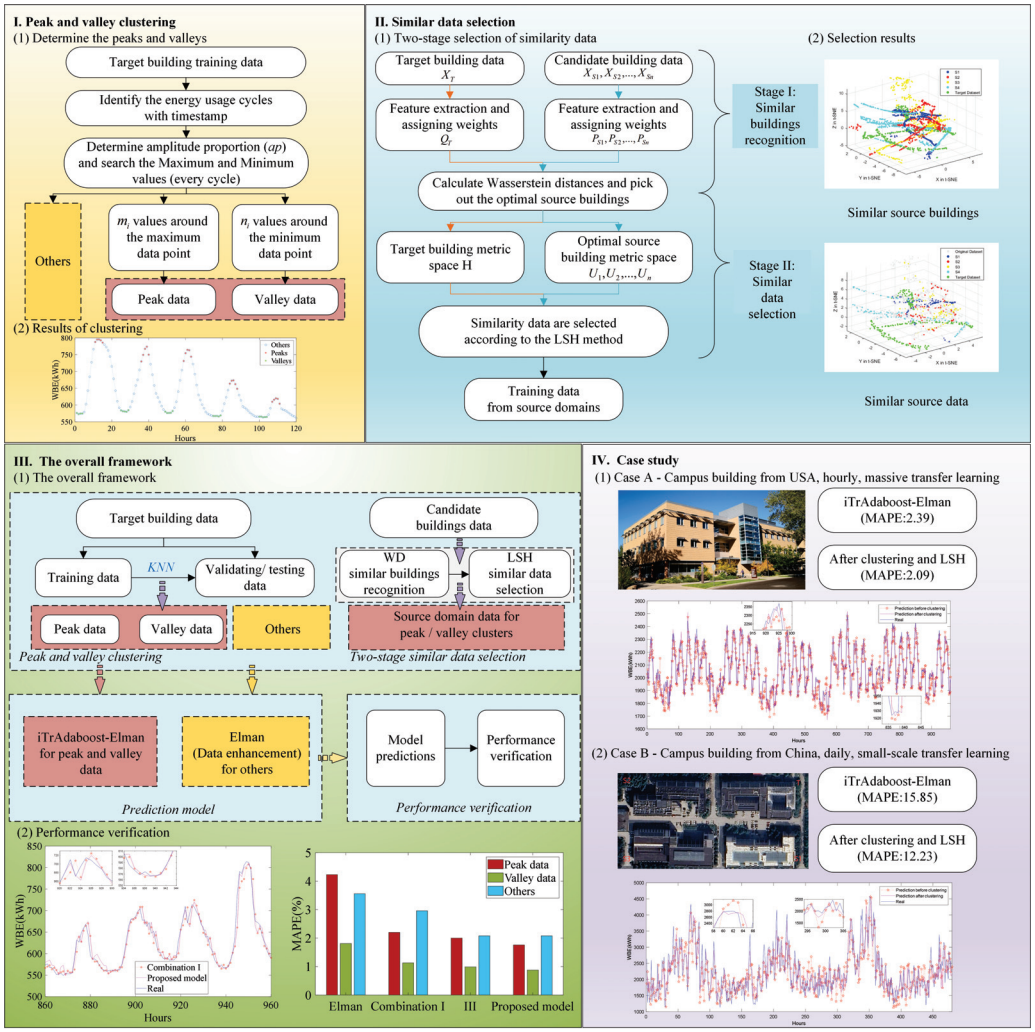


Figure 3. General framework of the study.

3. Case Studies

In this section, the performance of proposed method is first validated on a public dataset. Then, hourly/daily power loads from two real campus buildings in the USA and China will be used for prediction experiments. To objectively assess the performance, three commonly used indicators—mean absolute error (MAE), mean absolute percentage error (MAPE), and root mean square error (RMSE)—are calculated for this study. The mathematical formulas are provided as follows:

$$\mathrm{MAE} = \frac{\sum_{i=1}^{n} \left| Y_i - \hat{Y}_i \right|}{n}, \tag{5}$$

$$\text{MAPE} = \frac{1}{n}\sum_{i=1}^{n}\frac{\left|Y_i - \hat{Y}_i\right|}{Y_i}, \tag{6}$$

$$\text{RMSE} = \sqrt{\frac{\sum_{i=1}^{n}\left(Y_i - \hat{Y}_i\right)^2}{n}}, \tag{7}$$

where n is the data amount, Y_i is the measured data value, and $\hat{Y}_i$ is the predicted data value.

All calculations in this study were completed in MATLAB-R2023b software (Intel(R) Xeon(R) Gold 5222 CPU, 3.80 GHz, and 32 GB RAM). All figures and tables were output and sorted out by MATLAB software. Data processing methods and some parameters are set according to Section 2.

3.1. Benchmark Case

The dataset of this benchmark case is derived from the Great Energy Predictor III competition organized by ASHRAE [41]. The performance validation and model comparison are based on this case because of its good data integrity and openness.

3.1.1. Description of Target and Source Domain Buildings

(1) Target domain building

In the public dataset, we randomly select an academic building as the target building. The basic information about the building is provided in Table 2. The original features related to the energy usage include: air temperature (T_air), sea level pressure (S_p), time sine (sh), time cosine (ch), dew temperature (T_dew), holiday flag (H_flag), previous hourly loads ($y-1$), and previous two-hourly loads ($y-2$).

Correlation analysis is employed to screen the key features, and those with low correlation to the actual energy consumption values are removed. Figure 4 shows the Pearson correlation coefficient results, where WBE is the whole building electricity load. After feature selection, S_p and sh are eliminated and the other six features are retained.

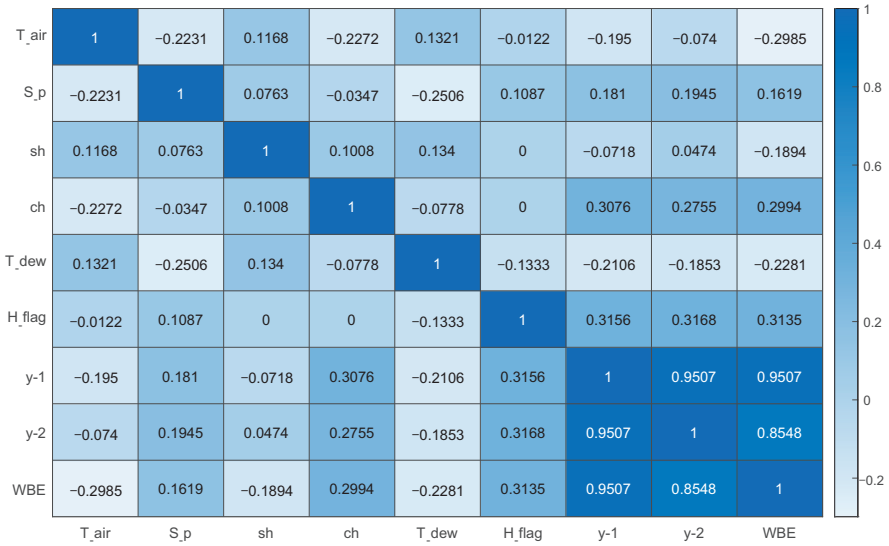


Figure 4. Results of Pearson correlation analysis, benchmark case.

A total of 1200 sets of hourly data since January 2016 are chosen for model construction. The dataset is divided into three parts (training, validation, and testing) with the ratio of 1:1:8. To simulate the data scarcity scenario, only the first 120 hours' data are for model training, and the remaining 1080 hours' data are for model validation and performance

testing. The time series of the target building's energy loads and corresponding data division are shown in Figure 5.

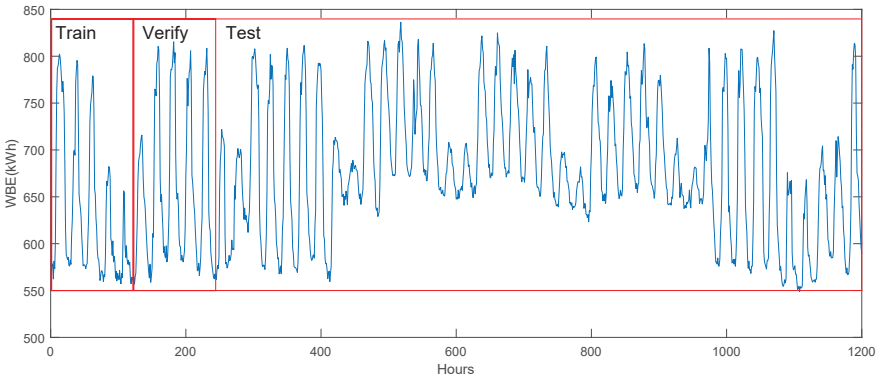


Figure 5. Hourly electrical loads' time series from target building, benchmark case.

(2) Source domain buildings

For this case study, the remaining 1000+ buildings in the public dataset form a candidate building pool for similar building selection. By calculating the WD value between each building in the candidate pool and the target building (only using training data), four buildings with the highest degrees of similarity (minimum WDs) are finally picked out (denoted as S1, S2, S3, and S4). Calculating the WD value between buildings in the public dataset, which has a storage size of about 1 GB, typically takes no more than half an hour. Table 2 lists the relevant information of similar buildings sorted by WD.

Table 2. Relevant information of similar buildings (sorted by WD), benchmark case.

Building No.	WD	Building Type	Square Feet	Air Temperature (°C)	Sea Level Pressure
Target	-	Education	182,943	0–38.3	987.3 –1035.9
S1(#1092)	1006.48	Office	105,167	−26.1–37.8	987.2–1046.5
S2(#1289)	1009.99	Education	194,441	−17.2–35.6	982.6–1043.4
S3(#780)	1011.23	Education	120,836	−16.1–36.7	986.8–1042.7
S4(#192)	1011.57	Education	151,637	2.2–48.3	996.1–1032.2
S5(#1328)	1014.73	Education	279,840	−28.8–11.8	983.6–1036.6
S1447(#803)	5093.44	Education	182,986	−28.8–33.9	983.6–1043.8
S1448(#794)	5151.56	Education	731,945	−28.8–33.9	983.6–1043.8
S1449(#801)	5326.67	Education	484,376	−28.8–33.9	983.6–1043.8

3.1.2. Data Clustering of Target Domain

Since hourly data have a strong 24-hour periodicity, a moving average filtering process on the training set is performed to prevent probable outliers from affecting the judgment of peak loads. Then, based on the data clustering method mentioned in Section 2.2, the training data from target domain is divided into three clusters: "peak", "valley", and "others". The amplitude proportion is set to 15%. The clustered result on the training set from the target domain is shown in Figure 6. The validating and testing sets are classified using KNN method based on the clustered features. The KNN classification is based on the procedure described in Section 2.2.

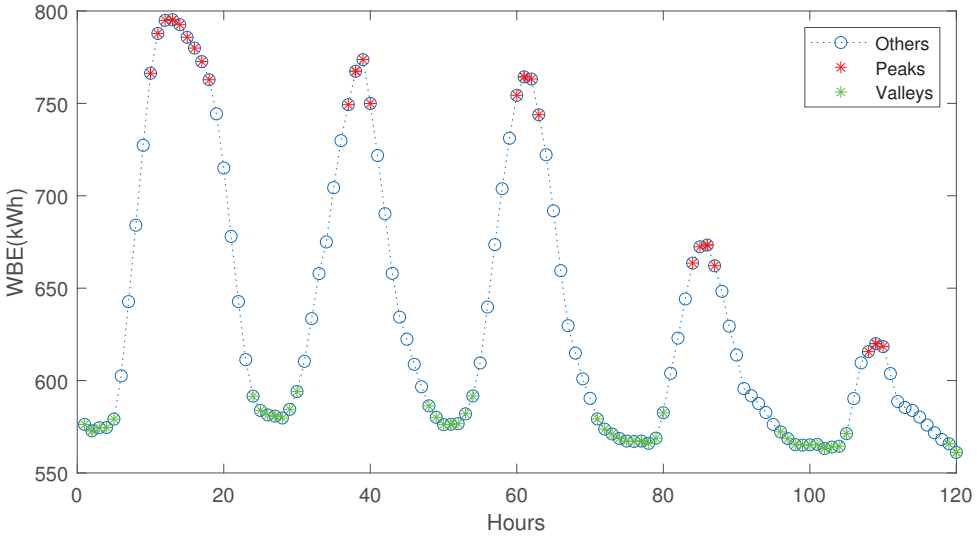


Figure 6. The clustered result of 120 hours' training data from target domain, benchmark case.

3.1.3. Data Selection from Similar Buildings

To enhance the target prediction's accuracy, only peak/valley clusters containing insufficient samples are supplemented with data from the source domains. The IBTL algorithm is carried out for these two clusters' prediction. From four similar buildings selected by the WD metric, similar data are chosen by the LSH method. A total of 523 sets of hourly data from these four source domains is retained and used for knowledge transfer learning. To show the high dimensional features more directly, the t-SNE algorithm is used to reduce the feature dimension, and the effect of similar data selection by LSH is shown in Figure 7.

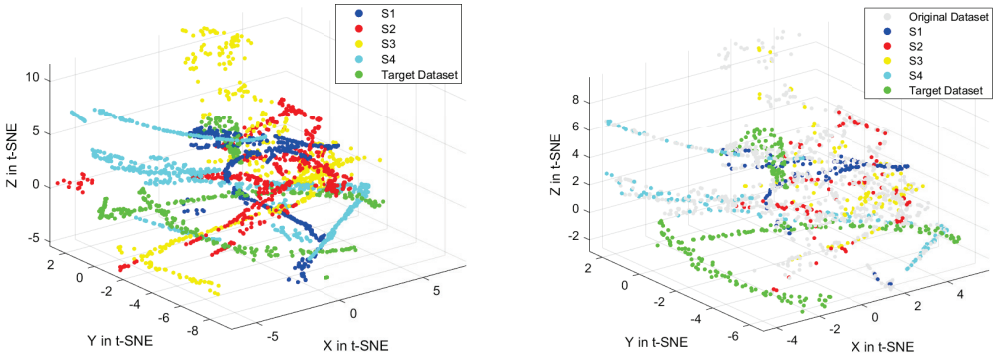


Figure 7. Effect of similar data selection by LSH (left: before LSH, right: after LSH), T-SNE, benchmark case.

3.1.4. Prediction Results

Base on the prediction strategy presented above, 120 hours' training data are clustered into three categories. Among them, "peak/valley" clusters carry out the proposed instance-based transfer learning model (iTrAdaboost-Elman). Considering that the "others" cluster has a strong cyclical trend, the data of this cluster are supplemented with Gaussian noise instead of knowledge transfer from a similar building, and the Elman network is used for this cluster's load prediction.

For performance investigation, 80% of the total data (960 hours' data) are used for model testing. The predicted loads are recorded in Figure 8. The fitted scatter validation results are recorded in Figure 9. Quantitative results show that, with only 120 hours'

training data, the MAE of the proposed model reaches 13.68 kWh (MAPE: 1.96%, RMSE: 19.31 kWh). The basic data-driven model Elman network and transfer learning iTrAdaboost-Elman model are also realized without data clustering. Compared with these two models, the MAE of the proposed model is reduced by 49.2% (Elman) and 25.6% (iTrAdaboost-Elman), respectively. The detailed results of the three models are all recorded in Table 3.

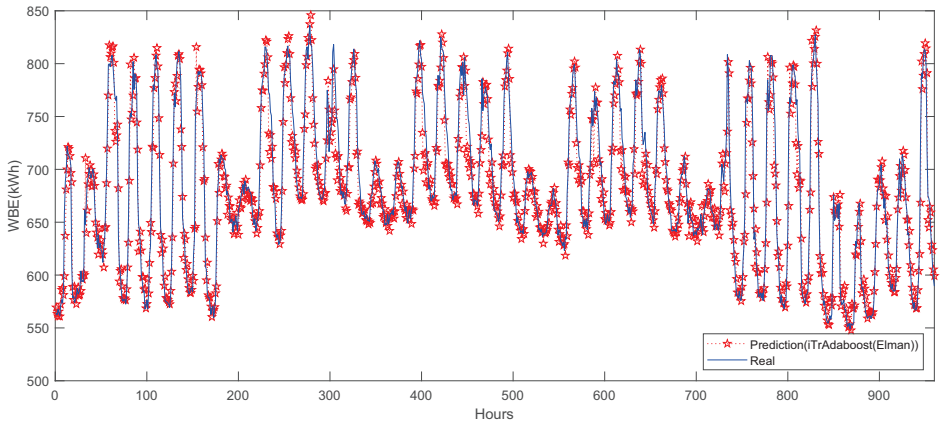


Figure 8. Prediction results of the proposed model, benchmark case.

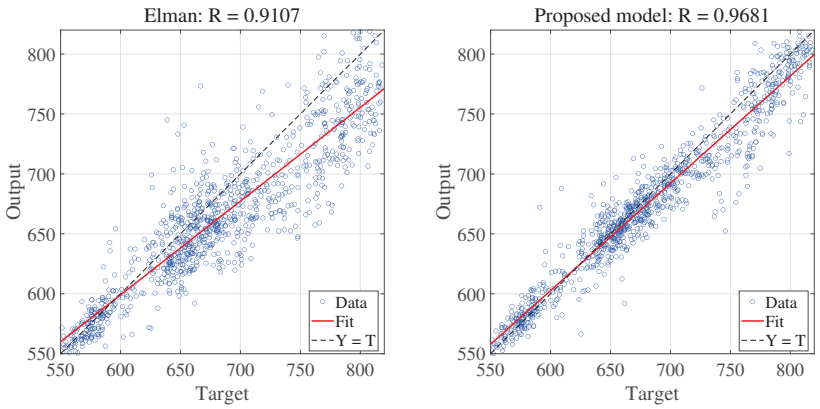


Figure 9. Fitted scatter validation plots of predictions (left: Elman, right: proposed model), benchmark case.

Table 3. Performance comparison with proposed model and Elman/iTrAdaboost-Elman, benchmark case.

Model	Transfer Learning	Data Clustering	MAE (kWh)	MAPE (%)	RMSE (kWh)
Elman	No	No	26.94	3.80	35.17
iTrAdaboost-Elman	Yes	No	18.39	2.63	24.31
Proposed model	Yes	Yes	13.68	1.96	19.31

3.1.5. Discussion and Analysis

To investigate the performance of the proposed model, a brief discussion is presented for the following four aspects:

(1) The combination effect of data clustering and transfer learning

To compare the combination effect, three different combinations of data clustering and transfer learning strategy are carried out as follows: (I) Transfer learning strategy (iTrAdaboost-Elman) is applied on all data without clustering; (II) Transfer learning strategy is applied on all data after data clustering; (III) Transfer learning strategy is only applied

on clusters of "Peak"/"Valley". The cluster of "Others" with a strong cyclical trend does not use training data from other buildings, and the traditional Elman model is applied. To show the effect of LSH data selection, the above three compared models do not use LSH-based similar data selection, and all data from similar buildings constitute the entire source domain dataset. The prediction results are compared with that of proposed model with LSH.

Results are all recorded in Figure 10 and Table 4. It is seen that: (1) Comparing results from Combination II and I, data clustering could enhance the transfer learning effect, and the whole prediction accuracy is improved (2.63 vs. 2.50, MAPE); (2) Comparing results from Combination III and II, the transfer learning strategy for peak/valley data is a more targeted and efficient prediction method, and the prediction accuracy is further improved to 2.05 (MAPE); (3) Comparing results from Combination III and I, the peak data after clustering (without LSH) can be better predicted (2.63 vs. 2.05, MAPE); (4) Using LSH-based similar data selection, the proposed model achieves the best prediction accuracy: 1.96 (MAPE).

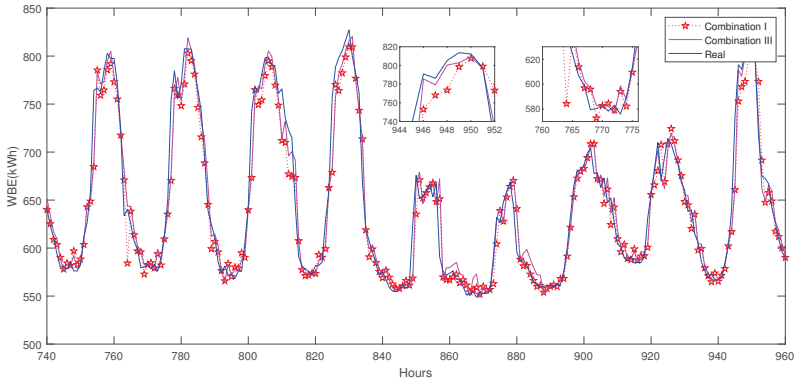


Figure 10. Prediction results before and after data clustering, iTrAdaboost-Elman, benchmark case.

Table 4. Prediction results for three combinations of data clustering and transfer learning (MAPE, %), benchmark case.

Transfer Learning	Data Clustering	LSH	"Peak" Data	"Valley" Data	"Others" Data	Integrated
I. All data	No	No	2.22	1.59	3.40	2.63
II. All clusters	Yes	No	2.10	1.43	3.26	2.50
III. Clusters of Peak/Valley	Yes	No	2.10	1.43	2.29	2.05
Proposed model	Yes	Yes	1.91	1.30	2.29	1.96

(2) The influence of KNN classification on the overall prediction accuracy

As we have mentioned, the realtime sampled data for model testing could not be clustered by the same method as historical data for training. The KNN method is used for these data, which would inevitably introduce the classification error to some extent. To analyze the influence of KNN classification on the overall prediction accuracy, three different values of KNN key parameter K are set, and their classification results are compared with that of the timestamp/extreme search method. Results are recorded in Table 5. It is seen that, supposing the testing data is sampled real-time in practice, the KNN method will result in a classification error around 27%. The prediction accuracy for peak/valley clusters tend to decrease compared with that of timestamp/extreme search method, but the impact on the overall prediction accuracy is not significant. When K is set to 5, the prediction accuracy achieves the best score (1.96%, MAPE), which is almost the same as that of timestamp classification (1.95%).

Table 5. Comparison of KNN classifications on the overall prediction accuracy, benchmark case.

Classification Method	Classification Accuracy (%)	Amounts of Clustered Data	Prediction Accuracy (MAPE, %) "Peak"	"Valley"	"Others"	Overall
Timestamp	100.0	226/243/491	1.63	1.13	2.50	1.95
KNN (K = 4)	71.9	349/172/439	2.02	1.40	2.34	2.06
KNN (K = 5)	74.2	317/198/445	1.96	1.30	2.29	1.96
KNN (K = 6)	72.8	347/181/432	2.02	1.37	2.32	2.03

(3) The influence of LSH data selection on the overall prediction accuracy

As Table 4 shows, the LSH similar data selection could enhance transfer learning-based prediction accuracy. The value of similarity threshold σ in LSH determines the amount of selected data for "Peak" and "Valley" source domains' construction, and its influence on the prediction accuracy is investigated here. Four feasible values of similarity threshold σ are set in LSH, and other model parameters remained consistent. The prediction results are compared in Table 6. As the similarity threshold changes from 0.3 to 0.45, the amount of selected data gradually decreases from 2024 to 183, and the calculation time also decreases accordingly from 120.9 s to 82.7 s (10 times average). The prediction accuracy does not exhibit a similar monotonic decrease. When σ is set to 0.4, 523 sets of similar data are selected and the predictive model achieves optimal accuracy (1.96%, MAPE).

Table 6. Comparison of different similarity threshold σ on overall prediction accuracy, benchmark case.

LSH Usage	Value of Threshold (σ)	Amount of Selected Data	MAE (kWh)	MAPE (%)	RMSE (kWh)	Time (s)
No	–	–	18.39	2.63	24.31	79.5
Yes	0.30	2024	14.00	2.01	19.48	120.9
Yes	0.35	1701	14.10	2.02	19.50	110.5
Yes	0.40	523	13.68	1.96	19.31	87.0
Yes	0.45	183	14.30	2.06	19.65	82.7

(4) Performance comparison with other reported models

Through the benchmark dataset, the previously reported data-driven models, including BP [42], ELM [43], RF [44], RBF [45], and LSTM [46], are also constructed for performance comparison. The parameter setting is consistent with the references. The average results of twenty runs per model are recorded in Table 7. Compared with these traditional data-driven models, the Elman model achieves the best prediction performance on the dataset, which is the reason why Elman is chosen as the sub-learners in the proposed transfer learning strategy.

Further, two previously reported transfer learning methods without data clustering are built according to the literature [14,30]. The model parameters are consistent with those in the literature, and the average results of twenty runs per model are recorded. The results are compared with the proposed strategy in Table 7. It is seen the proposed model reaches the best accuracy (1.96%, MAPE). From the respective of model complexity and time consumption, although the transfer learning models consume more time than traditional models, the prediction time of the proposed model is less than 100 s, which is acceptable for hourly load prediction.

Table 7. Performance comparison between the proposed model and the previous models, benchmark case.

Model	MAE (kWh)	MAPE (%)	RMSE (kWh)	Time (s)
Elman	26.94	3.80	35.17	1.72
BP [42]	32.11	4.71	40.70	1.25
ELM [43]	34.30	5.01	45.07	1.13
RF [44]	27.64	4.03	35.13	1.17
RBF [45]	27.39	3.97	37.51	19.12
LSTM [46]	32.13	4.68	40.43	16.78
MMD-iTrAdaboost-BP [14]	18.83	2.71	25.05	79.5
NNS-iTrAdaboost-LSTM [30]	17.81	2.56	23.00	436.7
Proposed model	13.68	1.96	19.31	87.0

3.2. Campus Building Case A

3.2.1. Description of Target Building Data

To verify the adaptivity and robustness of the model, a real campus building from University of Wyoming, USA, is selected. It has three floors, about 6000 square meters in total. Only 1200 hourly data from September to October, 2017 are picked from the Information Technology Center Building. All weather and power load data come from local sensing/metering devices. The data division for training/validating/testing is consistent with that of benchmark case (1:1:8), i.e., only the first 120 hours' data are considered as known historical data for training. Figure 11 shows the outside of the target building.

For the target building, the original data features include eight variables: outdoor dry-bulb temperature (T), the previous hourly temperature ($T-1$), the previous two hours ($T-2$), holiday-flag, time-sine (sh), time-cosine (ch), the energy consumption of the previous 1 hour ($y-1$), and the energy consumption of the previous 2 hours ($y-2$). By the Pearson's correlation coefficient analysis, time-sine (sh) is eliminated, and seven features are retained as model input features. The data clustering is carried out based on Section 2.2. For the training set, three data classes of peak/valley/others are clustered according to timestamp and extreme search. For the validating and testing sets, the KNN method is used for corresponding data's classification.



Figure 11. Outside of Information Technology Center building, University of Wyoming.

3.2.2. Two-Stage Selection of Source Domain Data

In this case, the same public dataset as the benchmark case is used as the candidate building pool for similar building selection. The WD metrics of more than 1000 buildings

are calculated, and the four similar buildings with minimum WD values are selected. Table 8 lists the relevant information about target and similar buildings.

Further, similar data from the source domain buildings are selected by the LSH method. According to the method described in Section 2.3.2, only peak/valley data from source domains are identified and picked by LSH. A total of 1338 sets of hourly data are selected and transferred to enhance the peak/valley clusters for target model training.

Table 8. Relevant information of similar buildings, case A.

Building No.	WD	Building Type	Square Feet	Air Temperature (° C)	Sea Level Pressure
S1 (#375)	1040.18	Office	850,354	−10.6–37.8	991.5–1040.9
S2 (#223)	1121.81	Education	261,188	2.2–47.2	999.3–1028.2
S3 (#365)	1181.60	Healthcare	819,577	−10.6–37.8	991.5–1040.9
S4 (#645)	1220.96	Education	304,333	1.1–35.0	999.8–1031.7

3.2.3. Results

According to the proposed method, the peak/valley clustered data are predicted by the transfer learning iTrAdaboost-Elman model, and the other clustered data are predicted by the Elman network without transfer leaning. The prediction errors on 960-hour testing data reach 42.95 kWh (MAE), 2.09% (MAPE), and 60.79 kWh (RMSE).

To validate the data clustering effect, three combinations of data clustering and transfer learning are compared as the benchmark case in Section 3.1.4. Results are recorded in Table 9. It is seen that compared with Combination I, Combination II's data clustering could improve prediction accuracy from 2.73 to 2.39 (MAPE). More efficiently, the transfer learning strategy only for peak/valley data (Combination III) achieves better accuracy: 2.14 (MAPE). Compared with all three combinations, the proposed model with LSH similar data selection reaches the best prediction accuracy: 2.09 (MAPE). It is demonstrated that by clustering the target domain data, we can distinguish the peak/valley data that need data enhancement by transfer learning. Targeted knowledge transfer only for these data can efficiently achieve higher prediction accuracy. To indicate performance improvement by different prediction models, Figure 12 extracts load prediction curves of the last 100 hours for comparison. Figure 13 shows the whole 960 hours' prediction results with and without the proposed data clustering method.

Table 9. Comparison of prediction load results, iTrAdaboost-Elman, case A.

Transfer Learning	Data Clustering	LSH	MAE (kWh)	MAPE (%)	RMSE (kWh)
I. All data	No	No	56.60	2.73	77.02
II. All clusters	Yes	No	49.29	2.39	67.70
III. Clusters of Peak/Valley	Yes	No	44.32	2.14	62.22
Proposed model	Yes	Yes	42.95	2.09	60.79

3.3. Campus Building Case B

3.3.1. Description of Target and Source Buildings

Different from case A, a campus building's daily energy usage data in China is selected for model validation. In benchmark case and case A, a public dataset from ASHRAE that contains more than 1000 buildings is treated as a candidate building pool for similar building selection. In order to prevent excessive differences in building datasets due to different regions, populations, and operation modes, other buildings in the local building group are used for small-scale knowledge transfer in this case study. Compared to hourly

data, the daily data have less regularity in peak and valley cycles, and the effectiveness of data clustering is investigated through this case.

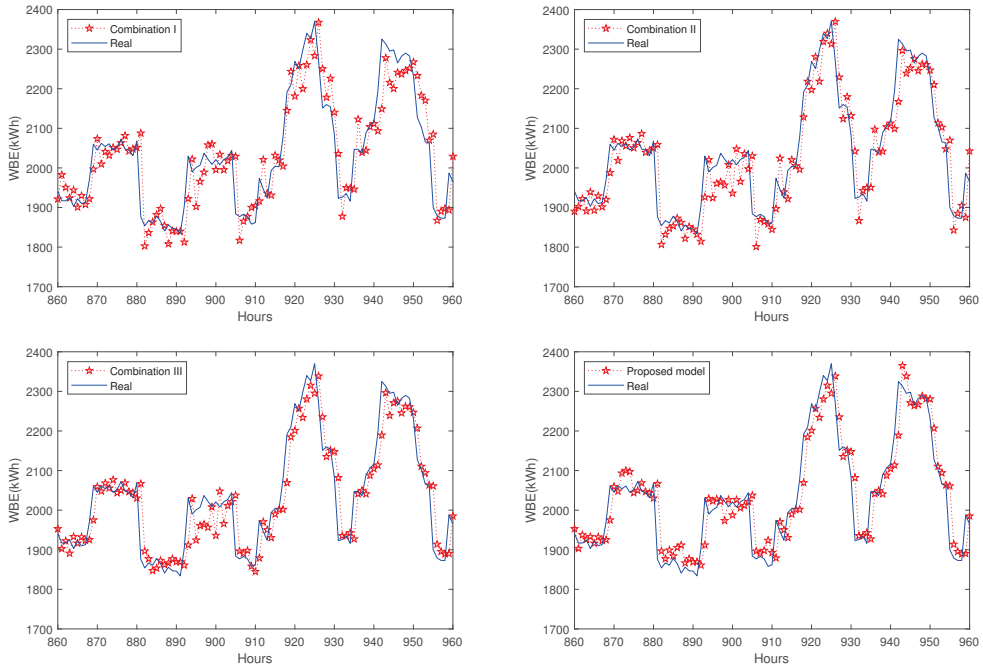


Figure 12. Comparison of prediction results for the proposed model and three combinations, iTrAdaboost-Elman, case A.

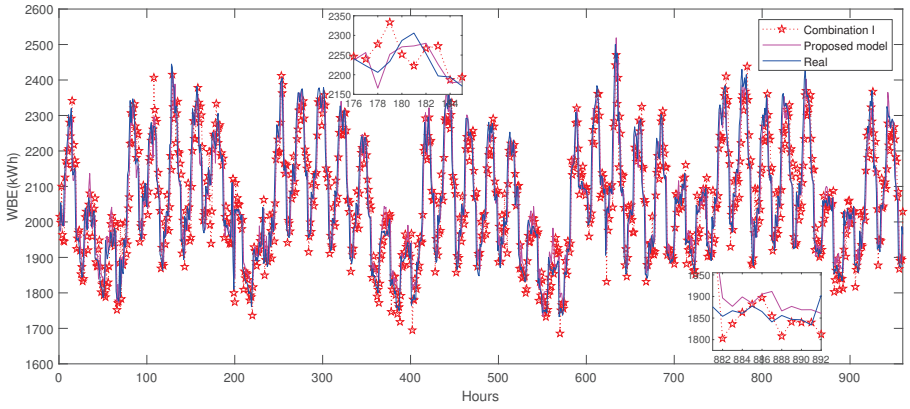


Figure 13. Prediction results with and without the proposed data clustering method, iTrAdaboost-Elman, case A.

The building of Electrical Information Engineering (EIE) at Jiangsu University, China, is selected as the target building. It has five floors, approximately 10,000 square meters in total. The other three buildings in the building group are selected as candidate source buildings (S1–S3). The top view of the building group and the outside of target building are both shown in Figure 14.

The electrical loads come from the database of the Energy Center of Jiangsu University, and the relevant meteorological data are collected from the website (WheatA V1.5.7j platform). The target building selects 600 days of data from 2018 to 2019 for model construction, and the division ratio of training/validating/testing is 1:1:8 by time series. The time series of the target building's energy loads and corresponding data division are shown in Figure 15. For candidate source buildings, 987 sets of daily data per building from January 2016 to October 2018 are selected. Considering the sensing and recording errors from the

field equipment, extra data preprocessing for data outliers and missing values is applied using the interquartile range (IQR) method.

The original input features for data-driven modeling include: mean air temperature, dew point temperature, total cloudiness, holiday flag, sea level pressure, humidity, $y-1$, and $y-2$. After feature selection by Pearson's method, the dew point temperature is eliminated and the other seven features are selected as model inputs.

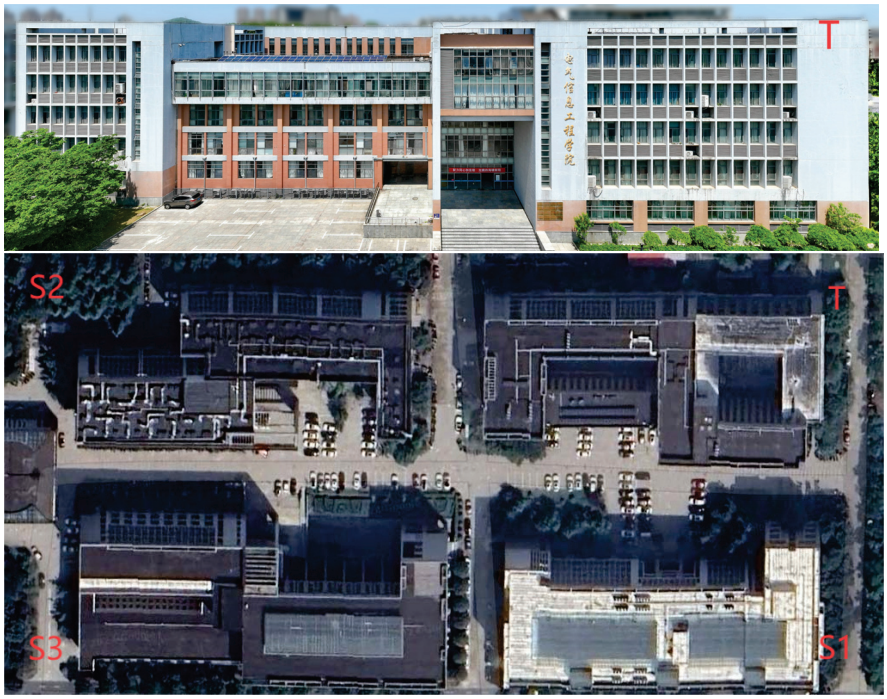


Figure 14. The outside of target building and the top view of the building group, Jiangsu University.

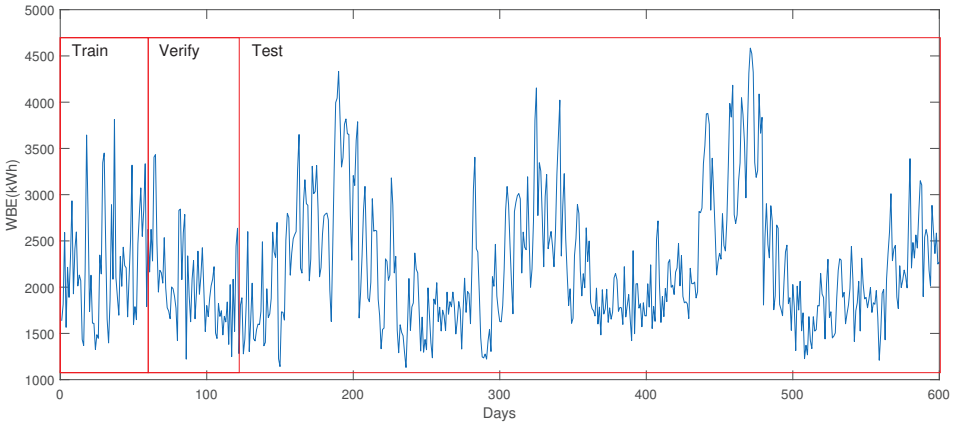


Figure 15. Daily electrical loads' time series from target building, case B.

3.3.2. Data Clustering for Target Domain and Data Selection from Similar Building

Different from hourly data clustering in the previous case studies, since the regularity of the daily data is not as pronounced as the hourly data, the way of extreme values searching is changed. For the training dataset, according to the energy consumption mode of the campus buildings, the non-working days (weekend) are determined as the energy usage's valley days, and the day with the most energy consumption is searched as the peak day in a weekly cycle. The one day before and after the peak day are also clustered into peak days together. The data in the validating and testing set are also classified by the KNN method.

For similar building selection, WD metrics are calculated to determine the similarity of the other three candidate buildings in the same group. Results show that the target building has the least distance from the S1 building, whereas the WDs with the other two buildings (S2, S3) are large. Therefore, the S1 building is selected as the source domain building, and, by the LSH method, 277 sets of daily data are picked from S1 as similar data for transfer learning.

3.3.3. Results

After the peak/valley data clustering and transfer learning, the daily electrical load prediction of the target building is performed. To investigate the effect of the proposed method on daily prediction, three different models' results are recorded in Table 10. The Elman model without data clustering and transfer learning has the worst accuracy (MAE: 489.16 kWh, MAPE: 21.94%, RMSE: 646.66 kWh). The proposed transfer learning model with data clustering still achieves the best accuracy (MAE: 254.60 kWh, MAPE: 12.23%, RMSE: 326.04 kWh). Figure 16 compares the effect of prediction results with and without data clustering.

Table 10. Comparison of prediction before and after data clustering, Elman/iTrAdaboost-Elman.

Model	Clustering	MAE (kWh)	MAPE (%)	RMSE (kWh)
Elman	No	489.16	21.94	646.66
iTrAdaboost-Elman	No	343.12	15.85	433.51
Proposed model	Yes	254.60	12.23	326.04

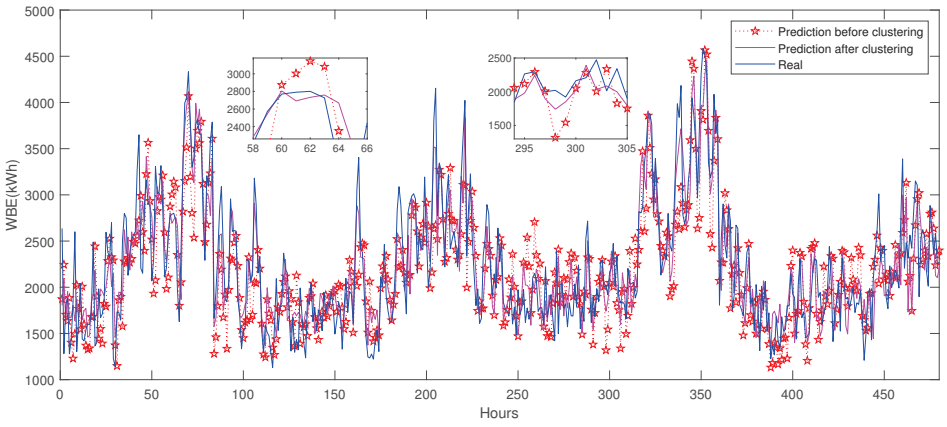


Figure 16. Prediction results with and without data clustering, iTrAdaboost-Elman, case B.

4. Conclusions

In this study, a clustering-based transfer learning method was proposed to address the problem of insufficient sampling of peak/valley data that affects short-term electrical load prediction performance. Through peak/valley data clustering from target domain and two-stage similar data selection from multi-source domains, the proposed transfer learning iTrAdaboost-Elman model for peak/valley data was built. Three case studies were provided for performance validation. In the benchmark case (public dataset), using only 120 hours' training data, the proposed model reached a prediction accuracy of 1.96% (MAPE) that was much better than the Elman model (3.80%) and the iTrAdaboost-Elman model without data clustering (2.63%). The effects of data clustering and LSH similar data selection were both investigated. Two other real campus building cases from the USA and China (Case A and B) were then studied to verify the adaptivity and robustness of the model. For different predictive time scales (hourly and daily) and knowledge transfer

scopes, the proposed method also had an accuracy advantage compared with other models. Especially for Case B of daily electrical load prediction, in which the energy usage pattern changed and only four buildings were used for similar domain selection, the proposed method still achieved better accuracy than the Elman model (12.23% vs. 21.94%, MAPE) and the iTrAdaboost-Elman model without data clustering (15.85%). For short-term building electrical load forecasting tasks with insufficient data for model training, the proposed method proved superior performance and thus had great application potential in the building energy management system. It should be noted that for proper data clustering, the energy usage cycle must be identifiable. Otherwise, the proposed timestamp and extreme search method would not be effective. Sensitivity analysis of model performance on different time scales and building types will be the next step of our research.

Author Contributions: All authors contributed to the study conception and design. Data analysis and modeling simulations were done by S.Z. Calibration of the simulation results was done by K.L., and the first draft of the manuscript was written by K.L. and S.Z. Data and literature collection was done by M.Z. and B.W. All authors have read and agreed to the published version of the manuscript.

Funding: This work was supported by "Six Talents Peak" High-level Talents Program of Jiangsu Province (Grant No. JZ-053).

Data Availability Statement: All data are available per request.

Acknowledgments: The authors would like to thank the staff of the University of Wyoming Information Technology Center and Jiangsu University for providing energy consumption data.

Conflicts of Interest: The authors declare that they have no known competing financial interests or personal relationships that could have appeared to influence the work reported in this paper.

Abbreviations

AdaBoost	adaptive boosting
ap	amplitude proportion
ASHRAE	American Society of Heating Refrigerating and Air-conditioning Engineers
BP	back propagation neural network
DTW	dynamic time warping
ELM	extreme learning machine
FCM	fuzzy C-mean
Elman	Elman recurrent neural network
iTrAdaBoost	improved transfer adaptive boosting algorithm
IBTL	instance-based transfer learning
KNN	K-nearest neighbors
LSH	locality sensitive hashing
LSTM	long short-term memory
MBTL	model-based transfer learning
MMD	maximum mean discrepancy
MIC	maximum information coefficient
MAE	mean absolute error
MAPE	mean absolute percentage error
MK-MMD	multi-core maximum mean discrepancy
NNS	nearest neighbor search
RBF	radial basis function
RF	random forest

RMSE	root mean square error
T-SNE	t-distributed stochastic neighbor embedding
WD	Wasserstein distance
Γ	label space
M	the set number of building data
N	the feature number of each set
W_p	p-Wasserstein distance
β_t	weighting update factor
γ	threshold
χ	domain feature space

References

1. Dechamps, P. The IEA World Energy Outlook 2022—A brief analysis and implications. *Eur. Energy Clim. J.* **2023**, *11*, 100–103. [CrossRef]
2. Al-Rakhami, M.; Gumaei, A.; Alsanad, A.; Alamri, A.; Hassan, M.M. An ensemble learning approach for accurate energy load prediction in residential buildings. *IEEE Access* **2019**, *7*, 48328–48338. [CrossRef]
3. Chen, Z.; Chen, Y.; Xiao, T.; Wang, H.; Hou, P. A novel short-term load forecasting framework based on time-series clustering and early classification algorithm. *Energy Build.* **2021**, *251*, 111375. [CrossRef]
4. Li, K.; Tian, J.; Xue, W.; Tan, G. Short-term electricity consumption prediction for buildings using data-driven swarm intelligence based ensemble model. *Energy Build.* **2021**, *231*, 110558. [CrossRef]
5. Filgueiras, D.B.; Coelho da Silva, F.L. A study on the prediction of electricity consumption considering the energy efficiency measures—Applied in case of the Brazilian public sector. *Energy Effic.* **2023**, *16*, 94. [CrossRef]
6. Zhou, X.; Sun, J.; Tian, Y.; Lu, B.; Hang, Y.; Chen, Q. Hyperspectral technique combined with deep learning algorithm for detection of compound heavy metals in lettuce—ScienceDirect. *Food Chem.* **2020**, *321*, 126503. [CrossRef]
7. Pavlatos, C.; Makris, E.; Fotis, G.; Vita, V.; Mladenov, V. Enhancing Electrical Load Prediction Using a Bidirectional LSTM Neural Network. *Electronics* **2023**, *12*, 4652. [CrossRef]
8. Chen, C.; Zhu, W.; Steibel, J.; Siegford, J.; Norton, T.J. Classification of drinking and drinker-playing in pigs by a video-based deep learning method. *Biosyst. Eng.* **2020**, *196*, 1. [CrossRef]
9. Liu, J.; Abbas, I.; Noor, R.S. Development of Deep Learning-Based Variable Rate Agrochemical Spraying System for Targeted Weeds Control in Strawberry Crop. *Agronomy* **2021**, *11*, 1480. [CrossRef]
10. Smola, A.J.; Gretton, A.; Borgwardt, K. Maximum mean discrepancy. In Proceedings of the 13th International Conference, ICONIP, Hong Kong, China, 3–6 October 2006; pp. 3–6.
11. Panaretos, V.M.; Zemel, Y. Statistical aspects of Wasserstein distances. *Annu. Rev. Stat. Appl.* **2019**, *6*, 405–431. [CrossRef]
12. Kinney, J.B.; Atwal, G.S. Equitability, mutual information, and the maximal information coefficient. *Proc. Natl. Acad. Sci. USA* **2014**, *111*, 3354–3359. [CrossRef] [PubMed]
13. Borgwardt, K.M.; Gretton, A.; Rasch, M.J.; Kriegel, H.P.; Schölkopf, B.; Smola, A.J. Integrating structured biological data by kernel maximum mean discrepancy. *Bioinformatics* **2006**, *22*, e49–e57. [CrossRef] [PubMed]
14. Li, K.; Wei, B.; Tang, Q.; Liu, Y. A data-efficient building electricity load forecasting method based on maximum mean discrepancy and improved TrAdaBoost algorithm. *Energies* **2022**, *15*, 8780. [CrossRef]
15. Lu, Y.; Wang, G.; Huang, S. A short-term load forecasting model based on mixup and transfer learning. *Electr. Power Syst. Res.* **2022**, *207*, 107837. [CrossRef]
16. Wei, N.; Yin, C.; Yin, L.; Tan, J.; Liu, J.; Wang, S.; Qiao, W.; Zeng, F. Short-term load forecasting based on WM algorithm and transfer learning model. *Appl. Energy* **2024**, *353*, 122087. [CrossRef]
17. Yuan, Y.; Chen, Z.; Wang, Z.; Sun, Y.; Chen, Y. Attention mechanism-based transfer learning model for day-ahead energy demand forecasting of shopping mall buildings. *Energy* **2023**, *270*, 126878. [CrossRef]
18. Tian, Y.; Sehovac, L.; Grolinger, K. Similarity-based chained transfer learning for energy forecasting with big data. *IEEE Access* **2019**, *7*, 139895–139908. [CrossRef]
19. Li, Y.; Bao, T.; Chen, H.; Zhang, K.; Shu, X.; Chen, Z.; Hu, Y. A large-scale sensor missing data imputation framework for dams using deep learning and transfer learning strategy. *Measurement* **2021**, *178*, 109377. [CrossRef]
20. Gao, N.; Shao, W.; Rahaman, M.S.; Zhai, J.; David, K.; Salim, F.D. Transfer learning for thermal comfort prediction in multiple cities. *Build. Environ.* **2021**, *195*, 107725. [CrossRef]
21. Li, A.; Xiao, F.; Fan, C.; Hu, M. Development of an ANN-based building energy model for information-poor buildings using transfer learning. *Build. Simul.* **2020**, *14*, 1–13. [CrossRef]

22. Pardamean, B.; Muljo, H.H.; Cenggoro, T.W.; Chandra, B.J.; Rahutomo, R. Using transfer learning for smart building management system. *J. Big Data* **2019**, *6*, 1–12. [CrossRef]
23. Gao, Y.; Ruan, Y.; Fang, C.; Yin, S. Deep learning and transfer learning models of energy consumption forecasting for a building with poor information data. *Energy Build.* **2020**, *223*, 110156. [CrossRef]
24. Pinto, G.; Wang, Z.; Roy, A.; Hong, T.; Capozzoli, A. Transfer learning for smart buildings: A critical review of algorithms, applications, and future perspectives. *Adv. Appl. Energy* **2022**, *5*, 100084. [CrossRef]
25. Zeng, P.; Sheng, C.; Jin, M. A learning framework based on weighted knowledge transfer for holiday load forecasting. *J. Mod. Power Syst. Clean Energy* **2019**, *7*, 329–339. [CrossRef]
26. Li, G.; Wu, Y.; Liu, J.; Fang, X.; Wang, Z. Performance evaluation of short-term cross-building energy predictions using deep transfer learning strategies. *Energy Build.* **2022**, *275*, 112461. [CrossRef]
27. Li, Z.; Liu, B.; Xiao, Y. Cluster and dynamic-TrAdaBoost-based transfer learning for text classification. In Proceeding of the 13th International Conference on Natural Computation, Fuzzy Systems and Knowledge Discovery (ICNC-FSKD), Guilin, China, 29–31 July 2017; IEEE: New York, NY, USA, 2017; pp. 2291–2295.
28. Tong, X.; Xu, X.; Huang, S.L.; Zheng, L. A mathematical framework for quantifying transferability in multi-source transfer learning. *Adv. Neural Inf. Process. Syst.* **2021**, *34*, 26103–26116.
29. Lu, H.; Wu, J.; Ruan, Y.; Qian, F.; Meng, H.; Gao, Y.; Xu, T. A multi-source transfer learning model based on LSTM and domain adaptation for building energy prediction. *Int. J. Electr. Power Energy Syst.* **2023**, *149*, 109024. [CrossRef]
30. Wei, B.; Li, K.; Zhou, S.; Xue, W.; Tan, G. An instance based multi-source transfer learning strategy for building's short-term electricity loads prediction under sparse data scenarios. *J. Build. Eng.* **2024**, *85*, 108713. [CrossRef]
31. Qian, F.; Ruan, Y.; Lu, H.; Meng, H.; Xu, T. Enhancing source domain availability through data and feature transfer learning for building power load forecasting. In *Building Simulation*; Springer: Berlin/Heidelberg, Germany, 2024; pp. 1–14.
32. Li, K.; Zhang, J.; Chen, X.; Xue, W. Building's hourly electrical load prediction based on data clustering and ensemble learning strategy. *Energy Build.* **2022**, *261*, 111943. [CrossRef]
33. Wu, X.; Zhou, J.; Wu, B.; Sun, J.; Dai, C. Identification of tea varieties by mid-infrared diffuse reflectance spectroscopy coupled with a possibilistic fuzzy c-means clustering with a fuzzy covariance matrix. *J. Food Process. Eng.* **2019**, *42*, e13298. [CrossRef]
34. Li, L. Combining Transfer Learning and Ensemble Algorithms for Improved Citrus Leaf Disease Classification. *Agriculture* **2024**, *14*, 1549. [CrossRef]
35. Dai, W.; Yang, Q.; Xue, G.R.; Yu, Y. Boosting for transfer learning. In Proceedings of the 24th International Conference on Machine Learning, Corvallis, OR, USA, 20–24 June 2007; pp. 193–200.
36. Elman, J.L. Finding structure in time. *Cogn. Sci.* **1990**, *14*, 179–211. [CrossRef]
37. Shen, T.; Zou, X.; Shi, J.; Li, Z.; Huang, X.; Yiwei, X.; Wu, C. Determination geographical origin and flavonoids content of goji berry using near-infrared spectroscopy and chemometrics. *Food Anal. Methods* **2016**, *9*, 68–79.
38. Che, J.; Wang, J.; Tang, Y. Optimal training subset in a support vector regression electric load forecasting model. *Appl. Soft Comput.* **2012**, *12*, 1523–1531. [CrossRef]
39. Andoni, A.; Indyk, P.; Nguyen, H.L.; Razenshteyn, I. Beyond locality-sensitive hashing. In Proceedings of the Twenty-Fifth Annual ACM-SIAM Symposium on Discrete Algorithms, SIAM, Portland, OR, USA, 5–7 January 2014; pp. 1018–1028.
40. Kalantari, I.; McDonald, G. A data structure and an algorithm for the nearest point problem. *IEEE Trans. Softw. Eng.* **1983**, *5*, 631–634. [CrossRef]
41. Ohlsson, M.B.; Peterson, C.O.; Pi, H.; Rognvaldsson, T.S.; Soderberg, B.P. Predicting System Loads with Artificial Neural Networks—Methods and Results from The Great Energy Predictor Shootout. *Ashrae-Trans. Am. Soc. Heat. Refrig. Airconditioning Engin.* **1994**, *100*, 1063–1074.
42. Huang, D.; He, S.; He, X.; Zhu, X. Prediction of wind loads on high-rise building using a BP neural network combined with POD. *J. Wind. Eng. Ind. Aerodyn.* **2017**, *170*, 1–17.
43. Liu, C.; Sun, B.; Zhang, C.; Li, F. A hybrid prediction model for residential electricity consumption using holt-winters and extreme learning machine. *Appl. Energy* **2020**, *275*, 115383. [CrossRef]
44. Wang, Z.; Wang, Y.; Zeng, R.; Srinivasan, R.S.; Ahrentzen, S. Random Forest based hourly building energy prediction. *Energy Build.* **2018**, *171*, 11–25. [CrossRef]
45. Zhang, A.; Zhang, L. RBF neural networks for the prediction of building interference effects. *Comput. Struct.* **2004**, *82*, 2333–2339. [CrossRef]
46. Zhou, X.; Lin, W.; Kumar, R.; Cui, P.; Ma, Z. A data-driven strategy using long short term memory models and reinforcement learning to predict building electricity consumption. *Appl. Energy* **2022**, *306*, 118078. [CrossRef]

Disclaimer/Publisher's Note: The statements, opinions and data contained in all publications are solely those of the individual author(s) and contributor(s) and not of MDPI and/or the editor(s). MDPI and/or the editor(s) disclaim responsibility for any injury to people or property resulting from any ideas, methods, instructions or products referred to in the content.

energies

MDPI

Article

A Decision-Making Tool for Sustainable Energy Planning and Retrofitting in Danish Communities and Districts

Muhyiddine Jradi

Center for Energy Informatics, The Maersk Mc-Kinney Moller Institute, University of Southern Denmark, Campusvej 55, 5230 Odense, Denmark; mjr@mmmi.sdu.dk

Abstract: This study presents a novel framework for city-level energy planning and retrofitting, tailored to Danish cities and neighborhoods. The framework addresses the challenges of large-scale urban energy modeling by integrating automated processes for data collection, energy demand prediction, and renewable energy integration. It combines open-source simulation tools and validated datasets, enabling efficient and scalable predictions of energy performance across urban areas, including streets, districts, and entire cities, with minimal user input. The key components include data collection and demand modeling, energy resource estimation, performance gap evaluation, and the design of retrofitting strategies with renewable energy integration. The DanCTPlan energy planning tool, developed based on this framework, was applied to two case studies in Denmark: a single street with 101 buildings and a district comprising five streets with 1284 buildings. In the single-street case, retrofitting all buildings to meet current regulations resulted in a 60.8% reduction in heat demand and a 5.8% reduction in electricity demand, with significant decreases in peak energy demands. The district-level retrofitting measures led to a 29.5% reduction in heat demand and a 2.4% reduction in electricity demand. Renewable energy scenarios demonstrated that photovoltaic systems supplying 30% of electricity demand and solar thermal systems meeting 10% of heating demand would require capacities of 2218 kW and 3540 kW, respectively. The framework's predictive capabilities and flexibility position it as a robust tool to support decision-makers in developing sustainable and cost-effective energy strategies, paving the way toward establishing energy-efficient and positive energy districts.

Keywords: urban energy planning; energy retrofitting; renewable energy integration; energy demand prediction; sustainable cities; positive energy districts; Danish energy planning; energy demand prediction

1. Introduction

As Europe strives toward a low-carbon and more sustainable future, improving building energy efficiency has become a key priority [1]. Buildings are responsible for a significant share of energy consumption and greenhouse gas emissions, making the push to enhance their energy performance more urgent across the continent. In this context, urban-scale energy modeling and planning are pivotal to achieving sustainable urban development. As cities grow at an unprecedented rate, they are transforming into major hubs of energy consumption, greenhouse gas emissions, and broader environmental impacts. To effectively tackle climate change, improve energy security, and foster socio-economic development, it is crucial to understand and manage energy dynamics at both district and city levels [2,3]. Through the use of advanced modeling techniques and comprehensive

planning frameworks, urban-scale energy initiatives offer a holistic solution to complex energy challenges, engaging various stakeholders and optimizing resource use across multiple sectors [4]. The core aim of urban-scale energy modeling is to examine energy flows, consumption patterns, and the interactions between different urban domains such as buildings, transportation, industry, and infrastructure. By analyzing these relationships, modeling tools provide valuable insights into the drivers of energy demand, identify opportunities for efficiency improvements, and map out pathways for low-carbon urban development. This knowledge empowers policymakers to create targeted interventions, prioritize investments, and adopt policies that support energy efficiency, renewable energy adoption, and sustainable land use planning, all of which contribute to building resilient and environmentally friendly cities [5]. Urban-scale energy planning acts as a catalyst for innovation, collaboration, and active stakeholder engagement within urban communities. These planning processes, ranging from participatory scenario development to collaborative decision-making platforms, emphasize inclusivity, transparency, and social equity in shaping the future of urban energy systems. Moreover, urban-scale energy modeling and planning are crucial for enhancing the resilience of energy infrastructure to climate change, natural disasters, and other external shocks [6]. By analyzing vulnerabilities, risks, and the adaptive capacity of energy systems, planners can devise robust strategies that bolster energy security, reliability, and flexibility in the face of uncertainty. These strategies may involve reinforcing critical infrastructure networks, promoting decentralized energy systems, and creating resilience-oriented approaches that allow cities to withstand disruptions, recover quickly from emergencies, and build the capacity to thrive in a rapidly changing climate [7].

In Denmark, the importance of urban-scale energy modeling and planning is especially important in the country's drive toward sustainability, energy security, and climate resilience. As a leader in renewable energy adoption and urban innovation, Denmark relies heavily on advanced modeling tools and comprehensive planning frameworks to optimize energy use, reduce carbon emissions, and bolster the resilience of urban infrastructure. With an ambitious goal to achieve fossil-free status by 2050 [8], urban-scale energy initiatives are instrumental in guiding the country's transition to renewable energy sources, advancing energy efficiency measures, and integrating decentralized energy systems at the local level. By leveraging cutting-edge modeling techniques and fostering stakeholder engagement, Danish cities can uncover synergies across energy sectors, prioritize investments in sustainable infrastructure, and encourage collaboration between government bodies, industry partners, and local communities.

Over the past two decades, substantial theoretical and experimental research has been dedicated to meeting standards and regulations within the building sector. However, much of this research has concentrated on individual buildings, systems, or components, with relatively few studies addressing the design, operation, and retrofitting of building clusters, streets, and urban areas [9,10]. To fill this gap, the present work introduces DanCTPlan, an innovative energy planning tool specifically designed to enhance energy efficiency and interconnectivity within urban areas in Denmark. The tool's methodology hinges on two key components: dynamic simulations of building energy performance using Energy Plus and data from the Danish building standard BR18 [11]. Furthermore, it takes into account factors such as building type, age, and usage to predict heating and electricity demands. By integrating data from the Danish Building and Housing Register (BBR) [12], the tool can access detailed building specifications for a given area, allowing for accurate predictions of energy consumption at the district and building cluster level. DanCTPlan also facilitates comparisons between predicted and actual performance, providing insights into the energy performance gap and helping identify discrepancies between expected and

observed energy consumption. The tool can also assess the impact of building envelope retrofitting on both the district and area levels, laying the groundwork for the integration of renewable energy supply systems, including photovoltaics (PV), wind power, and solar thermal units. This paper outlines the development and design of DanCTPlan, offering an in-depth explanation of its building cluster modeling and prediction methodology. The tool is then applied to real case studies in Denmark, predicting and reporting heating and electricity demands for streets and neighborhoods, and offering recommendations for optimizing energy-efficient operations.

The key innovative aspects of this work and the proposed framework and tool are as follows:

1. Automated Data Integration: A key innovation of the proposed energy consumption prediction framework is its ability to automatically extract and integrate data from the Danish Building and Housing Register (BBR) and building regulations, such as BR18. This automated data processing significantly reduces manual input, a major limitation of current tools, often requiring labor-intensive data collection. By leveraging open data sources, the framework streamlines the modeling process and makes energy consumption prediction more accessible and scalable.
2. Scalability Across Urban Areas: The framework is designed for scalability, making it applicable at the building level and at the district and city scales. This multi-level application enables urban planners and policymakers to model energy demand across different urban areas, providing insights into city-wide energy performance. The ability to scale predictions from individual buildings to entire cities is a notable advancement, filling a gap in existing tools, which are typically restricted to smaller, less complex scales.
3. Holistic Approach to Retrofitting and Renewable Energy Integration: One of the most distinguishing features of the framework is its holistic approach to retrofitting and renewable energy scenarios. It allows users to model both energy efficiency improvements (such as building envelope upgrades) and renewable energy integration (e.g., photovoltaics and solar thermal systems). This dual focus not only enhances the accuracy of energy predictions, but also provides a more comprehensive solution to meet sustainability and energy transition goals.
4. Actionable Metrics for Decision-Making: The framework outputs a wide range of actionable metrics that inform decision-making, including heating performance, peak energy demands, and renewable energy contributions. These metrics help guide strategic decisions about energy use and efficiency measures, making the tool a valuable asset for urban planners, policymakers, and energy consultants. By providing detailed data on energy performance, the tool directly supports the implementation of energy-saving measures and carbon reduction goals.
5. Contextual Relevance for Denmark: The framework is specifically designed to address Denmark's energy regulations and urban development needs, making it a highly relevant tool for Danish urban planners and policymakers. It takes into account the unique characteristics of Danish buildings, heating fuel types, and energy regulations, making it more applicable than generic frameworks. This localized approach ensures that the tool can help meet Denmark's energy efficiency goals while providing a foundation for adaptation to other regions facing similar energy challenges.

The rest of this paper is organized into five main sections. Section 2 provides an overview of urban-scale energy modeling, discussing its approaches and applications and the challenges that need to be addressed in the field. Section 3 outlines the approach and methodology used in the study, detailing the research process and the data that were utilized for energy modeling and energy evaluation. Section 4 presents and describes

the DanCTPlan tool with its various features and services. Section 5 implements the case study, applying the tool to both a single street and a district-level case, demonstrating how the approach works in actual scenarios. Finally, Section 6 presents a discussion of the main findings of the tool implementation and assessment, along with highlighting future insights, and Section 7 reports the main conclusions of this study.

2. Urban-Scale Energy Modeling

2.1. Background

Building energy modeling has long been a cornerstone in the research and design of energy-efficient buildings. It plays a crucial role in optimizing building performance [13], supporting the design process [14], managing operations [15], and guiding energy retrofitting efforts [16]. With a wealth of energy modeling tools and software now available, this field has matured, offering accurate simulations and forecasts to improve energy use in individual buildings. However, as the world rapidly transitions to more interconnected cities and communities, driven by advances in smart grids and flexible energy systems, there is an urgent need to shift focus beyond single buildings. The goal is to create energy-efficient, flexible urban environments that can adapt to the complexities of modern life. Urban-scale energy modeling addresses this need by simulating and analyzing energy consumption, generation, and distribution across an entire urban area [17,18]. This approach helps provide a deeper understanding of energy flows within cities, uncovering opportunities for efficiency improvements and enabling informed decision-making for urban planners and policymakers. In this regard, Figure 1 presents an overall urban-scale energy modeling workflow with various steps and components. With the increasing complexity of urban energy systems, due to population growth, climate change, and technological innovations, new modeling techniques and tools have been developed to overcome these challenges and support the creation of sustainable, energy-efficient cities [19].

Urban-scale energy models (USEMs) can be classified into top-down, bottom-up, and hybrid approaches, each with unique characteristics [20]. Top-down models use aggregate data, like macroeconomic and demographic trends, to estimate city-level energy consumption and emissions. While straightforward and useful for policy analysis, they lack spatial and temporal detail, often oversimplifying local energy dynamics. Bottom-up models, on the other hand, provide detailed analyses at the building or infrastructure level, using granular data to assess the impact of technological interventions. These models, though accurate, are data-intensive and computationally demanding. Hybrid models combine the strengths of both approaches, offering detailed insights alongside broader contextual analyses, though they are complex and resource-intensive to develop.

In recent decades, the field of urban-scale building energy modeling (UBEM) has advanced significantly, with numerous studies contributing to its evolution. Salvalai et al. [21] reviewed key UBEM tools, focusing on data workflows and simulation engines, guiding the development of zero-carbon communities. Sola et al. [20] analyzed tools modeling energy demand, generation, and distribution, highlighting the differences in their architectures. Wong et al. [22] examined urban-scale simulation methods, emphasizing the importance of spatial and environmental factors in dense urban areas. Another work by Reinhart et al. [23] introduced the concept of UBEM, establishing foundational simulation methods and validation techniques. A review by Kamel [24] explored physics-based models, stressing precise calibration, while Abbasabadi et al. [25] highlighted the need for integrated models to reflect urban energy systems' interconnectedness. Innovations like CityBES by Chen [26] and GIS-based modeling by Fonseca [27] advanced automated and spatial data-driven analyses.

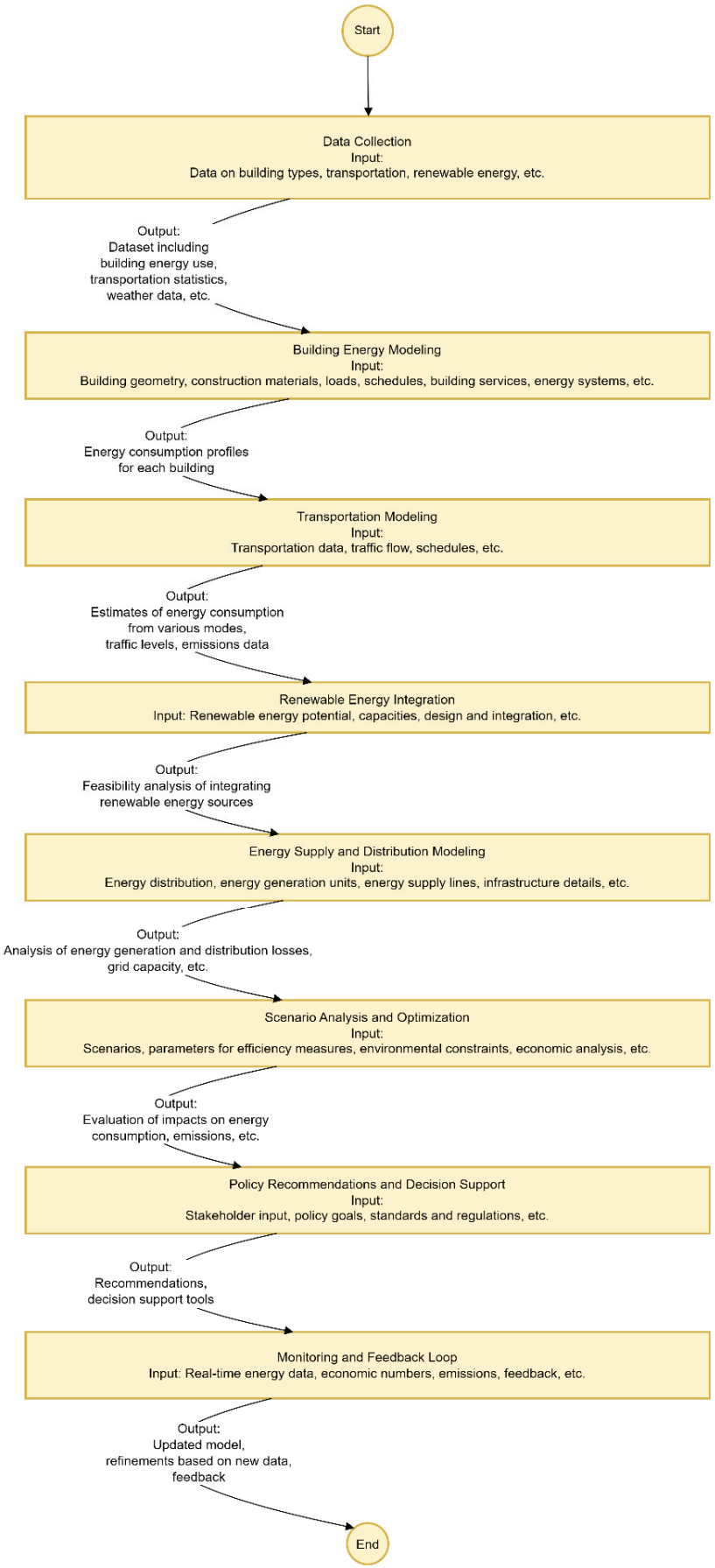


Figure 1. Urban-scale energy modeling workflow.

Machine learning has also influenced UBEM. Fathi [28] demonstrated its utility in predicting urban building energy performance, while Hong [29] reviewed its application in real-world environments. Zhang [30] integrated energy and carbon emission models, promoting zero-energy buildings, and Borràs [31] explored energy communities and decentralized solar projects. Deng [32] introduced AutoBPS, a BIM-based tool that simplifies urban-scale simulations. Research has also focused on Denmark's potential for positive energy districts (PEDs). Jradi et al. [33] modeled a district in Odense, demonstrating that retrofitting and renewable energy integration can achieve surplus energy production. Jepsen et al. [34] investigated transforming parts of an island into PEDs through energy system upgrades and renewable expansions. Advanced tools, ranging from detailed simulations to urban-scale systems, continue to support energy optimization and emission reductions in cities. These developments highlight the growing importance of UBEM in sustainable urban planning to establish broader urban energy systems, helping cities optimize energy use and reduce emissions.

2.2. Challenges to Be Addressed

Urban-scale energy models hold great potential for improving city energy performance and sustainability but face several challenges. The most significant is the availability and quality of data. Accurate models require detailed and up-to-date data on building characteristics, energy consumption, and local climate. Improving data-sharing practices, standardizing data, and fostering collaboration between stakeholders can help address these gaps. Another challenge is the integration of diverse models. Urban energy systems are complex, and for effective modeling, various systems like energy consumption and transportation must work together seamlessly. Standardized data formats and open-source platforms can help overcome this issue. The computational demands of these models also pose a challenge, as bottom-up and hybrid models require significant computing power. More efficient algorithms and computational tools are needed to make these models more accessible and practical. Lastly, for urban-scale models to be effective, they must be integrated into decision-making processes. This requires user-friendly models and platforms, effective communication, and collaboration with policymakers and stakeholders to ensure the models reflect real-world needs and produce actionable insights.

It is within this complex landscape of challenges and opportunities that the proposed tool in this work, DanCTPlan, becomes a vital asset. As a comprehensive energy planner tool specifically tailored for energy-efficient and interconnected urban areas in Denmark, DanCTPlan addresses many of the barriers that have traditionally hindered urban-scale energy modeling. The tool integrates dynamic simulations of building energy performance using advanced techniques like Energy Plus and incorporates data from the Danish building standard BR18 [11], offering accurate and location-specific predictions of heating and electricity demands. By incorporating data from the Danish Building and Housing Register (BBR) [12], DanCTPlan provides reliable insights into energy consumption across building clusters and districts. This helps to bridge the critical data gap that many energy models face.

Moreover, DanCTPlan is designed with interoperability in mind. It combines a range of data sources and modeling components, allowing different aspects of urban energy systems to be modeled cohesively. By using standardized data formats and protocols, it ensures that diverse models can work together seamlessly, enabling comprehensive analysis and informed decision-making. The tool's flexible architecture also allows it to adapt to future advancements in energy modeling and computational technologies, ensuring that it remains relevant as the field evolves. The DanCTPlan tool also addresses the computational challenges of urban-scale energy modeling by using simple and efficient

algorithms. Its design allows for detailed modeling of urban energy systems without overburdening computational resources, making it accessible to a wide range of users, including policymakers, urban planners, and energy professionals. By providing an easy-to-use interface and actionable insights, DanCTPlan empowers users to make informed decisions about energy use, building retrofits, and renewable energy integration at the district level. Additionally, it serves as a valuable resource for teaching students and supporting academic tasks, including educational demonstrations, research applications, and hands-on learning experiences.

Furthermore, DanCTPlan places a strong emphasis on stakeholder collaboration. By enabling local governments, energy providers, and community stakeholders to work together, the tool fosters a participatory approach to urban energy planning. This collaborative environment ensures that the insights generated by the model are not only scientifically sound but also aligned with local priorities and needs. Whether it is optimizing energy efficiency, integrating renewable energy systems, or planning for future urban development, DanCTPlan facilitates transparent, inclusive, and data-driven decision-making processes. The DanCTPlan tool represents a significant step forward in overcoming the challenges facing urban-scale energy modeling. By addressing data quality, integration, computational efficiency, and stakeholder engagement, it provides a comprehensive solution to the complex energy challenges facing urban areas in Denmark and beyond.

3. Approach and Methodology

Urban energy planning is a critical yet complex task, particularly when scaling from individual buildings to neighborhoods or city districts. While substantial research and tools exist for assessing single-building energy performance, there remains a gap in city-scale, user-friendly platforms. This study addresses the gap by introducing a framework for modeling and predicting the energy performance of building clusters, neighborhoods, and city districts in Denmark. The platform minimizes user input requirements by automating data collection and integrating robust validation methodologies. The framework's primary innovations include its automated data pipeline, predictive accuracy for diverse urban areas, and the incorporation of retrofitting and renewable energy scenarios.

3.1. Methodology

3.1.1. Framework Overview and Validation Mechanism

The methodology employs a modular framework (Figure 2) to facilitate efficient energy planning. The framework ensures reliability through a systematic validation process that compares predicted outputs with real-world data. This validation mechanism involves an analysis between modeled and actual energy usage at the street and neighborhood levels, providing confidence in its predictive accuracy and reliability. The respective validation involves baseline data comparison, where modeled energy usage is cross-referenced with baseline energy data derived from the Danish Building Regulations. Additionally, ground-truthing is conducted, with validation performed using real energy consumption data for heating and electricity from municipal datasets. Moreover, sensitivity analysis is conducted, with the key parameters varied, to evaluate the robustness of the prediction and planning approach.

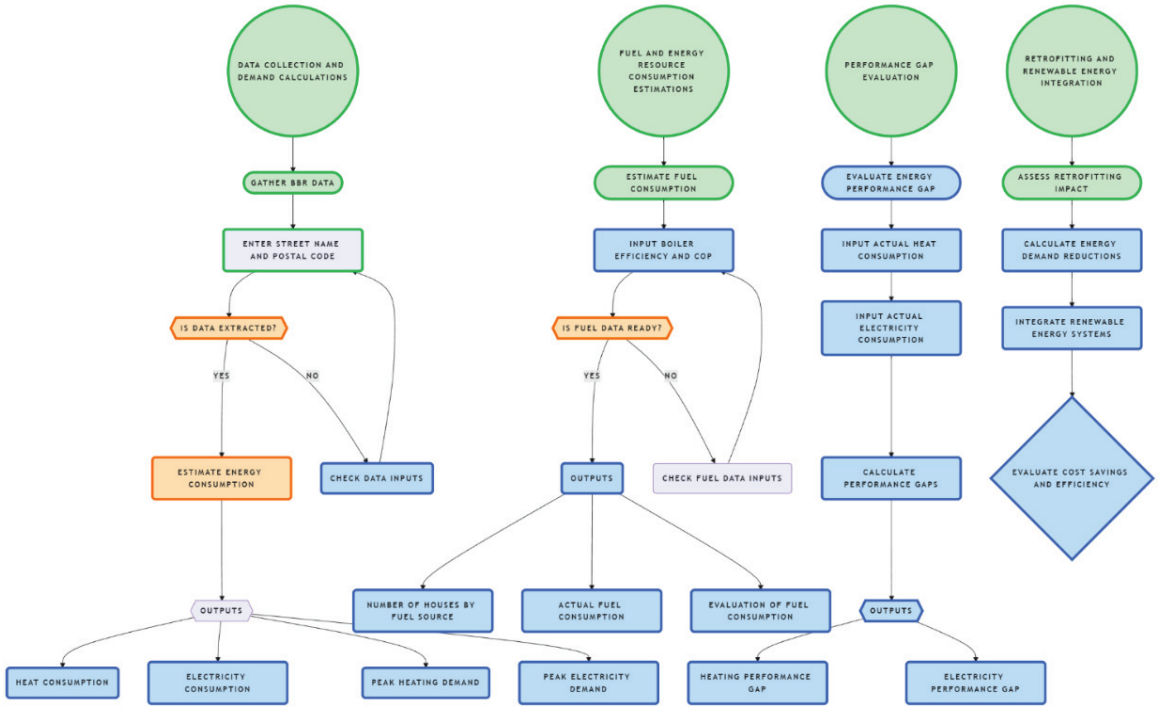


Figure 2. The overall methodology of the proposed holistic city energy planning tool.

3.1.2. Data Collection and Demand Calculations

The framework is designed to minimize user input while providing robust city-scale energy performance predictions. It leverages automated data extraction from the Danish Building and Housing Register (BBR) and integrates this with streamlined analytical processes. The user provides only the street name and postal code, and the platform processes detailed building-specific and aggregate energy performance metrics. The key outputs include the following:

- The heat consumption of the area;
- The electricity consumption of the area;
- The peak heating demand;
- The peak electricity demand.

To improve data reliability, the framework cross-references BBR data with auxiliary databases, such as meteorological datasets and energy usage profiles from the Danish Energy Agency. This multi-source integration ensures robust energy landscape insights, enabling planners to make informed decisions rapidly.

3.1.3. Fuel and Energy Resource Consumption Estimation

This component estimates fuel-specific energy resource consumption at the neighborhood level, enhancing the granularity of energy use profiles. The methodology expands beyond traditional tools by incorporating user-friendly workflows for dynamic fuel mix scenarios. Leveraging BBR data and Danish Energy Agency conversion factors, the framework evaluates resource consumption for various fuel types, such as wood pellets, oil, gas, and district heating. The inputs include the following:

- Boiler efficiency and heat pump COP (Coefficient of Performance);
- Fuel types associated with specific buildings, automatically extracted from BBR data.

The outputs from this functionality are as follows:

- The number of buildings using each fuel source;
- Total fuel consumption estimates by type;

- Scenarios evaluating fuel-specific consumption if the entire area transitions to a single fuel type.

These outputs offer granular insights into inefficiencies, enabling policymakers to prioritize areas for optimization, such as retrofitting older boiler systems or promoting district heating.

3.1.4. Performance Gap Evaluation

Performance gap analysis is a central innovation in the framework, enabling the evaluation of discrepancies between predicted and actual energy consumption at the street or neighborhood level. Using baseline energy benchmarks from Danish Building Regulations, the tool incorporates the following:

- Actual heat consumption for the area (e.g., from district heating records);
- Actual electricity consumption for the area (e.g., from utility providers);

By comparing predicted and actual consumption, the platform calculates the following:

- The heating performance gap (as a percentage);
- The electricity performance gap (as a percentage);
- The analysis supports targeted interventions by identifying areas with significant deviations, and guiding strategies for retrofitting or operational improvements.

3.1.5. Retrofitting and Renewable Energy Integration

The framework incorporates a scenario-based analysis module for retrofitting and integrating renewable energy systems. Unlike conventional tools, it simulates the impacts of retrofitting measures (e.g., insulation upgrades, window replacements) and models renewable energy systems (e.g., solar PV panels, solar thermal collectors) based on Danish energy standards. The outputs include the following:

- The renewable energy capacity required to meet demand;
- The contribution of renewables to heating and electricity needs;
- The associated emission reductions and cost savings.

This approach allows planners to evaluate both the financial and environmental benefits of transitioning to sustainable energy systems.

3.2. Input Data Description

The primary input for the proposed city-level model is data from the Danish Building and Housing Register (BBR) [12]. This extensive database contains detailed information on all buildings in Denmark, including year of construction, location, heating source, and usage. Companies, experts, or researchers can request these data in Excel format. The model requires the following seven specific inputs:

- The street name;
- The postal code of the street;
- The building usage type, simplified into eight categories: one-story houses, two-story houses, apartments, offices, public institutions, food stores, non-food stores, and others;
- The heating fuel type, divided into seven categories: electricity, gas, liquid fuels, solid fuels, straw, natural gas, and other sources;
- The year of construction, used to estimate energy performance;
- The year of renovation, used if the building has been renovated;
- The building area.

It is important to highlight that the Danish Building and Housing Register (BBR) categorizes building types into approximately 104 groups based on their usage. Recog-

nizing the similarity among many of these categories, we proposed consolidating them into eight distinct groups to streamline the workflow, as outlined earlier. Additionally, in the model, liquid fuels are presumed to be fuel oil, while solid fuels are assumed to be wood pellets for consistency. A pivotal input for the model is the building construction year or performance year, automatically extracted from the Danish BBR. This year serves as a foundation for estimating the expected performance through dynamic simulations and adherence to Danish building standards. In cases of building renovations, the energy renovation year is selected as the reference for performance evaluation.

3.3. Single-Building Energy Consumption Predictions

Each building along the street is categorized into one of eight types, each with its standard energy consumption based on its age and construction year. For the first four categories, one-story houses, two-story houses, apartments, and offices, detailed simulations using EnergyPlus analyze heating and electricity usage, considering construction years ranging from pre-1960 to post-2015. These simulations, along with their outcomes, have been previously validated by Foldager et al. [35]. Meanwhile, the energy consumption data for the remaining four categories are derived from historical averages between 1997 and 2002.

The standardized energy consumption per square meter for each category is given in Table 1 [35]. Additionally, the model predicts the peak heating and electricity demands, with capacities reported in Watts per square meter, as shown in Table 2. By organizing buildings into categories and construction periods, such as grouping all one-story buildings constructed before the 1960s, the model calculates the energy demand for each category by multiplying the standardized consumption and capacity values with the area of each category. Ultimately, these individual demands are summed to determine the total energy demand for the entire street or cluster.

Table 1. Energy consumption per square meter of different building categories and ages [35].

Energy [kWh/m^2]	**Pre-1960s**		**60–70s**		**1980s**		**1990s**		**2000s**		**2015s**	
	Elec	Heat	Elec	Heat	Elec	Heat	Elec	Heat	Elec	Heat	Elec	Heat
1-story	40	326	37	212	35	127	34	80	33	67	33	37
2-story	40	336	38	223	36	137	34	87	33	71	33	38
App	40	330	37	214	35	129	36	84	35	67	32	38
Office	46	384	42	250	41	153	41	94	40	81	39	44
Shop ÷ food	37	213	34	138	33	83	31	52	31	44	30	24
Shop + food	267	220	249	143	237	86	226	54	225	45	219	25
Public Inst.	33	293	31	190	30	114	28	72	28	60	27	33
	Not time-specific											
Other buildings	Electricity 44								Heat 100			

Table 2. The heating and electricity peak capacity for the eight different building categories [35].

Capacity [W/m^2]	**Pre-1960s**		**60–70s**		**1980s**		**1990s**		**2000s**		**2015s**	
	Elec	Heat	Elec	Heat	Elec	Heat	Elec	Heat	Elec	Heat	Elec	Heat
1-story	9	105	9	70	8	47	7	32	8	27	8	17
2-story	9	108	9	80	9	55	8	20	8	16	8	8
App	9	111	9	75	9	50	8	33	8	28	8	16
Office	9	123	9	90	9	61	6	30	8	27	8	13

Table 2. *Cont.*

Capacity [W/m^2]	**Pre-1960s**		**60–70s**		**1980s**		**1990s**		**2000s**		**2015s**	
Shop ÷ food	8	123	7	90	7	61	6	30	6	27	6	13
Shop + food	55	123	52	90	49	61	47	30	47	27	45	13
Public Inst.	7	123	6	90	6	61	6	30	6	27	6	13
Not time-specific												
Other buildings	Electricity 9							Heat 32				

4. DanCTPlan Tool

In the previous section, we discussed a method and approach for creating a tool tailored to energy planning and design at both the street and city levels in Denmark. This tool, DanCTPlan, is designed with the user in mind, aiming for ease of use and flexibility. It is essentially a software package that is built using Microsoft Excel spreadsheets and operates seamlessly, ensuring accessibility, comprehension, and implementation for users.

The DanCTPlan tool leverages open-source software to enhance the flexibility, accessibility, and scalability of the system. One of the key components of the tool is EnergyPlus, an open-source building energy simulation engine. By utilizing EnergyPlus, the tool benefits from a robust and well-supported platform that can simulate the energy performance of buildings based on dynamic inputs such as construction type, heating systems, and location. This open-source nature of EnergyPlus ensures that the simulation engine is highly customizable, adaptable to new building types, and continuously updated by a community of developers and researchers.

The open-source approach also allows for the integration of additional data sources and algorithms. For example, the use of data from the Danish Building and Housing Register (BBR), which is publicly accessible, is central to the tool's ability to estimate energy demand across various building types.

DanCTPlan comprises two main components: a user-friendly interface and a set of databases that run in the background to perform calculations. The interface serves as the user's window into the tool's functionality. Under the INPUT DATA tab of the interface, users input relevant data into designated yellow cells, as shown in Figure 3. This includes information such as building specifications, energy sources, and consumption patterns. Additionally, the user can include information on the expected coverage of renewable energy capacity installation in the case study considered. Under the OUTPUT DATA tab, users can view the output data generated by the tool, as noted in Figures 4 and 5. This includes details like the number and categorization of buildings, respective space areas, overall and specific heating and electricity consumption, estimates of peak heating and electricity capacity requirements, and overall energy consumption for the selected building cluster. Additionally, there is information on the types of heating sources and fuels utilized within the buildings, as well as the renewable energy systems installed, along with their corresponding capacities.

INPUT DATA	
Postal Code	5270
Roadname 1	Lille Rugbjerg vej
Roadname 2	Anderupvej
Roadname 3	
Roadname 4	
Roadname 5	Enggårdsvej
COP Heat Pump	3
Efficiency el. boiler	0.9
Efficiency Fuel Boilers	0.8
PERFORMANCE GAP INPUT DATA	
Actual Heating Consumption [MWh]	500.00
Actual Electricity Consumption [MWh]	100.00
RENEWABLE ENERGY PRODUCTION	
Input: Percentage of consumption covered by unit	
Photovoltaic panels [%]	0%
Solar thermal collecters [%]	30%
Onshore Wind capacity [%]	0%
Near shore capacity [%]	0%

Figure 3. DanCTPlan input data.

ɪtegory	Number of Buildings	Space area [m2]	Heat consumption [MWh]	Heat consumption [kWh/m2]	Electricity consumption [MWh]	Electricity consumption [kWh/m2]
Whole city	84,933		3,004,518,273	154,602	755,290,598	38,865
Total street(s)	325	14,397	**20,704**	**105**	**8526**	**105**
1-story	104	12,191	2531	164	553	36
2-story	0	0	0	0	0	0
Appartments	3	990	153	155	36	36
Offices	4	1216	272	185	61	41
Shops-food	2	0	70	34	63	31
Shops	0	0	0	0	0	0
Public Insitutions	0	0	0	0	0	0
Others	212	0	17,678	100	7813	44
Peak Capacity [kW]			6669	34	1774	9

Figure 4. DanCTPlan output data.

A useful feature of DanCTPlan is its ability to estimate fuel consumption based on the selected energy sources. For instance, if a specific street or cluster is to be heated using a particular energy source, the tool can calculate the expected fuel usage. This includes, for example, if the planner aims to install heat pumps instead of fuel oil and gas boilers in a certain area. Nevertheless, the output tab provides information on renewable electricity production in the considered case, including data on the installed capacities of PV, wind, and solar thermal collectors, as noted in Figure 5.

Moreover, the tool has an integrated holistic economic assessment feature, allowing reporting of the cost of operation of various energy supply systems in a certain area or district, including district heating, wood pellets, heat pumps, and electric boilers, among others. In addition to targeting energy system and network planning, the tool takes into account building envelope retrofitting, and there is a separate dedicated tab showing information on the energy retrofitting of existing buildings in the considered district to comply with the building regulation BR2018 in Denmark for building renovation to class 'C'. This tab, as shown in Figure 6, includes information on the cumulative area of the buildings corresponding to the categories year of construction/last retrofitted, along with estimated data on heat demand reduction, electricity consumption savings, and overall operational

cost reduction due to the adopted retrofitting. Similarly to the initial information shown in Figure 4 for the baseline buildings' initial consumption, this tab also shows data on the total and specific heating and electricity consumption of the different types of buildings, and the respective peak capacity demand, after retrofitting.

Heating sources			
	Consumption	Consumption if the whole street uses the same fuel	
District Heating [MWh]	12,674	20,704	
Natural Gas [m3]	0	2,258,601	
Diesel [m3]	-	2,493	
Fuel oil [kg]	5760	2,200,261	
Biogas [m3]	-	3,888,722	
Wood Chips [kg]	-	9,617,270	
Wood Pellets [kg]	42,689	5,110,892	
Heat Pump [kWhel]	0	6,901,337	
Electric Boiler [kWhel]	19,727	22,774,411	
RENEWABLE ELECTRICITY PRODUCTION			
Technology	Capacity [kW]	Output [MWh]	Area [m2]
PV *based on Odense/DK	0	0	0
Onshore Wind	0	0	
Near shore	0	0	
RENEWABLE HEAT PRODUCTION			
Solar Collectors	9662	6211	13,803

Figure 5. Heating source evaluation and renewable energy solution assessment.

Retrofit all buildings to follow BR2018		
Total area to be retrofitted:	12,388.00	m2
1960	3186.00	m2
1980	3871.00	m2
1990	5331.00	m2
Heat demand reduction	1567.89	MWh
Electricity demand reduction	38.18	MWh
Total achievable reduction	1606.07	MWh
Total achievable operational cost reduction	584,100.35 kr.	[DKK/year]

Figure 6. Energy retrofitting of the district's building envelope.

The output section also provides insights into the performance gap of the building cluster concerning heating and electricity consumption, as noted in Figure 7. This is achieved by comparing the tool's estimations with the actual data provided by the user. While providing these inputs is optional, doing so enables DanCTPlan to generate more accurate reports on energy performance.

PERFORMANCE GAP OUTPUT DATA		
	Heating Performance Gap	Electricity Performance Gap
Performance Gap [%]	4	-19

Figure 7. Heating and electricity performance gaps.

In addition to the input and output sections, DanCTPlan includes graphical representations. These graphs offer a visual overview of energy consumption patterns, highlighting trends such as heating and electricity usage across different building categories. They also depict the distribution of buildings based on the fuel and resources used for heating. Overall, DanCTPlan is a comprehensive tool that not only aids in energy planning and design, but also empowers users with insights to optimize energy efficiency and resource allocation within urban environments.

5. Case Study Implementation

In this section, the established DanCTPlan energy planning and reporting tool is implemented and assessed in two case studies in Denmark: a standard single street to highlight some of the basic features of the tool, and a district of five streets. The results of the base case scenarios are presented, and the findings of the energy retrofitting of the systems and buildings in both cases are reported and evaluated. The names of the different streets will be omitted for anonymity.

5.1. Single Street Case

In the first case study, a single street in Odense, Denmark, is selected and introduced to implement the DanCTPlan energy planning and retrofitting tool. The aim is to highlight the main features of the tool in evaluating the energy supply scheme in the street and evaluate the impact of retrofitting. The first step in the demonstration is reading the corresponding data for this specific street from the Danish BBR building registry.

Figure 8 illustrates the distribution of building types within the street tag. Specifically, 10 buildings are categorized as one-story houses, 34 as apartments, 1 as an office building, 2 as food-related shops, and 5 as public institutions. Additionally, 46 buildings are classified under the "others" category, which largely consists of very small, conditioned areas in addition to non-conditioned structures such as carports, storage boxes, and sheds that do not have any energy consumption.

Category	Number of Buildings	Heat consumption [MWh]	Heat consumption [kWh/m2]	Electricity consumption [MWh]	Electricity consumption [kWh/m2]
Whole city	84,933	3,003,597,299	154,555	755,119,863	38,856
Total street(s)	101	**4930**	**201**	**939**	**201**
1-story	10	431	294	57	39
2-story	0	0	0	0	0
Appartments	34	3581	217	614	37
Offices	1	16	384	2	46
Shops-food	3	115	208	20	37
Shops	2	41	143	72	249
Public Insitutions	5	715	133	161	30
Others	46	31	100	14	44
Peak Capacity [kW]		1860	76	208	8

Figure 8. DanCTPlan output data for the street case study.

As highlighted by the tool, the analysis covers 101 buildings within the designated street tag, with a total estimated annual heating consumption of 4929 MWh and annual

electricity consumption of 939 MWh. Furthermore, the tool calculates the peak capacities for heating at 1860 kW and for electricity at 208 kW. These peak capacity estimates are crucial for forming an initial understanding of the scale and requirements of future energy systems designed for the area, whether for new installations or when retrofitting existing systems. Specifically, these capacity outputs offer valuable insights for both heating energy systems and electricity generation systems.

In the context of fuel consumption, the tool also provides a comparative analysis of current and projected fuel usage under various scenarios. As depicted in Figure 9, the current heating demand for the area is predominantly met through district heating, with a cumulative supply of 4883 MWh, supplemented by a small amount of electricity supplied by electric boilers (45 MWh). The adjacent column in the figure illustrates the amount of fuel the area would consume if the entire street were to transition to a single heating fuel source. For example, if the street were to exclusively utilize electric boilers, the total annual electricity consumption would rise to 5422 MWh. Alternatively, if the heating were supplied by wood pellets, the annual consumption would amount to 1216 tons. It is noted here that the street has no current renewable electricity production installations. Furthermore, the economic evaluation highlights that the current cost of heating delivery is around 1529 k DKK for district heating and 67 k DKK for electric boiler operation.

Heating sources				Economics
	Consumption	Consumption if the whole street uses the same fuel		Cost of operation [DKK/year]
District Heating [MWh]	4883	4930		1,529,399
Natural Gas [m3]	0	537,769		0
Diesel [m3]	0	594		0
Fuel oil [kg]	0	523,878		0
Biogas [m3]	0	925,898		0
Wood Chips [kg]	0	2,289,855		0
Wood Pellets [kg]	0	1,216,894		0
Heat Pump [kWhel]	0	1,643,196		0
Electric Boiler [kWhel]	45,101	5,422,548		67,651
RENEWABLE ELECTRICITY PRODUCTION				
Technology	Capacity [kW]	Output [MWh]	Area [m2]	
PV *based on Odense/DK	0.00	-	0.0	-
Onshore Wind	0.00	-		
Near shore	0.00	-		
RENEWABLE HEAT PRODUCTION				
Solar Collectors	2300	1479	3286	

Figure 9. Heating demand breakdown and energy resource evaluation for the street case study.

These data provide a more precise foundation for planning purposes than the conventional use of tabulated static values, which often lead to oversized or undersized system designs. In the case of oversizing the system, unnecessary costs are incurred, while undersizing may result in an inability to meet the required energy demand. Therefore, this more dynamic approach enables better-informed decisions, ultimately contributing to cost-efficiency and energy reliability. Such detailed information is critical for energy planners, consultants, authorities, and decision-makers, enabling them to devise more accurate and cost-effective strategies for energy system implementation or upgrades. These figures offer an initial glimpse into the potential impacts of switching to different heating fuels, providing essential information for authorities, consultants, and decision-makers when

considering future modifications or upgrades to the street's heating infrastructure. This enables better foresight in determining the most cost-effective and sustainable fuel options, aligning with both energy demands and environmental goals.

Additionally, the tool provides representative graphs, for instance, Figure 10, that break down energy consumption for heating and electricity by building category. These visual representations allow for a clear understanding of how different building types contribute to overall energy consumption. Figure 11 further complements this by displaying the number of buildings aggregated by the heating source currently in use, providing an easy-to-read summary of energy consumption patterns across the street's various building types.

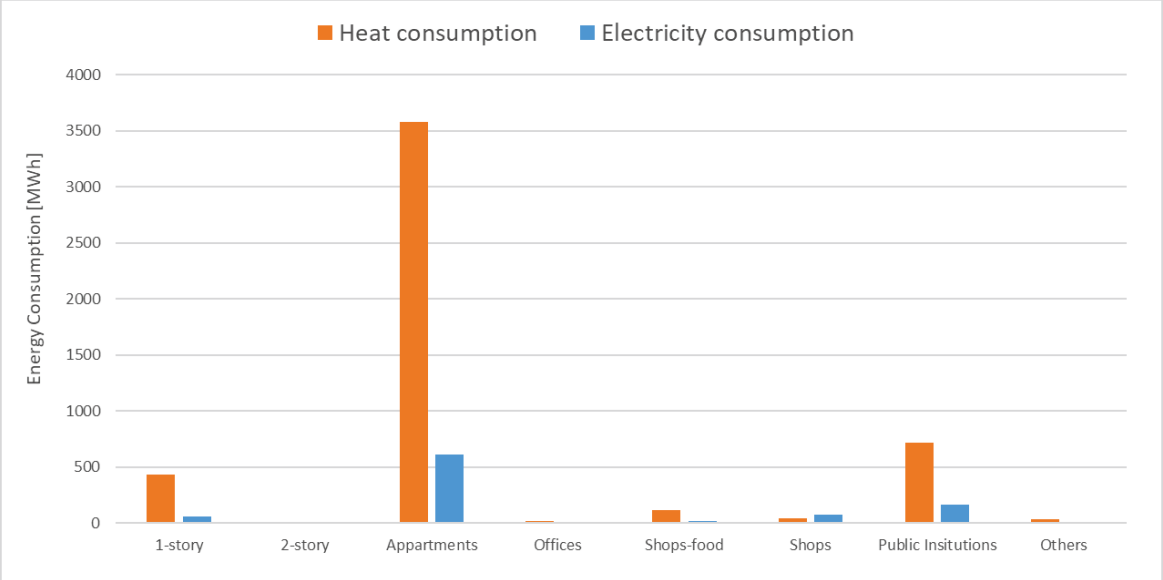


Figure 10. A breakdown of energy consumption for heating and electricity by building category for the street case study.

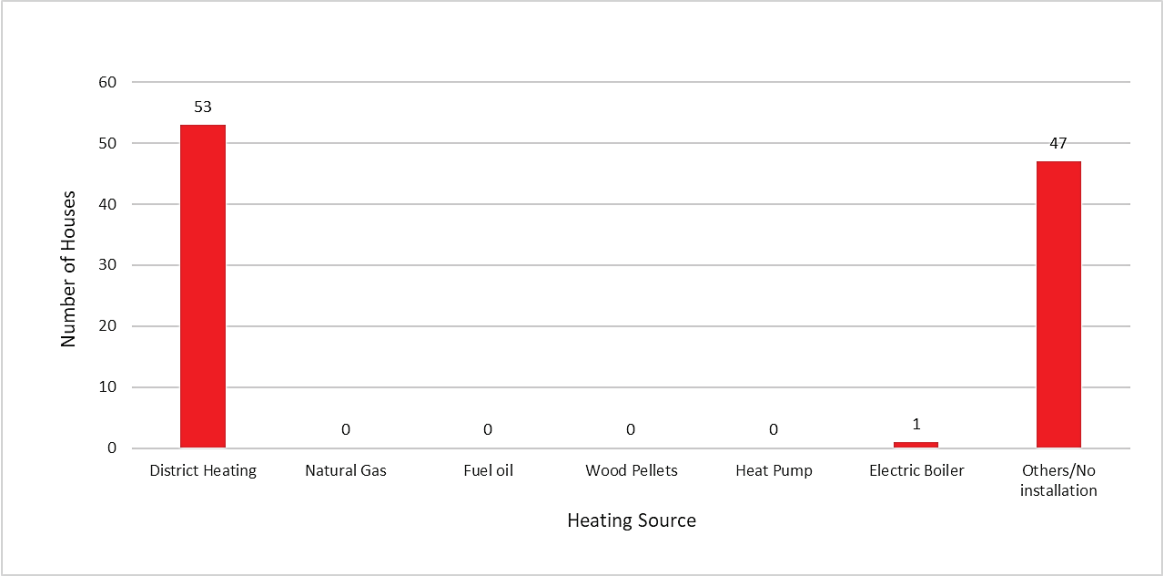


Figure 11. The number of buildings aggregated by the heating source for the street case study.

In terms of retrofitting, and adopting the approach described in the previous section, on retrofitting all existing buildings to the level of the current building regulation 'Class C', the results are provided in Figure 12, showing that the area of buildings to be retrofitted

at the moment is around 21169 m^2, allowing a heat demand reduction of 3001.35 MWh (60.8%), and an electricity demand reduction of around 54.2 MWh (5.8%). The overall and specific energy consumption of the buildings in the specific street after retrofitting are presented in Figure 13, showing a reduction in the peak capacity demand for heating from 1860 kW to 637 kW, while the electricity peak demand is reduced from 208 kW to around 192 kW.

Retrofit all buildings to follow BR2018		
Total area to be retrofitted:	21,169.00	m2
1960	9092.00	m2
1980	3539.00	m2
1990	8538.00	m2
Heat demand reduction	3001.35	MWh
Electricity demand reduction	54.20	MWh
Total achievable reduction	3055.55	MWh
Total achievable operational cost reduction	1,167,850.33 kr.	[DKK/year]

Figure 12. Building envelope retrofitting in the street case study.

	Heat Consumption reduction [MWh]	Heat Consumption reduction [%]	Heat consumption [MWh]	Heat consumption [kWh/m2]	Electricity consumption [MWh]	Electricity consumption [kWh/m2]
Total street(s)	**3001**	**61%**	**1928**	**79**	**885**	**36**
1-story	314	73%	116	79	49	34
2-story	0	0%	0	0	0	0
Appartments	2223	62%	1358	82	586	36
Offices	12	76%	4	94	2	41
Shops-food	86	75%	29	52	17	31
Shops	26	62%	15	54	65	226
Public Insitutions	340	48%	375	70	152	28
Others	0	0%	31	100	14	44
Peak capacity [kW]			637	26	192	8

Figure 13. Overall energy retrofitting results for the street case study.

5.2. District Case

In the second case study, a district consisting of five streets in Odense, Denmark, was selected to implement the DanCTPlan energy planning and retrofitting tool. The goal of this study is to showcase the core features of the tool in evaluating the district's energy supply systems and assessing the potential effects of retrofitting and integrating renewable energy sources. Much like the first case, the process begins by extracting the relevant data for this specific district from the Danish BBR building registry.

The district encompasses a total of 1284 buildings, with nearly half of them being small, conditioned spaces, along with various unconditioned sheds and storage rooms. Figure 14 illustrates the distribution of these building types within the district. Specifically, 549 of the buildings are categorized as one-story houses, 10 are apartment complexes, 9 are office buildings, 27 are food-related shops, and 4 are public institutions.

	Number of Buildings	Space area [m2]	Heat consumption [MWh]	Heat consumption [kWh/m2]	Electricity consumption [MWh]	Electricity consumption [kWh/m2]
Whole city	84,933		3,004,291,370	154,591	755,248,534	38,863
Total street(s)	1284	158,062	**22,755**	**107**	**7579**	**107**
1-story	549	86,855	13,069	128	3579	35
2-story	0	0	0	0	0	0
Appartments	10	9421	1225	105	408	35
Offices	9	15,480	2126	136	641	41
Shops-food	27	42,448	3077	64	1534	32
Shops	0	0	0	0	0	0
Public Insitutions	4	3858	614	70	250	28
Others	685	0	2644	100	1168	44
Peak Capacity [kW]			9029	42	1610	8

Figure 14. DanCTPlan output data for the district case study.

As highlighted in the output data tab of the figure, the district's estimated annual heating consumption is 22,754 MWh, with an annual electricity consumption of 7578 MWh. The tool also calculates the peak capacities for heating at 9029 kW and electricity at 1609 kW. These peak capacity estimates are essential for gaining an initial understanding of the scale and requirements of future energy systems for the district, whether in the form of new installations or retrofitting existing systems.

The tool also enables a detailed comparative analysis of current and projected fuel consumption under different scenarios. As shown in Figure 15, the district's heating demand is currently met by a mix of district heating, electric boilers, and heat pumps, with respective consumption figures of 22,629 MWh, 31,851 kWh, and 1464 kWh. Given that this district is situated in the heart of the city, district heating accounts for the largest share of heat supply. The adjacent column in the figure shows the potential fuel consumption if the district were to transition to a single fuel source for heating. If heat pumps were the exclusive heating source, the total annual electricity consumption would increase to about 7585 MWh. On the other hand, if heating were to be supplied by wood pellets, the annual consumption would amount to around 5617 tons. The economic evaluation further reveals that the current cost of delivering heating is approximately 7087 kDKK for district heating, 47 kDKK for electric boilers, and 2.2 kDKK for heat pumps.

Heating sources			Economics
	Consumption	Consumption if the whole street uses the same fuel	Cost of operation [DKK/year]
District Heating [MWh]	22,629.51	22,754.68	7,087,561.59
Natural Gas [m3]	0	2,482,309.32	0.00
Diesel [m3]	0	2740	0
Fuel oil [kg]	0	2,418,190.62	0
Biogas [m3]	0	4,273,889.08	0
Wood Chips [kg]	0	10,569,833.21	0
Wood Pellets [kg]	0	5,617,111.37	0
Heat Pump [kWhel]	1464	7,584,894.70	2197
Electric Boiler [kWhel]	31,851.67	25,030,152.50	47,777.50

Figure 15. Heating demand breakdown and energy resource evaluation for the district case study.

Figure 16 provides a detailed breakdown of energy consumption for heating and electricity by building category, offering a clear visualization of how different types of buildings contribute to the overall energy usage in the district. Complementing this, Figure 17 presents the number of buildings categorized by the heating source currently

in use, providing a straightforward summary of energy consumption patterns across the different building types in the area.

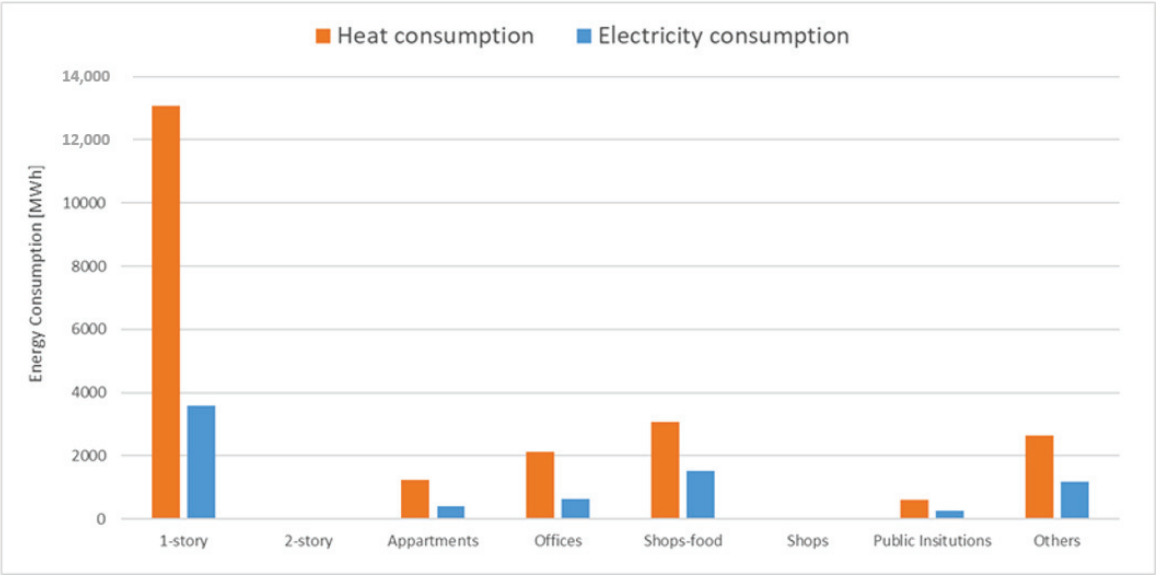


Figure 16. A breakdown of energy consumption for heating and electricity by building category for the district case study.

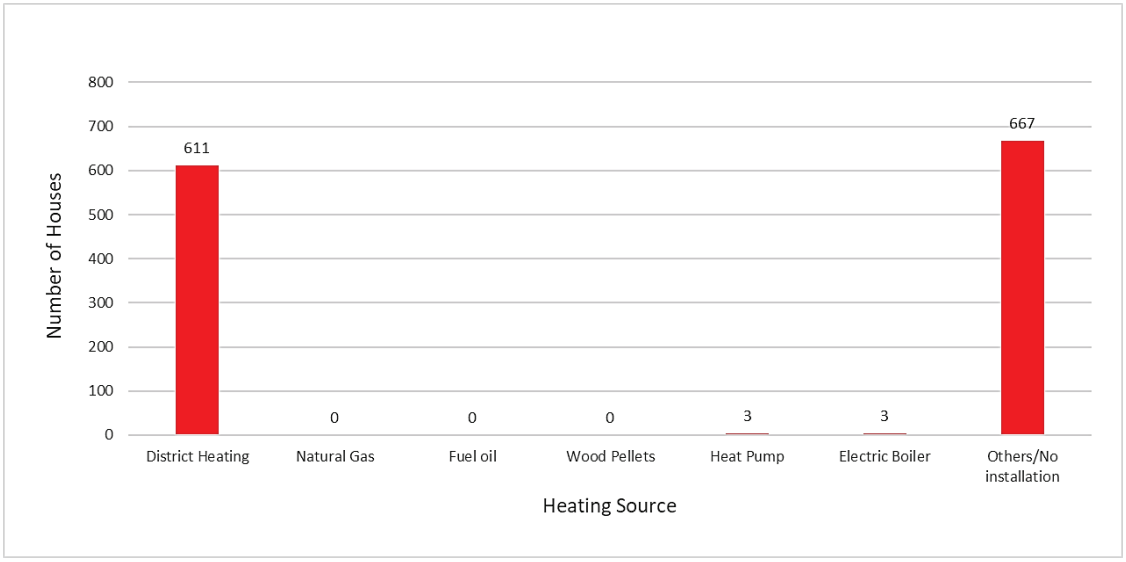


Figure 17. The number of buildings aggregated by the heating source for the district case study.

Regarding retrofitting, this study evaluates the impact of upgrading all buildings to meet the current building regulation standard, 'Class C'. As shown in Figure 18, the total area of buildings requiring retrofitting is approximately 104,969 m^2. This retrofitting would result in a reduction in heating demand by 6715.25 MWh (29.5%) and electricity demand by 183.95 MWh (2.4%). The overall and specific energy consumption of the buildings in the specific street after retrofitting are presented in Figure 19, showing a reduction in the peak heating and electricity demand to 4726 kW and 1357 kW, respectively.

Retrofit all buildings to follow BR2018		
Total area to be retrofitted:	104,969.00	m2
1960	1912.00	m2
1980	18,967.00	m2
1990	84,090.00	m2
Heat demand reduction	6715.25	MWh
Electricity demand reduction	183.95	MWh
Total achievable reduction	6899.20	MWh
Total achievable operational cost reduction	3,546,059.20 kr.	[DKK/year]

Figure 18. Building envelope retrofitting in the district case study.

	Heat Consumption reduction [MWh]	Heat Consumption reduction [%]	Heat consumption [MWh]	Heat consumption [kWh/m2]	Electricity consumption [MWh]	Electricity consumption [kWh/m2]
Total street(s)	**6715**	**30%**	**16,039**	**75**	**7395**	**35**
1-story	5120	39%	7949	78	3423	34
2-story	0	0%	0	0	0	0
Appartments	290	24%	936	80	413	35
Offices	666	31%	1460	94	633	41
Shops-food	601	20%	2476	51	1509	31
Shops	0	0%	0	0	0	0
Public Insitutions	39	6%	575	65	248	28
Others	0	0%	2644	100	1168	44
Peak capacity [kW]			4727	22	1358	6

Figure 19. The overall energy retrofitting results for the district case study.

Additionally, Figure 20 compares the impact of retrofitting on the district's monthly heating demand, providing an overall view of how retrofitting would improve energy efficiency and reduce consumption.

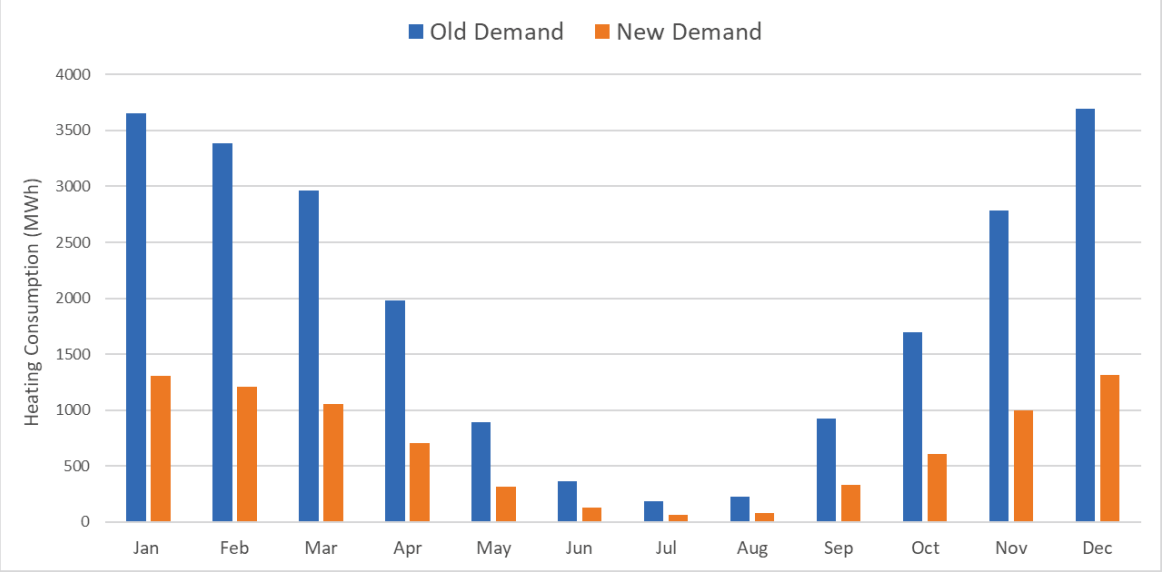


Figure 20. The impact of building envelope retrofitting on the district's building monthly heating demand.

To further illustrate the tool's capabilities, the study examines a scenario in which 30% of the district's electricity demand is met by photovoltaic (PV) systems, and 10% of the heating demand is provided by solar thermal-driven district heating. Figures 21 and 22 show the resulting heat and electricity balances for this scenario. According to our calculations, the district would need to install approximately 2218 kW of PV systems and around 3540 kW of solar thermal collector capacity. While these calculations are based on tabulated solar system generation data, as well as assumptions about the implementation process, these figures provide a foundation for future scenario planning. They can also guide the integration of various energy supply and storage solutions, paving the way for more sustainable and efficient energy systems in the district. This approach will not only support future energy scenarios, but also encourage the exploration of diverse renewable energy solutions, driving the district towards greater energy independence and environmental sustainability.

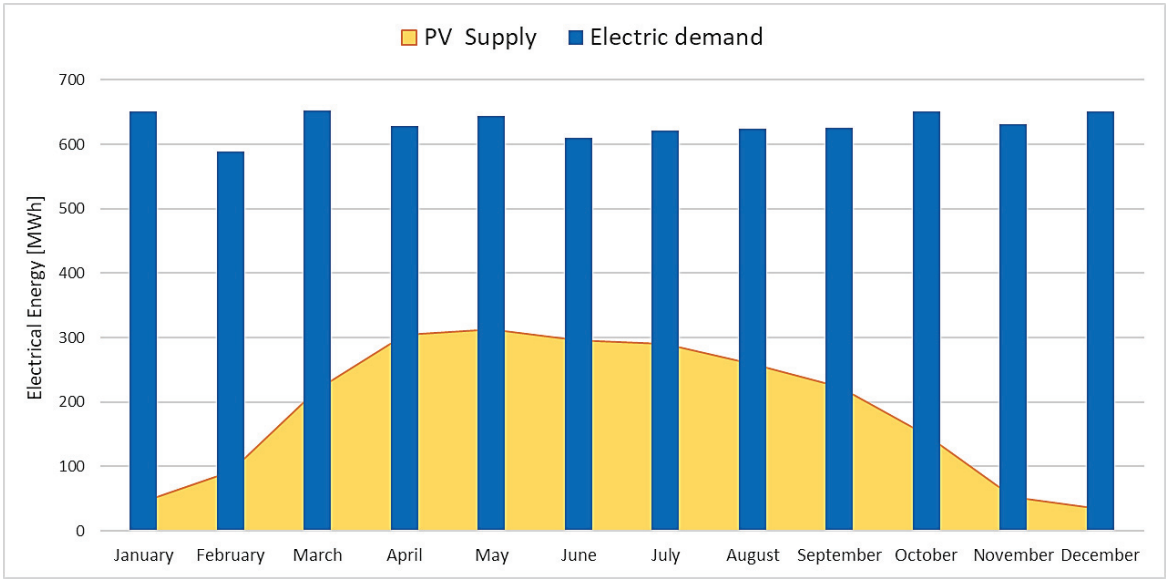


Figure 21. The electricity balance for the district under a scenario where 30% of the electricity demand is supplied by photovoltaic (PV) systems.

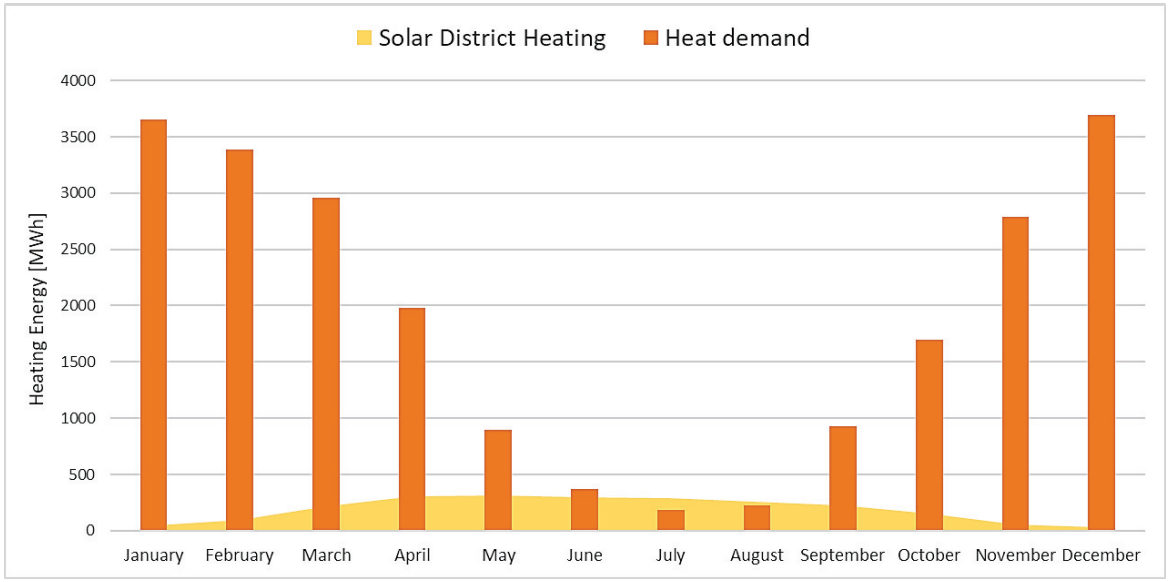


Figure 22. The heat balance for the district under a scenario where 10% of the heating demand is met by solar thermal-driven district heating.

6. Discussion and Future Insights

6.1. Strengths and Practical Applications

The DanCTPlan tool presents an innovative approach to urban energy planning, designed to tackle some of the most complex challenges in the field. Unlike traditional models that focus on individual buildings, DanCTPlan takes a big-picture approach, analyzing energy performance across streets, districts, and entire neighborhoods. By combining dynamic energy simulations using Energy Plus with data from the Danish Building and Housing Register (BBR) and the BR18 building standard, it delivers a good level of evaluation detail. It factors in critical details like building type, age, and usage, enabling accurate predictions for heating and electricity demands across a wide range of urban scenarios.

One of the tool's standout features is its ability to address the persistent energy performance gap between what is predicted and what happens in real life. By comparing simulated energy use with actual consumption, DanCTPlan helps identify where things are not adding up and points the way to smarter solutions. It also aids in evaluating retrofitting measures, showing how upgrades can affect energy use not just in one building but across an entire district. On top of that, it is equipped to assess how renewable energy sources, like solar panels, wind turbines, and solar thermal systems, can be integrated into the urban level, making it a potential tool for Denmark's ambitious sustainability goals.

The tool's applications are vast, spanning from a single street to a city district. It is designed to be intuitive and efficient, yet simple and user-friendly, making it accessible to urban planners, policymakers, and energy consultants. By leveraging actual information on the building level, its predictions are not only accurate but also directly actionable. Moreover, the modular nature of the tool means it can keep evolving, incorporating new energy technologies as they emerge.

The tool also uses comprehensive algorithms to deliver detailed simulations, avoiding the common pitfalls of static models that often oversimplify energy needs. For example, it provides precise calculations for peak demand, helping design energy systems that are both cost-effective and reliable. It also brings economic clarity to the table, allowing stakeholders to weigh the financial implications of retrofitting or transitioning to renewable energy. Urban planners can use the tool to optimize energy use in dense areas, while policymakers can rely on it to develop strategies for cutting emissions and improving energy resilience.

When compared to existing urban-scale energy tools, DanCTPlan stands out for its holistic urban focus. While these tools excel in detailed simulations for individual buildings and their integrations, they often require advanced technical expertise and are less suited for large-scale, integrated urban planning. Furthermore, conventional urban energy planning tools are characterized by a large level of complexity with exhaustive inputs, vast assumptions, and standardized evaluation metrics. In contrast, DanCTPlan combines the granularity of building-specific data with broader urban analyses, making it a valuable resource for municipalities and planners. Additionally, its dynamic validation mechanisms, comparing simulated data with real-world usage, help reduce the persistent performance gaps seen in many energy models. This capability sets it apart from conventional energy planning platforms, which rely heavily on static assumptions, offering a more adaptable and accurate tool for long-term urban energy planning.

One of DanCTPlan's most significant strengths is its accessibility and usability. Designed with an intuitive interface, the tool minimizes the technical barrier for stakeholders such as urban planners, policymakers, and energy consultants. By enabling straightforward data input, scenario configuration, and result analysis, it broadens its applicability, particularly in smaller municipalities or organizations with limited technical expertise. Its modularity allows adaptation to diverse urban contexts and energy planning scenarios, ranging from small neighborhoods to city-wide assessments. These attributes make

DanCTPlan a key enabler for municipalities striving to meet sustainability goals and carbon neutrality targets.

In addition, validation through case studies has demonstrated the tool's practical utility and reliability. Similarly, our district-level analyses provided actionable insights into the impact of retrofitting and renewable energy adoption. These applications illustrate the tool's potential to inform large-scale energy transitions, optimize resource allocation, and guide sustainable urban development.

6.2. Limitations and Challenges

Despite its strengths, DanCTPlan has several limitations that must be acknowledged. The tool relies on a range of assumptions to simulate complex urban dynamics, such as uniform weather conditions. While these assumptions ensure computational feasibility, they may oversimplify real-world scenarios. For example, dynamic events like disruptions or extreme weather are not fully accounted for, potentially impacting predictive accuracy in heterogeneous urban environments.

Additionally, the validation was conducted on a single street and a district within Denmark, limiting the generalizability of our findings. Variations in urban layouts, socio-economic conditions, and environmental factors across cities may require additional testing and calibration to extend the tool's applicability.

Furthermore, the accuracy of predictions is heavily reliant on the quality and resolution of input data. Inconsistent or incomplete datasets can undermine the reliability of outputs, emphasizing the need for robust data preprocessing and validation in future applications. One of the most significant challenges lies in the quality and availability of the Building and Housing Register (BBR) data, which serve as a cornerstone for the tool's analyses. These data often contain gaps or inaccuracies, particularly for older buildings or those with complex histories of renovation. For example, missing information about building materials, heating systems, or occupancy patterns can lead to discrepancies between the model's predictions and actual performance. Outdated data can be equally problematic, especially in dynamic urban environments where buildings are frequently updated or re-purposed. Without reliable and current input data, the tool's effectiveness is diminished, and its insights may lead to suboptimal planning decisions.

In the current version of the DanCTPlan tool, solar gains are estimated based on general assumptions related to building type, construction year, and location. However, building orientation is not considered, and shadows from neighboring buildings are not taken into account. This design choice was made to preserve the simplicity and applicability of the tool, ensuring it remains user-friendly and can be easily applied to large-scale urban scenarios without the need for complex inputs or detailed simulations. By omitting these details, the tool allows for quick, generalized assessments that can be applied across a variety of building types and locations without requiring extensive data or advanced expertise.

Moreover, to estimate solar radiation and wind energy for electricity generation, the tool utilizes tabulated data specifically tailored for Denmark. These data provide average solar radiation and wind speed values, which are used to predict potential renewable energy generation based on the location and type of building. The choice of using these data is driven by the goal of offering quick, generalized insights for urban energy planning, rather than requiring complex modeling of local factors like building shading or aerodynamic effects. While incorporating these aspects could improve the accuracy of predictions, the current design prioritizes the ability to scale and apply the tool across various urban scenarios with minimal data requirements.

Another area of concern is the way DanCTPlan calculates heating resource capacity. The tool employs simplified methods to estimate thermal performance, which, while effective for large-scale assessments, can sometimes overlook the intricacies of thermal dynamics. For instance, it may not fully account for variations in heat distribution within buildings, differences in thermal inertia, or the effects of specific operational conditions. These oversimplifications can result in less precise recommendations for heating system design, particularly for projects requiring tailored solutions to optimize energy use.

The tool's approach to retrofitting also has its limitations. While DanCTPlan excels at evaluating the overall energy efficiency of building envelopes, its analysis stops short of breaking down individual components such as windows, doors, walls, and roofs. This can be a drawback for stakeholders interested in more granular insights, such as the energy saving potential of replacing specific windows with higher-performance alternatives or adding insulation to a particular wall section. Such detailed assessments are often critical for ensuring that retrofitting projects achieve their maximum potential for energy savings and cost-effectiveness.

Furthermore, the tool's ability to model the long-term performance of decentralized energy solutions remains somewhat constrained. As these systems are highly sensitive to operational and environmental changes, a lack of real-time data integration means that predictions may fail to capture dynamic shifts in energy performance. For example, variations in local weather conditions or fluctuating occupancy levels can have significant effects on decentralized systems like solar panels or small-scale biomass boilers.

6.3. Future Directions

To address these limitations and enhance this tool's role as a comprehensive decision-support tool, the following future developments are proposed:

- Leveraging Real-Time Data Streams: Employing smart meter readings and IoT-enabled sensors, could enable the dynamic modeling of energy systems. This enhancement would allow the tool to respond to temporal variations and improve its adaptability to real-world urban energy dynamics.
- Expanding Validation and Scalability: Broader validation across diverse urban settings, including regions with varying climates, energy systems, and regulatory frameworks, will ensure greater generalizability. Future iterations should focus on refining algorithms to accommodate these variations and scaling the tool for larger urban areas.
- Enhancing Environmental and Socio-Economic Analysis: Integrating detailed lifecycle cost analyses, carbon footprint assessments, and equity-focused metrics will provide a more comprehensive framework for decision-making. This would align the tool with broader sustainability and social inclusion goals.
- User Interface Enhancements: Simplifying the interface with dashboards, interactive visualizations, and guided workflows will broaden the tool's accessibility, especially for non-expert users. This would make it a valuable resource for diverse stakeholders, including city planners and policymakers in resource-constrained settings.
- Multi-Scenario Analysis and Policy Support: Developing a multi-scenario analysis feature would enable users to model various "what-if" scenarios, such as the impact of integrating renewable energy systems or conducting large-scale retrofitting under different policy conditions. This capability would support data-driven policymaking and urban resilience planning.

Overall, the DanCTPlan tool represents a significant step forward in urban energy planning, offering a scalable, adaptable, and user-friendly platform for addressing energy challenges. By addressing its current limitations and integrating advanced features, DanCTPlan has the potential to evolve into a comprehensive decision-support system

that bridges the gap between energy forecasting and holistic urban energy planning. As cities worldwide strive to meet ambitious sustainability goals, DanCTPlan can play a pivotal role in empowering stakeholders to design energy-efficient, resilient, and low-carbon urban futures.

7. Conclusions

The DanCTPlan tool provides a robust platform for energy consumption forecasting and analysis, offering significant potential to support urban-scale energy planning and efficiency improvements. While the tool excels in delivering accurate energy predictions based on validated building energy models, its role extends beyond forecasting to contribute valuable insights that inform the energy planning process. The tool's integration of real, localized data from the Danish Building and Housing Register (BBR) and its ability to simulate the effects of energy retrofitting and renewable energy adoption strengthen its practical utility.

The results from the case studies demonstrate the tool's capability to analyze energy demand and evaluate retrofitting scenarios. For instance, in the Odense Street case study, retrofitting all buildings to the 'Class C' standard led to a 60.8% reduction in heating demand and a 5.8% reduction in electricity demand, alongside substantial reductions in peak heating capacity. Similarly, for the district-level case study of 1284 buildings, the tool projected a 29.5% reduction in heating demand and a 2.4% reduction in electricity demand under the same retrofitting scenario, showcasing its utility for large-scale applications.

However, it is essential to note that the DanCTPlan tool functions primarily as an energy forecasting and analysis platform, which provides foundational inputs to decision-making rather than encompassing the entire decision-making process itself. The insights generated by the tool enable stakeholders to assess energy system performance, allocate resources efficiently, and explore sustainable energy solutions. Yet, the tool's outputs must be integrated with broader decision-making frameworks involving economic, policy, and social considerations to fully align with the comprehensive theme of urban energy planning outlined in this study's title.

Future work will focus on advancing the tool's capabilities to better support holistic decision-making processes. This includes incorporating features for lifecycle cost analysis, carbon footprint evaluation, and socioeconomic impact assessments, thereby providing a more comprehensive framework for policymakers and urban planners. Enhancing the tool's scalability to cover larger regions and diverse building typologies, as well as integrating advanced machine learning algorithms and real-time data for predictive analytics and optimization, will further strengthen its impact.

By addressing these developments, DanCTPlan can evolve into a comprehensive decision-support system, empowering stakeholders to design and implement sustainable, resilient, and low-carbon urban energy systems. This evolution will bridge the current gap between energy forecasting and holistic energy planning, ensuring that the tool meets the needs of urban energy transitions in Denmark and beyond.

Funding: This research was carried out under the 'SDU Participation in IEA Annex 89—Ways to Implement Net-zero Whole Life Carbon Buil-dings' project, funded by the Danish Energy Agency (Energistyrelsen) under the Energy Technology Development and Demonstration Program (EUDP), ID number: 134234-511994.

Data Availability Statement: Data are contained within the article.

Acknowledgments: The authors would like to acknowledge the support of Barbara Jepsen, Tom Haut, and Emil Wang Nielsen in the establishment of the DanCTPlan tool.

Conflicts of Interest: The authors declare no conflicts of interest. The funders had no role in the design of the study; in the collection, analyses, or interpretation of the data; in the writing of the manuscript, or in the decision to publish the results.

References

1. Hernandez, J.L.; de Miguel, I.; Velez, F.; Vasallo, A. Challenges and opportunities in European smart buildings energy management: A critical review. *Renew. Sustain. Energy Rev.* **2024**, *199*, 114472. [CrossRef]
2. Muñoz, I.; Hernández, P.; Pérez-Iribarren, E.; García-Gusano, D.; Arrizabalaga, E. How can cities effectively contribute towards decarbonisation targets? A downscaling method to assess the alignment of local energy plans with national strategies. *Energy Strategy Rev.* **2023**, *49*, 101137. [CrossRef]
3. Soussi, A.; Zero, E.; Bozzi, A.; Sacile, R. Enhancing Energy Systems and Rural Communities through a System of Systems Approach: A Comprehensive Review. *Energies* **2024**, *17*, 4988. [CrossRef]
4. Amiri, S.S.; Mueller, M.; Hoque, S. Investigating the application of a commercial and residential energy consumption prediction model for urban Planning scenarios with Machine Learning and Shapley Additive explanation methods. *Energy Build.* **2023**, *287*, 112965. [CrossRef]
5. Wu, H.; Yang, C.; Liang, A.; Qin, Y.; Dunchev, D.; Ivanova, B.; Che, S. Urbanization and Carbon Storage Dynamics: Spatiotemporal Patterns and Socioeconomic Drivers in Shanghai. *Land* **2024**, *13*, 2098. [CrossRef]
6. Wu, W.; Wang, Z.; Wu, K.; Chen, Y.; Wang, S.; Niu, X. Urban resilience framework: A network-based model to assess the physical system reaction and disaster prevention. *Environ. Impact Assess. Rev.* **2024**, *109*, 107619. [CrossRef]
7. Camporeale, P.E.; Pilar, M.-M. Retrofit strategies to mitigate overheating linking urban climate modeling and urban building simulations with outdoor comfort: An urban sector in Malaga (Spain). *Energy Build.* **2023**, *298*, 113531. [CrossRef]
8. Lund, H.; Mathiesen, B.V. Energy system analysis of 100% renewable energy systems—The case of Denmark in years 2030 and 2050. *Energy* **2009**, *34*, 524–531. [CrossRef]
9. Jepsen, B.; Haut, T.; Jradi, M. Towards energy efficient planning of Danish cities and neighbourhoods. In Proceedings of the 34th International Conference on Efficiency, Cost, Optimization, Simulation and Environmental Impact of Energy Systems (ECOS 2021), Taormina, Italy, 28 June–2 July 2021.
10. Mutani, G.; Todeschi, V. Building energy modeling at neighborhood scale. *Energy Effic.* **2020**, *13*, 1353–1386. [CrossRef]
11. Danish Building Regulation (BR18). Available online: https://bygningsreglementet.dk/ (accessed on 3 December 2024).
12. The Central Register of Buildings and Dwellings (BBR). Available online: https://ncrr.au.dk/danish-registers/the-central-register-of-buildings-and-dwellings-bbr (accessed on 2 December 2024).
13. Khani, A.; Khakzand, M.; Faizi, M. Multi-objective optimization for energy consumption, visual and thermal comfort performance of educational building (case study: Qeshm Island, Iran). *Sustain. Energy Technol. Assess.* **2022**, *54*, 102872. [CrossRef]
14. Zhou, Y.; Tam, V.W.; Le, K.N. Developing a multi-objective optimization model for improving building's environmental performance over the whole design process. *Build. Environ.* **2023**, *246*, 110996. [CrossRef]
15. Maturo, A.; Vallianos, C.; Buonomano, A.; Athienitis, A. A novel multi-level predictive management strategy to optimize phase-change energy storage and building-integrated renewable technologies operation under dynamic tariffs. *Energy Convers. Manag.* **2023**, *291*, 117220. [CrossRef]
16. Jradi, M.; Madsen, B.E.; Kaiser, J.H. DanRETwin: A Digital Twin Solution for Optimal Energy Retrofit Decision-Making and Decarbonization of the Danish Building Stock. *Appl. Sci.* **2023**, *13*, 9778. [CrossRef]
17. Park, J.; Wang, T.-H. An Integrated Urban Building Energy Benchmarking Workflow to Support Urban Energy Evaluation: A Case Study of Sheffield UK. *Buildings* **2024**, *14*, 3398. [CrossRef]
18. Na, W.; Liu, S. Benchmarking building energy consumption for space heating using an empirical Bayesian approach with urban-scale energy model. *Energy Build.* **2024**, *320*, 114581. [CrossRef]
19. Haneef, F.; Pernigotto, G.; Gasparella, A.; Kämpf, J.H. Application of Urban Scale Energy Modelling and Multi-Objective Optimization Techniques for Building Energy Renovation at District Scale. *Sustainability* **2021**, *13*, 11554. [CrossRef]
20. Sola, A.; Corchero, C.; Salom, J.; Sanmarti, M. Simulation Tools to Build Urban-Scale Energy Models: A Review. *Energies* **2018**, *11*, 3269. [CrossRef]
21. Salvalai, G.; Zhu, Y.; Sesana, M.M. From building energy modeling to urban building energy modeling: A review of recent research trend and simulation tools. *Energy Build.* **2024**, *319*, 114500. [CrossRef]
22. Wong, C.H.H.; Cai, M.; Ren, C.; Huang, Y.; Liao, C.; Yin, S. Modelling building energy use at urban scale: A review on their account for the urban environment. *Build. Environ.* **2021**, *205*, 108235. [CrossRef]
23. Reinhart, C.F.; Cerezo Davila, C. Urban building energy modeling—A review of a nascent field. *Build. Environ.* **2016**, *97*, 196–202. [CrossRef]
24. Kamel, E. A Systematic Literature Review of Physics-Based Urban Building Energy Modeling (UBEM) Tools, Data Sources, and Challenges for Energy Conservation. *Energies* **2022**, *15*, 8649. [CrossRef]

25. Abbasabadi, N.; Ashayeri, M. Urban energy use modeling methods and tools: A review and an outlook. *Build. Environ.* **2019**, *161*, 106270. [CrossRef]
26. Chen, Y.; Hong, T.; Piette, M.A. Automatic generation and simulation of urban building energy models based on city datasets for city-scale building retrofit analysis. *Appl. Energy* **2017**, *205*, 323–335. [CrossRef]
27. Fonseca, J.A.; Nguyen, T.-A.; Schlueter, A.; Marechal, F. City Energy Analyst (CEA): Integrated framework for analysis and optimization of building energy systems in neighborhoods and city districts. *Energy Build.* **2016**, *113*, 202–226. [CrossRef]
28. Fathi, S.; Srinivasan, R.; Fenner, A.; Fathi, S. Machine learning applications in urban building energy performance forecasting: A systematic review. *Renew. Sustain. Energy Rev.* **2020**, *133*, 110287. [CrossRef]
29. Hong, T.; Chen, Y.; Luo, X.; Luo, N.; Lee, S.H. Ten questions on urban building energy modeling. *Build. Environ.* **2020**, *168*, 106508. [CrossRef]
30. Zhang, S.-C.; Yang, X.-Y.; Xu, W.; Fu, Y.-J. Contribution of nearly-zero energy buildings standards enforcement to achieve carbon neutral in urban area by 2060. *Adv. Clim. Change Res.* **2021**, *12*, 734–743. [CrossRef]
31. Mansó Borràs, I.; Neves, D.; Gomes, R. Using urban building energy modeling data to assess energy communities' potential. *Energy Build.* **2023**, *282*, 112791. [CrossRef]
32. Deng, Z.; Chen, Y.; Yang, J.; Causone, F. AutoBPS: A tool for urban building energy modeling to support energy efficiency improvement at city-scale. *Energy Build.* **2023**, *282*, 112794. [CrossRef]
33. Jradi, M.; Nielsen, E.W.; Lund, M. A Comprehensive Technical Analysis of Retrofitting a Danish Residential Area into a Positive Energy District. *Future Cities Environ.* **2023**, *9*, 18. [CrossRef]
34. Jepsen, B.K.H.; Haut, T.W.; Jradi, M. Design, Modelling and Performance Evaluation of a Positive Energy District in a Danish Island. *Future Cities Environ.* **2022**, *8*, 1. [CrossRef]
35. Engelbrecht Foldager, H.; Camillus Jeppesen, R.; Jradi, M. DanRETRO: A Decision-Making Tool for Energy Retrofit Design and Assessment of Danish Buildings. *Sustainability* **2019**, *11*, 3794. [CrossRef]

Disclaimer/Publisher's Note: The statements, opinions and data contained in all publications are solely those of the individual author(s) and contributor(s) and not of MDPI and/or the editor(s). MDPI and/or the editor(s) disclaim responsibility for any injury to people or property resulting from any ideas, methods, instructions or products referred to in the content.

MDPI AG
Grosspeteranlage 5
4052 Basel
Switzerland
Tel.: +41 61 683 77 34

Energies Editorial Office
E-mail: energies@mdpi.com
www.mdpi.com/journal/energies



Disclaimer/Publisher's Note: The title and front matter of this reprint are at the discretion of the Guest Editors. The publisher is not responsible for their content or any associated concerns. The statements, opinions and data contained in all individual articles are solely those of the individual Editors and contributors and not of MDPI. MDPI disclaims responsibility for any injury to people or property resulting from any ideas, methods, instructions or products referred to in the content.





Academic Open
Access Publishing

mdpi.com

ISBN 978-3-7258-4188-2